SENSOR TECHKNOWLEDGE

Sensors for Process Development: A Practical Guide

Govind Rao

CAST
Center for Advanced Sensor Technology
UMBC
Chemical
Biochemical and
Environmental
Engineering

Inspiration

How much better to get wisdom than gold! To get understanding is to be chosen rather than silver. The Bible

The greatest gift is to give people your enlightenment, to share it. It has to be the greatest. The Buddha

Ask a question and you're a fool for three minutes – don't ask a question and you're a fool all your life. Chinese proverb

Work for work's sake, not for yourself. Act but do not be attached to your actions. Be in the world, but not of it. Bhagavad Geetha

Burn worldly love, rub the ashes and make ink of it, make the heart the pen, the intellect the writer, write that which has no end or limit. Guru Nanak

My Lord! Enrich me with knowledge… The Quran

If thou lackest knowledge, what hast thou then acquired? Hast thou acquired knowledge, what else dost thou want? The Talmud

A knife of the keenest steel requires the whetstone, and the wisest man needs advice. Zoroaster

Acknowledgements

This book is dedicated to:

Taxpayers of America, who funded most of the work that led to the papers described here and to the taxpayers of Maryland, who gave my lab the means to do the work and finally, the taxpayers of India, who gave me an amazing and largely free public education.

Students, postdocs, collaborators whose work over the years advanced the state-of-the-art in bioprocess monitoring and are the co-authors of many of the publications.

UMBC colleagues for support and allowing the creation of the Center for Advanced Sensor Technology.

Friends in industry who kept pushing me to find better solutions to their problems and to Jim Swartz who started it with a seminar invitation to Genentech.

Patent licensees who enabled the work to be commercialized, in particular: Fluorometrix, Scientific Bioprocessing, Sartorius-Stedim and GE Healthcare. Joe Qualitz and Joe Cremonese, you inspire me.

Original copyright holders (Wiley and Elsevier) for generously granting me permission to reprint the papers.

Mentors for their guidance at every stage of my personal and professional life. Raj Mutharasan for taking a chance on me. Profs. Art Humphrey, Danny Wang, Jay Bailey and Mike Shuler for treating me as one of their own students and generously mentoring me at a critical early stage.

My faithful companions Xudong Ge, Dan Kostov and Leah Tolosa, all former students/postdocs who decided that staying at CAST was what they wanted to do even when they could have gone anywhere.

Family for their constant support.

My teacher for always reminding me that:

"God gave you the time, space, cause, material, idea, skill, chance, and fortune. Why should you feel as if you are the doer?"

- Bhagawan Sri Sathya Sai Baba

It is with this spirit that I have compiled this book and tried to distill insights gathered over almost 30 years of bioprocessing and sensor development. I am making the book available to anyone who wants to learn more about the field free of charge. The only hope and expectation I have is that it is useful to the reader and helps either give you some new knowledge and understanding or solves a practical problem that you may be facing.

Please send me any questions/comments/criticism via email to grao@umbc.edu.

Sincerely,

Govind Rao

Center for Advanced Sensor Technology
And
Department of Chemical, Biochemical and Environmental Engineering
University of Maryland, Baltimore County
Baltimore, MD 21250

Table of Contents

Introduction

Congratulations on opening this book and getting to this point. It appears that you have some interest in learning more about how to effectively grow cells in culture and to get a better handle on the environment that they are occupy. This book should help you understand how important it is to monitor the cellular environment and also to guide you towards the tools, tips and techniques to do so.

The papers are not presented in temporal order. Rather, I have chosen to tell the story of each sensor and its application. I have attempted to bring them to life by giving some background about each paper, the people involved and how the work ended up being done. Sometimes, the back story can be as illuminating as the main subject itself and I have tried to capture this aspect.

PART I: Non-invasive Sensors

It all began with trips to industry. Extending my doctoral work, I was working on the use of redox sensors for trying to gain an understanding of the relationship between the extracellular milieu (culture redox potential as measured by a platinum electrode) and intracellular parameters like NADH levels (measured by culture fluorescence), which give the cellular metabolism its reducing power. I was always interested in trying to connect the environment of the cell to its metabolic behavior. Given its obvious importance to bioprocess monitoring, I received several invitations from friends in industry to visit and give seminars. There was keen interest in our work, but at the time, the primary focus in industry was to measure oxygen and pH. The sensors for these parameters that were available were very bulky and expensive. They also did not work very well. Although the Clark electrode derived oxygen sensors had been refined to work as sterilizable probes in bioreactors, they tended to drift, be subject to electrical interference and not wholly reliable. And given that most processes were aerobic and that supplying oxygen to cells, especially at larger scales was critical, measuring oxygen accurately to control processes was probably the number one pain point experienced in industry. I listened to a litany of woes about various process development and manufacturing issues that had been caused by failing/inaccurate oxygen measurements. pH electrodes were a bit better, but also had their own issues including fragility. Given our nascent expertise in sensor development, a frequent wish expressed was that for better process monitoring sensors.

About this time (around 1990) I met Prof. Joseph Lakowicz, a pioneer in fluorescence measurements. As I learnt, oxygen is a potent quencher of fluorescence. Lakowicz had shown very intriguing data on a Ruthenium compound that showed a large change in fluorescence as a function of the oxygen level around it. It was also a molecule that had a long fluorescence lifetime, meaning that the electronics needed to measure the fluorescence could be economically constructed. However, what was more interesting to me was that the molecule could be immobilized in silicone. It was also heat-stable, which held the possibility of using it to create an oxygen sensor that could be steam-sterilized and also end up in a form factor suitable for use in place of a standard oxygen electrode that was in use in bioreactors. All these requirements led to the first paper here and describes how the sensor was fabricated, tested and demonstrated in a fermentation.

There is an interesting back story here as well. I had applied for NSF funding to create these new non-invasive optical sensors. However, I had proposed a $3,000 blue laser as the light source. The reviewers thought this to be impractical and so reduced the grant duration to two years, as they nevertheless considered the idea worthy of pursuit. Luckily, this period coincided with the first blue LEDs entering the market and we were able to use one of them instead of a laser. However, the first-generation LEDs were so dim, that we needed a photomultiplier tube to capture the emission. Thankfully, they rapidly got bright enough that subsequent generation instruments now use them along with low-cost detectors, making the optical instrumentation truly low-cost and widely useable. I have a profound sense of satisfaction because this body of work helped bring about a paradigm shift in the state-of-the-art in bioprocessing and biomanufacturing.

Chapter One: Oxygen and pH

The journey began with Bambot et al. In our quest to improve upon the current existing gold standard, the Ingold type steam sterilizable electrode, we decided to use the housing of one to build our optical sensor. There were two reasons for this. One was to use a form factor that was a standard in the bioprocessing world and the second was to make the sensor look like the familiar sensor and amenable to steam sterilization. The paper describes our detailed fabrication and validation of the system.

Shabbir Bambot came to the lab after a Ph.D. at the University of Pittsburgh. He was very bright, enthusiastic to learn new things and great with his hands. Along with a graduate student in Electrical Engineering (Raja Holvanahali) and his mentor Prof. Gary Carter, he modified a laboratory grade phase fluorometer to couple with a fiber optic bundle that he inserted into the gutted housing of an oxygen electrode. He put in an optical window and this allowed us to put the oxygen sensor outside the window, in contact with the fermentation media so it could be sterilized in an autoclave and the fiber bundle could be inserted later (see Figure 2). Prof. Lakowicz provided advice on the fluorescence measurements.

It was a weird setup. The phase fluorometer (ISS K2) was a black box about the size of a suitcase and it was on a large optical table. The fermentor was a 2 liter spinner flask where we had inserted a conventional oxygen sensor for comparison purposes. The lab had blacked out windows since it was used for sensitive optical measurements and so everything was dark to minimize stray light effects. So the entire setup looked like it was out of a Frankenstein movie, with lights, strange liquids bubbling away and lots of cables and tubes everywhere!

It worked right away. It was apparent that the optical sensor, by virtue of the non-linear calibration curve was going to be very useful in low-oxygen ranges and fortuitously that is where one wants the greatest accuracy in bioprocess applications.

This paper showed us that a compact oxygen sensor was not far away and set the stage for subsequent work.

Phase Fluorometric Sterilizable Optical Oxygen Sensor

Shabbir B. Bambot,[1] Raja Holavanahali,[2] Joseph R. Lakowicz,[3] Gary M. Carter,[2] and Govind Rao[1]*

[1]Department of Chemical and Biochemical Engineering and Medical Biotechnology Center of the Maryland Biotechnology Institute, University of Maryland Baltimore County, Baltimore, Maryland 21228; [2]Department of Electrical Engineering, University of Maryland Baltimore County, Baltimore, Maryland 21228; and [3]Center for Fluorescence Spectroscopy, Department of Biological Chemistry and Medical Biotechnology Center of the Maryland Biotechnology Institute, University of Maryland at Baltimore, Baltimore, Maryland 21201

Received September 1, 1993/Accepted December 15, 1993

We report here on a low-cost, optical oxygen sensor as an attractive alternative to the widely used amperometric Clark-type oxygen electrode for measuring dissolved oxygen tensions in cell cultures and bioreactors. Our sensor is based on the differential quenching of the fluorescence lifetime of a chromophore in response to the partial pressure of oxygen. This is measured as a phase shift in fluorescence emission from the chromophore due to oxygen quenching when excited by an intensity modulated beam of light. In this article we demonstrate the advantages of lifetime-based optical methods over both intensity based optical methods and amperometric electrodes. Our sensor is particularly suitable for measuring dissolved oxygen in bioreactors. It is autoclavable, is free of maintenance requirements, and solves the problems of long-term stability, calibration drifts, and reliable measurement of low oxygen tensions in dense microbial cultures that limit the utility of Clark-type electrodes.

Key words: fluorescence lifetime • phase modulation fluorometry • dissolved oxygen tension • oxygen measurement

INTRODUCTION

The monitoring and control of oxygen concentrations is of great importance in various commercial and scientific applications. The industry standard for oxygen measurement, the modified polarographic Clark electrode has now been available for more than three decades[6] and yet is still being constantly modified and perfected. The Clark electrode operates on the principle of oxygen reduction at a negatively biased platinum surface. The electrode is constructed with a silver anode, a platinum cathode, and a KCl or AgCl electrolyte. A Teflon or silicone membrane separates the electrode components from the surrounding medium. When the cathode is polarized with a negative voltage, oxygen diffusing through the membrane from the surrounding medium gets reduced at the surface of the cathode. The magnitude of the negative bias on the platinum electrode (–0.8 to –1 V) is maintained such that the electrode operates under conditions of membrane controlled diffusion. Since the diffusive flux is a function of the partial pressure of oxygen in the fluid, it is possible to calibrate the electrode current versus oxygen tension. Clark electrodes are calibrated by equilibrating a sample with nitrogen to read zero and followed with either air or oxygen to read 100%. The readings are usually expressed as a percentage of air saturation. Since the electrolyte is consumed during operation, over a period of time drifts in calibration occur. Despite these limitations and problems, the Clark electrode is widely used because it is the best available technique to date. We have briefly summarized the most critical issues, and for greater details the reader is directed to an excellent review by Lee and Tsao.[14]

1. Long-term stability: The polarographic Clark electrode utilizes an electrolyte that is eventually consumed. Consequently, long-term use (several days) results in gradual drift in the electrode signal due to electrolyte consumption.

2. Flow dependence: Since the electrode actually consumes oxygen, measurements in a stagnant sample cause the oxygen tension at the membrane sample interface to deplete, resulting in an extension of the diffusion layer into the sample (note that the electrode functions under conditions of membrane controlled diffusion). Thus controlling the sample renewal rate or flow rate at the membrane will affect the accuracy of the reading, the effect decreasing with increasing membrane thickness.

3. Response time: In the literature, response time is usually specified as the time taken for the electrode to reach >90% of the output. A fast response time is critical when one is measuring transient phenomena such as oxygen respiration rates in tissue or suspended cells or dynamic measurements of the volumetric mass transfer coefficient in bioreactors.

4. Electrical interface: When low-level electrical signals are measured, it is very likely that substantial error

* To whom all correspondence should be addressed.

CCC 0006-3592/94/0111139-07

may be introduced in the measurement by extraneous interferences such as ground loop currents and interaction with other electrodes (pH, redox, etc.). To circumvent this problem, one can either "float" the reference ground of the electrode by using an isolation amplifier[14] or a differential amplifier.

The problem with the Clark electrode is that some of these requirements have solutions that are opposing. For instance, flow dependence may be reduced by employing a thicker membrane, but this would occur at the cost of increased response time. As a result, most commercially available systems are design compromises that sacrifice a part of some desirable feature. It should be noted that an optical measurement technique where oxygen and/or electrolyte is not consumed will be free of the drawbacks mentioned above.

Optical sensing provides a promising alternative to amperometric methods in solving some of the problems mentioned above. A number of reports in recent years have demonstrated the feasibility of optical oxygen sensing using indicator molecules whose optical properties change with changing oxygen concentrations.[2,5,17,20] Additional advantages in using optical methods include small size, freedom from electrical interferences, no requirement of a reference cell, and the ability to do remote sensing using fiber optics.

The various optical methods available for general sensor applications can essentially be classified into three categories based on the following phenomena:

1. Absorbance
2. Fluorescence intensity
3. Fluorescence lifetime

The methods are listed in the order of increasing superiority. Fluorescence intensity sensing is clearly superior to absorbance based sensing because of higher sensitivity, selectivity (by choosing favorable excitation and emission wavelengths), and compatibility with laser excitation sources.[1,3] Most reports on optical oxygen sensing measure changes in fluorescence intensity upon oxygen quenching of the fluorophores. Although such a strategy yields near perfect results in an optically clean environment, most sensing applications required measuring oxygen in optically "dirty" systems like blood or microbial cultures in bioreactors.

Recent reports have shown fluorescence lifetime measurements to be superior to fluorescence intensity measurements.[4,13,15] This technique circumvents a variety of problems attributed to intensity based methods, including light losses, lamp drift, photobleaching, and leaching of the probe as well as optical properties of the environment.[13] At first, this seems to require more sophisticated and expensive instrumentation, but work by the authors and other laboratories has demonstrated the use of a long lifetime oxygen sensitive probe that can be excited using off-the-shelf blue light emitting diodes (LEDs) and electroluminescent light sources (ELLs). The long lifetime of the probe also permits the use of inexpensive electronics in collecting and measuring lifetime related information and allows the setup to be made compact and rugged. We have described the use of lifetime based sensing in making a workable and autoclavable optical oxygen sensor that is particularly adapted to measuring oxygen levels in bioreactors. As novel probes sensitive to other analytes (pH, CO_2, glucose, etc.) are synthesized, the technique described here could lead to a new generation of sensors.

Theory of Measurement

Fluorescence lifetime measurements can be accomplished using either of two methods: (1) time domain or (2) frequency domain fluorometry, often referred to as phase modulation fluorometry. Of the two the latter is preferable for sensing applications because of the possibility of constructing low cost instruments to measure even subnanosecond lifetimes. In a phase shift fluorometric sensor, the fluorescence lifetime is monitored by measuring the phase shift of the fluorescence radiation relative to the phase of the sinusoidally intensity modulated excitation light.[13] For a population of sensor molecules with a single exponential fluorescence decay, the measured phase angle shift θ depends on the fluorescence lifetime τ and on the modulation frequency f according to the expression

$$\tan \theta = 2\pi f\tau \qquad (1)$$

However, even if the intensity decay is multi- or nonexponential, there is a phase angle observable at each modulation frequency, which can be related to an apparent phase lifetime. Figure 1 shows the typical frequency response of phase for a single-exponential fluorescence decay. A change in fluorescence lifetime results in the shifting of the curve along the abscissa. Curves 1, 2, and 3 represent, respectively, the maximum, average, and minimum lifetimes encountered during the measurement. For a given error in

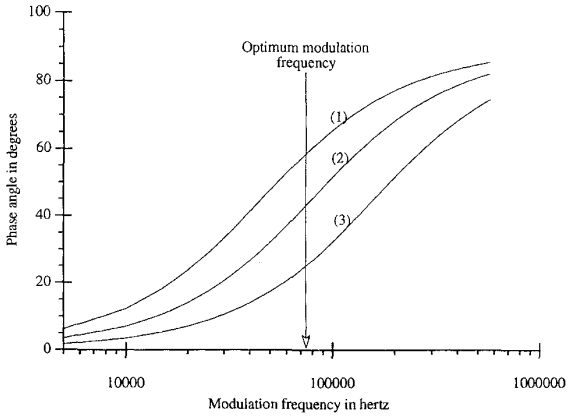

Figure 1. Typical frequency response of phase angles for a single-exponential decaying fluorophore. Curves 1 and 3 represent, respectively, the unquenched and quenched fluorescence lifetimes. Curve 2 is for an average fluorescence lifetime.

measuring θ, maximum lifetime measurement accuracy can be established by optimizing the modulation frequency of the light source. Thus, in Figure 1, this optimal frequency is that at which $\theta = 45°$ on the curve representing the average lifetime. From Equation (1) it follows that the optimum modulation frequency f_{opt} is given by

$$2\pi f_{opt}\tau = 1 \quad (2)$$

The oxygen sensitive molecular probe used in this study, tris [4,7-diphenyl-1,10-phenanthroline] Ru(II) complex,[7,8] was found to have an optimum modulation frequency of 76 kHz when immobilized in a silicone rubber membrane. The fluorescence of this complex is quenched by oxygen molecules resulting in a reduction of fluorescence lifetime. One can thus obtain a correlation between fluorescence lifetime and the partial pressure of oxygen (see Results section).

The long fluorescence lifetime of the ruthenium probe and hence the low modulation frequency permit the use of inexpensive electronics in collecting and measuring lifetime related information and allow the set up to be made compact and rugged. Furthermore, because of low light intensity requirements, the excitation light was provided using low-cost, off-the-shelf blue LEDs.

MATERIALS AND METHODS

Chemicals

The Ru(II) complex was synthesized at the Center for Fluorescence Spectroscopy, University of Maryland, Baltimore. All other reagents were purchased from Aldrich or Sigma. The silicone membrane was prepared by spreading a thin layer of GE Silicone II (Stock CE 5000, GE Silicones, General Electric Company, Waterford, NY) on a microscope slide using a blade. The thin layer (about 0.5 mm thick) was allowed to cure overnight and was then removed from the glass surface resulting in a thin transparent silicone membrane. The membrane was then soaked in a solution of the ruthenium complex in chloroform (typically 1.25 mg/mL) for 5 min allowing the silicone matrix to expand and absorb the fluorophore. The membrane was then removed and air dried for 5 min after which it shrank back to its original size. The membrane was washed with ethanol to remove surface fluorophore molecules and after drying was laid out on a circular glass window. In the final optrode configuration the membrane was held toward the sample with the glass window facing the excitation beam.

Optics and Electronics

Figure 2 shows a schematic of the experimental setup used to test the optical oxygen sensor. The excitation light from a blue silicon LED (CREE Research, Durham, NC) was coupled into one of the arms of a bifurcated fiber-optic bundle via a 450-nm low-wave-pass filter. The common

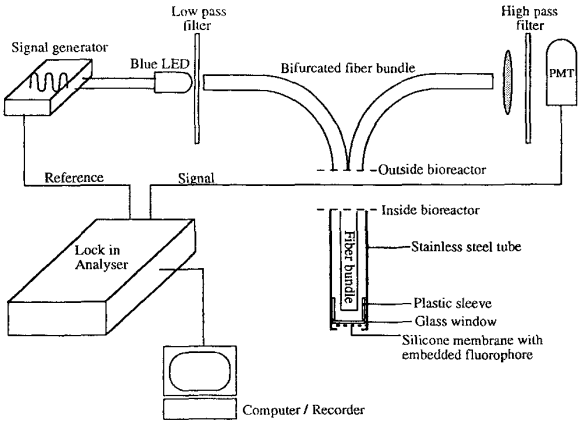

Figure 2. Experimental setup of optical oxygen sensor. The intensity modulated excitation light enters one arm of a bifurcated fiber bundle. The other arm carries the intensity modulated phase shifted fluorescence to a photomultiplier tube. The PMT signal phase is compared with the internal reference from the signal generator using a lock-in amplifier and the phase difference displayed on a computer.

end of the bifurcated fiber bundle had a core diameter of 4 mm whereas each arm had a core diameter of 3.5 mm. The peak emission wavelength of the LED was 470 nm with a spectral halfwidth of 70 nm. Inspite of the rather low optical output power, the small viewing angle (16°) of the LED enabled efficient coupling of the output into the fiber-optic, giving sufficient excitation light at the sensor. The emission was collected from the other arm of the bifurcated bundle. The detector used was a Hamamatsu R928 photomultiplier tube (PMT) in a Oriel PMT housing with a 8-mm-diamter entrance aperture. Stray excitation was prevented from entering by placing a 600-nm-long wave pass filter in front of the aperture. A focusing lens of 25 mm diameter helped in maximizing fluorescent light collection. The stem of the bundle was housed in a stainless steel tube which held the fluorophore embedded membrane in the excitation path.

The LED was sine wave modulated using a BK Precision Model 3020 sweep/function generator at 76 kHz. The circuit consisted of a 512-Ω resistance placed in series so as to limit the maximum current passing through the diode. The input voltage to the circuit was an AC voltage of 8.3 V (peak to peak) and DC voltage of 8.25 V. This ensured that the LED had a positive bias at all times. This operation of the LED resulted in an AC-to-DC light output of about 2.45 V AC (peak to peak) and DC voltage of 1.9 V. This is equivalent to 64% of light modulation. Note that light modulation percentage can be easily changed by changing the input voltages.

An EG&G 5206 two-channel heterodyning lock-in analyzer (Princeton, NJ) was used to detect the magnitude and phase of the PMT outlet. The lock-in amplifier affords the flexibility of measuring a pure signal using a narrow (1-Hz) bandwidth amplifier, thus eliminating any out-of-band

noise. Note that once parameters like frequency have been optimized, a simple single frequency phase discriminator can be used to build a significantly cheaper electronic circuit. As shown in Figure 2, the reference electrical signal against which the phase lag of the fluorescence signal can be determined was acquired directly from the signal generator.

Fermentation

The *Escherichia coli* fermentation experiments were conducted using a 2-L spinner flask equipped with both oxygen sensors, Clark-type and optical, at 25°C (controlled room temperature). The Clark-type electrode and oxygen preamplifier (OPA130) was purchased from Ingold Electrodes (Wilmington, MA). Two different media were used in the fermentation experiments, as explained in the Results section. The Luria–Bertani (LB) medium contained (in g/L) tryptone, 10; yeast extract, 5; and NaCl, 5. The GC medium contained (in g/L) casamino acids, 30; yeast extract, 20; glycerol, 40 (autoclaved separately); and $MgSO_4 \cdot 7H_2O$, 4 m*M*. Ampicillin, 0.01 g/mL (final), was added just before inoculation. The inocula were prepared using 100 mL of the same medium and grown overnight in a shake flask at 37°C. The stirring speed was maintained at 600 rpm and the gases were sparged at the rate of about 2 vvm (volume per volume per minute). The fermenter (including media and oxygen sensors) was autoclaved for 20 min at 120°C. The fermentation was carried out at room temperature and 1 mL antifoam (2.5%) was added when required. Optical density was measured at 660 nm.

The data from the two oxygen sensors was obtained on a Macintosh computer through an analog interface (Strawberry Tree Inc., Sunnyvale, CA). The capture rate was one data point per minute over a period of approximately 20 h.

Sensor Calibration

The sensors were calibrated both in the gaseous phase and in water at 25°C. The sensors were mounted inside a 2-L spinner flask which was sparged with a mixture of oxygen and nitrogen. The percentage of oxygen and nitrogen in the mixture was determined with the help of precision gas "flo-sensors" (model 310) from The McMillan Company, Coppers Cove, TX. Using needle valves, the flow rates of the two gases were controlled at different percentage combinations such that the total gas flow rate was always 5 L/min. The phase and voltage response of the optical and Clark-type electrode was recorded and plotted against percent oxygen (Fig. 3).

RESULTS AND DISCUSSION

Figure 3 shows the room temperature calibration curves for the Clark-type electrode and our optical sensor in (a) the gas phase and (b) water. Both environments show near identical calibrations. Whereas the Clark-type electrode shows a linear calibration the optical sensor shows a

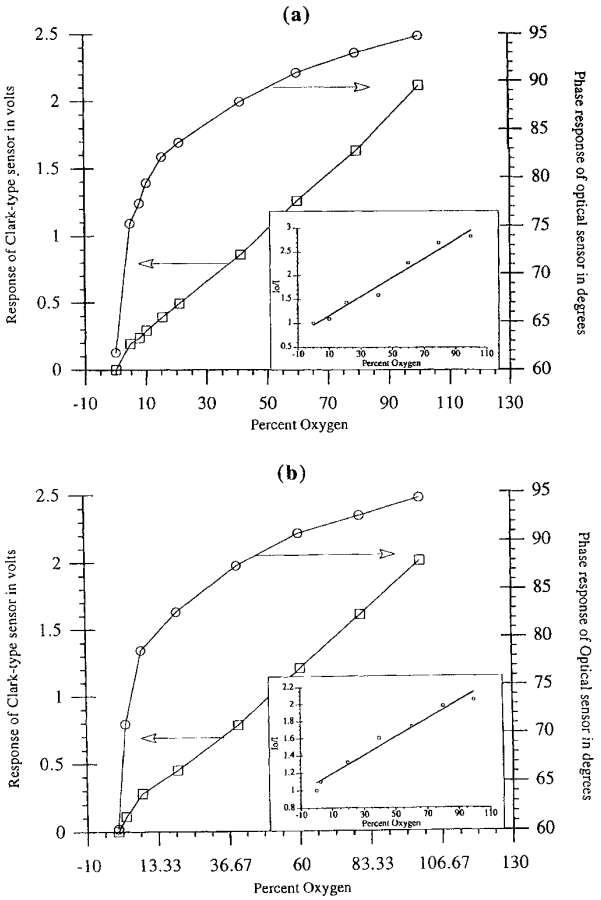

Figure 3. Calibration curves for optical sensor and Clark-type oxygen electrode. The phase response of the optical sensor and the voltage response of the Clark-type electrode is plotted against percent oxygen in the gas mixture (oxygen and nitrogen) sparged (a) directly) and (b) through water contained in a bioreactor at 25°C (controlled room temperature). Although the Clark-type electrode shows a linear calibration, the optical sensor shows a Stern–Volmer relationship (see text). Inset in each figure is the Stern–Volmer plot using intensity data collected in the respective calibration experiments.

hyperbolic response as predicted by the Stern–Volmer equation[18]

$$\tau_0/\tau = I_0/I = 1 + K_p O_2 \quad (3)$$

where τ_0 and τ are the unquenched (zero oxygen) and quenched lifetimes, I_0 and I are the corresponding unquenched and quenched fluorescence intensities, K is the overall quenching constant and pO_2 is the oxygen tension in the sample. The overall quenching constant K is an oxygen sensitivity parameter which in the case of lifetime measurement includes only the effect of dynamic quenching of fluorescence.

Significant deviations from the above theory are expected in real systems. First, in most real systems the probe molecules are immobilized in order to maximize response, minimize interference, and facilitate reuse. For this purpose

a suitable matrix or gel is used. However, it is difficult to mimic a solution like environment, and most often immobilization causes the probe molecules to exist in a microheterogeneous environment. This results in multi-exponential lifetimes that cannot be resolved accurately using a single exponential model.[5] Second, sensors based on fluorescence quenching undergo both static and dynamic quenching simultaneously, the relative contributions of which are not known.[15] Since fluorescence lifetimes are governed by dynamic quenching alone, the lifetime sensing method eliminates this uncertainty. In any case an exact fit of data to theory should not be expected. Although an attempt to fit the calibration data in Figure 3 with a Stern–Volmer equation gave a good fit at low oxygen tensions, the fit at higher levels of oxygen was not acceptable. In practice the use of an empirical calibration between observed phase angles and dissolved oxygen (DO) levels is recommended. Thus a cubic spline interpolated relation between phase angles and percent oxygen was used as the calibration for the optical sensor in converting phase angles to percent oxygen. A linear calibration was used to obtain percent oxygen from volts in the case of the Clark-type electrode.

Note that the sensitivity of the optical sensor at low oxygen tensions is significantly higher than that of the Clark-type electrode. This is partly due to the high oxygen permeability of silicone rubber membranes, which has the effect of increasing the overall quenching constant K in Equation (3). As a result higher oxygen sensitivities are obtained at low oxygen tensions, which is the operating regime for most bioreactor and wastewater treatment facilities. At high oxygen tensions, however, the optical sensor has a lower sensitivity because of the hyperbolic nature of the calibration curve. Consequently, in Figure 4 small errors in measuring phase angles result in large percent oxygen variations in this regime. The lock-in analyzer used in this study had a phase sensitivity of $\pm 0.5°$. As discussed earlier, building a dedicated phase discriminator with a higher sensitivity is possible and should alleviate this problem.

Figure 4 shows the transient response of the two sensors to alternate sparging of oxygen and nitrogen gases in water. As is apparent, large phase angle changes (and hence lifetime changes) are observed when the sparged gas is changed from nitrogen to oxygen and vice versa. Although the net response coincides with the response of the Clark-type electrode, the response time of the optical sensor was found to be superior (about 40% faster) to that of the Clark-type electrode at low (below 20% oxygen) oxygen tensions. At higher oxygen tensions the response time was comparable to that of the Clark-type electrode. However, at oxygen tensions above 75% the noise due to the given error in phase measurement by the lock-in analyzer (as discussed earlier) makes oxygen tension determination unreliable. Fortunately, oxygen tension measurement applications in this regime are rarely encountered.

To determine the autocalvability of the optical sensor, three different sensor membranes with varying probe concentrations (2.5, 1.25, and 0.625 mg/mL in chloroform) were autoclaved at 120°C for 40 min. In each case, an 8 to 10% reduction in dynamic range (difference in response between 0% oxygen and 100% oxygen) was observed after the first autoclaving. We attribute this to the "setting" of the silicone rubber membrane as evidenced by a change in texture as well as binding with the glass window on which the membrane is placed. Such a change could well affect the microheterogeneity of the environment in which the fluorophore is placed. However, this was a one-time effect, and subsequent autoclaving (up to 20 times) did not result in any measurable change in the dynamic range or in the absolute phase angles measured. This, combined with the fact that there is no long-term leaching of fluorophore from the membrane, allows this sensor to be used in applications which require repeated autoclaving. The absence of leaching was evidenced by the fact that there was no loss in fluorescence intensity after multiple autoclavings and extended use in aqueous media. This is not surprising considering the hydrophobicity of the matrix and the very low solubility of the fluorophore in water. An additional advantage of the optical sensor is that the calibration curve is absolute and only a one-time calibration is required after the first autoclaving.

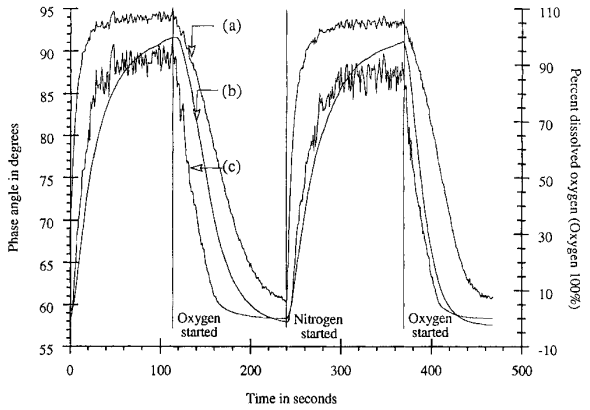

Figure 4. Response time analysis of DO sensors. Response of optical sensor and Clark-type electrode to DO levels in a 2-L vessel containing water (at 25°C) alternatingly sparged with oxygen and nitrogen: (a) optical sensor response in phase angles; (b) Clark-type electrode response in percent oxygen; (c) optical sensor response in percent oxygen. The noise in the phase data is due to the 0.5° resolution limit on the lock-in analyzer used.

To determine the applicability of our sensor in monitoring DO levels in a bioreactor, comparisons with a Clark-type electrode were carried out in *E. coli* batch fermentations. One of the major concerns was possible interference from other fluorescing species in the medium, particularly the yeast extract. Broadband fluorescence (450 to 600 nm) was observed upon excitation of a yeast extract solution in a spectrofluorometer with blue light at 450 nm. However, no detectable interference was observed when the optical sensor was used to measure DO in the solution. Clearly

the end-on optical configuration (Fig. 2) helps in significantly excluding extraneous fluorescence. Figure 5 shows the response profiles of the optical sensor and Clark-type electrode to DO in an overnight *E. coli* batch fermentation. The DO level slowly depletes as the cells grow to their maximum optical density. Both sensors track the decrease in oxygen, resulting in a strikingly similar DO profile. At this point, because of rapid cell growth, oxygen is consumed at least as fast as it is being supplied. Nutrient depletion and acetate accumulation ultimately lead to cell death, at which point oxygen consumption falls. This causes an increase in DO as indicated by both sensors. It must be noted that the local fluctuations in the sensor response is not noise but actual fluctuations in DO.

To ascertain the response limits of the sensors under low DO conditions, another batch fermentation was carried out using a relatively rich medium.[16] This resulted in a fast growth rate and consequently a rapid depletion in DO. Air was sparged at the same rate as above. As shown in Figure 6, both electrodes show a rapid decline in DO. However, although the Clark-type electrode reaches its lower limit, the optical sensor continues to track the low-DO levels since this is the regime (as shown in Fig. 3) in which the optical sensor is most sensitive. After remaining at zero for some time the DO level rises again toward the end of the fermentation, signaling nutrient depletion and cell death.

Furthermore, because of electrolyte consumption, the Clark-type electrode has a manufacturer specified drift in linearity of about 0.3% over 1 week. In practice, a significantly higher drift is observed. Upon continuous exposure to water saturated with oxygen for 2 weeks the response of the Clark-type electrode changed from 1.6 to 1.8 V, i.e., a 10% drift. On the other hand, the optical sensor is a non-consumption based system and as such showed no drift in calibration over the 2-week time period.

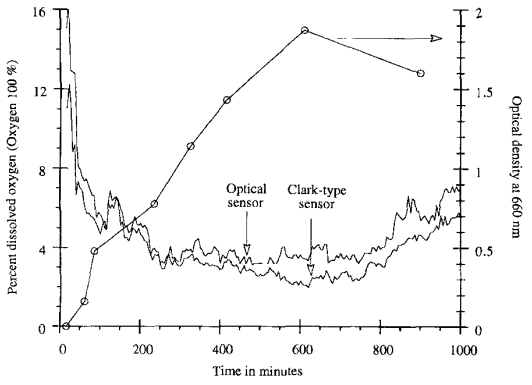

Figure 5. Dissolved oxygen profile during a typical *E. coli* fermentation. Using a cubic spline interpolation of the data shown in Figure 3, the responses of the two sensors have been converted into percent oxygen and plotted as shown. The optical sensor closely tracks the response of the Clark-type electrode throughout the fermentation. The fermentation was conducted at 25°C.

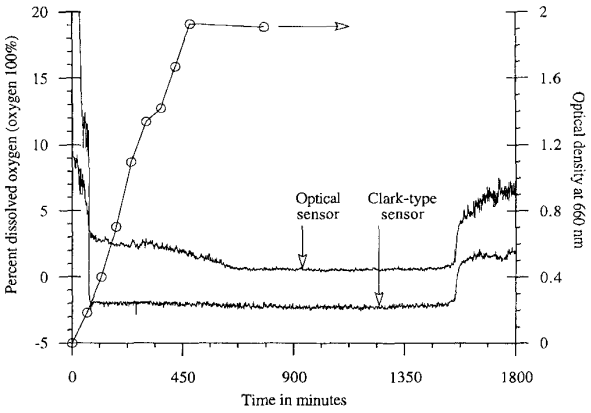

Figure 6. Transient response of DO sensors during *E. coli* fermentation in rich medium. Using a richer medium to obtain faster growth rates and low DO levels, the Clark-type electrode quickly drops to a zero reading whereas the optical sensor tracks the low DO levels. For clarity the Clark-type electrode response is shown offset by 3%. The fermentation was conducted at 25°C.

The optical sensor described here has an additional advantage because of its lack of drift and requirement for repeated calibration. Besides its generally superior performance, its accuracy and reliability make it more attractive for bioprocess manufacturing at a time when validation documentation and regulatory conditions are becoming more stringent.

CONCLUSIONS

In this article the application of fluorescence lifetime measurements to monitoring dissolved oxygen tensions in bioreactors was investigated. Lifetime based optical sensors, as mentioned earlier, have been shown to have particular advantages over intensity based optical sensors. Here, we have demonstrated the advantages of lifetime based optical methods over Clark-type amperometric electrodes. The optical sensor described is autoclavable, is maintenance free, has a fast response, and is particularly useful in the low-oxygen regime. The light source is an inexpensive blue LED. Since the sensor does not consume oxygen, it is independent of fluid flow rates around it, and because it is optical, the sensor is free of electrical interferences. Additional features include long-term stability and a one-time calibration requirement. Economically, the sensor compares well with the Clark-type sensor and preliminary estimates show that it can be built for less than $1000. We are currently in the process of making a prototype sensor.

The general methodology used above can also be extended to measure other analytes. The field of lifetime based sensing has advanced dramatically during the past year. New lifetime probes have become available. We are now aware of a wide variety of probes which change lifetime in response to pH,[11] pCO_2,[16] Ca^{2+},[12,19], Mg^{2+} (J. R. Lakowicz and H. Szmacinski, unpublished observation), K^+ and Cl^-,[10] and glucose.[9] The generic technology described

in this article can be directly ported over once effective immobilization methods are developed.

Support from National Science Foundation grants BCS9209157 and BCS9157852 is acknowledged with matching funds from Artisan Industries, Inc. Waltham, MA.

References

1. Angel, S. M. 1987. Optrodes: Chemically selective fiber-optic sensors. Spectroscopy **2**(4): 38–48.
2. Bacon, J. R., Demas, J. N. 1987. Determination of oxygen concentrations by luminescence quenching of a polymer immobilized transition metal complex. Anal. Chem. **59**: 2780–2785.
3. Baeyens, W. R. G., De Keukeleire, D., Korkidis, K. (eds.). 1991. Luminescence techniques in chemical and biochemical analysis. Marcel Dekker, New York.
4. Berndt, K. W., Lakowicz, J. R. 1992. Electroluminescent lamp-based phase fluorometer and oxygen sensor. Anal. Biochem. **201**: 319–325.
5. Carraway, E. R., Demas, J. N., DeGraff, B. A., Bacon, J. R. 1991. Photophysics and photochemistry of oxygen sensors based on luminescent transition metal complexes. Anal. Chem. **63**: 337–342.
6. Clark, Jr., L. C. 1956. Monitor and control of blood and tissue oxygen tension. Trans. Am. Soc. Artif. Int. Org. **2**: 41.
7. Demas, J. N., DeGraff, B. A. 1991. Design and applications of highly luminescent transition metal complexes. Anal. Chem. **63**(17): 829–837.
8. Kalyanasundaram, K., Nazeeruddin, Md. K., Gratzel, M., Viscardi, G., Savarino, P., Barni, E. 1992. Synthesis and photophysical characteristics of highly luminescent complexes of Ru(II) containing 4,4′-di-(*p*-carboxylphenyl)-2,2′-bipyridine. Inorg. Chim. Acta **198**: 831–839.
9. Lakowicz, J. R., Maliwal, B. P. 1993. Optical sensing of glucose using phase-modulation fluorimetry. Anal. Chim. Acta **271**: 155–164.
10. Lakowicz, J. R., Szmacinski, H. 1993. Fluorescence lifetime based sensing of pH, Ca^{2+}, K^+ and glucose. Peer reviewed for sensors and actuators as part of the first European Conference on Optical Chemical Sensors and Biosensors, Graz, Austria, April 12–16, 1992. Sensors and Actuators B **11**: 133–143.
11. Lakowicz, J. R., Szmacinski, H. 1993. Optical measurement of pH using fluorescence lifetime and phase modulation fluorimetry. Anal. Chem. **65**: 1674.
12. Lakowicz, J. R., Szmacinski, H., Nowaczyk, K., Johnson, M. L. 1992. Fluorescence lifetime quenching of calcium using Quin-2. Cell Calcium. **13**: 131–147.
13. Lakowicz, J. R. 1983. Principles of fluorescence spectroscopy. Plenum, New York.
14. Lee, Y. H., Tsao, G. T. 1979. Dissolved oxygen electrodes. pp. 35–86 In: T. K. Ghose, A. Fiechter, and N. Blakebrough (eds.), Advances in biochemical engineering, vol. 13. Springer Verlag, Berlin.
15. Lippitsch, M. E., Pusterhofer, J., Leiner, M. J. P., Wolfbies, O. S. 1988. Fiber optic oxygen sensor with the fluorescence decay time as the information carrier. Anal. Chim. Acta **205**: 1–6.
16. Lundell, D., Greenberg, R., Alroy, Y., Condon, R., Fosetta, J. D., Gewain, K., Kastelein, R., Lunn, C. A., Reim, R., Shah, C., Kimmenade, A., Narula, S. K. 1990. Cytoplasmic and periplasmic expression of a highly basic protein, human interlukin 4, in *Escherichia coli*. J. Ind. Microb. **5**: 215–227.
17. Opitz, N., Lubbers, D. W. 1987. Theory and development of fluorescence based optochemical oxygen sensors: Oxygen optodes. Int. Anasthesiol. Clin. **25**: 177–197.
18. Parker, C. A. 1968. Photoluminescence of solution. Elsevier, Amsterdam.
19. Szmacinski, H., Gryczynski, I., Lakowicz, J. R. 1993. Calcium dependent fluorescence lifetimes of Indo-1 for one- and two-photon excitation fluorescence. Photochemistry and Photobiology. **58**: 341–345.
20. Wolfbeis, O. S., Caroline, F. M. 1984. Long wavelength fluorescence indicators for the determination of oxygen partial pressures. Anal. Chim. Acta **160**: 301–304.

The next paper details our attempt to make a steam sterilizable optical pH sensor. This was particularly challenging, as the molecule used had to be held in an environment that protons could diffuse into. Given that we had rapidly developed a fairly robust oxygen sensor, I did not think that a pH sensor would take this long. However, the main challenge was to find a matrix that would allow protons to diffuse in and out. Unlike the oxygen sensor, where silicone rubber worked to immobilize the ruthenium-based sensor molecule, immobilizing the pH sensitive dye proved to be more difficult.

Luckily, Haley Kermis joined the lab as a postdoc and she had extensive experience in making hydrogels, which turned out to be the solution to immobilizing the pH dye. But as Figure 1 shows, this took some doing. By this time, Yordan Kostov had joined the lab as a postdoc and turned out to be an outstanding electrical engineer who had an unusual background, as it combined electrical engineering, chemistry and spectroscopy. Graduate student Peter Harms was a tinkerer and so we were able to successfully demonstrate an optical sensor for pH measurements in fermentation applications.

Biotechnol. Prog. **2002,** *18,* 1047–1053

Dual Excitation Ratiometric Fluorescent pH Sensor for Noninvasive Bioprocess Monitoring: Development and Application

Haley R. Kermis, Yordan Kostov, Peter Harms, and Govind Rao*

Department of Chemical and Biochemical Engineering, University of Maryland Baltimore County, 1000 Hilltop Circle, Baltimore, Maryland 21250

The development and application of a fluorescent excitation-ratiometric, noninvasive pH sensor for continuous on-line fermentation monitoring is presented. The ratiometric approach is robust and insensitive to factors such as source intensity, photobleaching, or orientation of the patch, and since measurements can be made with external instrumentation and without direct contact with the patch, detection is completely noninvasive. The fluorescent dye 8-hydroxy-1,3,6-pyrene trisulfonic acid was immobilized onto Dowex strongly basic anion-exchange resin, which was subsequently entrapped into a proton-permeable hydrogel layer. The sensor layer was polymerized directly onto a white microfiltration membrane backing that provided an optical barrier to the fluorescence and scatter of the fermentation medium. The ratio of emission intensity at 515 nm excited at 468 nm to that excited at 408 nm correlated well with the pH of clear buffers, over the pH range of 6−9. The sensor responded rapidly (<9 min) and reversibly to changes in the solution pH with high precision. The sterilizable HPTS sensor was used for on-line pH monitoring of an *E. coli* fermentation. The output from the indwelling sensor patch was always in good agreement with the pH recorded off-line with an ISFET probe, with a maximum discrepancy of 0.05 pH units. The sensor is easily adaptable to closed-loop feedback control systems.

Introduction

In recent years, there has been considerable research effort toward the development of techniques for continuous on-line monitoring of pH for environmental, biomedical, and bioprocess applications. In particular, optical techniques based on fluorescence measurements offer many advantages over conventional electrochemical approaches, including high sensitivity and ease of miniaturization. In addition, since fluorescence emission from an indwelling patch can be monitored without direct contact, in situ pH measurements can be made noninvasively with external instrumentation. The latter is highly desirable for bioprocesses using large, instrumented fermenters, by circumventing the cumbersome task of probe sterilization. For benchtop shake flasks and small scale, high throughput operations that do not readily accommodate the larger probes, in situ fluorescence-based patches delivering continuous real time pH values could be used to monitor and even control the acidity of the environment.

With judicious choice of the fluorescent indicator and immobilization conditions, measurements can be made over the desired region with high sensitivity. Sensors have been developed that measure the pH-dependent change in emission intensity, including those based on fluorescein, cyanine (*1*), and transition metal complexes (*2*−*4*). However, the inherent drawbacks of intensity-based measurements include signal variations due to probe photobleaching and fluctuations in source intensity and a sensitivity to position and orientation of the sensor patch that precludes noninvasive detection. Furthermore, measurements in highly scattering or fluorescent media are difficult at best, even with an opaque membrane backing (*5*). Sensors based on the pH-dependent change in fluorescent lifetime of an immobilized ruthenium metal ligand complex (*6*) do not suffer the same drawbacks but require more complicated instrumentation. In addition, sensitivity to collisional quenching by oxygen results in an additional calibration parameter or operation under anaerobic conditions.

An alternate approach that circumvents the problems associated with intensity-based measurements is ratiometric detection. Given a fluorescent indicator that exhibits a shift in excitation or emission wavelength with pH, the ratio of the emission intensity at the two wavelengths can be used as a robust measure of the pH that is insensitive to orientation, probe concentration, and background fluorescence. Fiber-optic sensors based on fluorescein (*7*), seminaphthofluorescein (*8*), and carboxynaphthofluorescein (*9*) have been described that rapidly and reliably correlate intensity ratios to pH. The extensive photobleaching that is observed for these dyes is accounted for by the ratiometric approach but would still limit the useful lifetime of the sensor.

The fluorescent dye 8-hydroxy-1,3,6-pyrene trisulfonic acid trisodium salt (HPTS) exhibits two excitation wavelengths, one UV ($\lambda_1 = 405$ nm) and one blue ($\lambda_2 = 457$ nm), that correspond to the acid and its conjugate base (*10*). The ratio of emission intensities, R, for these two

* To whom correspondence should be addressed. Tel: 410-455-3400. Fax: 410-455-6500. E-mail: grao@umbc.edu.

10.1021/bp0255560 CCC: $22.00
Published on Web 08/14/2002

wavelengths is related to the proton concentration according to (*11*)

$$[H^+] = k_a \frac{(R_{max} - R)}{(R - R_{min})} \frac{(\epsilon_{A^-}\Phi_{A^-})_{\lambda_2}}{(\epsilon_{HA}\Phi_{HA})_{\lambda_2}} \quad (1)$$

where R_{min} and R_{max} are the ratios for the acid (HA) and conjugate base (A^-), respectively, ϵ and Φ are the extinction coefficient and quantum yield of each species evaluated at λ_2, and k_a is the equilibrium dissociation constant. Experimentally, the apparent dissociation constant of the immobilized dye, $k_{a,app}$, is given by the product

$$k_{a,app} = k_a \frac{(\epsilon_{A^-}\Phi_{A^-})_{\lambda_2}}{(\epsilon_{HA}\Phi_{HA})_{\lambda_2}} \quad (2)$$

With a pK_a of 7.3, HPTS is suitable for ratiometric detection in the physiological range. This, together with a low toxicity (*12*) and insensitivity to oxygen concentration (*13*), makes HPTS an appropriate probe for physiological and bioprocess pH measurements. Furthermore, with the recent availability of low cost UV LEDs, the dye can be measured with relatively inexpensive instrumentation that combines UV and blue LEDs and a photodiode module. Such a setup has been described elsewhere (*14*) to detect the pH of a high throughput microbioreactor system via HPTS directly dissolved in the fermentation media. If HPTS were immobilized in a matrix with suitable optical and diffusion properties and fixed to the inside wall of the reaction vessel, ratiometric emission data could be collected externally and inexpensively. This report describes the preparation of an HPTS sensor patch and its use as an indwelling sensor to noninvasively monitor a fermentation process.

The value of HPTS as a fluorescent ratiometric pH indicator for optical sensors has been widely demonstrated in the literature. The dye has been covalently attached to controlled pore glass (*15*) and aminoethyl cellulose (*16*) in the development of fluorescence-based pH sensors that operate in neutral and acidic environments, as well as an intravascular blood gas monitoring system where it was used for both pH and pCO_2 detection (*17*). HPTS can also be immobilized by ionic binding to cationic supports, given its three strongly anionic sulfonic acid groups. Fiber-optic pH sensors have been described with HPTS bound to an anion exchange membrane (*13*) or resin (*18*) and fixed to the tip of the optical fiber. This simple technique has been adapted here in the preparation of an HPTS patch for noninvasive bioprocess monitoring, by polymerization of the HPTS-bound resin beads into a highly swollen poly(ethylene glycol) hydrogel layer. The hydrogel layer serves to fix the resin in place but still promotes proton diffusion in the vicinity of the dye. Additionally, poly(ethylene glycol) hydrogels are known for their excellent biocompatibility(*19*, *20*). Last, a white microfiltration membrane backing has been used to provide an optical barrier between the sensing layer and the background media. The entire setup was used to monitor the pH of an *E. coli* fermentation.

Experimental Section

Materials. The fluorescent dye 8-hydroxy-1,3,6-pyrene trisulfonic acid trisodium salt (HPTS) was obtained from Molecular Probes Inc. (Eugene, OR). Dowex 1 × 8-400 strongly basic anion-exchange resin was obtained from Sigma Chemical Co. (St. Louis, MO). Poly(ethylene glycol) diacrylate with an average molecular weight of 3400 was obtained from Shearwater Polymers (Huntsville, AL). The photoinitiator Darocur 1173 was supplied by Ciba Specialty Chemicals (Tarrytown, NY). White microfiltration membranes in mixed esters of cellulose with a nominal pore diameter of 0.2 μm (Kimble) were used as a support backing. Analytical grade sodium chloride, sodium dihydrogen phosphate, and tris(hydroxymethyl)-aminomethane (Tris) were obtained from Sigma Inc. (St. Louis, MO). Tryptone and yeast extract (Difco) used in the preparation of nutrient broth were from Beckton-Dickinson (Sparks, MD).

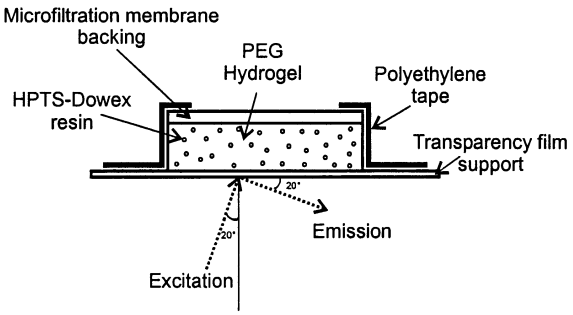

Figure 1. Schematic diagram of the HPTS-PEG-Dowex sensor assembly affixed to transparency film.

Sensor Fabrication. Dowex resin (1 g) was suspended in 10 mL of a 50 μM solution of HPTS in deionized water. The resin suspension was allowed to equilibrate at room temperature for 24 h with occasional stirring. Polymer precursor solution was prepared by combining 50 mg of PEG-diacrylate, 0.2 mL of the HPTS-Dowex suspension, and 2 μL of Darocur and vortexing for 10 min. The precursor solution was polymerized directly on the membrane backing to promote adhesion and between glass slides to prevent oxygen inhibition. The microfiltration membrane was cut to 2 cm × 4 cm and placed on a glass microscope slide. The precursor solution was pipetted directly onto the membrane backing and covered with a second glass slide, using aluminum spacer tape at the edges to control the gap thickness. Free radical polymerization of the acrylate end groups was initiated by exposure to a 100-W long wave UV spot lamp (UVP, Inc.; Upland, CA) for 30 s. After polymerization, the PEG-Dowex layer was peeled from the glass slides with the microfiltration membrane attached to the bottom surface and allowed to hydrate in deionized water for 24 h. Sensors constructed in this manner were approximately 250 μm thick. For comparison, control PEG-Dowex layers without HPTS were also prepared.

To facilitate insertion of the sensor into cuvettes for reproducible analysis, the PEG-Dowex layer was affixed to rigid transparency film. A 0.8-cm square of hydrogel was blotted dry and placed backing-up on a transparency film. The layer was fixed to the surface with black polyethylene waterproof tape (3M; St. Paul, MN) from which a 0.5 cm square had been removed to provide exposure to the sample solution. With this setup, the sensor assembly could be easily attached to the inside surface of polystyrene disposable cuvettes using adhesive or double-sided tape, enabling front face measurement of the PEG-Dowex layer. A schematic diagram of the sensor assembly is depicted in Figure 1.

Instrumentation. Fluorescence measurements were performed using a Varian Cary Eclipse fluorescence spectrophotometer with a solid sample/cuvette holder designed for front-face measurements with excitation light at an angle of incidence between 20° and 35°.

Uncorrected excitation and emission spectra of both solutions and sensor assemblies were recorded in polystyrene disposable cuvettes fixed at 20° from the incident beam. For measurement of the PEG-Dowex sensor, the assembly was mounted to the inside front surface of the cuvette using double-sided adhesive tape. Unless otherwise stated, all measurements were performed at room temperature (25 ± 2 °C).

To measure the response time of the sensor, buffer solutions were continuously pumped from larger reservoirs into a sealed cuvette containing a sensor assembly, using a peristaltic pump operated at 40 mL/min. At this flow rate, the well-stirred solution inside the cuvette (~4 mL) would be replaced in approximately 40 s (6τ).

Since the solid sample/cuvette holder is not equipped for temperature control, a separate single-cell Peltier accessory was used to collect excitation spectra at temperatures other than ambient. Temperature control in the jacket surrounding the cuvette was varied between 10 and 40 °C. Since the single-cell Peltier unit is not adapted for front-face measurements, the sensor assembly was suspended in the cuvette from a rubber stopper at 20° from the incident beam.

Sensor Calibration. For calibration of the sensor assemblies, buffered saline solutions (0.15 or 0.3 M overall ionic strength) were prepared by reconstitution of sodium chloride and the appropriate base (10 mM) in deionized water and titration to the desired pH using 1 M HCl or 1 M NaOH. Calibration buffers with pH between 6.2 and 8.2 were buffered with phosphate, while those solutions of higher pH (>8.2) were buffered with Tris. Luria-Bertani (LB) nutrient broth was prepared that contained sodium chloride (5 g/L), tryptone (10 g/L), and yeast extract (5 g/L) with pH adjusted to 7.2 with strong acid or base. The pH of each solution was recorded using a model IQ240 Benchtop/Portable ISFET sensor pH probe (IQ Scientific Instruments; San Diego, CA). For each set of conditions, the collected data were fit to the following rearrangement of eqs 1 and 2:

$$R = \frac{[H^+]R_{min} + k_{a,app}R_{max}}{k_{a,app} + [H^+]} \qquad (3)$$

using a least-squares linear regression to determine the parameters R_{min}, R_{max}, and $k_{a,app}$.

Fermentation. The overnight seed culture consisted of a 1% inoculum of *E. coli* JM105 strain frozen stock in 20 mL of LB nutrient broth, incubated at 37 °C with shaking at 260 rpm (Orbit Environ Shaker, Lab-Line Instruments; Melrose Park, IL). The fermentation was carried out at room temperature in a 500-mL shake flask containing 100 mL of LB broth that was inoculated with 2.5% seed culture. The shake flask was placed on a rotating shaker (LaPine Scientific Co.; Berkeley, CA) set at 100 rpm. Dissolved oxygen and pH were not controlled. A polystyrene disposable cuvette containing a sensor assembly was sterilized thoroughly with 70 v/v % ethanol solution (*21*), rinsed extensively in sterile water and mounted in the spectrophotometer. To prevent optical interference from the media beyond the edges the sensor, the outside of the cuvette was covered with black tape except for a small square that exposed the sensor. The fermentation broth was pumped into the cuvette and recirculated to the shake flask by a peristaltic pump operating at 40 mL/minute. The spectrophotometer recorded the emission intensity at 515 nm with excitation at 408 and 468 nm, at 1-min intervals. The ratiometric data collected by the instrument were converted to pH using eqs 1 and *2* with the previously determined calibration parameters. At 20-min intervals, samples of the media were removed and analyzed for pH using the ISFET probe and optical density (600 nm) using a Milton Roy Spectronic 401.

Results and Discussion

The Dowex resin beads used to immobilize HPTS consist of a polystyrene support with quaternary ammonium groups capable of ionic binding with the sulfonic acid groups of HPTS. The beads are then physically entrapped in a hydrogel layer formed by the free radical polymerization of poly(ethylene glycol) diacrylate. The resulting matrix is highly swollen, at approximately 85% water content (*22*), and promotes proton diffusion. As depicted schematically in Figure 1, fluorescence spectra were recorded with the sensor fixed at 20° from the excitation beam. This configuration was chosen by comparison of the excitation spectrum for HPTS solution at 90° with the spectra collected in the solid sample/cuvette holder at incident angles between 20° and 35°. At 20°, scatter and reflection were reduced with minimal loss of emission intensity.

Figures 2a and 2b compare the excitation and emission spectra of HPTS solution and HPTS immobilized in the PEG-Dowex sensor assembly, both in pH 7.2 buffer. In the immobilized form, the two characteristic pH-sensitive excitation wavelengths of HPTS are preserved, however, both the excitation and emission maxima are slightly red-shifted to 408, 468, and 515 nm, respectively. This effect has been reported elsewhere for HPTS immobilized on Dowex anion-exchange resin (*18*). In addition, an increase in emission intensity with excitation at the UV wavelength relative to the blue wavelength is observed for the immobilized dye. This may be attributed to background fluorescence and scatter from the PEG-Dowex matrix. The excitation spectra of the control layer prepared without HPTS is also depicted in Figure 2a, and shows preferential excitation in the UV region. The white membrane backing on the sensor patch also contributes to the measured scatter and reflection, although this is minimized with the sensor orientation fixed at 20° from the excitation beam. Elsewhere (*5*), similar membranes have been stained black to circumvent this difficulty. However, the presence of the white, reflective surface serves to enhance the signal output from the sensor by reflection of both incident and emitted light back through the HPTS layer, rather than allowing transmission beyond the patch. This effectively doubles the path length of the beam, resulting in emission intensities that are considerably (up to four times) higher than those from similar sensors with no membrane backing (data not shown).

Figure 3 depicts the pH-dependent excitation spectra of HPTS immobilized in the PEG-Dowex sensor assemblies measured at a fixed emission wavelength of 515 nm and normalized to the intensity with excitation at 408 nm. As in solution, the immobilized HPTS exhibits a positive pH dependence in the normalized emission intensity with blue excitation, with more than a 10-fold increase between pH 6.2 and 8.8. The ratio of the intensity with excitation at 408 nm to the intensity with excitation at 468 nm was calculated at each pH for three identical but separately constructed sensor assemblies to produce the data listed in Table 1. Despite slight differences in sensor orientation, thickness, or local resin concentration, the standard error is consistently low, demonstrating the reproducibility of sensor construction and the robustness of the ratiometric technique. In

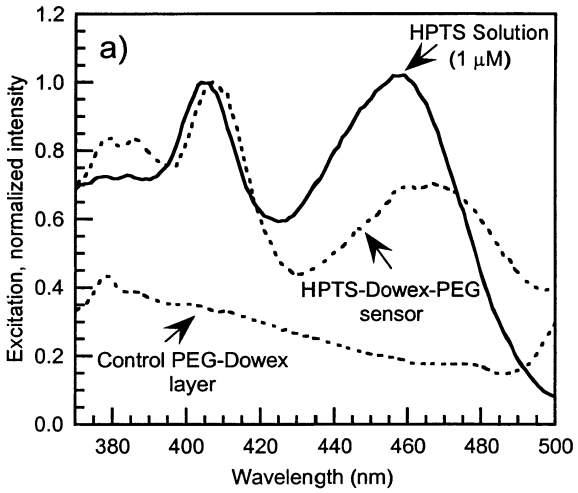

Figure 2. Normalized (a) excitation spectra ($\lambda_{emission} = 515$ nm) and (b) emission spectra ($\lambda_{excitation} = 408$ nm) of 1 μM HPTS solution, HPTS-PEG-Dowex sensor, and control PEG-Dowex sensor in pH 7.2 PBS (0.15 M).

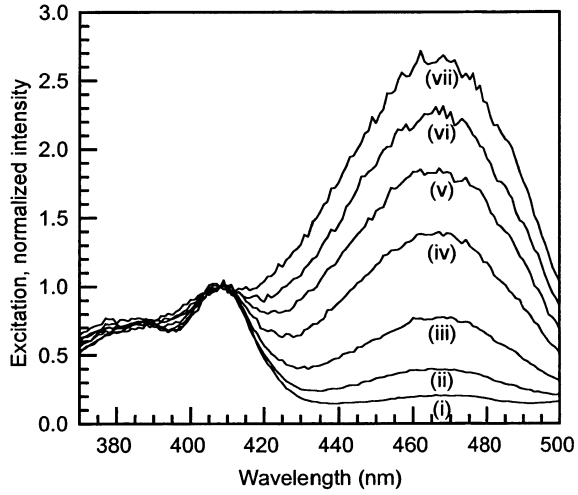

Figure 3. Normalized excitation spectra ($\lambda_{emission} = 515$ nm) of HPTS immobilized in the PEG-Dowex sensor at pH: (i) 6.2, (ii) 6.69, (iii) 7.16, (iv) 7.66, (v) 8.0, (vi) 8.42, (vii) 8.81; 0.15 M buffer, $T = 25$ °C.

addition, the precision of these measurements indicates that the scatter described earlier is consistent and does not interfere with the operation of the sensor. The apparent pK_a of the immobilized dye is approximately 7.7, slightly higher than that of HPTS in solution. This shift toward a more basic value is not surprising. Given that both the highly anionic sulfonic acid groups on the dye and the polyether segments of the PEG hydrogel are attractive to protons, the apparent pH inside the sensor matrix is reduced. The range of linearity of the HPTS-PEG-Dowex sensor extends from approximately 6.7 to 8.7. The increase in apparent pK_a is therefore favorable in terms of bioprocess measurement, as it corresponds to a working range that is consistent with that observed during many microbial and mammalian fermentations including *E. coli* and *Klebsiella pneumoniae* (*5, 14*).

Table 1. Intensity Ratio of Sensor Measured at 515 nm ($\lambda_{ex} = 468$ nm/$\lambda_{ex} = 408$ nm) in 0.15 M PBS and Quantitative Fitting Parameters for This Data Set

pH	intensity ratio (mean ± SD; $n = 3$)
6.20	0.22 ± 0.025
6.69	0.41 ± 0.013
7.16	0.78 ± 0.012
7.66	1.39 ± 0.02
8.00	1.84 ± 0.05
8.42	2.32 ± 0.07
8.81	2.67 ± 0.03

Quantitative Fitting Parameters

parameter	value ± error
R_{min}	0.19 ± 0.042
R_{max}	2.84 ± 0.060
p$k_{a,app}$	7.75 ± 0.045
χ^2	0.010412

The effect of various operating parameters on the performance of the HPTS-PEG-Dowex was evaluated. Figure 4 compares the calibration curve of intensity ratio of a sensor assembly in 0.15 and 0.3 M buffers. Sensitivity to ionic strength has been reported elsewhere (*23*) for HPTS covalently bound to porous glass via a sulfonamide. The intensity ratio of HPTS immobilized in the PEG-Dowex matrix is clearly affected by the ionic strength of the buffer, which is not surprising given the highly charged nature of the dye. With increased ionic strength, the apparent pK_a of the immobilized dye and the range of linearity are slightly more basic at 8.1, requiring a simple recalibration of the sensor at these conditions. The performance of the HPTS-PEG-Dowex assembly is also sensitive to temperature. Figure 5 depicts the emission intensities measured with excitation at 408 and 468 nm and the combined intensity ratio, as the temperature is increased from 10 to 40 °C. At both excitation wavelengths, the increase in temperature corresponds to an increase in emission intensity. However, since the blue excitation wavelength (468 nm) responds with greater sensitivity, the increase in temperature also corresponds to an increase in intensity ratio. Admittedly, changes in temperature and ionic strength influence the degree of hydration of both the Dowex resin and the PEG hydrogel and therefore the local dye concentration. However, such a change in swelling alone would be expected to affect both the UV and blue excitation peaks equally. It is also interesting to note that this trend is contrary to what is expected on the basis of the increase in nonradiative decay at higher temperatures, suggesting either a change in the ground or excited state kinetic parameters or some interactions between the dye and the immobilization resin. This unexpected result is currently under investigation in our laboratory to determine if this effect can be harnessed to develop a temperature-independent sensor (since emission intensities normally decrease with increasing temperature), a technique described elsewhere

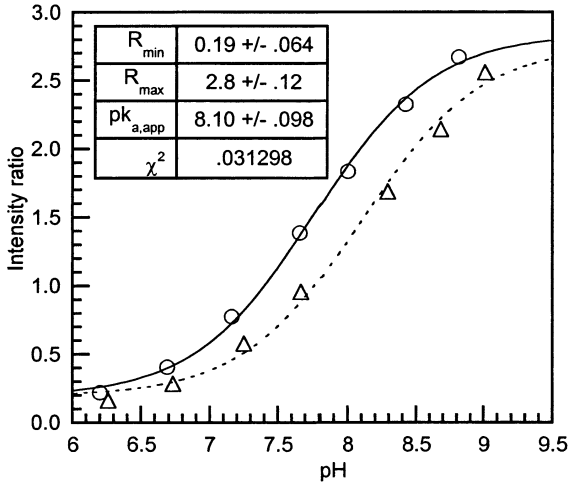

Figure 4. Calibration curve of the sensor measured in (○) 0.15 M PBS and (△) 0.3 M PBS; $T = 25$ °C; fitting parameters listed for the sensor in 0.3 M buffer.

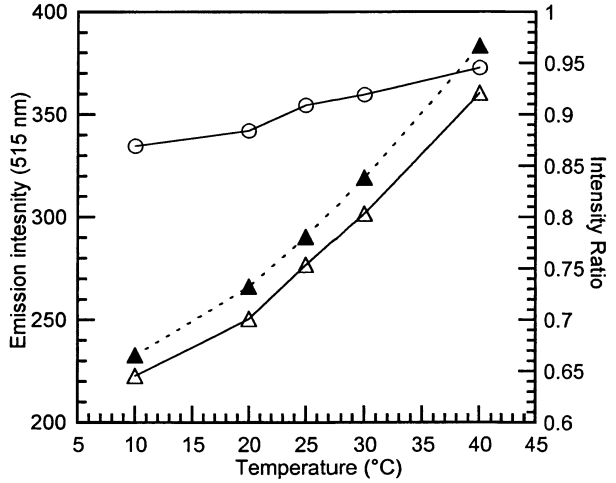

Figure 5. Effect of temperature on the properties of HPTS immobilized in PEG-Dowex in 0.15 M PBS: emission at 515 nm with excitation at (○) 408 nm and (△) 468 nm and (▲) intensity ratio.

for a ruthenium-pyrene complex in a similar hydrogel (*24*). For now, since the sensor is targeted for use in bioprocesses that are largely temperature-controlled, the impact is minimal. The effect of aging on sensor performance was also evaluated. Since PEG hydrogels must be stored hydrated to prevent cracking of the matrix, it is important to monitor the potential for leaching of HPTS into the soaking solution. Sensor assemblies were shielded from light and stored in deionized water for 3 weeks at ambient temperature. While loss of signal intensity was minor (<10%) and expected, owing to equilibrium leaching of HPTS from the matrix into the storage solution, there was no observable change in the sensor calibration curve. Since neither the ion-exchange resin nor the microfiltration membrane backing is suitable for sterilization by autoclave, the sensor assembly was exposed to 70% ethanol/water to determine the feasibility of this method of sterilization. Apart from temporary and reversible dehydration of the hydrogel matrix, no change in the performance of the sensor was detected. Though not tested here, other methods of sterilization such as ethylene oxide treatment may be suitable provided the hydrogel is kept hydrated.

The dynamic behavior of the sensor was investigated by pumping different pH buffers into the cuvette. The

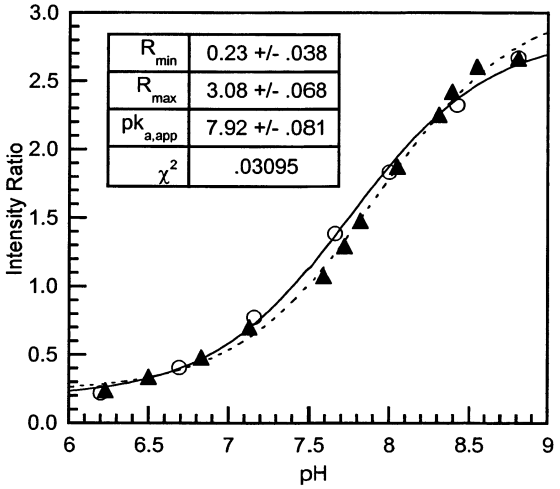

Figure 6. Intensity ratio measured in (○) clear 0.15 M PBS and (▲) LB nutrient broth with *E. coli* ($OD_{600nm} = 0.25$); $T = 25$ °C; fitting parameters listed for the sensor in cell/media suspension.

sensor was allowed to equilibrate in each buffer with constant, open-loop circulation from a larger reservoir while the excitation intensity ratio was monitored. The response time for a 95% change was approximately 9 min. While this is adequate for the purpose of bioprocess monitoring, the faster response times that are desirable for control schemes should be easily attained with a reduction in sensor thickness. The change in intensity ratio was completely reversible and could be cycled back and forth with no observable drift, i.e., the signal returned to within 1% of the original value with each cycle.

In preparation for use in a batch fermentation, the performance of the HPTS-PEG-Dowex sensor was evaluated in spent nutrient broth from an *E. coli* fermentation. LB broth containing *E. coli* at an optical density (600 nm) of 0.25 was titrated to produce samples of varying pH between 6 and 9. Figure 6 compares the intensity ratio of the sensor measured in the spent media samples with the calibration curve in clear buffer. Qualitatively, the experimental results in media are similar to those in PBS; however, the quantitative fitting parameters are significantly different than those determined in clear buffer. While the presence of the opaque backing combined with the ratiometric technique reduces the optical interference associated with media background fluorescence and scatter from the cell suspension, some interference is observed owing to the diffusion of colored species into the sensing layer, with significant absorption at the excitation wavelengths. This effect may be overcome by increasing the concentration of HPTS within the patch.

The PEG-Dowex sensor assembly was used to perform continuous on-line measurement of the pH during an *E. coli* fermentation. Figure 7 depicts the pH of the media recorded on line by the sensor and compared with that measured offline by a conventional pH probe. The optical density of the media is also shown as a measure of biomass production. The fermentation began at the initial media pH of 7.2 and remained relatively stable during the lag phase. As the cells enter the exponential growth phase, a dramatic increase in optical density is observed, followed by a corresponding increase in pH that is consistent with the accumulation of metabolic waste. The ensuing stationary phase is accompanied by a leveling in the pH at approximately 8.4. After an initial equilibra-

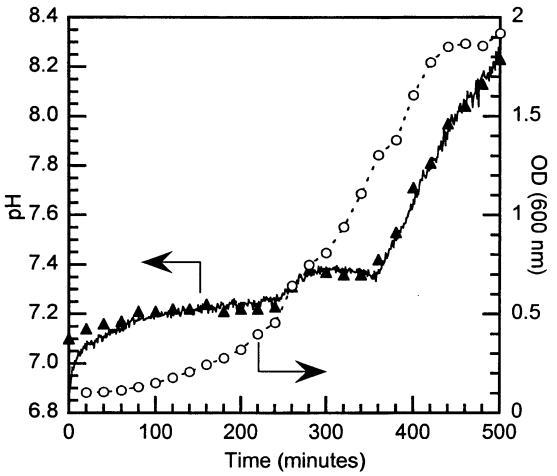

Figure 7. Fermentation of *E.coli*: (○) OD_{600nm}, pH measured (—) on-line by sensor and (▲) off-line with ISFET pH probe.

tion period of approximately 20 min, the pH recorded on line by the sensor was always in excellent agreement with that measured off line over the course of the 8-h fermentation, with a maximum discrepancy of 0.05 pH units. Although a signal loss of approximately 35% was observed, owing to an increase in the optical density of the media and the equilibrium loss of HPTS from the patch, the intensity ratio was unaffected and remained a reliable measure of the pH. It is also worthwhile to note that the raw intensities recorded by the sensor, as well as the calculated ratio, were remarkably stable with very little noise, despite the high flow rate (40 mL/min) and degree of mixing inside the cuvette. Toward the end of the fermentation (>8 h), a consistent overprediction of the pH was observed. Examination of the used patch revealed evidence of microbial growth on the inside surface of the hydrogel, which was poorly sealed to the transparency film in the current setup. While the polyethylene tape used here to fix the patch in place is sufficient for the purpose of proof-of-principle, entrapment of the media components in the stagnant region beneath the hydrogel layer would limit the useful lifetime of the patch to approximately 8 h. It is difficult to attach a highly swollen layer to a hydrophobic surface. Improved methods of attachment will be investigated for further work including cyanoacrylate adhesives and heterofunctional cross-linkers.

Conclusions

The pH sensor consisting of HPTS-bound resin entrapped in a poly(ethylene glycol) hydrogel is capable of timely and reversible pH measurement and demonstrates linearity and sensitivity over a physiologically and bioprocess-relevant range. The sensor was successfully used in a shake-flask setup to provide continuous, on-line measurements of the pH of an *E. coli* fermentation. The robustness of the dual-excitation ratiometric technique, combined with the presence of an opaque membrane backing for optical isolation eliminate any interference from the nutrient broth and cells. The pH recorded by the sensor on line was in good agreement with samples measured off line with a conventional pH electrode. The HPTS-PEG-Dowex sensor is suitable for bioprocess monitoring and can be easily adapted for pH control with a decrease in thickness and corresponding response time.

The instrumentation for detection of the HPTS sensor patch using UV and blue LEDs and a photodiode module is currently under construction in our laboratory. The components are inexpensive and represent a simple and potentially portable way to obtain reliable, on-line pH information from a bioprocess without the use of an invasive probe or optical fiber. While the pH range overlapped by the HPTS sensor patch is somewhat narrow, it is suitable for many industrially relevant microbial fermentations. Nonetheless, other probes such as Rhodol Green and the LysoSensor dyes (*25*) are under consideration for monitoring of the lower operating pH of yeasts and fungi in the same, noninvasive manner.

Acknowledgment

This work was sponsored by NSF grant BES0091705 and unrestricted funding from Dupont, Fluorometrix, Genentech, Merck and Pfizer.

References and Notes

(1) Zen, J.-M.; Patonay, G. Near-infrared fluorescence probe for pH determination. *Anal. Chem.* **1991**, *63*, 2934−2938.
(2) Chan, C.-M.; Fung, C.-S.; Wong, K.-Y.; Lo, W. Evaluation of a luminescent ruthenium complex immobilized inside Nafion as optical pH sensor. *Analyst* **1998**, *123*, 1843−1847.
(3) Price, J. M.; Xu, W.; Demas, J. N.; DeGraff, B. A. Polymer-supported pH sensors based on hydrophobically bound luminescent ruthenenium(II) complexes. *Anal. Chem.* **1998**, *70*, 265−270.
(4) Malins, C.; Glever, H. G.; Keyes, T. E.; Vos, J. G.; Dressick, W. J.; MacCraith, B. D. Sol−gel immobilised ruthenium(II) polypyridyl complexes as chemical transducers for optical pH sensing. *Sens. Actuators, B* **2000**, *67*, 89−95.
(5) Chan, C.-M.; Lo, W.; Wong, K.-Y. Application of a luminescence-based pH optrode to monitoring of fermentation by *Klebsiella pneumoniae*. *Biosens. Bioelectron.* **2000**, *15*, 7−11.
(6) Clarke, Y.; Xu, W.; Demas, J. N.; DeGraff, B. A. Lifetime-based pH sensor system based on a polymer-supported ruthenium(II) complex. *Anal. Chem* **2000**, *72*, 3468−3475.
(7) Agayn, V. I.; Walt, D. R. Fiber-optic sensor for continuous monitoring of fermentation pH. *Bio/Technology* **1993**, *72*, 6−9.
(8) Xu, Z.; Rollins, A.; Alcala, R.; Marchant, R. E. A novel fiber-optic pH sensor incorporating carboxy SNAFL-2 and fluorescent wavelength-ratiometric detection. *J. Biomed. Mater. Res.* **1998**, *39*, 9−15.
(9) Song, A.; Parus, S.; Kopelman, R. High-performance fiber-optic pH microsensors for practical physiological measurements using a dual-emission sensitive dye. *Anal. Chem.* **1997**, *69*, 863−867.
(10) Wolfbeis, O. S.; Fuerlinger, E.; Kroneis, H.; Marsoner, H. Fluorimetric analysis. I. Study on fluorescent indicators for measuring near neutral ("physiological") pH values. *Fresenius' J. Anal. Chem.* **1983**, *55*, 119−124.
(11) Tsien, R. Y. Fluorescent indicators of ion concentrations. *Methods Cell Biol.* **1989**, *30*, 127−156.
(12) Lutty, G. A. The acute intravenous toxicity of stains, dyes, and other fluorescent substances. *Toxicol. Pharmacol.* **1978**, *44*, 225−229.
(13) Zhujun, Z.; Seitz, W. R. A fluorescence sensor for quantifying pH in the range from 6.5 to 8.5. *Anal. Chim. Acta* **1984**, *160*, 47−55.
(14) Kostov, Y.; Harms, P.; Randers-Eichhorn, L.; Rao, G. Low-cost microbioreactor for high-throughput bioprocessing. *Biotechnol. Bioeng.* **2001**, *72*, 346−352.
(15) Offenbacher, H.; Wolfbeis, O. S.; Furlinger, E. Fluorescence optical sensors for continuous determination of near-neutral pH values. *Sens. Actuators* **1986**, *9*, 73−84.
(16) Schulman, S. G.; Chen, S.; Bai, F.; Leiner, M. J. P.; Weis, L.; Wolfbeis, O. S. Dependence of the fluorescence of immobilized 1-hydroxypyrene-3,6,8-trisulfonate on solution pH: extension of the range of applicability of a pH fluorosensor. *Anal. Chim. Acta* **1995**, *304*, 165−170.
(17) Gehrich, J. L.; Lubbers, D. W.; Opitz, N.; Hansmann, D. R.; Miller, W. W.; Tusa, J. K.; Yafuso, M. Optical fluorescence and its application to an intravascular blood gas monitoring system. *IEEE Trans Biomed. Eng.* **1986**, *BME-33*, 117−132.

(18) Zhang, S.; Tanaka, S.; Wickramasinghe, Y. A. B. D.; Rolfe, P. Fibre-optical sensor based on fluorescent indicator for monitoring physiological pH values. *Med. Biol. Eng. Comput.* **1995**, *33*, 152−156.
(19) Shoichet, M. S.; Winn, S. R.; Athavale, S.; Harris, J. M.; Gentile, F. T. Poly(ethylene oxide)-grafted thermoplastic membranes for use as cellular hybrid bio-artificial organs in the central nervous system. *Biotechnol. Bioeng.* **1993**, *43*, 563−572.
(20) Zhang, M.; Desai, T.; Ferrari, M. Proteins and cells on PEG immobilized silicon surfaces. *Biomaterials* **1998**, *19*, 953−960.
(21) Brauker, J. H.; Carr-Brendel, V. E.; Martinson, L. A.; Crudele, J.; Johnston, W. D.; Johnson, R. C. Neovascularization of synthetic membranes directed by membrane microarchitecture. *J. Biomed. Mater. Res.* **1995**, *29*, 1517−1524.
(22) Cruise, G. M.; Scharp, D. S.; Hubbell, J. A. Characterization of permeability and network structure of interfacially photopolymerized poly(ethylene glycol) diacrylate hydrogels. *Biomaterials* **1998**, *19*, 1287−1294.
(23) Wolfbeis, O. S.; Offenbacher, H. Fluorescence sensor for monitoring ionic strength and physiological pH values. *Sens. Actuators* **1986**, *9*, 85−91.
(24) Ji, H.-F.; Shen, Y.; Hubner, J. P.; Carroll, B. F.; Schmehl, R. H.; Simon, J. A.; Schanze, K. S. Temperature-independent pressure-sensitive paint based on a bichromophoric luminophore. *Appl. Spectrosc.* **2000**, *54*, 856−863.
(25) Haugland, R. P. *Handbook of Fluorescent Probes and Research Chemicals*; Molecular Probes, Inc.: Eugene, OR, 2000.

Accepted for publication July 11, 2002.

BP0255560

Now that we had a non-invasive oxygen sensor, we were eager to learn how oxygen levels varied in the most ubiquitous of systems used to culture cells- the T-flask (widely used for animal cells). The T-flask has an interesting history. Per the National Museum of American History, they were developed by Wilton Earle at the National Cancer Institute (https://americanhistory.si.edu/collections/search/object/nmah_333869). They were named T-flasks since they were blown from glass tubing. Unlike today's flasks, they had conical ends to allow the cells to settle at the bottom for facile media changes.

The other design feature was to allow a large surface area for gas diffusion. It had long been assumed that the surface/volume ratio of a T-flask was such that cells would receive sufficient oxygen by diffusion (assuming that the liquid depth was not too great). It was also standard practice to slightly crack open the cap to allow for air exchange with the incubator atmosphere.

The first author of the paper is Lisa Randers-Eichhorn. She had a B.S. in Biological Sciences from UMBC and joined the lab right after graduation as a technician. She was extremely careful with setting up experiments and was very good at cell culture. I paired her with an extremely sharp undergraduate, Roscoe A. Bartlett. Ross was extremely enthusiastic and had an interesting background. He was the son of Roscoe Bartlett, a Maryland member of the US House of Representatives and one of the very few Ph.Ds to ever hold office. He was an extremely involved parent and once when Ross' grades dropped, he stopped by to meet the instructor! Added to the mix was Professor Douglas Frey, who has excellent modeling skills and we continue to use him to explain mathematically what it is that our experiments are telling us.

The results were astonishing. First of all, cracking open the cap made no difference (Figure 3). When we thought that perhaps our liquid depth might be too high and ran another experiment with one quarter the depth, the cells still experienced oxygen limitation (Figure 4). Furthermore, a substantial fraction of the oxygen appears to come via diffusion through the flask wall (Table 1).

Another interesting observation. Figure 4 shows spikes in the oxygen concentration. We believe that these were caused to agitation introduced by a faulty lab-door closer that slammed the door hard. If you forgot to catch the door, it would slam shut and we believe that this introduced slight vibration in the liquid in the T-flask and it improved mixing to allow greater oxygen diffusion. We had unwittingly discovered a simple way to improve oxygen mass transfer in T-flasks!

Noninvasive Oxygen Measurements and Mass Transfer Considerations in Tissue Culture Flasks

Lisa Randers-Eichhorn,[1] Roscoe A. Bartlett,[1] Douglas D. Frey,[1] and Govind Rao[1,2]*

[1]Department of Chemical and Biochemical Engineering, University of Maryland Baltimore County, Baltimore, Maryland; and [2]Medical Biotechnology Center of the Maryland Biotechnology Institute, University of Maryland, Baltimore, Maryland 21201

Received November 21, 1995/Accepted March 5, 1996

Murine hybridomas were cultivated in tissue culture flasks. Dissolved oxygen tensions in the gas and liquid phases during cell growth were monitored. Oxygen levels were measured noninvasively by interrogating an oxygen-sensitive patch mounted on the interior surface of the tissue culture flask with an optrode from outside the tissue culture flask. Readings were made in tissue culture flasks with caps both cracked open and completely closed. Although the oxygen in the gas phase remained near atmospheric oxygen levels in both flasks, over time the liquid-phase oxygen tension at the bottom of the flasks reached zero during cell growth in both the open and closed tissue culture flasks. These results suggest that the widespread practice of cracking open tissue culture flask caps during cell growth with a view to supplying adequate oxygen to cells is ineffective and probably unnecessary.

The mass transfer characteristics of the tissue culture flask were also studied. The dominant resistance to oxygen mass transfer to the sensor and the cells was through the liquid media. The mass transfer rates through the liquid layer under standard laboratory conditions were found to be greater than those predicted by diffusion alone. This suggests that mixing at a microscale occurs. Volumetric and specific oxygen consumption rates were also calculated from the sensor data. These consumption rates were comparable with values published elsewhere.

Key words: optical oxygen sensor • tissue culture flask • cell culture • oxygen mass transfer

INTRODUCTION

Tissue culture flasks (T-flasks) are commonly used as a convenient vehicle for cell propagation and preliminary scale-up due to their varying available sizes. Oxygen supply to cells growing in T-flasks is thought to be primarily liquid-phase diffusion limiting, as the cell suspension is not agitated. This is the reason for the commonly available high surface area-to-volume ratio of the various sizes of T-flasks encountered (typically 25, 75, 150, and 225 cm^2) where the approximate ratio of the surface available for gas diffusion to the culture volume is held constant. Typically, T-flasks are inoculated and transferred every other day. Because there is no agitation, cells tend to settle and grow on the bottom surface. In the case of anchorage-dependent cells, they are obligated to grow on the bottom and side surfaces in contact with the medium.

For both productivity during scale-up and experimental results to be dependable, it is important that the cells be treated in a consistent manner from transfer to transfer. However, several factors can affect the consistency between transfers. Gas composition can affect the lag phase which in turn affects productivity.[14] It has been previously reported that cells growing in partially opened T-flasks are not oxygen limited.[5,8]

For the most part, the Clark oxygen electrode has been utilized to measure oxygen levels in growing cultures of cells. However, because cells, suspension or attachment dependent, grow only on the bottom surface of the T-flask, size and design constraints of the Clark electrode may limit its accuracy in measuring oxygen in the thin cell layer. At low oxygen tensions, the Clark electrode is prone to erroneous readings because the measurement itself depends on oxygen consumption by the electrode.[3] An additional disadvantage of using a Clark electrode to measure oxygen levels in a T-flask is the need for a penetration which compromises the sterility of the environment and requires careful sealing to minimize oxygen diffusion around it.

Recently, two optical sensors have been described that incorporate thin, fluorophore-containing silicone patches, which can be used to measure oxygen tension in both open and closed systems. One sensor is based on luminescence intensity measurements and was used to measure oxygen in transparent vessels.[10] The other optical sensor's measurements are based on fluorescence lifetime measurements, and it has been used in a small-scale fermentor to monitor dissolved oxygen in a growing bacterial culture.[2] The sensor, which is based on

* To whom all correspondence should be addressed at: University of Maryland Baltimore County, Department of Chemical and Biochemical Engineering, Room 252 TRC Building, 5200 Westland Boulevard, Baltimore, MD 21227. Telephone (410) 455-3415; fax (410) 455-6500; e-mail grao@umbc.edu

CCC 0006-3592/96/040466-13

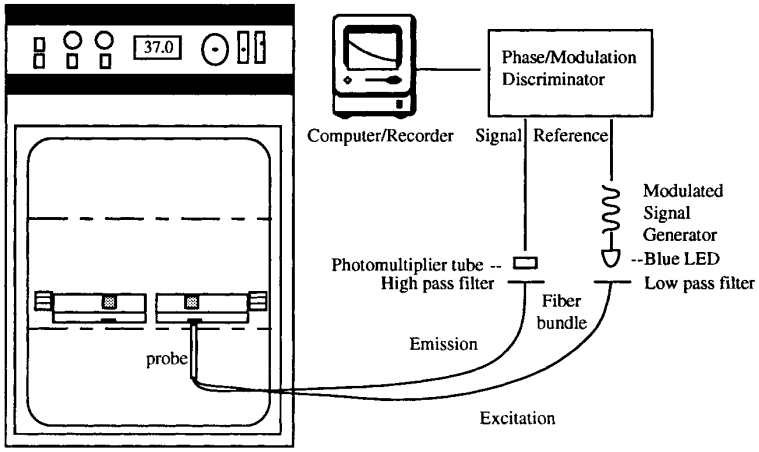

Figure 1. Experimental setup of the optical oxygen sensor.

changes in fluorescence lifetime, has several advantages over the intensity-based sensor. Fluorescence lifetime measurements are independent of problems commonly associated with intensity-based measurements such as photobleaching, probe concentration, lamp drift, and inner filter effects.[3,9] Furthermore, the small size, flexibility, and autoclavability of the sensor used to measure fluorescent lifetimes affords it a diversity of uses, and measurements can be made in ambient light without a black box as required for intensity-based measurements. An additional advantage over intensity-based measurements is that the positioning of the fiber-optic optrode is not critical, and thus one instrument is sufficient for making readings at multiple sensor patch sites. By placing a thin oxygen sensor on the bottom of the T-flask under the cell layer and by following changes in fluorescence lifetimes during a 7-day growth cycle, we were able to follow oxygen consumption in open and closed T-flasks of hybridoma cultures.

The experimental setup is shown in Figure 1. The sensor patch was attached to the inner surface of the bottom (for monitoring oxygen tension around the cells) and the side of the T-flask (for monitoring headspace oxygen tension). An optical probe was placed against the outside of the T-flask to illuminate the sensor patch and collect the emission light from the fluorophore. Data were recorded as phase angle readings and subsequently converted to percent oxygen values.

THEORY

Oxygen Supply to Cells

To characterize the mass transport of oxygen to the sensor patch and the cells, four distinct regions of the T-flask must be considered: the cell layer; the bulk media liquid layer; the headspace gas; and the T-flask wall (Fig. 2).

The formation of the oxygen gradients associated with the T-flask originate within the individual cells in the cell layer where oxygen is being consumed. Due to these oxygen concentration gradients, oxygen is transported from the gas phase through the liquid and cell layers to the sensor patch. Oxygen is also transported to the cells and the sensor patch through the bottom of the T-flask wall adjacent to the cell layer. Oxygen transport into the T-flask also takes place through the walls of the T-flask adjacent to the gas phase. To determine the significance of the mass transfer resistance in each of the regions it is necessary to first compare the liquid, gas, and cell layers. To quantitate the mass transfer through the liquid layer, the experimental and theoretical mass transfer rate through the liquid media must be considered. These rates are then compared with oxygen consumption of the cells.

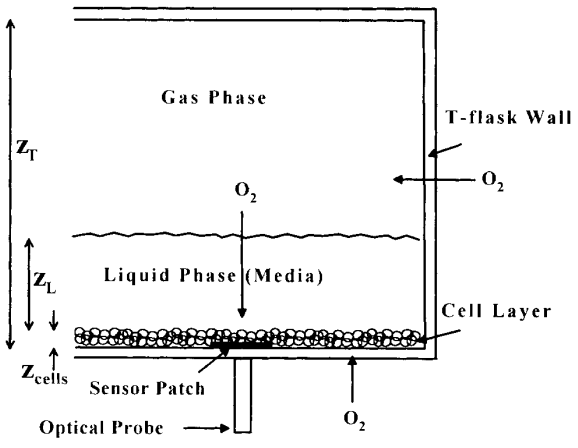

Figure 2. T-flask mass transfer system.

Liquid and Gas Phase Mass Transfer Resistance

The liquid and gas phase mass transfer resistances are often compared using the parameter $k_x/(k_y \cdot m)$ where m is the equilibrium coefficient for the species being transported and k_x and k_y are the liquid and gas phase mass transfer coefficients, respectively.[7] If $k_x/(k_y \cdot m) \gg 1$ then the mass transport is gas-phase limited, and if $k_x/(k_y \cdot m) \ll 1$ then it is liquid phase limited. To compare the gas and liquid phase mass transfer resistances, k_x and k_y are estimated from diffusion limitations, and $k_x/(k_y \cdot m)$ is given in Eq. (1):

$$\left(\frac{k_x}{k_y m}\right) = \left(\frac{D_L}{D_g}\right)\left(\frac{C_L^*}{C_g^*}\right)\left(\frac{z_T - z_L}{z_L}\right) \tag{1}$$

Diffusivities for oxygen in water (D_L) and in air (D_g) were taken from Geankoplis[7] and adjusted for temperature (T) using the proportionalities $D_L \propto T$/viscosity and $D_g \propto T^{1.75}$/pressure. The diffusivities used were $D_L = 0.103$ cm^2/h and $D_g = 720$ cm^2/h. The concentration of oxygen in air of 8.23×10^{-3} mmol O_2/mL at 37°C and 1 atm was calculated using the ideal gas law. The concentration of oxygen in water in equilibrium with air used was 2.14×10^{-4} mmol O_2/mL.[7]

For $z_L = 0.4$ cm, $k_x/(k_y \cdot m) = 3.16 \times 10^{-5} \ll 1$. The mass transfer resistance through the liquid phase is therefore much more significant than through the gas phase, and the gas phase will be approximately uniform.

Cell Layer Mass Transfer Resistance

It is also important to consider how much mass transfer resistance there will be through the cell layer. If the mass transfer resistance through the cell layer is significant, the dissolved oxygen (DO) the sensor will read beneath the cell layer will be less than the liquid phase DO just above the cell layer.

The mass transfer resistances for the bulk liquid and cell layers can be compared using the ratio of the diffusion coefficient for the layer divided by the thickness of the layer. For this comparison, the thickness of the cell layer (z_{cells}) and the effective diffusivity of oxygen through the cell layer (D_{cells}) must be estimated. To estimate D_{cells} the cell layer was modeled as a layer of unconsolidated solid particles (cells) in which oxygen diffuses through the interstitial liquid to reach the sensor patch. An average voidage (ε) for unconsolidated particles is around 0.5 with a tortuosity (τ) of about 1.5. Therefore, $D_{\text{cells}} = (\frac{\varepsilon}{\tau})(D_L) = 0.33D_L$.

The ratio of the thickness of the cell layer to the bulk liquid layer can be calculated as follows. The volume of the cell layer is equal to the volume occupied by the cells divided by the fraction of cell volume to total volume:

$$\textit{Volume of cell layer} = (A_o)(z_{\text{cells}}) = \frac{(X)(A_o)(z_L + z_{\text{cells}})(V_{\text{cells}})}{(1 - \varepsilon)} \tag{2}$$

Solving Eq. 2 for the ratio of z_{cells}/z_L gives Eq. (3):

$$\frac{z_{\text{cells}}}{z_L} = \frac{(X)(V_{\text{cells}})}{((1 - \varepsilon) - (X)(V_{\text{cells}}))} \tag{3}$$

It has been observed that the average cell diameter for these hybridoma cells is 13 μm (13×10^{-6} m). This gives the cells an average volume of $\frac{\pi}{6}(13 \times 10^{-4}\text{ cm})^3 = 1.15 \times 10^{-9}$ cm^3. The maximum cell concentration has not been shown to exceed 2×10^6 cells/mL. Using the given values in Eq. (3), $z_{\text{cells}}/z_L = 2.3 \times 10^{-3}$.

The ratio of the diffusivities and the thickness for each layer are compared in Eq. (4):

$$\left(\frac{D_L}{D_{\text{cells}}}\right)\left(\frac{z_{\text{cells}}}{z_L}\right) = \left(\frac{D_L}{0.33D_L}\right)(2.3 \times 10^{-3}) = 6.90 \times 10^{-3} \ll 1 \tag{4}$$

This means that more than 99% of the gradient exists in the bulk liquid layer and the resistance in the cell layer is negligible. The dominant mass transfer resistance for oxygen reaching the cells and the sensor patch is therefore the liquid layer. The mass transfer resistance through the liquid layer must now be quantitated.

Experimental and Theoretical Mass Transfer Resistances through the Liquid Media

Determining the mass transfer rate of oxygen through the liquid layer is an important factor in determining whether or not a cell culture will be mass transfer limited, and strongly it influences the dissolved oxygen concentration at the bottom of the T-flask as the cells are growing. It is common practice to model the liquid layer as diffusion limited.[11] The diffusion limited mass transfer coefficient per unit area ($k_{L,\text{diff}}$) through the liquid layer to the bottom of the T-flask is derived by integrating Fick's law at steady state:

$$N = \left(D_L\left(\frac{C_L^* - C_{L,z_L}}{z_L}\right)\right) = k_{L,\text{diff}}\left(C_L^* - C_{L,z_L}\right) \tag{5}$$

To test the hypothesis that the liquid layer is diffusion limited, a method is devised by which the experimental and theoretical diffusion-limited oxygen mass transfer rates can be compared.

Numerical Diffusion-Limited Dissolved Oxygen Profiles

Comparison of theoretical and experimental liquid layer mass transfer rates is facilitated by a simple unsteady-state experiment. This experiment is described by the following differential equation with the given boundary conditions [see Eq. (6)]. The coordinate system used in Eq. (6) is $z = 0$ at the surface of the liquid layer and $z = z_L$ at the bottom of the liquid layer:

$$\frac{\partial C_L}{\partial t} = -D_L\frac{\partial^2 C_L}{\partial z^2} \tag{6}$$

where the boundary conditions are: (1) $C_L = C_{L,\text{initial}}$, for $t = 0$, $0 < z < z_L$; and (2) $C_L = C_L^*$, for $t > 0$, $z = 0$.

To obtain the theoretical $DO_{L,zL}$ profiles, this equation was numerically solved using a program written in Visual Basic (Microsoft) that uses an explicit finite difference method where $\delta C_L/\delta t$ and $\delta^2 C_L/\delta z^2$ were estimated using forward and divided difference formulas, respectively.[7] This numerical model was also modified to account for the mass transfer of oxygen through the bottom of the T-flask.

Calculation of the Specific Cellular Oxygen Consumption Rate from DO Data

The approximate specific cellular oxygen consumption rate profile for a period of cell growth in a closed T-flask can be calculated from the DO versus time profiles for the gas phase and cell layer. First, the volumetric oxygen consumption rate (Q_{O_2}) is calculated from the DO data and then the specific oxygen consumption rate (q_{O_2}) is found by dividing by the cell concentration (X).

The consumption of oxygen by the cells over any particular time interval can be calculated from an overall mass balance on the T-flask. This mass balance (millimoles of O_2) is given in Eq. (7):

$$\begin{array}{c} O_2 \\ \text{Consumed} \\ \text{by cells} \end{array} = \begin{array}{c} O_2 \\ \text{Depleted} \\ \text{in the gas} \\ \text{phase} \end{array} + \begin{array}{c} O_2 \\ \text{Depleted} \\ \text{in the} \\ \text{liquid} \\ \text{phase} \end{array} + \begin{array}{c} O_2 \\ \text{Transported} \\ \text{through} \\ \text{the T-flask} \\ \text{wall} \end{array} \quad (7)$$

The value of Q_{O_2} for each time interval is the oxygen consumed by the cells divided by $A_o \cdot z_L \cdot \Delta t$ and q_{O_2} is given by Q_{O_2}/X.

MATERIALS AND METHODS

Cell Culture

Experiments were conducted using suspension-cultured SP2/0-derived murine hybridomas, HyHEL-10 secreting a monoclonal isotype 1 heavy-chain antiavian lysozyme IgG.[16] Cells were maintained at 37°C, 5% CO_2 in Dulbecco's modified Eagle's medium and Ham F-12 nutrient (1:1 mixture DMEM/F-12) supplemented with L-glutamine, 2-mercaptoethanol, $NaHCO_3$, and 4% (v/v) fetal bovine serum (Sigma Chemical Co., St. Louis, MO). Cells were transferred every 2 days, in the midexponential growth phase, as a 1:6 ratio in 25-cm^2 sterile Corning T-flasks. Cells were amplified in 225-cm^2 T-flasks with a total volume of 90 mL for the 4-mm liquid depth and 350 mL for the 15.6-mm experiments.

Assays

A 4-mL sample was aseptically removed of which 50 to 100 μL was used for cell viability and cell density measurements and 2 mL for glucose and lactate analysis. Cell viability and density was determined by simultaneous fluorescent staining with fluorescein diacetate and propidium iodide.[1] The culture broth was centrifuged at 13,500g for 30 s, and the supernatant was analyzed for glucose and lactate with a YSI-2700 Select Biochemistry Analyzer.

Optical Oxygen Sensor and Calibration

An optical oxygen sensor based on the differential quenching of the fluorescence lifetime of a fluorophore in response to the partial pressure of oxygen was used to monitor gas and liquid phase oxygen tensions in T-flasks.[2,3] The sensor consists of a thin silicone membrane containing an oxygen-sensitive ruthenium complex, which indicates changes in oxygen levels as a phase shift in the fluorescence emission when excited by an intensity-modulated beam of light.

The sensor was prepared as previously described[2] by spreading a thin layer of silicone (GE Silicone II, General Electric Co., Waterford, NY) on a microscope slide and allowing it to cure overnight. The silicone membrane was incubated in 2.5 mg/mL of Tris-[4,7-diphenyl-1,10-phenanthroline] ruthenium (II) complex in phenol for 5 min, allowed to dry for 5 min, and then surface fluorophores were rinsed off with ethanol. It was allowed to dry completely, yielding a sensor approximately 0.4 mm thick. The silicone matrix adheres very well to both plastic and glass without the need for adhesives, as long as both surfaces are dry at installation. The probe and electronics were the same as described by Bambot et al.,[2] with the exception that the sensor patch was installed on the inside of the T-flask instead of at the end of the fiber bundle and the 450-nm lowpass filter was 500 nm.

Readings of the patch were ascertained through the clear, polystyrene T-flask with the optical probe placed directly against the T-flask at the center of the patch. Continuous measurements were taken in the incubator with the door closed and intermittent readings with the door open. Sensor phase angle measurements only require a few seconds per sensor and readings are nearly instantaneous. Since changes in probe alignment angle and rotation produced minor variations in sensor readings due to variability within the patch, the probe was positioned at the center of each patch and was held approximately 90° to the sensor.

Because the optical sensor senses oxygen tension or partial pressure, it has identical calibrations in the gas and liquid phase.[2] The sensors were calibrated in the gas phase at 37°C. The sensors were mounted inside a 225-cm^2 T-flask which was sparged with a mixture of air (100% DO) and nitrogen (0% DO). The percentage and flow rates of the two gases were controlled with gas flow meters such that the total gas flow rate was always 0.3 L/min. The phase response of the optical electrode was recorded and plotted against percent DO. The hy-

perbolic response of the optical probe calibration is similar to the Stern–Volmer equation.[13]

Experimental Oxygen Measurement

For the experiments, autoclaved sensors were aseptically mounted on the inner surface of the T-flasks. We simply placed the sensor on the inside of the T-flask with sterile forceps and gently moved the forceps over the membrane to remove air bubbles between the sensor and the flask. The sensor remained completely attached to the T-flask surface for the duration of the experiment. No modifications to the T-flasks were required because the patches were installed inside the T-flasks, and readings could be taken through the clear plastic. One patch was placed above the liquid level (gas phase), the other below (liquid phase) on the T-flask's bottom surface.

Prewarmed media, 37°C, was added to the T-flasks, an initial sensor reading was taken, the medium was inoculated with the hybridomas, and a sample was removed for analysis. The T-flasks were then placed in an incubator controlled at 37°C and 5% CO_2. One lid was cracked open approximately one-half of a turn to allow oxygen transfer, the other lid remained closed. Readings of each sensor were taken intermittently during the experiment while one sensor was monitored continuously. The experiment was repeated and the results from both experiments were the same. Data of continuous readings were logged every 2 min using a Strawberry Tree data acquisition system (Strawberry Tree, Sunnyvale, CA). Experiments were carried out for 160 h.

The Corning T-flasks used in this experiment were two position plug seal caps which can be used open or closed. To operate in the open mode, the cap needs to be backed off and then tightened until a slight resistance is obtained to allow the breathing tabs to engage and support the lid permitting gas exchange, approximately one-half of a turn.

Liquid Phase Mass Transfer Rates

Mass transfer rates through different thicknesses of water were measured experimentally. Water was used instead of media since it has essentially the same diffusivity. For liquid thicknesses of 4, 10, and 15.6 mm, the corresponding volumes of water were added to a T-flask with an optical sensor patch attached to the bottom. The T-flask was then placed in an incubator maintained at 37°C. The contents of each T-flask were then sparged with nitrogen for about 2 h to flush the oxygen from the liquid and gas phases. After sufficient time was given to allow the contents to reach 37°C, the cap was removed and oxygen was allowed to diffuse into the T-flask while the DO at the bottom of the liquid layer was recorded. The gas phase DO profile above the sensor patch was determined by a similar experiment in which no water was put into the T-flask.

Mass Transport of Oxygen through the T-Flask Walls

To compensate for the mass transfer of oxygen into the T-flask, the permeability and the thickness of the T-flask walls were measured. The permeability of the polystyrene T-flask wall was determined using a simple unsteady-state experiment in which oxygen was removed from a 225-cm^2 T-flask by sparging with nitrogen; the T-flask was then sealed and the gas-phase DO in the T-flask was monitored using the optical sensor as oxygen diffused back in through the T-flask walls. Eqs. (8a) and (8b) describe the mass transport of oxygen into the T-flask during this experiment. In Eq. (8b), A is the entire surface area of the T-flask wall and Vol is the volume of the T-flask:

$$\frac{\partial DO_g}{\partial t} = K(100\% - DO_g) \tag{8a}$$

$$K = \left(\frac{P_M}{x_T}\right)\left(\frac{A}{Vol}\right)\left(\frac{p^*}{C_g^*}\right) \tag{8b}$$

The variable K in Eq. (8a) is assumed not to be a function of concentration or time, and Eq. (8a) was separated, integrated, and rearranged to give Eq. (9), where $DO_{g,to}$ is the dissolved oxygen concentration in the gas phase at time t_o.

$$\ln(100\% - DO_g) = -(K)(t) + (\ln(100\% - DO_{g,t_o}) + (K)(t_o)) \tag{9}$$

Using Eq. (9) the negative slope of $\ln(100\% - DO_g)$ vs. t gives K. The experimentally determined permeability was calculated by solving Eq. (8b) for P_M.

RESULTS

Cell Settling

It was observed that cells settled to the bottom of the T-flask shortly after inoculation and sampling. To determine experimentally if the cells physically obstructed the oxygen sensor from accurately measuring the dissolved oxygen in the liquid phase, a 4-mm liquid depth, 4-day-old culture was mixed and placed on an inverted microscope. A 4-day-old culture was chosen for maximal cell density. Cells settled to the T-flask bottom within approximately 1.5 h but did not attain densities high enough to affect the dissolved oxygen readings due to mass transfer resistance through the cell layer. It was interesting to note that the T-flasks were slightly concave and the cells tended to settle in higher densities toward the center of the flask probably with the aid of

external vibrations. Most movement caused vibration in the liquid layer of the T-flask. Vibrations were most pronounced by opening and closing the incubator door, walking in front of the incubator, and even gently closing a nearby refrigerator. Even the lab laminar flow hood and air conditioning unit caused minor vibrations. Based on the cell layer calculations developed in the Theory section, supported with experiment observation, in all experiments the liquid phase sensor was positioned at a point of intermediate cell density where for the 4-mm liquid depth there was never a full layer of cells covering the sensor, and for the 15.6-mm depth there was a maximum of three layers of cells.

Liquid Depth Experiments at 15.6 mm

Figure 3a shows the oxygen and growth profiles of the cell layer in an open T-flask with a liquid depth of 15.6 mm. The liquid phase DO was monitored continuously while readings of gas phase DO were ascertained daily just before cell samples were taken for analysis (indicated by spikes in DO). The DO under the cell layer began to decrease shortly after inoculation and

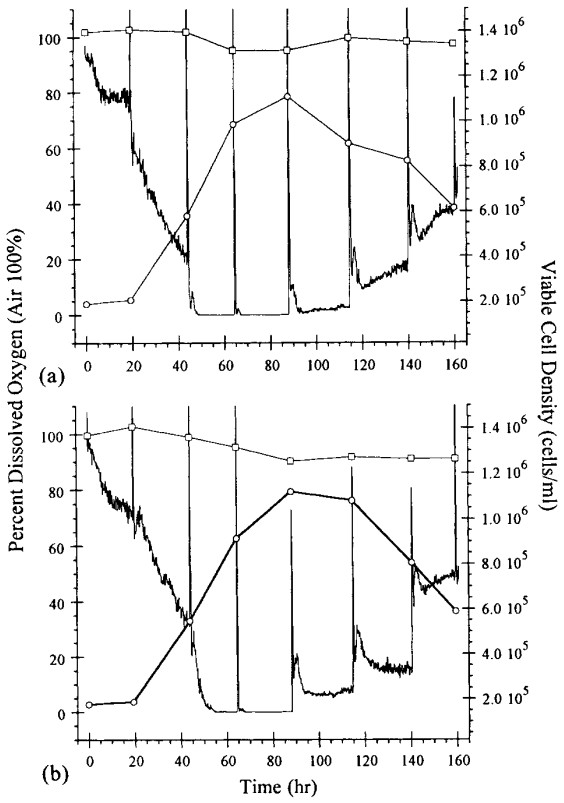

Figure 3. Profiles of gas-phase (□) and bottom of liquid-phase (—) dissolved oxygen and viable cell density (○) of a growing hybridoma culture in a (a) partially open and (b) closed 225-cm^2 T-flask of 15.6-mm liquid layer depth. Spikes in dissolved oxygen indicate cell sampling.

reached 0% approximately 50 h later when the cells were in the rapid phase of cell growth. An increase in DO of the liquid phase occurred after sampling at 90 h and continued to increase through the stationary and death phases. The daily readings of the gas phase showed little change in DO throughout the experiment.

To determine if there were decreased oxygen levels under the cell layer of a closed T-flask, the same experiment was conducted with the T-flask lid closed. The cell growth and oxygen profiles are shown in Figure 3b. The liquid phase dissolved oxygen decreased to reach 0% dissolved oxygen at around 52 h, approximately the same time as in the open T-flask, and increased at approximately 90 h as in the open T-flask. In both cases, from the time of inoculation to 20 h, there was little measurable increase in cell density, while the liquid phase dissolved oxygen decreased approximately by 30%. As the rate of cell growth increased, the rate of oxygen consumption increased and, consequently, the DO at the bottom of the T-flask decreased. At this time the cells were still in exponential growth. The level of oxygen began to increase at approximately 90 h in the stationary phase and continued to increase through the death phase. As in the case of the open T-flask (Fig. 3a), the gas phase DO in the closed T-flask showed little change between daily sampling (Fig. 3b).

The glucose utilization, lactate production, culture viability, and total cell density in both the open and closed T-flasks were also similar throughout the growth cycle (data not shown). The viable cell density profile of the open T-flask was nearly identical to that of the closed T-flask (Fig. 3a and b). For both flasks, the cell density increased as the liquid phase dissolved oxygen was consumed and decreased as the liquid phase dissolved oxygen increased.

Liquid Depth Experiments at 4 mm

To determine the effect of thinner liquid depths on the oxygen profile under the cell layer during growth and to determine if the gas phase in the 15.6-mm experiments showed no oxygen depletion during cell growth due to the T-flasks being mixed and sampled every day, experiments were carried out in both open and closed T-flasks with 4-mm liquid depth. An initial and final cell sample was taken and intermittent readings of the gas phase sensor (of the open T-flask) and the liquid phase sensor (of the closed T-flask), otherwise, the T-flasks were not disturbed during the experiment.

In the open 4-mm-liquid-depth T-flask (Fig. 4), the initial and final dissolved oxygen readings of the gas phase indicated no decrease in oxygen. The dissolved oxygen in the liquid phase decreased during the experiment to near 0% at around 60 h and began to increase at 107 h.

In the closed 4-mm-liquid-depth study, over the duration of the experiment the dissolved oxygen in the gas

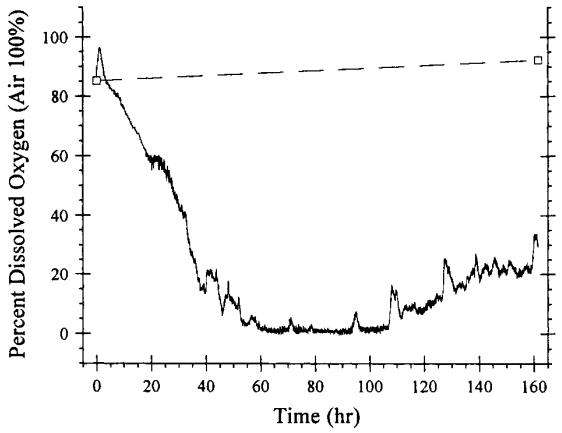

Figure 4. Profiles of gas-phase (□) and bottom of liquid-phase (—) dissolved oxygen of a growing hybridoma culture in a partially open 225-cm^2 T-flask of 4-mm liquid layer depth. Cells were not sampled throughout growth.

phase decreased by approximately 20% (Fig. 5—shown are smoothed profiles for determination of oxygen consumption). The dissolved oxygen in the liquid phase decreased to near 0% between 40 and 68 h, and even at 160 h remained below 10% dissolved oxygen.

The initial and final values for viable and total cell density, glucose consumption, and lactate production for both experiments utilizing the 4-mm liquid depth showed no significant differences.

Glucose consumption, lactate production, and both viable and total cell density did not differ significantly between open and closed T-flasks. The glucose consumption by the cells was the same for the 4- and 15.6-mm liquid depths, but for the 4-mm-liquid-depth experiments the lactate production was approximately 20% lower, the viable cell density 75% higher, and the total cell density was 51% higher than in the 15.6-mm-liquid-depth T-flasks (data not shown).

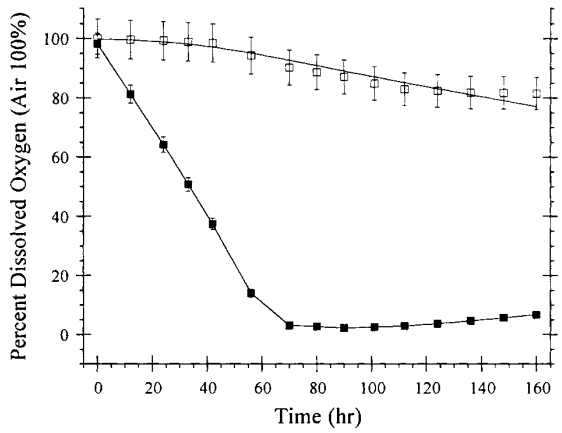

Figure 5. Profiles of experimental (□) and the smoothed (—) gas-phase (DO_g) and bottom of liquid-phase dissolved oxygen ($DO_{L,zL}$) (■), of a growing hybridoma culture in a closed 225-cm^2 T-flask of 4-mm liquid layer depth. Cells were not sampled throughout growth. Error bars represent maximum error in DO_g and $DO_{L,zL}$ due to fluctuations in incubator temperature upon sensor reading.

Liquid Phase Mass Transfer Resistance

The theoretical and experimental DO profiles for the unsteady-state mass transfer of oxygen into liquid layers of 4, 10, and 15.6 mm in thickness are shown in Figure 6. The theoretical profiles were determined by solving

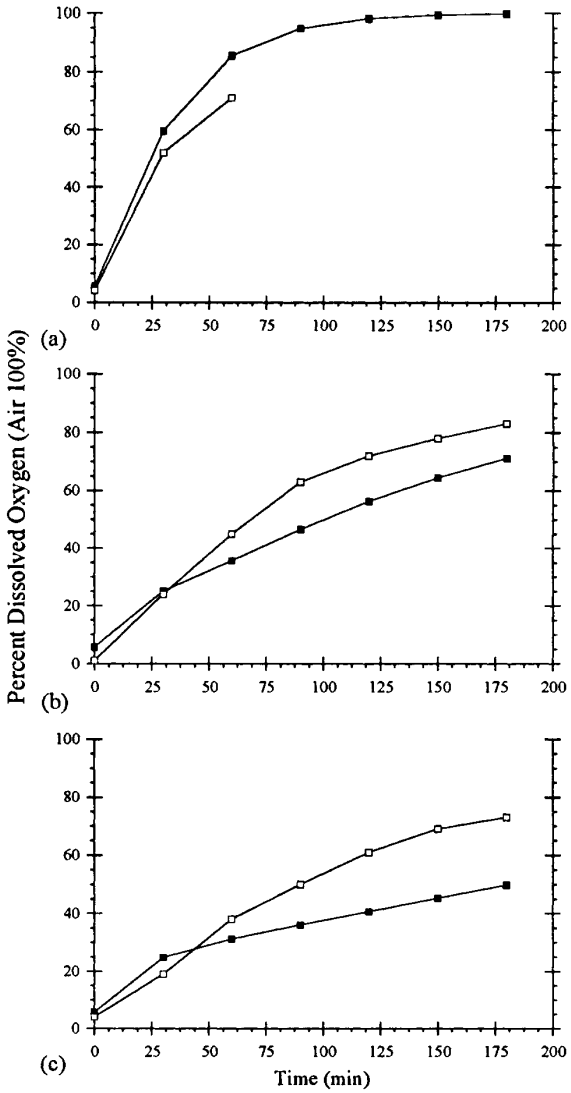

Figure 6. Comparison of experimental (□) and theoretical (■) $DO_{L,zL}$ vs. time profiles at the bottom of the 225-cm^2 T-flask for oxygen diffusion through different thicknesses of liquid: (a) 4 mm; (b) 10 mm; and (c) 15.6 mm.

the differential equation given earlier [Eq. (6)] with the exception that the surface concentration of oxygen used in the program was not the instantaneous step change indicated in boundary condition 1 of Eq. (6), but instead was the experimentally determined gas-phase DO profile. This gas-phase DO increased very quickly and reached 80% within 24 min (data not shown). The program was also modified to account for mass transport of oxygen through the bottom of the T-flask. These modifications insured that the program solution was subjected to the same conditions as the liquid in the T-flask where the DO at the bottom of the T-flask was being measured.

The theoretical DO profile for the 4-mm liquid thickness was slightly greater than the experimental value (Fig. 6a). The theoretical DO profiles for the 10-mm (Fig. 6b) and 15.6-mm (Fig. 6c) experiments were both lower than the experimental profiles with the variation in the 15.6-mm experiment being greater than that of the 10-mm case.

To check the accuracy of the finite difference program, the results of the program were compared to published graphical solutions.[7] The finite difference and published solutions were nearly identical for each of the liquid thicknesses for the same boundary and initial conditions (the mass transport of oxygen through the bottom of the T-flask was not included for this comparison).

Theoretical (as determined by the program) and experimental oxygen mass transfer rates through the liquid film were compared by the negative slope of the plot of $\ln(100\% - DO_{L,\,zL})$ vs. time for each thickness of liquid. The negative slope of this plot will hereby be denoted as alpha. The slope of this plot is not a function of the initial dissolved oxygen concentration. This method was used because it is similar to how the results of the numerical solution were correlated in Geankoplis[7] and it seemed reasonable to apply the same method to the experimental data. These plots (not shown) were approximately linear over a large region for both the experimental and theoretical data. The maximum slopes (alpha) of these plots are graphed in Figure 7.

Both the experimental and theoretical alphas decreased as the liquid layer thickness (z_L) increased. For the 4-mm liquid thickness, the theoretical alpha was greater than the experimental alpha. However, the theoretical alphas decreased more substantially with increasing z_L than did the experimental alphas. This trend is shown in Figure 7 by the increase in the ratio of experimental to theoretical alphas with increasing z_L.

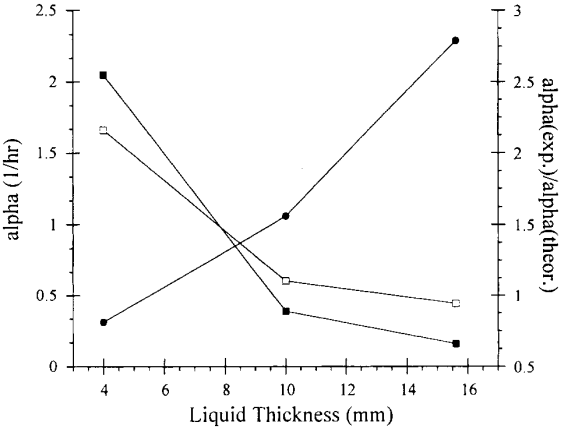

Figure 7. Slopes of $\ln(100\% - DO_{L,zL})$ vs. time (alpha) for experimental (□) and theoretical (■) $DO_{L,zL}$ profiles for unsteady-state oxygen mass transport through 4-mm-, 10-mm-, and 15.6-mm-thick layers of liquid in a 225-cm^2 T-flask. Also graphed is the ratio of experimental-to-theoretical slopes [alpha (exp)/alpha (theor.)] for each liquid layer thickness (●).

Permeability of the T-Flask Wall

The negative slope of the least-squares line of $\ln(100\% - DO_g)$ vs. time from the DO_g data for oxygen mass transfer through the T-flask wall mentioned earlier, gave $K = 1.77 \times 10^{-3}$ 1/h [Eq. (6b)]. The total volume of the 225-cm^2 T-flask (Vol) was 900 cm^3 and the total surface area (A) was approximately 671.2 cm^2. The T-flask wall thickness (x_T) was measured to be 1.8 mm. By rearranging Eq. (6b), and using these values, the permeability was calculated to be $P_M = 2.20\times 10^{-6}$ mmol O_2 · mm/(cm^2 · h · cm Hg).

Calculation of Specific Cellular Oxygen Consumption Rate from DO Data

The DO data used to calculate Q_{O_2} is plotted in Figure 5. Only half of the data points (0, 24, 42, 70, 90, 112, 136, and 160 h) in Figure 5 were directly calculated from the experimental data. The error bars for the experimental DO_g data represent the uncertainty associated with the variability of the sensor calibration with fluctuations in temperature which is presented in the Discussion section. The intermediate data points were interpolated. A smoothed gas-phase DO_g profile is also plotted in Figure 5. The smoothed DO_g curve was produced by minimizing the sum of the squared error subject to the constraint that k_L was constant during the calculation of Q_{O_2}. Lotus 123r4 software was used for this curve fit. Using Solver, the smoothed gas-phase DO_g points ($DO_{g,\,s}$) were determined minimizing the sum of the squared error of $(DO_g - DO_{g,\,s})^2$ subject to the constraint that the average k_L values for each time period were equal. The mass balance (millimoles O_2) showing how this average k_L for each time period relates to Q_{O_2} and the mass transport through the bottom of the T-flask is given in Eq. (10).

$$Q_{O_2}(A_o)(z_L)(\Delta t) = k_L(A_o)\left(C_L^*\right)\left(\frac{DO_{g,\,s,\,t} + DO_{g,\,s,\,t+\Delta t}}{2}\right) - \left(\frac{DO_{L,\,z_L,\,t} + DO_{L,\,z_L,\,t+\Delta t}}{2}\right) + \frac{P_M(A_0)(p^*)}{x_T(100\%)}\left[100\% - \left(\frac{DO_{L,\,z_L,\,t} + DO_{L,\,z_L,\,t+\Delta t}}{2}\right)\right] \quad (10)$$

The subscripts of t and $t + \Delta t$ denote the dissolved oxygen values at the beginning and at the end of the time period. The k_L for this optimal curve smoothing was 0.37 cm/h. Each point for Q_{O_2} in Figure 8 is the average for the preceding time interval. The error curves for Q_{O_2} (Fig. 8) and q_{O_2} (Fig. 9) were calculated from the maximum and the minimum possible slopes of the smoothed $DO_{g,\,s}$ curves. The maximum slope of the smoothed $DO_{g,\,s}$ curve was found by fixing the endpoints at the highest ($DO_{g,\,s} = 100 + 3.45$, $t = 0$ h) and the lowest ($DO_{g,\,s} = 81.5 - 1.17$, $t = 160$ h) possible values, as determined by the error bars in the DO_g data discussed earlier, then minimizing the sum of the squared error of $(DO_g - DO_{g,\,s})^2$ subject to the constraint that the average k_L values for each time period were equal. The minimum slope of the smoothed $DO_{g,\,s}$ curve was found in a similar manner except the lowest ($DO_{g,\,s} = 100 - 3.45$, $t = 0$ h) and highest ($DO_{g,\,s} = 81.5 + 1.17$, $t = 160$ h) endpoints were fixed.

The q_{O_2} profile was calculated as described in the Theory section using the estimated viable cell concentration (X) profile shown in Figure 9. The endpoints of X were fixed by the experimentally determined initial and final viable cell concentrations. The maximum X for the 4-mm experiment was estimated by assuming the ratio of the maximum viable concentration divided by the final total cell concentration for the 15.6-mm experiment shown in Figure 3b (data not shown for total cell density) of 0.93 was equal to this same ratio for the 4-mm cell growth experiment. Using this assumption, the maximum X for the 4 mm was 1.7×10^6 cells/mL. The shape of the 4-mm X profile was estimated from the shape of the X profile for the 15.6-mm case (Fig. 3b). The results of these calculations are shown in Figure 8. Again, each point for q_{O_2} is the average for the preceding time interval. The calculated totals of the oxygen depletion and the mass transfer of oxygen through the T-flask walls are given in Table I.

DISCUSSION

Although this oxygen sensor was extremely useful in aseptically ascertaining the dissolved oxygen values of both the bottom of the cell layer and the gas phase in T-flasks, since it is still being developed and is a prototype, it did have some inherent errors associated with its use. Phase angle readings were significantly affected by changes in temperature. When the incubator door was opened for intermittent sensor readings, the temperature of the incubator decreased and to less of an extent the temperature inside the T-flasks decreased. As the temperature decreased, the dissolved oxygen reading decreased. Most reduction in dissolved oxygen readings was noted when gas-phase sensor readings (up to 13% decrease) and liquid-phase sensor readings (up to 7% decrease) were 100%. The effect of temperature was less significant in both gas- and liquid-phase readings when measured at 0% DO (up to 2% decrease). The phase discriminator used in these experiments had a sensitivity of ±0.5°. This also had a more significant effect on dissolved oxygen readings at higher dissolved

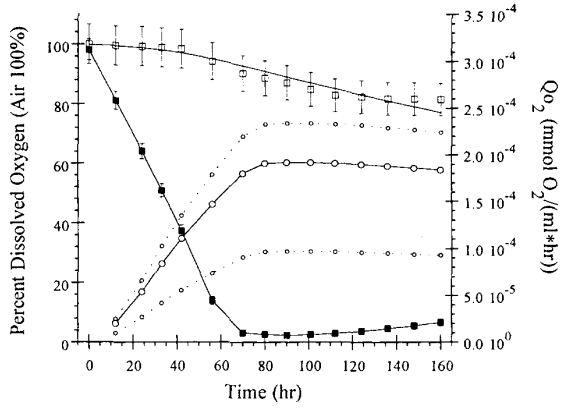

Figure 8. Volumetric (○, Q_{O_2}) oxygen consumption rate for murine hybridoma cells growing in 4 mm of media in a closed 225-cm² T-flask calculated from DO data. Open circle, dotted lines (○) represent the maximum error in Q_{O_2} due to fluctuations in incubator temperature upon sensor reading. Shown also is the dissolved oxygen concentration at the bottom of the T-flask (■) and smoothed (—) and experimental (□) gas-phase dissolved oxygen with error bars.

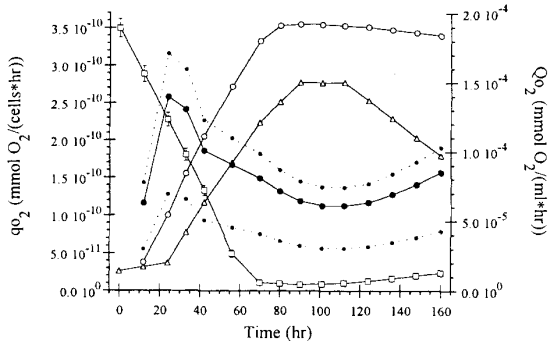

Figure 9. Specific (●, q_{O_2}) and volumetric (○, Q_{O_2}) oxygen consumption rates for murine hybridoma cells growing in 4 mm of media in a closed 225-cm² T-flask calculated from DO data. Dotted line, closed circles (●) represent the maximum error in q_{O_2} due to fluctuations in incubator temperature upon sensor reading. Shown also is the dissolved oxygen concentration at the bottom of the T-flask (□, max = 98.5%) with corresponding error bars and the estimated viable cell concentration profile (△, max = 1.7×10^6 cells/mL).

Table I. Contributions to the oxygen consumed by hybridoma cells growing in 4 mm of media in a closed 225-cm^2 T-flask (t = 160 h).

Oxygen source	Millimoles O_2
Gas-phase depletion	1.49
Liquid-phase depletion	0.01
Mass transfer through T-flask wall, gas-phase surface area	0.13
Mass transfer through T-flask wall, bottom of liquid-phase surface area	0.54
Total	2.17

oxygen levels due to the hyperbolic nature of the sensor calibration curve. One-half of a degree phase at dissolved oxygen values near 100% could be equivalent to a maximum variation in dissolved oxygen readings of ±10%, whereas this would only have a maximum variation of ±1.5% at dissolved oxygen values near 0%.

In testing this sensor in cell culture flasks, we noted that the dissolved oxygen values in the cell layer during cell growth decreased to 0% dissolved oxygen. To examine this further, experiments were conducted in T-flasks with lids both open and closed in 15.6 mm of liquid depth. This depth was chosen primarily to enable cell sampling without significantly affecting final volume, but also because it was the common thickness employed by this lab for cell scale-up into bioreactors, and the volume was below the 370-mL working volume, equivalent to 16.4-mm liquid layer thickness, recommended by the manufacturer. Because it is generally recommended that the layer of media in the T-flask be in the range of 2 to 5 mm in thickness to ensure adequate oxygen transfer to the cells growing on the bottom of the T-flask,[6] experiments were also carried out in 4 mm of liquid depth in open and closed T-flasks in which only an initial and final cell sample were taken. Cells growing in a closed system are thought to be limited by the availability of headspace oxygen.[8]

It was surprising to note that both the open and closed T-flasks in all experiments (Figs. 3a and b, 4, and 5) exhibited similar gas- and liquid-phase oxygen trends throughout the growth cycle with only small decreases in the gas phase, indicating that headspace oxygen was not a limiting factor in these experiments. An interesting observation is the sharp increase in dissolved oxygen that appeared to take place immediately after the sampling process (Fig. 3a and b). We believe that this is a result of the mixing that takes place as the T-flasks are handled. It appears that an inexpensive vibrating device that could be affixed to the trays in CO_2 incubators may improve the performance of T-flask cultures by providing better mixing.

Although the liquid-phase dissolved oxygen profiles for both the closed and open 4-mm-liquid-depth T-flasks were similar throughout growth (Figs. 4 and 5), oxygen in the cell layer of the open flask appeared to be consumed faster than in the closed T-flask. This was very likely due to increased vibration from intermittent liquid-phase readings of the closed T-flask when the incubator door was open and shut and slight vibration when the probe was placed against the T-flask for readings. By increasing vibration to the T-flask, there should be increased mixing in the liquid layer increasing the rate of oxygen transfer and thereby allowing more oxygen to reach the cells. Because the open T-flask was only sampled at the start and end of the experiment, the dissolved oxygen profile through the liquid layer was not disturbed during cell growth.

The similar glucose uptake and lactate production profiles indicate that, in all T-flasks, the yield of lactate on glucose was approximately 1 g/g, suggesting that sealing the T-flask had no significant effect on cell metabolism. Although the growth and metabolism profiles did not differ between open and closed T-flask experiments, there did appear to be a significant difference in these profiles between the 4- and 15.6-mm liquid depths. The lower lactate production and higher final cell densities in the 4-mm-liquid-depth T-flasks indicates that the cells growing in the 4-mm liquid depth may have been less oxygen limited than those in the 15.6-mm condition. The 4- and 15.6-mm-liquid-depth experiments were not conducted simultaneously; therefore, further studies would need to be done to verify differences in growth profiles with liquid thickness.

Because our data indicate no significant variations in cell density, glucose consumption, and lactate production in open and closed T-flasks, we assume there would be no effect on specific antibody production, although further studies are needed to confirm this.

Usually media is replaced every 2 to 4 days in closed vessels to reduce the CO_2 produced by the cells during growth and the associated increase in lactate and decrease in pH.[8] Since there were no significant differences in cell growth and lactate production between the open and closed flasks over 7 days, this would indicate that CO_2 from cell respiration was no more a limitation in closed T-flasks than in the open ones.

The cells used for these experiments grew in suspension as a thin layer (less than three cells thick in the 15.6-mm liquid layer). Therefore, it is assumed their presence had a minimal effect on sensor readings. The significance of mass transfer resistance for anchorage-dependent cells needs to be determined on a case-by-case basis since it will depend on the void fraction of the cells. Usually T-flasks are treated to give them a net negative or less commonly a net positive charge for a substrate on which anchorage-dependent cells can grow.[4] The silicone patch used in these experiments carries a net neutral charge. Furthermore, it is common practice[6] to coat substrates with water-repellent silicone to inhibit attachment by cells; therefore, it would be expected that anchorage-dependent cells would attach

poorly to the patch and, therefore, should not significantly effect sensor readings.

It is unclear why the experimental DO profile for the 4-mm unsteady-state experiment in Figure 6 dropped below the theoretical profile. Several sources of error could account for this discrepancy: the experimentally measured permeability for the T-flask wall could have been higher than it actually was and there could have been inaccuracies associated with the sensor and inaccurate values for the property data used in the numerical solution. There seemed to be an increase in the mass transfer rates of oxygen through the liquid layer as the liquid layer thickness increased. This trend is shown qualitatively in Figure 6 and quantitatively in Figure 7 by the increase in alpha (exp.)/alpha (theor.). It is believed that deviations between the experimental and theoretical mass transfer rates (alphas) were due to convective currents in the liquid layer, possibly caused by the vibrations produced in the lab mentioned earlier. It takes very little convection to significantly increase the mass transfer of oxygen in this system. It also appears that the effect of this disturbance on the oxygen mass transfer rate is more pronounced in thicker layers of liquid. The actual quasi-steady state mass transfer rate through the liquid layer is probably a function of $k_{L,\text{diff}}$, z_L, and alpha (exp.)/alpha (theor.). With further study, the exact functionality of this relation could be determined.

The results of these mass transfer experiments seem to suggest that the practice of modeling the liquid phase as a stagnant layer[11] in ordinary lab conditions could be inaccurate, especially for thicker layers. Further study in this area is clearly warranted.

The permeability of the T-flask wall had to be determined experimentally, because this information was not available from the manufacturer. The permeability for the polystyrene T-flask wall determined in this experiment was comparable to a value found in literature of $P_M = 7.47 \times 10^{-10}$ (cm^3 [STP] · cm)/(s · cm^2 · cm Hg) at 30°C.[7] Converting this permeability into the same units as used in this study (0.0454 mmol O_2/cm^3 (STP)) gives $P_M = 1.22 \times 10^{-6}$ (mmol O_2 · mm)/(cm^2 · h · cm Hg). This published value at 30°C is more than half the experimentally determined value of 2.20×10^{-6} (mmol O_2 · mm)/(cm^2 · h · cm Hg) at 37°C. Because the permeability increases with temperature the experimental and published values are even closer in magnitude.

The results show that the largest portion of the oxygen consumed by the cells growing in 4 mm of media in the closed 225-cm^2 T-flask was taken from the headspace gas phase as expected (see Table I). What is surprising, however, was the relatively large calculated portion of oxygen that was transported through the walls of the T-flask during the cell growth experiment. The oxygen transported through the T-flask wall accounted for approximately 30% [(0.13 + 0.54)/2.17 ≈ 0.30] of the total amount of oxygen consumed by the cells. It was expected that more oxygen would be transported through the bottom of the T-flask than through the walls exposed to the gas phase since the bottom of the T-flask was exposed to a much larger gradient and accounted for about one third of the total surface area of the T-flask wall. This was indeed the case as shown in Table I. It appears that oxygen transport through the walls is a significant source of oxygen in closed T-flasks.

Despite the fluctuations and uncertainty in the gas phase DO data, calculated values for q_{O_2} were very similar to values published in other sources. For example, Miller et al.[12] reported a q_{O_2} of 2.00×10^{-10} mmol O_2/(cell · h) at 10% DO in a continuous culture.[12] This published q_{O_2} is in the range of q_{O_2} values calculated for this article as shown in Figure 9. It is also interesting to note that Miller et al.[12] reported q_{O_2} to be 1.30×10^{-10} mmol O_2/(cell · h) at 0.5% DO in the same study, and the average q_{O_2} when the DO reached zero between 70 and 80 h in this experiment was 1.32×10^{-10} mmol O_2/(cell · h). This was very close to the value reported by Miller et al.[12]

The decline in q_{O_2} after 30 h is expected for two reasons. First, it has been previously reported that the q_{O_2} of hybridoma cells decreases as DO decreases for DOs below the critical DO.[12] Second, the DO at the bottom of the T-flask reached near zero and the mass transfer rates reached maximum values while the cells were estimated to still be growing. With Q_{O_2} at its maximum rate and cells continuing to grow, q_{O_2} must decrease because q_{O_2} is inversely proportional to the cell concentration. It is also interesting to note that, as the cells were estimated to be in the early death phase at around 110 h and the viable cell concentration decreased, q_{O_2} began to rise. This is consistent with Miller et al.'s work,[12] since he also reported elevated q_{O_2} when the DO level increased from near zero. These conclusions cannot be completely substantiated, however, since Miller et al.'s work[12] was with continuous cultures while the T-flask is a batch system.

If more reliable DO measurements at higher DO concentrations could be obtained of the gas phase, the oxygen consumption rates calculated would be as accurate as those DO measurements. This suggests that the procedure used in this experiment could be utilized as an easy non-labor-intensive method for measuring the specific oxygen consumption rates of cells growing in closed T-flasks.

Calculations involving the cellular oxygen consumption rates and the DO profiles for the bottom of the liquid phase for the 15.6-mm cell growth experiment is also consistent with increased mass transfer rates through the liquid layer. For example, the mass transfer coefficient through the liquid layer in the 15.6-mm experiment shown in Figure 3b was calculated by equating the volumetric consumption rate by the cells to the sum of the mass transfer rates through the liquid layer and the bottom of the T-flask. From Figure 3b at 50 h, using

$q_{O_2} = 1.30 \times 10^{-10}$ mmol O_2/(cell · h) for low DO, the calculated k_L was 0.298 cm/h. The theoretical diffusion-limited $k_{L,diff}$ = (0.103 cm^2/h)/(1.56 cm) = 0.066 1/h. Therefore, the experimental k_L was 0.298/0.066 = 4.51 times greater. This suggests that some disturbance caused an increase in the liquid layer mass transfer rates and it had a greater effect in the thicker layers of liquid.

To clarify this discussion, even though the dissolved oxygen is zero in both the 4- and 15.6-mm liquid depths, since there are more cells in the 15.6-mm liquid depth, there will be more mass transfer resistance and therefore a lower specific oxygen consumption rate than in the 4-mm case.

CONCLUSIONS

The use of an autoclavable sensor which could be placed in the cell layer of T-flasks enabled us to determine that whether the T-flask lid was partially opened or completely closed did not affect the oxygen level in the growing layer of cells. During growth, cells in the closed T-flask utilized nearly all available oxygen in the cell layer while depleting little oxygen from the gas phase, indicating that the low level of oxygen in the cell layer was not due to headspace oxygen limitations and the mass transfer process of diffusion of oxygen from the gas phase into the liquid phase is far too slow to adequately meet the oxygen demand of the cells.

Since oxygen limitation can affect cell growth, cell lines should be carefully monitored throughout scale-up to ensure higher productivity and consistent results. By keeping T-flasks closed during incubator cultivation, the risk of contamination to the culture will be significantly minimized. A means of providing gentle agitation during T-flask culture is likely to create a less oxygen limited environment for cells and could expedite and improve scale-up protocols. We are currently conducting related experiments. Similar studies are being planned to also monitor CO_2 levels during cell culture using a recently described fluorescence-lifetime-based sensor.[15]

Several conclusions regarding the mass transfer characteristics of the T-flask are supported from these experiments. The T-flask is overwhelmingly liquid phase mass transfer limited. Therefore, liquid layer thickness is an important consideration when setting up a cell growth experiment in a T-flask. Also, the mass transfer resistance through the cell layer is insignificant as compared to the resistance through the bulk liquid layer. The mass transfer rates of oxygen through the liquid layer are greater than predicted by the diffusion-limited model, especially for thicker layers of liquid. This increase in mass transfer rates was supported by the theoretical DO profiles and the calculations involving the oxygen consumption rates. This suggests that experimentally determined mass transfer rates through the liquid layer are necessary to accurately scale-up T-flasks. The mass transfer of oxygen through the T-flask wall appears to be significant in closed T-flasks. Specific oxygen consumption rates calculated from DO data collected using the optical sensor that were similar to values published in other sources demonstrates the possible usefulness of this optical sensor in calculating oxygen consumption rates for cells growing in closed T-flasks.

Support from NSF grants (BCS9157852 and BES9413262) with matching funds from Genentech, Inc., is acknowledged. We thank Dr. Shabbir B. Bambot for oxygen sensor setup and assistance with initial testing, both Dr. Jeffrey Sipior and Dr. Gregory F. Payne for helpful discussions, and Dr. Sipior for sensor electronics optimization.

NOMENCLATURE

A_o	cross-sectional area of the T-flask (cm^2)
alpha	negative slope of the plot of ln(100% − $DO_{L,zL}$) vs. time for unsteady-state oxygen mass transfer into a liquid layer (1/h)
C_g	concentration of oxygen in the uniform gas phase of the T-flask (mmol O_2/mL)
C_L	concentration of oxygen at some position in the liquid phase (mmol O_2/mL)
$C_{L,\,zL}$	concentration of oxygen at the bottom of the liquid phase at z_L (mmol O_2/mL)
C_g^*	concentration of oxygen in air (1 atm, 37°C) (mmol O_2/mL)
C_L^*	concentration of oxygen in water in equilibrium with air (1 atm, 37°C) (mmol O_2/mL)
$DO_g = (C_g/C_g^*) \times 100\%$	percent concentration of oxygen in the uniform gas phase referenced to air (1 atm, 37°C) (%)
$DO_{L,\,zL} = (C_{L,z_L}/C_L^*) \times 100\%$	percent concentration of oxygen at the bottom of the liquid phase referenced to equilibrium with air (1 atm, 37°C) (%)
D_g	diffusivity of oxygen in air (1 atm, 37°C) (cm^2/h)
D_L	diffusivity of oxygen in water (1 atm, 37°C) (cm^2/h)
D_{cells}	effective diffusivity of oxygen in the cell layer (1 atm, 37°C) (cm^2/h)
k_L	actual oxygen mass transfer coefficient per unit area for the liquid layer (cm/h)
$k_{L,\,diff}$	D_L/z_L, the diffusion-limited oxygen mass transfer coefficient per unit area for the liquid layer (cm/h)
N	flux of oxygen (mmol O_2/cm^2 · h)
P_M	permeability of oxygen through the T-flask wall [mmol O_2 · mm/(cm^2 · h · cm Hg)]
p^*	partial pressure of oxygen in air (1 atm, 37°C) (cm Hg)
q_{O_2}	specific cellular oxygen consumption rate [mmol O_2/(cells · h)]
Q_{O_2}	volumetric cellular oxygen consumption rate [mmol O_2/(mL · h)]
t	time (h)
V_{cells}	average volume per cell (cm^3)
X	average viable cell concentration in the liquid phase (cells/mL)
x_T	thickness of the T-flask wall (mm)
z	distance down from the surface of the liquid phase (cm)

z_L	height of the bulk liquid layer above the cell layer and z at the bottom of the liquid layer (cm)
z_{cells}	height of the cell layer (cm)
z_T	total height of the T-flask (cm)
ε	voidage fraction for the cell layer (1 − total cell volume/total cell layer volume)
τ	tortuosity for the cell layer

References

1. Altman, S. A., Randers, L., Rao, G. 1993. Comparison of trypan blue dye exclusion and fluorometric assays for mammalian cell viability determination. Biotechnol. Prog. **9**: 671–674.
2. Bambot, S. B., Holavanahali, R., Lakowicz, J. R., Carter, G., Rao, G. 1994. Phase fluorometric sterilizable optical oxygen sensor. Biotechnol. Bioeng. **43**: 1139–1145.
3. Bambot, S. B., Lakowicz, J. R., Rao, G. 1995. Potential applications of lifetime based, phase-modulation fluorimetry in bioprocess and clinical monitoring. TIBTECH **13**: 106–115.
4. Barngrover, D. 1986. Substrata for anchorage-dependent cells, pp. 131–150. In: W. G. Thilly (ed.), Mammalian cell technology. Butterworth, Boston, MA.
5. Cherry, R. S. 1989. Oxygen transport in animal cell bioreactors, pp. 107–128. In: M. L. Shuler (ed.), Chemical engineering problems in biotechnology, vol. 1. AICHE, New York.
6. Freshney, R. I. 1987. Culture of animal cells. Liss, New York.
7. Geankoplis, C. J. 1993. Transport process and unit operations. 3rd edition. Prentice-Hall, Englewood Cliffs, NJ.
8. Griffiths, B. 1992. Scaling-up of animal cell cultures, pp. 47–93. In: R. I. Freshney (ed.), Animal cell culture a practical approach. 2nd edition. IRL Press, New York.
9. Lakowicz, J. R. 1983. Principles of fluorescence spectroscopy. Plenum, New York.
10. Li, X.-M., Ruan, F.-C., Ng, W.-Y., Wong, K.-Y. 1994. Scanning optical sensor for measurement of dissolved oxygen and BOD. Sensors and Actuators **21**: 143–149.
11. McLimans, W. F., Blumenson, L. E., Tunnah, K. V. 1968. Kinetics of gas diffusion in mammalian cell culture systems. II. Theory. Biotechnol. Bioeng. **10**: 741–763.
12. Miller, W. M., Wilke, C. R., Blanch, H. W. 1988. Transient responses of hybridoma metabolism to changes in the oxygen supply rate in continuous culture. Bioproc. Eng. **3**: 103–111.
13. Parker, C. A. 1968. Photoluminescence of solutions. Elsevier, Amsterdam.
14. Shuler, M. L. 1989. Bioprocess engineering, pp. 1–28. In: M. L. Shuler (ed.), Chemical engineering problems in biotechnology, vol. 1. AICHE, New York.
15. Sipior, J., Bambot, S., M, R., Carter, G. M., Lakowicz, J. R., Rao, G. 1995. A lifetime-based optical CO_2 gas sensor with blue or red excitation and stokes or anti-stokes detection. Anal. Biochem. **227**: 309–318.
16. Smith-Gill, S. J., Mainhart, C. R., Lavoie, T. B., Rudikoff, S., Potter, M. 1984. V_L–V_H expression by monoclonal antibodies recognizing avian lysozyme. J. Immunol. **132**: 963–967.

Once the non-agitated T-flask experiments showed conclusively that the cells experienced oxygen limitation, we turned our attention to measuring oxygen levels in shake flasks, which are the workhorse "bioreactor" of the microbial and fungal fermentation research world. For microbial cells, it was assumed that the fact that a shake flask was being vigorously agitated would suffice to deliver adequate oxygen; if you look at the fairly violent agitation that a shake flask is subjected to, it is hard to believe that there would be any oxygen limitation. Wrong again, as the next paper showed that this assumption was not true and that even in an agitated shake flask, oxygen limitation can and does occur. This topic was explored in greater detail and is addressed later in the book.

Leah Tolosa had just joined the lab and became part of the core team at CAST. I have already introduced the other authors.

COMMUNICATION TO THE EDITOR

Noninvasive Measurement of Dissolved Oxygen in Shake Flasks

Leah Tolosa, Yordan Kostov, Peter Harms, Govind Rao

Department of Chemical and Biochemical Engineering, University of Maryland, Baltimore County, 1000 Hilltop Circle, Baltimore, Maryland 21250; telephone: (410) 455-3415; fax: (410) 455-6500; e-mail: grao@umbc.edu

Received 4 March 2002; accepted 14 May 2002

DOI: 10.1002/bit.10409

Abstract: Shake flasks are ubiquitous in cell culture and fermentation. However, conventional devices for measuring oxygen concentrations are impractical in these systems. Thus, there is no definitive information on the oxygen supply of growing cells. Here we report the noninvasive, nonintrusive monitoring of dissolved oxygen (DO) in shake flasks using a low-cost optical sensor. The oxygen-sensitive element is a thin, luminescent patch affixed to the inside bottom of the flask. The sensitivity and accuracy of this device is maximal up to 60% DO, within the range that is critical to cell culture applications. By measuring actual oxygen levels every 1 or 5 min throughout the course of yeast and *E. coli* fermentations, we found that a modest increase in shaker speed and a decrease in culture volume slowed the onset of oxygen limitation and reduced its duration. This is the first time that in situ oxygen limitation is reported in shake flasks. The same data is unattainable with a Clark type electrode because the presence of the intrusive probe itself changes the actual conditions. Available fiber optic oxygen sensors require cumbersome external connections and recalibration when autoclaved. © 2002 Wiley Periodicals, Inc. *Biotechnol Bioeng* **80:** 594–597, 2002.

Keywords: oxygen sensor; non-invasive sensor; shake flask fermentation

INTRODUCTION

Shake flasks are arguably the most widely used apparatus in fermentation and cell culture experiments and yet have changed little since their inception. For this reason, the continuous monitoring of culture conditions in shake flasks has remained a challenge that needs to be addressed. Keeping track of optical density, pH, available nutrients, carbon dioxide, and DO are presently achieved by off-line measurements or by inserting submersible probes in the culture media (Scheper and Lammers, 1994; Royce, 1993; Locher et al., 1992). In this article, we report the in situ measurement of dissolved oxygen (DO) using an optical sensor.

Oxygen availability is a very critical issue during microbial growth in submerged fermentations because of the poor solubility of oxygen in water. This is a more significant issue in shake flasks, where oxygen availability is dependent mainly on the surface area to liquid volume ratio. Several studies during the past decades have dealt with the oxygen availability in shake flasks and the effects on cell growth and product formation (Dahlgren et al., 1993; Visser et al., 1990; Tunac, 1989; McDaniel and Bailey, 1969; Schultz, 1964; Gaden, 1962; Smith and Johnson, 1954). However, in routine shake flask experiments a general assumption persists even today that adequate oxygen is provided to the growing cells. This assumption is made out of convenience because of the lack of suitable means to measure oxygen levels in situ. Measuring oxygen in shake or spinner flasks is not easy with conventional electrode or fiber-optic technology. The difficulty lies in the need to insert the cumbersome probe into the culture media while trying to maintain aseptic conditions. When inserted, the electrode or fiber optic probe acts as a baffle, changing the flow conditions (Tunac, 1989); thereby the amounts of DO measured may differ from the actual levels in the absence of a probe. Additionally, a Clark-type electrode consumes oxygen during measurement, thus skewing the data at low oxygen levels. More importantly, as the flask is rotated at high speeds for long periods of time, mechanical failure of the probe becomes unavoidable. This can lead to large drifts and even leakage of probe electrolytes into the culture. With fiber-optic probes, mechanical failure is also possible with continuous, high-speed shaking. Recalibration is necessary after autoclaving fiber-optic probes. External connections can be awkward, especially when multiple probes are employed to several shake flasks. This effort can also be very expensive. Additionally, commercially available fiber-optic probes and oxygen-sensitive membranes for multi-well plates rely on luminescence intensity changes that are easily

Correspondence to: Govind Rao
Contract grant sponsor: NSF
Contract grant number: BES 0091705
Contract grant sponsors: Fluorometrix, Genentech, Merck, and Pfizer

affected by dye concentrations, photobleaching, or variations in excitation light intensities. In contrast, the sensor that is reported here relies on lifetime changes that are generally insensitive to the conditions mentioned above.

We circumvented the problems associated with invasive electrodes and fiber optic sensors by using an oxygen-sensitive luminophore immobilized in an autoclavable polymer and affixed to the bottom of the vessel. The patch is fractions of a millimeter thick and does not interfere with the flow pattern of the media. Figure 1 shows the details of the oxygen-sensing system. The flask is placed on top of a coaster-like enclosure containing the modulated light sources (light-emitting diodes or LEDs) and the detector, which are interfaced to a computer. A conventional environmental shaker with standard four-pronged flask clamps accommodates and stabilizes the flask–coaster setup. With this arrangement the oxygen levels during fermentation can be automatically followed as often as every 5 sec.

MATERIALS AND METHODS

The patch included in the oxygen-sensing system as supplied by Fluorometrix Corp. (Stow, MA) contained the oxygen-sensitive dye [1,2-bis(diphenylphosphino)ethane-Pt $\{S_2C_2(CH_2CH_2$-*N*-2-pyridinium)$\}][BPh_4]$ (Kostov et al., 2000a,b; Van Houten et al., 1998). This patch was attached to the bottom of a dry 250-mL Erlenmeyer flask, hydrated with distilled water and autoclaved. The measured amount of media (50 or 75 mL) was inoculated with 10% v/v of an overnight seed culture. Luria-Bertani (LB) broth (Quality Biological, Gaithersburg, MD) and YPD broth (Sigma-Aldrich, St. Louis, MO) were used for *E. coli* and yeast cultures, respectively. Milk filters were used as closures in all the experiments since these are shown to provide the greatest oxygen diffusion (data not shown). Initialization of the instrument was done in two steps: 1) sampling in the absence of patch (i.e., in air), and 2) sampling in the presence of a short-lived fluorophore (essentially the zero decay rate reference) dispersed in a polymer disk (bicycle reflector). The flask was placed on top of the coaster and held in place with the flask clamp on a G24 Environmental Incubator Shaker (New Brunswick Scientific, New Brunswick, NJ). Readings were taken every 5 min, although the instrumentation is capable of taking readings every 5 sec. The software corrects for the values obtained in the initialization step described above and automatically calculates the DO from the calibration curve in Figure 2. An important aspect of this approach is that the calibration data for a single lot of patches may be simply entered as the coefficients of a second-order polynomial into the software and no actual nitrogen/air calibrations are required, thus simplifying use even more. Measuring DO at 100% N_2 gas saturation and at 100% air saturation provided additional assessment of the calibration of the patch and instrument prior to fermentation. Fermentations were done at 25–27°C. The optical densities (OD) and pH were measured before and after fermentation.

RESULTS AND DISCUSSION

The measurement of DO is based on Stern-Volmer quenching of emission as described previously (Lakowicz, 1999). Briefly, the excited state of the luminescent dye [1,2-bis(diphenylphosphino)ethane-Pt $\{S_2C_2(CH_2CH_2$-*N*-2-pyridinium)$\}][BPh_4]$ is quenched proportionately to the oxygen concentrations. Intensity-modulated light at a frequency ($\omega = 2\pi \times$ Hz) generated from the LEDs serves as

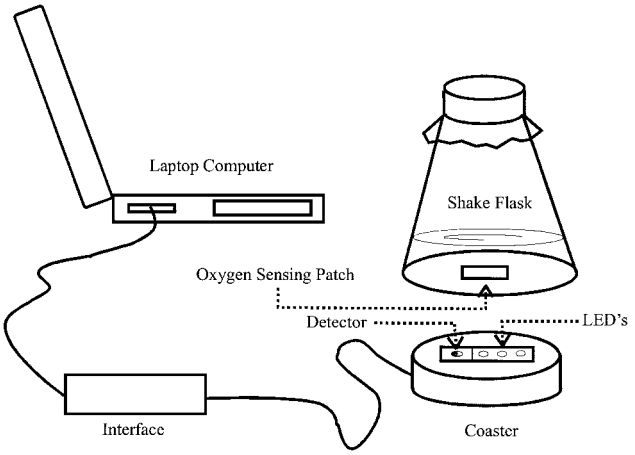

Figure 1. Setup of the noninvasive oxygen-sensing system used in the shake-flask experiments. The oxygen-sensing patch was fixed to the bottom of the flask that sits snugly on top of the coaster containing the light sources (LEDs) and the detector. The flask and coaster are held in place in the shaker with conventional four-pronged flask clamps.

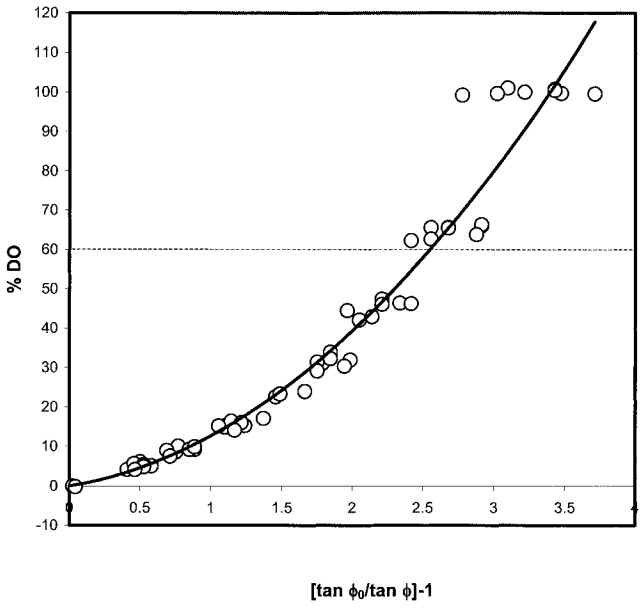

Figure 2. Calibration plot of %DO as a function of phase angles, ϕ. The data is obtained by measuring the phase angles at various mixtures of air and nitrogen gas bubbled in water. The phase at 100% N_2 gas saturation is designated ϕ_0. The DO is measured with an Ingold® oxygen electrode.

the excitation source. The phase shift (ϕ) of the resulting emission is related to the decay time (τ) by:

$$\tan \phi_\omega = \omega\tau \quad (1)$$

Collisional quenching by oxygen is described by the Stern-Volmer equation,

$$\tau_0/\tau = \tan \phi_0/\tan \phi = 1 + Ksv[Q] \quad (2)$$

where τ_0 and ϕ_0 are the decay time and phase in the absence of oxygen, respectively, *Ksv* is the Stern-Volmer constant and *Q* is the oxygen concentration. The calibration plot of phase, ϕ, as a function of DO (Fig. 2), where 0% DO is N_2 gas saturated and 100% DO is air saturated, gives a nonlinear plot. This is due to the inherent property of this dye, in which there are dual emitting species (Kostov et al., 2000a,b). A cursory examination of Figure 2 shows that the spread of values is greater at higher oxygen levels. Above 60%, smaller phase changes result in larger errors in DO readings. Nevertheless, oxygen levels below 60% are of greater significance in fermentation and cell culture than the higher oxygen concentrations.

Figures 3 and 4 show the measurements of oxygen levels during yeast and *E. coli* culture, respectively. In both cases there is a marked difference in oxygen profiles, depending on the culture conditions. In the yeast fermentation, a moderate decrease in the culture volume and increase in the shaker speed alters the conditions from microaerobic to aerobic. As shown in Figure 2, when the culture volume is 50 ml and the shaker speed is 350 rpm in yeast, the oxygen levels decrease with time but are never totally depleted. In the 75-mL and 250 rpm fermentations, oxygen-limiting conditions persist for hours. As oxygen begins to increase, this may signal the onset of cell lysis, or the depletion of the energy source. In the *E. coli* culture, a similar occurrence is observed. Additionally, the pH of the culture became increasingly more basic. A change in culture volume from 75 mL to 50 mL (Fig. 4A) significantly decreased the onset of oxygen limitation and shortened its duration. This can be attributed to the increase in surface area to liquid volume ratio, thereby promoting more efficient aeration of the media. In Figure 4B, the volume was kept constant at 75 mL, while the speed of the shaker was increased incrementally. As expected, at the slowest speed of 150 rpm oxygen supply was highly limited, resulting in an almost immediate approach to microaerobic conditions. Increasing the shaker speed from 250 to 350 rpm did not radically decrease the onset of oxygen depletion, but the duration was shorter at a faster shaker speed. Interestingly, inflections in DO are seen consistently and have previously been observed in *E. coli* fermentations (Anderson et al., 2001).

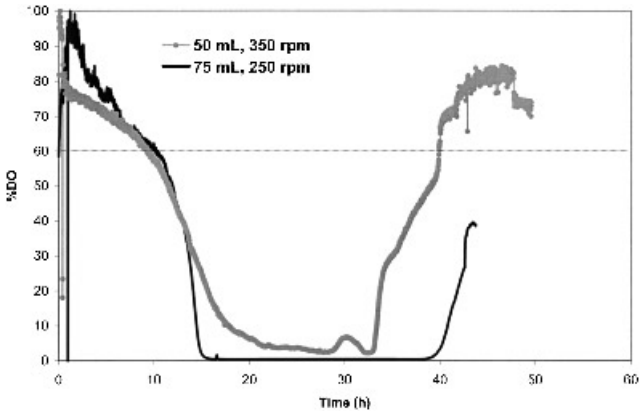

Figure 3. *Saccharomyces cerevisae* fermentation in 250-mL shake flasks. Larger volumes at slower shaker speeds lead to oxygen-limiting conditions. Above 60% DO, the sensor becomes less sensitive to increases in DO and is subject to larger errors.

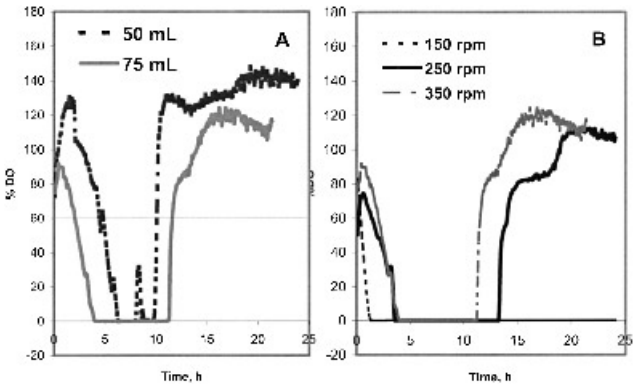

Figure 4. *Escherichia coli* fermentation in 250-mL flasks. **A:** %DO of 50 and 75 mL culture volumes at 350 rpm shaker speed. **B:** %DO of 75 mL culture at 150, 250, and 350 rpm shaker speeds. Above 60% DO, the sensor becomes less sensitive to increases in DO and is subject to larger errors.

Figures 3 and 4 show the oxygen concentrations available to cells during fermentation in shake flasks. Attempts to duplicate the same information using a small Clark-type electrode proved futile, as mechanical failure became inevitable after some time in the shaker. We believe that the same outcome can be expected with fiber-optic sensors, particularly the micrometer-sized probes. To date, we know of no other successful attempt to acquire noninvasive in situ DO data in shake flasks. Stability tests at ~30% DO (data not shown) ran for 6 straight days with sampling every 5 min showed a drift of no more than 3% DO values, comparable to a Clark-type electrode. Fouling was not observed in yeast or *E. coli* fermentation, most likely due to the Teflon-like backing on the patch. Used patches have been reautoclaved and reused twice with no detectable degradation in performance, although the signal becomes increasingly noisy due to photobleaching of the patch. Next-generation versions of this instrumentation will allow DO monitoring of several shake flasks simultaneously, a configuration that is difficult to design with submersible probes. Finally, noninvasive sensors for other analytes (individually and in multiplex) are being designed following the same overall instrumentation design.

References

Anderson DC, Swartz J, Ryll T, Lin N, Snedecor B. 2001. Metabolic oscillations in an Escherichia coli fermentation. Biotechnol Bioeng 72:212–218.

Dahlgren ME, Powell AL, Greasham RL, George HA. 1993. Development of scale-down techniques for investigation of recombinant Escherichia coli fermentations: acid metabolites in shake flasks and stirred bioreactors. Biotechnol Prog 9:580–586.

Gaden EL. 1962. Improved shaken flask performance. Biotechnol Bioeng 4:99–103.

Kostov Y, Harms P, Pilato RS, Rao G. 2000a. Ratiometric oxygen sensing: detection of dual-emission ratio through a single emission filter. Analyst 125:1175–1178.

Kostov Y, Van Houten KA, Harms P, Pilato RS, Rao G. 2000b. Unique oxygen analyzer combining a dual emission probe and a low-cost solid-state ratiometric fluorometer. Appl Spectrosc 54:864–868.

Lakowicz JR. 1999. Principles of fluorescence spectroscopy, 2nd ed. New York: Kluwer Academic/Plenum Publishers.

Locher G, Sonnleitner B, Fiechter A. 1992. On-line measurement in biotechnology: techniques. J Biotechnol 25:25–53.

McDaniel LE, Bailey EG. 1969. Effect of shaking speed and type of closure on shake flask cultures. Appl Microbiol 17:286–290.

Royce PN. 1993. A discussion of recent developments in fermentation monitoring and control: a practical perspective. Crit Rev Biotechnol 13:117–149.

Scheper T-H, Lammers F. 1994. Fermentation monitoring and process control. Curr Opin Biotech 5:187–191.

Schultz JS. 1964. Cotton closure as an aeration barrier in shaken flask fermentations. Appl Microbiol 12:305–310.

Smith CG, Johnson MJ. 1954. Aeration requirements for the growth of aerobic microorganisms. J Bacteriol 68:346–350.

Tunac JB. 1989. High-aeration capacity shake-flask system. J Ferment Eng 68:157–159.

Van Houten KA, Heath DC, Barringer CA, Rheingold AL, Pilato RS. 1998. Functionalized 2-pyridyl-substituted metallo-1,2-enedithiolates. Synthesis, characterization, and photophysical properties of $(dppe)M\{S_2C_2(2\text{-}pyridine(ium))(CH_2CH_2OR'')\}$ and $(dppe)M[\{S_2C_2(CH_2CH_2\text{-}N\text{-}2\text{-}pyridinium)\}]^+$ (R" = H, Acetyl, Lauroyl; M = Pd, Pt; dppe = 1,2-Bis(diphenylphosphino)ethane). Inorg Chem 37:4647.

Visser W, Scheffers WA, Batenburg-van der Begte WH, van Dijken JP. 1990. Oxygen requirements of yeasts. Appl Environ Microbiol 56: 3785–3792.

Finally, for tissue culture, it was believed that one could control oxygen level around cells by dialing the appropriate level of oxygen in the gas phase. This would work, but only if the rate of oxygen supply exceeds that of the rate of consumption by the cells.

We lucked out in getting Linda Bambrick, an enthusiastic collaborator who was then at the school of medicine and working with neurons and astrocytes and looking at the effects of oxygen levels. To obtain a controlled oxygen level, Linda had an expensive incubator where one could dial in the desired oxygen tension in the gas phase and the assumption was that the liquid medium around cells would of course be in equilibrium with the gas phase.

As the paper shows, this is not the case. Ironically, the Nobel prize in physiology and medicine for 2019 was awarded for the fundamental discoveries in how cells sense oxygen levels. However, most people do not measure this vital parameter!

It was also our first attempt at measuring oxygen levels in tissue growing in a petri dish and ended up working quite well.

AIChE

In vitro Cell Culture pO_2 is Significantly Different from Incubator pO_2

L. L. Bambrick
Dept. of Anesthesiology, University of Maryland School of Medicine, Baltimore. MD 21201

Y. Kostov and G. Rao
Center for Advanced Sensor Technology, Dept. of Chemical and Biochemical Engineering, University of Maryland Baltimore County, Baltimore, MD 21250

DOI 10.1002/btpr.622
Published online Month 00, 2011in Wiley Online Library (wileyonlinelibrary.com).

Continuous noninvasive monitoring of peri-cellular liquid phase pO_2 in adherent cultures is described. For neurons and astrocytes, this approach demonstrates that there is a significant difference between predicted and observed liquid phase pO_2. Particularly at low gas phase pO_2s, cell metabolism shifts liquid phase pO_2 significantly lower than would be predicted from the O_2 gas/air equilibrium coefficient, indicating that the cellular oxygen uptake rate exceeds the oxygen diffusion rate. The results demonstrate the need for direct pO_2 measurements at the peri-cellular level, and question the widely adopted current practice of relying on setting the incubator gas phase level as means of controlling pericellular oxygen tension, particularly in static culture systems that are oxygen mass transfer limited. © 2011 American Institute of Chemical Engineers *Biotechnol. Prog.,* 000: 000–000, 2011
Keywords: oxygen, neurons, astrocytes, sensor, adherent cells, cell culture

Introduction

In vitro cell culture technology is little changed from its inception. An incubator with temperature/humidity/CO_2 control and simple plastic disposable vessels filled with sterile media are typically employed. The vast majority of cultures are done under static conditions, where the vessels are simply placed in the incubator. Recently, techniques to dynamically regulate the incubator atmosphere and thereby the conditions experienced by cells have become available. However, it is unclear to what extent the incubator atmosphere affects the pericellular environment of static culture vessels. This question is the subject of the present study.

Cell survival, proliferation, and differentiation are all regulated by the extracellular pO_2. In vivo, arterial blood pO_2 is 90–110 mm Hg while in venous blood it is 35–40 mm Hg. The extracellular pO_2 seen by cells outside the vasculature varies from tissue to tissue and depends on blood flow, distance from the vasculature and tissue oxygen consumption. Mean tissue pO_2 is about 22 mm Hg (3%) in adult, less in embryo.[1] Measurements with oxygen microelectrodes have given values of 10–40 mm Hg in brain, depending on brain region.[2]

Because pO_2 regulates differentiation, gene expression, and metabolism, there is a need to measure and control this critical variable. This may be particularly true when considering the potential differences between the pO_2 experienced by a cell in vivo and the pO_2 seen by the cell in tissue culture medium exposed to room air (20.8% oxygen). Most in vitro cell studies are done in a 95% air, 5% CO_2 incubator environment. In the absence of cells, the resulting 20% O_2 gives a liquid phase pO_2 of 156 mm Hg—which would mean that cultured cells are exposed to extremely hyperoxic conditions. In fact, the actual pO_2 in close proximity to the cells, the pericellular pO_2, is dependent on two variables: oxygen supply to the cells by diffusion through the media/vessel walls and oxygen consumption by the cells. For example, one study found that although primary cultures of endothelial and mesangial cells were hyperoxic (78–110 mm Hg), several passaged cell lines were hypoxic in a 20% O_2, atmosphere due to their higher density and higher metabolic rates.[3] In another study, microelectrodes were used to record depth profiles for oxygen in cell cultures under static conditions, and the authors found significant differences between measured pericellular oxygen tension and that in ambient air.[4] Typically, the actual pO_2 is an unmonitored and uncontrolled variable in most in vitro experiments.

Standard methods for measuring pO_2 in vitro have included the Clarke-type electrode and, more recently, the use of optical probes with immobilized fluorophores on the tip of an optical fiber. Another option is the use of oxygen sensitive fluorophores dissolved in the medium (see, e.g., Ref. [5]). Both optical probes and Clarke-type electrodes have the disadvantage of needing to be positioned in the tissue culture dish (or flask) with an open connection back to their recorder, exposing the cells to contamination. Furthermore, their reading reflects the concentration in their immediate vicinity (i.e., at the probe immersion depth) and may not be representative of the actual oxygen concentration around the

Conflicts of interest: G.R. and Y.K. have an equity position in Fluorometrix, Corporation.

Correspondence concerning this article should be addressed to G. Rao at grao@umbc.edu.

cells. Additionally, the Clarke-electrode itself consumes oxygen and the pO_2 reported will be lower than that seen by cells in the absence of the electrode. Protein in media can also foul Clarke-type electrodes. Cultures with media loaded with oxygen sensitive fluorophores can be read without opening the tissue culture system but must be removed from the incubator and placed in a recorder (e.g., a fluorescence plate reader) to measure the pO_2. A problem with this approach is that the reader will read the total fluorescence across the liquid layer; therefore, the result is somewhat distorted, as there will be contributions from both the well bottom (where the cells reside) as well as from the top surface of the liquid, where the medium is in direct contact with the atmosphere.

A method for the continuous noninvasive monitoring of liquid phase pO_2 at the bottom of the well has been previously reported.[6] This study describes a reaction-diffusion model for oxygen transport and consumption and estimates the mass transfer contribution of oxygen diffusion through the vessel wall. In contrast to an invasive microelectrode, the measurement system relies on a system that includes a sterilizable oxygen sensitive patch that is placed inside a culture vessel. The patch incorporates a fluorophore which changes its optical parameters in response to variations in pO_2. The patch is monitored noninvasively through the bottom of the well by a miniature, low-profile fluorescence analyzer connected to a computer. The patch is comprised of a top gas-permeable layer (50 μm), a 500 μm thick layer of the O_2 sensitive fluorophore embedded in a silicon matrix and a bottom adhesive layer.[7] A miniature fluorometer built like a coaster fits right under the culture dish and monitors the changes in the fluorescence decay rate by quantifying the phase shift between the excitation and emission light. In this approach, the cells are cultured directly on the top of the oxygen sensing patch. In suspension-cultured hybridomas, a similar approach showed that liquid phase pO_2 varied with cell density and viability.[8]

In the present communication, we report continuous noninvasive monitoring of pericellular liquid phase pO_2 in adherent cultures. It is demonstrated that in neuron and astrocyte cultures, cell metabolism shifts liquid phase pO_2 significantly lower than would be predicted from the O_2 gas/air equilibrium coefficient. This is especially true at low gas phase pO_2s, substantiating the need for monitoring and possibly control of liquid rather than gas phase pO_2.

Methods

Cortical astrocytes and hippocampal neurons were prepared from embryonic day 15.5 mouse brain (C57Bl6J) as previously described.[8,9]

The sensing patches were placed on 25 mm glass coverslips and autoclaved. Patch-loaded coverslips were placed in 35 mm petri dishes, the hydrophobic top layer was coated with poly-L-lysine (Sigma, 0.2 mg mL^{-1}, 20 min) and laminin (Sigma, 8 μg mL^{-1}, 5 h) to promote cell adhesion. Astrocytes or neurons in 4 mL of medium, 25,000–500,000 cells mL^{-1} were added to the p35 dish in DMEM/F12 10% FBS, penicillin/streptomycin (astrocytes), or Neurobasal medium 10% FBS, penicillin/streptomycin (neurons). For neurons, the medium was changed to Neurobasal + B27 serum free supplement at 1 day in vitro. A total of 5 μM cytosine arabinofuranoside (Sigma) was added at 3 days in vitro to inhibit cell division and the medium changed to fresh Neurobasal + B27 at 4 days in vitro. Cultures were used at 5–12 days in vitro.

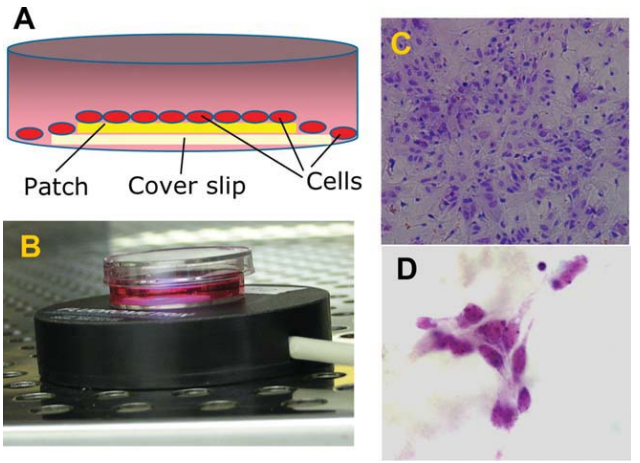

Figure 1. Experimental setup for the continuous, noninvasive measurement of pericellular pO_2 of adherent cells.

(A) Cartoon of the sensing patch with adherent cells cultured directly on top. The cover slip serves as patch carrier. The coverslip rests on the bottom of the petri dish. The measured distance from the surface of the medium to the top of the patch was 5 mm. (B) 35 mm dish with the patch and cells placed on a minifluorometer coaster inside the incubator. (C) Images of astrocytes and (D) neurons grown on the oxygen sensing patch.

To visualize cell growth on the patches, coverslips were rinsed in warmed PBS and fixed in ethanol at 4°C for 30 min. Cells were stained in cresyl violet for 5 min. After rehydration through 95 and 75% ethanol, cells were rinsed in distilled H_2O and immediately photographed on a Nikon E800 microsope with an Optronics video camera.

Cultures were maintained in Xvivo environmental control chamber (Biospherix, NY). This consisted of a buffer chamber connecting to an enclosed glove box and incubator. Control of pO_2 in the glove box and incubator ensured that gas phase pO_2 did not change when cells were taken out of the incubator for manipulations such as drug addition.

Oxygen sensitive patches and fluorescence analyzer were from Fluorometrix (Stow, MA). Patches were calibrated according to the manufacturer's protocol. Data were collected every 15 min, unless other noted.

Unless noted, all reagents were from Invitrogen. Antimycin A (Sigma) was made up in ethanol at 10 mM. An addition of 0.5 μL mL^{-1} gave a final concentration of 5 μM. Addition of vehicle alone had no effect in these experiments.

Results

Pericellular measurement of pO_2 implies placement of the sensor as close to the growing cells as possible. This was achieved by growing the cells on the sensing patch surface (Figure 1A). Figure 1B shows the culture dish on top of the coaster inside an incubator. The cable connecting the coaster to the analyzer is passed out through the gasket sealing the incubator door. Visualization of the cells with Cresyl Violet showed that both astrocytes and neurons adhered well to the patch and grew normally (Figures 1C,D).

Using two coaster arrays, pericellular oxygen was measured in parallel for mouse hippocampal neurons seeded at either 125,000 or 250,000 cells mL^{-1} at 20% O_2 (room air plus 5% CO_2). In Figure 2A, seeding density had a significant effect on pO_2 with lower pO_2 in the presence of higher

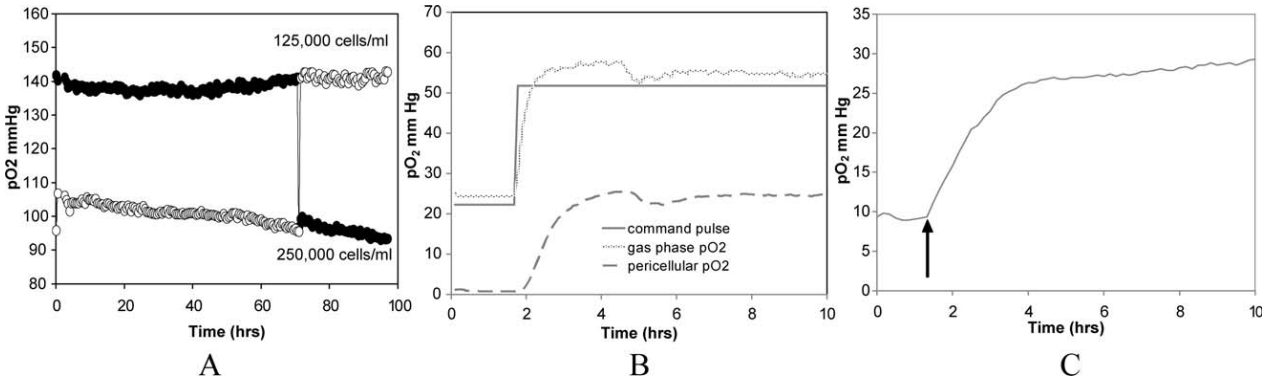

Figure 2. Time profiles of pericellular pO_2.

(A) Parallel pO_2 monitoring of neuron cultures with different cell densities on two coasters (coaster 1, open circles, coaster 2, closed circles). Neurons cultured at densities of 250,000 cells mL^{-1} or 125,000 cells mL^{-1} had pO_2 of 90–100 or 130–140 mm Hg, respectively. Recordings were stable for over 30 h. Dishes were swapped between the coasters at 70 h; (B) Change in pericellular pO_2 in response to gas phase pO_2 in an astrocyte culture; (C) Change in pericellular pO_2 in an astrocyte culture following antimycin A treatment (arrow).

cell density. The recordings were stable for 70 h. At that time, the dishes were swapped between the coasters and the results showed that the recorded pO_2 was independent of the coaster and stable for a further 30 h. The results verified the stability and reliability of the measurement approach.

Changes in gas phase pO_2 are reflected in the measured pericellular pO_2. Figure 2B shows a representative experiment with astrocytes at 50,000 cells mL^{-1} where the gas phase pO_2 in the Biospherix chamber was changed from 22.5 mm Hg to 52.5 mm Hg (from 3 to 7% O_2). The incubator chamber pO_2 follows the command pulse to the chamber with a slight lag. The liquid phase pO_2 measured in a culture dish with media and cells lag slightly behind the gas phase, as expected. Note that the liquid phase pO_2s with cells present are lower than the gas phase pO_2s, consistent with cell O_2 consumption lowering pericellular pO_2. Gentle agitation of the dish allowed oxygen to enter the medium more rapidly and achieve a reading closer to the gas phase (data not shown). This agitation approach could be used to control pO_2 levels in incubator cultures. The effect of cell density on pericellular pO_2 was greater at lower gas phase pO_2s. For astrocytes, the difference between the gas and liquid phase pO_2s was 149 and 100 mm Hg, respectively, for cells (125,000 mL^{-1}) incubated in 20% O_2 (room air plus 5% CO_2) and 37 and 8 mm Hg, respectively, for astrocytes incubated at 5% O_2. Similar results were found for hippocampal neurons. At room air and 5% O_2 in the incubator gas phase, neurons (100–200,000cells mL^{-1}) experienced pO_2s of 35 and 2–3 mm Hg, respectively. This finding demonstrates that direct measurement of liquid phase pO_2 becomes more critical as experiments are done at lower gas phase pO_2s.

Reference measurements performed with patches under the same conditions but without any cells showed 134 (room air+5% CO_2 in the gas phase) and 31 mm Hg (5% O_2) for parallel patches in cell-free dishes. The values from cell-free patches are in agreement with the finding that the pO_2 at the bottom of a 24 well polystyrene plate (with 1 mL medium) was 91–98% of the gas phase pO_2 (Metzen et al.[3]) and consistent with cell metabolism causing the lower observed liquid phase pO_2.

To confirm that the difference in liquid phase pO_2 was due to cellular O_2 consumption and not to cell coating of the patch limiting O_2 diffusion, mitochondrial oxidative phosphorylation was blocked with the metabolic poison antimycin A. Figure 2C shows a representative experiment, where pO_2 was measured for 125,000 mL^{-1} astrocytes in 37 mm Hg gas phase pO_2 (5% O_2). Upon the addition of 5 μM antimycin, pO_2 rose from 9 to 30 mm Hg over a period of 2 h. Antimycin A inhibition of metabolism is expected to be rapid. Data from PC12 cells loaded with a fluorescent O_2 reporter show changes within 10 min of antimycin addition.[10] The slow rate of rise of the pO_2 in Figure 2C is due to the rate of oxygen diffusion into the p35 dish, consistent with Allen et al.[11]

Table 1. Liquid Phase pO_2 (Measured in mm Hg) for Patches with 0, 50,000, and 125,000 astrocytes/mL

Chamber pO_2	Cell Free	50,000	125,000
20% O_2 148 mm Hg	134 ± 14	128 ± 3	100 ± 6
5% O_2 37 mm Hg	31 ± 1	20 ± 3	8 ± 2
5% O_2 Plus 5 μM Antimycin A	30 ± 1	30 ± 1	29 ± 1

Measurements were made at gas phase pO_2 values of 148 and 37 mm Hg and in the absence and presence of the metabolic inhibitor antimycin A. Results are the means +/− SEM for 3–5 experiments. Two-way ANOVA showed a significant effect of cell density, chamber pO_2 and antimycin treatment on liquid phase pO_2.

Table 1 shows comparable results in three further experiments. For astrocytes at 25,000 or 125,000 cells mL^{-1}, initial pO_2 values were lower than those recorded for the cell free patch, and the effect of cell density was more profound at lower gas phase pO_2s. Addition of antimycin A had no effect on the cell-free patch but raised pO_2 levels for the cell-containing patches to cell-free levels. This is consistent with cellular metabolism affecting pericellular pO_2, as has been reported for cell lines.

Discussion

The present results demonstrate the continuous noninvasive monitoring of pericellular pO_2 for adherent cells. The extracellular pO_2 is shown to be dependent not just on gas phase pO_2 but also on cell density and cell metabolism.

In many experiments, the goal of tissue culture is to recreate as closely as possible the in vivo conditions in an accessible in vitro model. Given that in vivo measurements of brain pO_2 are between 10 and 40 mm Hg, depending on brain region, the present results clearly show that neurons and astrocytes under the tissue culture conditions most commonly used (room air, 5% CO_2) are significantly hyperoxic. Studies of neuron and astrocyte death after oxygen-glucose deprivation (to model ischemia) have shown that oxidative injury and cell death are greater at 20% O_2, when compared with 5% O_2, demonstrating that the hyperoxia of culturing the cells at 20% O_2 has a measurable effect on cell function.[12,13] Furthermore, the finding that the pericellular pO_2 was sensitive to cell density (Table 1, Figure 2A) makes it clear that calculating a theoretical liquid phase pO_2 and setting the gas phase pO_2 to achieve that is not a sufficient answer to the problem of hyperoxia and may lead to cells being grown under hypoxic conditions. Finally, the fact that cells proliferate and density may change during an experiment supports a need for continuous monitoring and control of pericellular pO_2 over time.

The lag between a change in gas phase pO_2 and pericellular pO_2 in Figure 2B and the slow re-equilibration of the pericellular pO_2 after antimycin A treatment (Figure 2C), together with other studies,[14] are consistent with the diffusion resistance of the stagnant media layer being so high that hours are required for equilibration of the media with the headspace gas. This may not be a problem for simple culturing of cells at a target pO_2 where feedback between the pO_2 signal from the patch and control of the gas phase pO_2 (as could be achieved in a Biospherix-type chamber) would be sufficient, even with cell proliferation. However, it is a constraint if the experiment requires more rapid changes in pO_2, perhaps to model the changes that occur during a hypoxic episode, in vivo. Here, any strategy of rapid control of pO_2 would require some form of convective enhancement of the oxygen diffusion.[14] Even for cell culture at a single pO_2, the diffusion lag makes it clear that media changes must always be done with media pre-equilibrated to the target pO_2 to avoid giving the cells a hyper- or hypoxic shock.

Oxygen concentration affects the production of oxygen radicals, which are important in cell signaling and cell damage. Oxygen concentration is also one of the major factors regulating cell metabolism and protein expression. Furthermore, low oxygen concentration interferes with hydroxylation and further polyubiquitination of hypoxia-inducible factor 1-α (HIF 1-α), which prevents its rapid degradation. The up-regulated HIF 1-α then binds to specific regulatory sequences, known as hypoxia responsive elements, in the promoter regions of a number of genes.[15] Examples are, among others, genes encoding erythropoietin, vascular endothelial growth factor, and some glycolytic enzymes, e.g., phosphoglycerate kinase.

The response to pO_2 varies by cell type. For example, epithelial cells typically have more pronounced up-regulation of HIF-1α than mesenchymal cells.[16] Oligodendrocyte precursor cells prematurely differentiate when exposed to hypoxia.[17] For some cells, hypoxynemia at pO_2 of 35 mm Hg and below may lead to lactate-induced acidosis.[18] Lower pO_2 may inhibit the growth, differentiation, and bone-forming capacity of rat osteoblasts, while acting as a powerful stimulator of osteoclast formation.[19] Lower pO_2 also influences the proliferation of human mesenchymal stem cells, resulting in ~30-fold higher cell expansion over 6 weeks without loss of multi-lineage differentiation capabilities.[20] And stem cells in general are routinely grown in 5–6% O_2 because culturing at 20% results in poorer proliferation.[21,22]

Previous data and the present report show that changes in the media layer thickness, number of cultured cells or environmental gas composition can lead to pO_2 levels in the medium around the cells that may be quite different from the intended culturing conditions. Because a wide range of cellular responses are sensitive to pO_2, experiments will need to monitor and possibly control pericellular pO_2. This study provides a model of direct, continuous measurement of O_2 concentration in close proximity to the cells to provide exact information on this critical experimental condition.

Acknowledgment

This paper is dedicated to Professor Michael Shuler in grateful appreciation for his unstinting generosity and support to anybody that needed it. Funding was provided by Sartorius-Stedim Biotechnology.

Literature Cited

1. Boveris DL, Boveris A. Oxygen delivery to the tissues and mitochondrial respiration. *Front Biosci*. 2007;12:1014–1023.
2. Erecińska M, Silver IA. Tissue oxygen tension and brain sensitivity to hypoxia. *Respir Physiol*. 2001;128:263–276.
3. Metzen E, Wolff M, Fandrey J, Jelkmann W. Pericellular pO_2 and O_2 consumption in monolayer cell cultures. *Respir Physiol*. 1995;100:101–106.
4. Pettersen EO, Larsen LH, Ramsing NB, Ebbesen P. Pericellular oxygen depletion during ordinary tissue culturing, measured with oxygen microsensors. *Cell Proliferation*. 2005;38:257–267.
5. Swartz HM. On tissue oxygen and hypoxia. *Anitox Redox Signal*. 2007;9:1111–1113.
6. Randers-Eichhorn L, Bartlett RA, Frey DD, Rao G. Noninvasive oxygen measurements and mass transfer considerations in tissue culture flasks. *Biotechnol Bioeng*. 1996;51:466–478.
7. Ge X, Hanson M, Shen H, Kostov Y, Brorson KA, Frey DD, Moreira AR, Rao G. Validation of an optical sensor-based high-throughput bioreactor system for mammalian cell culture. *J Biotechnol*. 2006;122:293–306.
8. Bambrick LL, Fiskum G. Mitochondrial dysfunction in mouse trisomy 16 brain. *Brain Res*. 2008;1188:9–16.
9. Bambrick LL, Golovina VA, Blaustein MP, Yarowsky PJ, Krueger BK. Abnormal calcium homeostasis in astrocytes from the trisomy 16 mouse. *Glia*. 1997;4:352–358.
10. O'Riordan TC, Zhdanov AV, Ponomarev GV, Papkovsky DB. Analysis of intracellular oxygen and metabolic responses of mammalian cells by time-resolved fluorometry. *Anal Chem*. 2007;79:9414–9419.
11. Allen CB, Schneider BK, White CW. Limitations to oxygen diffusion and equilibration in in vitro cell exposure systems in hyperoxia and hypoxia. *Am J Physiol Lung Cell Mol Physiol*. 2001;281:L1021–L1027.
12. Danilov CA, Fiskum G. Hyperoxia promotes astrocyte cell death after oxygen and glucose deprivation. *Glia*. 2008;56:801–808.
13. Fiskum G, Danilov CA, Mehrabian Z, Bambrick LL, Kristian T, McKenna MC, Hopkins I, Richards EM, Rosenthal RE. Post-ischemic oxidative stress promotes mitochondrial metabolic failure in neurons and astrocytes. *Ann NY Acad Sci*. 2008;1147:129–138.
14. Baumgardner JE, Otto CM. In vitro intermittent hypoxia: challenges for creating hypoxia in cell culture. *Respir Physiol Neurobiol*. 2003;136:131–139.
15. Brown JM. Exploiting the hypoxic cancer cell: mechanisms and therapeutic strategies. *Mol Med Today*. 2000;6:157–162.

16. Chi J-T, Wang Z, Nuyten DSA, Rodriguez EH, Schaner ME, Salim A, Wang Y, Kristensen GB, Helland A, Borresen-Dale A.-L., Giaccias A. Longaker MT, Hastie T, Yang GP, van de Vijver, MJ, Brown PO. Gene expression programs in response to hypoxia: cell type specificity and prognostic significance in human cancers. *PLoS Med*. 2006;3:e47. doi:10.1371/journal.pmed. 0030047.
17. Akundi RS, Rivkees SA. hypoxia alters cell cycle regulatory protein expression and induces premature maturation of oligodendrocyte precursor cells. *PLoS ONE*. 2009;4:e4739. doi:10.1371/journal.pone.0004739.
18. Sher PK. The effects of acidosis on chronically hypoxic neurons in culture. *Exp Neurol*. 1990;107:256–262.
19. Utting JC, Robins SP, Brandao-Burch A, Orriss IR, Behar J, Arnett TR. Hypoxia inhibits the growth, differentiation and bone-forming capacity of rat osteoblasts. *Exp Cell Res*. 2006; 312:1693–1702.
20. Grayson WL, Zhao F, Bunnell B, Ma T. Hypoxia enhances proliferation and tissue formation of human mesenchymal stem cells. *Biochem Biophys Res Commun*. 2007;358:948–953.
21. Csete M. Oxygen in the cultivation of stem cells. *Ann NY Acad Sci*. 2005;1049:1–8.
22. Peura TT, Bosma A, Stojanov T. Derivation of human embryonic stem cell lines. *Theriogenology*. 2007;67:32–42.

Manuscript received Nov. 4, 2010, and revision received Dec. 21, 2010.

When several of these papers had been published and at conference presentations, a question that repeatedly arose was “how do they compare with traditional sensors?” To answer this question, we ran the traditional sensors in a head-to-head comparison in the same bioreactor. Mike Hanson was a Ph.D. student who started validating the newly emerging sensor technology and its application to minibioreactors (shown later). Tony Moreira is a colleague who first introduced me to the world of regulatory sciences, with all its complications. It became clear the sensors could play a key role in getting a better handle on bioprocesses and a fertile collaboration with Kurt Brorson at FDA ensued. The following paper describes the results and they conclusively showed that the optical sensors gave results that were identical to the conventional sensors.

ARTICLE

BIOTECHNOLOGY and BIOENGINEERING

Comparisons of Optical pH and Dissolved Oxygen Sensors With Traditional Electrochemical Probes During Mammalian Cell Culture

Michael A. Hanson,[1,2] Xudong Ge,[1] Yordan Kostov,[1] Kurt A. Brorson,[2] Antonio R. Moreira,[1] Govind Rao[1]

[1]Center for Advanced Sensor Technology, Department of Chemical and Biochemical Engineering, University of Maryland Baltimore County, 1000 Hilltop Circle, Baltimore, Maryland 21250; telephone: 410-455-3415; fax: 410-455-6500; e-mail: grao@umbc.edu

[2]Office of Biotechnology Products, Center for Drug Evaluation and Research, Food and Drug Administration, Rockville Pike, Bethesda, Maryland

Received 17 October 2006; accepted 27 December 2006

Published online 10 January 2007 in Wiley InterScience (www.interscience.wiley.com). DOI 10.1002/bit.21320

ABSTRACT: Small-scale upstream bioprocess development often occurs in flasks and multi-well plates. These culturing platforms are often not equipped to accurately monitor and control critical process parameters; thus they may not yield conditions representative of manufacturing. In response, we and others have developed optical sensors that enable small-scale process monitoring. Here we have compared two parameters critical to control in industrial cell culture, pH and dissolved oxygen (DO), measured with our optical sensors versus industrially accepted electrochemical probes. For both optical sensors, agreement with the corresponding electrochemical probe was excellent. The Pearson Correlations between the optical sensors and electrochemical probes were 98.7% and 99.7%, for DO and pH, respectively. Also, we have compared optical pH sensor performance in regular (320 mOsm/kg) and high-osmolality (450 mOsm/kg) cell culture media to simulate the increase in osmolality in pH-controlled cultures. Over a pH range of 6.38–7.98 the average difference in pH readings in the two media was 0.04 pH units. In summary, we have demonstrated that these optical sensors agree well with standard electrochemical probes. The accuracy of the optical probes demonstrates their ability to detect potential parameter drift that could have significant impact on growth, production kinetics, and protein product quality. We have also shown that an increase in osmolality that could result from controlling pH or operating the reactor in fed-batch mode has an insignificant impact on the functionality of the pH patches. Biotechnol. Bioeng. 2007;97: 833–841.

KEYWORDS: optical sensor; electrochemical probe; mammalian cell culture; process monitoring; scale-up

Introduction

Bioprocess cell culture development requires many experiments to select and genetically engineer production organisms and to optimize media and growth conditions. This may lead to high material costs and long development timelines. An obvious solution to expedite development is to carry out multiple experiments simultaneously. This is easily accomplished at small scale in disposable multi-well plates and tissue-culture flasks. Unfortunately, three major (and related) setbacks are repeatedly associated with these small-scale culturing platforms. First, it has proven difficult to equip them with the capabilities to monitor environmental conditions which are critical to cell growth and product formation, such as DO concentration (Chotigeat et al., 1994; Kunkel et al., 1998; Ozturk and Palsson, 1990) and pH (Borys et al., 1993; Hayter et al., 1992; Muthing et al., 2003; Ozturk and Palsson, 1991). Second, without the ability to monitor these important parameters, accurately controlling them is impossible. If pH and DO concentration are left to vary freely, the value of cell culture models is suspect given no relationship can be established between the other critical development variables and product quality attributes. Finally, a major goal in bioprocess development is to design a process that scales up appropriately. However, scale-up is impossible if even minimal information like pH or DO is unavailable from the small-scale culture. Problems with scale-up and mass production have been identified by the FDA as a critical defect that historically led to slow development and escalated costs (FDA, 2004a).

Correspondence to: G. Rao

Ideally, during process development, hundreds of experiments would be carried out simultaneously to matrix all potential variables in order to achieve an optimized manufacturing process. Statistical design of experiments (DOE) can be used to lessen the number of experiments needed to identify key parameters, their optimal values, and process parameter interactions (Li et al., 2006). But with the above limitations of the small-scale culture platforms, process developers are forced to use mid-scale culturing platforms, such as liter-scale bioreactors, equipped with traditional electrochemical probes for pH and DO concentration. In this case, labor cost and time commitments increase with scale, limiting the number of experiments that can be carried out concurrently. The ultimate effect is further lengthening the development timeline.

The development of fluorescence-based sensing technologies has aided in remedying this fundamental flaw in the process development paradigm. The promise of fluorescence sensing in bioprocessing was first demonstrated by Junker et al. (1988) where during yeast fermentation pH and DO were measured online using fiber optics and analyte-sensitive fluorophores that were dissolved in the medium. Over the last decade, we have built on this theme and developed an arsenal of optical sensors capable of being deployed at any scale. However, the fluorophores used in these sensors are immobilized in a patch that gets affixed to the inside of the reactor vessel. Of these, the DO and pH sensors have been used extensively for monitoring cells in culture. The DO sensor utilizes a fluorescent dye whose emission is quenched by oxygen at a rate dependent upon oxygen concentration. An early version of this sensor was first used during *E. coli* fermentation by submerging the patch and the necessary fiber-optic excitation and detection instrumentation into a 2 L spinner flask along with an electrochemical DO probe (Bambot et al., 1994). Using submerged fiber optics to bring the patch and instrumentation to sufficient proximity was only an optical sensing proof-of-concept as it does not fulfill the goal of sensor miniaturization. By affixing the <1 mm thick patches on the inside of clear culturing containers and placing the optical instrumentation immediately outside, the sensor becomes essentially noninvasive. The latter configuration has been used to measure DO tension in *E. coli* and yeast shake-flask fermentations (Tolosa et al., 2002) and to analyze the impact of shake-flask enclosure on the oxygen mass transfer coefficient, k_La (Gupta and Rao, 2003). The pH sensor uses a fluorescent dye whose absorbance spectrum changes with respect to pH. Initial usage during shake-flask *E. coli* fermentation consisted of circulating culture broth from the flask through a sensor-equipped cuvette in a fluorometer and then back into the flask for continuous online monitoring (Kermis et al., 2003).

The optical DO and pH sensors were first used in tandem in an *E. coli* fermentation carried out in a 1 mL cuvette microbioreactor (Kostov et al., 2001). The cell densities and profiles of pH and DO were compared to those obtained in a 1 L bioreactor equipped with electrochemical probes and it was found that matching k_La in the two vessels was sufficient for scale-up. Next the sensors were implemented in several high throughput bioreactor systems. First, DO and pH were monitored in 1 and 6 mL *E. coli* cultures carried out in a 24-well plate and a discrete 24-station high throughput reactor system, respectively (Harms et al., 2006). Next the sensors were used to monitor 30 mL mouse hybridoma cultures in a 12-station high throughput reactor system (Ge et al., 2006).

Scale up is a complex task consisting of several stages and implementation of new technology between stages. Consistency in analytical instruments at the different scales is key to assure seamless transitions between the different stages and that process performance is consistent between different scales. Process and product consistency through monitoring of critical process parameters is at the core of the process analytical technology (PAT) initiative (FDA, 2004b). Implementation of PAT as early as the development phase could contribute heavily to understanding the impact of process parameters. An example of undesirable results that can happen if inconsistency occurs during technology transfer happened at a cGMP pilot plant. In this case, a poorly executed transfer from a development lab to the pilot plant resulted in, a seemingly minor 0.2 pH unit discrepancy between the two cell culture systems; this discrepancy led to a 30% reduction in volumetric productivity (Bhatia et al., 2006). To test consistency between our small scale optical DO and pH sensors and widely accepted traditional electrochemical probes for larger vessels, we evaluated the performance of both using a murine hybridoma culture grown for over 100 h in a 5 L bioreactor. Also, the performance of the optical pH sensors was evaluated in media of normal (320 mOsm/kg) and high osmolality (450 mOsm/kg) to simulate pH-controlled and fed-batch environments where osmolality increases substantially with time.

Materials and Methods

Cell Line and Culture Media

A SP2/0 based myeloma/mouse hybridoma cell line (2055.5) secreting an IgG_3 monoclonal antibody (MAb) specific for the *Neisseria meningitides* capsular-polysaccharide (MCPS) (Rubinstein and Stein, 1988) was selected as our model cell culture process. The cells were maintained in a 250 mL spinner flask (Kontes, Vineland, NJ) in CD Hybridoma protein-free media (Gibco Brand, Carlsbad, CA) supplemented with 2 mM glutamine (HyClone, Laboratories Inc., Logan, UT), 100 U/mL penicillin (HyClone), 100 g/mL streptomycin (HyClone), 1 g/L PF-68 (MP Biomedicals, LLC, Aurora, OH), and 3.5×10^{-4}% β-mercaptoethanol (v/v) (Sigma, St. Louis, MO). During cell culture maintenance the flask was kept in a water-jacketed incubator (Napco, Winchester, VA) at 37°C and 50% relative humidity with a headspace CO_2 composition of

DOI 10.1002/bit

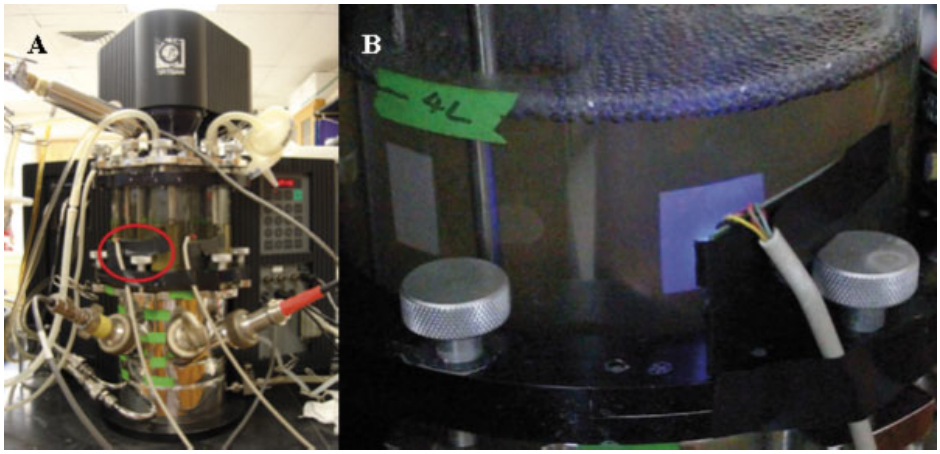

Figure 1. Pictures of the bioreactor retrofitted with optical sensors for DO and pH. **A**: Entire system with external optical sensor instrumentation circled in red. **B**: Up-close picture of a pH sensor patch being illuminated during a measurement. [Color figure can be seen in the online version of this article, available at www.interscience.wiley.com.]

5% in air. During bioreactor operation, the media were slightly modified by replacing 75% of the CD Hybridoma media with RPMI 1640 (Mediatech Inc., Herndon, VA), and adding fetal bovine serum (5% of the total media volume).

Bioreactor Set-Up and Operation

The sensor comparison experiment was carried out in the 5 L bioreactor system (Artisan, Waltham, MA) shown in Figure 1A. Two sets of optical sensor patches for both DO (Lumet, Bethesda, MD) and pH (Fluorometrix, Stow, MA) were attached to the inside of the reactor vessel. The first set was for calibration. Since calibration requires near-continuous excitation of the sensing fluorophores, the possibility of photobleaching exists. Therefore, the second set was used for monitoring during culture. The gel-electrolyte filled electrochemical pH probe (Mettler-Toledo, Columbus, OH) was calibrated using pH 4 and 7 buffers (Fisher Scientific, Pittsburgh, PA) as references. This pH probe and the Clark-type DO probe (Mettler-Toledo) were inserted into the reactor vessel which was then sterilized with an attached bottle of 2 M NaOH by autoclaving for 30 min at 121°C. Following sterilization, the electrochemical DO probe was calibrated at 0 and 100% air saturation by sparging with nitrogen and air. The LEDs and detectors (both described below) for fluorophore illumination and quantification, respectively, were positioned adjacent to the patches, but outside the vessel (red circle, Fig. 1A). Shown in Figure 1B is an up-close view of an exterior LED emitting blue light to excite the fluorophore in a sensor patch during data acquisition. The optical sensors were calibrated as described below using the already calibrated electrochemical probes as references. After optical sensor calibration, the PBS buffer and cell culture media were aseptically pumped out and in of the reactor, respectively, by flowing through 0.22 μm in-line filters (Millipore, Billerica, MA). Cells in mid-exponential growth phase were inoculated into the reactor to a final concentration of approximately 1.5×10^5 cells/mL. Optical sensor measurements were taken every 15 min. The temperature and agitation speed were controlled at 37°C and 75 rpm, respectively, for the duration of the experiment. At no point was pH controlled. From inoculation until approximately 88 h into the experiment, the culture was aerated through the vessel headspace by a 5% CO_2 in air–gas mixture, but DO was not controlled. At 88 h aeration was switched to sparging and a set-point of 30% air saturation was assigned. The set-point was dropped to 15% air saturation 6 h later. Samples were drawn from the reactor approximately every 8 h for cell counting and antibody quantification.

Monitoring Cell Growth and MAb Production

Cell viability was determined by counting trypan blue (Sigma) excluding cells utilizing a microscope and a hemacytometer (Hausser, Horsham, PA). MAb-containing supernatant was clarified prior to analysis for −20°C storage by centrifugation at 500*g* for 10 min at 4°C. MAb concentration was quantified by a mouse IgG3 specific ELISA. Briefly, anti-κ chain capture antibody (Southern Biotech, Birmingham, AL) was first immobilized in 96-well plates (Thermo, Waltham, MA). After several washes and plate blocking with fish gelatin (Sigma), the supernatant was serially diluted into the wells, where the capture antibody selectively binds the IgG_3. After further washes, an anti-IgG_3 alkaline phosphatase conjugated antibody (Southern Biotech) was added to the plate were it in turn bound the captured IgG_3. After a final wash, the plate-associated

enzyme was then allowed to cleave a substrate, 4-methylumbelliferyl phosphate (Sigma), producing a measurable fluorescent molecule. Sample IgG_3 concentrations were determined by comparing their fluorescence curves to that from serially diluted IgG3 standards of known concentrations (Becton, Dickinson and Co., Palo Alto, CA) by conducting parallel line analyses.

Optical Sensor Calibration

The oxygen sensor patches used in this study were provided by Lumet LLC (Bethesda, MD). Detailed descriptions of the oxygen-sensitive fluorophore, patch construction and the associated opto-electronic instrumentation have been documented previously (Harms et al., 1999; Kostov et al., 2000a,b; Tolosa et al., 2002). The pH sensor patches used in this study were developed by the authors' laboratory (Kermis et al., 2002, 2003).

Normally, the optical sensors are available as pre-calibrated patches. However, for this study we wanted to do a vigorous comparison versus electrochemical probes. DO patch calibration was done in PBS by sequentially measuring the phase shift at 0, 20, 40, 60, 80, and 100% air saturation (as measured by the already-calibrated DO electrode). Air and nitrogen were sparged into the vessel to obtain the desired concentrations. The pH sensors were calibrated by sequentially measuring the fluorophore emission ratio at pH 6.5, 6.8, 7.15, and 7.5 (as measured by the already-calibrated pH electrode). These values were achieved by sparging CO_2 and pumping 2 M NaOH into the reactor. The temperature was maintained at 37°C during both calibrations. The mathematically modified phase shift and fluorophore emission ratio were fit to second degree polynomial functions with r^2 values of 0.7371 and 0.9995, in order for optical sensing software to calculate dissolved oxygen concentration and pH, respectively.

Accelerated Stability Studies of Sensor Patches

The stability of the DO patches was tested in pH 7.2, 0.15 M PBS at 37°C for 15 h. During the test, the DO concentration was maintained at 10% by bubbling a gaseous mixture of air and nitrogen through the buffer. The gas mixture composition was obtained by mixing air and nitrogen whose flow rates were adjusted by flow meters. The stability of the pH patches was tested in pH 7.8, 0.15 M PBS at 37°C for 60 h. Five patches were used for each kind of patches. The DO concentrations and the pH values were read every 3 min.

Effect of Osmolality of pH Sensor Performance

All solution osmolalities were determined using a vapor pressure osmometer (Wescor, Logan, UT). In the first experiment either 0.5 M NaCl or cell culture media (described above) was titrated into reactor vessels with starting volumes of 20 mL cell culture media. pH was measured in both reactor vessels using the patches described above. Next, high-osmolality media (450 mOsm/kg) was made by adding 0.54 mL of 2 M NaCl to 20 mL of media (320 mOsm/kg) described above. The pH of both media and high-osmolality media was step-changed from 6.38 to 7.98 by sequential 0.5 mL additions of 0.1 M NaOH.

Results and Discussion

Electrochemical probes are the standard means for in process monitoring of DO and pH during fermentation and cell culture. Unfortunately their size prevents their use in very small-scale culture applications. To address this limitation in process monitoring, small optical sensors have been developed by us and others (Ge et al., 2003; Weidgans et al., 2004) and are available commercially by such companies as Fluorometrix (www.fluorometrix.com) and Ocean Optics (www.oceanoptics.com). In the work presented here, we test optical sensor performance by comparing with industry-accepted electrochemical probes.

For our sensor comparison, we used a model mammalian culture of murine hybridoma cells expressing an anti-MCPS IgG_3 MAb. The viable cell density and MAb profile for the duration of the experiment are shown in Figure 2. At 88 h of culture, aeration by sparging commenced to provide O_2 to the cells, but an abrupt drop in viable cell density occurred. This drop can be attributed to cell damage caused by severe energy dissipation during bubble breakage (Chisti, 2000). Otherwise, cell growth and rate of product formation proceeded as expected, providing a typical situation for the sensor comparisons.

The DO profiles from the optical sensor and electrochemical probe are shown in Figure 3. The oxygen concentration dropped at an increasing rate for the first 38 h (necessitating the eventual sparging). During this time, the optical sensor slightly overestimated the DO. From 34–88 h the cells consumed all available oxygen in the reactor. To perturb and provide O_2 to the system, at 88 h the aeration method was switched to sparging and control of DO was initiated at a set-point of 30% air saturation. Both sensors responded to the change in DO. The optical sensor again overestimated the DO, initially by 9.7% but then drifting back to within 5% DO of the electrochemical probe. At 96 h the set-pointed was shifted to 15% DO. At this lower DO concentration, agreement between the two sensors improved. After several hours at 15%, oxygen delivery rate surpassed consumption and the DO concentration increased until the end. In retrospect it may have perturbed the system less with an earlier but lower rate of sparge; additional steady state DO concentrations could have been compared.

The calibration data (not shown) for the DO sensor indicate that the sensing properties of the oxygen sensitive fluorophore change as a function of DO concentration. With this in mind, a sensitivity plot was constructed that

DOI 10.1002/bit

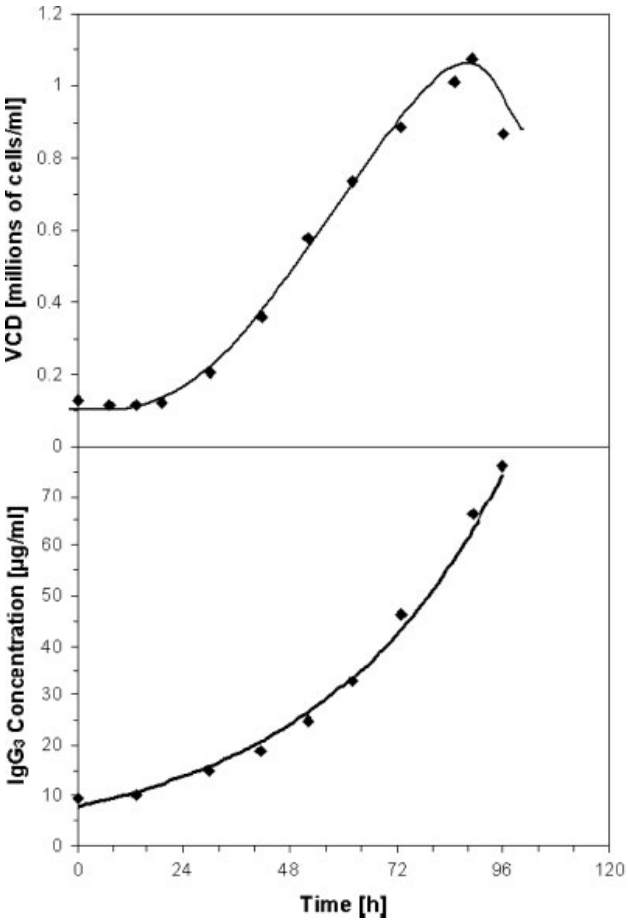

Figure 2. Viable cell density (VCD) and IgG_3 titer throughout the experiment.

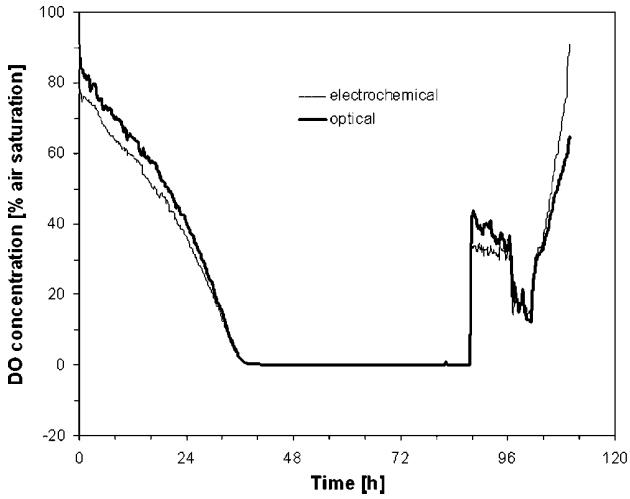

Figure 3. Dissolved oxygen (DO) profiles. (▬) optical and (—) electrochemical. Method of aeration was changed at 88 h from headspace to sparging in order to achieve a DO set-point of 30% DO. Set-point was changed to 15% DO at 96 h.

shows how well the optical sensor and electrochemical probe agreed at different DO concentrations (Fig. 4). Overall, there was a 98.7% Pearson Correlation between the two DO probes. The general trend is that as DO increases, the agreement between the two probes decreases. This is expected to be the case as the calibration showed that the sensor is less sensitive at higher DO concentrations. When the data are examined temporally, the trend appears to hold less true for data after 88 h. Early on in the experiment, the difference between the two probes was just under 5% at 30% DO. However, at the same DO level late in the experiment, the difference varied from 1 to 10%. One possible cause for this change in sensor performance late in the experiment could be photo-bleaching of the oxygen sensitive fluorophore.

While it is always desirable to maximize precision and accuracy in sensors such as those that measure DO, the degree of needed accuracy and precision hinges on the real impact of cell culture DO concentrations on cell growth and product quality characteristics. As a practical example, hybridoma cells can be grown in DO concentrations ranging from 5 to 80% DO without impacting growth and IgG specific productivity. However, DO concentration at more extreme set points does have an impact. In one study, DO varied between 0 and 1% and the growth rate and metabolic rate of key nutrients in hybridoma cells was dramatically affected (Ozturk and Palsson, 1990, 1991). Also, as DO concentration increased from 10 to 50 to 100% in another hybridoma cell line, galactosylation of the produced IgG_1 changed dramatically (Kunkel et al., 1998). Modifications in sialylation also occurred on recombinant human follicle

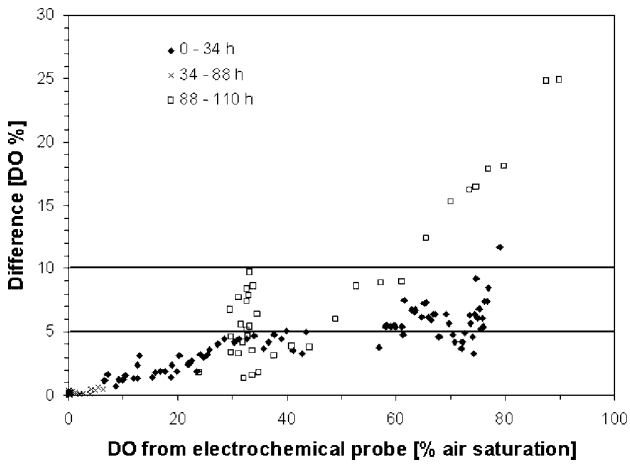

Figure 4. Dissolved oxygen (DO) sensitivity plot. Absolute difference between data obtained using optical and electrochemical probe versus DO concentration.

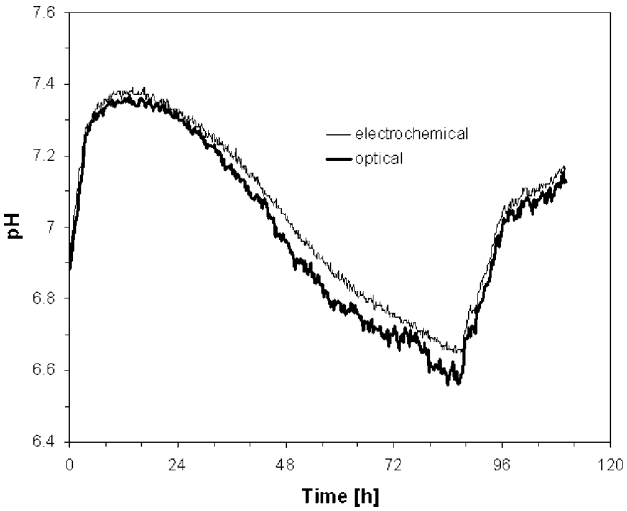

Figure 5. pH profiles. (——) optical and (—) electrochemical.

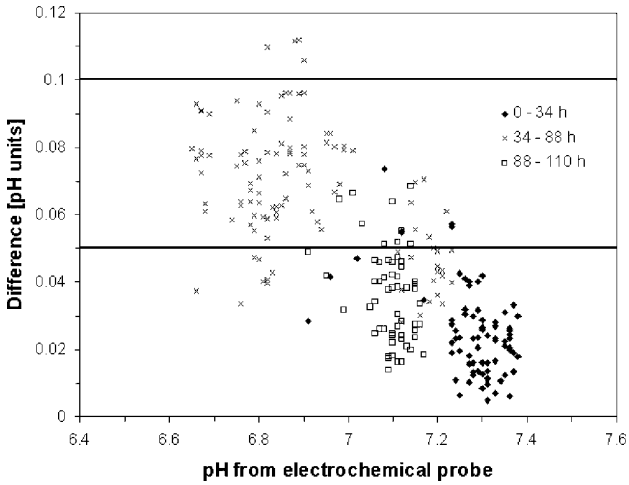

Figure 6. pH sensitivity plot. Absolute difference between data obtained using optical and electrochemical probe versus pH concentration.

stimulating hormone produced in Chinese hamster ovary (CHO) cells as DO concentration increased from 10 to 90% DO (Chotigeat et al., 1994). Conversely, fucosylation and specific productivity of CHO-produced recombinant human erythropoietin only varied under hypoxic (3%) and hyperoxic (200%) conditions (Restelli et al., 2006). Taken together, these examples suggest, first, that a DO sensor must be sensitive and accurate at low DO concentrations (<5% DO). Also for product quality considerations, the sensor must be functional in the range of 0–100% DO. It is unclear how sensitive the sensor must be at mid- to high-DO concentrations as the studies above employed relatively large changes in DO concentration of 20–30% DO. In the work presented here, 97% of the data showed less than a 10% difference in DO concentration between the two probes. The remaining 3% of the data with a difference greater than 10% DO occurred in the last 2 h of the experiment. These late deviations support the hypothesis of patch fluorophore photo-bleaching, but inaccuracy introduced by the calibration function cannot be ruled out. A new DO sensing fluorophore is currently being developed in-house with improved stability over time. And a more accurate calibration can be achieved by incorporating more data points, especially in the more sensitive lower-DO regime.

The pH profiles from the two probes are shown in Figure 5. The pH in the reactor rose from an initial value of 6.9 to its peak of 7.4 over the first 15 h which coincided with the lag phase of cell growth. Once the cells started growing exponentially the pH started dropping and continued to do so until 88 h into the experiment when the method of aeration was switched to sparging. At that point, based on the rate of increase in pH, it appears that the sparging of 5% CO_2 in air resulted in stripping of the cell culture medium of gaseous acidic species, most likely CO_2. At 96 h, as the DO set-point was switched to 15% air saturation, less gas was being sparged and the pH increased at a slower rate.

For the duration of the experiment, the optical sensor underestimated the pH in the reactor. The agreement between the two pH probes as a function of time and pH is shown in Figure 6. Overall, there was a 99.7% Pearson Correlation between the two pH probes. As pH increases so does the agreement between the two probes. As described earlier the pH responsive fluorophore exists in two forms based on its protonation (Kermis et al., 2002). The pKa of the fluorophore is 7.4, thus the sensor is most sensitive around pH 7.4. The agreement between the two pH sensors does not appear to be time dependent; that is, data taken after 88 h agree with the electrochemical probe data as well or better than earlier data. This supports the precision, accuracy and robustness of the pH patch and sensor instrumentation.

Mammalian cells are extremely sensitive to changes in extracellular pH with tight optima. Also, optimal pHs for specific growth rate and specific protein production are not necessarily the same. For instance, it has been documented that hybridoma cells grow optimally at pH 7.2 but produce the most MAb per cell around pH 6.9 (Hayter et al., 1992; Muthing et al., 2003; Ozturk and Palsson, 1991). Of the literature cited here, the smallest change in pH tested was a very modest 0.15 pH units (Ozturk and Palsson, 1991). Shifts of 0.15 units from the optimal growth and production pHs resulted in reductions in specific growth and production rates of 13 and 16%, respectively. Larger changes in pH during culture of hybridoma and other cell lines has resulted in more severe reductions in growth and protein production (Hayter et al., 1992; Jardon and Garnier, 2003), impacted protein glycosylation (Borys et al., 1993;

DOI 10.1002/bit

Muthing et al., 2003), and endogenous virus-like particle production (Brorson et al., 2002). As demonstrated in the pH sensitivity plot (Fig. 6), optical sensors were accurate (with respect to accepted electrochemical probes) within 0.05 pH units 60% of the time and within 0.1 pH units 99% of the time. These data, taken in view of literature citing the impact of changing pH, suggest that these optical sensors are sensitive enough to prohibit substantial decreases in growth and productivity as a result of inaccurate pH monitoring.

The 4-day culture carried out is typical of batch cultures. The aim of the study was to demonstrate that optical sensors monitor comparably to electrochemical probes in that setting. In other bioreactor configurations, such as fed-batch or perfusion, culture longevity may last from weeks to several months. In terms of stability, the major concern with the sensor patches is photobleaching of the patch-encapsulated fluorophore. The rate at which the fluorophore bleaches is proportional to its exposure to excitation light. For our experiment, the optical sensor measurements were taken every 15 min. To test the long-term stability of the sensor patches, accelerated stability tests were carried out where the fluorophores were excited at an increased rate, every 3 min. Figure 7A shows the stability results for the DO patches. After several initial set-point changes, DO was set at approximately 10%. The noise associated with the readings in all five bioreactors decreased over time. There was also a gradual downward drift of 2–3% DO over the duration of the study. How often the fluorophores are excited during culture depend how quickly one would expect the pH and DO concentration to change. For example, these parameters tend to change more rapidly in microbial fermentation than mammalian cell culture. Where in the latter, one could optically sample every 30–60 min and still be able to enforce corrective actions to maintain pH and DO set-points. At a sampling rate of 1–2 times per hour, the stability plots in Figure 7 could be extrapolated 10–20 times longer than what is shown.

In cultures where pH is being controlled (not here), addition of corrective solutions (e.g., NaOH, CO_2, HCl) results in an increase in media osmolality. This is also the case in fed-batch cultures where concentrated feed solutions are added. MA-HPDS, the pH sensitive fluorophore, exists in protonated and unprotonated forms. The distribution of these two forms, and thus the absorption spectrum, is a function of solution pH. However, a shift in local ionic strength alters the pK_a value of the dye, thus impacting the relationship between the structure distribution and pH (Kermis et al., 2003). Several experiments were carried out to determine if and to what extent relevant changes in osmolality may impact pH sensor performance. First, cell culture media (320 mOsm/kg) in two reactor vessels was titrated with either pH adjusted 0.5 M NaCl or additional cell culture media. Plotted in Figure 8 is the difference between the pH measured in the two vessels versus the osmolality in the NaCl titrated vessel. The baseline difference in the two vessels is 0.017 ± 0.005 pH units until an osmolality of 438 mOsm/kg was reached. From that point

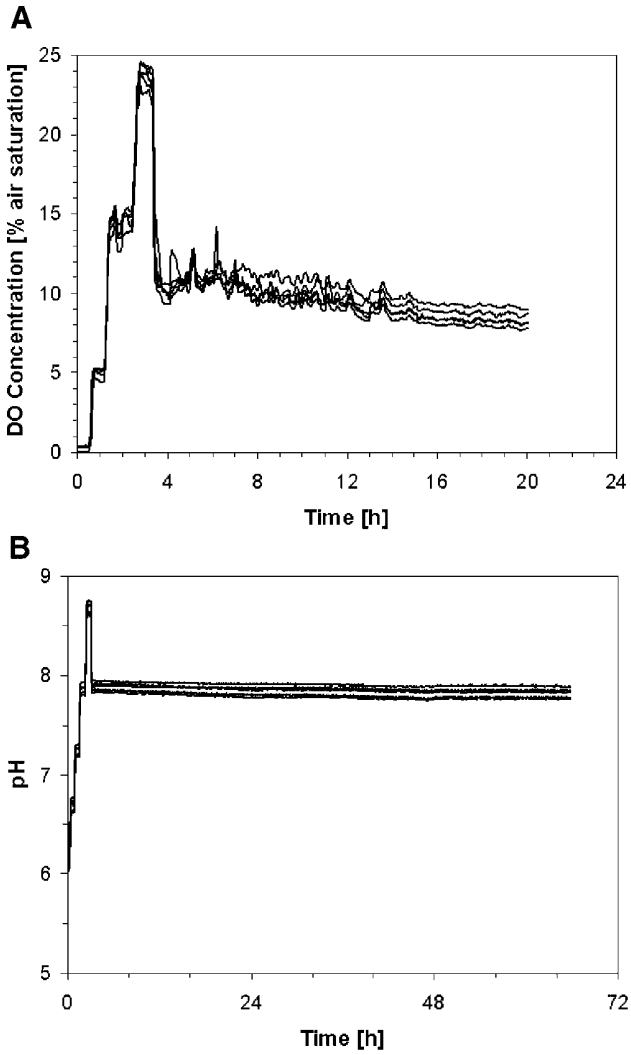

Figure 7. Accelerated stability tests of DO and pH sensor patches. In these studies, patch encapsulated fluorophores were excited every 3 min.

to 480 mOsm/kg, the difference in pH increased linearly with media osmolality. From a process point of view, it would be advantageous to keep media osmolality under 450 mOsm/kg in order to avoid pH discrepancies of 0.05 units or more. A second experiment was carried out to see if observed differences were pH dependent (Fig. 9). Here, the pH in control media (320 mOsm/kg) and high-osmolality media (450 mOsm/kg) was increased from 6.38 to 7.98 step-wise by sequential equivolume additions of 0.1 NaOH. The average difference in the two media over the tested range was 0.036 ± 0.018 pH units and there appears to be no pH dependence. The extent to which controlling pH or adding media concentrates increases osmolality is system dependent. For instance, certain cells may produce more acidic metabolites and thus might need more NaOH to

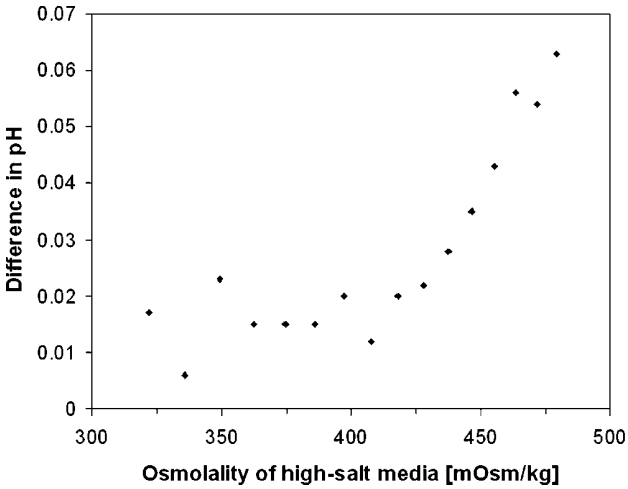

Figure 8. Difference in pH measurements in control media (320 mosm/kg) and media titrated with 0.5 M NaCl. Difference plotted versus osmolality of NaCl titrated media.

maintain a certain pH. Here, we have demonstrated the impact on pH sensor performance of solution osmolalities nearing 500 mOsm/kg, more than a 50% increase over our standard media. In what would be more commonly encountered situations of near neutral pH and moderate osmolality, pH differed by less than 0.05 pH units on average.

In summary, our optical sensors enable small-scale monitoring of critical process parameters. When pH and DO measurements obtained with optical sensors are compared to measurements from standard industrial electrochemical probes, there is a good agreement. The accuracy as compared to electrochemical probes is sufficient to prohibit any significant impact on growth, production kinetics, and protein product quality. Agreement between these two technologies is necessary to ensure consistent productivity when transferring technology from development into larger scales, as the standard probes are much more expensive and can't be used in very small scale cell culture platforms. Furthermore, these patch-type disposable sensors can be deployed in virtually any transparent/translucent reactor, thereby opening the way for their adoption in large-scale disposable reactors.

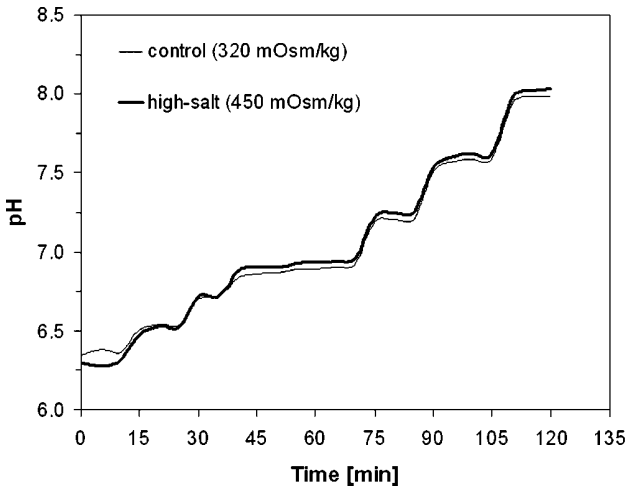

Figure 9. Impact of media osmolality on optical pH sensor performance. Step-changes in pH from 6.38 to 7.98.

The technology described in this paper has been licensed to Fluorometrix, in which some of the authors (X.G., Y.K., and G.R.) have an equity position. We thank Wendy Lea for assisting with the reactor set up and photography. Views expressed in this article are those of the authors and not necessarily those of the US FDA or the US government. Discussion of individual cell culture devices does not constitute an endorsement by the US FDA or US government. Michael Hanson is partially funded by a PDA Pre-doctoral Fellowship. We dedicate this paper to Prof. Danny Wang on the occasion of his 71th birthday.

References

Bambot SB, Holavanahali R, Lakowicz JR, Carter GM, Rao G. 1994. Phase fluorometric sterilizable optical oxygen sensor. Biotechnol Bioeng 43:1139–1145.

Bhatia R, Chiang B, Jan D, Cammaart E, Wood C, Haddock H, Ozsoy N, Ozturk SS. 2006. The devil is in the details: A tale of process scale-up and technology transfer for a cell culture process. 232nd ACS National Meeting. San Francisco, CA.

Borys MC, Linzer DI, Papoutsakis ET. 1993. Culture pH affects expression rates and glycosylation of recombinant mouse placental lactogen proteins by Chinese hamster ovary (CHO) cells. Biotechnology (N Y) 11(6):720–724.

Brorson K, De Wit C, Hamilton E, Mustafa M, Swann PG, Kiss R, Taticek R, Polastri G, Stein KE, Xu Y. 2002. Impact of cell culture process changes on endogenous retrovirus expression. Biotechnol Bioeng 80(3):257–267.

Chisti Y. 2000. Animal-cell damage in sparged bioreactors. Trends Biotechnol 18(10):420–432.

Chotigeat W, Watanapokasin Y, Mahler S, Gray PP. 1994. Role of environmental conditions on the expression levels, glycoform pattern and levels of sialyltransferase for hFSH produced by recombinant CHO cells. Cytotechnology 15(1–3):217–221.

FDA. 2004a. Challenge and Opportunity on the Critical Path to New Medical Products. http://www.fda.gov/oc/initiatives/criticalpath/whitepaper.html

FDA. 2004b. Guidance for Industry: PAT—A Framework for Innovative Pharmaceutical Development, Manufacturing, and Quality Assurance.

Ge X, Tolosa L, Simpson J, Rao G. 2003. Genetically engineered binding proteins as biosensors for fermentation and cell culture. Biotechnol Bioeng 84(6):723–731.

Ge X, Hanson M, Shen H, Kostov Y, Brorson KA, Frey DD, Moreira AR, Rao G. 2006. Validation of an optical sensor-based high-throughput bioreactor system for mammalian cell culture. J Biotechnol 122(3):293–306.

Gupta A, Rao G. 2003. A study of oxygen transfer in shake flasks using a non-invasive oxygen sensor. Biotechnol Bioeng 84(3):351–358.

Harms P, Sipior J, Ram N, Carter GM, Rao G. 1999. Lowcost phase-modulation measurements of nanosecond fluorescence lifetimes using a lock-in amplifier. Rev Sci Instrum 70:1535–1539.

DOI 10.1002/bit

Harms P, Kostov Y, French JA, Soliman M, Anjanappa M, Ram A, Rao G. 2006. Design and performance of a 24-station high throughput microbioreactor. Biotechnol Bioeng 93(1):6–13.

Hayter PM, Kirkby NF, Spier RE. 1992. Relationship between hybridoma growth and monoclonal antibody production. Enzyme Microb Technol 14(6):454–461.

Jardon M, Garnier A. 2003. PH, pCO2, and temperature effect on R-adenovirus production. Biotechnol Prog 19(1):202–208.

Junker BH, Wang DIC, Hatton TA. 1988. Fluorescence sensing of fermentation parameters using fiber optics. Biotechnol Bioeng 32(1):55–63.

Kermis HR, Kostov Y, Harms P, Rao G. 2002. Dual excitation ratiometric fluorescent pH sensor for noninvasive bioprocess monitoring: Development and application. Biotechnol Prog 18(5):1047–1053.

Kermis HR, Kostov Y, Rao G. 2003. Rapid method for the preparation of a robust optical pH sensor. Analyst 128(9):1181–1186.

Kostov Y, Harms P, Pilato RS, Rao G. 2000a. Ratiometric oxygen sensing: Detection of dual-emission ratio through a single emission filter. Analyst 125(6):1175–1178.

Kostov Y, Van Houten KA, Harms P, Pilato RS, Rao G. 2000b. Unique oxygen analyzer combining a dual emission probe and a low-cost solid-state ratiometric fluorometer. Appl Spectrosc 54:864–868.

Kostov Y, Harms P, Randers-Eichhorn L, Rao G. 2001. Low-cost microbioreactor for high-throughput bioprocessing. Biotechnol Bioeng 72(3):346–352.

Kunkel JP, Jan DC, Jamieson JC, Butler M. 1998. Dissolved oxygen concentration in serum-free continuous culture affects N-linked glycosylation of a monoclonal antibody. J Biotechnol 62(1):55–71.

Li F, Hashimura Y, Pendleton R, Harms J, Collins E, Lee B. 2006. A systematic approach for scale-down model development and characterization of commercial cell culture processes. Biotechnol Prog 22(3):696–703.

Muthing J, Kemminer SE, Conradt HS, Sagi D, Nimtz M, Karst U, Peter-Katalinic J. 2003. Effects of buffering conditions and culture pH on production rates and glycosylation of clinical phase I anti-melanoma mouse IgG3 monoclonal antibody R24. Biotechnol Bioeng 83(3):321–334.

Ozturk SS, Palsson BO. 1990. Effects of dissolved oxygen on hybridoma cell growth, metabolism, and antibody production kinetics in continuous culture. Biotechnol Prog 6(6):437–446.

Ozturk SS, Palsson BO. 1991. Growth, metabolic, and antibody production kinetics of hybridoma cell culture: 2. Effects of serum concentration, dissolved oxygen concentration, and medium pH in a batch reactor. Biotechnol Prog 7(6):481–494.

Restelli V, Wang MD, Huzel N, Ethier M, Perreault H, Butler M. 2006. The effect of dissolved oxygen on the production and the glycosylation profile of recombinant human erythropoietin produced from CHO cells. Biotechnol Bioeng 94(3):481–494.

Rubinstein LJ, Stein KE. 1988. Murine immune response to the Neisseria meningitidis group C capsular polysaccharide. II. Specificity. J Immunol 141(12):4357–4362.

Tolosa L, Kostov Y, Harms P, Rao G. 2002. Noninvasive measurement of dissolved oxygen in shake flasks. Biotechnol Bioeng 80(5):594–597.

Weidgans BM, Krause C, Klimant I, Wolfbeis OS. 2004. Fluorescent pH sensors with negligible sensitivity to ionic strength. Analyst 129(7):645–650.

Chapter Two: Glucose, Glutamine and CO_2

Oxygen and pH were a good start. However, particularly for mammalian cells, glucose, glutamine, CO_2, ammonia and lactate were frequently presented as targets for sensors. We list the first three where we have had some success and are continuing to work on the rest.

The glucose and glutamine sensors were offshoots of ongoing work to develop highly sensitive sensors for diabetes and metabolism, where the idea was to develop sensors that could be used to make transdermal measurements in human subjects. They were based on binding proteins that nature had evolved over millions of years to help microbes transport these molecules into the cell. Since they are present in very low concentrations in the environment, natural selection favored the evolution of the most sensitive proteins, with micromolar binding capabilities. In contrast, an enzyme such as glucose oxidase binds glucose at millimolar levels, which is the typical glucose/glutamine level in cell culture media. What this meant practically was that either extremely small sample sizes (since they would have to be diluted a thousand-fold) or dialysate with very low concentrations could be assayed. The next two papers demonstrate both applications.

Leah Tolosa was ideally positioned to build on this project. A biochemist by training, she had begun to work with he binding proteins and had demonstrated in previous work that they could in fact be fluorescently labeled and could reliably and reproducibly work as “reagentless” sensors since the transduction of the signal was based on reversible binding of the target analyte to the sensor protein. Xudong Ge had started his Ph.D. in the lab and helped to get the sensors to work in a bioreactor application. Jen Simpson was a talented student who could culture mammalian cells, so we had all the ingredients to demonstrate the application of this new class of sensors for bioprocess applications.

There were some surprises. Because the sensors were so sensitive, we were able to detect trace glucose in LB media. Also, because the samples were diluted 1000x, any optically interfering media components were also correspondingly diluted, so no extensive sample preparation was required. We could also monitor glucose and glutamine from very small volume cultures in well-plates because the sample volume requirement was very small. We also saw that commercially available slow-release glutamine formulations did not work as advertised.

Genetically Engineered Binding Proteins as Biosensors for Fermentation and Cell Culture

Xudong Ge, Leah Tolosa, Jen Simpson, Govind Rao

Department of Chemical and Biochemical Engineering, University of Maryland, Baltimore County, 1000 Hilltop Circle, Baltimore, Maryland 21250; telephone: 410-455-3415; fax: 410-455-6500; e-mail: grao@umbc.edu

Received 21 April 2003; accepted 14 August 2003

Published online 21 October 2003 in Wiley InterScience (www.interscience.wiley.com). DOI: 10.1002/bit.10830

Abstract: The signal-transduction properties and the potential applications of two engineered binding proteins from *E. coli* were extensively studied. Both proteins have a single cysteine mutation in their polypeptide chains, which allow the introduction of an environmentally sensitive fluorophore: ANS for glucose-binding protein (GBP) and acrylodan for glutamine-binding protein (QBP). Both proteins respond to their ligands in the micromolar range. The proteins can be stored at 4°C for at least 5 months. Apparent binding constant, protein concentration, and fluorophore are three major factors that affect the biosensor's responsive ranges. The binding of the ligand is quick and reversible in solution, but the unfavorable dissociation equilibrium and mass-transfer resistance for encapsulated proteins can delay the response to several minutes and the recovery to hours. Simulated results show that using dialysis tubing with a diameter of 1 mm or less is possible to reduce the recovery time to less than 30 minutes. The potential applications of GBP were studied in yeast fermentation and *E. coli* fermentations in three different scales: 150 mL, 5 mL, and 100 μL. The results were compared with an YSI 2700 Chemistry Analyzer. Although the latter could not give reliable results for the *E. coli* fermentations as the glucose concentration in LB medium is close to its lower detection limit, the glucose biosensor presented here was successfully applied to each situation. Glutamine-binding protein was tested in cell cultures of two different scales (100 mL and 100 μL) and the results were also compared with those obtained with YSI. Both QBP and YSI gave good results for the 100-mL cell culture, but the relatively large sample volume requirement of YSI (at least 5 μL) prevented it from being used in the 100-μL cell culture. Because of their small sample volume requirements (less than 1 μL) and high sensitivity, the assays described here might find wide applications in high-throughput bioprocessing. © Wiley Periodicals, Inc. *Biotechnol Bioeng* **84**: 723–731, 2003.

Keywords: fermentation; cell culture; glucose; glutamine; sensor

Correspondence to: Govind Rao

Contract grant sponsors: Juvenile Diabetes Research Foundation International; the National Institutes of Health; National Science Foundation; Fluorometrix, Genentech, Merck, Pfizer

Contract grant number: 4-1999-793; DK062990; BES 0091705

INTRODUCTION

Research on biosensors has greatly increased in recent years because of biosensors' widespread potential applications and remarkable ability to measure the presence of a single molecular species in a complex mixture. However, before the invention of protein-engineering techniques, the only available biomolecules to construct biosensors were naturally occurring macromolecules. With this limitation, what one could do in developing biosensors was to find a naturally occurring macromolecule with a proper signal transduction mechanism and the desired analyte specificity from a number of candidates, and then devise a detector to adapt to that mechanism (Hellinga and Marvin, 1998). Although a number of biosensors have been developed in this manner, this method is case-specific and laborious. With the advent of protein-engineering techniques, the number of strategies for developing biosensors has been greatly increased. We can now develop biosensors not only in the way described above, but also by incorporating reporter groups, such as fluorophores, directly into biological molecules with desired analyte specificity, thus making them suitable to the available detectors (Dattelbaum and Lakowicz, 2001; Gilardi et al., 1994, 1997; Marvin and Hellinga, 1998; Salins et al., 2001; Tolosa et al., 1999).

The ligand-specific periplasmic binding proteins are a superfamily of such macromolecules that are responsible for active transport of biochemical substances such as ions, amino acids, and sugars, and can be engineered to sense these substrates (Hsiao et al., 1996; Sun et al., 1998). Previous biological and biochemical studies have shown that these binding proteins share some common properties although their size and amino acid sequences may be quite different (Quiocho, 1990). Each periplasmic binding protein is composed of a single polypeptide chain with a molecular mass of 22,000 to 59,000 Da. The binding affinity in terms of dissociation constants is in the micromolar or submicromolar range. Most binding proteins have a two-domain

structure connected by a hinge (Quiocho, 1990). The binding site is in the interface of the two domains. It has been shown in a number of proteins that binding of the ligand can induce a large conformational change, from an ''open'' ligand-free structure to a ''closed'' ligand-bound structure (Hsiao et al., 1996; Sun et al., 1998). By introducing single fluorophores into such proteins, this conformational change upon ligand binding can be taken advantage of to construct biosensors that respond to their respective ligands. These binding proteins include glucose-binding protein (GBP) (Marvin and Hellinga, 1998; Salins et al., 2001; Tolosa et al., 1999), maltose-binding protein (Gilardi et al., 1994; 1997), phosphate-binding protein (Brune et al., 1994), and glutamine-binding protein (QBP) (Dattelbaum and Lakowicz, 2001).

The choice of labeling sites is generally based on the identification of specific sites on the protein that undergo maximum conformational change upon substrate binding (Marvin and Hellinga, 1998). However, this approach neglects the effects of the dye conjugated to the protein. Thus, it is common to observe different environment-sensitive dyes conjugated to the same site showing varying response to analyte concentrations (Dattelbaum and Lakowicz, 2001; Marvin and Hellinga, 1998). Consequently, there is a degree of empiricism in the design of binding protein-based biosensors.

In this study, two engineered binding proteins, Q26C GBP and S179C QBP, were prepared and labeled with environment-sensitive fluorophores showing maximum signal change as previously reported (Dattelbaum and Lakowicz, 2001; Tolosa et al., 1999). These single-labeled binding proteins allow for intensity-based measurements. To make the sensors more robust, a dual-emitting QBP was also prepared by dual-labeling, i.e., besides the environment-sensitive fluorophore labeled at the single cysteine mutation, a long-lived reference fluorophore was also labeled at the N-terminal of the binding protein, where minimal environmental changes may be expected. Upon ligand binding, the environment-sensitive fluorophore is more exposed to the solvent, resulting in a decrease in its fluorescence intensity. On the other hand, the fluorescence intensity of the reference fluorophore is unaffected, and thereby serves as an internal standard. A detailed description of this dual-labeled QBP has been reported elsewhere (Tolosa et al. 2003). Our emphasis here is placed on the elucidation of the signal transduction properties and the potential applications of these two binding proteins.

MATERIALS AND METHODS

Materials

2-(4′-iodoacetamidoanilino)naphthalene-6-sulfonic acid (ANS) and 6-acryloyl(di-methylamino)naphthalene (acrylodan), tris(2-carboxyethyl)phosphine (TCEP) were purchased from Molecular Probes (Eugene, OR). Glucose, mannose, galactose, sucrose, fructose, maltose, glutamine, Sephadex G-25, DEAE Sephadex A-50, *N*, *N*-dimethylformamide (DMF), chloroform, NaCl, K_2HPO_4, KH_2PO_4, Na_2HPO_4, NaH_2PO_4, M_gSO_4 were purchased from Sigma-Aldrich. Tryptone and yeast extract were obtained from Becton Dickinson (Sparks, MD). Soy peptone was obtained from DIFCO Laboratories (Detroit, MI). All chemicals were used without further purification. Dialysis membrane tubing was obtained from Spectrum Medical Industries, Inc. (Los Angeles, CA). Slide-A-lyzer® dialysis cassettes were purchased from PIERCE (Rockford, IL).

Protein Expression, Purification, and Fluorophore Coupling

The plasmids encoding the mutants were constructed by site-directed mutagenesis as described previously (Dattelbaum and Lakowicz, 2001; Tolosa et al., 1999). Two different host *E. coli* cells, NM303 and HB101, were used for the production of GBP. NM303 does not produce the wild type of GBP, but has a low productivity for mutant GBP. Although HB101 produces the wild type of GBP, its presence does not interfere with the labeling of the dye because it does not contain reactive cysteine residues. Transformation and expression of S179C QBP was carried out in *E. coli* strain HB101.

Glutamine-binding protein was released by using the chloroform shock method (Dattelbaum and Lakowicz, 2001). The amount of S179C QBP was estimated by using sodium dodecyl sulfate-polyacrylamide gel electrophoresis, which showed that the content of QBP in the periplasmic extract was more than 80%. GBP was released by using the osmotic shock method (Dattelbaum and Lakowicz, 2001). The GBP content in the supernatant was about 50%. The total concentration of the binding proteins was determined using Micro Protein Determination (Sigma Diagnostics, Inc., St. Louis, MO). A slight excess of TCEP was added into the protein solutions to prevent the oxidation of the thiol groups.

The S179C QBP was labeled with acrylodan and separated from the unreacted dye by gel-permeation chromatography (Dattelbaum and Lakowicz, 2001). The labeling of Q26C GBP with ANS was conducted in a similar manner except that an additional purification step was needed because unreacted ANS tends to adsorb on the protein, which cannot be completely removed with Sephadex G-25. The adsorbed free dye gives a higher baseline signal and decreases the relative signal change. To remove the remaining free dye and further purify the protein, the protein solution was applied to a DEAE Sephadex A-50 column (Boos and Gordon, 1971). The total protein concentration was determined and the labeling efficiency was estimated from the total protein concentration and the concentration of protein-bound fluorophore, which was calculated from its absorbance and extinction coefficient (Haughland, 1996). The final product was 0.2 μm filter-sterilized, and stored at 4°C.

Fluorescence Measurements

The emission spectra were recorded on a Varian Cary Eclipse fluorescence spectrophotometer (Varian Instruments, Walnut Creek, CA). All samples were measured in quartz cuvettes (Starna Cells, Inc. Atascadero, CA).

Response and Recovery Time Measurements

The response and recovery times of the binding proteins were studied in Slide-A-lyzer® dialysis cassettes (PIERCE, Rockford, IL). Three cassettes were used for each measurement so that the error could be estimated. To measure the response time, 1 mL of protein solution (1.7 μ*M* GBP, 1.3 μ*M* QBP) was injected into each cassette, to which a buoy was then attached. A clean 500-mL beaker was filled with 400 mL of 10 m*M* phosphate buffer with the desired glucose or glutamine concentration. The dialysis cassettes were then put into the beaker and gently stirred. The fluorescence intensity of the protein solutions was measured every 2–5 min until equilibrium was reached. To measure the recovery time, the cassettes were removed from the beaker and then placed into another beaker filled with 400 mL of fresh 10 m*M* phosphate buffer. Thereafter, the fluorescence intensity was measured every 20–60 min until new equilibrium was reached. Meanwhile, the buffer was replaced with fresh buffer every 30 min.

Fermentation and Cell Culture

The yeast seed culture consisted of 4 mg dry yeast cells (SAF Consumer Company, Atlanta, GA) in 20 mL of YEHD-rich medium (2% yeast extract, 1% soy peptone, and 2% glucose). The culture was incubated at 30°C with shaking at 260 rpm for 8–10 h. The fermentation was carried out at 30°C in a 500-mL shake flask containing 147 mL of YEHD medium and 3 mL of seed inoculum. Then 1.0 mL of broth sample was taken for analysis every 30–60 minutes. To avoid the change in glucose concentration after sampling, the samples were quickly cooled on ice to quench the cellular metabolism. After the optical density (OD) was measured with a Milton Roy Spectronic 401 spectrophotometer at 600 nm, the sample was centrifuged and the supernatant glucose concentrations were measured directly with an YSI 2700 chemistry analyzer and concurrently with the glucose biosensor described here by diluting 1 μL of sample 10,000 to 40,000 times.

The *E. coli* (JM105) seed culture consisted of 2% inoculum in 5 mL of LB medium incubated at 37°C with shaking at 260 rpm for 8–10 h. The fermentations were carried out at 37°C in a 500-mL shake flask, a 15-mL polypropylene tube and on a 96-well plate. The volume of LB medium added to each fermentor was 150 mL, 5 mL, and 100 μL with 3% seed culture for the 150-mL fermentation and 5% for the other two. Samples were taken every 30–60 min. For the 150-mL fermentation, 1 mL of sample was taken each time and the glucose concentration and optical density were measured thereafter. For the 5-mL and 100-μL fermentations, only 1 μL of sample was taken each time and the optical density was measured only at the end of the fermentation. Glucose analysis was conducted in the same manner as in the yeast fermentation except that all samples were diluted 250 times.

The cells used in the cell culture came from two different cell lines, GM010178 and GM14649, both lymphoblasts from adult breast tissue. These cell lines were obtained commercially from Coriell Cell Repositories, and have been grown in a solution of 15% Fetal Bovine Serum in RPMI Medium 1640 with GlutaMAX™ (Gibco™, Grand Island, NY). For the 100- mL cell culture, 50 mL of fresh medium was mixed with 50 mL of inoculum in a 250- mL polystyrene flask, and then incubated in a CO_2 incubator (Precision Scientific, Chicago, IL) until the color of the medium turned from red to yellow. 1 mL of sample was taken from the culture every 2 h for analysis. After sampling, the sample was quickly cooled on ice to quench the cellular metabolism. The glutamine concentration was then measured with a YSI 2700 Chemistry Analyzer and concurrently with the glutamine biosensor described in this paper by diluting a small volume of sample 1,000 times. For the 100-μL cell culture, 50 μL of fresh medium was mixed with 50 μL of inoculum in a well on a 96-well plate, and then incubated in the CO_2 incubator. One microliter of sample was taken each time and the glutamine concentration was measured with the present biosensor thereafter.

RESULTS AND DISCUSSION

Optical Spectrum

The mutant GBP and QBP each have a single cysteine residue at position 26 and position 179, respectively. The cysteine mutation allows the proteins to be labeled with sulfhydryl-reactive dyes that exhibit polarity sensitive photophysical properties with lower fluorescence intensity in more polar environment.

The QBP labeled with acrylodan exhibits one emission maximum at 515 nm, which decreases in intensity with increasing concentration of glutamine (Fig. 1). This decrease in intensity suggests that acrylodan is displaced into the more polar aqueous phase upon ligand binding. Like the acrylodan-labeled QBP, GBP labeled with ANS exhibits one emission maximum at 466 nm, which decreases in intensity with increasing concentration of glucose (Fig. 2). The calibration curves of these two biosensors are shown in the insets in Figures 1 and 2.

The apparent binding constants were calculated by fitting the experimental results to the binding isotherm (Dattelbaum and Lakowicz, 2001). The binding constants for the single-labeled and double-labeled QBP were calculated to be 0.23 ± 0.01 μ*M* and 0.28 ± 0.03 μ*M*, respectively. Both are in agreement with the reported value of 100–300 n*M* for the wild type (Sohanpal et al., 1993). The reason for this agreement is that the position of the fluorophore is far

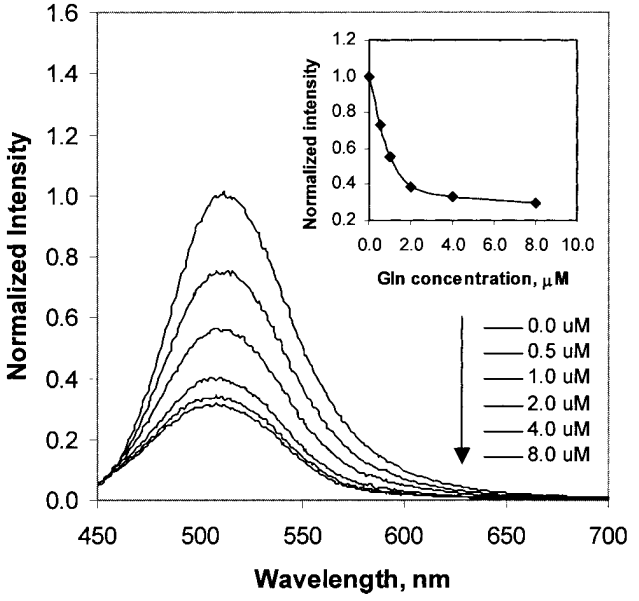

Figure 1. Emission spectra of Acr-QBP in increasing concentrations of glutamine. QBP concentration = 1.01 μM. Excitation wavelength = 360 nm. Inset: Changes in normalized emission intensity at 515 nm with glutamine concentrations.

from the binding site, consequently, the binding affinity is not greatly affected. The binding constant of GBP for glucose was calculated to be 0.78 $\pm$ 0.07 μM, which also agrees well with the reported value of 0.8 μM (Hellinga and Marvin, 1998).

Stability and Reproducibility

The stability of the binding proteins was determined by binding assays. The labeled binding proteins can be stored in phosphate buffer at 4°C for at least 5 months. The reproducibility of the calibration curves is shown in Figure 3. It can be seen that the sensitivity of GBP did not undergo any change during the testing period of 2 months. It also shows that the labeled QBP underwent some changes in 5 months after preparation, but was still responsive to glutamine. Factors that could have caused this change include fluorophore or protein degradation, or fluorophore dissociation from the protein. Although it is not clear what caused this change in sensitivity after 5 months, it is obvious that recalibration of the biosensor during its use in fermentation or cell culture is unnecessary because fermentation or cell culture usually lasts from only several hours to a few days. This long storage life makes the system very attractive commercially.

Responsive Ranges

The lower and upper detection limits are important properties of a sensor. The lower detection limit of the present sensing strategy was calculated from the experimental data according to its definition (Signal/Noise = 3). From the results shown in Table I, we can see that the detection limit was mainly affected by the binding affinity of the protein, the concentration of the protein, and the quantum yield of the fluorophore. The binding affinity determines the magnitude of the responsive ranges. Therefore, the most effective way to change the responsive ranges is to modify the structure of the binding site by mutagenesis. It should also be noted that the apparent binding constant may be affected by the fluorophore and the labeling position (Brennan et al., 2000; Dattelbaum and

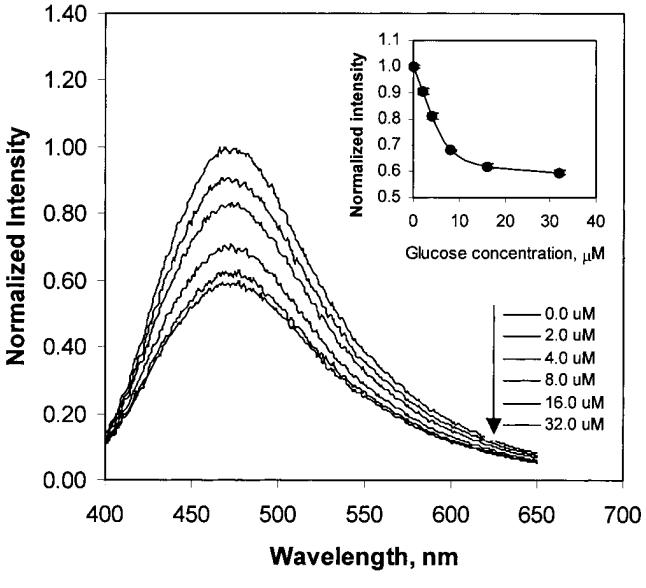

Figure 2. Emission spectra of ANS-GBP in increasing glucose concentration. GBP concentration = 8.1 μM; Excitation wavelength = 330 nm. Inset: Changes in normalized emission intensity with glucose concentrations.

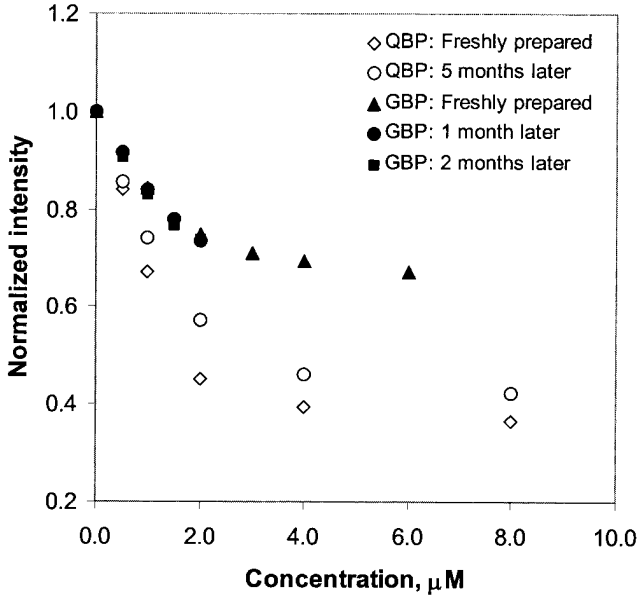

Figure 3. Reproducibility of QBP and GBP. QBP: Concentration = 1.01 μM, Excitation wavelength = 360 nm, Emission wavelength = 515 nm; GBP: Concentration = 1.7 μM, Excitation wavelength = 330 nm, Emission wavelength = 466 nm.

Table I. Lower and upper detection limits.

Protein	Affinity constant μM	Dye	Conc μM	LDL[a] μM	UDL[b] μM	LDL/UDL
GBP	0.78	ANS	1.7	0.3	10	33
			5.5	0.5	32	64
QBP	0.23	Acrylodan	0.87	0.03	3.2	107
			3.54	0.07	16	229

[a]LDL-Lower detection limit.
[b]UDL-Upper detection limit.

Lakowicz, 2001; Hellinga and Marvin, 1998), which, in turn, affects the responsive ranges.

The effect of protein concentration on the responsive ranges is illustrated in Table I. Although both detection limits increased with the protein concentration, the lower detection limit increased only slightly while the upper detection limit increased almost proportionately. If we define the ratio of the upper detection limit and lower detection limit as the flexibility of the sensing range, the flexibility of the sensing range can increase greatly if the concentration of the binding protein is increased. The decrease of the lower detection limit with decreasing the protein concentration allows us to adjust the sensing sensitivity. The lower the protein concentration, the higher the sensitivity but the responsive range will be narrower.

Comparing the detection limits of GBP and QBP, we can see that the lower detection limit of QBP is about 10 times lower than that of GBP. This big difference was mainly caused by the difference between the quantum yields of the two fluorophores. The acrylodan on the QBP has a much higher quantum yield than the ANS on the GBP. The reason is that a fluorophore with a higher quantum yield can give a much stronger signal for the same strength of excitation. As a result, the lower detection limit of the sensor can be greatly lowered and the flexibility of the sensing range can be significantly improved.

Response and Recovery Times

Although the soluble binding proteins have complete freedom of movement in solution, and thereby exhibit their maximum activity, only after immobilization can these proteins be used repeatedly or continuously. In the literature, the immobilization of binding proteins has been reported in only two articles. Zhou and Cass (1991) studied the immobilization of maltose binding protein (MBP) labeled with IAEDANS. MBP-IAEDANS was immobilized onto PCG by glutaraldehyde coupling, carbodiimide coupling, and diazonium coupling. Unfortunately, even for the least inactivating method, only 25% of the native binding activity left after immobilization. Wenner et al. (2001) studied the possibility of immobilizing phosphate-binding protein (PBP) labeled with MDCC in sol-gel. The maximum signal change is again only 25% of that in solution. The restricted mobility upon immobilization, which severely limits the conformational change that is necessary for a binding protein to function, is the major reason for this low binding affinity. Among the principal methods for biological immobilization—adsorption, covalent binding, crosslinking, entrapment, and encapsulation—encapsulation is the method that least interferes with the binding process. So it seems to be the best possible method for the immobilization of the binding proteins reported here.

To verify the feasibility of the encapsulation method, the response and recovery times of the two binding proteins were studied in Slide-A-lyzer® dialysis cassettes with a molecular weight cut off of 10,000 (PIERCE, Rockford, IL). Experimental results (Fig. 4) show that the response was fairly rapid for both binding proteins (around 5–12 min). However, compared with the extremely fast response in liquid (less than 1 s), the response time in dialysis cassettes suggested that this process was diffusion-limited. Compared with the relatively fast response, the recovery times for both binding proteins were extremely long. To facilitate the signal recovery, the effect of ultrasonic agitation on this process was tested. Unexpectedly, the signal recovery was actually delayed in ultrasound field. The reasons for this delay might be that agitation altered the positioning of the dye on the protein, making the dye more exposed to the environment.

To find a rationale for the slow signal recovery, computer simulations were conducted by using the reported kinetic parameters for the binding reaction between glutamine and QBP (Weiner and Heppel, 1971). The reported value of k_a for the binding is $9.8 \times 10^7\ M^{-1}s^{-1}$ and the k_d for the dissociation is $16\ s^{-1}$. These two values can yield a

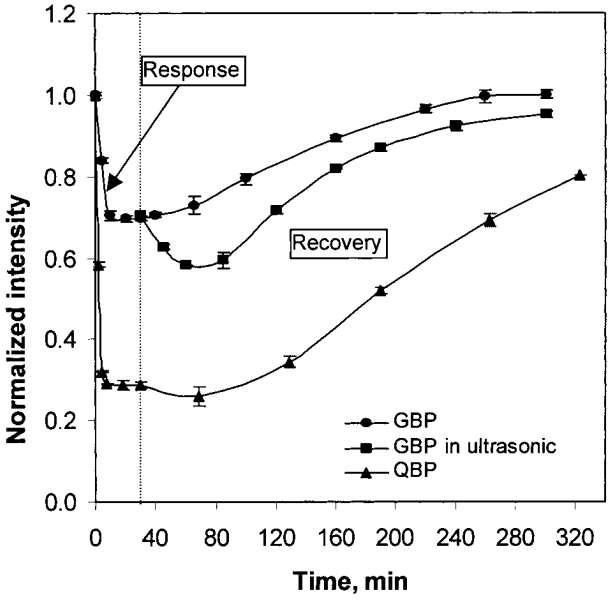

Figure 4. Response and recovery times of GBP and QBP in dialysis cassettes. GBP: Concentration = 1.7 μM; Excitation wavelength = 330 nm; Emission wavelength = 466 nm. QBP: Concentration: 1.3 μM; Excitation wavelength = 360 nm; Emission wavelength = 515 nm.

dissociation constant of 0.163 μ*M*, which is very close to that obtained in this study.

The mathematical model used for simulation is based on the following three reasonable assumptions:

1. The mass transfer resistance across the dialysis membrane is the only major resistance. All other mass transfer resistances are negligible.
2. No concentration difference exists throughout the space inside the dialysis membrane.
3. The concentration of the free substrate is always in equilibrium with the concentration of the bound substrate.

Based on the above assumptions, the following equation can be obtained by doing the mass balance of the substrate:

$$V\frac{d([A]+[EA])}{dt} = KS([A]_0 - [A]) \tag{1}$$

where V is the volume of the binding protein solution inside the dialysis membrane. $[A]$, $[EA]$ are the concentrations of the substrate in free and bound state, respectively. t is time. K is the overall mass transfer coefficient. S is the area for mass transfer. $[A]_0$ is the concentration of the substrate outside the dialysis membrane. According to the third assumption, we have:

$$\mathrm{A} + \mathrm{E} \Leftrightarrow \mathrm{EA} \tag{2}$$

$$k_a[A][E] = k_d[EA] \tag{3}$$

$$[A] = \frac{k_d[EA]}{k_a([E]_T - [EA])} \tag{4}$$

where k_a, k_d are the rate constants for binding and dissociation, respectively. $[E]$ is the concentration of the binding protein with no bound substrates. $[E]_T$ is the total concentration of the protein. Substitution of Eq. (4) into Eq. (1) gives:

$$\frac{d[EA]}{dt} = -\frac{KS}{V}\frac{k_d[EA]([E]_T - [EA])}{k_d[E]_T + k_a([E]_T - [EA])^2} \tag{5}$$

Equation (5) was used to simulate the response and recovery process.

The calculated results show that when there is no mass-transfer resistance, the response and recovery both take less than 1 s (results not shown), showing that the binding of the ligand is completely reversible and the time needed to reach equilibrium is actually very fast in liquid. However, when the binding protein is encapsulated in a dialysis cassette, the response time is delayed by several minutes and the recovery time is delayed even longer to several hours (see Fig. 5). The simulated results for 90% response and 90% recovery times were calculated based on Eq. (5) and listed in Table II. From these results, we can see that the binding constants and the mass transfer resistance are the two major factors that affect the response and recovery times. Because of the extremely low dissociation constant, very few free ligands exist in equilibrium with the bound ligands, resulting in a very small mass transfer driving force in the recovery process. Increasing the binding constants through mutagenesis and decreasing the mass transfer resistance are two solutions to this problem. Comparatively, the latter is much easier and more efficient in reducing the response and recovery times. Simulated results show that using dialysis tubing with a diameter of 1 mm or less and 10,000 MWCO, it is possible to reduce the recovery time to less than 30 min (Table II). Approaches to immobilization of the binding proteins are under investigation in our lab. These results will be reported separately.

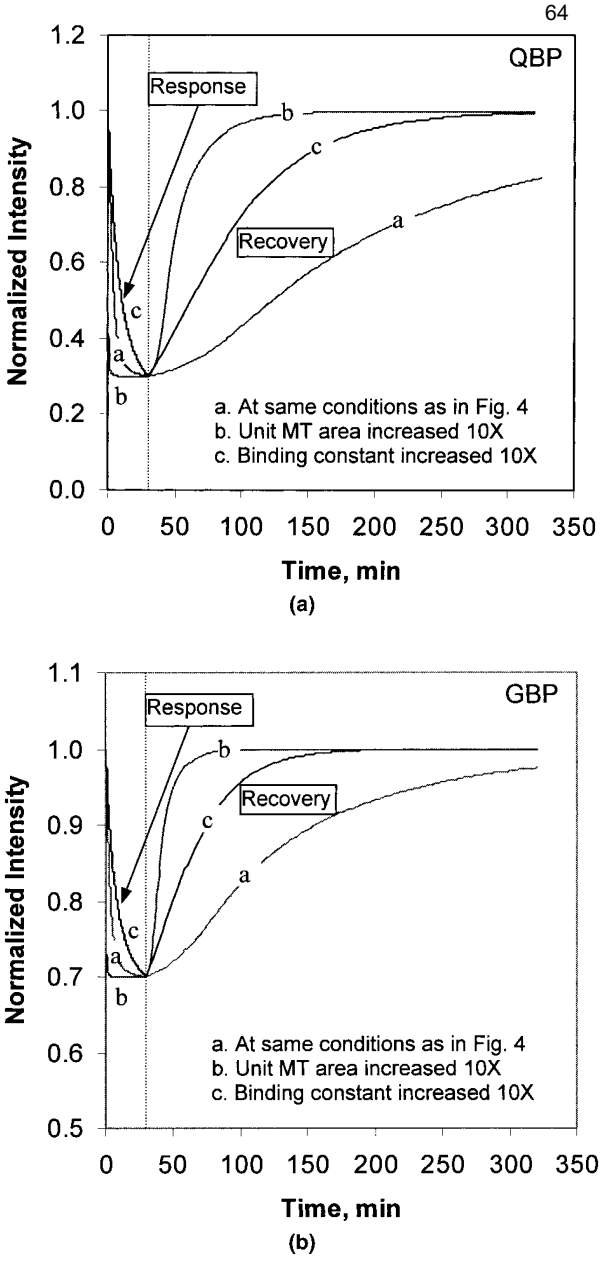

Figure 5. Simulated response and recovery curves for QBP (a) and GBP (b).

Table II. Simulated results for 90% response and 90% recovery times.

	QBP		GBP	
	Response, min	Recovery, min	Response, min	Recovery, min
At same conditions as Fig. 4	8	515	8	266
K_d increased 10×	19	146	18	82
Unit MT area increased 10×	0.8	52	0.6	26

Applications in Fermentation and Cell Culture

The applicability of the present sensing strategy was tested in a yeast fermentation, *E. coli* fermentation and mammalian cell culture. The glucose concentrations were measured with both an YSI 2700 Chemistry Analyzer (Yellow Springs Instrument Co., Inc.) and the biosensor presented here. The YSI 2700 Chemistry Analyzer has a responsive range up to 140 m*M* and a lower detection limit (based on signal/noise = 3) of 0.1 m*M*. GBP has a lower detection limit between 0.3–0.5 μ*M* (Table I). Because of this extremely high sensitivity, the responsive range of GBP can be expanded to several orders of magnitude by simply diluting the sample. For example, the samples analyzed using GBP were diluted 10,000 to 40,000 times while the samples analyzed with YSI were aspirated into the instrument as is (Fig. 6). This dilution step does not only expand the responsive range. Just as importantly, it leads to the elimination or minimization of fluorescent interference in optically ''dirty'' media. For this reason, it is not difficult to obtain reliable data even from the UV-excitable ANS label of GBP. As we can see in Figure 6, although the glucose concentration readings were not completely identical for the two different methods, the trend was similar. The presence of ascorbic acid in the baker's yeast, which tends to increase the YSI signal, might be one of the reasons for the disagreement. Ascorbic acid is added to the SAF yeast as a dough conditioner to help dough stretch easily (http://www.safyeast.com/catalog.html).

For the *E. coli* fermentation in 500-mL shake flask, the trend in glucose consumption as the cell density increases was clearly established from the data determined using the binding protein (Fig. 7a). In contrast, the YSI 2700 chemistry analyzer could not give reliable results because the glucose concentration in LB medium was close to the lower detection limit of YSI, which was measured to be 0.1 m*M*. Clearly, GBP is better at monitoring glucose

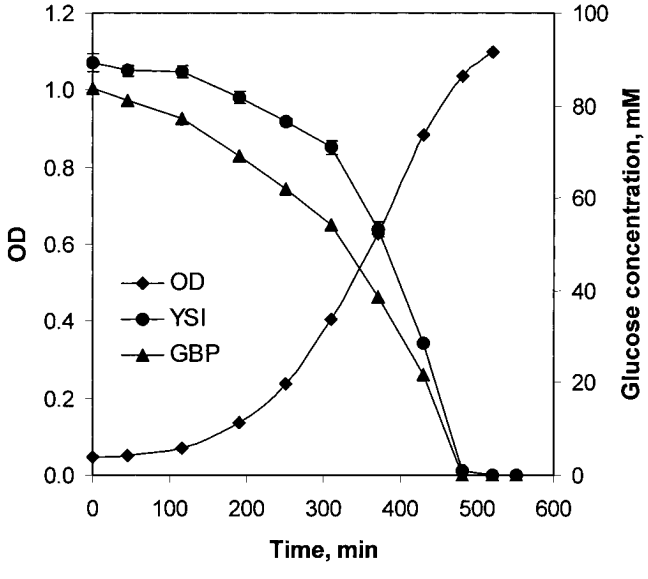

Figure 6. Comparison of glucose concentrations measured with a YSI 2700 Chemistry Analyzer® and GBP in yeast fermentation.

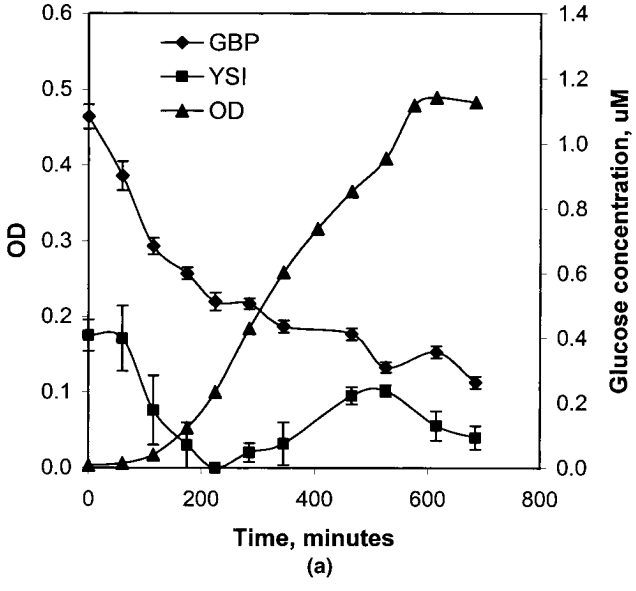

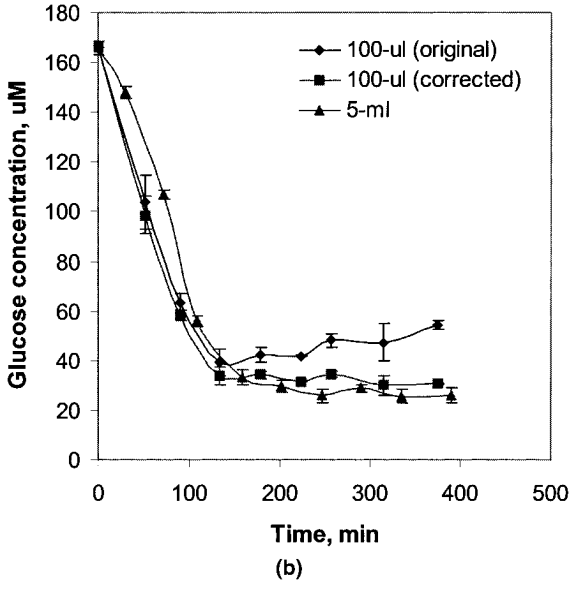

Figure 7. Changes in glucose concentration measured with GBP in *E. coli* fermentations (a) in a 500-mL shake flask, (b) in a 15-mL plastic tube and on a 96-well plate.

concentrations at submillimolar levels. We note that monitoring of glucose levels in fermentations using LB medium is not yet routine because of the lack of a sensitive and simple measuring technique.

Another advantage afforded by the high sensitivity of GBP is that very small sample volumes (<1 μL) are required for analysis. This makes it applicable to microbioreactors (≈100 μL). This application is impossible for the YSI Chemistry Analyzer because its minimum sample volume is 5 μL, which is too high for microbioreactors. The changes in glucose concentration during the 5-mL fermentation and the 100-μL fermentation are shown in Figure 7b. For the 100-μL fermentation, it was noted that the glucose concentration was somewhat affected by the evaporation of the medium, which tends to increase the concentrations of the solutes. However, after correcting the effect of volume change caused by evaporation, it was found that the glucose concentration profiles for the two different scales of fermentations are actually quite similar. Effective measures to prevent the evaporation of the medium will be taken during future experiments although it is not a problem of the sensor itself. Another remarkable observation from these fermentation experiments is that the glucose concentration in different batches of LB medium is quite different. Although *E. coli* cells may be able to adapt to this difference very quickly, it may have a profound impact on the productivity and purity of products. Thus, monitoring of glucose concentration should become routine in fermentations using LB media, particularly in industrial bioprocesses.

The QBP sensor described here was tested in a lymphoblast culture. The glutamine concentration profiles during the 100-mL cell culture are shown in Figure 8a. The gradual increase in glutamine concentration in the sterile medium in the absence of cells is caused by the gradual release of glutamine from GlutaMAX™, a dipeptide conjugate (*L*-alanyl-*L*-glutamine) used as the *L*-glutamine source in a stabilized form (www.invitrogen.com). The dissociation of the GlutaMAX™ dipeptide is accelerated by aminopeptidases within the cell. At the early stage of the cell culture, the concentration of the dipeptide is high. The dissociation rate of the dipeptide is greater than the utilization rate of the glutamine released. As a result, some of the glutamine molecules diffuse out of the cells and accumulate in the medium (Brand et al., 1989). We believe this to be the reason why the glutamine concentration increased more rapidly when cells were present. As in the determination of glucose, analysis of glutamine by the QBP sensor was compared to the YSI Chemistry Analyzer. Determination of glutamine using YSI is a complicated process. The YSI glutamine biosensor is a glutaminase and glutamate oxidase dual enzyme sensor (www.ysi.com). The glutaminase converts glutamine to glutamate and ammonia. The glutamate thus produced is then oxidized by glutamate oxidase to α-ketoglutarate, ammonia, and hydrogen peroxide. The hydrogen oxide that is released is detected at the platinum electrode. Since glutamate oxidase can also detect the glutamate that is already present in the media, the

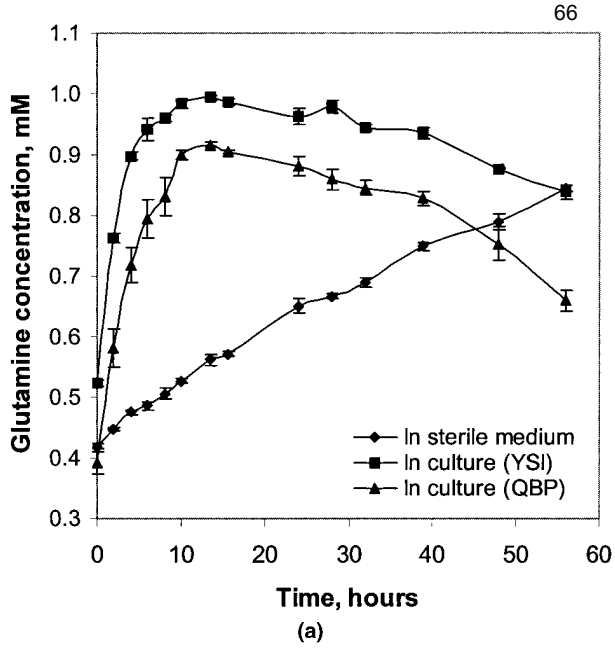

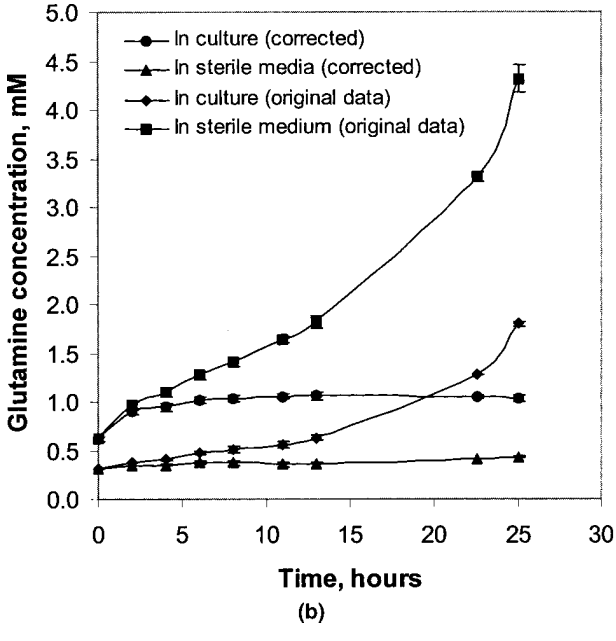

Figure 8. Changes in glutamine concentration measured with a YSI 2700 Chemistry Analyzer and QBP in cell culture (a) in a 250-mL polystyrene flask for cell culture (cell line GM14649), and (b) on a 96-well plate (cell line GM010178).

reading of the glutamine sensor is actually the sum of glutamine and glutamate in the media. To determine the concentration of glutamine alone, a second sensor containing only the glutamate oxidase has to be used initially to determine the glutamate concentrations. This value is then subtracted from the sum to get the glutamine concentration. For the present experiment, only the glutamine sensor was used, and therefore includes both glutamine and glutamate. QBP on the other hand, is responsive to glutamine but not to glutamate. This explains the higher readings of YSI compared to those of QBP as seen in Figure 8a. We believe

that the highly sensitive, more straightforward and highly selective measurement of glutamine by QBP is a vast improvement from the current industry standard for glutamine analysis.

The 0.03–0.07 μ*M* lower detection limit (Table I) for the acrylodan-labeled QBP allows for sample volumes smaller than those for GBP. The sample volume for the assay described here can be as small as 500 nL or even less. This makes it applicable to microscale cell cultures as shown in Figure 8b for the glutamine concentration profile in a 100-μL cell culture. In this case, the relatively large sample volume requirement of YSI (at least 5 μL) prevented its application. As in the small-scale *E. coli* fermentation described previously, the glutamine concentration was also affected by evaporation of the medium in small-scale cell cultures. Thus, the effect of volume change must be taken into account. The effect in this case was much greater as the duration of the experiment was much longer. To correct the effect of volume change, the volume of the medium was measured at the beginning and the end of the cell culture. The volume of the medium during the cell culture was then estimated by assuming a linear decrease in volume. This assumption of linear decrease in volume is reasonable because the surface area for evaporation is constant. In future cell culture experiments, we will take effective measures, e.g., using a water-saturated atmosphere, to reduce or eliminate this volume change. We did not do the cell culture experiments described above over the entire growth phase because it was not our main objective here. This aspect will certainly be studied in the future.

CONCLUSION

The engineered glutamine-binding protein (QBP) and glucose-binding protein (GBP) described in this article could accurately and reliably measure their respective ligands. Both proteins have sensitivity in the micromolar ranges. The successful applications of these binding proteins in different scales of fermentation and cell culture suggest that they can be used to measure their respective ligands from micromolar levels to as many orders of magnitude as required. The only requirement is that the sample should be diluted accordingly. An extra benefit from diluting the samples from cell culture or fermentation applications is that the dilution virtually eliminates the interference of the autofluorescence, which is usually a problem for ordinary optical sensors. The sample volume required for the biosensors described here is less than 1 μL; this makes them applicable to microbioreactors and small-scale cell cultures. The small sample volume requirements together with the high sensitivity may allow them to be widely applied in high-throughput bioprocessing.

References

Boos W, Gordon AS. 1971. Transport properties of the galactose-binding protein in *Escherichia coli*. J Biol Chem 246(3):621–628.

Brand K, Fekl W, Hintzenstern J, Langer K, Luppa P, Schoerner C. 1989. Metabolism of glutamine in lymphocytes. Metabolism 38(8), suppl 1:29–33.

Brennan JD, Flora KK, Bendiak GN, Baker GA, Kane MA, Pandey S, Bright FV. 2000. Probing the origins of spectroscopic responses to analyte-induced conformational changes in fluorescently-labeled cod iii parvalbumin. J Phys Chem B 104:10100–10110.

Brune M, Hunter JL, Corrie JET, Webb MR. 1994. Direct, real-time measurement of rapic inorganic phosphate release using a novel fluorescent probe and its application to actomyosin subfragment 1 ATPase. Biochemistry 33:8262–8271.

Dattelbaum JD, Lakowicz JR. 2001. Optical determination of glutamine using a genetically engineered protein. Anal Biochem 291:89–95.

Gilardi G, Mei G, Rosato N, Agro AF, Cass AEG. 1997. Spectroscopic properties of an engineered maltose binding protein. Prot Eng 10(5): 479–486.

Gilardi G, Zhou LQ, Hibbert L, Cass AEG. 1994. Engineering the maltose binding protein for reagentless fluorescence sensing. Anal Chem 66: 3840–3847.

Haughland RP. 1996. Handbook of fluorescent probes and research chemicals. Eugene, OR: Molecular Probes, Inc.

Hellinga HW, Marvin JS. 1998. Protein engineering and the development of generic biosensors. Trends Biotechnol 16:183–189.

Hsiao CD, Sun YJ, Rose J, Wang BC. 1996. The crystal structure of glutamine binding protein from *Escherichia coli*. J Mol Biol 262: 225–242.

Marvin JS, Hellinga HW. 1998. Engineering biosensors by introducing fluorescent allosteric signal transducer: Construction of a novel glucose sensor. J Am Chem Soc 120:7–11.

Quiocho FA. 1990. Atomic structure of periplasmic binding proteins and the high-affinity active transport systems in bacteria. Phil Trans Roy Soc London, ser B 326:341–351.

Salins LLE, Ware RA, Ensor CM, Daunert S. 2001. A novel reagentless sensing system for measuring glucose based on the glucose/galactose-binding protein. Anal Biochem 294:19–26.

Sohanpal K, Watsuji T, Zhou LQ, Cass AEG. 1993. Reagentless fluorescence sensors based upon specific binding proteins. Sensors Actuators B 11:547–552.

Sun YJ, Rose J, Wang BC, Hsiao CD. 1998. The structure of glutamine binding protein complexed with glutamine at 1.94A resolution: Comparisons with other amino acid binding proteins. J Mol Biol 278:219–229.

Tolosa L, Ge X, Rao G. 2003. Reagentless optical screening of glutamine using fdual-emitting glutamine-bending protein. Anal Biochem 314: 199–205.

Tolosa L, Gryczynski I, Eichhorn LR, Dattelbaum JD, Castellano FN, Rao G, Lakowicz JR. 1999. Glucose sensor for low-cost lifetime based sensing using a genetically engineered protein. Anal Biochem 267:114–120.

Weiner H, Heppel LAA. 1971. Binding protein for glutamine and its relation to active transport in *Escherichia coli*. J Biol Chem 246(22): 6933–6941.

Wenner BR, Douglass PM, Shrestha S, Sharma BV, Lai S, Madou MJ, Daunert S. 2001. Genetically designed biosensing systems for high-throughput screening of pharmaceuticals, clinical diagnostics, and environmental monitoring. Proc SPIE 4252:59–70.

Zhou LQ, Cass AEG. 1991. Periplasmic binding protein based biosensors 1. Preliminary study of maltose binding protein as sensing element for maltose biosensor. Biosens Bioelectr 6:445–450.

Now that we had shown that the binding proteins could be used in complex fermentation and cell culture media, it was time to tackle measurements that could be done in an automated fashion in bioreactors. Here, we decided that one could use dialysis tubing to get the samples from the bioreactors. One could insert a sterile sample loop into a bioreactor and simply rely on glucose diffusion from the medium into the carrier buffer in the loop (Figure 1). The surface area and length of the loop became additional variables that could be optimized in addition to the loop's membrane thickness. Essentially, the sensor relied on glucose mass transfer into the lumen of the sampling membrane.

Xudong's excellent modeling skills guided us in this effort and all of Leah's careful development of the sensor paid off and as the data in Figure 8 show, we were able to demonstrate real time glucose sensing in a minibioreactor culture. The approach is completely generic and applicable to any cell culture system. Furthermore, multiple analytes can be targeted. Of course, this is not new in the sense that flow injection analysis has been around for a while, but the use of a highly sensitive sensor means that as in the previous paper, very low analyte concentrations can be measured.

Biotechnol. Prog. **2008,** *24,* 691–697

On the Possibility of Real-Time Monitoring of Glucose in Cell Culture by Microdialysis Using a Fluorescent Glucose Binding Protein Sensor

Xudong Ge, Govind Rao, and Leah Tolosa*

Center for Advanced Sensor Technology, Department of Chemical and Biochemical Engineering, University of Maryland Baltimore County, 1000 Hilltop Circle, Baltimore, Maryland 21250

Although glucose sensors with millimolar sensitivity are still the norm, there is now a developing interest in glucose sensors with micromolar sensitivity for applications in minimally invasive sampling techniques such as fast microdialysis and extraction of interstitial fluid by iontophoresis and laser poration. In this regard, the glucose binding protein (GBP) with a binding constant for glucose in the micromolar range is of particular relevance. GBP is one of the soluble binding proteins found in the periplasmic space of Gram-negative bacteria. Because of its hinge-like tertiary structure, glucose binding induces a large conformational change, which can be used for glucose sensing by attaching a polarity sensitive fluorescent probe to a site on the protein that is allosterically responsive to glucose binding. Correspondingly, the resulting optical biosensor has micromolar sensitivity to glucose. Because binding is reversible, the biosensor is reusable and can be stored at 4 °C for 6 months without losing its sensitivity. In this paper, we show the feasibility of using the GBP biosensor to monitor glucose in microdialysis. The effect of perfusion rate, bulk glucose concentration and temperature on microdialysis efficiency was determined. Additionally, the glucose concentrations in mammalian cell culture were monitored to demonstrate the applicability of this sensor in complex and dynamic processes over a period of time. As the sensor is sensitive to micromolar glucose, high dialysis efficiency is not required when the bulk glucose concentration is within the millimolar physiological range. Thus, a perfusion rate of 10 μL/min or faster can be used, resulting in delay times of 1 min or less.

Introduction

Glucose monitoring is very important in bioprocesses such as fermentation and mammalian cell culture. As glucose is the major energy source for cells, optimal glucose concentrations are crucial in healthy cell growth and efficient product yield. In addition, glucose analysis is of importance as a clinical indicator of diabetes. Because the glucose concentration in cell culture media and human blood is in the millimolar range, currently available glucose sensors predictably have millimolar sensitivities. Most of these glucose sensors utilize glucose oxidase as the biological element. In this design, the enzyme is immobilized in a polymer or a porous membrane (*1*−*11*) in close contact with a polarized electrode. When exposed to glucose, the enzyme converts glucose into gluconolactone and hydrogen peroxide, which is then detected by the electrode. Another protein that has been investigated as a possible glucose sensor is concanavalin A (*12*−*15*). This sensor utilizes the competition between glucose and a sugar-containing macromolecule like dextran for binding to the ConA. In addition, D'Auria et al. used coenzyme-depleted enzymes labeled with ANS as the signal transducers (*16*−*18*).

With advancements in diabetes research, it became apparent that continuous monitoring of blood glucose levels is far superior to the intermittent testing from finger pricks that is now accepted practice. Additionally, relatively painless and minimally invasive sampling promotes patient compliance. Thus, novel sampling techniques such as fast microdialysis (*19*), extraction of interstitial fluid by iontophoresis (*20*) and laser poration (*21*, *22*) have emerged in recent years. However, these technologies have inherent barriers that do not allow full extraction of glucose from blood and tissue. For example, to achieve millimolar concentrations of glucose in microdialysis, the dimensions of the probe should be large, which may not be practical for a subcutaneous device. Alternatively, the perfusion rate should be slow which can result in a long lag time. In iontophoresis, the skin itself acts as a barrier when the weak electromotive force is applied to extract glucose from the interstitial fluid. Consequently, it has become necessary to develop new glucose sensors with submillimolar glucose sensitivities.

In the search for glucose sensors with submillimolar sensitivities, ligand-specific periplasmic binding proteins have drawn much attention (*23*−*38*). These binding proteins have a two-domain structure connected by a hinge (*39*). The binding of the ligand at the binding site close to the hinge can induce a large conformational change from an "open" ligand-free structure to a "closed" ligand-bound structure (*40*, *41*). By introducing a polarity-sensitive fluorophore into such a protein, the conformational change in response to ligand binding can be indirectly detected. The result is an optical biosensor that responds in submillimolar concentrations of the ligand (*42*). Many of the papers on the binding proteins have focused on the construction of the biosensors such as the introduction of the mutation, the expression and purification of the protein and labeling of the protein with fluorescent probes. Little has been written on the useful characteristics of such sensors and none on their application in conjunction with novel sampling techniques.

* To whom correspondence should be addressed. Tel: 410-455-3432. Fax: 410-455-6500. E-mail: leah@umbc.edu.

10.1021/bp070411k CCC: $40.75
Published on Web 04/19/2008

The construction and fluorescent labeling of this biosensor has been described previously (*36*, *37*). Monitoring of glucose consumption in cell culture and fermentation through direct assay of the media was shown to be feasible in both large (hundreds of mL) and small (hundreds of μL) culture volumes (*34*). The small cultures in particular are impossible to monitor for glucose concentration using the gold standard glucose oxidase electrodes. We have shown that the micromolar sensitivity and submicromolar limit of detection of the GBP biosensor allowed for dilution of minute volumes of the cell culture media to within the analytical range of GBP. On the basis of this result, we concluded that any sampling technique that inherently dilutes the sample from millimolar to micromolar glucose will work appropriately with the sensor. In this paper, the characteristics of the GBP-based glucose biosensor and its application in fast microdialysis for bioprocess monitoring are investigated. The sensor characteristics including sensitivity, stability, accuracy, reversibility, selectivity and temperature sensitivity were scrutinized further. Additionally, the effects of bulk glucose in the media, perfusion flow rates and temperature on dialysis efficiency were studied.

Materials and Methods

Materials. 6-Acryloyl-2-dimethylaminonaphthalene (acrylodan) and tris(2-carboxyethyl) phosphine (TCEP) were purchased from Invitrogen. Fructose, fucose, galactose, glucose, maltose, mannose, sucrose, DEAE Sephadex A-50, *N*,*N*-dimethylformamide (DMF), NaCl, KH_2PO_4, Na_2HPO_4, NaH_2PO_4, and $MgCl_2$ were purchased from Sigma-Aldrich (St. Louis, MO). Tryptone and yeast extract were obtained from Becton Dickinson (Sparks, MD). All chemicals were used without further purification. Snakeskin pleated dialysis tubing (10 K MWCO) was purchased from PIERCE (Rockford, IL).

GBP Expression, Purification and Fluorophore Coupling. The preparation of the engineered protein and the labeling of the fluorescent probe have been described previously (*30*, *34*−*37*). The plasmid expressing the wild-type GBP was constructed by cloning the *E. coli* K12 MglB gene into vector pTZ18U. The single-cysteine mutation at position 255 was introduced by using the Quick-Change mutagenesis kit from Stratagene (Cedar Creek, TX). The mutated plasmid was then transformed into *E. coli* NM303. The protein was overexpressed by growing the cells in LB media overnight. The cells were then collected by centrifugation and the periplasmic binding protein was released by osmotic shock method (*23*). After the protein was purified on a DEAE Sephadex A-50 column, the protein was labeled with acrylodan by reacting with 10- to 20-fold dye at pH 7.5 for 2 h at room temperature or overnight at 4 °C in the presence of 10-fold TCEP. Unreacted acrylodan was removed by passing through a Sephadex G-25 column. The total protein concentration was determined and the labeling efficiency was estimated from the total protein concentration and the concentration of protein-bound probe, which was calculated from its absorbance and extinction coefficient (*43*). The final product was 0.2 μm filter-sterilized. The filtered protein can be stored at 4 °C for over 6 months without losing its sensitivity (*34*).

Experimental Setup. The experimental setup for microdialysis of buffer solutions and mammalian cell culture is shown in Figure 1. The minibioreactor was produced by Fluorometrix (Stowe, MA). The bioreactor has a volume of 40 mL and has disposable pH and oxygen-sensing patches attached to the bottom for pH and dissolved oxygen monitoring (*44*). It is capable of temperature control. The agitation speed can be adjusted smoothly from 0 to 1000 rpm. The microinjector and

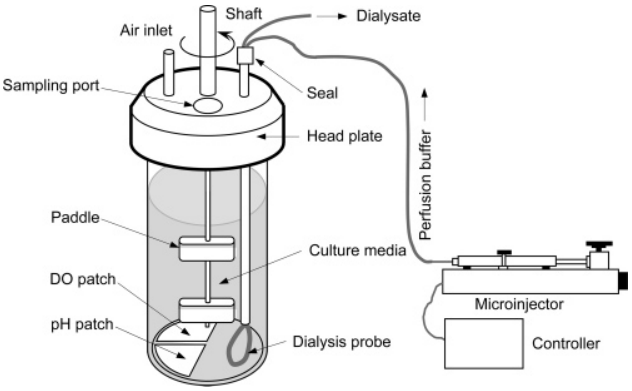

Figure 1. Experimental setup for mammalian cell culture and microdialysis.

controller (Bioanalytical Systems, West Lafayette, IN) is connected through plastic tubing to the dialysis probe (MWCO 10 000), which is immersed in the buffer solution or cell medium. The glucose concentration in the dialysate and the dialysis efficiency were determined as a function of the glucose concentration in the medium, the flowrate of the perfusion buffer, and temperature. In the buffer experiments, the flowrate was adjusted stepwise from 0.1 to 100 μL/min.

Mammalian Cell Culture. A SP2/0 based myeloma/mouse hybridoma cell line (2055.5) secreting an IgG3 antibody specific for the *Neisseria meningitides* capsular-polysaccharide (MCPS) (Rubinstein and Stein, 1988) was maintained in a 250-mL spinner flask (Kontes, Vineland, NJ) in CD Hybridoma protein-free media (Gibco Brand, Carlsbad, CA) supplemented with 2 mM glutamine (HyClone, Laboratories Inc., Logan, UT), 100 U/mL penicillin (HyClone), 100 g/mL streptomycin (HyClone), 1 g/L PF-68 (MP Biomedicals, LLC, Aurora, OH), and 3.5×10^{-4}% mercaptoethanol (v/v) (Sigma, St. Louis, MO). The flask was kept in a water-jacketed incubator (Napco, Winchester, VA). Before performing the cell culture in the bioreactor (Figure 1), the air inlet was covered with a 0.22 μm syringe filter (Millex-GV, Millipore, Bedford, MA). The bioreactor except the dialysis probe, which was ethanol sterilized separately, was then steam sterilized at 121 °C for 25 min. Upon cooling, the vessel was first rinsed with media and then filled with 35 mL of cell culture media inoculated with 7.2×10^4 cells/mL in a laminar flow hood. The process was monitored by DO and pH sensors. The temperature and agitation speed was controlled at 37 °C and 100 rpm. The vessel headspace was open to the atmosphere via the 0.22 μm syringe filter. Dialysate samples were taken twice a day for glucose measurement using a 10 μL/min perfusion rate. Culture samples were withdrawn twice a day with syringes through the sampling port on the vessel for cell counting. Cells in the samples were counted using a hemocytometer.

Fluorescence Measurements. The fluorescence intensity of the labeled protein was measured either in cuvettes on Varian Cary Eclipse fluorescence spectrophotometer (Varian Instruments, Walnut Creek, CA) or in 96-well plates on a SpectraMax M5 plate reader (Molecular Devices, Sunnyvale, CA). To measure the fluorescence intensity in cuvettes, 200 μL of GBP solution was added to a 1.5-mL poly(methylmethacrylate) cuvette (BrandTech Scientific, Essex, CT). After the intensity was measured 10 times, 2.0 μL of glucose standard or sample was added. The mixture was gently vortexed for 10 s, and the intensity was measured again 10 times. The assay was performed in triplicate for each standard or sample. All measurements were made at the same instrumental conditions: excitation wavelength

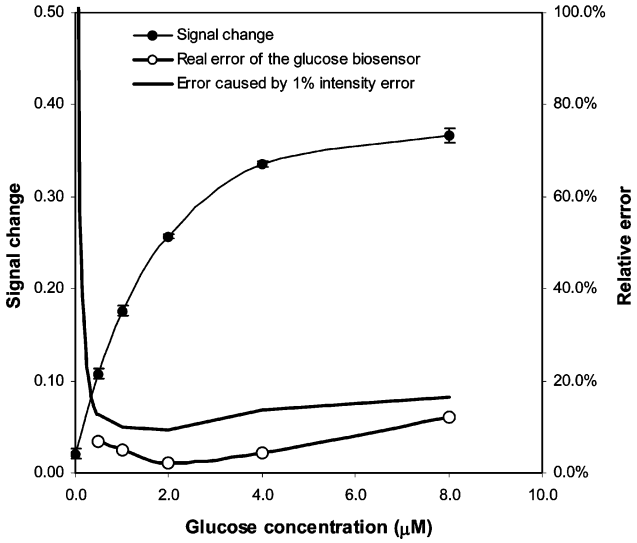

Figure 2. Typical calibration curve and relative measurement error.

380 nm, emission wavelength 510 nm, excitation slit width 5 nm, emission slit width 5 nm, PMT detector voltage 750 V, and average time 0.1 s. To measure the fluorescence intensity in 96-well plates, 200 μL of GBP solution was added to each of the designated wells, and the fluorescence intensities were measured 3 times. Volumes of 2.0 μL of glucose standard or sample were then added to each of the wells. The plate was gently shaken for 10 s, and the intensities were measured 3 times.

Results and Discussion

Characteristics of the GBP-Based Glucose Assay. The engineered glucose binding protein described here has a single cysteine mutation at 255 where a polarity sensitive probe acrylodan is covalently attached. The labeled acrylodan emits strong green fluorescence (510 nm) when excited with violet light (380 nm). In the presence of glucose, the fluorescence intensity of acrylodan decreases with glucose concentration. A typical calibration curve of the glucose biosensor is shown in Figure 2. It can be seen that the calibration curve is almost linear at low glucose concentrations but gradually saturates at higher glucose concentration. The thick black line with circles shows the average relative error of the biosensor at different glucose concentrations. The average relative error is defined as

$$\text{error (\%)} = \frac{\Delta G}{\overline{G}} \times 100 \qquad (1)$$

where ΔG is the standard deviation of the measured glucose concentrations, and $\overline{G}$ is the average of the measured glucose concentrations. Obviously, the average relative error reaches its minimum, which is 2.1%, at glucose concentration of 2.0 μM. If the slope of the calibration curve in Figure 2 is defined as the sensitivity of the assay, the standard deviation of the measured glucose concentrations in eq 1 is then equal to

$$\Delta G = \frac{\Delta S}{m} \qquad (2)$$

where ΔS is the standard deviation of the measured signal changes, and m is the sensitivity of the assay at measured glucose concentration. Substitution of eq 2 into eq 1 gives

$$\text{error (\%)} = \frac{\Delta S}{m\overline{G}} \times 100 \qquad (3)$$

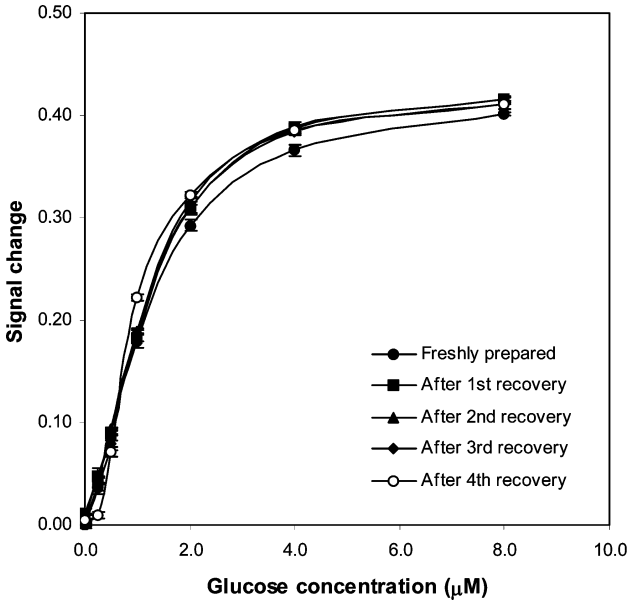

Figure 3. Reusability of the labeled glucose binding protein.

It can be seen that the average relative error of the measured glucose concentrations is proportional to the standard deviation of the measured signal changes and inversely proportional to the measured glucose concentration and the sensitivity of the assay at that concentration. At low glucose concentrations, the average relative error is higher because $\overline{G}$ is small although the sensitivity of the assay, m, is high. On the other hand, the average relative error is also higher at high glucose concentrations because of low sensitivity. At medium glucose concentrations, the two factors offset somewhat and the average relative error of the measured glucose concentrations is lower. The thick black line without symbols gives the average relative error of the measured glucose concentrations caused by 1% standard deviation of fluorescence intensity measurements. It can be seen that 1% intensity measurement error can cause a relative error of 10% or higher for glucose concentrations. This means that it is very critical to accurately measure the fluorescence intensity. One way to effectively decrease the errors is to read the fluorescence intensity many times and then average the data (*38*). Accordingly, averaging reduces the lower limit of detection (*45*) up to 5 times depending on how many measurements are averaged.

As shown in Figure 2, the biosensor has micromolar sensitivity for glucose. Although the detection range can be broadened by increasing the concentration of the GBP as previously described (*34*−*38*), it cannot be easily extended to measure millimolar glucose solely by increasing the GBP concentration because of the concentration limit. Therefore, physiological concentrations of glucose, which are in the millimolar range, require a dilution step prior to measurement with this biosensor. Alternatively, sampling techniques that inherently dilutes the sample such as microdialysis and iontophoresis are especially applicable. In clinical diagnostics applications, these techniques generally sample the interstitial fluid rather than venous blood. Although the glucose concentration in interstitial fluid is similar to blood, when extracted by iontophoresis the concentration is reduced to 0−30 μM (*20*). Note that these concentrations fit the responsive range of the glucose sensor discussed here. In the case of microdialysis, the concentration of glucose in the dialysate depends on the dimensions of the microdialysis membrane, properties of the membrane material, the perfusion flow rate and the temperature. However, in general, practical

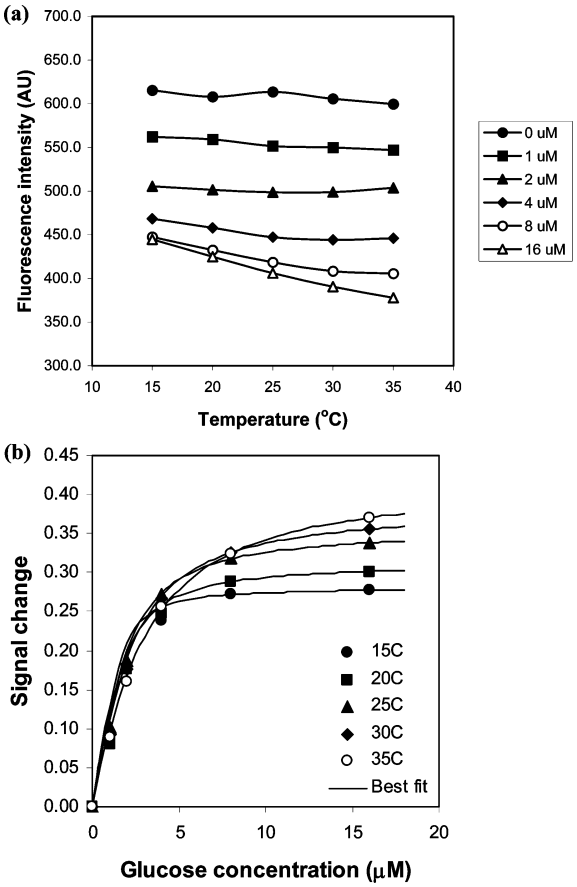

Figure 4. Change of the fluorescence intensity with temperature at different glucose concentrations (a) and the best fits to the calibration data at different temperatures (b).

considerations give rise to submillimolar concentrations of glucose in the dialysate. For dialysates at such low glucose levels, the conventional glucose oxidase-based methods are more difficult to implement as these concentrations approach the limit of detection. It is clear that, in contrast, GBP can be used for glucose measurements in these submillimolar concentrations. Nevertheless, some preliminary measurements may be required to determine the proper dilution of the samples and appropriate calculations to determine the concentration of glucose in the original sample.

To check if the labeled GBP is reusable, used GBP was recovered after the assay and its reusability was studied. After the assay, the GBP was no longer responsive to glucose because of the bound glucose. To remove the bound glucose, used GBP solution was injected into a dialysis bag, which was then dialyzed in PBS buffer at 4 °C for 2 h. After that, the PBS buffer was replaced with fresh buffer and the GBP solution was dialyzed for another 2 h. After that, 99.99% of the bound glucose was removed from the GBP solution. The GBP solution could then be transferred from the dialysis bag to a sterile plastic tube for tests. Results show that the calibration curves do not change significantly after several recoveries (Figure 3). These experiments prove that should the protein sensor be immobilized on a solid surface, it will result in a reversible and reusable sensor.

For any analytical method, it is very important to study what factors affect the measurements and, thus, should be controlled or set. For the GBP glucose biosensor, the temperature is a very important factor because it affects both the fluorescence as well as the protein structural dynamics. Figure 4a shows the changes in fluorescence intensity of the labeled GBP with temperature at different glucose concentrations. As expected, the fluorescence intensity of the labeled protein decreases with temperature. The data in Figure 4a can be re-plotted to get Figure 4b. The apparent binding constants could be calculated by fitting the experimental results to the binding isotherm:

$$\Delta F = \frac{\Delta F_{\max} G}{K_d + G} \tag{4}$$

where ΔF is the normalized signal change at any glucose concentration, $\Delta F_{\max}$ is the normalized signal change at saturating glucose concentration, K_d is the apparent binding constant, and G is the glucose concentration in free state. The symbols in Figure 4b represent the experimental data and the lines are the best nonlinear fit to eq 4. The results for $\Delta F_{\max}$ and K_d at different temperatures are listed in Table 1. Further analysis of this data was not done to determine the contributions of nonradiative deactivation of the fluorophore and fluctuations in the protein structure to the observed decrease in intensity. Nevertheless, it is clear that temperature control is absolutely imperative in using this biosensor.

Figure 5 shows the calibration curves for glucose and five other sugars. It can be seen that in addition to glucose the GBP biosensor also responds to galactose although to a lesser extent. The GBP biosensor is significantly less sensitive to other sugars, although they show some minor effects at these concentrations. It should be noted that culture media, blood and interstitial fluid usually have negligible amounts of these other sugars in comparison to glucose. Exceptions are patients with galactosemia and some newborns, whose blood contains elevated galactose (6−10 mg/dL).

Microdialysis. Figure 6a shows the relationship between the dialysis efficiency (E) and the perfusion rate at two different temperatures. The dialysis efficiency is defined as

$$E = \frac{C}{C_b} \times 100\% \tag{5}$$

where C is the glucose concentration in the dialysate, and C_b is the glucose concentration in the media. It can be seen that the glucose concentration in the media has no effect on the dialysis efficiency but temperature and perfusion flow rate have a great effect.

Suppose that the glucose concentration in the bioreactor is well-mixed and the perfusion buffer in the dialysis probe is a plug flow, then the mass balance for the glucose diffusing across the probe membrane yields the flowing equation:

$$\upsilon dC = k2\pi r dx(C_b - C) \tag{6}$$

where C is the glucose concentration in the perfusion buffer at position x, k is mass transfer coefficient, r is the radius of the dialysis probe, and υ is the perfusion rate. Integration of eq 6 gives

$$\ln(1 - E) = -\frac{2\pi rkL}{\upsilon} \tag{7}$$

where L is the length of the dialysis probe. Figure 6b shows that the glucose concentration in the dialysate agrees very well with eq 7.

Figure 7 shows the delay time and dialysis efficiency at different perfusion rates. The delay time is defined as the time needed for the perfusion buffer to flow from the dialysis probe to the collection tube. Both delay time and dialysis efficiency change inversely with the perfusion rate. Because the GBP

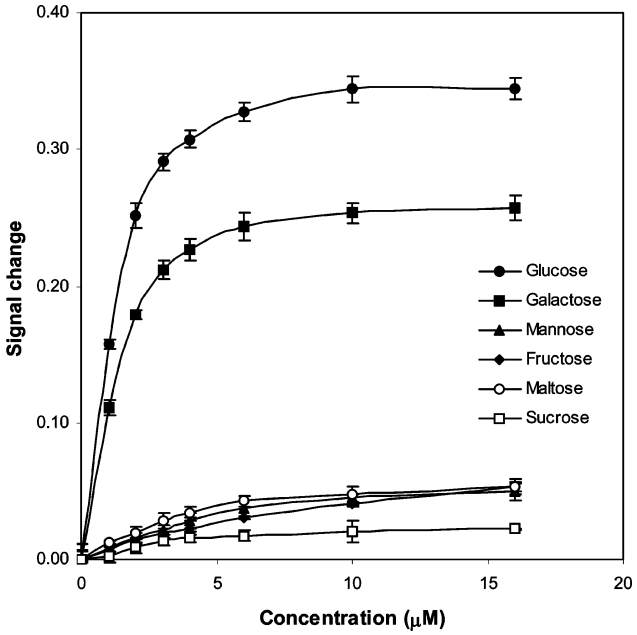

Figure 5. Sensitivity of the labeled GBP to different sugars.

Table 1. Best Nonlinear Fit Results of Maximum Signal Changes (ΔF_{max}) and Apparent Binding Constants (K_d) at Different Temperatures

temp, °C	ΔF_{max}	K_d, μM
15	0.282 ± 0.002	0.25 ± 0.06
20	0.313 ± 0.002	0.56 ± 0.07
25	0.357 ± 0.001	0.82 ± 0.04
30	0.385 ± 0.002	1.20 ± 0.06
35	0.421 ± 0.002	1.99 ± 0.06

biosensor is sensitive at very low concentrations, high dialysis efficiency (i.e., approaching 100%) is not required. In fact, at a limit of detection (LOD) of 0.04 μM (*38*), a dialysis efficiency of 0.02% will provide glucose concentrations that are about 100X the LOD. The commercially available microdialysis system used in this study even at the fastest perfusion rate is still too efficient. Thus, future work will require adjustment of the microdialysis conditions to decrease efficiency by either decreasing the dimensions of the probe or fabricating new material for the microdialysis membrane. Nevertheless, in the mammalian cell culture experiments, though not ideal, a perfusion rate of 10 μL/min was selected. Accordingly, collection of the dialysate and further dilution to within the sensitivity range of the GBP sensor was required. Even at this rate, the delay time is less than 1 min. Other glucose analysis methods that require high dialysis efficiencies are reported to have a lag time of 30−35 min. Thus, with further optimization our method can approach real time monitoring of glucose.

At 10 μL/min perfusion rate, the dialysis efficiency is about 5%. Thus, if 100 μL of dialysate is collected each time, the glucose concentration in the bioreactor decreases by only 0.14% because of the dialysis. Therefore, the effect of dialysis itself on the glucose concentration in the bioreactor is negligible.

Mammalian Cell Culture. A SP2/0 based myeloma/mouse hybridoma cell line was grown in the bioreactor shown in Figure 1 at 37 °C and 100 rpm. The pH and dissolved oxygen concentration were monitored by disposable sensing patches. The cell density reached its maximum at about 100 h and then declined rapidly (Figure 8). As the cells grew and consumed more oxygen before reaching the highest cell density, the dissolved oxygen gradually declined from 100% air saturation to 76% and then recovered rapidly to 100% at the end of the culture process due to the death of the cells. As the seed culture was originally maintained in 5% CO_2, pH quickly increased at the beginning of the culture process due to the loss of the dissolved CO_2 from the culture.

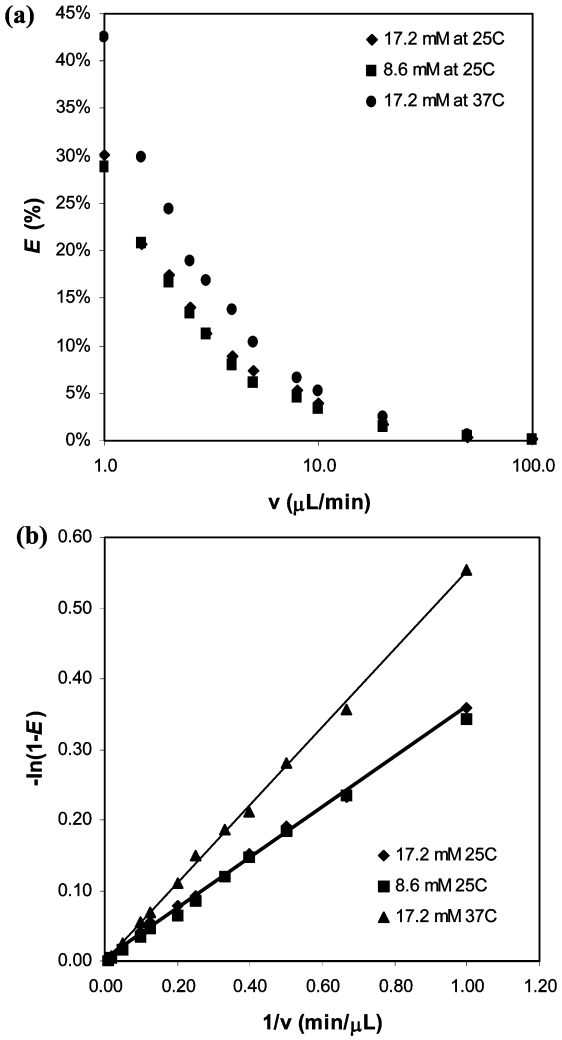

Figure 6. Relation between dialysis efficiency and bulk glucose concentration, perfusion rate, and temperature.

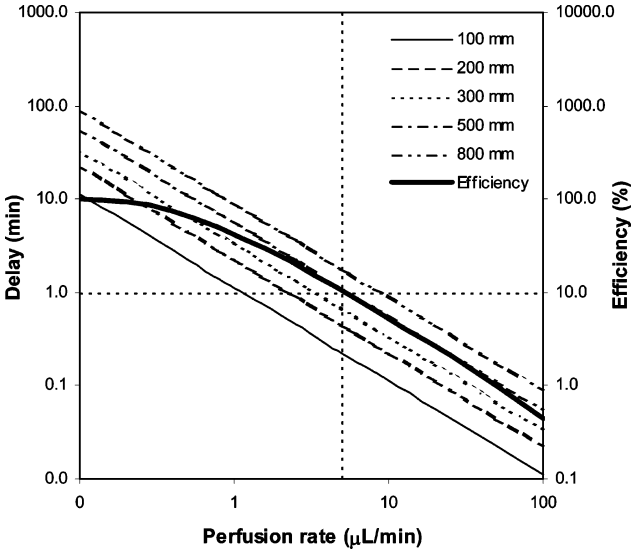

Figure 7. Delay time and dialysis efficiency at different perfusion rates.

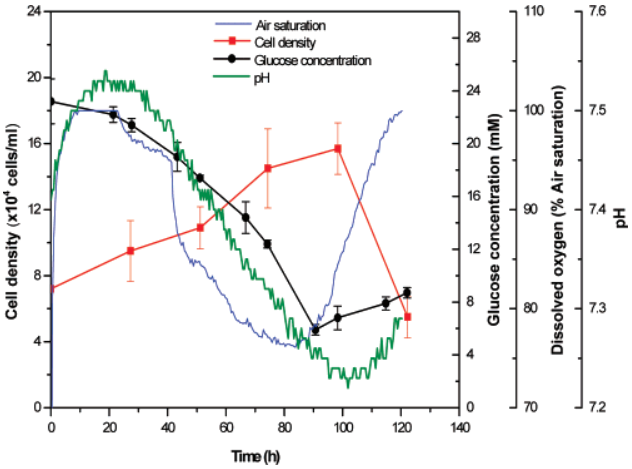

Figure 8. Glucose concentration, DO, pH, and cell density profiles in mammalian cell culture.

Although the glucose concentration in the dialysate agrees very well with eq 5, the mass transfer coefficient k can be affected by many factors such as temperature, the viscosity of the media, stirring speed, etc. Additionally, the presence of cells or macromolecules in the media may also affect the dialysis efficiency as some of the pores in the dialysis probe may be blocked by the cells or macromolecules. In this study, the beginning dialysis efficiency was determined by the glucose concentrations in the beginning culture and the first dialysis sample taken immediately after the start of the cell culture. The ending dialysis efficiency was determined by the glucose concentrations in the final culture and the last dialysis sample taken immediately before the end of the culture. The beginning dialysis efficiency is higher than the ending dialysis efficiency, showing that some of the pores were blocked during the cell culture. Assuming a linear decline for the dialysis efficiency, the glucose concentrations in the culture were calculated and shown in Figure 8. Results show that the glucose concentration decreased as the cells grew and consumed glucose. At the late stage of the cell culture, the glucose concentration gradually increased. As the cells begin to lose viability, they undergo lysis thereby discharging their contents into the surrounding medium.

Conclusion

We have shown that the fluorescent GBP is a potential sensor for real-time monitoring of glucose in cell culture using microdialysis. The submicromolar limit of detection of GBP allows for minimal microdialysis efficiency. Thus, the fast perfusion flow rates utilized in this work resulted in time lags of about 1 min. Less sensitive sensors like those using glucose oxidase require slower flow rates, resulting in much longer time lags. Nonetheless, flow rates beyond the capability of the microdialysis device used here (>100 μL/min) should provide glucose levels well above the limit of detection of GBP. Thus, further work is needed to customize either the dimensions of the microdialysis probe or the material of the semipermeable membrane to allow for lower glucose concentrations in the dialysate while approaching real-time monitoring. Additionally, material that will resist cell-adhesion and biofouling will be investigated.

Acknowledgment

The authors acknowledge the support of the National Institutes of Health through grants DK062990 and DK072465 and the U.S. Army Medical Research and Materiel Command through grant W81XWH-04-1-0781. The *E. coli* NM303 was from cultures originally provided by Dr. W. Boos, University Konstanz, Germany.

References and Notes

(1) Campuzano, S.; Gálvez, R.; Pedrero, M.; Manuel de Villena, F J.; Pingarrón, J M. Preparation, Characterization and Application of Alkanethiol Self-Assembled Monolayers Modified with Tetrathiafulvalene and Glucose Oxidase at a Gold Disk Electrode. *J. Electroanal. Chem.* **2002**, *526*, 92−100.

(2) Chen, T.; Friedman, K. A.; Lei, I.; Heller, A. In Situ Assembled Mass-Transport Controlling Micromembranes and Their Application in Implanted Amperometric Glucose Sensors. *Anal. Chem.* **2000**, *72*, 3757−3763.

(3) Gouda, M. D.; Kumar, M. A.; Thakur, M. S.; Karanth, N. G. Enhancement of Operational Stability of an Enzyme Biosensor for Glucose and Sucrose Using Protein Based Stablizing Agents. *Biosens. Bioelectron.* **2002**, *7*, 503−507.

(4) Haouz, A.; Stieg, S. Continuous Monitoring of D-Glucose and L-lactate by Flow Injection Analysis. *Enzyme Microb. Technol.* **2002**, *30*, 129−133.

(5) Miscoria, S. A.; Desbrieres, J.; Barrera, G. D.; Labbé, P.; Rivas, G. A. Glucose Biosensor Based on the Layer-by-Layer Self-Assembling of Glucose Oxidase and Chitosan Derivatives on a Thiolated Gold Surface. *Anal. Chim. Acta* **2006**, *578* (2), 137−144.

(6) Mignani, A.; Scavetta, E.; Tonelli, D. Electrodeposited Glucose Oxidase/Anionic Clay for Glucose Biosensors Design. *Anal. Chim. Acta* **2006**, *577* (1), 98−106.

(7) Endo, H.; Yonemori, Y.; Musiya, K.; Maita, M.; Shibuya, T.; Ren, H.; Hayashi, T.; Mitsubayashi, K. A Needle-Type Optical Enzyme Sensor System for Determining Glucose Levels in Fish Blood. *Anal. Chim. Acta* **2006**, *573*−*574*, 117−124.

(8) Kang, X.; Mai, Z.; Zou, X.; Cai, P.; Mo, J. A Novel Glucose Biosensor Based on Immobilization of Glucose Oxidase in Chitosan on a Glassy Carbon Electrode Modified with Gold-Platinum Alloy Nanoparticles/Multiwall Carbon Nanotubes. *Anal. Biochem.* **2007**, *369* (1), 71−79.

(9) Dai, Z.; Fang, M.; Bao, J.; Wang, H.; Lu, T. An Amperometric Glucose Biosensor Constructed by Immobilizing Glucose Oxidase on Titanium-Containing Mesoporous Composite Material of no. 41 Modified Screen-Printed Electrodes. *Anal Chim Acta* **2007**, *591* (2), 195−199.

(10) Ekanayake, E. M.; Preethichandra, D. M.; Kaneto, K. Polypyrrole Nanotube Array Sensor for Enhanced Adsorption of Glucose Oxidase in Glucose Biosensors. *Biosens. Bioelectron.* **2007**, *23* (1), 107−113.

(11) Henninger, N.; Woderer, S.; Kloetzer, H. M.; Staib, A.; Gillen, R.; Li, L.; Yu, X.; Gretz, N.; Kraenzlin, B.; Pill, J. Tissue Response to Subcutaneous Implantation of Glucose-Oxidase-Based Glucose Sensors in Rats. *Biosens. Bioelectron.* **2007**, *23* (1), 26−34.

(12) Ballerstadt, R.; Schultz, J. S. A Fluorescence Affinity Hollow Fiber Sensor for Continuous Transdermal Glucose Monitoring. *Anal. Chem.* **2000**, *72*, 4185−4192.

(13) Meadows, D. L.; Schultz, J. S. Design, Manufacture and Characterization of an Optical Fiber Glucose Affinity Sensor Based on an Homogeneous Fluorescence Energy Transfer Assay System. *Anal. Chim. Acta* **1993**, *280*, 21−30.

(14) McCartney, L. J.; Pickup, J. C.; Rolinski, O. J.; Birch, D. J. S. Near-Infrared Fluorescence Lifetime Assay for Serum Glucose Based on Allophycocyanin-Labeled Concanavalin A. *Anal. Biochem.* **2001**, *292* (2), 216−221.

(15) Russell, R. J.; Pishko, M. V. A Fluorescence-Based Glucose Biosensor Using Concanavalin A and Dextran Encapsulated in a Poly(ethylene glycol) Hydrogel. *Anal. Chem.* **1999**, *71*, 3126−3132.

(16) D'Auria, S.; Di Cesare, N.; Gryczniski, Z.; Gryczniski, I.; Rossi, M.; Lakowicz, J. R. A Thermophilic Apo-Glucose Dehydrogenase as Non-Consuming Glucose Sensor. *Biochem. Biophys. Res. Commun.* **2000**, *274*, 727−731.

(17) D'Auria, S.; Herman, P.; Rossi, M.; Lakowicz, J. R. The Fluorescence Emission of Apo-Glucose Oxidase from Aspergillus Niger as Probe to Estimate Glucose Concentrations. *Biochem. Biophys. Res. Commun.* **1999**, *263*, 550−553.

(18) D'Auria, S.; Lakowicz, J. R. Enzyme Fluorescence as a Sensing Tool: New Perspectives in Biotechnology. *Curr. Opin. Biotechnol.* **2001**, *12*, 99−104.
(19) Heinemann, L. Continuous Glucose Monitoring by Means of the Microdialysis Technique: Underlying Fundermental Aspects. *Diabetes Technol. Ther.* **2003**, *5* (4), 545−561.
(20) Sieg, A.; Guy, R. H.; Delgado-Charro, M. B. Noninvasive Glucose Monitoring by Reverse Iontophoresis in Vivo: Application of the Internal Standard Concept. *Clin. Chem.* **2004**, *50* (8), 1383−1390.
(21) Gebhart, S.; Faupel, M. D.; Fowler, R.; Kapsner, C.; Lincoln, D.; Mcgee, V.; Pasqua, J.; Steed, L.; Steed, M.; Wangsness, M.; Xu, F.; Vanstory, M.; Burdick, J.; Chase, B. A.; Faupel, M.; Schultz, B.; Gebhart, S. Real-Time Glucose Sensing using Transdermal Fluid under Continuous Vacuum Pressure in Children with Type 1 Diabetes. *Diabetes Tech. Therap.* **2003**, *5*, 159−166.
(22) Burdick, J.; Chase, B. A.; Faupel, M.; Schultz, B.; Gebhart, S. Real-Time Glucose Sensing using Transdermal Fluid under Continuous Vacuum Pressure in Children with Type 1 Diabetes. *Diabetes Tech. Therap.* **2005**, *7*, 448−455.
(23) Dattelbaum, J. D.; Lakowicz, J. R. Optical Determination of Glutamine Using a Genetically Engineered Protein. *Anal. Biochem.* **2001**, *291*, 89−95.
(24) Gilardi, G.; Mei, G.; Rosato, N.; Agro, A. F.; Cass, A. E. G. Spectroscopic Properties of an Engineered Maltose Binding Protein. *Protein Eng.* **1997**, *10* (5), 479−486.
(25) Gilardi, G.; Zhou, L. Q.; Hibbert, L.; Cass, A. E. G. Engineering the Maltose Binding Protein for Reagentless Fluorescence Sensing. *Anal. Chem.* **1994**, *66*, 3840−3847.
(26) Kubo, I. Potentiometric Phosphate-Sensing System Utilizing Phosphate-Binding Protein. *Anal. Bioanal. Chem.* **2002**, *372*, 273−275.
(27) Marvin, J. S.; Hellinga, H. W. Engineering Biosensors by Introducing Fluorescent Allosteric Signal Transducers: Construction of a Novel Glucose Sensor. *J. Am. Chem. Soc.* **1998**, *120*, 7−11.
(28) Naal, Z.; Park, J. H.; Bernhard, S.; Shapleigh, J. P.; Batt, C. A.; Abruna, H. D. Amperometric TNT Biosensor Based on the Oriented Immobilization of a Nitroreductase Maltose Binding Protein Fusion. *Anal. Chem.* **2002**, *74*, 140−148.
(29) Salins, L. L. E.; Ware, R. A.; Ensor, C. M.; Daunert, S. A Novel Reagentless Sensing System for Measuring Glucose Based on the Galactose/Glucose-Binding Protein. *Anal. Chem.* **2001**, *294*, 19−26.
(30) Tolosa, L.; Gryczynski, I.; Eichhorn, L. R.; Dattelbaum, J. D.; Castellano, F. N.; Rao, G.; Lakowicz, J. R. Glucose Sensor for Low-Cost Lifetime Based Sensing Using a Genetically Engineered Protein. *Anal. Biochem.* **1999**, *267*, 114−120.
(31) Tian, Y.; Cuneo, M. J.; Changela, A.; Hocker, B.; Beese, L. S.; Hellinga, H. W. Structure-Based Design of Robust Glucose Biosensors using a Thermotoga maritima Periplasmic Glucose-Binding Protein. *Protein Sci.* **2007**, *16* (10), 2240−2250.
(32) Cuneo, M. J.; Changela, A.; Warren, J. J.; Beese, L. S.; Hellinga, H. W. The Crystal Structure of a Thermophilic Glucose Binding Protein Reveals Adaptations That Interconvert Mono and Disaccharide Binding Sites. *J. Mol. Biol.* **2006**, *362* (2), 259−270.
(33) Ye, K.; Schultz, J. S. Genetic Engineering of an Allosterically Based Glucose Indicator Protein for Continuous Glucose Monitoring by Fluorescence Resonance Energy Transfer. *Anal. Chem.* **2003**, *75*, 3451−3459.
(34) Ge, X.; Tolosa, L.; Simpson, J.; Rao, G. Genetically Engineered Binding Proteins as biosensors for Fermentation and Cell Culture. *Biotechnol. Bioeng.* **2003**, *84* (6), 723−731.
(35) Tolosa, L.; Ge, X.; Rao, G. Reagentless Optical Sensing of Glutamine using a Dual-Emitting Glutamine-Binding Protein. *Anal. Biochem.* **2003**, *314* (2), 199−205.
(36) Ge, X. Development of novel optical sensors for fermentation and cell culture. Ph.D. dissertation. University of Maryland, Baltimore County, 2004.
(37) Ge, X.; Tolosa, L.; Rao, G. Dual-labeled Glucose Binding Protein for Ratiometric Measurements of Glucose. *Anal. Chem.* **2004**, *76* (5), 1403−1410.
(38) Ge, X.; Lam, H.; Modi, S. J.; LaCourse, W. R.; Rao, G.; Tolosa, L. Comparing the Performance of the Optical Glucose Assay Based on the Glucose Binding Protein with High Performance Anion-exchange Chromatography with Pulsed Electrochemical Detection: Efforts to Design a Low-Cost Point-of-Care Glucose Sensor. *J. Diabetes Sci. Technol.* **2007**.
(39) Quiocho, F. A. Atomic Structure of Periplasmic Binding Proteins and the High-Affinity Active Transport Systems in Bacteria. *Philos. Trans. R. Soc. London, Ser. B* **1990**, *326*, 341−351.
(40) Hsiao, C. D.; Sun, Y. J.; Rose, J.; Wang, B. C. The Crystal Structure of Glutamine-binding Protein from Escherichia coli. *J. Mol. Biol.* **1996**, *262*, 225−242.
(41) Sun, Y. J.; Rose, J.; Wang, B. C.; Hsiao, C. D. The Structure of Glutamine-binding Protein Complexed with Glutamine at 1.94 A Resolution: Comparisons with other Amino Acid Binding Proteins. *J. Mol. Biol.* **1998**, *278*, 219−229.
(42) Hellinga, H. W.; Marvin, J. S. Protein Engineering and the Development of Generic Biosensors. *TIBTECH* **1998**, *16*, 183−189.
(43) Haughland, R. P. *Handbook of Fluorescent Probes and Research Chemicals*; Molecular Probes, Inc.: Eugene, OR, 1996.
(44) Ge, X.; Hanson, M.; Kostov, Y.; Moreira, A. R.; Rao, G. Validation of an optical sensor-based high-throughput bioreactor system for mammalian cell culture. *J. Biotechnol.* **2006**, *122* (3), 293−306.
(45) Long, G. L.; Winefordner, J. D. Limit of detection − a closer look at the IUPAC definition. *Anal. Chem.* **1983**, *55* (7), 712A−724A.

Received October 30, 2007. Accepted March 5, 2008.

BP070411K

For CO_2, the problem was more complex. Our initial attempt is shown in the first paper. Clearly, the lifetime-based approach demonstrated worked, but the modulation frequency meant that the instrumentation involved would be expensive.

Therefore, we had to come up with an alternative that would satisfy the demands of bioreactor application (autoclavable, stable) but yet allow for the possibility of low-cost instrumentation. I was lucky to have Qing Chang join the lab as a postdoc. For his Ph.D., Qing had worked on developing optical CO_2 sensors with Andrew Mills. Those were based on absorbance (colorometric) principles and we built on that to make it a fluorescent sensor.

326 *Biotechnol. Prog.* **1998,** *14,* 326–331

Steam-Sterilizable, Fluorescence Lifetime-Based Sensing Film for Dissolved Carbon Dioxide

Qing Chang,[†,‡] Lisa Randers-Eichhorn,[†,‡] Joseph R. Lakowicz,[†,§] and Govind Rao*[,†,‡]

Medical Biotechnology Center, University of Maryland Biotechnology Institute, Second Floor, 725 West Lombard Street, Baltimore, Maryland 21201, Department of Chemical and Biochemical Engineering, University of Maryland Baltimore County, TRC Building, 5200 Westland Boulevard, Baltimore, Maryland 21227, and Center for Fluorescence Spectroscopy, Department of Biochemistry and Molecular Biology, University of Maryland at Baltimore, 725 West Lombard Street, Baltimore, Maryland 21201

An autoclavable sensing film was developed for monitoring dissolved CO_2. The sensing film, based on fluorescence resonance energy transfer (FRET), consisted of a fluorescent donor, an acceptor, and a quaternary ammonium hydroxide, which were doped in a two-component silicone film. As no aqueous solution was used in the sensing film matrix, the sensing film was unaffected by osmotic pressure. Fluorescence lifetime was selected as the sensing parameter, and measured in frequency domain using phase fluorometry. Upon exposure to 20% CO_2-saturated water, a 43° increase in phase angle was observed at 100 MHz. The process was fully reversible when the sensing film was exposed to nitrogen-saturated water. The estimated response and recovery times for 90% signal change were 1 min (for a step change from 0 to 6.7% CO_2-saturated water) and 1.5 min (for a step change from 6.7 to 3.3% CO_2-saturated water). When used for on-line monitoring of dissolved CO_2 produced by a culture of *Escherichia coli*, the sensing film showed a similar trend to that obtained from off-line measurements using a wet chemistry analyzer.

Introduction

There is a great demand for sensors in the field of biotechnology (*1*, *2*). The demand comes from the fact that the success of fermentation is highly dependent on real-time determination of the key analytes, such as glucose, pH, and dissolved O_2 and CO_2, during the process. On-line compositional analysis of fermentation broth is critical for high product yields and helpful for minimizing deleterious metabolic byproducts. To date, electrochemical sensors have been used predominantly as a means of measuring these parameters. However, the lack of autoclavability for many electrochemical sensors prevents their use in situ. As an alternative, optical sensors (*3*−*5*) have been widely studied and developed; these sensors are inexpensive, miniature, robust, easy to fabricate, suitable for simultaneous analysis of multianalytes, and autoclavable in most cases. Among examples of autoclavable optical sensors are fluorescence sensors for sensing dissolved O_2 in bioreactors (*6*, *7*), a fiber-optic pH sensor for fermentation monitoring (*8*), and a fiber-optic CO_2 sensor for beer fermentation monitoring (*9*).

In this paper, we describe an autoclavable fluorescence lifetime-based sensing film capable of on-line fermentation monitoring of dissolved CO_2. The monitoring of carbon dioxide is important in bioprocess development because its elevated presence or absence has been shown to affect cell growth and product formation in prokaryotic and eukaryotic cells alike (*10*−*14*). Recently, Uttamlal and Walt (*9*) have first reported a steam-sterilizable fiber-optic CO_2 sensor for on-line fermentation monitoring, which is based on entrapped fluorophore-buffer solution in a Gore-Tex membrane. Although novel and useful, this sensor, like any other buffer-solution-based sensors, is subject to the osmotic pressure difference between the internal buffer solution and the external sample solution, and therefore needs preconditioning by either storing for several days or autoclaving the sensor for a few cycles in the external solution prior to use. To solve this problem, in our work we adopted another approach to sensing film preparation methodology; that is, the ion-pair indicator technique (*15*−*20*). In this technique, a quaternary ammonium hydroxide is used to not only help dissolve the indicator dye (and other hydrophilic chemical components) into a hydrophobic polymer membrane by the formation of an ion pair between the quaternary ammonium cation and the indicator dye anion, but also to provide in the membrane the initial basic environment that is essential for a CO_2-sensing film to work. This technique results in near solid-state sensing films that exhibit fast response and recovery (typically in seconds, when exposed to gaseous CO_2), and that are insensitive to changes in osmotic pressure. In an earlier study by our group (*20*), we demonstrated that a fluorescence lifetime-based FRET CO_2-sensing film based on ion-pair technique could be used for fermentation off-gas monitoring. The sensing film, however, could not be autoclaved because of the problems of dye leaching out from the polymer matrix, ethyl cellulose, and decomposition of the quaternary ammonium hydroxide, tetraoctylammonium hydroxide, which destroyed the initial basic environment

* Corresponding author: Department of Chemical and Biochemical Engineering. Telephone: (410) 455-3415. Fax: (410) 706-2623. E-mail: grao@umbc.edu.

[†] Medical Biotechnology Center.

[‡] Department of Chemical and Biochemical Engineering.

[§] Center for Fluorescence Spectroscopy.

S8756-7938(97)00119-7 CCC: $15.00
Published on Web 02/18/1998

and left the film permanently insensitive to CO_2. In the present paper, we demonstrate that these problems can be solved by using different polymer matrix and quaternary ammonium hydroxide.

The proposed sensing mechanism (*15*, *16*) for such a CO_2 sensing film can be summarized with following equations:

$$\{Q^+D^-\cdot xH_2O\} + CO_2 \leftrightarrows \{Q^+D^-\cdot xH_2O\cdot CO_2\} \quad (1)$$

$$\{Q^+D^-\cdot xH_2O\cdot CO_2\} \leftrightarrows \{Q^+D^-\cdot (x-1)H_2O\cdot H_2CO_3\} \quad (2)$$

$$\{Q^+D^-\cdot (x-1)H_2O\cdot H_2CO_3\} \leftrightarrows \{Q^+HCO_3^-\cdot (x-1)H_2O\cdot HD\} \quad (3)$$

where, $\{Q^+D^-\cdot xH_2O\}$ represents the quaternary ammonium cation and the indicator dye anion ion pair associated with x water molecules, and $\{Q^+HCO_3^-\cdot(x-1)H_2O\cdot HD\}$ is for the quaternary ammonium cation and the hydrogen carbonate anion ion pair associated with $x-1$ water molecules and the dye in its free acid form, HD. When the indicator used is a colorimetric dye, the change of the dye from its deprotonated form, Q^+D^-, to protonated form, HD, produces a color change, and therefore a change in the absorption spectra. If one of the absorption spectra can overlap with the emission spectrum of a fluorophore added as a fluorescence donor, and if the distance between the molecules of the colorimetric dye and those of the fluorophore meets Förster distance, the fluorescence resonance energy transfer from the fluorescence donor to the colorimetric dye, now called fluorescence acceptor, may occur (*21*). In this way, the spectrum change of the acceptor, which is induced by the presence or absence of CO_2, is reflected in the fluorescence intensity and lifetime change of the donor. Lifetime measurement is preferred because of its unique advantages of being insensitive to signal drift resulting from the variation of light source intensity, instability of the photodetector, and photobleaching of the fluorophore (*22*). In our studies, the lifetime measurements were performed in frequency domain using a light-emitting diode (LED) as the excitation light source.

Materials and Methods

Materials. The *m*-cresol purple (MCP), sulforhodamine 101 hydrate (SR101), silver(I) oxide, cetyltrimethylammonium bromide (CTMABr), hydrogen hexachloroplatinate hydrate, methanol, and chloroform were purchased from Aldrich and used without further purification. Poly(dimethylsiloxane), vinyldimethyl terminated (product no.: PS443) and (30−35%) methylhydro-(65−70%) dimethylsiloxane copolymer (product no. PS123) were obtained from United Chemical Technologies, Inc. (Bristol, PA). Gases (i.e., pure nitrogen and pure carbon dioxide) were from Potomac Airgas (Linthicum, MD). Gas mixtures with certain $\%CO_2$ were obtained by blending the nitrogen with carbon dioxide through two flowmeter tubes (FM4332 and FM4333, Advanced Specialty Gas Equipment Corp., South Plainfield, NJ).

Sensing Film Preparation. The preparation of the sensing film involved three steps: preparing the silicone film, preparing the dye solution, and doping the film with the dye solution. To prepare the silicone film, 0.9 g of PS443 was mixed with 66 mg of hydrogen hexachloroplatinate-saturated PS443 and 43 mg of PS123. After shaking for 10 min, the viscous solution was smeared on a glass microscope slide, and allowed to stand under nitrogen for 1 week. The curing of the polymer typically started in ∼1 h, and finished in 1 week. The resulting film was highly clear and nontacky to touch. Before use, the film was removed with a razor blade from the glass slide, and shaped into the desired size. To prepare the dye solution, a 0.5 M solution of cetyltrimethylammonium hydroxide (CTMAOH) in methanol was first prepared by the following procedures: 0.1822 g of CTMABr was dissolved in 1 mL of methanol, into which an excess amount (0.1160 g) of silver(I) oxide was added. The suspension was shaken for half an hour, and then the solid phase was removed by centrifugation. Next, the acceptor solution was prepared by dissolving 2.2 mg of MCP in 1.5 mL of chloroform, with addition of 20 μL of the 0.5 M CTMAOH solution. Similarly, the donor solution was made up by dissolving 3.5 mg of SR101 in 1.5 mL of chloroform, with addition of 20 μL of the 0.5 M CTMAOH solution. The final dye solution consisted of 0.5 mL of the acceptor solution, 0.2 mL of the donor solution, 0.1 mL of the 0.5 M CTMAOH solution, and 0.3 mL of chloroform. To dope the silicone film with the dye solution, the silicone film was first soaked in chloroform and then moved into the dye solution. After shaking for 1 min, the expanded, dyed film was removed from the solution and allowed to dry in ambient atmosphere. The dried film shrank back to its original size and was washed with methanol until the washout was colorless. After drying, a blue transparent film, which displayed fluorescence intensity and lifetime change when exposed to CO_2, was obtained.

Measurements. Absorption spectra were taken using a Beckman DU640 spectrophotometer (Fullerton, CA). Fluorescence spectra and phase-modulation measurements were carried out using an ISS K2 multifrequency phase and modulation fluorometer (Champaign, IL). In the emission spectrum measurements, a xenon arc lamp was used as the light source with the band-pass settings of 8 and 16 nm for the excitation and emission monochromators, respectively. In the phase-modulation measurements, the light source used was a blue LED (NSPB500, Nichia America Co., Lancaster, PA) with an emission maximum of ∼450 nm. The light output of the LED was amplitude-modulated as described previously (*23*). Light from the LED with a wavelength >500 nm was cut off by placing a set of short-wave-pass filters (500FL07, 600FL07, and 700FL07; Andover, Salem, NH) in the excitation path. The fluorescence was collected at wavelengths >600 nm through an Andover 600FH90 long-wave-pass filter. The lifetime reference solution used was a 10^{-5} M solution of Texas Red in water, with an assumed reference lifetime of 4 ns. The reference intensity was adjusted by adding proper neutral density filter(s) in its emission path to match the emission light intensity from the sensing film. In all phase angle measurements (except the time-dependent measurements), the measurement error was statistically preset as 0.2°. The instrument collected and averaged the signal until this criterion was met. The measurement apparatus setup was very similar to that described in our previous paper (*24*). The sample solution (∼20 mL), saturated with the desired gas, was circulated into the cuvette containing the sensing film via a circulation pump (MasterFlex, model 7520-10, Cole-Parmer, Chicago, IL). In the cuvette, the sensing film self-adhered to the front wall of the quartz cuvette. Front-face-measurement geometry was adopted at an orientation of ∼60° between the excitation light beam and the film surface to validate the measurement in the highly turbid fermentation media. Whereas naked sensing films were

used for characterization, a white PTFE gas-permeable membrane (cat. no.: 951204, Orion, Cambridge, MA) was put behind the sensing film in the cuvette to block the excitation light in validation and fermentation studies, because of the auto-fluorescing of the fermentation media. This approach greatly prevented the excitation light from coming into the media and therefore minimized the interference of the medium fluorescence. The cuvette containing the sensing film and the PTFE membrane was then steam-sterilized at 121 °C and 20 psi for 20 min. Unless otherwise specified, all the experiments were conducted at 23.0 °C.

Fermentation. Sensing film validation and fermentation experiments were conducted using *E. coli* strain JM105. The seed culture consisted of 1% inoculum in 50 mL of Luria-Bertani (LB) medium (10 g/L bacto-tryptone, 5 g/L bacto-yeast extract, 10 g/L NaCl) in a 250-mL shake flask, pH 7.2, incubated at 35.0 °C at 260 rpm for 6 h in an environmental incubator shaker (model G24, New Brunswick Scientific Co., Inc., Edison, NJ). Sensing film validation and fermentation studies were carried out in a 500-mL Bellco glass spinner vessel submerged in a 34.5 °C water bath. The spinner vessel was inoculated with 200 μL of seed inoculum in 200 mL of M9 minimal medium (*25*) containing 0.01% thiamine for the sensing film validation study and 300 μL of seed inoculum and 300 mL of M9 medium for the fermentation study. Aeration was controlled at 1 VVM (VVM = volume per volume per minute). Agitation was controlled with a Whatman Controller 1000 submersible stirrer. pH was monitored with an Accumet pH meter (model 915). As before, the broth was circulated to the cuvette containing the sensing film for on-line dissolved CO_2 measurements. Experiments were conducted at ~18 h when all glucose was utilized and the culture just stopped producing carbon dioxide. This time will be referred to as time zero.

For the sensing film validation experiment, 20 min after the recording was started, 32% CO_2 was sparged into the broth, after which air was sparged, and then the cycle was repeated. On-line dissolved CO_2 samples were collected continuously by the fluorometer, and 1-mL samples were removed at various times for off-line dissolved CO_2 analysis.

For the fermentation experiment, 2 g/L glucose was added to the culture 15 min after the recording was started. Approximately every 15 min, a 1-mL sample was removed for off-line analyses (200 μL was used for optical density measurement, 50 μL for glucose analysis, and 50 μL for carbon dioxide measurement).

The off-line sample analysis was carried out as follows: cellular optical density (OD) was measured with a Milton Roy Spectronic 401 spectrophotometer at 600 nm, and glucose was analyzed with a YSI 2700 Select Biochemistry Analyzer (Yellow Springs, OH). Off-line carbon dioxide was measured with a Kodak Biolyzer Rapid Analysis System (Eastman Kodak Co., New Haven, CT).

Results and Discussion

Autoclavability of the Sensing Film. The failure of autoclavability of the ion-pair-type CO_2-sensing films is mainly caused by two things: dye leaching out from polymer matrix during autoclaving and permanent loss of the internal basic condition in the matrix. By choosing a proper polymer, however, the dye may be retained in the matrix. We found that the two-component silicone used was superb for this purpose. Once the silicone-expanding-solvent, chloroform, was evaporated, both the donor and acceptor could not be washed out from the film even with methanol, which is known as a good solvent for these dyes. Furthermore, dye leaching out was not found during autoclaving of the film.

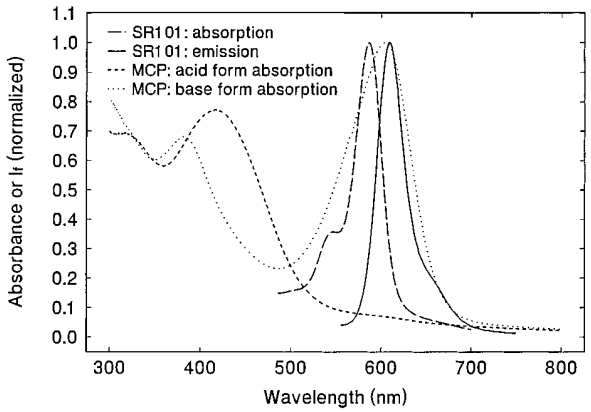

Figure 1. Spectral characteristics of SR101 and MCP in silicone film.

It was suggested (*15*) that the loss of the internal basic condition in the polymer matrix was probably due to degradation of the quaternary ammonium hydroxide through a Hofmann β-hydrogen elimination reaction (*26*). Therefore, it is logical to think that the fewer the available β-hydrogens in a quaternary ammonium cation, the slower the degradation rate should be. By comparing the films containing the same quantity but different quaternary ammonium hydroxides [i.e., tetraoctylammonium hydroxide (TOAOH, β-hydrogen: 8), cetyltrimethylammonium hydroxide (CTMAOH, β-hydrogen: 2), and tetramethylammonium hydroxide (TMAOH, β-hydrogen: 0)], we found that the stability was of the order TOAOH < CTMAOH < TMAOH, which was indicated by the time for the films to lose their initial blue color in a basic environment. The TMA^+ cation, however, bonds to the dye, MCP, anion so strongly that even 100% CO_2 could not turn the deprotonated dye into its protonated form. Hence, CTMAOH was selected for the fabrication of the sensing film. The combination of the silicone with CTMAOH made the sensing film not only autoclavable, but stable for continuous use in liquid phase for 2−3 weeks.

Characterization of the Sensing Film. Figure 1 shows the spectral characteristics of the fluorescence donor, SR101, and acceptor, MCP, in silicone film. The perfect spectral overlap between the emission of SR101 (solid line) and the absorption of the deprotonated MCP (dotted line) indicates that SR101 and the deprotonated MCP can be a very good pair of FRET donor−acceptor. In contrast, the spectral overlap between the emission of SR101 and the absorption of the protonated MCP (short dashed line) is very limited. This result means that we can expect significant signal change with MCP as the indicator. The excitation peak (at 587 nm) of SR101 (see the long dashed line) is somewhat away from that of our excitation light source (i.e., ~450 nm). However, the near unity quantum yield of rhodamine compounds (*27*) enabled us to collect strong fluorescence even when we excited the compound at 450 nm with the LED.

Figure 2 illustrates the phase angle and modulation versus frequency profile in the absence (solid lines) and presence (dashed lines) of dissolved CO_2. In this experiment, the sensing film was exposed to nitrogen-saturated water, and then 20% CO_2-saturated water. At 100 MHz, this exposure yielded a 43° increase in phase angle and

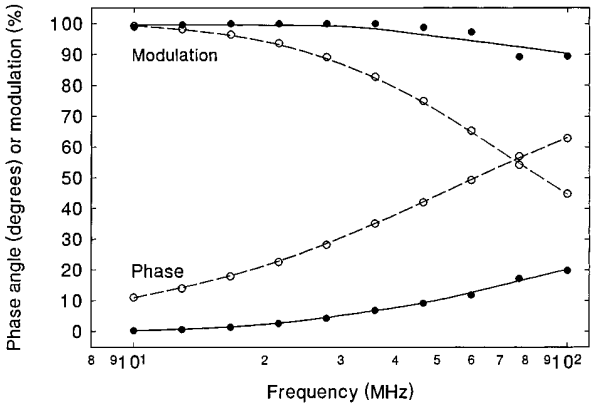

Figure 2. Frequency-dependent phase angle and modulation profile for the sensing film in water solutions saturated with pure nitrogen (solid lines) and 20% CO_2 in nitrogen (dashed lines). Modulation is plotted at the top of the figure and phase at the bottom.

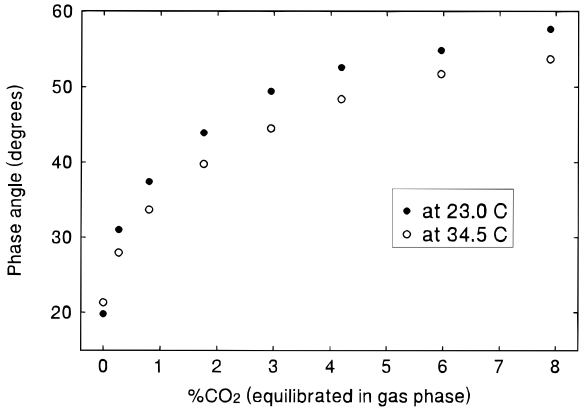

Figure 3. Equilibrium response of the sensing film to water solutions saturated with various amounts of CO_2 at 23.0 °C (closed circle) and 34.5 °C (open circle). Values of the phase angle were measured at 100 MHz.

a 45% decrease in modulation, indicating an increase in the lifetime of the fluorophore, SR101. The upper limit at which the LED could be modulated was 100 MHz.

Further calibrations were carried out at 100 MHz under two different temperatures (Figure 3). Compared with nitrogen-saturated water, 8% CO_2-saturated water caused increases of ~37° and ~33° in phase angle at 23.0 and 34.5 °C, respectively. Increasing temperature appears to reduce the phase angle range of the sensing film, and therefore the sensitivity that is defined as $\Delta\phi/\Delta(\%CO_2)$, where ϕ represents phase angle. This reduction is a collective result of the temperature effect on many factors, such as Henry's law constant, equilibrium constants for eqs 1−3, and the solubility of CO_2 in the silicone film. The response of the sensing film to the dissolved CO_2 is fully recoverable, which can be seen from Figure 4a. Figure 4a illustrates the time-dependent response and recovery profile of the sensing film to dissolved CO_2. When the water, saturated with gases switched between nitrogen and 6.9% CO_2, was pumped through the cuvette containing the sensing film, the phase angle changed accordingly. The typical increase and decrease in phase angle were completed in about 2 and 15 min, respectively. These times obviously depend on how fast the water can be saturated with the specific gas. The real response and recovery times were estimated from Figure 4b. In this experiment, a small magnetic stirring bar was placed on the bottom of the cuvette containing the sensing film, which was capped with a PTFE lid and sealed with Parafilm. Then, 1.5 mL of nitrogen-saturated water was injected into the cuvette through a small hole in the lid and the recording was started. When the reading was steady, with stirrer on, 0.1 mL of 100% CO_2-saturated water was injected, giving a diluted mixture equivalent to 6.7% CO_2-saturated water. Four minutes later, another 1.5 mL of nitrogen-saturated water was added, resulting in a 3.3% CO_2-saturated water solution. With an assumption that all mixing could be accomplished in seconds, the response and recovery times for 90% signal change were estimated as 1 min (for a step change from 0% to 6.7% CO_2-saturated water) and 1.5 min (for a step change from 6.7% to 3.3% CO_2-saturated water), respectively.

Sensing Film Validation in Fermentation. To validate the sensing film in fermentation monitoring, 32% CO_2 in air and pure air were alternately sparged into a culture of *E. coli*, and the on- and off-line dissolved CO_2 were measured with the sensing film and Biolyzer,

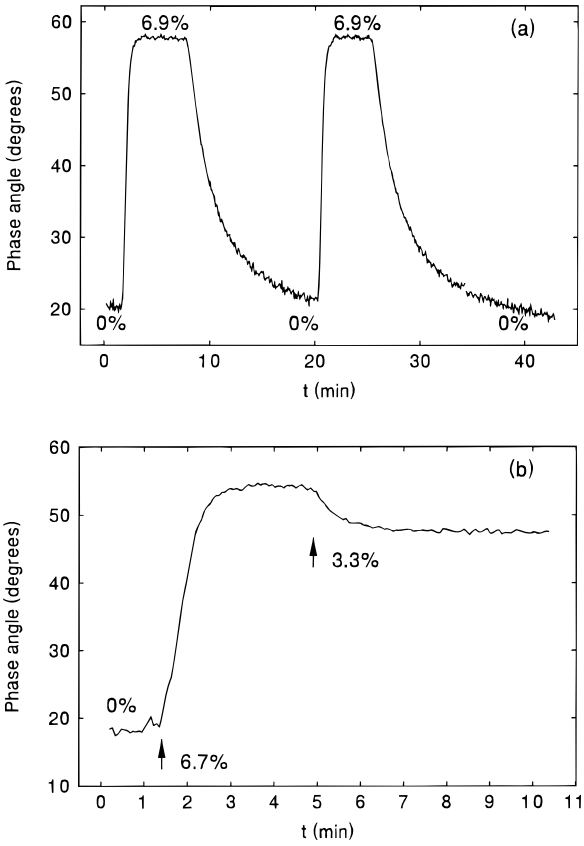

Figure 4. Time-dependent response of the sensing film to the water solutions saturated with various amounts of CO_2. Phase angle was measured at 100 MHz. The gases were introduced into the solutions through (a) bubbling and (b) liquid-to-liquid mixing.

respectively (Figure 5a). The dissolved CO_2 measurements by the sensing film were not affected by changes in pH, because little phase angle difference was observed when the sensing film was placed in pH 6 and 8 buffer solutions. On the other hand, the Biolyzer, which is a wet chemistry measurement of dissolved CO_2, displayed a sensitivity to pH as evidenced by the deviation from the initial and final peaks in the measured dissolved CO_2 concentration (Figure 5a,b). The pH meter was calibrated at the beginning and end of the experiment, and it was noted that the calibration shifted −0.12 unit over the course of the experiment, further indicating that the

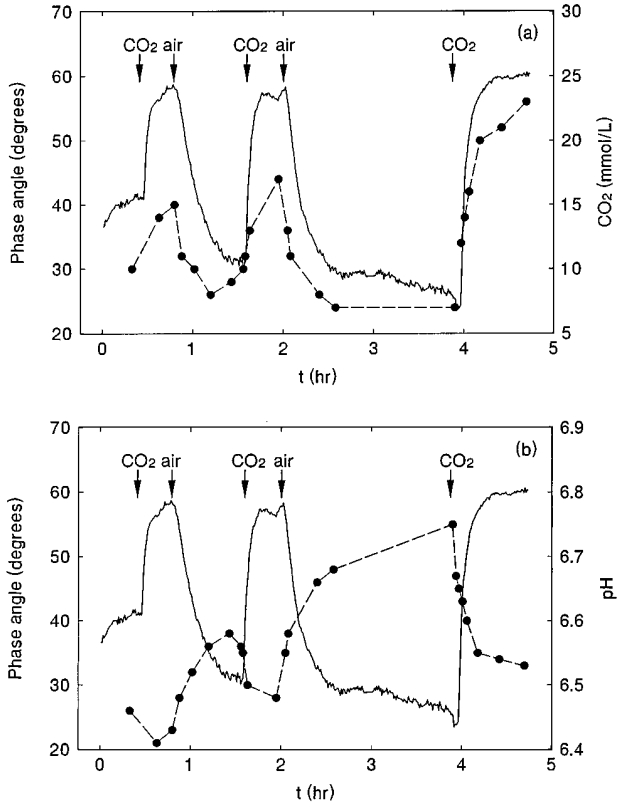

Figure 5. (a) On-line (solid line) and off-line (dashed line) dissolved CO_2 measurements. Arrows indicate addition of 32% CO_2 or air. (b) On-line dissolved CO_2 (solid line) and pH (dashed line). Arrows indicate addition of 32% CO_2 or air.

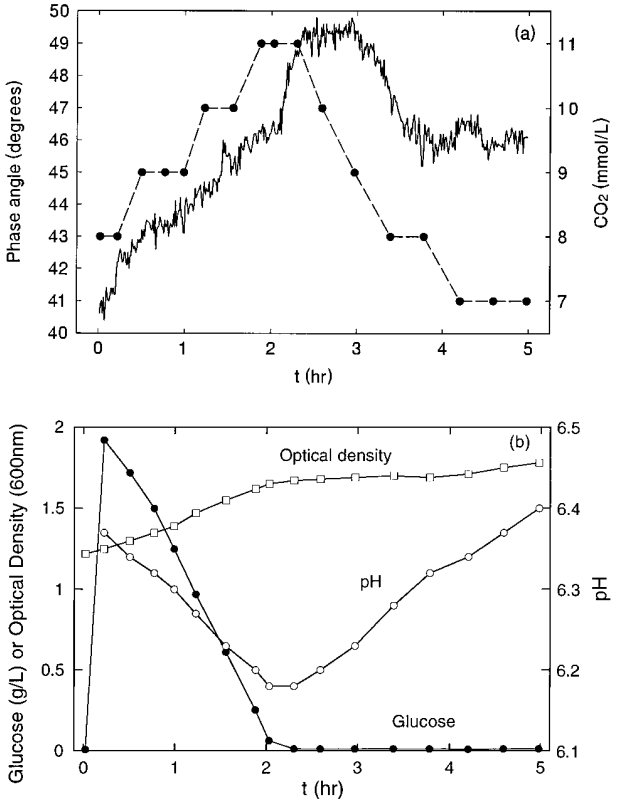

Figure 6. (a) Carbon dioxide measurements during a fermentation of *E. coli*. The dissolved CO_2 was measured on-line by the sensing film (solid line) and off-line by the Biolyzer (dashed line). (b) On-line pH (open circle) and off-line glucose (closed circle) and optical density (open square) measurements during the fermentation.

Biolyzer was affected by changes in pH. The Biolyzer also could have been affected by inhibitory compounds released by the cells as they entered the stationary phase of growth. Most importantly, Figure 5a shows that the on-line dissolved CO_2 profile closely followed that of the off-line profile.

Finally, we tested the sensing film in a batch fermentation of *E. coli* JM105. The cells were grown in a bioreactor at constant aeration, agitation, and temperature. The culture was aseptically pumped from the bioreactor to the sensing film positioned in the cuvette of the phase fluorometer and back at a rate of 30 mL/min. This allowed the carbon dioxide to be continuously monitored on-line by the sensing film. Glucose (2 g/L) was added to the culture. As seen in Figure 6a, the dissolved CO_2 profile measured on-line with the sensing film follows the off-line measurements made with the Biolyzer, with a shift that could have been due to differences in mixing and sampling between the on- and off-line measurements. Because off-line samples were removed directly from the bioreactor and on-line samples were required to travel from the bioreactor through tubing to the sensing film in the fluorometer, a lag in the measurement of the true dissolved CO_2 could have occurred with the sensing film. We have noted this shift consistently in experiments utilizing an actively growing culture. Almost immediately after glucose addition, the cells began to metabolize the glucose and produce CO_2 (Figure 6a,b). Both the on- and off-line dissolved CO_2 increased, production peaked around 2 h when glucose was exhausted, and the cells reached the late log phase of growth, and within 45 min the CO_2 began to decrease. As would be expected, the pH profile somewhat inversely reflects that of the dissolved CO_2 (Figure 6a and b). As the cells utilized the glucose, the culture became more acidic until the glucose was exhausted and the cells entered into the stationary phase of growth. Again, the Biolyzer appeared to be affected by either pH or an accumulation of interferring compounds, as evidenced by the downward shift in dissolved CO_2 measured at the end of the experiment compared with initial readings. Over the course of the experiment, the sensing film closely monitored the dissolved CO_2 of the culture, qualifying this sensing film as an on-line measure of dissolved CO_2.

Conclusion

An autoclavable sensing film for on-line monitoring of dissolved CO_2 in fermentation has been developed based on FRET. No aqueous solution was involved in the sensing film matrix, so the sensing film was not affected by osmotic pressure. Fluorescence lifetime was selected as the sensing parameter and was measured in frequency domain by phase-fluorometry. Upon exposure to 20% CO_2-saturated water, a 43° increase in phase angle was observed at 100 MHz. The process was fully reversible when the sensing film was exposed to nitrogen-saturated water. The estimated response and recovery times for 90% signal change were 1 min (for a step change from 0% to 6.7% CO_2-saturated water) and 1.5 min (for a step change from 6.7% to 3.3% CO_2-saturated water). When used for on-line monitoring of dissolved CO_2 produced by a culture of *E. coli*, the sensing film showed a similar trend to that obtained from off-line measurements using a Biolyzer. Such a sensing film will allow the dissolved CO_2 in bioreactors to be monitored, controls to be applied, and thereby decrease the potential deleterious effects on

cell growth and product formation. In addition, the sensing film may obviously be used for numerous biomedical and environmental applications.

Acknowledgment

Financial support for this research from the National Science Foundation (Grants BES-9413262 and BCS-9157852) and Genentech, Inc., is gratefully acknowledged. The authors also thank Dr. Tracey R. Pulliam for providing the *E. coli* JM105, and Dr. Konstantin Konstantinov of Bayer Inc. for his encouragement.

References and Notes

(1) Rao, G.; Bambot, S. B.; Kwong, C. W.; Szmacinski, H.; Sipior, J.; Holavanahali R.; Carter, G. Application of Fluorescence Sensing to Bioreactors. In *Topics in Fluorescence Spectroscopy. Volume 4: Probe Design and Chemical Sensing*; Lakowicz, J. R., Ed.; Plenum: New York, 1994; pp 417−448.

(2) Twork, J. V., Yacynych, A. M., Eds. *Sensors in Bioprocess Control*; Marcel Dekker: New York, 1990.

(3) *Topics in Fluorescence Spectroscopy. Volume 4: Probe Design and Chemical Sensing*; Lakowicz, J. R., Ed.; Plenum: New York, 1994.

(4) *Fiber Optic Chemical Sensors and Biosensors*, Vols. I and II; Wolfbeis, O. S., Ed.; CRC: Boca Raton, FL, 1991.

(5) *Handbook of Chemical and Biological Sensors*; Taylor, R. F., Schultz, J. S., Eds., Institute of Physics Publishing: Bristol, U.K., 1996.

(6) Bambot, S. B.; Holavanahali, R.; Lakowicz, J. R.; Carter, G. M.; Rao, G. Phase Fluorometric Sterilizable Optical Oxygen Sensor. *Biotechnol. Bioeng.* **1994**, *43*, 1139−1145.

(7) Kroneis, H. W.; Marsoner, H. J. A Fluorescence-Based Sterilizable Oxygen Probe for Use in Bioreactors. *Sens. Actuators* **1983**, *4*, 587−592.

(8) Agayn, V. I.; Walt, D. R. Fiber-Optic Sensor for Continuous Monitoring of Fermentation pH. *Bio/Technology* **1993**, *11*, 726−729.

(9) Uttamlal, M.; Walt, D. R. A Fiber-Optic Carbon Dioxide Sensor for Fermentation Monitoring. *Bio/Technology* **1995**, *13*, 597−601.

(10) Haddadin, J.; Morin, D.; Ollivier, P. Effect of Different Carbon Dioxide Concentrations on Ferrous Iron and Pyrite Oxidation by a Mixed Culture of Iron and/or Sulfur-oxidizing Bacteria. *Enzymol. Microb. Technol.* **1993**, *15*, 832−841.

(11) Jones, R.; Greenfield, P. Effect of Carbon Dioxide on Yeast Growth and Fermentation. *Enzymol. Microb. Technol.* **1982**, *4*, 210−223.

(12) Kuriyama, H.; Mahakarnchanakur, W.; Matsui, S.; Kobayashi, H. The Effects of pCO_2 on Yeast Growth and Metabolism under Continuous Fermentation. *Biotechnol. Lett.* **1993**, *15*, 189−194.

(13) McLimans, W. F. The Gaseous Environment of the Mammalian Cell in Culture. In *Growth, Nutrition and Metabolism of Cells in Culture*; Rothblat, G. H., Cristofalo, V. J., Eds.; Acamdemic: New York, 1972; Vol. 1, pp 137−170.

(14) Royce, P. N. Effect of Changes in the pH and Carbon Dioxide Evolution Rate on the Measured Respiratory Quotient of Fermentations. *Biotechnol. Bioeng.* **1992**, *40*, 1129−1138.

(15) Mills, A.; Chang, Q.; McMurray, N. Equilibrium Studies on Colorimetric Plastic Film Sensors for Carbon Dioxide. *Anal. Chem.* **1992**, *64*, 1383−1389.

(16) Mills, A.; Chang, Q. Fluorescence Plastic Thin Film Sensor for Carbon Dioxide. *Analyst (Cambridge)* **1993**, *118*, 839−843.

(17) Mills, A.; Chang, Q. Tuning Colorimetric and Fluorimetric Gas Sensors for Carbon Dioxide. *Anal. Chim. Acta* **1994**, *285*, 113−123.

(18) Mills, A.; Chang, Q. Colorimetric Polymer Film Sensors for Dissolved Carbon Dioxide. *Sens. Actuators, B* **1994**, *21*, 83−89.

(19) Weigl, B. H.; Wolfbeis, O. S. New Hydrophobic Materials for Optical Carbon Dioxide Sensors Based on Ion Pairing. *Anal. Chim. Acta* **1995**, *302*, 249−254.

(20) Sipior, J.; Randers-Eichhorn, L.; Lakowicz, J. R.; Carter, G. M.; Rao, G. Phase Fluorometric Optical Carbon Dioxide Gas Sensor for Fermentation Off-Gas Monitoring. *Biotechnol. Prog.* **1996**, *12*, 266−271.

(21) Lakowicz, J. R. *Principles of Fluorescence Spectroscopy*; Plenum: New York, 1983.

(22) Bambot, S. B.; Lakowicz, J. R.; Rao, G. Potential Applications of Lifetime-based Phase-modulation Fluorimetry in Bioprocess and Clinical Monitoring. *Trends Biotechnol.* **1995**, *13*, 106−115.

(23) Sipior, J.; Carter, G. M.; Lakowicz, J. R.; Rao, G. Single Quantum Well Light Emitting Diodes Demonstrated as Excitation Sources for Nanosecond Phase-Modulation Fluorescence Lifetime Measurements. *Rev. Sci. Instrum.* **1996**, *67*, 1−4.

(24) Chang, Q.; Lakowicz, J. R.; Rao, G. Fluorescence Lifetime-Based Sensing of Methanol. *Analyst (Cambridge)* **1997**, *122*, 173−177.

(25) Rodriguez, R. L.; Tait, R. C. *Recombinant DNA Techniques: An Introduction*; Benjamin/Cummings Publishing: Reading, MA, 1983; p 150.

(26) March, J. *Advanced Organic Chemistry: Reactions, Mechanism, and Structure*, 4th ed.; John Wiley & Sons: New York, 1992; pp 1015−1017.

(27) Drexhage, K. H. Fluorescence Efficiency of Laser Dyes. *Nat. Bur. Stand. (U. S.) Spec. Pub.* **1977**, *466*, 33−40.

Accepted November 20, 1997.

BP970119K

For his Ph.D. work, Xudong took on the challenge of making the CO_2 sensor robust. The next paper describes these efforts and resulted in a stable, long-lived sensing film that was sterilizable. We also demonstrated its use in a fermentation.

ELSEVIER

Biosensors and Bioelectronics 18 (2003) 857–865

BIOSENSORS & BIOELECTRONICS

www.elsevier.com/locate/bios

High-stability non-invasive autoclavable naked optical CO_2 sensor

Xudong Ge, Yordan Kostov, Govind Rao *

Department of Chemical and Biochemical Engineering, University of Maryland, Baltimore County, 1000 Hilltop Circle, Baltimore, MD 21250, USA

Received 4 April 2002; accepted 1 August 2002

Abstract

The fabrication and characterization of a high-stability non-invasive autoclavable naked optical CO_2 sensor is described in this report. The sensor was made by using 8-hydroxypyrene-1,3,6-trisulfonic acid trisodium salt (HPTS) as the fluorescence dye and cetyltrimethylammonium hydroxide (CTMAOH) as the phase transfer agent (the base). A highly hydrophobic two-component silicone film was used as the polymer matrix, which overcame some of the limitations of the existing plastic type CO_2 sensors, such as dye leaching and cross-sensitivity to ions. To improve the stability of the sensor, several affecting factors were investigated. Experimental results showed that sufficient base and a small amount of water in the sensing film were critical factors that affected the stability of the sensor. Although the sensor was more stable when kept in water, the function of the sensor could recover when the sensor kept in air was transferred into water. The sensor has a lifetime of several months. The detection limit of the sensing film was about 0.03%. The average response and recovery times were 0.66 and 1.94 min, respectively. It had no cross-sensitivity to salt concentrations in the range of 0–0.2 M and to pH in the range of 5.6–8.0, so it can be used in processes with changing ion concentration and pH. It was sterilizable and could be autoclaved many times without losing its sensitivity. The applicability of the sensor in real application was successfully tested in the fermentation of *Escherichia coli*.

Keywords: Carbon dioxide; Sensor; Ratiometric; Fluorescence; Fermentation

1. Introduction

Measurements of dissolved or gaseous CO_2 are important in many fields (Wolfbeis, 1990). For example, CO_2 sensor is a necessary device for monitoring the CO_2 concentrations in air or water, which is a key parameter in environmental analysis and atmospheric pollution control. The success of fermentation or cell culture is highly dependent on real-time determination of the dissolved CO_2 (Chang et al., 1998; Pattison et al., 2000). Carbonated beverages and modified atmospheres in food packaging or storage are also examples of current applications of CO_2 monitors (Marazuela et al., 1998).

The two most common devices used for the detection of CO_2 are the infrared detector (Patel, 1990), and the Severinghaus electrode (Severinghaus and Bradley, 1958). While infrared absorption detector produces quick response times and the results are reliably quantitative, they are bulky, expensive, and only applicable to gaseous CO_2. The Severinghaus type CO_2 electrode comprises a pH electrode in contact with a thin layer of bicarbonate buffer solution with the whole system encapsulated by a thin, gas-permeable membrane. CO_2 in the sample under test diffuses through the gas permeable membrane and equilibrates with the internal aqueous solution thereby altering its pH. The change in pH is monitored by the pH electrode. Although it can be used to measure dissolved CO_2, the Severinghaus type CO_2 electrode has a long response time (typically 5–15 min) and suffers from the same drawbacks of the pH electrode upon which it is based. Other devices (Sipior et al., 1996) for CO_2 measurements include gas chromatograph (GC) and mass spectrometer (MS). MS is capable of producing measurements in near real time but its price is prohibitively high. GC, while less expensive, requires 10–20 min to complete an analysis of a sample and can not be used for real-time measurements.

* Corresponding author. Tel.: +1-410-455-3415; fax: +1-410-455-6500

E-mail address: grao@umbc.edu (G. Rao).

0956-5663/02/$ - see front matter
PII: S0956-5663(02)00159-8

To overcome the drawbacks of these methods, two types of optical CO_2 sensors have been investigated. The first type of optical CO_2 sensors (Uttamlal and Walt, 1995; Wolfbeis et al., 1988; Munkholm et al., 1988; Lubbers and Opitz, 1983; Zhang and Seitz, 1984; Weigl et al., 1993 Wolfbeis, 1991) has similar design features to the Severinghaus type CO_2 electrode except that a pH-sensitive dye replaces the pH electrode to detect the change in pH caused by the diffusion of CO_2. Just like Severinghaus type CO_2 electrode, this kind of sensor is based on the reaction of CO_2 with a bicarbonate buffer contained behind a hydrophobic polymer. The reaction results in a shift in the pH of the buffer, causing a change in absorption or fluorescence intensity of a pH indicator dye added to the buffer. The gas-permeable polymer acts not only as a matrix for immobilizing the buffer and dye, but also as a barrier for ions. Unfortunately, the response time of this kind of sensors is usually long, due to the introduction of the gas-impermeable membrane. Additionally, although the hydrophobic coating of the CO_2 sensors is impermeable to both liquid water and ions, it is permeable to water vapors. As a result, there is a tendency to establish an osmotic equilibrium between internal buffer and sample solution (Weigl et al., 1993), which can give rise to a gradual drift (Wolfbeis, 1991). In practice, this has limited their use to situations where the osmolarity of the sample is fairly constant, such as in blood gas analysis or detection of bacteria in blood.

A recent approach to CO_2 sensing uses a phase transfer agent (a quaternary ammonium hydroxide) to replace the previously required sodium bicarbonate buffer solution (Chang et al., 1998; Sipior et al., 1996; Mills and McMurray, 1993; Sipior et al., 1995; Weigl and Wolfbeis, 1995; Mills and Chang, 1994a; Mills et al., 1992; Mills and Chang, 1992, 1994b), In this technique, the quaternary ammonium hydroxide is used not only to help dissolve the indicator dye into a hydrophobic polymer by the formation of an ion pair between the quaternary ammonium cation and the indicator dye anion, along with the water required for production of carbonic acid and deprotonation of the dye, but also to provide in the membrane the initial basic environment that is essential for a CO_2-sensing film to work. As the hydrophobic polymer itself can act as a barrier to ions, no additional gas-permeable membrane is needed, so this kind of sensor is also called naked sensor by some researchers. The naked sensor shows a very promising behavior in many respects, especially its extremely short response time.

Less hydrophobic polymers such as ethylcellulose have been used as the matrix for the ion pair by some authors (Mills and McMurray, 1993; Mills et al., 1992; Mills and Chang, 1994b). It is relatively easier to incorporate the ion-pair into such polymers. However, as such polymers are generally permeable to ions, this causes a cross-sensitivity to electrolytes and pH. Thus, these films are good only when applied to measure gaseous CO_2 (Sipior et al., 1996). For this reason, incorporation of the ion pair directly into a hydrophobic polymer such as silicone is a highly desirable alternative (Chang et al., 1998).

In our lab, a CO_2 sensing system based on the principle of fluorescence resonance energy transfer (FRET) was previously investigated (Chang et al., 1998; Sipior et al., 1995, 1996). Two dyes are involved in such sensors: a fluorescent dye and a pH-sensitive dye. The change in pH induces a color change in the pH-sensitive dye, decreasing the overlap of its absorbance spectrum with the emission spectrum of the fluorescence dye. This decrease in spectral overlap decreases the rate of FRET from the excited fluorescent donor dye to the pH-sensitive acceptor dye, resulting in an increase of both the fluorescence intensity and lifetime (Lakowicz, 1999). Lifetime measurement is preferred because of its unique advantages of being insensitive to signal drift resulting from the variation of light source intensity, instability of the photodetector, and photobleaching of the fluorophore. However, the device for lifetime measurements is relatively expensive. The advantage of using FRET is that it removes the limitation that the fluorescent dye must be sensitive to the changes in pH. Thus, one has many more choices when selecting the dye used to fabricate the CO_2 sensor. However, as at least two dyes are involved in the sensing film, the interactions between components would be more complex and this adds some uncertainties to the stability of the sensor.

To overcome the drawbacks of the CO_2 sensors made previously and further improve their performance, we fabricated a new naked CO_2 sensor by using 8-hydroxypyrene-1,3,6-trisulfonic acid trisodium salt (HPTS) as the fluorescence dye. HPTS exhibits two excitation wavelengths, corresponding to its protonated and deprotonated form, respectively. This property makes it extremely suitable for steady-state ratiometric measurements, thus eliminating the inherent drawbacks of intensity-based measurements including signal variations due to probe photobleaching and fluctuations in light source intensity, etc. Another advantage of ratiometric measurements is that the device used in measurements is relatively simple and cheap, compared with lifetime measurements. Experimental results show that the CO_2 sensor developed in our lab not only has a very long stability, but also is insensitive to ion concentration and pH. Further more, it is sterilizable and can be autoclaved many times without losing its sensitivity. Because of the above advantages, it should find wide applications in many fields such as biotechnology, environmental protection, healthcare and food processing.

2. Experimental

2.1. Materials

Cetyltrimethylammonium hydroxide solution (25 w/w%) in methanol (CTMAOH) was purchased from Fluka. HPTS was obtained from Molecular Probes Inc. (Eugene, OR). Hydrogen hexachloroplatinate, methanol, and chloroform were purchased from Aldrich and used without further purification. Polydimethylsiloxane, vinyldimethyl terminated (PS443) and (30–35%) methyl-hydro- (65–70%) dimethylsiloxane copolymer (PS 123) were obtained from United Chemical Technologies, Inc. (Bristol, PA). Pure nitrogen and pure CO_2 were obtained from Potomac Airgas (Linthicum, MD). Gas mixtures with known CO_2 contents were obtained by blending pure CO_2 with nitrogen through two flowmeters (FM4332 and FM4333, Advanced Specialty Gas Equipment Corp., South Plainfield, NJ).

2.2. Preparation or the sensing films

The sensing film was prepared in three steps: preparing the silicone film, preparing the dye solution, and doping the silicone film with the dye solution. The silicone film was made in a way similar to that described in our previous paper (Chang et al., 1998). First, a hydrogen hexachloroplatinate-saturated mixture was made by dissolving sufficient hydrogen hexachloroplatinate into PS443. Then, 220 mg of this mixture was blended with 3.0 g of PS443 and 143 mg of PS123. After shaking sufficient long for the mixture to be well mixed, the viscous solution was smeared on a glass microscope slide. After that, the glass microscope slide with the viscous mixture was placed under nitrogen for 1 week. The curing of the polymer started soon after it was smeared on the glass and finished in 1 week. The resulting film was highly transparent, clear or slightly yellowish if it was more than 0.5 mm thick. Before use, the film was removed with a razor blade from the glass slide, and shaped into the desired size. To prepare the dye solution, some amount of HPTS, varying for different patches, was dissolved into chloroform. Some amount of 25% (w/w) CTMAOH solution in methanol, also varying for different patches, was added. After that, the dye solution was placed for about 1 h so that the dye and the base had sufficient time to form ion-pair. Before the silicone film was doped with the dye solution, another some amount of CTMAOH solution was added, whose function was to stabilize the sensing film and to adjust the sensitivity. About 30 min after the silicone film was put into the dye solution, the expanded, dyed film was removed from the dye solution and allowed to dry in ambient atmosphere. The dried film shrank back to its original size and was washed with methanol or water thoroughly. After drying, a greenish transparent film was obtained.

2.3. Instrumentation

Fluorescence spectra and ratiometric measurements were carried out using a Varian Gary Eclipse fluorescence spectrophotometer for front face measurements with excitation light at an angle of 20°. Before being measured, the CO_2 sensing film was affixed to one of the inside walls of a cuvette (Fig. 1a). Distilled water was added into the cuvette if it was intended to validate the application of the sensing film in water. Sample gases with different CO_2 contents flowed into and out of the cuvette through two needles and bubbled through the water. The position of the cuvette in the fluorometer was adjusted to get the maximal fluorescence. For fermentation experiment, a more complicated sensor assembly structure was adopted (Fig. 1b). A piece of sensing film was first affixed to a piece of transparency film. Then, the sensing film was covered by a piece of white filter paper slightly larger than the sensing film to block off the background fluorescence from the broth. A piece of black tape with a small square window in the middle was used to fix the sensing film and the white filter paper onto the transparency film. After that, the whole sensor assembly was inserted into a polystyrene cuvette and fixed onto one of the inside walls with silicone grease (Fig. 1b).

2.4. Fermentation

The fermentation experiment was carried out using *Escherichia coli* JM105. The seed culture consisted of 1% inoculum in 20 ml LB medium incubated at 37 °C with shaking at 260 rpm (Orbit Environ Shaker, Labline Instruments; Melrose Park, IL) for 8–10 h. The

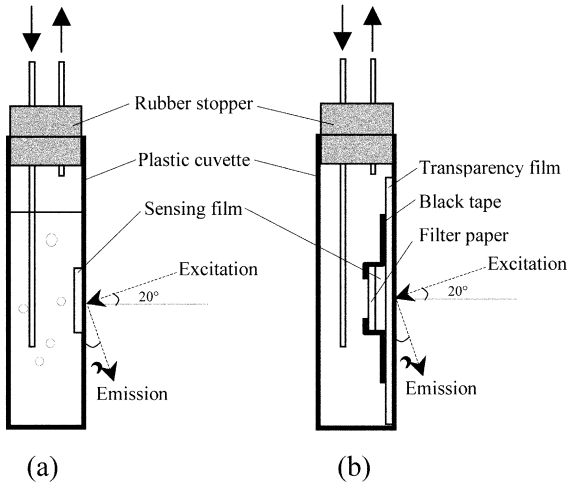

Fig. 1. Schematic diagrams of the experimental setups. (a) For measurements other than fermentation. (b) For fermentation.

fermentation was carried out at room temperature in a 500 ml shake flask containing 145 ml of LB medium and 5 ml of seed inoculum. The shake flask was placed on a rotating shaker (LaPine Scientific Co.; Berkeley, CA) at 80 rpm. The cuvette containing the sensing film and the tubing were thoroughly rinsed with 70 v/v% ethanol solution for sterilizing before connecting to the fermentation flask. The sensing film had been previously autoclaved. However, as the supporting components (black tape, transparency film) were not steam-sterilizable, it was necessary to ethanol sterilize the whole assembly. To solve this problem, another new naked optical CO_2 sensing with the ability to block off the background fluorescence is being developed. The broth was then aseptically circulated between the cuvette containing the sensing film and the shake flask for on-line dissolved CO_2 measurements, 1.0 ml of broth sample was taken form the flask every 15–30 min for biomass analysis. The cellular optical density (OD) was measured with a Milton Roy Spectronic 401 spectrophotometer at 600 nm.

3. Results and discussion

3.1. Long-term baseline stability

The excitation and emission spectra of HPTS in bicarbonate buffer solution and in silicone polymer are shown in Fig. 2. It can be seen that it possesses two maximum excitation wavelengths and one maximum emission wavelength. The silicone film used here almost does not affect the maximum excitation wavelengths of HPTS (405 and 459 nm), but the maximum emission wavelength in the silicone film is slightly red-shifted from 512 to 523 nm. So the Stokes' shift of HPTS is slightly bigger in silicone film than in bicarbonate buffer. The fluorescence intensity of the silicone film itself is very low, too low to be clearly shown on the figure. This figure also shows that the ratio of the fluorescence intensity at 405 nm to the fluorescence intensity at 459 nm is very sensitive to the CO_2 concentration in the gas phase in equilibrium with the buffer or sensing film. The different sensitivities for these two different situations are due to the different bases and their different concentrations.

Although the ion-pair type CO_2 sensor is very promising, the best sensor previously made in our lab or by other researchers has a usable lifetime from only several hours to a few days. This severely limits its use in real applications, in order to fabricate a long lifetime sensor, we investigated the effects of important affecting factors on the long-term stability of the sensor. These factors include the base concentration in the dye solution (or the molar ratio of base to dye in the film),

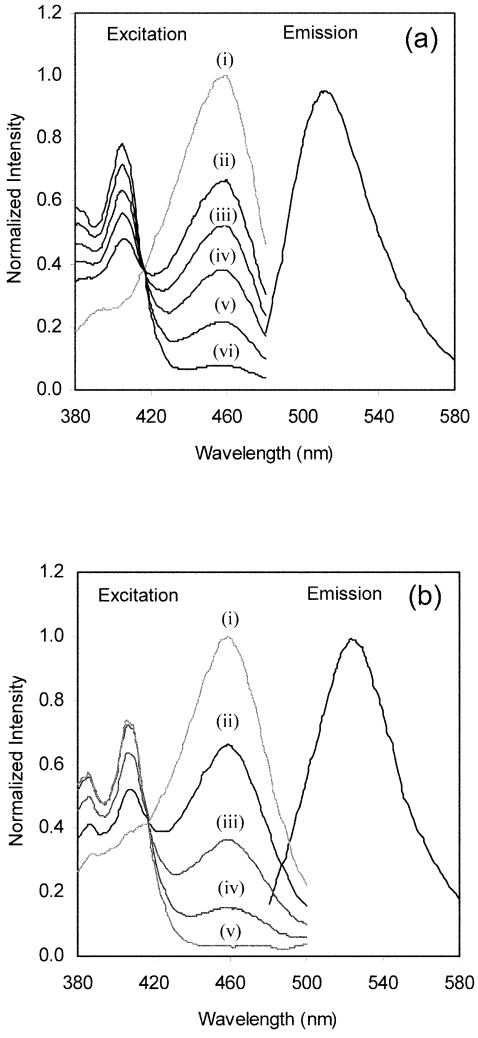

Fig. 2. Normalized fluorescence spectra of HPTS in (a) 0.01 M biocarbonate buffer and (b) silicone polymer membrane. CO_2 contents in gas phase in equilibrium with the liquid: (a) (i) 0.0%, (ii) 0.37%, (iii) 0.87%, (iv) 1.73%, (v) 3.81%, (vi) 15.30%; (b) (i) 0.0%, (ii) 0.13%, (iii) 0.37%, (iv) 0.58%, (v) 18.15%.

the water content in the sensing film and the storage method.

The effect of molar ratio of base to dye in the sensing film on the stability of the sensing film is shown in Fig. 3. It can be seen that the CO_2 sensing film was much more stable when more base CTMAOH was used. The reason for this might be that although the silicone film is almost neutral, there are some acidic functions or groups in it which will react with the base in the sensing film. There are also a lot of acidic vapors in air, especially in chemical laboratories. Adding more bases in the dye solution can neutralize the acid groups in the sensing film and the acidic vapors in air. As a result, the composition or structure of the CO_2 sensor would remain unchanged for a longer time.

Fig. 4 illustrates the effect of water content in the sensing film on its baseline stability. Two different

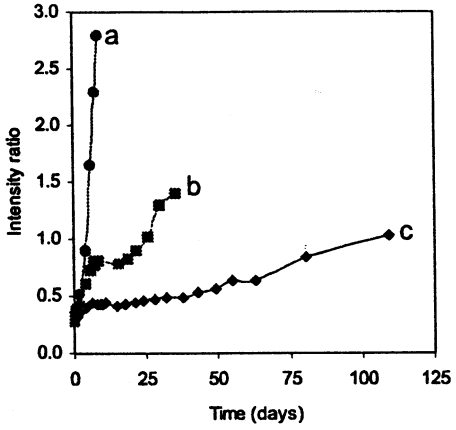

Fig. 3. Effect of base concentration on the baseline stability of the sensing membrane. Molar ratios of base to dye: (a) 72:1; (b) 84:1; (c) 100:1.

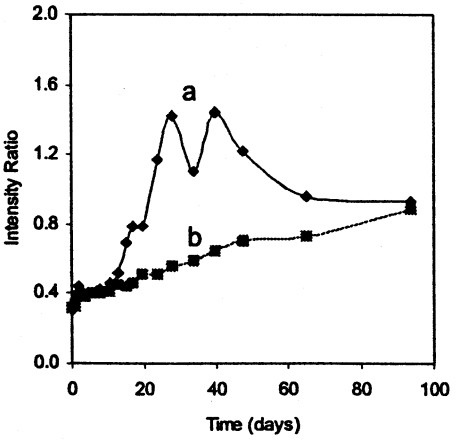

Fig. 4. Effect of water content in dye solution on the baseline stability of the sensing membrane: a, dehydrated chloroform; b, water-saturated chloroform.

sensing patches were made under exactly the same conditions except that one of them was made in dehydrated chloroform, while the other one was made in water-saturated chloroform, thus having a higher water-content. From Fig. 4, it can be seen that the sensor with a higher water-content is much more stable. This shows that although the sensing film is almost solid, a small amount of water is still necessary for the sensor to function properly. If the water content in the sensing film is not enough, then only a small fraction of the dye molecules {DH} will be hydrated and exist in their deprotonated form $\{Q^+D^- \cdot xH_2O\}$. As a result, the sensor will appear more sensitive to CO_2 because less CO_2 is needed to change the dye from its deprotonated form to its protonated form. After a long time of storage in water, the sensitivities of the two patches tend to be identical because the water contents in both sensing patches reach equilibrium with water.

Fig. 5 shows the effect of storage method on the stability of the CO_2 sensor. After two sensing patches

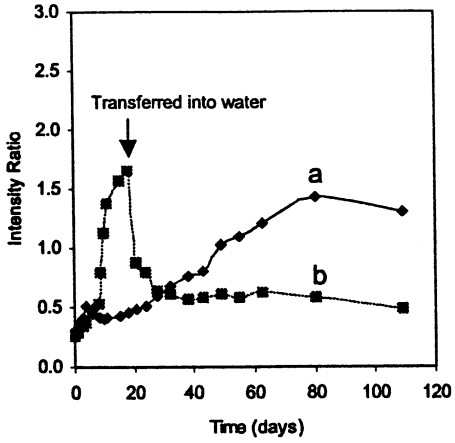

Fig. 5. Effect of storage method on the baseline stability of the sensing membrane: a, stored in distilled water; b, transferred into water after being stored in air for 20 days.

were made under exactly the same conditions, one of the two patches was kept in water and the other one was kept in air. The patch stored in air was transferred into water after 20 days. We can see that when kept in water, the sensor was more stable. However, when the sensor kept in air was transferred into water, we can see a gradual return towards its original sensitivity. The fast change in sensitivity for the sensor stored in air may be caused by the change in water content in the polymer film. When the sensing film was stored in air, some of the water contained in the polymer film would be lost gradually. As a result, only part of the base or/and ion-pair could interact with the CO_2 diffusing into the polymer and less CO_2 would be needed to reach equilibrium with the base or/and ion-pair The sensor would be more sensitive. After the sensor was transferred into water, the water content in the sensing film would gradually increase. This figure implies that storing the sensing film in air for some time might be beneficial to its long-term stability. The reason for this is being investigated.

From Figs. 3–5, we can see that the sensing film made under appropriate conditions could last about 120 days. Although the drift patterns were not exactly the same for different sensing patches made under different conditions, the total drift within the 120 days, which is about 0.7 U, was actually very small, compared with the large signal change shown in Figs. 7–9, which is about 20 U for a change in CO_2 from 0 to 20%. This is an excellent result for a naked sensing film, compared with the commercialized YSI 8500 CO_2 Monitor (http://www.YSI.com), which has a usable lifetime of 45 days.

Other experiments show that the maximum excitation intensities of HPTS and their ratio in water solution do not change with time (not shown). Therefore, the reason for the baseline drift of the sensor might be caused by the interaction between the dye and/or the base and

some of reactive groups in the silicone polymer, changing the amount or structure of the base or/and ion pair.

3.2. Detection limit and repeatability

Fig. 6 shows the detection limit of the sensing film. It can be seen that the sensing film is very sensitive to CO_2. Although the sensing film is exposed to a gas mixture with a CO_2 concentration as low as 0.05%, which is the lowest concentration we can obtain with our available devices, the signal is still very large. According to the definition of detection limit, the detection limit is about three times of the noise level. So the detection limit should be less than 0.03%. The response times for 90% signal change for gas-phase measurements are 0.9 min for a step change from 0 to 1.08% CO_2, and 0.5 min for a step change from 0 to 8.28%, respectively. The recovery times for 90% signal change are 1.8 min for a step change from 6.98 to 0% and 2.2 min for a step change from 2.31 to 0%, respectively. The good repeatability of the sensing film is shown in Fig. 7. The response and recovery times for 90% signal change calculated from Fig. 7, are 2.8 and 3.6 min, respectively. However, as the gas was bubbling through the liquid phase in this case, the above time includes the time needed to reach equilibrium between the gas and the liquid.

3.3. Cross-sensitivity of the sensing film to ion and pH

Fig. 8 illustrates the effect of salt concentration on the sensitivity of the sensing film. When the salt concentration [NaCl] changes within the range of (0–0.2 M), the readings of the sensing film do not change significantly with the salt concentration. This is a very good property because it can be used in processes with changing salt concentration without the need to re-calibrate the sensor during the process. Most of the previously made sensors, especially those using bicarbonate buffer, are cross-reactive to ionic strength or osmotic pressure. As a result, they can only be used in processes with constant salt concentrations. However, if the salt concentration is too high, the intensity ratio of the sensing film will slightly decrease for the same gas-phase CO_2 concentration. According to the reference Stephen and Stephen (1964) the solubility of CO_2 is lower in water solution of salt than in pure water. As the sensing film actually measures the concentration of dissolved CO_2, the decrease in reading of the sensing film at high salt concentrations may be caused by the decrease in solubility of CO_2.

The cross-reactivity of the sensing film to pH was also tested by calibrating the sensing film in phosphate

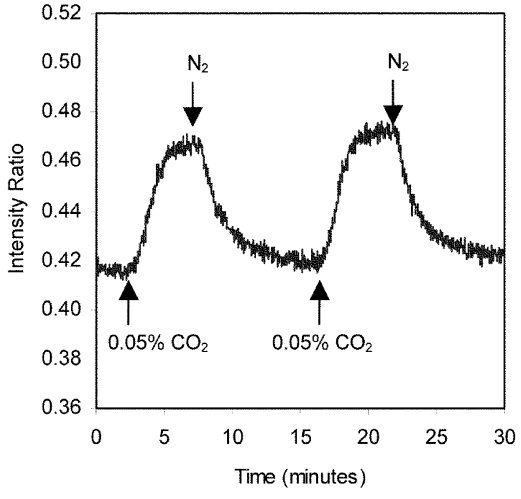

Fig. 6. Detection limit of the sensing film.

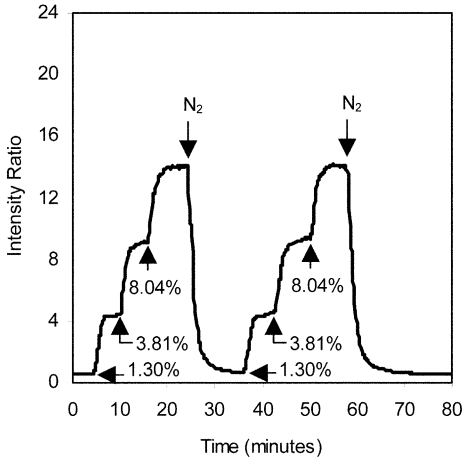

Fig. 7. Repeatability of the sensing film.

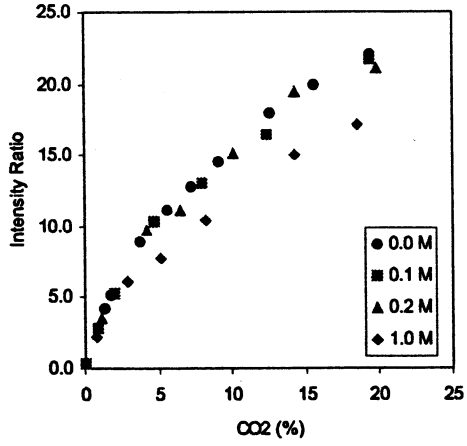

Fig. 8. Effect of ion concentration on the sensitivity of the sensing membrane.

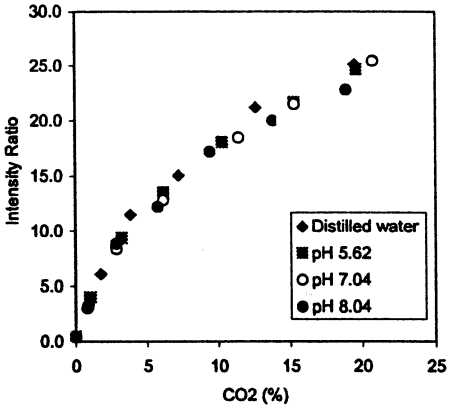

Fig. 9. Effect of pH on the sensitivity of the sensing film.

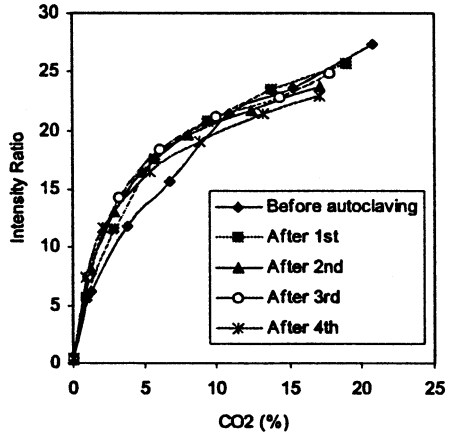

Fig. 10. Autoclavability of the sensing film.

buffers with different pH. As can be seen from Fig. 9, no signal change occurred within the tested pH range.

3.4. Autoclavability and sterilizability of the sensing film

Fig. 10 shows the calibration curves of the sensing film before and after autoclaving. It can be seen that this sensing film can be autoclaved many times without losing its sensitivity. Although the sensitivity of the sensing film changed slightly before and after the first autoclaving, it almost remained constant after the following autoclavings.

Dye leaching out of the polymer matrix during autoclaving and permanent loss of the internal basic condition in the matrix are two major reasons that could cause the failure of autoclavability of the ion-pair-type CO_2 sensing films. To prevent the dye from leaching out of the polymer matrix during autoclaving, a two-component highly hydrophobic silicone film was used. Once the silicone expanding solvent, chloroform, was evaporated, both the fluorescent dye (HPTS) and the base (CTMAOH) were retained in the matrix firmly. Due to the strong hydrophobic property, water molecules and ions cannot easily go into or come out of the polymer matrix. As a result, no dye leaching was found during the autoclaving of the sensing film. The formation of ion-pairs also decreases the possibility of dye leaching. Owing to its greater affinity to the hydrophobic polymer matrix, the ion pair is less subject to leaching than HPTS alone. Additionally, the high stability of HPTS was also beneficial to the stability of the sensing film.

Besides its autoclavability, this sensing film can also be sterilized in 70 v/v% ethanol. However, the sensitivity of the sensing film increased slightly after being sterilized (see Fig. 11). So it might be necessary to recalibrate the sensor after sterilizing. This change in sensitivity after being ethanol-sterilized may be caused by the partial loss of water or base in the sensing film due to the extraction of ethanol.

3.5. Application of the sensing film in fermentation

The sensing film was tested in a batch fermentation of *E. coli* JM105 at room temperature in a 500 ml shake flask. The broth was aseptically circulated between the cuvette containing the sensing film (Fig. 1b) and the shake flask for on-line dissolved CO_2 measurements. Measurements were made with external instrumentation without direct contact with the sensing film, so the detection was non-invasive. About 1.0 ml of broth sample was taken from the flask every 15–30 min for biomass analysis. Fig. 12 shows the CO_2 concentration in the media recorded online by the sensor and the optical density of the media, which was used as a measure of the biomass production. The figure clearly shows that the fermentation process underwent three different stages: the lag phase, the exponential growth

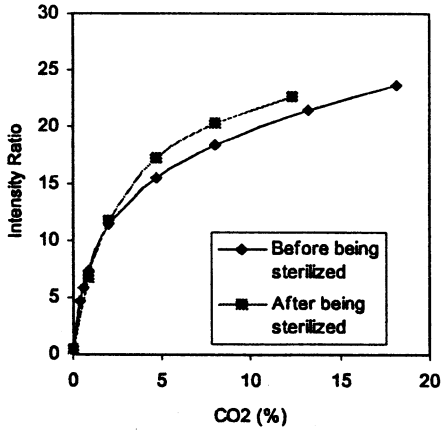

Fig. 11. Ethanol-sterilizability of the sensing film.

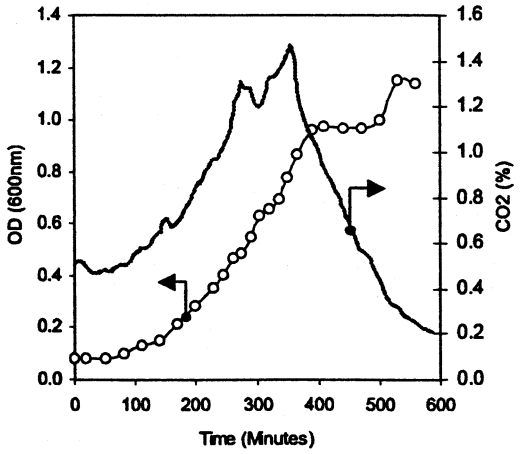

Fig. 12. Application of the sensing film in fermentation.

phase and the stationary phase. During the lag phase, the CO_2 concentration remained relatively stable. As the cells entered the exponential growth phase, a sharp increase in optical density was observed, followed by a corresponding increase in CO_2 concentration due to active respiration. As the cells entered the stationary phase, the cells stopped growing and the CO_2 concentration in the flask began to decline. This ability to track dissolved CO_2 simply should be of great utility in fermentation and cell culture applications.

4. Conclusions

A high-stability non-invasive autoclavable naked optical CO_2 sensor was made by using HPTS as the fluorescence dye and CTMAOH as the phase transfer agent (or base). The sensor was successfully used in an *E. coli* fermentation to provide continuous, on-line measurements of CO_2 concentration. Investigations of the factors affecting the stability of the sensing film showed that as more base was added, the sensing film was more stable but less sensitive. Although the sensing film was almost solid, sufficient water should be present in the sensing film for the sensor to function properly. When kept in water, the sensor was more stable. However, when the sensor kept in air was transferred into water, the function of the sensor could recover. The sensor could last more than several months with only little drift. The detection limit of the sensing film was about 0.03% CO_2. The average response and recovery times were 0.7 and 2.0 min, respectively. It was insensitive to ion concentration in the range of 0–0.2 M and to pH in the range of 5.6–8.0, so it can be used in processes with changing ion concentration and pH. It was sterilizable and could be autoclaved many times without losing its sensitivity. Due to the above advantages, it should find wide applications in many fields such as biotechnology, environmental protection, healthcare and food processing.

Acknowledgements

This work was sponsored by NSF Grant BES0091705 and unrestricted funding from Genentech, Merck and Pfizer.

References

Chang, Q., Randers-Eichhorn, L., Lakowicz, J.R., Rao, G., 1998. Steam-sterilizable, fluorescence lifetime-based sensing film for dissolved CO_2. Biotechnol. Prog. 14 (2), 326–331.

Lakowicz, J.R., 1999. Principles of Fluorescence Spectroscopy, second ed.. Kluwer Academic/Plenum Publishers, New York.

Lubbers, D.W., Opitz, N., 1983. Blood gas analysis with fluorescence dyes as an example of their usefulness as quantitative chemical sensors. Anal. Chem. Symp. Ser. 17, 609–619.

Marazuela, M.D., Moreno-Bondi, M.C., Orellana, G., 1998. Luminescence lifetime quenching of a ruthenium(II) polypyridyl dye for optical sensing of carbon dioxide. Appl. Spectrosc. 52 (10), 1314–1320.

Mills, A., Chang, Q., 1992. Modelled diffusion-controlled response and recovery behavior of a naked optical film sensor with a hydrophobic-type response to analyte concentration. Analyst 117, 1461–1466.

Mills, A., McMurray, N., 1993. Fluorescence plastic film sensor for carbon dioxide. Analyst 118, 839–843.

Mills, A., Chang, Q., 1994. Tuning colourimetric and fluorimetric gas sensors for carbon dioxide. Anal. Chim. Acta 285, 113–123.

Mills, A., Chang, Q., 1994. Colorimetric polymer film sensors for dissolved carbon dioxide. Sens. Actuat. B21, 83–89.

Mills, A., Chang, Q., McMurray, N., 1992. Equilibrium studies on colorimetric plastic film sensors for carbon dioxide. Anal. Chem. 64, 1383–1389.

Munkholm, C., Walt, D.R., Milanovich, F.P., 1988. A fiber-optic sensor for CO_2 measurement. Talanta 35, 109–112.

Patel, M., 1990. Chem. Br. 26, 640.

Pattison, R.N., Swamy, J., Mendenhall, B., Hwang, C., Frohlich, B.T., 2000. Measurement and control of dissolved carbon dioxide in mammalian cell culture processes using an in situ fiber optic chemical sensor. Biotechnol. Prog. 16, 769–774.

Severinghaus, J.W., Bradley, A.F., 1958. Electrodes for blood pO_2 and pCO_2 determination. J. Physiol. 13, 515–520.

Sipior, J., Bambot, S., Romauld, M., Carter, C.M., Lakowicz, J.R., Rao, G., 1995. A lifetime-based optical CO_2 gas sensor with blue or red excitation and stokes or anti-stokes detection. Anal. Biochem. 227, 309–318.

Sipior, J., Randers-Eichhorn, L., Lakowicz, J.R., Carter, C.M., Rao, G., 1996. Phase fluorometric optical carbon dioxide gas sensor for fermentation off-gas monitoring. Biotechnol. Prog. 12, 266–271.

Stephen, J., Stephen, T. (Eds.), Solubilities of Inorganic and Organic Compounds, Tertiary Systems, Part 2, vol. 2. Pergamon Press, London 1964.

Uttamlal, M., Walt, D.R., 1995. A fiber-optic carbon dioxide sensor for fermentation monitoring. Biotechnology 13, 597–601.

Weigl, B.H., Wolfbeis, O.S., 1995. New hydrophobic materials for optical carbon dioxide sensors based on ion pairing. Anal. Chim. Acta 302, 249–254.

Weigl, B.H., Holobar, A., Rodriguez, N.V., Wolfbeis, O.S., 1993. Chemically and mechanically resistant carbon dioxide optrode based on a covalently immobilized pH indicator. Anal. Chim. Acta 282, 335–343.

Wolfbeis, O.S., 1990. Fiber-optic sensors in bioprocess control. In: Twork, J.V., Yacynych, A.M. (Eds.), Sensors in Bioprocess Control. Marcel Dekker, New York, pp. 95–125.

Wolfbeis, O.S. (Ed.), Fiber Optical Chemical Sensors and Biosensors, vol. 2. CRC Press, Boca Raton, FL 1991, p. 61.

Wolfbeis, O.S., Weis, L.J., Leiner, M.J.P., Ziegler, W.E., 1988. Fiber-optic fluorosensor for oxygen and carbon dioxide. Anal. Chem. 60, 2028–2030.

Zhang, Z., Seitz, W.R., 1984. A carbon dioxide sensor based on fluorescence. Anal. Chim. Acta 160, 305–309.

But what good could a CO_2 sensing film be if it could not be used broadly? So we turned to Dan Kostov's expertise and came up with associated low-cost opto-electronics and came up with a CO_2 sensing system for fermentation applications. The following paper describes its construction and use.

Low-Cost Noninvasive Optical CO_2 Sensing System for Fermentation and Cell Culture

Xudong Ge, Yordan Kostov, Govind Rao

Center for Advanced Sensor Technology, Department of Chemical and Biochemical Engineering, University of Maryland, Baltimore County, 1000 Hilltop Circle, Baltimore, Maryland 21250; telephone: 410-455-3415; fax: 410-455-6500; e-mail: grao@umbc.edu

Received 13 May 2004; accepted 9 September 2004

Published online 29 December 2004 in Wiley InterScience (www.interscience.wiley.com). DOI: 10.1002/bit.20337

Abstract: High-throughput bioprocessing is a very promising technique for bioprocess development and optimization because of its high efficiency. The key to its development has been the availability of simple and inexpensive sensors to monitor the bioprocesses conducted in its small-scale bioreactors. Here we report on a low-cost noninvasive CO_2 sensing system suitable for any transparent vessel. The system was composed of a CO_2 sensing patch, a coaster, an interface, and a computer. The sensing film was prepared using the ion-pair technique. The coaster was a small self-made device with necessary optics and electronics for ratiometric measurements with a component cost of less than $100. Results show that the system was stable and reliable despite its simplicity and low cost. The sensitivity of the CO_2 sensing system was not affected by pH, media type, or temperature. It was shown to be stable for at least 10 days, long enough for most bioprocesses. © 2004 Wiley Periodicals, Inc.

Keywords: CO_2; sensor; fluorescence; high-throughput bioprocessing

INTRODUCTION

Although fermentation has been practiced by mankind since prehistoric times, it is since the advent of genetic engineering and the recent advances in computer science and process control that biotechnology began to boom very rapidly. Now bioprocesses are extremely important in a variety of industries such as biopharmaceutical, food, and environment (Bakoyianis and Koutinas, 1996; Bylund et al., 2000; Handa-Corrigan et al., 1998).

In conventional bioprocessing, the cost for process development and optimization makes up a large part of the total investment because of its low efficiency. To determine the optimal environmental and nutritional conditions, a large number of experiments under varying conditions have to be conducted. Four different scales of equipment can be used for process optimization; each has its advantages and disadvantages. The cost is prohibitively high if the process optimization is performed in large-scale bioreactors. Although process optimization can be performed in lab-scale bioreactors (1–100 L), it is still costly and time-consuming (Kennedy and Krouse, 1999). As a result, only a limited number of experiments can be conducted. Process optimization performed in shake flasks is less costly and can be conducted in parallel, but the cultivation conditions are generally not controlled except for temperature and agitation. Thus, such studies can only provide limited information about the bioprocess. It would be greatly beneficial to instrument shake flasks to extract more process information from them. We have previously reported on a non-invasive oxygen sensor designed to monitor oxygen levels in shake flasks (Gupta and Rao, 2003; Tolosa et al., 2002). In this article we describe a similar sensor developed for monitoring pCO_2.

Monitoring of carbon dioxide in bioprocesses is of importance because it affects microbial growth in various ways (Dixon and Kell, 1989; Kato and Tanaka, 1998; Shang et al., 2003; Sparringa et al., 2002). It is a product of cell respiration and can pass through cell membranes to influence the pH inside cells. Thus, variations of dissolved CO_2 concentration can affect the cells' morphology, their metabolic products, and rates.

The CO_2 sensor commonly used in bioprocess at present is the YSI 8500 CO_2 monitor (Yellow Springs Instrument Co., Inc., Youngstown, OH). Although it can monitor the dissolved CO_2 concentration continuously on-line, it is bulky and invasive, and as such not very suitable for small-scale bioreactors. Here we report a low-cost noninvasive CO_2 sensing system suitable for any transparent vessels. For convenience, it was tested in *E. coli* (NM303) fermentation conducted in a 250-mL shake flask. However, because of its noninvasiveness and miniature scale, this technique can be easily transferred to other types of transparent bioreactors (Harms et al., 2002; Kostov et al., 2001).

Correspondence to: Govind Rao

Contract grant sponsors: National Science Foundation; Genentech; Merck; Pfizer

Contract grant number: BES0091705

EXPERIMENTAL

Materials

Cetyltrimethylammonium hydroxide solution (25 w/w %) in methanol (CTMAOH) was purchased from Fluka. 8-hydroxypyrene-1,3,6-trisulfonic acid trisodium salt (HPTS) was obtained from Molecular Probes Inc. (Eugene, OR). Methanol and chloroform were purchased from Aldrich and used without further purification. Platinum divinyl complex (PC074), polydimethylsiloxane, vinyldimethyl terminated (PS443) and (30–35%) methyl-hydro-(65–70%) dimethylsiloxane copolymer (PS123) were obtained from United Chemical Technologies, Inc. (Bristol, PA). Pure nitrogen and pure CO_2 were obtained from Potomac Airgas (Linthicum, MD). Gas mixtures with known CO_2 contents were obtained by blending pure CO_2 with nitrogen through two flow meters (FM4332 and FM4333; Advanced Specialty Gas Equipment Corp., South Plainfield, NJ).

CO_2 Sensing System

The low-cost noninvasive CO_2 sensing system is shown in Figure 1. The system is composed of a CO_2 sensing patch, a coaster, an interface, and a computer. The sensing patch was fabricated as reported previously (Ge et al., 2003) except that a different catalyst, PC074, was used. This catalyst is more efficient and colorless, so it is more suitable for optical applications. To prepare the CO_2 sensing patch, a hydrophobic silicone membrane was first produced using PS123, PS443 as monomers, and PC074 as catalyst. Then, a dye solution was prepared by dissolving a certain amount of HPTS in chloroform. To this dye solution, a certain amount of organic base, CTMAOH, was added to form ion pairs with the dye. A piece of silicone membrane was dropped into the dye solution, and soaked for 30 minutes. Finally, the swollen dyed silicone membrane was removed from the dye solution, allowed to dry at room temperature, and washed with deionized water. The patch was then stored in phosphate buffer (pH7.5) before test. During the patch preparation, the formation of the ion pairs has two important functions. First, it can easily diffuse into the expanded silicone membrane that has been soaked in the dye solution. Thus, it helps transfer the polar dye molecules into a hydrophobic membrane. Second, the dye in the ion pairs exists in its deprotonated form. This initial state is essential for a CO_2-sensing patch to work.

The coaster that is developed is a miniature dual wavelength fluorometer specifically designed to measure the excitation ratio of the patch in small form factor. It consists of two commercially available LEDs with emissions at 400 (Bivar, Irvine, CA) and 450 nm (Nichia, Japan), respectively. The "red tail" in the LED emission was filtered using a common short pass filter BG-12 (Schott, Germany). The emission detection was performed by a photodiode, filtered with a band pass filter (center wavelength 550nm, 40 nm FWHM). The LED light was modulated at approximately 10 kHz, which helps to suppress the influence of the ambient light. The light intensity was converted into a voltage by a transimpedance amplifier, and the fluorescence amplitude was quantified using an onboard synchronous detector (Fig. 2). The LEDs were fired sequentially, and the fluorescence intensity was measured. The digital control and the analog-to-digital conversion were performed by a U12 LabJack digital acquisition (DAQ) card (LabJack Corp., Lakewood, CO). The digital signals were recorded by a computer, which also calculates

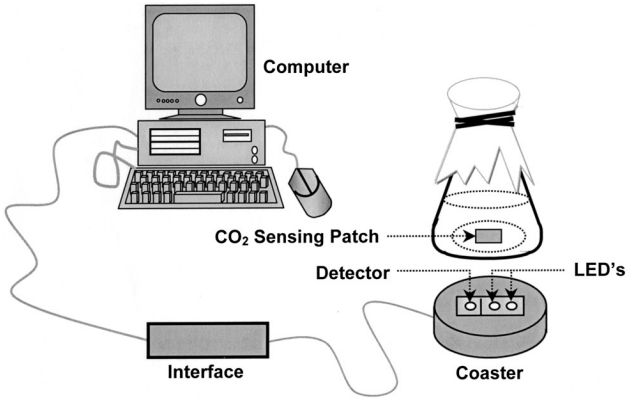

Figure 1. Low-cost noninvasive CO_2 sensing system.

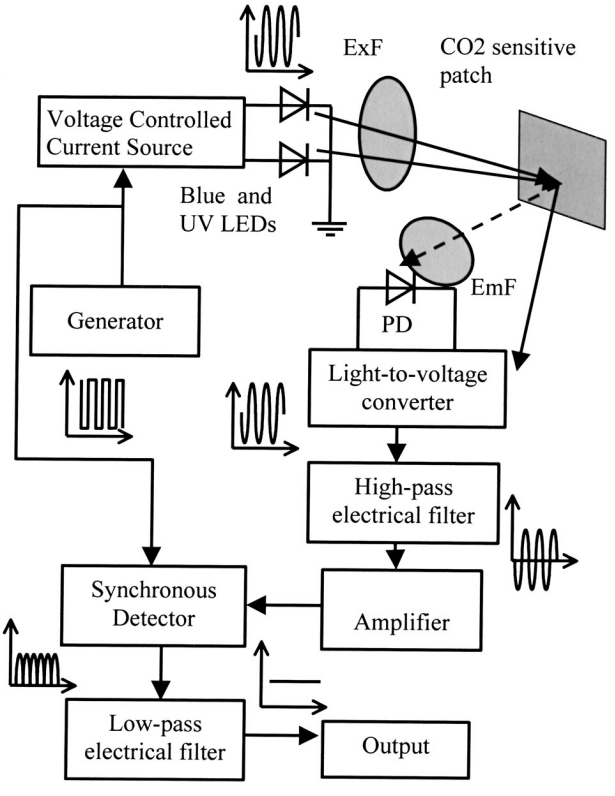

Figure 2. Block schematics of the optoelectronics. The shapes of the electrical signals throughout the stages are also shown.

the emission ratio. The cost of the electronics (without the DAQ card) was under $100 .

Before the whole sensing system was tested, a piece of sensing film was first affixed to a piece of transparency film. Then, the sensing film was covered by a piece of white filter paper slightly larger than the sensing film to block off the background fluorescence from the broth. A piece of black tape with a small square window in the middle was used to fix the sensing film and the white filter paper onto the transparency film. After that, the whole sensor assembly was inserted into the bioreactor and fixed onto the bottom with silicone grease. Although the sensing patch is autoclavable (Ge et al., 2003), the supporting components (black tape, silicone grease) are not. Thus, the whole assembly has to be sterilized with alcohol. To make the CO_2 sensing system easier to use and more useful, an autoclavable, ready-to-use CO_2 sensing assembly is being developed. The successful preparation of such an assembly will greatly expand the usage of the CO_2 sensing system, especially in cell culture and high-throughput bioprocessing.

Fermentation

The seed culture consisted of 1% of inoculum in 5 mL of LB medium incubated at 37°C in a 15-mL plastic tube with shaking at 260 rpm (Orbit Environ Shaker; Lab-line Instruments; Melrose Park, IL) for 8–10 h. Before fermentation, the shake-flask containing the sensing film was thoroughly rinsed with 70 v/v % ethanol solution for sterilization. Then, 48 mL of LB medium was added and inoculated with 2 mL of seed inoculum. The shake-flask was placed on a shaker with the coaster positioned underneath for online dissolved CO_2 measurements. The fermentation was carried out at 37°C with shaking at 260 rpm. 1.0 mL of broth sample was taken from the flask every 20–40 minutes for biomass analysis. The cellular optical density (OD) was measured with a Hewlett Packard 8452A Diode Array Spectrophotometer at 600 nm. pH was measured with an IQ240 pH meter (IQ Scientific Instruments, San Diego, CA). For comparison, the broth sample was also analyzed off-line for dissolved CO_2 concentrations with a DT60 IBI Biolyzer.

RESULTS AND DISCUSSION

This CO_2 sensing system uses HPTS as the sensing element because of its large Stoke's shift, high photo-stability, low toxicity, and relatively low cost. More important, this pH sensitive probe has two excitation maxima at 405 nm and 460 nm, corresponding to its protonated and deprotonated forms, respectively. This property allows for ratiometric measurements, i.e., we can use the ratio of the two maximum fluorescence intensities instead of the fluorescence intensity at a single wavelength to correlate the CO_2 concentrations. The advantage of ratiometric measurement over single-intensity-based measurement is that it is insensitive to the fluctuations in intensity of the excitation source, leaching or photo bleaching of the probe, and positioning of the sample. When the sensing membrane contacts a sample, the CO_2 molecules in the sample diffuse into the membrane and react with the ion pairs inside. This reaction reverses the dye back to its protonated form, inducing a change in the relative magnitude of the two excitation maxima. The hydrophobic nature of the silicone membrane prevents hydrogen ions from entering, and thus prevents pH interference.

Compared with commercially available CO_2 sensing devices, which typically cost several thousand dollars, this system is very inexpensive. The electronics use mass-produced components manufactured for the telecom industry and are designed specifically to be powered up and interfaced with a low-cost ($110), USB powered DAQ card. In this way, any computer with an USB port can be used together with the sensor. Another important feature of the system is its minimal invasiveness. The coaster is positioned outside the bioreactor, and the measurements are made without direct contact with the media except for the sensing patch, which can be alcohol or radiation sterilized before the fermentation is conducted.

In this article we describe the performance of the system specially related to bioprocess applications such as cross-sensitivity to media type, effect of temperature, and long-term stability.

Cross-Sensitivity of the Sensing Film to the Type of the Media

Figure 3 illustrates the effect of different media on the sensitivity of the sensing system. One of the calibration curves shown in this figure was measured in LB media while the other in phosphate buffer with the same ionic strength. It can be seen that the type of the media has no effect on the sensitivity of the sensing patch. This property is very good for a sensor as it makes calibration much easier. LB media is an undefined media prepared with tryptone, yeast extract, sodium chloride, and potassium phosphates. Although the ionic strength can be prepared precisely, its composition is never known, and may be different from batch to batch. If the composition of the media affects the sensitivity of the sensing patch, it will be necessary to calibrate the sensing system for each batch of media. Here, as the CO_2 sensing patch is not affected by the type of the media, only a one-time calibration, which can be done in buffers with the same ionic strength, is required. Thus, the use of the sensor is very facile.

Effect of Temperature on the Sensitivity of the Sensing System

Besides media, temperature is another important factor affecting the bioprocess. The effect of temperature on the sensitivity of the sensing system is shown in Figures 4 and 5.

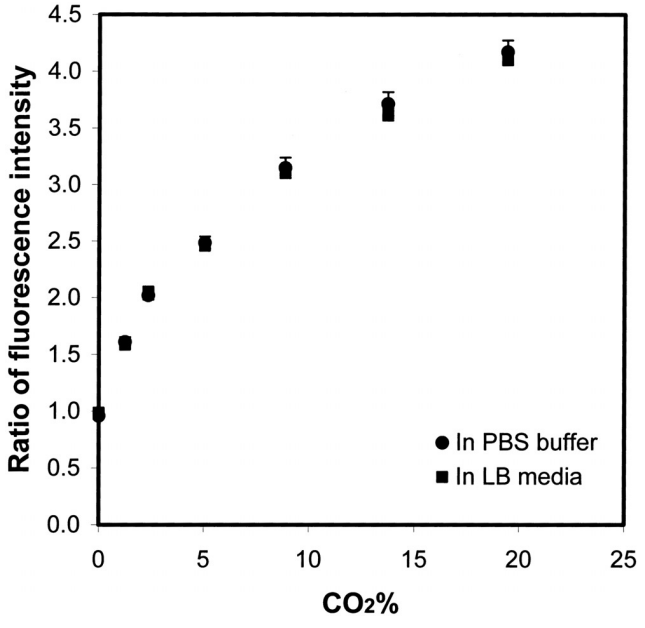

Figure 3. Effect of media on the sensitivity of the sensing system at room temperature. pH: 6.94; ionic strength: 0.244M.

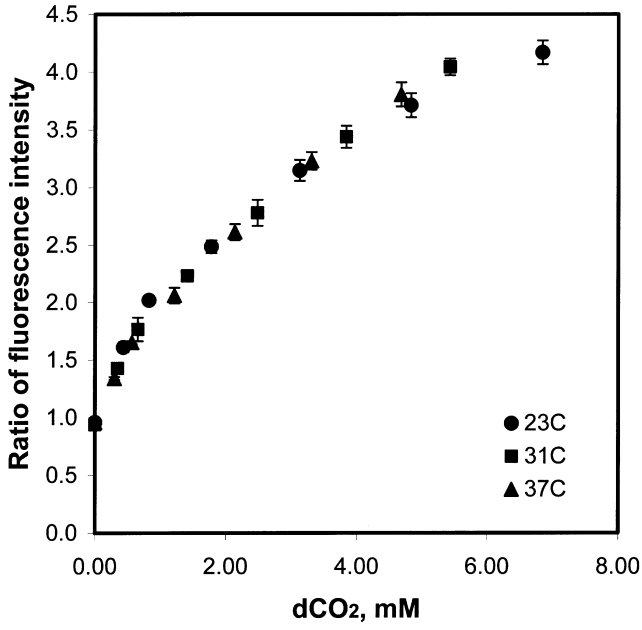

Figure 5. Ratio of fluorescence intensity plotted against dissolved CO_2 concentration in 10 mM, pH 7.0 phosphate buffer.

It can be seen that the ratio of fluorescence intensity decreases with temperature at the same gas-phase CO_2 concentrations (Fig. 4). However, when the ratio of fluorescence intensity is plotted against the dissolved CO_2 concentrations calculated by Henry's Law (Stephen and Stephen 1964), it is not affected by temperature at all (Fig. 5), showing that the effect of temperature is only caused by the change in solubility of CO_2 in water. This result suggests that together with a temperature sensor, the CO_2 sensing system described here can monitor the dissolved CO_2 concentrations at different temperatures without need for recalibration. Importantly, most bioprocesses are run under temperature control, so temperature sensitivity is a non-issue.

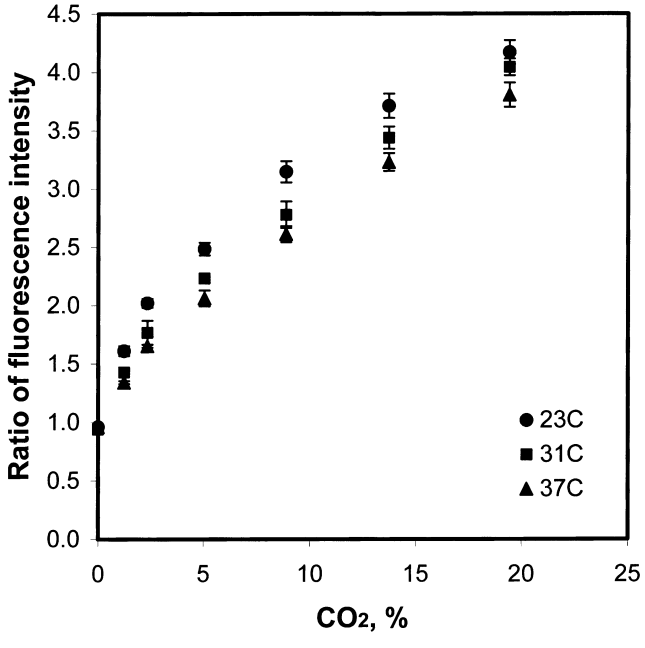

Figure 4. Ratio of fluorescence intensity plotted against gas-phase CO_2 concentration in 10 mM, pH 7.0 phosphate buffer.

Long-Term Stability of the Sensing System

Long-term stability is an important requirement for on-line measurements when repeated recalibration is not possible. When used in *E. coli* fermentations, a sensor should be stable for at least several hours. For cell-culture applications, however, it may be necessary to be stable for several days. To test the long-term stability of the CO_2 sensing system, the system was run continuously for several days, and meanwhile, challenged occasionally by changes in pH and ionic strength (Fig. 6). Results show that the CO_2 sensing system is not affected by changes in pH at all as long as the change in pH is not accompanied by a significant change in ionic strength. Without changes in ionic strength, the CO_2 sensing system was stable for at least 10 days, showing the coaster itself is stable although it is very simple and low cost. For fermentations with no significant changes in ionic strength (i.e., no or minimal pH control), this CO_2 sensing system can be used with no need for recalibration during the process. However, when the ionic strength significantly increases, results show that the sensitivity of the sensing patch decreases, and the effect of the ionic strength is different at different gas-phase CO_2 concentrations. The lower the gas-phase CO_2 concentration, the less the effect of the ionic strength. The cross-sensitivity of the sensor to ionic strength may be caused by changes in water content in the sensing patch. Because

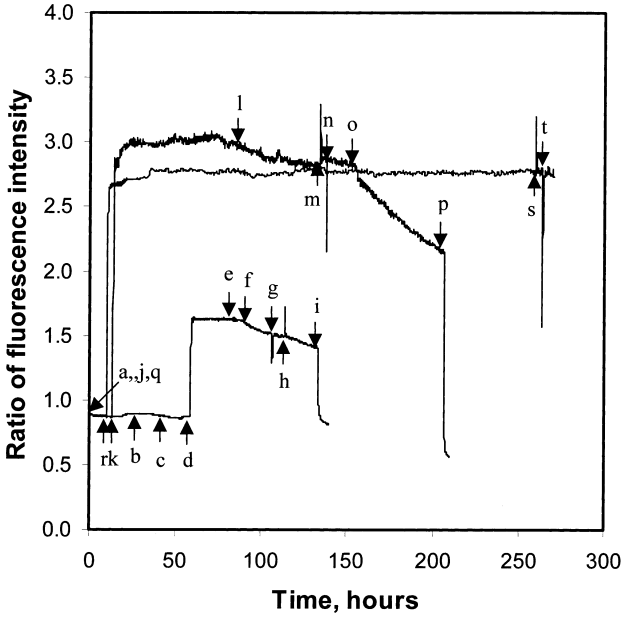

Figure 6. Long-term stability of the sensing system at room temperature. CO_2%: 0.0% at a–c, i, j, p, and q; 1.2% at d–h; 5.0% at r–t; and 6.8% at k–o. pH: 6.0 at h, i, m, and s; 7.0 at a–f, j–l, q, and r; and 8.0 at g, n–p, and t; ionic strength: 0.022M at a, j, k, q, and r; 0.026M at s; 0.030M at t; 0.122M at b and l; 0.124M at m; 0.128M at n; 0.222M at c and d; 0.228M at o and p; 0.322M at e; 0.422M at f; 0.457M at g; and 0.525M at h and i.

the sensing patch is not hydrophobic enough, it may be partially permeable to water vapor or liquid water. The change in ionic strength in the outer environment induces a gradual change in inner environment, which, in turn, causes a drift in sensitivity. Using a more hydrophobic silicone may be helpful to removing this cross-sensitivity. This approach is also being investigated.

Application of the Sensing System in *Escherichia coli* Fermentation

The sensing film was tested in a batch fermentation of *E. coli* NM303 at 37°C in a 250-mL shake flask. The coaster was placed under the shake flask for on-line dissolved CO_2 measurements. Figure 7 shows the pH profile, the optical density profile, and the dissolved CO_2 concentration profile recorded on-line by the CO_2 sensing system. For comparison, the dissolved CO_2 concentrations were also measured off-line with an available device, an IBI DT60 Biolyzer. The biolyzer analyzes CO_2 by using a procedure called differential potentiometry. The slide contains two identical ion-selective electrodes. Each consists of a silver and a silver chloride layer over which additional film layers have been added to make the electrodes selective for CO_2 ions (Ortho-Clinical Diagnostics, 1999). Results show that the biolyzer gave a much higher CO_2 concentration than the CO_2 patch. Two reasons may explain this big difference. On one hand, the biolyzer measures the total CO_2 concentration while the CO_2 sensing patch measures the CO_2 concentration only in unassociated

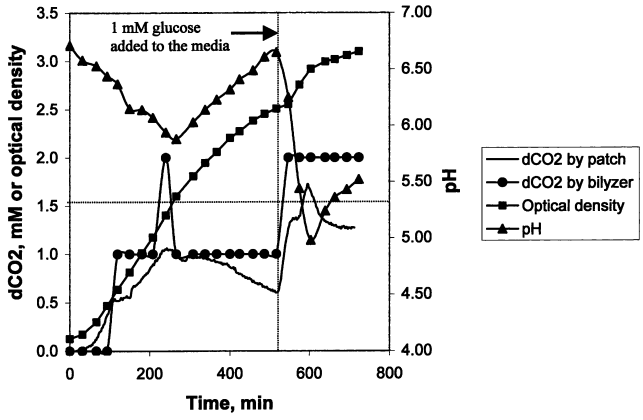

Figure 7. Application of the sensing system in *E. coli* fermentation at 37°C. The ionic strength of the LB medium is 0.244M.

form. On the other hand, many factors including nitrate, lactate, hippurate, and proteins, etc., may significantly increase the CO_2 results of the biolyzer (Ortho-Clinical Diagnostics, 1999). These substances may plentifully exist in the LB media. The difference between the CO_2 results of the biolyzer and its initial CO_2 concentration in fresh media reflects the CO_2 evolution during the fermentation (Fig. 7). Compared with the CO_2 concentration profile recorded by the CO_2 sensing patch, it can be seen that both devices give exactly the same trends in CO_2 evolution. Comparatively, the CO_2 patch has a much better resolution than the biolyzer. After examining the pH profile, we can see that it inversely reflects the profile of the CO_2 concentration. This shows that the CO_2 concentration was correctly tracked by the sensing system from another perspective. After 1 mM of glucose was added to the media, all profiles change as expected, showing again the ability of the sensing system to simply track the dissolved CO_2 concentration.

CONCLUSIONS

A low-cost noninvasive CO_2 sensing system suitable for any transparent vessels was constructed. The system consists of a CO_2 sensing patch, a coaster, an interface, and a computer. It is very simple and has a low cost. It is stable for at least 10 days, stable enough for most situations requiring CO_2 monitoring. The sensitivity of the system is not affected by the type of the media, pH, or temperature. Thus, it is not necessary to recalibrate when no significant changes in ionic strength occur. This system can correctly track the trends in CO_2 evolution in *E. coli* fermentation with a much higher resolution than IBI DT60 biolyzer.

The technology described in this article has been licensed to Fluorometrix, in which the authors have an equity position.

References

Bakoyianis V, Koutinas AA. 1996. A catalytic multistage fixed-bed tower bioreactor in an industrial-scale pilot plant for alcohol production. Biotechnol Bioeng 49:197–203.

Bylund F, Castan A, Mikkola R, Veide A, Larsson G. 2000. Influence of scale-up on the quality of recombinant human growth hormone. Biotechnol Bioeng 69:119–128.

Dixon NM, Kell DB. 1989. The control and measurement of "CO_2" during fermentations. J Microbiol Meth 10:155–176.

Gupta A, Rao G. 2003. A study of oxygen transfer in shake flasks using a non-invasive oxygen sensor. Biotechnol Bioeng 84(3):351–358.

Ge X, Kostov Y, Rao G. 2003. High-stability non-invasive autoclavable naked optical CO2 sensor. Biosensors Bioelectr 18:857–865.

Handa-Corrigan A, Hayavi S, Ghebeh H, Mussa NA, Chadd M. 1998. Novel porous matrix and bioreactors for high density cultures of insulinoma cell lines: Insulin secretion and response to glucose. J Chem Technol Biotechnol 71:51–56.

Harms P, Kostov Y, Rao G. 2002. Bioprocess monitoring. Curr Opin Biotechnol 13:124–127.

Kato I, Tanaka H. 1998. Influence of CO_2 ventilation on microbial cultivation in shake-flasks. Biotechnol Techniques 12(4):325–328.

Kennedy M, Krouse D. 1999. Strategies for improving fermentation medium performance: A review. J Industr Microbiol Biotechnology 23: 456–475.

Kostov Y, Harms P, Randers-Eichhorn L, Rao G. 2001. Low-cost microbioreactor for high-throughput bioprocessing. Biotechnol Bioeng 72(3):346–352.

Ortho-Clinical Diagnostics. 1999. Operator's Manual for Vitros DT II system. Rochester, NY: Ortho-Clinical Diagnostics.

Shang L, Jiang M, Ryu CH, Chang HN, Cho SH, Lee JW. 2003. Inhibitory effect of carbon dioxide on the fed-batch culture of *Ralstonia eutropha*: Evaluation by CO_2 pulse injection and autogenous CO_2 methods. Biotechnol Bioeng 83(3):312–320.

Sparringa RA, Kendall M, Westby A, Owens JD. 2002. Effects of temperature, pH, water activity and CO_2 concentration on growth of *Rhizopus oligosporus* NRRL 2710. J Appl Microbiol 92:329–337.

Stephen J, Stephen T. (Eds.). 1964. Solubilities of inorganic and organic compounds, vol. 2: tertiary systems, part 2. London: Pergamon Press.

Tolosa L, Kostov Y, Harms P, Rao G. 2002. Noninvasive measurement of dissolved oxygen in shake flasks. Biotechnol Bioeng 80(5):594–597.

PART II: Bioreactor Applications

The term “bioreactor” is used in its broadest sense and in this case, we mean any vessel or system designed to culture cells. Non-invasive sensors are agnostic and as long as one can get light in/out of the desired space and a sensor patch can be mounted, then any imaginable system can be converted into an instrumented bioreactor. We start out with the broadest class of vessels: T-flasks and shake (Erlenmeyer) flasks and then proceed to spinner flasks, bag reactors, minibioreactors. Finally, we show how there are particular genes that can used as markers for successful scale-up/down in the sense that if the cell behaves in the same manner across different scales, then the holy grail of seamless scale-up has been realized.

In all these instances, we have attempted to connect the dots where critical engineering parameters are measured across different scales and how the bioreactor operating conditions can be manipulated to achieve successful process transfers across many types and scales of bioreactors. In every case, accurate parametric monitoring is critical.

Chapter Three: Process Scouting Devices

Most “bioreactors” tend to be simple culture vessels with no instrumentation. These are widely used in early stage process development and tend to be either static, shaken or stirred configurations. In my trips to industry, I have seen all combinations used. When asked as to the rationale of a particular culture vessel over another (i.e. T-flask, shake- or spinner-flask), the answer tended to be along the lines either of “if it ain’t broke, don’t fix it” or a legacy effect where “this is how its always been done.” Consequently, the most critical part of the evolution of a process, the large number of media or strain screenings end up being done in un-instrumented vessels. This is largely true to this day, since the shift to instrumented minibioreactors tends to be too expensive for most people to adopt. Given this reality, we attempted to add sensors to a number of process scouting vessels and analyze them for various engineering parameters that are typically used during fermentation and cell culture in bioreactors. We also tried to see how the cellular environment behaved as a function of growth in these systems. The following papers address these aspects.

We had already seen that even in a vigorously agitated shake flask, oxygen limitation was observed. The shake flask is the mainstay and probably the most widely used bioreactor in fermentation process development. It has long been studied and modified to increase oxygen transfer using a variety of schemes such as changing the geometry, adding baffles, improving the closure etc. However, what was lacking in the literature was a systematic study of how much these factors affected oxygen levels.

The following study quantitatively characterizes these effects and was performed meticulously by Atul Gupta. Figure 3 shows the enormous variation in the time that growing cells experience oxygen limitation depending on the type of plug and the presence of baffles. If there were ever a data-driven case to be made for the need for monitoring oxygen levels in shake flaks fermentations, this is it.

Finally, if the shake flask is used for screening, it is important to consider the eventual scaled-up fermentor environment that cells will find themselves in. This study also demonstrated that by matching k_La one can approximate equivalent performance in the two systems (Figure 6).

A Study of Oxygen Transfer in Shake Flasks Using a Non-Invasive Oxygen Sensor

Atul Gupta, Govind Rao

Department of Chemical and Biochemical Engineering, University of Maryland Baltimore County, 101 ECS Building; 1000 Hilltop Circle, Baltimore, Maryland 21250; telephone: 410-455-3415; fax: 410-455-6500; e-mail: grao@umbc.edu

Received 26 February 2003; accepted 17 April 2003

Published online 21 August 2003 in Wiley InterScience (www.interscience.wiley.com). DOI: 10.1002/bit.10740

Abstract: We describe a study of oxygen transfer in shake flasks using a non-invasive optical sensor. This study investigates the effect of different plugs, presence of baffles, and the type of media on the dissolved oxygen profiles during *Escherichia coli* fermentation. We measured the volumetric mass transfer coefficient (k_La) under various conditions and also the resistances of the various plugs. Finally, we compared shake flask k_La with that from a stirred tank fermentor. By matching k_La's we were able to obtain similar growth and recombinant protein product formation kinetics in both a fermentor and a shake flask. These results provide a quantitative comparison of fermentations in a shake flask vs. a bench-scale fermentor and should be valuable in guiding scale-up efforts. © 2003 Wiley Periodicals, Inc. *Biotechnol Bioeng* **84**: 351–358, 2003.

Keywords: shake flasks; oxygen transfer; stirred tank fermentor; oxygen sensor

INTRODUCTION

Shake flasks are used in the biotechnology industry for a variety of tasks including the screening of wild-type strains, strain development, elucidation of metabolic pathways, media optimization, investigations of basic process conditions, and evaluation of fundamental growth kinetics. These studies are performed in shake flasks because of the sheer number of experiments involved (Kennedy et al., 1994). Experimental investigations in these vessels are often the first step in fundamental studies as well as in developing a large-scale fermentation process.

Aeration in shake flasks is achieved by simple gas liquid contact aided by shaking the vessels in reciprocating or rotary shaking machines. Shake flasks are traditionally sealed with different types of plugs to prevent contamination. These plugs however are not good closures with regard to air permeability (McDaniel and Bailey, 1969; McDaniel et al., 1965; Tunac, 1989). It has been shown that a cotton plug in the shake flask can limit the mass transfer significantly such that the oxygen in the headspace may fall to as low as 6% and carbon dioxide may accumulate up to as high as 15% (Schultz, 1964). Oxygen transfer in shake flasks partly depends on the flow of air through the plug and so the length of the neck of the flask or the type of closure greatly affects the oxygen transfer to the surface of the liquid. Many workers have demonstrated that the use of baffled flasks result in increase in oxygen transfer (Gaden, 1962; McDaniel et al., 1965; Smith and Johnson, 1954). Baffles increase the agitation in the liquid as well as the available surface area for oxygen transfer at the air–liquid interface. Oxygen availability is very critical during microbial growth in submerged fermentations because of the poor solubility of oxygen in water. Changes in oxygen availability may lead to drastic effects on fermentation kinetics (Clark et al., 1995; Delgado et al., 1989; Hopkins et al., 1987). However, neither the plugs nor the geometry of flasks have been standardized for use in bioprocess development. This can be attributed to the lack of bioprocess monitoring in these vessels which has led to a poor understanding of physical parameters that characterize the culture growth conditions (Buchs, 2001; Henzler and Wuppertal, 1991) in shake flasks.

To assess if a given culture vessel would be able to supply oxygen at a nonlimiting rate, it is essential to have a good estimate of the oxygen transfer capacity of the vessel. This can be measured in terms of the oxygen mass transfer coefficient (k_La). The k_La often serves to compare the efficiency of bioreactors and their mixing devices, as well as being an important scale-up factor in the bioprocess industry. It is the measure to quantify the effects of operating variables on the provision of oxygen. Hence, it becomes extremely important to measure the oxygen mass transfer coefficient in a bioreactor. So far, shake flasks have not been used to perform the scale-up of fermentation processes due to the lack of knowledge of the conditions under which shake-flask fermentations are performed. However, with the use of modern optical sensors and bioprocess monitoring devices, the role of shake flasks in bioprocess development may be further improved.

The transfer of oxygen from outside of the flask to the

Correspondence to: Govind Rao

Contract grant sponsor: National Science Foundation; DuPont; Fluorometrix; Genentech; Merck; Pfizer

Contract grant number: BES0091705

inside takes place through diffusion through the plug. The headspace air diffuses into the liquid in the flask. The oxygen balance for the headspace in the flask can thus be written as follows:

Increase in gas phase oxygen in the flask = (rate of diffusion through cotton plug) – (rate of transfer across gas liquid interface)

Increase in gas phase oxygen in the flask =

$$k(C_G - C_H) - k_L a\left(\frac{C_H}{M} - C_L\right) \cdot V_L \quad (1)$$

where k = plug transfer coefficient; $k_L a$ = gas–liquid interface transfer coefficient; C_H = concentration of oxygen in headspace; C_G = concentration of oxygen outside flask; C_L = concentration of oxygen in liquid; V_L = volume of liquid in flask; M = equilibrium constant.

When the steady state is achieved the total flux across the plug would be same as the flux across the gas liquid interface. Rearranging the above equation thus:

$$\phi = \left[\frac{1}{Mk} + \frac{1}{k_L a V_L}\right]^{-1}\left(\frac{C_G}{M} - C_L\right) \quad (2)$$

At equilibrium across the cotton plug $\frac{C_G}{M}$ can be replaced with C_L^* (saturation concentration of oxygen in liquid). The resulting equation can be compared with the *OTR* equation given as:

$$OTR = k_L a(C_L^* - C_L) \quad (3)$$

and hence the equivalent mass transfer coefficient for a shake flask can be defined as:

$$(k_L a)_{eq} = \frac{1}{V_L}\left[\frac{1}{Mk} + \frac{1}{V_L k_L a}\right]^{-1} \quad (4)$$

The above expression for mass transfer coefficient is equivalent to the sum of resistances at the sterile plug and at the gas–liquid interface. In previous studies, others have tried to measure the two transfer coefficients separately (Maier and Buchs, 2001; Mrotzek et al., 2001) using the sulfite oxidation method (Corman et al., 1957; Smith and Johnson, 1954; Tunac, 1989) or gassing-out method with a Clark-type electrode (Hirose et al., 1966; Schultz, 1964) but the combined mass transfer coefficient has not been reported. The previously used methods have their limitations (Schell et al., 2001). The sulfite oxidation method requires sampling at regular intervals thus limiting its utility. To avoid regular sampling some workers (Hermann et al., 2001) have used an optical online system for a sulfite-oxidation method of oxygen transfer measurement. Clark electrodes used in other studies for OTR measurements in shake flasks are not appropriate for a variety of reasons (Tribe et al., 1995). Non-invasive optical sensors are a better alternative to measure oxygen concentration in small bioreactors because they circumvent a variety of problems associated with the conventional probes.

In this study, we have retrofitted the shake-flask system with a luminescence-based sensor for online measurement of oxygen (Tolosa et al., 2002). This is a non-invasive sensor that measures the dissolved oxygen concentration in a shake flask with minimal perturbation of the actual conditions of a growing culture.

MATERIALS AND METHODS

Optical Oxygen Sensor

The optical sensor system (Fluorometrix, Stow, MA) used for oxygen measurement consists of two parts: a coaster and a patch (Tolosa et al., 2002). The coaster contains LEDs for excitation and photo detector for light detection. The patch is paper-thin, autoclavable, and contains an oxygen-sensitive luminescent dye, [1,2-bis(diphenyl phosphino)ethane Pt[$S_2C_2(Ch_2\text{-}CH_2\text{-}N\text{-}2\text{-pyrimidine}](BPh_4)$, immobilized in a silicone matrix. The patch is mounted on the interior surface of the flask (Fig. 1). The flask sits on top of the coaster, which is connected to a computer. The computer runs a Lab View (National Instruments Inc., Austin, TX) program to acquire the data online. This sensor is based on the dynamic quenching of excited-state of the luminescent metal-ligand complex by molecular oxygen. Dynamic quenching usually follows the Stern-Volmer equation:

$$\frac{I_0}{I} = \frac{\tau_0}{\tau} = 1 + k_{sv}\tau_0[Q] \quad (5)$$

where I = emission intensity, τ = decay lifetime, k_{sv} = stern volmer constant, $[Q]$ = quencher concentration, subscript 0's indicate the absence of quencher (oxygen). The concentration of the quencher (O_2 in this case) is determined by measuring the change in the lifetime of the luminophore (Bambot et al., 1994; Lakowicz, 1999).

The luminescent oxygen sensor was calibrated with water in the flask and the temperature controlled at 37°C. The sensor was mounted in the shake flask, which was sparged with a mixture of nitrogen and oxygen. The mixture ratio

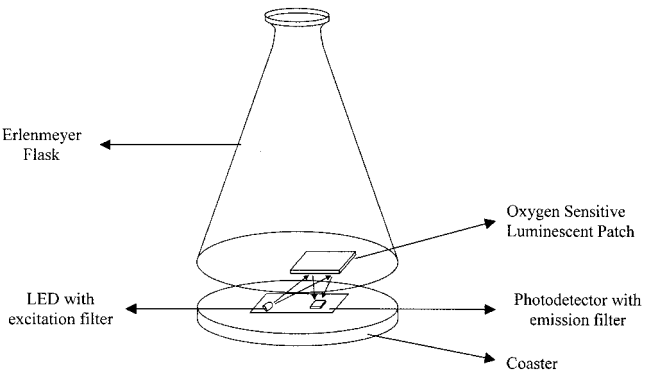

Figure 1. The above schematic is a close view of the flask and the coaster. The flask is equipped with a paper-thin luminescent patch mounted on the interior of the flask. Underneath the flask is the coaster with light-emitting diode (LED) with an excitation filter, which emits the excitation light, and detector with an emission filter, which receives the emission light from the patch.

was controlled with the help of precision gas mass flow meters (Emerson Electric Co., Brooks Instrument division, Hatfield, PA).

Response Time Correction for k_La Measurement

The gassing-out method of k_La measurement (described later) is associated with a limitation. This method necessitates the use of membrane-type electrodes, the response time of which may be inadequate to reflect the true change in the rate of oxygenation over a short period of time (Tribe et al., 1995). The probe response-time is the time needed to record 63% of a stepwise change and this should be much smaller than the mass transfer response time of the system ($1/k_La$) (Stanbury and Whitaker, 1989).

Assuming the diffusion of oxygen through the membrane of the probe as a first-order response (Brown, 2001), the diffusion process can be defined as:

$$\frac{dC_p}{dt} = \frac{1}{\tau_p}(C_L - C_p) \tag{6}$$

where C_p = the concentration of oxygen at the probe tip, C_L = concentration of oxygen in bulk fluid and τ_p is the time constant of the probe.

The time constant (63% response) of the fluorescence sensor was calculated to be 30 s and that of the Clark electrode used in this study to be 3 s at 37°C.

Substituting C_L from Eq. (3) in Eq. (6) and solving for C_P, we get:

$$C_p(t) = C_L^*\left(1 + \frac{k_La}{k_p - k_La}e^{-k_pt} - \frac{k_p}{k_p - k_La}e^{-k_Lat}\right) \tag{7}$$

where, k_La = response time corrected mass transfer coefficient and k_p = mass transfer coefficient of the probe (inverse of the probe time constant).

All the values of transfer coefficient reported in this text were corrected for the delay due to the response time of the oxygen-measuring device.

Mass Transfer Coefficient Measurements

In this study we used the method of gassing out for the measurement of mass transfer coefficient due to the simplicity of the method. The culture vessel was first filled to working volume with a reference medium. The medium was then purged of oxygen by bubbling nitrogen through it until the medium was oxygen-free. Finally, the system was sparged with air and the resulting oxygen concentration was measured (Stanbury and Whitaker, 1989). We used this method of measurement of oxygen transfer coefficient in shake flasks to measure the two transfer coefficients of the two resistances in a shake flask separately.

Experiment 1

The gas–liquid mass transfer coefficient in a shake flask was measured by the method described by Suijdam et al. (1978). In this method the oxygen in the shake flask was first displaced by nitrogen. After this the gas phase above the liquid was replaced by air, the shaker was turned on and the oxygen tension in the liquid in shake flask was registered with time.

Experiment 2

The plug transfer coefficient was measured by placing the oxygen sensor in the headspace of the flask. The flask was filled to working volume with water. Oxygen in the headspace was displaced by nitrogen. When the headspace oxygen concentration reached zero, the shaker was switched on to allow the gas to diffuse in and the oxygen concentration was recorded in the gas phase.

The optical sensor system (Fluorometrix, Stow, MA) was placed under the 250 mL conical flask (Bellco Glass Inc., Vineland, NJ) mounted on the Lab-line orbit environ shaker (Lab-line Instruments Inc., Melrose Park, IL) with a 1.6-cm shaking diameter. The flask equipped with the oxygen sensitive patch (Fluorometrix, Stow, MA) was filled with 100 mL distilled water. The flask was closed with an appropriate plug (cotton plug, sponge plug, and milk filter) and a thin plastic tube [3 mm O.D. (outer diameter) and 1.5 mm I.D. (inner diameter)] was passed through the plug to sparge nitrogen through it. The baffled flask used in this study had four indentations, each 6 cm long and 1.5 cm deep. The various plugs used were cotton plug (manually made with 1 g of absorbent cotton), sponge plug (S/P diSPo plugs for openings 28- to 35-mm outer diameter; Baxter Healthcare Corporation, Deerfield, IL) and milk filters (16.5 cm disks non-gauze; Ken AG, Ashland, OH).

For the mass transfer coefficient measurement in the fermentor, the 1.5 L New Brunswick Scientific Bioflo III (Edison, NJ) was used. The fermentor was filled with 1 L distilled water and equipped with a Clark type electrode (Model 21800-022, Control Company, Friendswood, TX) to measure oxygen. The reactor was set at a particular agitation speed, aeration rate, and 37°C. House air and nitrogen was used for k_La measurement using the static gassing out method.

Fermentation

Escherichia coli strain JM105 was transformed with the pBAD-GFP construct. (Lu et al., 2002). The seed culture was prepared by growing 1% inoculum overnight in 10 mL buffered Luria Bertani (LB) in a 50 mL culture tube at 250 rpm and 37°C. A 4% inoculum was used from the seed culture to start a shake-flask fermentation in LB (10 g/L bacto tryptone, 5 g/L bacto yeast extract, 10 g/L NaCl, pH 7.2, 4 g/L K_2HPO_4, 0.5 g/L KH_2PO_4) or minimal media (Glucose: 5 g/L^{-1}, NH_4Cl: 1 g/L^{-1}, K_2HPO_4: 1 g/L^{-1}, $MgCl_2$: 200 mg/L^{-1}, $FeSO_4$: 10 mg/L^{-1}, $CaCl_2$: 10 mg/L^{-1}) at 250 rpm and 37°C in a 250 mL baffled/unbaffled shake flask with 100 mL media volume. This amount of media was used in 250 mL flasks for these experiments to avoid

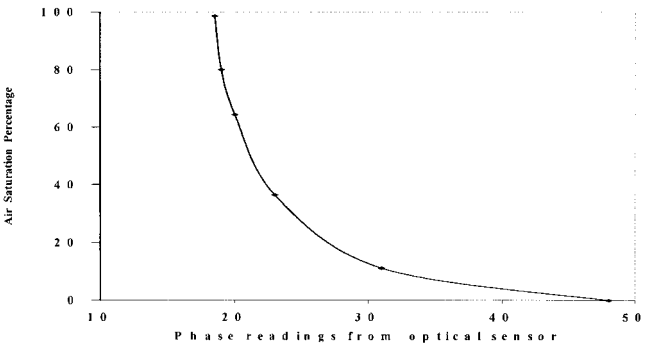

Figure 2. The calibration curve for the optical sensor shows a hyperbolic relation with the dissolved oxygen measurement from the Clark electrode. The sensitivity of the sensor is high for low DO values.

the exposure of the patch to air caused by vortex formation during agitation.

Stirred-tank fermentations were performed in the 1.5-L New Brunswick Scientific Bioflo III (Edison, New Jersey) fermentors. Dissolved oxygen probe (Ingold) was calibrated to read 0% with nitrogen gas and 100% with air. The fermentor was filled with 1 L LB media and autoclaved at 121°C and 15 psi for 30 min.

The seed culture was begun using 1% inoculum in 50 ml LB media in a 250 mL flask incubated overnight at 35°C and 250 rpm. The fermentor was inoculated with 4% seed culture of *E. coli* pBAD-GFP construct. Aeration in the fermentor was set at 1 volume of gas/volume of culture/minute (VVM) and temperature at 37°C for all the fermentations. Each fermentation was performed at a constant speed of the impeller throughout the fermentation time.

After 5 doublings (about 3 h), when the culture reached exponential phase, GFP was induced with 0.2% arabinose solution. The optical density of the culture was measured at 600 nm with Milton Roy Spectronic 401 spectrophotometer. The fluorescence intensity was measured offline using Varian Cary Eclipse fluorescence spectrophotometer (Varian Inc., Australia).

RESULTS AND DISCUSSION

The phase response of the fluorescence sensor was recorded and plotted against percentage DO (Fig. 2). The hyperbolic nature of the calibration curve of the oxygen sensor leads to higher sensitivity at low DO levels. This property of the sensor is advantageous for DO measurements in fermentation and cell culture work (Tolosa et al., 2002). However, the sensor has low sensitivity for DO levels above 60%. Thus, only the data below 60% DO were used for the mass transfer coefficient measurements.

Table I. Plug mass transfer coefficient obtained with Experiment 2 in an unbaffled shake flask with 100 mL water at 37°C and 250 rpm.

Closure	k (m^3/h)
Sponge plug	2.7 E –04 ± 1.4 E –04
Cotton plug	9.1 E –04 ± 3.3 E –04
Milk filter	5.7 E –03 ± 8.6 E –04

Table II. Gas–liquid mass transfer coefficient obtained with Experiment 1 in an open shake flask with 100 mL water at 37°C and 250 rpm.

Type of flask	k_La (h^{-1})
Baffled	59.2 ± 7.4
Unbaffled	30.8 ± 6.7

Using the oxygen sensor the mass transfer coefficient was measured for the individual resistances in a shake flask (Table I and Table II). A comparison between the oxygen transfer through the plug and the gas–liquid interface was made by calculating the two resistances separately. The transfer resistance of the shake-flask closure can be expressed by (1/k); and the resistance of the gas–liquid interface by ($M/V_L \cdot k_La$). From Table I it follows that for the sponge plug the transfer resistance is: $3.7 \cdot 10^3$ h/m^3 and from Table II the transfer resistance of the gas–liquid interface in an unbaffled flask is: $1.33 \cdot 10^4$ h/m^3 ($M = 41$, $V_L = 10^{-4}$ m^3). Clearly, the resistance provided by the gas–liquid interface was much higher than that of the plug. The individual plug resistances when compared with each other showed a large difference among them. In Table II, the transfer coefficient of the gas–liquid interface changed twofold with the introduction of baffles.

The corrected equivalent mass transfer coefficient values (Table III) under different conditions in the shake flask were obtained by substituting individual transfer coefficients in Eq. (4). The equivalent mass transfer coefficient is expected to be a better estimate of the transfer capacity of a shake flask as it accounts for both the gas–liquid interface resistance and the plug resistance.

The effect of baffles and different sterile closures in a shake flask was tested on the cell growth during *E. coli* fermentation. An experiment performed with three unbaffled flasks covered with different plugs (cotton, sponge, and milk filter) and a baffled flask covered with milk filter showed that the difference in the oxygen transfer rate in a shake flask under varying conditions led to different oxygen profiles during fermentation (Fig. 3a). All the unbaffled flasks reached zero-dissolved-oxygen level in the broth while the baffled flask maintained dissolved oxygen level above the critical value at all times during the fermentation. (Critical value of dissolved oxygen concentration is a char-

Table III. Equivalent mass transfer coefficient calculated from Equation (4) using the two transfer coefficients separately from Tables I and II.

Closure	Flask	k_La (h^{-1})
Sponge plug	Unbaffled	24 ± 3
Cotton plug		28.4 ± 6
Milk filter		30.4 ± 6
Sponge plug	Baffled	40.3 ± 5
Cotton plug		53.9 ± 8
Milk filter		57.6 ± 7

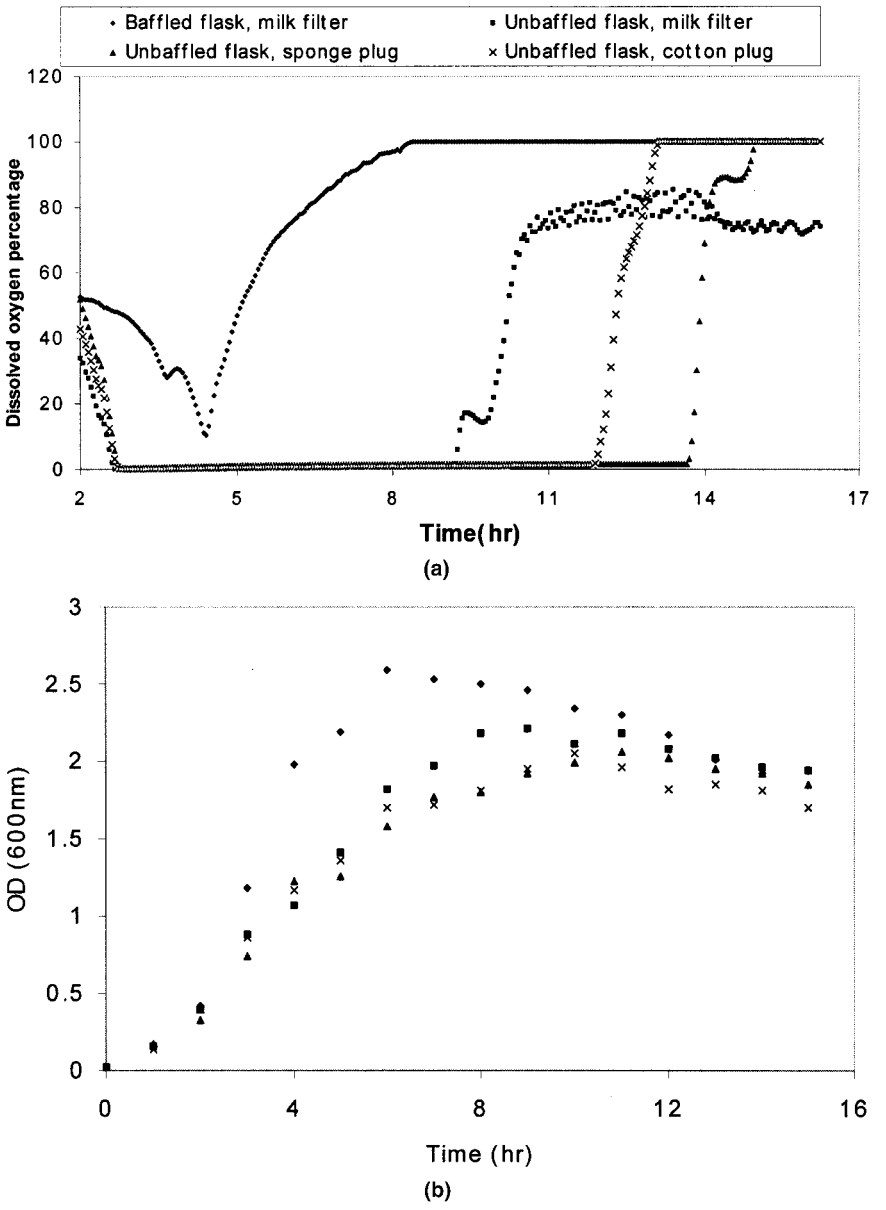

Figure 3. (a) DO during *E. coli* fermentation in four flasks with 100 mL LB media performed in parallel at 37°C and 250 rpm. The DO in the unbaffled flasks falls below critical value while the baffled flask does not get oxygen-limited. (b) Growth curve of *E. coli* fermentation in four flasks with 100 mL LB media carried out in parallel at 37°C and 250 rpm. Growth rate is higher for the flask with higher oxygen transfer rate.

acteristic of each microorganism and for *E. coli* the value is around 4% air saturation) If the dissolved oxygen concentration falls below the critical level then the cells may be metabolically disturbed.

Table IV. Duration of oxygen limitation in the shake flask during *E. coli* fermentation calculated from Figure 3a. Oxygen limitation in the flask is very sensitive to the change of plug and the introduction of baffles.

Closure	Flask	Duration (h)
Sponge plug	Unbaffled	10.5
Cotton plug		9
Milk filter		7.2
Milk filter	Baffled	0

The equivalent overall mass transfer coefficient of the unbaffled flasks with different plugs in Table III ranged from 24 h^{-1} to 30.4 h^{-1} while the mass transfer coefficient of the baffled flask with milk filter cap was close to 57.6

Table V. Volumetric mass transfer coefficient in a 1.5-L stirred-tank fermentor with 1 L distilled water and 37°C at an aeration rate of 1 vvm.

Impeller speed (rpm)	k_La (h^{-1})
25	9.8 ± 2.2
50	10.4 ± 1.8
100	14.2 ± 1.9
200	19.9 ± 3.0
300	25.7 ± 1.8
350	33.9 ± 2.2

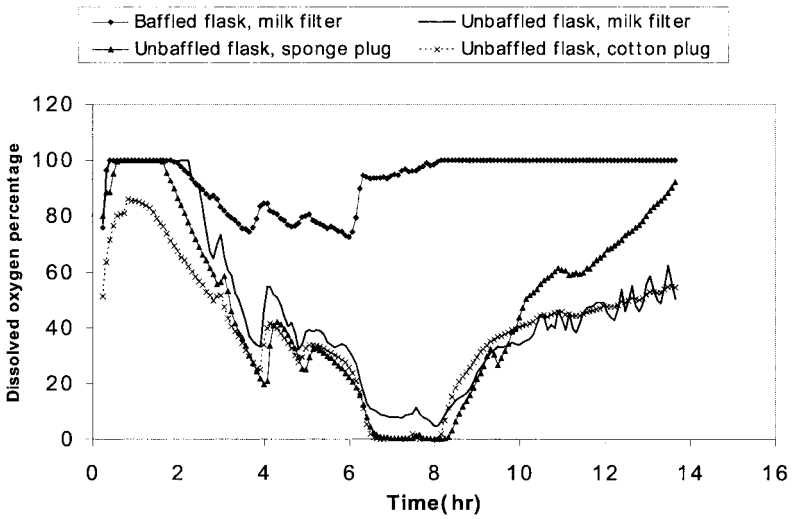

Figure 4. DO during *E. coli* growth in four flasks with 100 mL minimal media run at 37°C and 250 rpm. The flasks with high equivalent mass transfer coefficient, i.e., with milk filter cap, do not get oxygen-limited. The DO keeps oscillating in all the four flasks during *E. coli* growth.

h^{-1}. This difference in the oxygen transfer capacity of the shake flasks under different conditions resulted in the different dissolved oxygen profiles during fermentation (Fig. 3a). The dissolved oxygen in the unbaffled flask with sponge cap remains below critical level for around 10.5 h while for the same flask with milk filter cap, this duration is 7.2 h (Table IV). This shows that the change of plug of a shake flask affects the mass transfer coefficient, which, in turn, changes the duration of oxygen limitation during cell growth in them.

The effect of different oxygen transfer rates were also apparent on the biomass growth in the LB media. In Figure 3b the baffled shake flask with milk filter cap, which had the highest oxygen transfer rate, resulted in the fastest biomass growth rate during *E. coli* fermentation. Shake flasks with lower oxygen transfer rate had slower growth rates in their exponential phase. The impact of oxygen transfer was not limited only to the biomass growth rate but it also affected the extent of total biomass formation. Maximum biomass accumulated in the flask with the highest oxygen transfer while the biomass formation was lowest in the flask with the lowest oxygen transfer (Fig. 3b).

Interestingly, the DO profile in *E. coli* fermentation in minimal media in a similar experiment as above was observed to be oscillating in all the four flasks (Fig. 4). These variations in the oxygen consumption rate may be due to metabolic oscillations (Anderson et al., 2001). A comparison between Figures 3a and 4 shows that the DO was below critical value for a longer duration in LB media than in minimal media. This is probably due to lower oxygen demand in the minimal media caused by carbon source limitation. However, in both the figures, duration of oxygen limitation was minimal in the baffled flask as compared to the other flasks. Thus, the online monitoring of DO gives a

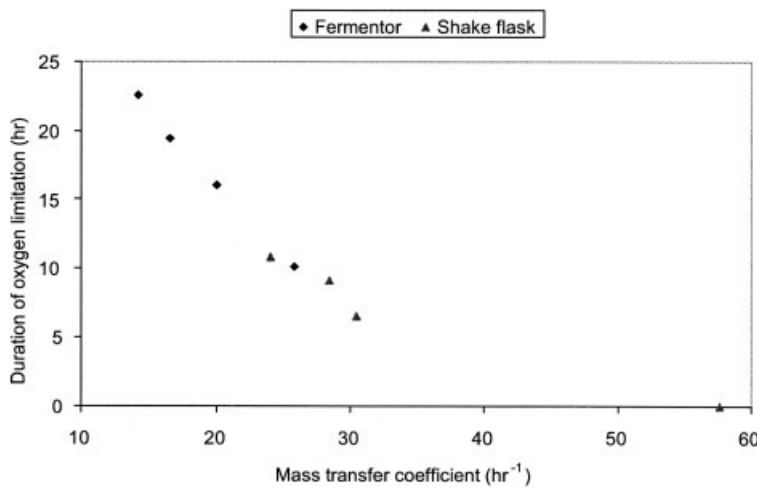

Figure 5. The effect of mass transfer coefficient in a shake flask and a fermentor on the duration that oxygen remains limiting during culture growth of *E. coli.*

good indication of the effect of change of media components on cell metabolism.

Table V lists the corrected volumetric mass transfer coefficient in a bench scale fermentor with 1 L distilled water operated at different impeller speed. The volumetric mass transfer coefficient in the stirred-tank fermentor was measured using the gassing-out method, to compare shake-flask fermentations with those performed in a stirred-tank fermentor. The mass transfer coefficient in the fermentor increased almost linearly with the speed of the impeller at a constant aeration rate.

Figure 5 illustrates the effect of the mass transfer coefficient in the reactor vessel on the duration for which oxygen remains below critical value during *E. coli* fermentation. Both the stirred-tank fermentor and the shake flask showed a decrease in the duration of oxygen limitation with increase in the mass transfer coefficient of the bioreactor. In the bench-scale fermentor operated at 100 rpm, the volumetric mass transfer coefficient was 14 h^{-1} and the oxygen remains limited for around 25 h for *E. coli* under these conditions. With an increase of agitation speed to 300 rpm, the mass transfer coefficient increased to 25.7 h^{-1} and the duration of oxygen limitation dropped down to around 10 h. Similarly for the unbaffled shake flask, with a sponge plug the mass transfer coefficient was 24 h^{-1} and the oxygen remained limiting for around 10.9 h for *E. coli* fermentation. With a change of plug to the milk filter under the same conditions, the mass transfer coefficient increased to 30.4 h^{-1} and the duration of oxygen limitation dropped down to around 6.5 h. This shows that the dissolved oxygen profile in a growing culture is very sensitive to the mass transfer coefficient of the bioreactor.

To compare the shake-flask fermentation with a stirred-tank fermentor the two vessels were run in parallel under the same fermentation conditions of k_La temperature, inoculum percentage, and media composition. The plug of the shake flask was chosen (cotton plug) such that the equivalent mass transfer coefficient was approximately equal to the k_La of the bench-scale fermentor operated at 300 rpm agitation and 1 vvm aeration ($\approx$ 26 h^{-1}). Both the shake flask and the fermentor were inoculated at the same time with an overnight grown seed culture in a common shake flask. After 3 h of inoculation, the GFP was induced with 2% arabinose in both the fermentors. The fermentation in the two vessels was compared by observing the cell growth, the dissolved oxygen profile, and the GFP formation. Figure 6a shows the dissolved oxygen concentration profile in the shake flask and the fermentor. The DO profile had a similar pattern for fermentation in both the bioreactors. The period of oxygen depletion and the recovery of the dissolved oxygen to 100% were similar and reproducible in the two bioreactors. The curves of the data comparing the biomass and GFP formation in the two vessels show good agreement (Fig. 6b, c). Hence, we can deduce that the equivalent mass transfer coefficient measured using the optical oxygen sensor, can be used as the scale-up criteria of fermentation from the shake flask to the stirred-tank fermentor. This method of process scale-up is comparatively simpler and easier than the power consumption model suggested in other studies (Buchs et al., 2000a; 2000b).

Shake flasks are well established and have proven to be a very useful and valuable tool for initial culture experiments and screening purposes. However, the lack of fundamental knowledge of the physical background and the controling parameters in shake flasks is still a problem. This is mainly due to the lack of custom made bioprocess-monitoring devices for shake flasks. Shake flasks will quite certainly continue to be the most applied bioreactors for mass screening in the future and there is an acute need for the improvement of shake flasks by providing on-line bioprocess monitoring in them. With the use of the optical oxygen sensor used in this study for on-line measurement of dissolved oxygen un-

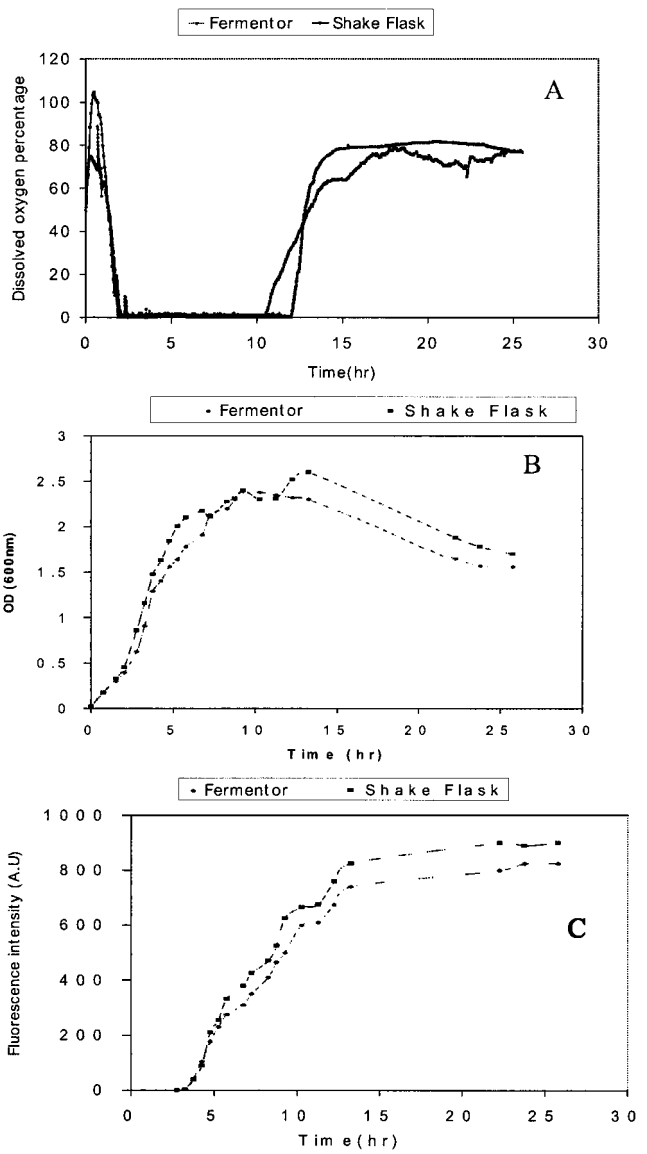

Figure 6. Time profiles of fermentation variables in shake flask in comparison with a standard 1 L bioreactor at same culture conditions during *E. coli* growth. (A) Dissolved oxygen profiles. (B) Optical density profiles. (C) GFP production profiles.

der sterile conditions, much information about the culture and the fermentation conditions can be gained. In this study, the sensor was used to perform the mass transfer coefficient measurements in the shake flask and also to understand the process of oxygen transfer into the flask. The sensor was used to compare the DO profiles in *E. coli* fermentation under different conditions and to quantify the effect of physical conditions of operation of the shake flask on the cellular growth in them. Also, with an understanding of the equivalent mass transfer coefficient in a shake flask and the effect of different conditions on k_La, *E. coli* fermentation in a shake flask was scaled-up to a bench-scale fermentor under identical conditions namely k_La, media composition, inoculum percentage, and temperature. Thus, it can be deduced that the new device for online oxygen monitoring in shake flask will play an increasing and promising role in reactor characterization and bioprocess development. The device will support both the screening of media or strains and be an important part of a scale-up procedure in research in the bioprocess industry.

We thank Dr. Yordan Kostov, Dr. Leah Tolosa and Peter Harms for their helpful suggestions.

NOMENCLATURE

k_G	Gas side mass transfer coefficient (hr^{-1})
k_L	Liquid side mass transfer coefficient (hr^{-1})
M	Equilibrium constant
C_L	Saturation oxygen concentration in liquid (g O_2/m^3)
C_p	Oxygen concentration at probe tip (g O_2/m^3)
D_{O2}	Diffusivity constant of oxygen through the plug
ϕ	Flux of oxygen (g O_2/hr)
τ_p	Time constant of probe (s)
k_La	Volumetric mass transfer coefficient (hr^{-1})
$(k_La)_{eq}$	Equivalent mass transfer coefficient (hr^{-1})
τ	Decay lifetime (ns)
k_q	Bimolecular quenching constant
OTR	Oxygen transfer rate
DO	Dissolved oxygen
I	Emission intensity

References

Anderson DC, Swartz J, Ryll T, Lin N, Snedecor B. 2001. Metabolic oscillations in an Escherichia coli fermentation. Biotechnol Bioeng 75: 212–218.

Bambot SB, Holavanahali R, Lakowicz JR, Carter GM, Rao G. 1994. Phase fluorometric sterilizable optical oxygen sensor. Biotechnol Bioeng 43:1139–1145.

Brown WA. 2001. Developing the best correlation for estimating the transfer of oxygen from air to water. Chem Eng Educ 35:134–147.

Buchs J. 2001. Introduction to advantages and problems of shaken cultures. Biochem Eng J 7:91–98.

Buchs J, Maier U, Milbradt C, Zoels B. 2000a. Power consumption in shaking flasks on rotary shaking machines: I. Power consumption measurement in unbaffled flasks at low liquid viscosity. Biotechnol Bioeng 68:589–593.

Buchs J, Maier U, Milbradt C, Zoels B. 2000b. Power consumption in shaking flasks on rotary shaking machines: II. Nondimensional description of specific power consumption and flow regimes in unbaffled flasks at elevated liquid viscosity. Biotechnol Bioeng 68:594–601.

Corman J, Tsuchiya HM, Koepsell HJ, Benedict RG, Kelly SE, Feger VH, Dworschack RG, Jackson RW. 1957. Oxygen absorption rates in laboratory and pilot plant equipment. Appl Microbiol 5:313–318.

Clark GJ, Langley D, Bushell ME. 1995. Oxygen limitation can induce microbial secondary metabolite formation: Investigations with miniature electrodes in shaker and bioreactor culture. Microbiol 141: 663–669.

Delgado G, Topete M, Galindo E. 1989. Interaction of cultural conditions and end-product distribution in *Bacillus subtilis* grown in shake flasks. Appl Microbiol Biotechnol 31:288–292.

Gaden EL Jr. 1962. Improved shaken flask performance. Biotechnol Bioeng 4:99–103.

Henzler HJ, Wuppertal MS. 1991. Suitability of the shaking flask for oxygen supply to microbiological cultures. Bioproc Eng 7:123–131.

Hermann R, Walther N, Maier U, Buchs J. 2001. Optical method for the determination of the oxygen-transfer capacity of small bioreactors based on sulfite oxidation. Biotechnol Bioeng 74:355–363.

Hirose Y, Sonada H, Kinoshita K, Okada H. 1966. Studies on oxygen transfer in submerged fermentations. Part IV: Determination of oxygen transfer rate and respiration rate in shaken cultures using oxygen analyzers. Agr Biol Chem 30:49–58.

Hopkins DJ, Betenbaugh MJ, Dhurjati P. 1987. Effects of dissolved oxygen shock on the stability of recombinant *Escherichia coli* containing plasmid pKN401. Biotechnol Bioeng 29:85–91.

Kennedy MJ, Reader SL, Davies RJ, Roades DA, Silby HW. 1994. The scale up of mycelial shake flask fermentations: A case study of g-linolenic acid production by Mucor Hiemalis IRL 51. J Ind Microbiol 13:212–216.

Lakowicz JR. 1999. Principles of fluorescence spectroscopy, Kluwer Academics, Plenum Publishers. New York, 2nd Ed.

Lee YH, Tsao GT. 1979. Dissolved oxygen electrodes. In: Ghose, TK, Fiechter, A, Blackborough, N, editors. Advances in biochemical engineering. Berlin: Springer-Verlag. p. 35.

Lu C, Albano CR, Bentley WE, Rao G. 2002. Differential rates of gene expression monitored by green fluorescent protein. Biotechnol Bioeng 79:429–437.

Maier U, Buchs J. 2001. Characterization of the gas–liquid mass transfer in shaking bioreactors. Biochem Eng J 7:99–106.

McDaniel LE, Zimmerli A, Bailey EG. 1965. Effect of oxygen supply rates on growth of *Escherichia coli*. I. Studies in baffled and unbaffled shake flasks. Appl Microbiol 13:109–114.

McDaniel LE, Bailey EG. 1969. Effect of shaking speed and type of closure on shake flask cultures. Appl Microbiol 17:286–290.

Mrotzek C, Anderlei T, Henzler HJ, Buchs J. 2001. Mass transfer resistance of sterile plugs in shaking bioreactors. Biochem Eng J 7: 107–112.

Schell DJ, Farmer J, Hamilton J, Lyons B, McMillan JD, Saez JC, Tholudur A. 2001. Influence of operating conditions and vessel size on oxygen transfer during cellulase production. Appl Biochem Biotechnol 91–93:627–642.

Schultz JS. 1964. Cotton closure as an aeration barrier in shaken flask fermentations. Appl Microbiol 4:305–310.

Smith CG, Johnson MJ. 1954. Aeration requirements for the growth of aerobic microorganisms. J Bacteriol 68:346–350.

Stanbury PF, Whitaker A. 1989. Principles of fermentation technology. 1st Ed.

Suijdam JCV, Kossen NWF, Joha AC. 1978. Model for oxygen transfer in a shake flask. Biotechnol Bioeng XX:1695–1709.

Tolosa L, Kostov Y, Harms P, Rao G. 2002. Non-invasive measurement of dissolved oxygen in shake flask. Biotechnol Bioeng 80:594–597.

Tribe LA, Briens CL, Margaritis A. 1995. Determination of the volumetric mass transfer coefficient (KLa) using the dynamic "Gas out gas in" method: Analysis of errors caused by dissolved oxygen probes. Biotechnol Bioeng 46:388–392.

Tunac JB. 1989. High aeration capacity shake flask system. J Ferm Bioeng 68:157–159.

Jose Vallejos had done a Master's degree in our lab under a Fulbright scholarship and showed the importance of mixing in minibioreactors and showed how a small milliliter scale system could replicate mixing patterns in larger scale systems and this work is described later in the minibioreactor section. However, the scholarship required him to return to his home country of Nicaragua for a couple of years where he worked in a large-scale ethanol fermentation plant at the million-liter scale. Jose is probably one of a handful of people on the planet who has worked with bioreactors that span such an enormous range!

Luckily for the profession, Jose came back to the lab to complete his Ph.D and decided to put a quantitative framework to the largely empirical world of small scale cell culture vessels, that our FDA collaborator Kurt Brorson described as "process scouting devices." A fertile and productive collaboration ensured.

The first problem that Jose tackled was that of oxygen and pH envoronments that a cell sees upon being thawed from a cryo-vial as it begins its seed train journey. I still find it remarkable that nobody had tried to build on our earlier work and start routinely measuring oxygen and pH, now that such sensors were commercially available. Jose was the first to document the changes in cellular environment during routine passaging of cells in T-flasks and the implications for cell stability. This is of critical importance, as the seed-train eventually ends up being scaled-up and produces the final cell culture product. The next paper has those details.

ARTICLE

BIOTECHNOLOGY and BIOENGINEERING

Dissolved Oxygen and pH Profile Evolution After Cryovial Thaw and Repeated Cell Passaging in a T-75 Flask

Jose R. Vallejos,[1] Kurt A. Brorson,[2] Antonio R. Moreira,[1] Govind Rao[1]

[1]Center for Advanced Sensor Technology, and Department of Chemical and Biochemical Engineering, University of Maryland, Baltimore County, 1000 Hilltop Circle, Baltimore, Maryland 21250; e-mail: grao@umbc.edu; fax: 410-455-6500; telephone: 410-455-3415

[2]Office of Biotechnology Products, Center for Drug Evaluation and Research, Food and Drug Administration, Silver Spring Maryland

Received 31 July 2009; revision received 3 November 2009; accepted 14 December 2009

Published online 31 December 2009 in Wiley InterScience (www.interscience.wiley.com). DOI 10.1002/bit.22649

ABSTRACT: Routine cell culture is done in small-scale disposable vessels (typically 0.1–100 mL volumes) in academia and industry. Despite their wide use in bioprocess development (i.e., process optimization and process validation), miniature process scouting devices (PSDs) are considered "black boxes" because they are generally not equipped with sensors. In this study, we show that on-line monitoring of dissolved oxygen (DO) and pH in a T-75 flask-based PSD can be achieved during cell passaging and that this information can be linked to different cellular metabolic states. In this case, on-line monitoring of DO and pH show three distinctive metabolic regions in passages 1–18, 19–28, 29–54 and in particular, the shift in the pH curve, the specific oxygen uptake rate (q_{O_2}), and the lactate production rate to the oxygen consumption rate yield ($Y_{Lac/ox}$) confirm the existence of these distinctive metabolic regions. These findings are particularly useful because they show that sensor equipped PSDs can help to monitor cell culture behavior after thaw, in pre- and seed culture prior to scale-up and in development/optimization studies. Such routine monitoring will help to develop more consistent cell culture techniques.

Biotechnol. Bioeng. 2009;105: 1040–1047.

KEYWORDS: monitoring; cell culture; T-flask; passaging; oxygen; pH

Introduction

Cell passaging is a common practice in bioprocess development and takes place after a cell vial from a cell bank is thawed from liquid nitrogen. In general, mammalian cells are passaged initially in static devices (T-flasks) and transferred to agitated devices (spinner/shake flasks) for subsequent passaging and scale-up to bench-scale bioreactors. In T-flasks, cells are expected to get adapted to the environmental/nutritional conditions after thaw and robust enough for transferring to agitated systems. Commonly used adaptation parameters are doubling times (Richieri et al., 1991) and antibody production (Fitzpatrick et al., 1993; Schmid et al., 1990). The number of passages required to start scale-up varies from three or more passages (Diao et al., 2008; Hiller et al., 1993; Lee and Palsson, 1993), depending on the cell line and medium composition.

Tissue culture flasks (T-flask) are among the most commonly used culture devices. T-flasks are characterized by their high surface area-to-volume ratio that compensates for the lack of agitation. They are mainly used as preliminary cell propagation and scale-up vehicles (Randers-Eichhorn et al., 1996), but a T-flask based screening platform (Lu et al., 2007), medium optimization studies (Gramer and Poeschl, 2000), and hepatocyte aggregation experiments (Glicklis et al., 2004) have also been reported. Mass transfer studies and on-line measurements of dissolved oxygen (DO) using patch-optical probe-based sensor have been reported by Randers-Eichhorn et al. (1996). They found that the DO concentration at the bottom of the flask reached zero during cell growth which indicates that mixing and mass transfer is not optimal for T-flask cultured cells. Despite these significant achievements, on-line monitoring of both DO and pH changes during cell passaging or subculturing in T-flasks and how they may affect cellular metabolism is not routine.

On-line monitoring of critical process parameters such as DO and pH in miniature process scouting devices (PSDs) confers important advantages to bioprocess development during scale-up (Hanson et al., 2007; Rao et al., 2009), automation (Puskeiler et al., 2005), mass transfer characterization (Gill et al., 2008; Zhang et al., 2006, 2008), and

Correspondence to: G. Rao

Contract grant sponsor: Sartorius-Stedim Biotech

scale-down (Betts et al., 2006). The ultimate goal is to integrate miniature PSDs with bench-scale devices by a data-driven scale strategy (Hermann et al., 2002). Significant advances have also been made equipping PSDs such as 24-well microtiter plates (Kensy et al., 2005; Naciri et al., 2008) and stirrer devices (Kostov et al., 2000) with DO and pH sensors. However, the work-horse static PSD, the T-flask, has not been equipped with sensors for monitoring of both DO and pH. Monitoring of critical process parameters in currently unmonitored devices such as T-flasks is critical to achieve process and product consistency as well as process understanding from PSDs (0.1–100 mL) to bench-scale devices. This is consistent with the process analytical technologies (PAT) initiative (Food and Drug Administration, 2004) where designing, analyzing, and controlling manufacturing as early as possible in the development phase (i.e., from cell vial thaw) is encouraged.

The main aim of this paper is to achieve on-line monitoring of both DO and pH in T-flasks to increase the process development/manufacturing understanding from cell vial thaw but prior to scale-up to agitated devices. Here we demonstrate that on-line monitoring of DO and pH can be incorporated in a T-flask to monitor growth of murine hybridoma after cell thaw and after extended passaging.

Materials and Methods

Cell Culture

The cell line used is a non-adherent SP2/0-based myeloma/mouse (2055.5) secreting an IgG3 antibody specific for the *Nisseria meningitides* capsular-polysaccharide (MCPS). A 1 L CD Hybridoma GT^{TM} (Invitrogen, Carlsbad, CA) stock media solution supplemented with 8 mM L-glutamine (GIBCO) and 2×10^{-4}% β-mercaptoethanol (v/v) (Sigma, St. Louis, MO) was prepared and stored at 4°C. New media was prepared as needed. The cell culture was kept in a CO_2 incubator at 37°C and 5% CO_2 in air. Cells were thawed from liquid nitrogen and cultured in a T-flask (75 cm^2) containing a total of 20 mL of media with an initial cell concentration of approximately 0.2×10^6 cells/mL. Cells were passaged every 3 days with three (3) consecutive passages in each T-flask and then transferred to a new T-flask. Cells were counted using a hemocytometer and viability was determined using the trypan blue exclusion method. Sample volumes of 0.5 mL were withdrawn from the flasks on days 0 and 3 (72 h after a passage started).

Dissolved Oxygen and pH Measurements

Oxygen and pH patches-based sensors, as described by Tolosa et al. (2002) and Kermis et al. (2003), were used in this study (see Fig. 1). The oxygen and pH sensors were obtained from Flurometrix (Stow, MA). Both oxygen and pH patches were autoclaved at 120°C for 25 min and then placed on the inside of the T-flasks with sterile forceps by removing the adhesive liner (that protects the adhesive layer) from the patches. Our patches are unaffected by cell density (Randers-Eichhorn et al., 1996). For these DO patches a drift study was performed in our laboratory at 100% DO and it was found that this drift was approximately 7% for the number of readings equivalent to our 9 days use. The same study was also performed for the pH patches and no apparent drift was observed. Our DO sensors are at their highest accuracy at low DO (Gupta and Rao, 2003).

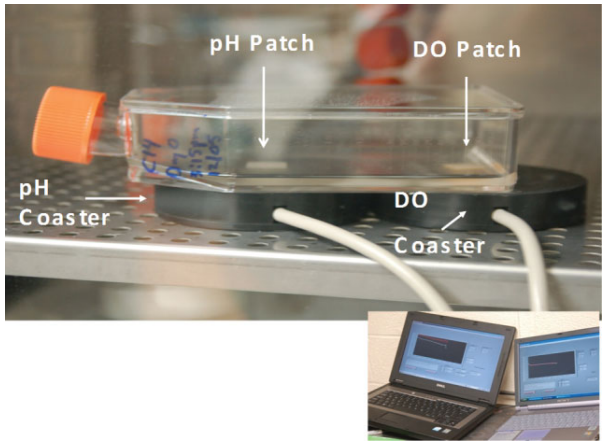

Figure 1. Dissolved oxygen and pH monitoring in a T-75 flasks inside a CO_2 incubator. [Color figure can be seen in the online version of this article, available at www.interscience.wiley.com.]

The patches were kept at the same positions inside T-flasks (see Fig. 1) during all experiments. DO and pH coasters were aligned with their respective patches from the outside. After sampling, this alignment was controlled in such a way that the excitation beam light shone upon the same patch spot. The DO and pH patches were used for three consecutive passages (9 days total) with a logging in rate of every 5 min in each T-flask.

Analytical Measurements

At time zero and at the end of each passage, 0.5 mL of sample was taken. Samples were centrifuged at 2,300 rpm for 2 min and the supernatant frozen for later lactate and glucose analysis in an YSI 2700 Analyzer (Yellow Springs, OH) (Yellow Springs Instrument Company).

Determination of Growth Rate and Metabolic Quotients

Net specific growth rate (μ_{net}), the number of population doublings or number of generations (N_p), specific oxygen uptake rate (q_{O_2}), specific metabolic rates for glucose (q_{Glu}) and lactate (q_{Lac}), the ratio of lactate production rate to the oxygen consumption rate ($Y_{Lac/oc}$), and the molar yield coefficient of glucose consumed to lactate produced

($Y_{Lac/Glu}$) were estimated from previously reported equations as proposed by Shuler Michael and Fikret (2002), Moran et al. (2000), Randers-Eichhorn et al. (1996), Ozturk and Palsson (1991a), Collins et al. (1998), Lee et al. (1991), and Jang and Barford (2000), respectively.

Results

The ability to equip small-scale PSDs with sensors that monitor important parameters like DO or pH will confer great advantages to development studies and early pre-culture. This includes tracking cell culture consistency over extended pre-culture durations and assuring that these important parameters remain within physiological levels in early culture, for example, immediately after thaw. To enable a model small-scale device with this utility, we aseptically placed laser-based DO and pH sensor patches in a conventional T-75 tissue culture flask and integrated the resultant PSD with a computer interface (Fig. 1).

Comparability Study of T-Flaks With and Without Patches

An initial cell culture comparability study was carried out in order to validate that sensor patches by themselves do not adversely impact cells. This is important because in theory autoclaving and the incorporation procedure into the T-flasks could release harmful leachables, poisoning the culture. Although similar studies have been performed previously with mini-bioreactors (Ge et al., 2006), the technology is novel enough to warrant this repeat study. This comparability study shows that no significant metabolic differences were noted between cell cultures grown in T-flasks with and without patches (see Table I). In particular, the $Y_{Lac/Glu}$ found in this study is similar in both T-flasks with and without patches and these $Y_{Lac/Glu}$ values are in the range of $Y_{Lac/Glu} = 1.68–1.88$ found by Ozturk and Palsson (1991b) and approximate to the $Y_{Lac/Glu} = 1.5$ reported by Miller et al. (1988a,b) for hybridoma batch cultures. In another similar comparability study, Ge et al. (2006) showed that the presence of pH and DO patches did not affect transcriptional profiling, HPLC analysis, viable cell count, and viability inspection of the same hybridoma cell line used in this study. As a result, the results presented in Table I are in good agreement with previous reported data and overall they show that the presence of pH and DO patches have no apparent effect on the metabolism of the cells.

Dissolved Oxygen and pH Evolution During Cell Passaging

On-line monitoring of DO and pH patches in this study enabled us to detect DO concentration and pH profile changes at different passages intervals. For example, under normal cell culture conditions the DO reached approximately 1% but at passages 18–20, 27–29, and 54–55 the DO level was above 1% (Fig. 2). In addition, observing the pH curves, it is possible to see that there is a shift in pH slope at each passage and it was found (data not shown) that this shift takes place when the cells are reaching their maximum specific lactate production rate. As lactate accumulation can destroy the buffering capacity of the medium by lowering the pH (Chen et al., 2001; Newland et al., 1990) and lactate is mainly produced from the glycolytic pathway, the pH curve provides real-time valuable data that can be linked to cellular metabolic activities, as shown in Figure 3, where three distinctive regions are observed.

Figures 3 and 5 show that during passages 1–18 (Region I), the glycolytic pathway rate is slower compared to oxidative phosphorylation. Inversely, from passages 18 to 28 (Region II, $N_p = 67–104$, respectively) the glycolytic pathway is favored over oxidative phosphorylation. This observation is supported by $Y_{Lac/ox}$ data as given by Figure 7 where by passage 18, the $Y_{Lac/ox}$ is higher than previous passages. In the third region (passages 29–54) the oxygen uptake rate increases for a couple of passages and then it decreases but the maximum lactate production rate is reached at slower rate. The increase and then decrease of the oxygen uptake rate is somehow unexpected as the $Y_{Lac/ox}$ value is kept constant during this region. This event illustrates how our monitoring system can provide an early warning system against metabolic shift. While we did not attempt to dissect the molecular and metabolic events in this shift we

Table I. Metabolic parameters during exponential growth phase during batch cultivation of a myeloma/mouse hybridoma cell line in a T-75 flask.[a]

Metabolic parameters	T-flask control (no patches)	T-flask patches	References
μ_{app} (day^{-1})	0.85 ± 0.0850	0.85 ± 0.0637	0.7[b]–1.0[c]
τ (day^{-1})	0.82 ± 0.0805	0.82 ± 0.0644	0.7[c]–1.0[b]
q_{Glu} ($\mu molGlu/\times 10^6$ cells day)	3.4 ± 0.53	3.64 ± 0.42	0.00216–0.01824[d]
q_{Lac} ($\mu molLac/\times 10^6$ cells day)	6.18 ± 1.0	6.57 ± 0.91	0.0036–0.0343[d]
$Y_{Lac/Glu}$ (molLac/molGlu)	1.83 ± 0.2439	1.82 ± 0.3096	1.68–1.88[d]

μ_{net} is net growth rate; τ is doubling time; q_{Glu} is specific glucose consumption rate; q_{Lac} is specific lactate production rate; and $Y_{Lac/Glu}$ is the molar yield coefficient of glucose consumed to lactate produced.

[a]Average and standard deviation values.
[b]Franek and Dolnikova (1991).
[c]Ozturk and Palsson (1991a).
[d]Ozturk and Palsson (1991b).

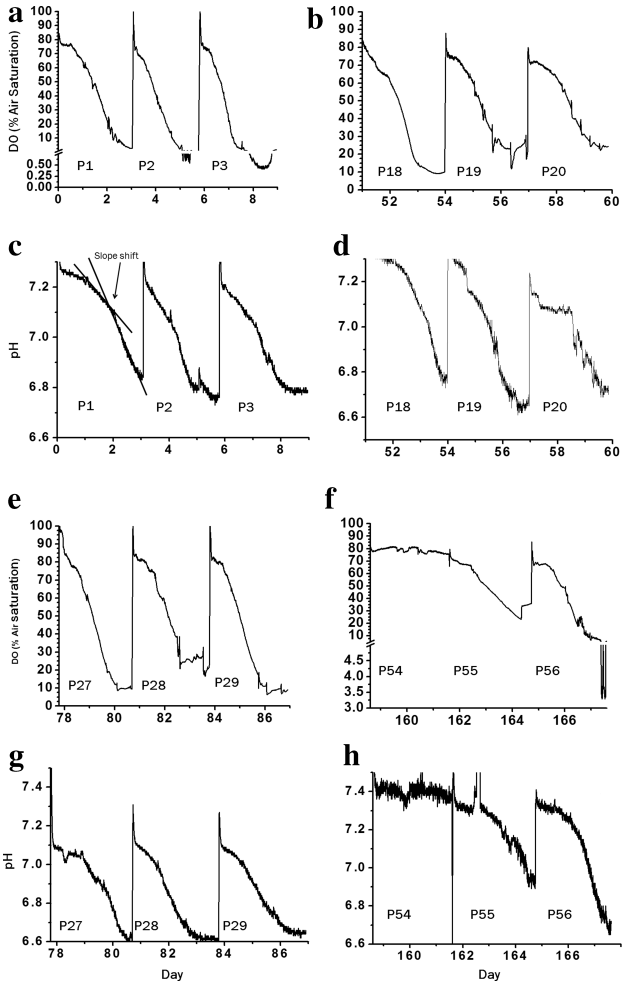

Figure 2. Dissolved oxygen and pH during cell passaging. Under normal cell culture conditions the DO reached approximately to 1% but at passages 18–20, 27–29, and 54–56 the minimum DO was above 1%.

show that T-flasks can be equipped with DO and pH sensors in a way that monitors for such undesirable changes.

Our DO and pH monitoring system also allowed us to see how cells responded to addition of fresh media. By passage 50, the medium that was being used was exhausted. A fresh lot of medium was used from passage 51 onwards. There appears to be some difference in medium composition (unknown) that resulted in the cells behaving differently as compared to previous passages. Growth rate dropped (Fig. 8) and $Y_{Lac/Glu} > 2$ (Fig. 6) within the same passage interval of 51–56. In this particular case, our on-line-monitoring system agreed with off-line-based monitoring such as $Y_{Lac/Glu}$ and growth rate but with the advantage of showing this different growth profile in real-time. This experience further indicates the value of continued monitoring.

Monitoring pH in T-flasks shows that the final pH reached at the end of each passage changes from passages 1

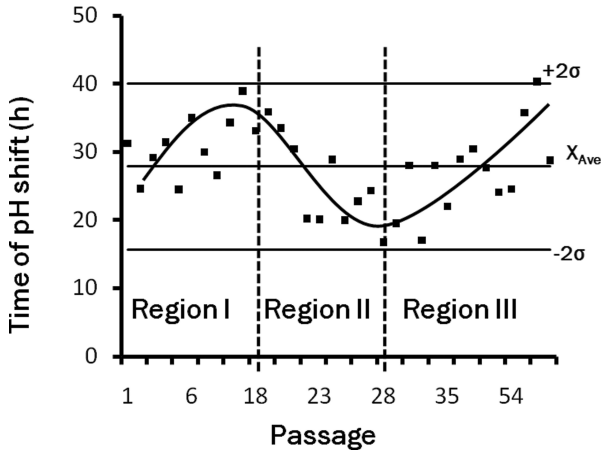

Figure 3. Time of pH shift as described in Figure 2c. Region I: 1–18, Region II: 19–28, and Region III: 29–54. Average (X_{Ave}).

to 18 but level off at around pH = 6.6 after passage 18. In summary, our sensor enabled T-flasks allowed us to detect some subtle evolution of the culture. Nevertheless, from Figure 4 it can be observed that a 2-day media change schedule or base addition would have been better from the standpoint of keeping pH within the optimal pH range of 7.1–7.4 as reported by Miller et al. (1988a). As a result, the PSD data can be used to design a better feeding schedule in further studies.

Specific Oxygen Uptake Rate During Passages

As previously shown by Randers-Eichhorn et al. (1996) and confirmed in this study, specific oxygen uptake rate for cells

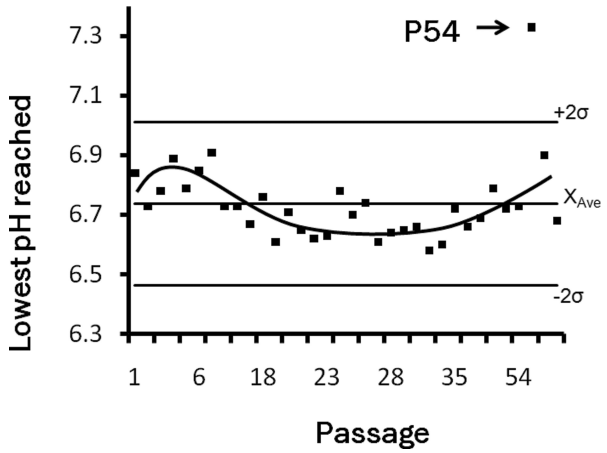

Figure 4. Lowest pH reached at the end of each passage. This pH is below the optimal pH range of 7.1–7.4 found by Miller et al. (1988a) but within the range of cell survival. Average (X_{Ave}).

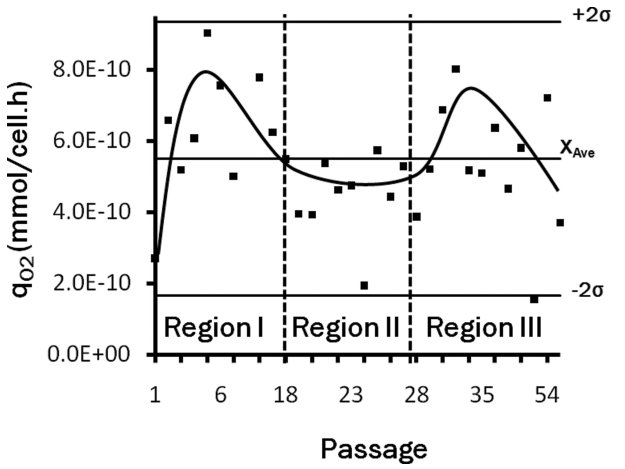

Figure 5. Specific oxygen consumption rate during cell passaging. Three distinctive regions I, II, and III are observed. Average (X_{Ave}).

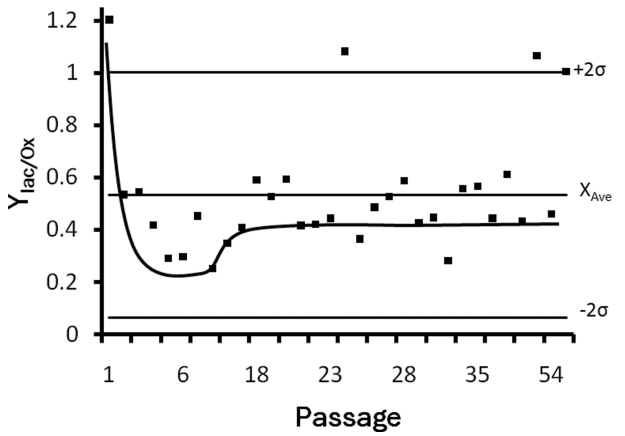

Figure 7. Lactate production rate to the oxygen consumption rate during cell passaging. Average (X_{Ave}).

cultured in T-flasks can be accomplished. By monitoring DO during passages the specific oxygen uptake rate was estimated using the equation proposed by Randers-Eichhorn et al. (1996). Results are presented in Figure 5 and similar to Figure 3, Figure 5 shows the same three distinctive regions I, II, and III from passages 1 to 18, 19 to 28, and 29 to 56, respectively. On-line monitoring of DO during cell passaging after thaw enabled us to quantitatively determine the relative low oxygen consumption rate of 2.7×10^{-10} (mmol/cell h) experienced by the cells immediately after thaw (passage 1) when compare to the maximum of 9×10^{-10} mmol/cell h (passage 5, $N_p = 19$).

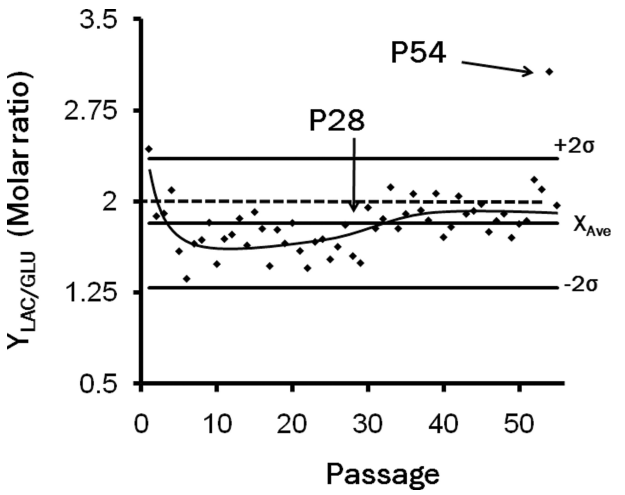

Figure 6. Lactate to glucose molar ratio during cell passaging. Average (X_{Ave}). $Y_{Lac/Glu} = 2$ (. . .) is the maximum theoretical value.

Lactate to Glucose Molar Ratio and Growth Rate

The metabolic shift observed from on-line monitoring data of DO and pH was compared to the lactate to glucose molar ratio ($Y_{Lac/Glu}$) and growth rate. Figure 6 shows that after passage 28 there is a shift in trend for $Y_{Lac/Glu}$ toward a higher value close to $Y_{Lac/Glu} = 2$. To the contrary, growth rate and cell viability (Fig. 8) do not seem to be affected much during cell passaging except by passage 50.

Discussion

Bioprocess Implications

The results presented in this study have important bioprocess implications. With on-line monitoring of DO and pH in T-flasks, for example, one can decide at what cellular energy production metabolic pathway, cells will be transferred to agitated devices (e.g., spinners or shake flasks). Plus, on-line monitoring of DO and pH can aid developing a process control strategy that would assure process consistency between PSDs (i.e., T-flasks) and bench-scale devices. As cells evolve to different cellular metabolic rates after thaw, a seamless cell transition would require keeping cells from shifting to different metabolic states as they are scaled-up from T-flasks to other devices (e.g., spinner or shake flasks). This approach could have a positive impact on maintaining productivity and product quality and consistency between different scales and systems. In an ongoing project in our laboratory, we are investigating how the cellular respiration is affected when cells are transferred from a T-flask to a 250 mL spinner flask and shake flasks in order to find out when the metabolic activity in the spinner or shake flasks matches the T-flask's prior to scale-up to larger devices.

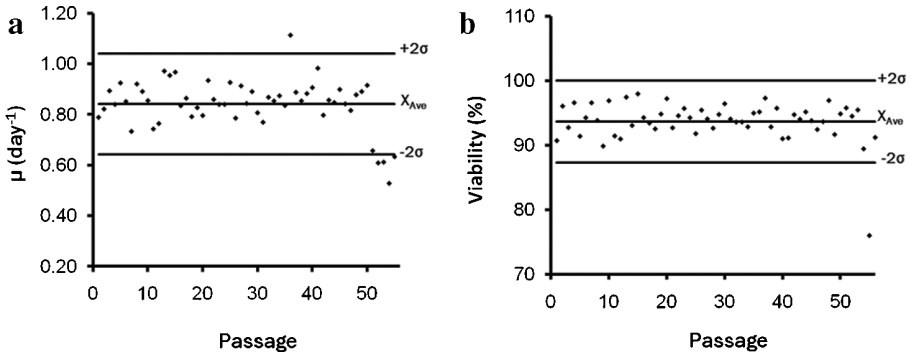

Figure 8. **a**: Specific growth rate versus passage. **b**: Cell viability versus passage. Average (X_{Ave}).

Our sensor enabled PSD showed that subtle evolution occurs in culture behavior during prolonged post-thaw passaging. This study showed that on-line monitoring of DO and pH can be linked to different cellular metabolic activities during cell passaging after thaw and prior to scale-up (Figs. 3 and 7). More involved studies (e.g., gene expression) with additional sensors (e.g., lactate and glutamine patches) are needed to really understand the impacts on the glycolytic and oxidative phosphorylation pathways, but here we show that metabolic shift can be detected and tracked in real time by on-line monitoring of DO and pH. Thus we provide a quantitative process information tool for early stages of bioprocess development (i.e., cell passaging after cell bank vial thaw) that is currently missing and it would be useful for further scale-up from T-flasks to other cell culture devices. This on-line data would assist pharmaceutical industry researchers designing a robust bioprocess development strategy with process information incorporated from PSDs to bench-scale devices (and beyond). It will also allow pre-culture facilities to monitor and eliminate early cultures experiencing drift in a manner that carries a trivial economic impact (i.e., the T-flask a few days after thaw). As a result, subsequent unpleasant manufacturing surprises during cell transfer and scale-up from the mL-scale to bench-scale could potentially be avoided and not only shorten the bioprocess development timeline but also lead to more consistent product quality.

Dissolved Oxygen and pH Evolution During Cell Passaging

Our sensor enabled PSD showed that pH and DO profile changes in our particular cell culture evolve from thaw. On-line monitoring of DO shows that after passage 2, cells were exposed to anoxic conditions of DO below 0.5% (critical DO, Miller et al., 1987) for 18.5 h (average per passage). This cyclic exposure to anoxic conditions can be detrimental for the cells as it can decrease the level of antioxidant molecules thus sensitizing cells to oxidant damage (Mercille and Massie, 1994) or increase reactive oxygen species (ROS) generation (Guzy et al., 2005). Thus, the combination of exposure to high DO levels and anoxic conditions may partially explain the change in DO (and pH) profile occurred during passages 18–20, 27–29 (Fig. 2). In this regard, the pH and DO profile evolution after cell thaw can be reflecting cells' response to oxidative stress. While these attributes may vary from culture to culture, the main point is that our PSD allows monitoring of this evolution. Monitoring this is important from a process control standpoint because subtle changes in seed culture can have broad impacts on subsequent production cultures.

Specific Oxygen Uptake Rate During Cell Passaging

The oxygen uptake values reported in this study are similar to those previously reported in the literature (Ozturk and Palsson, 1991a,b; Randers-Eichhorn et al., 1996; Zupke et al., 1995). This is important because it shows that our DO on-line monitoring enabled PSD can also mimic oxygen uptake rate found in larger cell culture devices and in the future a control strategy at the PSD scale can be developed to keep similar specific oxygen uptake rates between PSDs and bench-scale devices.

Lactate to Glucose Molar Ratio and Growth Rate

Our on-line DO and pH monitoring enabled PSDs were able to detect different cellular metabolic states (passages 1–18, 19–28, 29–54) even before that the shift in $Y_{Lac/Glu}$ took place (Fig. 6). In fact, another parameter such as growth rate (Fig. 8) did not show any significant change during cell passaging (except by passage 50). Figure 6 shows a trend shift in the $Y_{Lac/Glu}$ curve that takes place after passage 28 when the cells have been in the high glycolytic energy production rate (as shown by Figs. 3, 5, and 7) for about 10 passages. These results suggest that the $Y_{Lac/Glu}$, as a metabolic shift indicator, is 10 passages late as compared to our on-line monitoring of DO and pH. A $Y_{Lac/Glu} \geq 2$ has

been considered a metabolic shift parameter (Fitzpatrick et al., 1993; Meleady, 2007; Mercille and Massie, 1994; Miller et al., 1988a,b) and under this metabolic shift a high amount of glycolytic metabolites are converted to lactate. This is important because at higher $Y_{Lac/Glu}$ values, cells are in a less energy-efficient state which may alter their productivity and product quality attributes negatively. Consequently, having on-line DO and pH monitoring enabled PSDs can provide valuable data for developing a control strategy that could keep cells in the desired metabolic state longer.

As very early pre-culture in commercial settings is often performed in unmonitored T-flasks prior to scaling-up to spinner vessels and/or bench-scale bioreactors, the present work shows the importance of monitoring critical process parameters such as DO and pH. This can help design control strategies that would integrate unmonitored PSDs with fully instrumented laboratory-scale devices and allow for more consistent transfer protocols for seed-train development. For research use, it would allow for more consistent experimental design by ensuring that cells are studied under similar conditions.

Conclusion

The results presented in this study show that on-line monitoring of critical process parameters such as DO and pH can be accomplished in PSDs such as T-flaks. These PSDs can quantitatively track the dynamic behavior of a hybridoma cell line during extended subculturing after thaw, for example, from a cell bank vial. In our model culture, on-line monitoring of DO and pH show three distinctive regions in passages 1–18, 19–28, 29–54 that are linked to different cellular metabolic activities. Our DO and pH data show that as this cell culture evolved from thaw they begin preferring the oxidative phosphorylation pathway over glycolytic pathway for energy production in the first 18 passages ($N_p \leq 67$). While culture behavior will vary from cell-line to cell-line, on-line monitoring of DO and pH during cell passaging in a T-flask provides useful information to help to understand the manufacturing process at early bioprocess development stages and early pre-culture. This should aid the scaling-up process to bench-scale bioreactors, provide the process information to develop process control strategies, and provide assurance that cell culture drift does not occur during extended pre- and seed culture in commercial settings.

Funding from Sartorius-Stedim Biotech is gratefully acknowledged. G. Rao has an equity position in Flurometrix. Views expressed in this article are those of the authors and not necessarily of the US FDA or the US government. Discussion of the individual cell culture devices does not constitute endorsement by the US FDA or the US government.

References

Betts JI, Doig SD, Baganz F. 2006. Charcaterization and application of a miniature 10 mL stirred-tank bioreactor, showing scale-down equivalence with a conventional 7 L reactor. Biotechnol Prog 22:681–688.

Chen K, Liu Q, Xie L, Sharp PA, Wang DIC. 2001. Engineering of a mammalian cell line for reduction of lactate formation and high monoclonal antibody production. Biotechnol Bioeng 72:55–61.

Collins PC, Nielsen LK, Patel SD, Papoutaskis ET, Miller WM. 1998. Characterization of hematopoietic cell expansion, oxygen uptake, and glycolysis in a controlled, stirred-tank bioreactor system. Biotechnol Prog 14:466–472.

Diao J, Young L, Zhou P, Shuler ML. 2008. An actively mixed minibioreactor for protein production from suspended animal cells. Biotechnol Bioeng 100:72–81.

Fitzpatrick L, Jenkins HA, Butler M. 1993. Glucose and glutamine metabolism of a murine B-lymphocyte hybridoma grown in batch culture. Appl Biochem Biotechnol 43:93–116.

Food and Drug Administration. 2004. PAT. Framework for Innovative-Pharmaceutical Development, Manufacturing and Quality Assurance, 2004 (http://www.fda.org/cder/guidance).

Franek F, Dolnikova J. 1991. Hybridoma growth and monoclonal antibody production in iron-rich protein-free medium: Effect of nutrient concentration. Cytotechnology 7:33–38.

Ge X, Hanson M, Shen H, Kostov Y, Brorson KA, Frey DD, Moreira AR, Rao G. 2006. Validation of an optical sensor-based high-throughput bioreactor system for mammalian cell culture. J Biotechnol 122:293–306.

Gill NK, Appleton M, Baganz F, Lye GJ. 2008. Design and characterization of a miniature stirred bioreactor system for parallel microbial fermentations. Biochem Eng J 39:164–176.

Glicklis R, Merchuk JC, Cohen S. 2004. Modeling mass transfer in hepatocyte spheroids via cell viability, spheroid size, and hepatocellular functions. Biotechnol Bioeng 86:672–680.

Gramer M, Poeschl DM. 2000. Comparison of cell growth in T-flasks, in micro hollow fiber bioreactors, and in an industrial scale hollow fiber bioreactor system. Cytotechnology 34:111–119.

Gupta A, Rao G. 2003. A study of oxygen transfer in shake flasks using a non-invasive oxygen sensor. Biotechnol Bioeng 84(3):351–358.

Guzy RD, Hoyos B, Robin E, Chen H, Liu L, Mansfield KD, Simon MC, Hammerling U, Schumacker PT. 2005. Mitochondrial complex III is required for hypoxia-induced ROS production and cellular oxygen sensing. Cell Metab 1:401–408.

Hanson MA, Ge X, Kostov Y, Brorson KA, Moreira AR, Rao G. 2007. Comparison of optical pH and dissolved oxygen sensors with traditional electrochemical probes during mammalian cell culture. Biotechnol Bioeng 97:833–841.

Hermann R, Lehmann M, Buchs J. 2002. Characterization of gas–liquid mass transfer phenomena in microtiter plates. Biotechnol Bioeng 81:178–186.

Hiller GW, Clarck DS, Blanch HW. 1993. Cell retention-chemostat studies of hybridoma cells-analysis of hybridoma growth metabolism in continuous suspension culture in serum-free medium. Biotechnol Bioeng 42:185–195.

Jang JD, Barford JP. 2000. An unstructured kinetic model of macromolecular metabolism in batch and fed-batch cultures of hybridoma cells producing monoclonal antibody. Biochem Eng J 4:153–168.

Kensy F, John GT, Hofmann B, Büchs J. 2005. Characterisation of operation conditions and online monitoring of physiological culture parameters in shaken 24-well microtiter plates. Bioprocess Biosyst Eng 75:75–81.

Kermis HR, Kostov Y, Harms P, Rao G. 2003. Rapid method for the preparation of a robust optical pH sensor. Analyst 128:1181–1186.

Kostov Y, Harms P, Randers-Eichhorn L, Rao G. 2000. Low-cost microbioreactor for high-throughput bioprocessing. Biotechnol Bioeng 72(3):346–352.

Lee GM, Palsson BO. 1993. Stability of antibody productivity is improved when hybridoma cells are entrapped in calcium alignate beads. Biotechnol Bioeng 42:1131–1135.

Lee GM, Varma A, Palsson BO. 1991. Production of monoclonal antibody using free-suspended and immobilized hybridoma cells: Effect of serum. Biotechnol Bioeng 38:821–830.

Lu C, Gonzalez C, Gleason J, Gangi J, Yang JD. 2007. A T-flask based screening platform for evaluating and identifying plant hydrolysates for a fed-batch cell culture process. Cytotechnology 55:15–29.

Meleady P. 2007. Proteomic profiling of recombinant cells from large-scale mammalian cell culture processes. Cytotechnology 53:23–31.

Mercille S, Massie B. 1994. Induction of apoptosis in oxygen-deprived cultures of hybridoma cells. Cytotechnology 15:117–128.

Miller WM, Wilke CR, Blanch HW. 1987. Effects of dissolved oxygen concentration on hybridoma growth and metabolism in continuous culture. J Cell Physiol 132:524–530.

Miller WM, Blanch HW, Wilke CR. 1988a. A kinetic analysis of hybridoma growth and metabolism in batch and continuous suspension culture: Effect of nutrient concentration, dilution rate, and pH. Biotechnol Bioeng 32:947–965.

Miller WM, Wilke CR, Blanch HW. 1988b. Transient responses of hybridoma cells to nutrient additions in continuous culture: I. Glucose pulse and step changes. Biotechnol Bioeng 33:477–486.

Moran EB, McGowan ST, McGuire JM, Frankland JE, Oyebade IA, Waller W, Archer LC, Morris LO, Pandya J, Nathan SR, Smith L, Cadette ML, Michalowski JT. 2000. A systematic approach to the validation of process control parameters for monoclonal antibody production in fed-batch culture of a murine myeloma. Biotechnol Bioeng 69(3):242–255.

Naciri M, Kuystermans D, Al-Rubeai M. 2008. Monitoring pH and dissolved oxygen in mammalian cell using optical sensors. Cytotechnology 57:245–250.

Newland M, Greenfield PF, Reid S. 1990. Hybridoma growth limitations: The role of energy metabolism and ammonia production. Cytotechnology 3:215–229.

Ozturk SS, Palsson BO. 1991a. Growth, metabolic, and antibody production kinetics of hybridoma cell culture: 1. Analysis of data from controlled batch reactors. Biotechnol Prog 7:471–480.

Ozturk SS, Palsson BO. 1991b. Growth, metabolic, and antibody production kinetics of hybridoma cell culture: 2. Effects of serum concentration, dissolved oxygen concentration, and medium pH in a batch reactor. Biotechnol Prog 7(6):481–494.

Puskeiler R, Kaufmann K, Weuster-Botz D. 2005. Development, parallelization, and automation of a gas-inducing milliliter-scale bioreactor for high-throughput bioprocess design (HTBD). Biotechnol Bioeng 89(5):512–523.

Randers-Eichhorn L, Bartlett RA, Frey DD, Rao G. 1996. Noninvasive oxygen measurements and mass transfer considerations in tissue culture flasks. Bioetchnol Bioeng 51:466–478.

Rao G, Moreira A, Brorson K. 2009. Disposable bioprocessing: The future has arrived. Biotechnol Bioeng 102(2):348–356.

Richieri RA, Willimas LS, Chao PC. 1991. Cell cycle dependency of monoclonal antibody production in asynchronous serum-free hybridoma cultures. Cytotechnology 5:243–254.

Schmid G, Blanch HW, Wilke CR. 1990. Hybridoma growth, metabolism, and product formation in HEPES-buffered medium: II. Effect of pH. Biotechnol Lett 12(9):633–638.

Shuler Michael L, Fikret K. 2002. Bioprocess engineering. Basic concepts. 2nd edition. New Jersey: Prentice-Hall Publishing, p. 163.

Tolosa L, Kostov Y, Harms P, Rao G. 2002. Noninvasive measurement of dissolved oxygen in shake flasks. Biotechnol Bioeng 80:594–597.

Zhang Z, Szita N, Boccazzi P, Sinskey A, Jensen KF. 2006. A well-mixed, polymer-based microbioreactor with integrated optical measurements. Biotechnol Bioeng 93:286–296.

Zhang H, Lamping SR, Pickering SCR, Lye GJ, Shamlou PA. 2008. Engineering characterisation of a single well from 24-well and 96-well microtiter plates. Biochem Eng J 40:138–149.

Zupke C, Sinskey AJ, Stephanopoulus G. 1995. Intracellular flux analysis applied to the effect of dissolved oxygen on hybridomas. Appl Microbiol Biotechnol 44:27–36.

At the large bioreactor scale, there are a wealth of data on engineering parameters such as k_La, mixing time, power-to-volume ratios, impeller tip speed etc, However, not so much at the small scale where the vast number of process development studies are carried out, particularly for media optimization. We chose to use a 250 mL spinner flask, which was the workhorse stirred bioreactor widely used in cell culture process development as a model to characterize in detail and see if its utility could be upgraded by careful analysis of its mass transfer characteristics using sensors,

Interestingly, we found that there were significant oxygen gradients in a 5 liter bioreactor, which is where a large number of process development studies at the laboratory scale are conducted. We were only able to make this determination by measuring oxygen at multiple points in the bioreactor. These studies helped us later in designing our minibioreactor system to be representative of the laboratory scale bioreactor, as is discussed elsewhere in this book.

Integrating a 250 mL-Spinner Flask with Other Stirred Bench-Scale Cell Culture Devices: A Mass Transfer Perspective

Jose R. Vallejos
Center for Advanced Sensor Technology, Dept. of Chemical and Biochemical Engineering, University of Maryland, Baltimore County, Baltimore, MD 21250

Kurt A. Brorson
Office of Biotechnology Products, Center for Drug Evaluation and Research, Food and Drug Administration, Silver Spring, MD 20903

Antonio R. Moreira and Govind Rao
Center for Advanced Sensor Technology, Dept. of Chemical and Biochemical Engineering, University of Maryland, Baltimore County, Baltimore, MD 21250

DOI 10.1002/btpr.578
Published online April 26, 2011 in Wiley Online Library (wileyonlinelibrary.com).

The bioprocess development cycle is a complex task that requires a complete understanding of the engineering of the process (e.g., mass transfer, mixing, CO_2 removal, process monitoring, and control) and its affect on cell biology and product quality. Despite their widespread use in bioprocess development, spinner flasks generally lack engineering characterization of critical physical parameters such as k_La, P/V, *or mixing time. In this study, mass transfer characterization of a 250-mL spinner flask using optical patch-based sensors is presented. The results quantitatively show the effect of the impeller type, liquid filling volume, and agitation speed on the volumetric mass transfer coefficient (*k_La*) in a 250-mL spinner flask, and how they can be manipulated to match mass transfer capability at large culture devices. Thus, process understanding in spinner flasks can be improved, and these devices can be seamlessly integrated in a rational scale-up strategy from cell thawing to bench-scale bioreactors (and beyond) in biomanufacturing.* © 2011 American Institute of Chemical Engineers *Biotechnol. Prog.,* 27: 803–810, 2011
Keywords: bioprocess development, mass transfer, minibioreactors, scale-up, spinner flasks

Introduction

Bioprocess development typically involves the following stages (1) strain/clone screening, (2) early R&D studies, (3) process optimization, and (4) manufacturing. Strain/clone screening and early R&D studies are often carried out in unmonitored process scouting devices (PSDs) at the mL-Scale (<1 L). In contrast, process optimization and manufacturing stages are typically carried out in fully instrumented bioreactors (>1 L) that allow cell culturists to implement rigorous process control on critical process parameters such as dissolved oxygen (DO) and pH. As a result, there is a process information gap between PSDs and fully instrumented bioreactors that makes the transition from strain/clone screening to early process optimization stages more of an art than science. In this article, we provide quantitative process information data in a 250-mL spinner flask to enable a rational scale-up process development strategy (i.e., constant k_La) from strain/clone screening to manufacturing stage.

Correspondence concerning this article should be addressed to G. Rao at grao@umbc.edu.

Engineering Characterization of PSDs and Upstream Bioprocess Development

Mass transfer characterization of bioreactors at the bench, pilot, and manufacturing scales is a common task in equipment selection and design to ensure comparability across scales during bioprocessing development. In fact, scale-up at constant volumetric mass transfer coefficient (k_La) is typical for relative large fermentors.[1] But this is not always possible at the mL scale for PSDs, such as 250-mL spinner flasks, because they often lack monitoring capabilities for DO. As a result, understanding how equipment operational engineering aspects correlate between this PSD and laboratory-scale devices[2,3] is still a major challenge. This is despite the fact that novel optical-based DO sensors (based on quenching of fluorescence light[4]) have been used successfully for studies of stirred and shaken PSDs[5–9] as scale-down models of laboratory-scale bioreactors.

Spinner Flasks as PSDs

For many years, spinner flask applications have existed in the preculture of therapeutic proteins. But in recent years, tissue engineering and embryonic stem cell development are

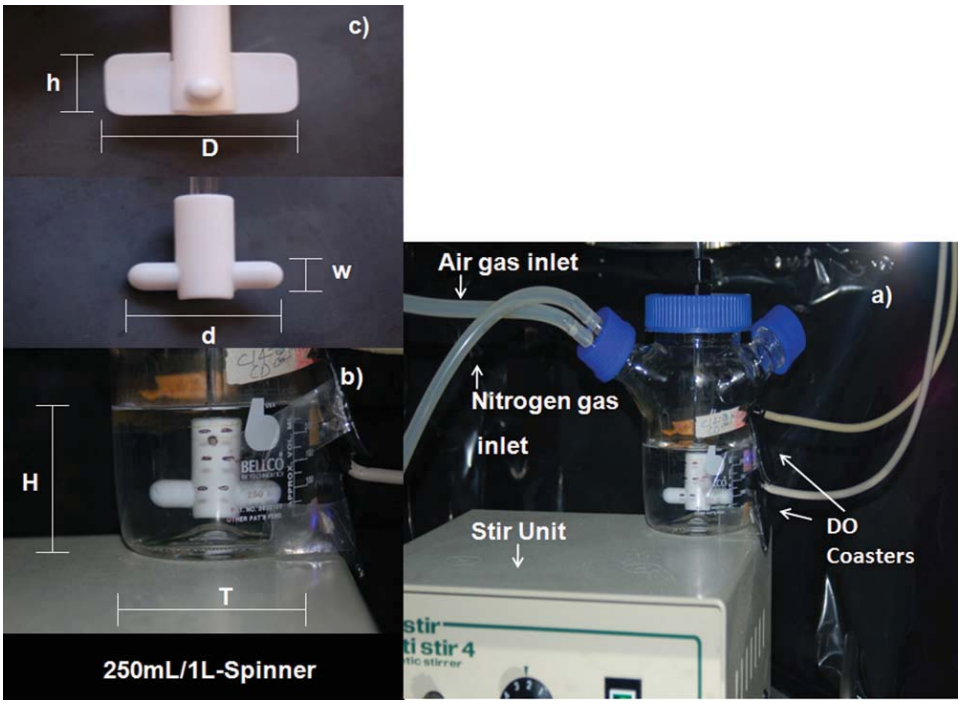

Figure 1. k_La **measurement experimental set-up.**

(**a**) 250-mL Spinner flask and sensor, (**b**) 250-mL spinner flask-close up, and (**c**) impeller most relevant geometrical parameters.

extensively carried out in spinner flasks. Spinner flasks also are key process linking cell culture devices which bridge the strain/clone screening and early process optimization stages. Spinner flasks have been extensively characterized for shear effects on shear-sensitive cells[10–12], but little engineering characterization of critical physical parameters has been performed for these devices.[13]

In this study, mass transfer characterization of 250-mL and 1-L spinner flasks using optical patch-based sensors is presented. These results are benchmarked to k_La values obtained in a 5-L stirred bioreactor Biostat® (Sartorius, Bohemia, NY) and compared with other cell culture devices (well plates, shake flasks, and spinner flasks) reported in the literature. The aim of this work is to generate process information (i.e., k_La) in spinner flasks that would provide the basis for developing a scale-up strategy (i.e., constant k_La) for the entire bioprocess development cycle.

Materials and Methods

Experimental set-up

Spinner flasks were placed on a magnetic stirrer (Bellco Glass, Vineland, NJ), and a gas tubing line was connected to one of the arms of the flask using a two-port sampler assembly (Bellco Glass, Vineland, NJ). A DO patch (Fluorometrix, Stow, MA) was affixed on the inside wall close to the bottom of the flask. This sensor system has previously been used to study oxygen transfer in shake flasks.[9] Briefly, this sensor system consists of a long-lifetime ruthenium-based fluorophore immobilized in the DO patch. After excitation from an intensity-modulated light source (blue LED), this fluorophore emits light at the same frequency but with lower modulation and a phase shift. This fluorescence is quenched by the presence of oxygen, and the DO concentration is estimated from the phase shift values (Stern Volmer equation).

In some cases where a spinner was filled to the maximum working volume, a second patch was placed close to liquid surface (i.e. top). In the case of our benchmarking 5-L stirred bioreactor Biostat®, three patches were used with one in the top section, one in the middle section, and one more in the bottom section (at the same level of a DO probe) of the vessel and air was sparged at 0.01 vvm.[14] The LEDs for excitation and photo detector for light detection were placed outside the cell culture devices (Figure 1a) and the most relevant geometrical parameters of the spinner flasks used in this study are shown in Figures 1b,c. To compare mass transfer capabilities of spinner flasks with smaller cell culture devices we used a minibioreactor that has previously been described in detail.[15] Briefly, this minibioreactor is 30 mm in diameter and 78 mm in height equipped with two 6 $\times$ 18 mm^2 paddles powered by an agitation motors placed on the top of the vessel.

Volumetric mass transfer coefficient measurements

We used the unsteady-state method[16], also known as the "gassing out" method, with no cells present. Briefly, deionized water at 37°C was deoxygenated with nitrogen, and then air was swept at the head space for 45 s until air saturation was reached (an oxygen patch was placed at the head space). Experiments were carried out in a Certomat BS-1 temperature control incubator (Sartorius, Bohemia, NY).

Because of the low k_La values reported in this study, the criterion that the response time of optical patch-based sensor (generally in the seconds scale) should be $\leq 1/k_La$ was applied throughout the range of measurements.[17] Consequently, response time of the optical sensor was disregarded in k_La calculations.

Liquid mass transfer coefficient (k_L)

In our study, k_L for headspace aeration was estimated using the equation proposed by Lavery and Nienow[18]:

$$k_L = \frac{k_L a \bullet V}{A} \quad (1)$$

where $k_L a$ value is the volumetric mass transfer coefficient, V is the filling volume, and A is the surface area.

Volumetric mass transfer coefficient correlations

For each flask, $k_L a$ was determined experimentally using the gassing-out method at different volumes and stir speeds. Then, the $k_L a$ experimental data were fitted to Eqs. 2 and 3 (see below) allowing the empirical constants (m, a, b, a_2, b_2, and c) to be estimated from the experimental data by nonlinear regression analysis of the $k_L a$ data using an Excel (Microsoft®) spreadsheet with equations based on the method proposed by Brown.[19]

The volumetric mass transfer coefficient ($k_L a$) model equations used to correlate our experimental data are as follow:

$$k_L a = mV^a N^b \quad (2)$$

$$k_L a = \frac{a_2 D_{O_2}}{T \bullet H} Re^{b_2} \mathrm{Fr}^c \quad (3)^{20})$$

where V is the liquid filling volume, N the stir speed, D_{O_2} the diffusion coefficient for oxygen, T the vessel internal diameter, H the liquid height, Re the Reynolds number, Fr the Froude number, and m, a, b, a_2, b_2, and c are empirical constants estimated from the data and Eqs. 2 and 3 by the method indicated above.

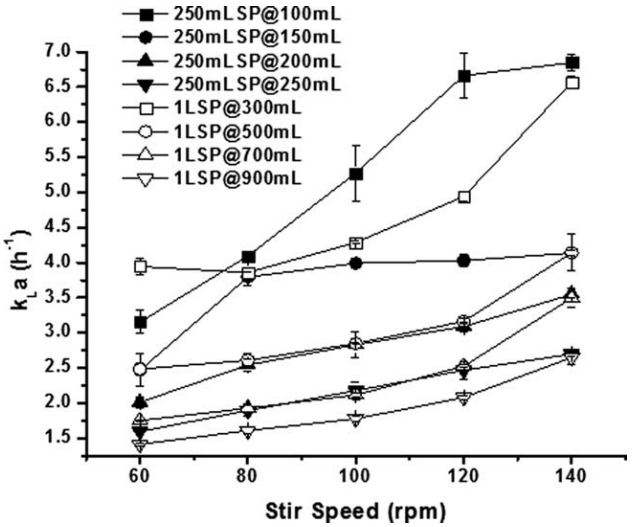

Figure 2. $k_L a$ comparability between a 250-mL and 1-L Spinner flask at different filling volumes and stir speeds under headspace aeration.

Results

Our patch based study shows that a 250-mL spinner flask can be operated in a manner such that it has similar $k_L a$ and OTR_{max} to a 1-L spinner flask (Figure 2), a 5-L Biostat® under air sparging conditions (Table 1) or larger stirred vessels.[21,22] Our DO patch-based sensor allows use of more representative test fluids and measurement methods (i.e., gassing out) that has previously been used in manufacturing scale bioreactors.[21] In contrast, our literature search found that estimations of volumetric mass transfer coefficient ($k_L a$) in shaken devices (e.g., microtiter plates and Erlenmeyer flasks) were done in electrolyte solutions using the sulfite method at room temperatures. Having a "standard" $k_L a$ estimation method for PSDs across the scales using more representative test fluids could significantly help in integrating different PSDs with trains of bioreactors.

Mass transfer equivalence of spinner Flasks

In this study, we evaluated 250-mL and 1-L spinner flasks, a 5-L Bioreactor and historical data in terms of $k_L a$, OTR_{max}, and Sherwood number (Sh) vs. Reynolds number (Re). To show this comparison, the $k_L a$ dependence on liquid filling volume, stir speed, Re number, and Fr number was

Table 1. Comparison of k_La and OTR_{max} Results Using Cell Culture Devices from our Study (under Headscape Aeration) with Published Data of other Systems

	Measurement conditions					Measured parameters	
Reference	Device	Liquid medium	Temperature (°C)	Filling Volume (L)	Agitation speed (rpm)	$k_L a$ range (h^{-1})	OTR_{max} (mmol/mL h) × 10^4
Stirred Devices							
This work	Minibioreactor	DI water	37	0.015–0.035	100–1000	0.97–10.73	2.08–23.0*
This work	250-mL spinner flask With paddle	DI water	37	0.10–0.25	60–140	1.59–6.85	3.41–14.30*
	No paddle	DI water	37	0.10–0.25	60–140	1.05–4.79	2.25–10.30*
This work	1-L spinner flask	DI water	37	0.30–1.0	60–140	1.26–6.75	2.69–14.10*
This work	5-L Biostat	DI water	37	4.5	60–300 1.1–5.7***	0.23–0.88** 2.44–12.1	0.49–1.88*
Aunins et al.[22]	1-L spinner flask	DMEM	37	0.50	25–250	0.75–4.40	1.61–9.42*
Lavery and Nienow[18]	LH Fermenter 500 series	DI water	37	1.5	100–350	0.65–2.05	1.39–4.39*
Shaken Devices							
Hermann et al.[33]	96-well microtiter plates	Electrolyte	22	0.00014–0.0002	0–1000	25–160	50–1500
Kensy et al.[34]	48-well microtiter plates	Electrolyte	25	0.0003–0.0006	0–2000	25–1600	50–2570
Maier et al.[35]	Shake flasks	Waterlike	22.5	0.002–0.16	50–500	3.6–432	7.70–900*
Gupta and Rao[8]	250-mL shake flask	Water	37	0.10	250	24–59.2	51.4–100*

* C* used to calculate OTR_{max} was 2.14 × 10^{-4}mmol O_2/mL.[7] ** Data obtained under headspace aeration conditions. *** Data obtained under air sparging conditions (0.01 vvm).

Table 2. Empirical Constants for k_La Correlation in Eqs. (2) and (3) Under Headspace Aeration and No Vortex[36]

	Device	m	a	b	D/T	Notes
Equation 2	Stirred Mini-bioreactor	0.0017	−0.79	0.81	0.67	Volume range: 0.015–0.035 L; Stir speed range: 100–900 rpm; $R^2 = 0.98$
	250-mL Spinner (w/paddle)	0.0074	−0.97	0.94	0.65	Volume range: 0.1–0.25 L; Stir speed range: 60–140 rpm; $R^2 = 0.97$
	250-mL Spinner (w/o paddle)	0.0041	−1.04	0.94	0.50	Volume range: 0.1–0.25 L; Stir speed range: 60–140 rpm; $R^2 = 0.97$
	1-L Spinner	0.028	−0.68	0.94	0.63	Volume range: 0.3–1.0 L; Stir speed range: 60–140 rpm; $R^2 = 0.99$
	5-LBiostat	0.74	−3.19	1.15	0.46	Volume: 4.5 L; Stir speed: 60–400 rpm; $R^2 = 0.99$
		a_2	b_2	c	Sh[36]$=1.4Re^{0.76}$	Notes
Equation 3	250-mL spinner(w/paddle) $Sh = 1.2\text{Re}^{0.76}$	0.76	0.86	0.13	D/T same as in Eq. 2	Volume and stir speed same as in Eq. 2. $R^2 > 0.97$
	250-mL spinner(w/o paddle) $\text{Sh}=1.5\text{Re}^{0.74}$	636	0.16	0.31		
	1 L-spinner $Sh = 3.3Re^{0.65}$	1586	0.10	0.25		
	5-L biostat $Sh = 0.59Re^{0.81}$	1.86	0.72	0.074		

These empirical constants were determined by fitting the experimental k_La data obtained using the gassing out method with process input physical measurable variables (V, N, T, H, etc.) using nonlinear regression (See Materials and Method sections for more details).

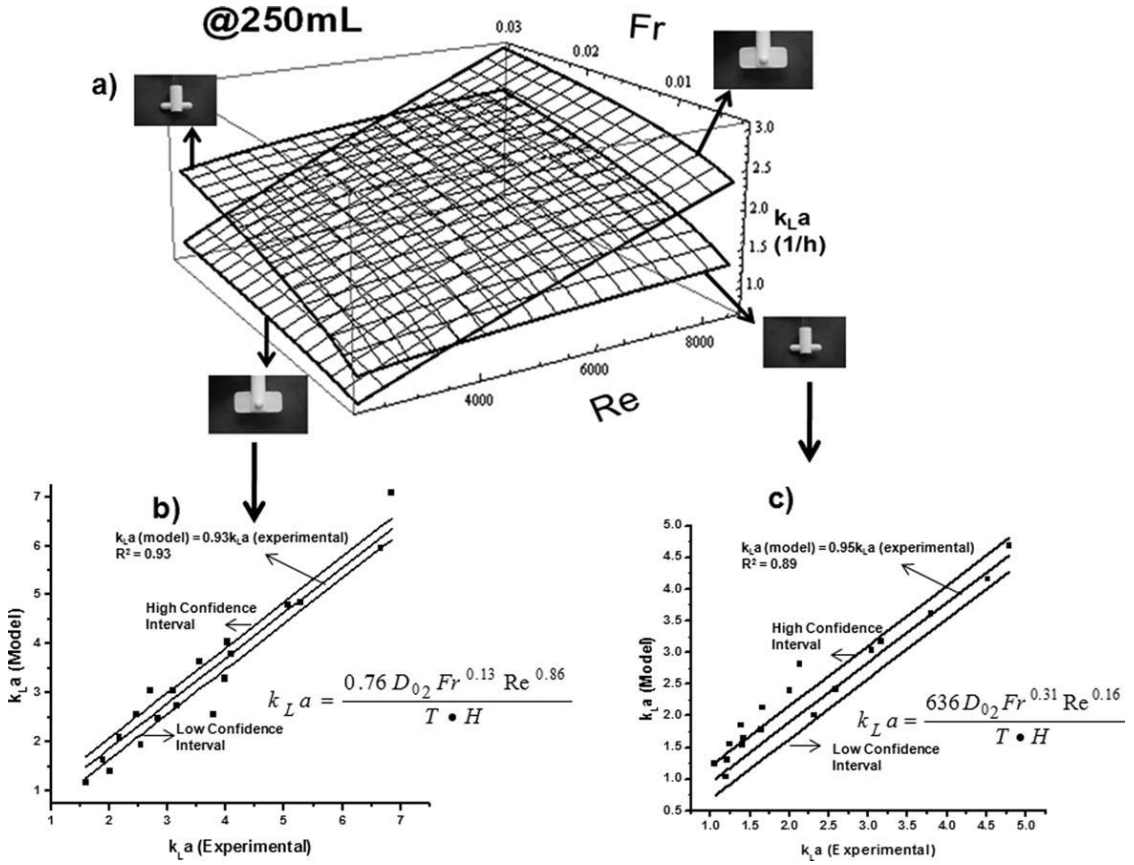

Figure 3. (a) k_La as a function of Reynolds (Re) and Froude (Fr) number in a 250-mL spinner flask for two type of impellers, (b) model vs. experimental for Paddle + Stirbar, and (c) model vs. experimental for Stirbar.

investigated experimentally in our optical patch enabled spinner flasks. The Sherwood (Sh) number relationship to Reynolds number (Re) in the 250-mL spinner flask was found to be similar to those reported in the literature (See Table 2 for similar devices). We observed in Figure 3 that when $Re > 4000$ and $Fr \approx 0.004$ there is an intersection point in the curves where the stirbar impeller starts to become less efficient than the paddle + stirbar impeller. Equation 2 was also plotted (Figure 4), and it shows that at low volumes (below 0.15 L) and high stir speed (above 100 rpm), the paddle + stirbar impeller enhances k_La up to two-fold when compared with the stirbar impeller. Both Figures 3 and 4 show that our model Eq. 2 can predict k_La in the 250-mL spinner flask with more reasonable accuracy than Eq. 3 at a critical t value of 2.1 (with 17 degrees of freedom using the 0.05 significance level) for both paddle and stir bar impeller, respectively. Thus, we recommend the use of Eq. 2 over Eq. 3 for estimating k_La or OTR_{max}, because it is more

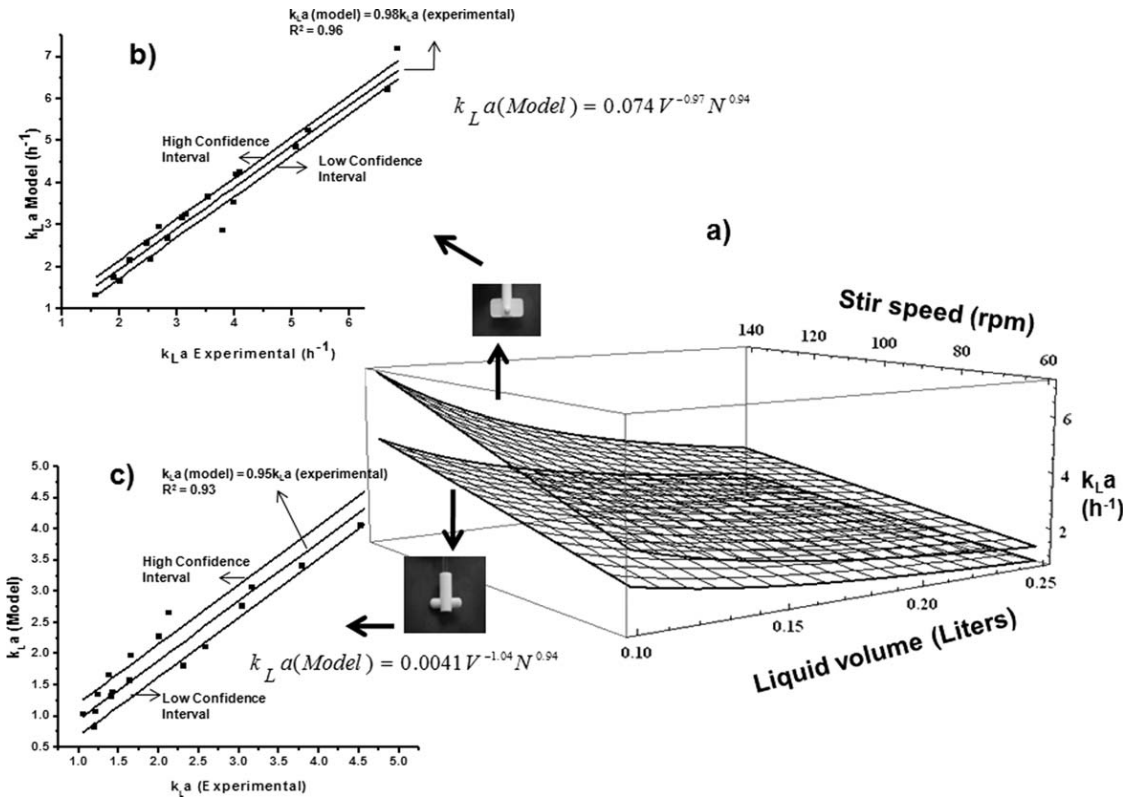

Figure 4. (a) k_La as a function of volume (L) and stir speed (rpm) in a 250-mL spinner flask for two type of impellers, (b) Model vs. experimental for Paddle +Stirbar, and (c) Model vs. experimental for stirbar.

Table 3. Comparison of k_L (m/s × 10^5) Results for Unbaffled and Baffled Cell Culture Devices under Headspace Aeration with Published Data[18]

Reference	Physical device characteristics			Measured values
	Vessel diameter (m)	Impeller diameter (m)	Type of impellers	Range of k_L
Unbaffled systems				
This work (250-mL spinner flask with paddle)	0.08	0.052	Paddle + Stirbar	1.74–4.28*
This work (250-mL spinner flask no paddle)	0.08	0.04	Stirbar	1.17–3.20*
This work (1-L spinner flask)	0.128	0.08	Paddle + Stirbar	2.6–5.9*
Lavery and Nienow[18]	0.233	0.06	Three-Bladed propeller	1.18–3.54*
Baffled systems				
This work (5-L Biostat)-Filling volume = 4.5 L	0.17	0.06	Pitched blade	1.45–5.54*
Lavery and Nienow[18]	0.10	0.05	Three-Bladed propeller	1.50–4.0
Lavery and Nienow[18]	0.10	0.05	Three-Bladed propeller	2.70–4.50

* $k_L = k_La \bullet V/A$ (See Materials and Method section).

accurate and practical using easily measurable parameters (i.e., volume and stir speed) as inputs.

Effect of impeller type on mass transfer in the 250-mL spinner flask

Our DO patches allowed us to investigate the effect of impeller type on mass transfer in spinner flasks. This dependence was determined by physical measurements followed by calculations using the method proposed by Xing et al.[22] our approach was shown to be useful. Data given in Table 2 led us to believe that the absolute value of coefficient parameters "*a*" and "*b*" for process variables such as filling volume and stir speed, respectively, may not be as critical as expected because with or without a paddle the dependence of k_La on these variables is very similar (10% difference maximum). These findings suggest that from the perspective of enhancing k_La, the type of impeller (given by coefficient "m") is more relevant. The measurements were 0.0074 vs. 0.0041 (80% difference) for spinner with paddle and without paddle, respectively.

The direct effect of impeller type on the liquid mass transfer coefficient (k_L) was also investigated, and the results are shown in Table 3. Comparison with literature values of k_L for both impellers used in our study showed reasonable agreement with other stirred devices, validating the utility of our sensor-patch based optical sensor.

Effect of patch position in the vertical axis on mass transfer

For the 250-mL spinner flask (i.e., filling volume of 250 mL) regardless of the impeller type, Figure 5 shows that there is no significance difference between the DO profiles at the bottom and top sections of the vessel. We used these DO profiles to estimate k_La and we also observed that k_La at the bottom and top sections are essentially the same. These results were similar to those found in the 1-L spinner flask (i.e.,

filling volume of 1 L) at 60 and 140 rpm as shown in Figure 6. In the 5-L stirred bioreactor, our results indicate that even a relative good mixing time does not guarantee a uniform air bubble distribution. We observed that at typical operational conditions (235 rpm and 0.01 vvm air sparging rate), the 5-L Biostat® showed significant oxygen distribution profile differences within the vessel vertical axis (Figure 7). This experiment was carried out at a relative low mixing time of 3.65 s estimated by pH-tracer technique (data not shown).

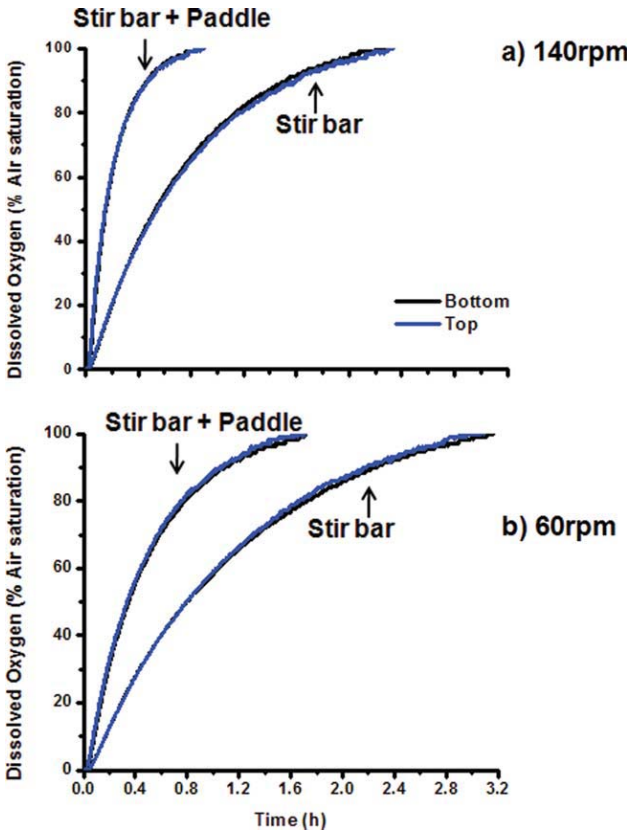

Figure 5. DO profiles at the bottom and top sections of a completely full 250-mL spinner flask and two types of impellers (stir bar + paddle, stir bar only).

(**a**) At 140 rpm and (**b**) At 60 rpm. The figure shows that for both type of impellers, there is no significant difference between DO profiles at the bottom or tops sections of the spinner flask.

Discussion

Bioprocess implications

Despite the significance of 250-mL spinner flasks in bioprocess settings, little engineering characterization of critical physical parameters has been performed for these devices. Most of the studies reported in the literature has focus on relative larger spinner flasks.[10–14,23,24]

The results presented in this study show that using optical patches, PSDs such as 250-mL spinner flasks can be chosen and set to successfully match k_La values observed in larger devices.[1,22] Thus, scalability is desirable because one could design seamless process transfer (i.e., scale-up) from currently unmonitored PSDs (wells plates, T-flasks, minibioreactor, and spinner flasks) to fully instrumented bench-scale bioreactors at either constant k_La or OTR_{max}. We and others have previously shown using *E. coli* fermentations[9,25,26] and hybridoma cells[27] that k_La can be used as a successful scale-down criterion for PSDs and bench-scale cell culture devices. These reported studies were carried out in different types of PSDs such as shake flasks, microwell plates, and stirred miniature bioreactors. Thus, our current mass transfer study, which extends these observations to spinner flasks shows the potential of these PSDs for developing a rationale scale-up strategy from strain/clone screening to early process optimization in bench-scale bioreactors (and beyond).[28]

Effect of impeller type on mass transfer

Using our patch-based DO sensor, we were able to show in a quantitative way for the first time the effect of impeller type on mass transfer in 250-mL spinner flasks. As expected, having a paddle as stirrer enhances both the liquid mass transfer coefficient (k_L) and the volumetric mass transfer coefficient (k_La). Further experiments could be designed to investigate the effect of, for example, shear stress (at constant k_La) or k_La (at constant shear rate) for both impellers on cell growth, product titer, and product quality attributes. These results further support the concept of a "data-driven bioprocessing" where even a "simple" decision such as what impeller is the best choice (i.e., k_La or shear stress) is best made based on experimental data.

Maximum oxygen transfer rate (OTR_{max}) in stirred PSDs

One should be cautious when comparing OTR_{max} in different cell culture devices under different conditions such medium composition, measurement method, and so on.

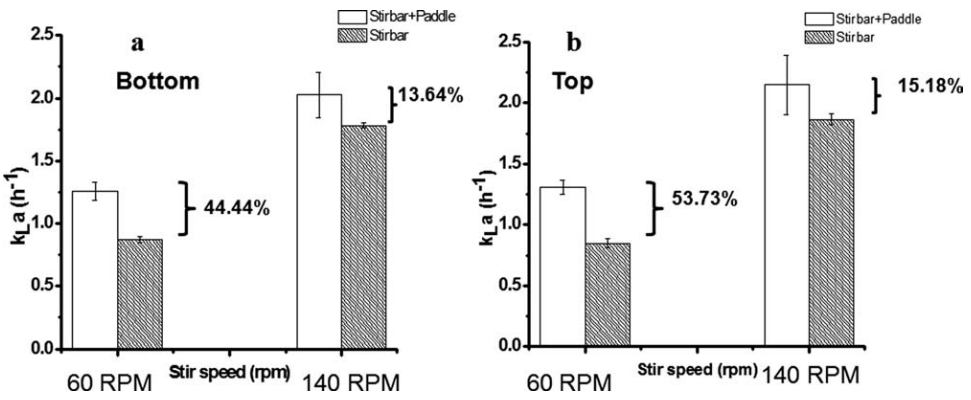

Figure 6. Local k_La in the bottom and top section of a 1-L standard spinner flask.

(**a**) Bottom and (**b**) Top.

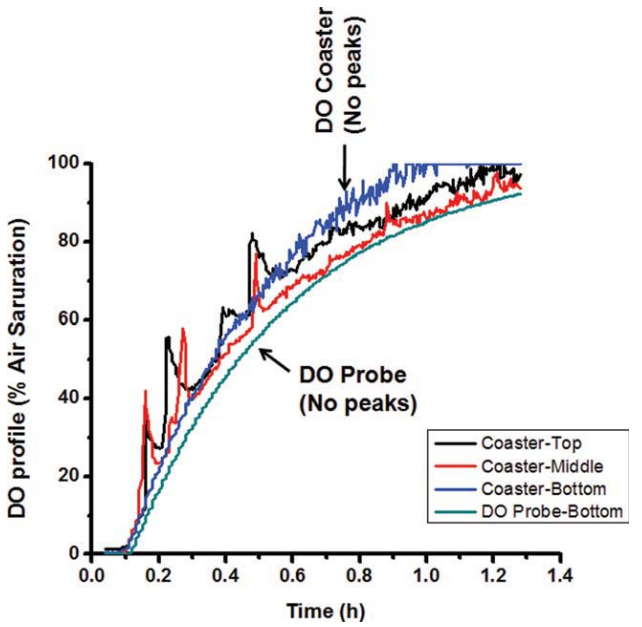

Figure 7. DO gradients in the bottom, middle, and top section of 5- L Biostat in the absence of cells.

This figure shows differences in the air bubbles distribution between the bottom (no transient peaks) and middle/top sections (transient peaks). Note: The coaster/patch located at the bottom of the vessel was located at the same level and close to a conventional DO probe. This experiment was carried out at a k_La of 2.3 h^{-1}, 235 rpm, and 0.01 vvm air sparging rate with a liquid filling volume of 4.5 L.

Stirred vessels used in this and other studies have similar OTR_{max}, but they differ from those reported for shaken PSDs. As shown in Table 1, stirred PSDs used in this study have significantly lower k_La and OTR_{max} than shaken PSDs. This argues that stirred devices are more useful for culture scale-up. Nevertheless, it is important to point out that we are comparing data from multiple studies using different methods. In fact, k_La is a strong function of medium composition and an ionic medium may give higher k_La over pure water under identical conditions.[17,29,30] However, our k_La measurement method and test media allowed us to compare our findings with previously reported data for other stirred cell culture devices both at the bench-scale and manufacturing-scale.[21,22]

DO gradients in spinner flasks

Our optical patch generated study shows that in the 60–140 rpm range, DO gradients are not likely to be found in either 250-mL spinner flasks (with or without paddle as stirrer) or the 1-L standard spinner flask. Our observations in the 5-L Biostat® suggest that even a relative low-mixing time value (as in this case of 3.65 s) as the sole criteria for scale-up is not enough to guarantee uniform bubble distribution in stirred vessels. This is further supported by findings of oxygen limitation in highly agitated and aerated laboratory-scale fermentors.[31] More importantly, the change in DO profile in the 5-L Biostat suggests that if cells are cultured and adapted to free bubble environment (current PSDs) and then transferred to sparged bioreactors, there could be some physiological or biological (i.e., apoptosis timing and rate) effects on the cells as suggested by Krampe and Al-Rubeai.[32] In theory, these biological effects on the cells during early seed expansion in PSDs could have a negative impact on the product titer and product quality attributes at the bench-scale bioreactors.

Conclusions

This study shows how patch-based DO sensors and mass transfer studies in spinner flasks can help in integrating these uncharacterized PSDs to fully instrumented bench-scale bioreactors filling the process information gap that currently exist among these cell culture devices. In addition, this study supports the concept of a "data-driven bioprocessing" in PSDs where the criteria (i.e., k_La or shear stress) for even a "simple" decision such as what impeller is the best choice is best made based on experimental data. This study also shows that k_La values in spinner flasks are similar to those previously found in larger stirred cell culture devices. As a result, a rational scale-up strategy at matched k_La from currently uncharacterized PSDs (during early seed expansion including cell thawing) such as spinner flasks to fully instrumented bench-scale bioreactors can be implemented. This approach could potentially reduce the bioprocess development timeline.

Acknowledgments

Funding from Sartorius-Stedim Biotech is gratefully acknowledged. G. Rao has an equity position in Flurometrix. Views expressed in this article are those of the authors and not necessarily of the US FDA or the US government. Discussion of the individual cell culture devices does not constitute endorsement by the US FDA or the US government.

Notation

A = surface area (m^2)
C_{in} = CO_2 concentration of inlet liquid (mol/L)
C_L = the oxygen concentration in liquid (% of air saturation)
C_{out} = CO_2 concentration of outlet liquid (mol/L)
C^* = the equilibrium oxygen concentration (% of air saturation)
C_0 = the oxygen initial concentration at $t = 0$ (% of air saturation)
D = impeller diameter (m)
D_{O_2} = diffusion coefficient of oxygen in water (m^2/s)
Fr = Froude number ($Fr = N^2 D/g$)
g = gravitational force (9.8 m/s^2)
H = liquid height (m)
k_L = liquid mass transfer coefficient (m h^{-1})
k_La = overall volumetric mass transfer coefficient (h^{-1})
N = stir speed (s^{-1} or min^{-1})
N_P = power number (no dimensional number)
OTR = oxygen transfer rate (mmol/mL h)
OTR_{max} = maximum oxygen transfer rate (mmol/mL h)
P/V = volumetric power input (Wm^{-3})
Re = Reynolds number ($Re = \rho ND^2/\mu$)
Sc = Schmidt number ($Sc = \mu/\rho D_{O_2}$)
Sh = Sherwood number ($Sh = k_L D/D_{O_2}$)
T = vessel internal diameter (m)
V = filling volume (m^3)

Greek Symbol

ρ = liquid density (kg/m^3)
μ = liquid viscosity (N s/m^2)

Literature Cited

1. Flores ER, Perez F, de la Torre M. Scale-up of *Bacillus thuringiensis* fermentation based on oxygen transfer. *J Ferment Bioeng*. 1997;83:561–564.
2. Rao G, Moreira A, Brorson K. Disposable bioprocessing: the future has arrived. *Biotechnol Bioeng*. 2009;102:348–356.
3. Betts JI, Baganz F. Miniature bioreactors: current practices and future opportunities. *Microb Cell Fact*. 2006;5:21–34.

4. Bambot SB, Holavanahali R, Lakowicz JR, Carter GM, Rao G. Phase fluorometric sterilizable optical oxygen sensor. *Biotechnol Bioeng*. 1993;43:1139–1145.
5. Kostov Y, Harms P, Randers-Eichhorn L, Rao G. Low-cost microbioreactor for high-throughput bioprocessing. *Biotechnol Bioeng*. 2000;72:346–352.
6. Lamping SR, Zhang H, Allen B, Shamlou PA. Design of a prototype miniature bioreactor for high throughput automated bioprocessing. *Chem Eng Sci*. 2003;58:747–758.
7. Kumar S, Wittmann C, Heinzel E. Minibioreactors. *Biotechnol Lett*. 2004;26:1–10.
8. Randers-Eichhorn L, Barlett RA, Frey DD, Rao G. Noninvasive oxygen measurement and mass transfer consideration in tissue culture flasks. *Biotechnol Bioeng*. 1996;51:466–478.
9. Gupta A, Rao G. A study of oxygen transfer in shake flasks using a non-invasive oxygen sensor. *Biotechnol Bioeng*. 2003;84:351–358.
10. Croughan MS, Sayre ES, Wang DIC. Viscous reduction of turbulent damage in animal cell culture. *Biotechnol Bioeng*. 1988;33:862–872.
11. Cherry RS, Papoutsakis ET. Hydrodynamic effects on cells in agitated tissue culture reactors. *Bioprocess Eng*. 1986;1:29–41.
12. Gooch KJ, Kwon JH, Blunk T, Langer R, Freed LE, Vunjak-Novakovic G. Effects of mixing intensity on tissue-engineered cartilage. *Biotechnol Bioeng*. 2001;72:402–407.
13. Sucosky P, Osorio DF, Brown JB, Neitzel GP. Fluid mechanics of a spinner-flask bioreactor. *Biotechnol Bioeng*. 2004;85:34–46.
14. Zhu H, Nienow AW, Bujalski W, Simmons MJH. Mixing studies in a model aerated bioreactor equipped with an up- or down-pumping 'Elephant Ear' agitator: power, hold-up and aerated flow field measurements. *Chem Eng Res Des*. 2009;87:307–317.
15. Ge X, Hanson M, Shen H, Kostov Y, Brorson KA, Frey DD, Moreira AR, Rao G. Validation of an optical sensor-based high-throughput bioreactor system for mammalian cell culture. *J Biotechnol*. 2005;122:293–306.
16. Shuler ML, Kargi F. Selection, scale-up, operation, and control of bioreactors. In: Amundson NR, editor. *Bioprocess Engineering. Basic Concepts*. 2nd ed. New Jersey:Prentice-Hall Publishing; 2001; 294 p.
17. Van't Riet K. Review of measuring methods and results in non-viscous gas-liquid mass transfer stirred vessels. *Ind Eng Chem Process Des Dev*. 1979;18:357–364.
18. Lavery M, Nienow AW. Oxygen transfer in animal cell culture medium. *Bioetchnol Bioeng*. 1987;30:368–373.
19. Brown AM. A step-by-step guide to non-linear regression analysis of experimental data using a Microsoft Excel spreadsheet. *Comp Prog Meth Biomed*. 2001;65:191–200.
20. Croughan MS, Chiou T-W, Wang DIC. Immobilized animal cell bioreactors. In: Asenjo JA, Merchuck JC, editors. *Bioreactor System Design*. New York: Marcel Dekker, Inc.; 1995;377–411.
21. Fuchs R, Ryu DY, Humphrey AE. Effect of surface aeration on scale-up procedures for fermentation processes. *Ind Eng Chem Des Dev*. 1971;10:190–196.
22. Xing Z, Kenty BM, Li ZJ, Lee SS. Scale-up analysis for CHO cell culture process in large-scale bioreactors. *Biotechnol Bioeng*. 2009;103:733–746.
23. Aunins JG, Woodson BA, Jr, Hale TK, Wang DIC. Effects of paddle impeller geometry on power input and mass transfer in small-scale animal cell culture vessels. *Bioetchnol Bioeng*. 1989;34:1127–1132.
24. Bonhenkamp H, Hilbert U, Noll T. Bioprocess development for the cultivation of human T-lymphocytes in a clinical scale. *Cytotechnology*. 2002;38:135–145.
25. Islam RS, Tisi D, Levy MS, Lye GJ. Scale-up of *Escherichia coli* growth and recombinant protein expression conditions from microwell to laboratory and pilot scale based on matched. *Biotechnol Bioeng*. 2008;99:1128–1139.
26. Gill NK, Appleton M, Baganz F, Lye GJ. Quantification of power consumption and oxygen transfer characteristics of a stirred miniature bioreactor for predictive fermentation scale-up. *Biotechnol Bioeng*. 2008;100:1144–1155.
27. Hanson M, Brorson KA, Moreira AR, Rao G. Comparison of optically monitored small-scale stirred tank vessels to optically controlled disposable bag bioreactors. *Microb Cell Fact*. 2009;8:44–50.
28. Miller WM, Wilke CR, Blanch HW. Effects of dissolved oxygen concentration on hybridoma growth and metabolism in continuous culture. *J Cell Physiol*. 1987;132:524–530.
29. Nienow AW. Reactor engineering in large scale animal cell culture. *Cytotechnology*. 2006;50:9–33.
30. Linek V, Kordač M, Moucha T. Evaluation of the optical sulfite oxidation method for the determination of the interfacial mass transfer area in small-scale bioreactors. *Biochem Eng J*. 2006;27:264–268.
31. Garcia JR, Cha HJ, Rao G, Marten MR, Bentley WE. Microbial nar-GFP cell sensors reveal oxygen limitations in highly agitated and aerated laboratory-scale fermentors. *Microb Cell Fact*. 2009;8:6–12.
32. Krampe B, Al-Rubeai M. Cell death in mammalian cell culture: molecular mechanisms and cell line engineering strategies. *Cytotechnology*. 2010;62:175–188.
33. Hermann R, Lehmann M, Büchs J. Characterization of gas-liquid mass transfer phenomena in microtiter plates. *Biotechnol Bioeng*. 2003;81:178–186.
34. Kensy F, Zimmermann HF, Knabben I, Anderlei T, Trauthwein H, Dingerdissen U, Büchs J. Oxygen transfer phenomena in 48-well microtiter plates: determination by optical monitoring of sulfite oxidation and verification by real-time measurement during microbial growth. *Biotechnol Bioeng*. 2005;89:698–708.
35. Maier U, Losen M, Büchs J. Advances in understanding and modeling the gas-liquid mass transfer in shake flasks. *Biochem Eng J*. 2004;17:155–167.
36. Aunins JG, Henzler HJ. In: Rehm H-J, Reeds G, editors. Aeration in Cell Culture Bioreactors. *Biotechnology*, Vol. 3, 2nd ed. Weinheim: VCH; 1993:219–281.

Manuscript received Oct. 18, 2010, and revision received Jan. 28, 2011.

Jose continued the work and started systematically characterizing process scouting devices. In this paper, the focus was to see if a T-flask could be placed on a rocker and if this innovation would lead to a reasonable scale-down model of a wave type bag reactor, which had taken over the cell culture industry as the preferred bioreactor largely due to its simplicity and convenience.

Our sensors had found their way into the wave bioreactor design and so by conducting parallel studies we were able to show the utility of a scale-down model for rocking bioreactors. However, because the T-flask is rigid, the cells did not grow as well in them and this suggested that a small rocked bag would be necessary to match the hydrodynamic factors and that matching k_La alone was insufficient for successful scale-down. We also enlisted Martina Micheletti, an expert in fluid dynamics to collaborate on this effort.

ARTICLE

BIOTECHNOLOGY and BIOENGINEERING

Optical Sensor Enabled Rocking T-Flasks as Novel Upstream Bioprocessing Tools

Jose R. Vallejos,[1] Martina Micheletti,[2] Kurt A. Brorson,[3] Antonio R. Moreira,[1] Govind Rao[1]

[1]Center for Advanced Sensor Technology, Department of Chemical, Biochemical and Environmental Engineering, University of Maryland, Baltimore County, 1000 Hilltop Circle, Baltimore, Maryland 21250; telephone: 410-455-3415; fax: 410-455-1049; e-mail: grao@umbc.edu

[2]The Advanced Centre for Biochemical Engineering, Department of Biochemical Engineering, University College London, Torrington Place, London, UK

[3]Office of Biotechnology Products, Center for Drug Evaluation and Research, Food and Drug Administration, Silver Spring, Maryland

ABSTRACT: During the past decade, novel disposable cell culture vessels (generally referred to as Process Scouting Devices or PSDs) have become increasingly popular for laboratory scale studies and seed culture generation. However, the lack of engineering characterization and online monitoring tools for PSDs makes it difficult to elucidate their oxygen transfer capabilities. In this study, a mass transfer characterization (k_La) of sensor enabled static and rocking T-flasks is presented and compared with other non-instrumented PSDs such as CultiFlask 50®, spinner flasks, and SuperSpinner D 1000®. We have also developed a mass transfer empirical correlation that accounts for the contribution of convection and diffusion to the volumetric mass transfer coefficient (k_La) in rocking T-flasks. We also carried out a scale-down study at matched k_La between a rocking T75-flask and a 10 L (2 L filling volume) wave bioreactor (Cultibag®) and we observed similar DO and pH profiles as well as maximum cell density and protein titer. However, in this scale-down study, we also observed a negative correlation between cell growth and protein productivity between the rocking T-flask and the wave bioreactor. We hypothesize that this negative correlation can be due to hydrodynamic stress difference between the rocking T-flask and the Cultibag. As both cell culture devices share key similarities such as type of agitation (i.e., rocking), oxygen transfer capabilities (i.e., k_La) and disposability, we argue that rocking T-flasks can be readily integrated with wave bioreactors, making the transition from research-scale to manufacturing-scale a seamless process.

Jose R. Vallejos's present address is Martek Biosciences Corporation (a DSM Nutritional Lipids Division), Kingstree, SC.
Correspondence to: G. Rao
Contract grant sponsor: Sartorius-Stedim Biotech
Received: 5 January 2012; Revision received: 5 March 2012;
Accepted: 19 March 2012
Accepted manuscript online 3 April 2012;
Article first published online 11 April 2012 in Wiley Online Library (http://onlinelibrary.wiley.com/doi/10.1002/bit.24508/abstract)
DOI 10.1002/bit.24508

Biotechnol. Bioeng. 2012;109: 2295–2305.

KEYWORDS: disposable bioreactors; optical sensors; T-flasks; mass transfer; scale-down; seed train

Introduction

During the past decade, novel disposable cell culture vessels have become increasingly popular in both R&D and biomanufacturing settings. Static, rocked and shaken non-instrumented Process Scouting Devices (PSDs) have been available for many years. However, limited engineering characterization and lack of online monitoring of PSDs makes it challenging to evaluate their oxygen transfer capabilities. Nonetheless, adaptation of low cost disposable dissolved oxygen (DO) and pH patch-based sensors (Kostov et al., 2001) to these disposable PSDs allows them to function as small disposable bioreactors. Among these non-instrumented disposable PSDs, T-flasks are primarily used under static conditions which restrict their bioprocessing applications to routine cell passaging. In this study, we have adapted low cost disposable DO and pH sensors to non-instrumented rocking T-flasks allowing matching of k_La and comparison with a 10 L-wave bioreactor.

We have previously described small scale mass transfer characterization using optical sensors (Bambot et al., 1993; Kostov et al., 2001) and non-instrumented PSDs such as static T-flasks (Randers-Eichhorn et al., 1996), shake flasks (Gupta and Rao, 2003) and spinner flasks (Vallejos et al., 2011). The volumetric mass transfer coefficient (k_La) has also been evaluated in systems such as 96-well plates (Hermann et al., 2003), 48-well plates (Kensy et al., 2005a), and 24-well plates (Kensy et al., 2005b) using the sulfite

oxidation method. However the mass transfer areas reported by Hermann et al. (2003) and Kensy et al. (2005a) have been shown to be significantly overestimated (Linek et al., 2006). Our studies leveraged the advanced fluorescence optical technology to make it possible to convert these PSDs into bioreactors capable of growing cells and at the same time monitoring DO and pH (Ge et al., 2006; Harms et al., 2006).

At the mL-scale (<100 mL) there is a need for novel disposable bioreactors with simpler process control and engineering characteristics that can be easily related to manufacturing-scale bioreactors in scale-down studies. The driving force is the need to increase the rate at which clones and processes are developed for clinical and commercial process selection (Heath and Kiss, 2007). Recently, a wide variety of novel mechanically driven disposable bioreactors between the 1.5 mL and 3,000 L scale have been developed. These include (1) wave-mixed, (2) stirred, (3) orbitally shaken, (4) vertically oscillating, (5) pneumatically driven as well as (6) hybrid systems. However at the mL-scale (<100 mL), very few disposable bioreactor types are available and they mostly rely on orbital shaking (Eibl et al., 2010). Among these only the μ24 Microbioreactor (Applikon, Schiedam, The Netherlands) and the μ96 Biolector (m2p-labs GmbH, Aachen, Germany) are equipped with DO and pH monitoring and control capabilities (Funke et al., 2010). Recently Sartorius and PreSens have launched a disposable version of larger Erlenmeyer flasks (125–1,000 mL flasks) traded as Sensolux® (Sartorius AG, Goettingen, Germany) and Shake Flask Reader (PreSens GmbH, Regensburg, Germany), respectively, that have monitoring capabilities for DO and pH. In addition to these options, Respiration Activity Monitoring System (RAMOS) for shake flasks is also available (Anderlei et al., 2004) that is being commercialized by Kühner AG (Adulf Kühner AG, Basel, Switzerland). In spite of these few examples, overall there is a lack of disposable rocking and stirring systems with DO and pH monitoring capabilities at the mL-scale (<100 mL) that can be seamlessly integrated with larger rocking and stirred cell culture devices.

Typically, wave bioreactors are used as seed expansion stage and the scale-up is mostly based on cell density and cell physiology. However, some attempts have been made to characterize these wave bags in terms of mass transfer and mixing capabilities (Mikola et al., 2007; Singh, 1999). This approach has provided a more robust scale-up strategy as it warrantees that wave bags will provide enough oxygen to achieve a target cell density during seed expansion. These studies have been carried out in the range of 2–200 L but rocking systems at the mL-scale have not been reported yet.

In this work, the possibility of sensor-enabled rocking T-flasks as a disposable bioreactor alternative at the mL-scale is demonstrated. As wave bioreactors are becoming increasingly popular at small and medium volume scale manufacture (Eibl et al., 2010), it would be desirable to create a scale-down tool that can mimic and predict cell culture performance of wave bioreactors. In bioprocessing, T-flasks are mainly used for preliminary cell propagation and as scale-up vehicles (Randers-Eichhorn et al., 1996), while in process development they have been used for platform screening (Lu et al., 2007), medium optimization studies (Gramer and Poeschl, 2000), and hepatocyte aggregation experiments (Glicklis et al., 2004). Recently, Vallejos et al. (2010) showed that sensor-enabled static T-flasks used for cell passaging after an initial vial thaw, can significantly aid in monitoring for clone instability based on DO and pH profile evolution.

In this study mass transfer and cell performance of a rocking T-flask equipped with patch-based optical sensors is investigated. The data obtained were successfully compared to larger scale novel disposable bioreactors, for example, a 10 L wave bioreactor (Biostat® Cultibag RM).

Materials and Methods

Experimental Set-Up

During our experiments, T-flasks were positioned on top of a rocker platform (Bellco Glass, Inc., Vineland, NJ) inside a CO_2 incubator. A DO patch and a pH patch (Fluorometrix, Stow, MA) were affixed on the inside walls of the flasks. This sensor system has been previously described in oxygen transfer studies in T-flasks (Randers-Eichhorn et al., 1996), shake flasks (Gupta and Rao, 2003) as well as spinner-flasks (Vallejos et al., 2011). The light emission diodes (LEDs) for excitation and photo detector for light detection were placed outside the wall of the T-flaks, aligned with the patches (shown in Fig. 1).

Volumetric Mass Transfer Coefficient Measurements and Correlations

For T-flasks, a gas tubing line was connected via a needle to the vent cap. A detailed description of the techniques used to measure the volumetric mass transfer coefficient and of the methodology used to correlate the data obtained in small scale devices can be found in Vallejos et al. (2011). In this work the "unsteady-state method" (Shuler and Kargi, 2001) also known as the "gassing out" method (i.e., combining nitrogen and air) has been used for k_La estimations in both T-flasks and wave bioreactors. Deionized water at 37°C was the test medium. In cases of low k_La ($<50\,h^{-1}$), as in this study, the response time of the optical sensor was considered negligible for the purpose of calculating k_La (Van't Riet, 1979) and thus can be disregarded.

With this assumption, the general volumetric mass transfer coefficient (k_La) model equation used to correlate the experimental data can be described by Equation (1):

$$k_La(\text{Model}) = mND + bD_{O_2}\left(\frac{A}{V}\right)^C \qquad (1)$$

where m, b, and c are empirical constants, N is the rocking speed, D is the length scale the liquid travels inside the T-flasks and wave bioreactor when rocking motion is

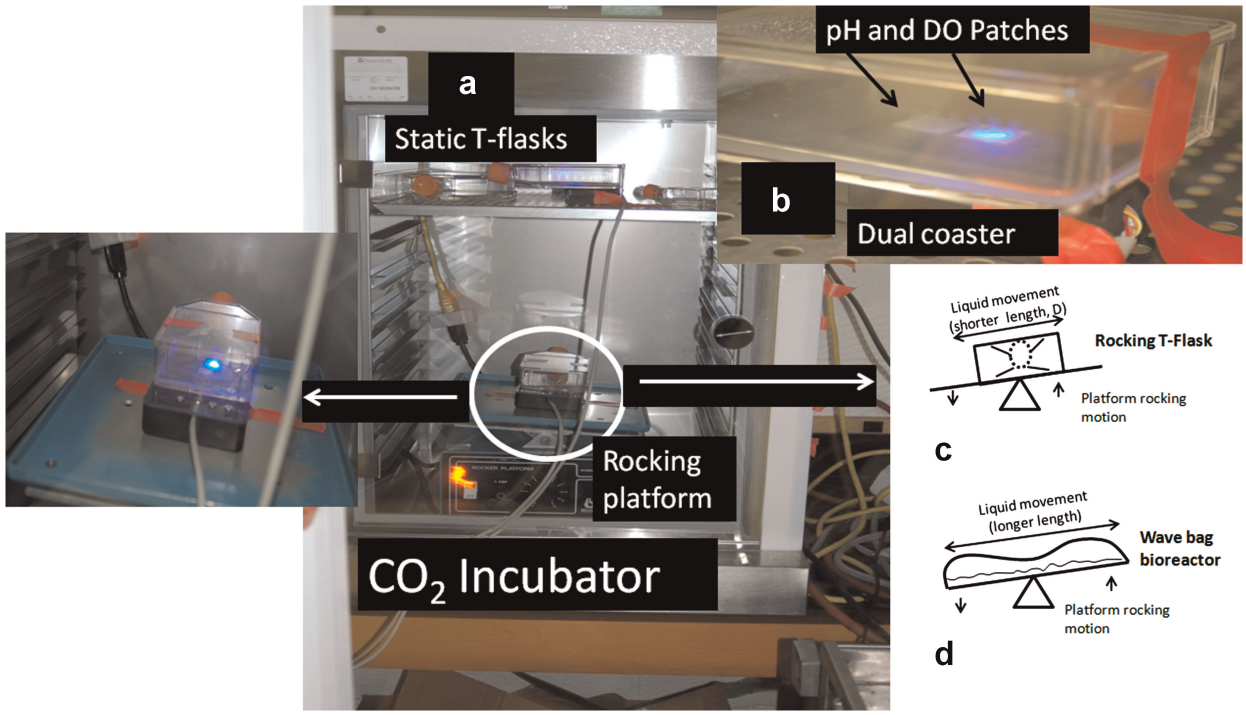

Figure 1. Cell culture experimental set-up inside CO_2 incubator. The Figure shows a static T75-flask (on the inside top) and a second T75-flask mounted on the top of a rocker platform inside a CO_2 incubator (**a**), optical sensors (**b**), liquid displacement in T-flasks (**c**), and wave bioreactor (**d**). [Color figure can be seen in the online version of this article, available at http://wileyonlinelibrary.com/bit]

applied, D_{O_2} is the oxygen diffusivity coefficient and A/V is the surface area to volume ratio.

The k_La experimental data obtained in this study were fitted to Equation (1) and the empirical constants (m, b, and c) were estimated by nonlinear regression analysis. Statistical equations based on the method proposed by Brown (2001) were used to estimate the empirical constants. The first and second terms in Equation (1) are convection and diffusion terms, respectively, and quantitatively estimate their contribution to the volumetric mass transfer coefficient.

In the case of the wave bioreactor, k_La was estimated using the "gassing out" method with our DO optical sensors (one sensor was in the liquid and other in the head space) and alternating the use of nitrogen and air to gas out the test medium. The bag headspace was flushed with nitrogen until DO reached zero. After holding DO at zero for 5 min, rocking agitation was stopped and air was introduced into the bag headspace until the reading from our sensor (in the headspace) reached saturation levels. As soon as saturation level was reached, rocking agitation was set at the desired value and the DO monitored for k_La estimation. All mass transfer studies were done in triplicate.

Cell Culture Experiments

The cell culture used in this study was a non-adherent SP2/0-based mouse hybridoma (2055.5) secreting an IgG3 antibody. Culture parameters used in this study are identical to those used in the previous work (Vallejos et al., 2010). To maintain consistency between experiments, a single CD Hybridoma AGT^{TM} (Invitrogen, Carlsbad, CA) medium lot was employed for all studies. Cells were taken from early post-thaw passages (i.e., at passage 4) in 250 mL-spinner flask to seed both the T-flask and the wave bioreactor. The inoculum seed (180 mL) was transferred into the wave bioreactor and, after mixing, the entire volume was split in between the wave bioreactor and the T75-flask to ensure that the same starting culture was used for both devices. The wave bioreactor was operated with acidic pH control (CO_2) during the first 18 h of cell culture but not with active DO control. We agitated both the wave bioreactor and rocking T-flask to match a k_La of 13.5 h^{-1} and maintain similar DO profiles. This scale-down study was done in duplicate (i.e., two consecutive runs) Sterility assurance was provided for glass vessels and patches by standard autoclaving procedures (i.e., 121°C for 22 min). Pre-autoclaved patches were attached inside laminar flow hood using sterile forceps to the purchased pre-sterilized T-flasks. As stated previously (Vallejos et al., 2010), our patches are un-affected by cell density (Randers-Eichhorn et al., 1996). For these DO patches a drift study was performed in our laboratory at 100% DO and it was found that this drift was approximately 7% for the number of readings equivalent to our nine days use. A similar study was also performed for the pH patches

and no apparent drift was observed. Our DO sensors are at their highest accuracy at low DO (Gupta and Rao, 2003).

Analytical Measurements

Samples were taken from the cultures at intervals of approximately 12 h and analyzed for viable cell density (VCD) and viability. Samples were centrifuged at 2,300 rpm for 2 min to remove cells and then analyzed for lactate and glucose using an YSI 2700 Analyzer (Yellow Springs Instrument Company, Yellow Springs, OH). In order to quantify the antibody protein titer a standard ELISA protocol was run on the supernatants as described by Kondragunta et al. (2010). Test articles were stored frozen (-20°C) when not analyzed immediately.

Results

Mass Transfer

The aim of this work is to demonstrate that rocking T-flasks can be used as scale-down models of bench-scale wave bags. In order to do this, k_La values, mixing and cell culture performance needed to be quantified and compared between the two systems. As a first step, the patch-based DO sensor (Fluorometrix) was used to accurately estimate the volumetric mass transfer coefficient (k_La) in rocking T-flasks allowing us to match it to a wave-type bioreactor. The volumetric mass transfer coefficient was measured in three different T-flask geometries (T25, T75, and T150) for a range of rocking speeds (up to 10 rocks per minute) and the results are compared in Figure 2 with k_La coefficients measured under static and shaking conditions. For each T-flask geometry three fill volumes were investigated to evaluate the impact of surface to volume ratio on the oxygen transfer rates. By applying a gentle (2–10 rpm) rocking agitation to T-flasks their oxygen transfer capabilities were significantly improved (Fig. 2a–c). This marked improvement results from the fact that these cell culture devices have a high surface area to volume ratios (A/V) and thus agitation enables mixing and oxygen transfer into the bulk liquid. The effect of the type of agitation (rocking versus shaking) on k_La was also tested in T-flasks and the main results are presented in Figure 2d–f. When A/V is maintained constant and agitation is kept low (i.e., 0–10 rpm, $Re < 3 \times 10^3$), rocking agitation provides higher k_La values than those obtained when shaking agitation is used (Fig. 2). For shaking conditions, an inflection point is present for curves in Figure 2d and e, corresponding to a critical shaking agitation rate of 40 rpm at which k_La starts to increase exponentially. This behavior has been observed in different shaken geometries (Hermann et al., 2003; Kensy et al., 2005a).

The data obtained using the rocking T-flask geometry at different operating conditions were used to estimate the coefficients m and b in Equation (1) and the following values were obtained:

$$k_La(\text{model}) = 0.0007\left(\frac{A}{V}\right)ND + 2.14D_{O_2}\left(\frac{A}{V}\right)^2 \quad (2)$$

These studies used T25, T75, and T150-flasks with a value of A/V belonging to the ranges 2.27–5.0 cm^{-1}, 1.88–3.75 cm^{-1}, and 1.88–2.5 cm^{-1}, respectively (Fig. 3). The critical t-distribution for Equation (2) fit is 2.01 at a significance level of 95% and a degree of freedom of 53. The confidence interval at this significant level is 0.89 h^{-1}. As can be seen from Figure 3, two points (i.e., k_La (model) of 16.83 and 16.28 h^{-1}) are far away from the upper confidence level (CL) but they are 23% and 10% higher than the experimental data, respectively. This behavior can be explained by the significant vibration experienced at these high rocking speeds by the platform.

It can also be observed from Equation (2), that the convection term (mND) from Equation (1) takes the form of $0.0007(A/V)ND$ and its contribution to k_La was also estimated (Fig. 4). The convection term is generally regarded as being important because it is associated with the bulk liquid movement that perturbs the gas-liquid interface. Equation (2) shows that the non-dimensional convection to diffusion ratio is directly proportional to rocking speed and length scale (D) but inversely proportional to A/V (Fig. 4). In addition, when A/V is constant, the convection term contribution is proportional to the Reynolds number (the ratio of convection to viscous forces). Overall, the results obtained in this work suggest that rocking T-flasks can be run in a predictable manner if all these terms are understood and controlled and thus can be used as novel engineering tools to improve understanding of how convection and diffusion affect mass transfer at the mL-scale. This information is critical to relate these devices to manufacturing-scale processes.

Mass Transfer in Rocking T-Flasks Versus Other PSDs

To show that rocking T-flasks can have superior mass transfer capabilities in comparison to traditional and novel PSDs, a comparison of the volumetric mass transfer coefficients (k_La) obtained in our rocking sensor-enabled T-flasks with other PSDs operated under stirring and shaking conditions was carried out and results are presented in Figure 5. It is clear from Figure 5 that rocking T-flasks have superior oxygen transfer capabilities than the other PSDs evaluated in this study. In fact, the data presented in Figure 5 shows that the surface area to volume ratio (A/V, cm^{-1}) is of critical importance for enhancing k_La at the mL-scale. This could be useful for culturing shear sensitive cells or tissues. It can also be observed that k_La increases as A/V increases, T-flasks are generally characterized by A/V values one order of magnitude higher than other PSDs and thus k_La is generally higher in these devices even at low Re values.

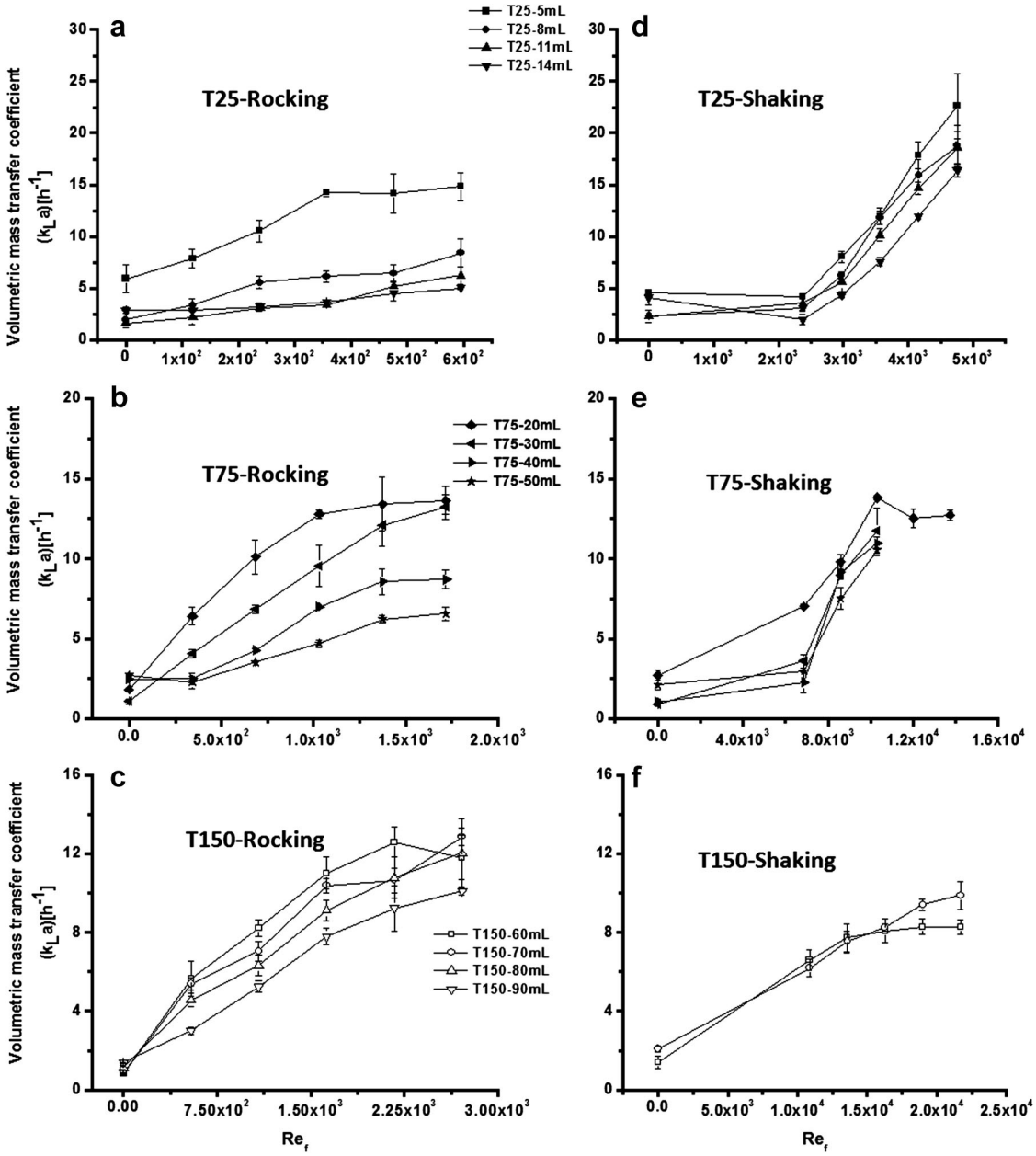

Figure 2. Volumetric mass transfer coefficient in rocking T-flasks (**a**–**c**) and shaking T-flasks (**d**–**f**). Similar $k_L a$ are observed between both systems except for T25-flasks at 5 and 8 mL under shaking agitation that show significant higher $k_L a$ than rocking T-flask. Note: Data in "e" T75 from 30 to 50 mL (for 70–80 rpm) are missing due to liquid spilling out of the flask under these conditions. Same phenomenon was observed for T150 from 80 to 90 mL (for 40–80 rpm) in "f."

Sensor Enabled Rocking T-Flasks as Potential Upstream Tools

Clone stability studies

As a proof of concept case study for the utility of rocking T-flasks, a direct comparison of hybridoma cells growth performance in rocking T-flasks, static T-flasks, and wave bioreactors was performed. A cell vial was thawed and split it into a static and a rocking T75-flask ($k_L a = 13.5\,h^{-1}$, 20 mL, 10 rpm). Figure 6 shows that cell cultures grew faster and more densely in rocking T75-flasks versus static T75-flasks, giving higher maximum VCD (1.8-fold increase) and producing less amount of lactate (25% less). This can be attributed to a culture conditions where high DO levels (Fig. 6c) were maintained by agitation in the rocking T75-flask and DO never decreased below 70%. In contrast, in static T-flasks DO levels fell to zero within two days (Vallejos et al., 2010) leaving them anoxic for hours at a time. The

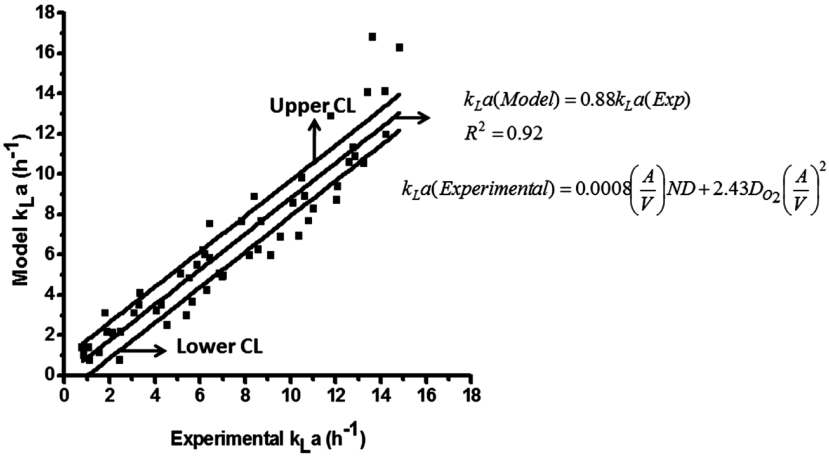

Figure 3. Statistical comparability between model (Equation 2) and experimental k_La in rocking T-flasks. The critical t (Student's t-test) for k_La model equation fit is 2.01 at a significance level of 95% and a degree of freedom of 53. The confidence interval at this significant level is 0.89 h^{-1}. The model fits best the experimental data at $k_La \leq 8\,h^{-1}$. $k_La \geq 16\,h^{-1}$ were obtained at the highest rocking speed with the rocker platform vibrating intensively. The slope of 0.88 argues that the model slightly underestimates k_La on a consistent basis.

agitated environment also had a positive impact on the pH of the culture, increasing the minimum pH by 0.2 units (Fig. 6d).

Antibody titers were also measured and it was observed that at the end of the culture the rocking T75-flask culture produced 31% higher antibody titer (106.1 ± 1.4 mg/L) than the static T75-flask (81.2 ± 1.5 mg/L).

Scale-down studies

A scale-down study at matched k_La conditions was carried out and hybridoma culture was grown in our sensor enabled rocking T75-flask (25 mL and 10 rpm) and in a 10 L-Cultibag® (2 L, 25 rpm and 4.5°) at a k_La of 13.5 h^{-1}. Results are shown in Figure 7 and summarized in Table I. By operating at conditions that provide the same k_La, both systems had similar DO profiles as well as maximum VCD and antibody titer. These are critical attributes studied usually as off-sample cell culture performance end points (Dutton et al., 1998). In addition, the pH profiles (Fig. 7d) between both the rocking T-flask and wave bioreactor were very similar although the pH was actively controlled (acidic control, CO_2) in the wave bioreactor during the first 18 h of cell culture. Slightly higher final lactate accumulation in the wave bioreactor is observed (Fig. 7b) but with no apparent effect on the pH profile presumably because of differences in dCO_2 between both systems. Despite most profiles matching, the protein productivity was in average 44% higher in

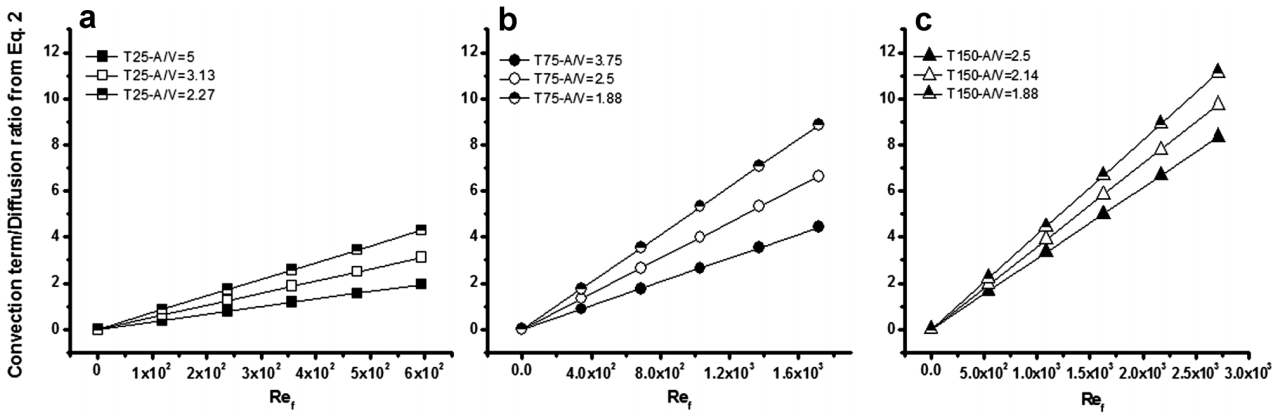

Figure 4. Convection term to diffusion term ratio as a function of rocking speed and A/V in T25 (**a**), T75 (**b**), and T150 (**c**) rocking T-flasks. The convection term to diffusion term ratio contribution to k_La is directly proportional to the rocking speed but inversely proportional to A/V. For similar A/V, the convection term contribution is proportional to Re number (data not shown). Also note that the slope of the lines increases with increase in the size of the flasks.

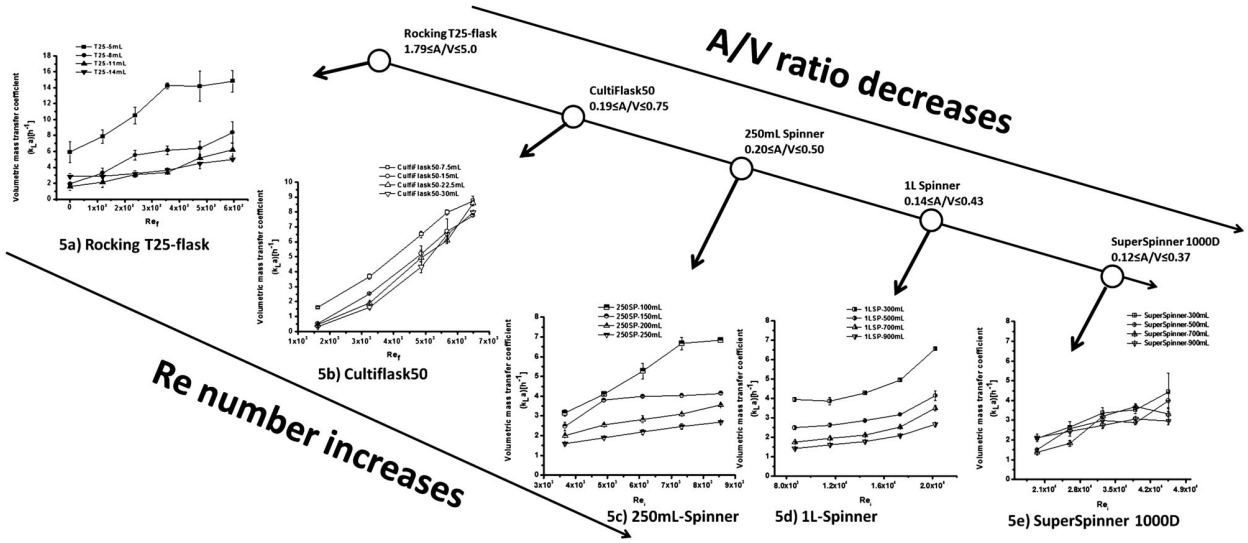

Figure 5. k_La comparability between rocking T25-flask (**a**) and other PSDs (CultiFlask50 (**b**), 250 mL Spinner (**c**), 1 L Spinner (**d**) and SuperSpinner 100D (**e**)) at 37°C. Rocking T-flasks show the highest oxygen transfer capabilities even at relative low Re_f. k_La is directly proportional to the initial area to volume ratio (A/V) as well as Re_f/Re_i. The non-overlapping nature of the curves shows that while k_La can be matched between the devices it will be very difficult to match both k_La and Re at the same time. In this case matching shear rate would be more important during scale up modeling. Note: Re_f ($Re_f = D^2\rho N/\mu$) and Re_i ($Re_i = D_i^2\rho N/\mu$) are the flask and impeller Reynolds number, respectively.

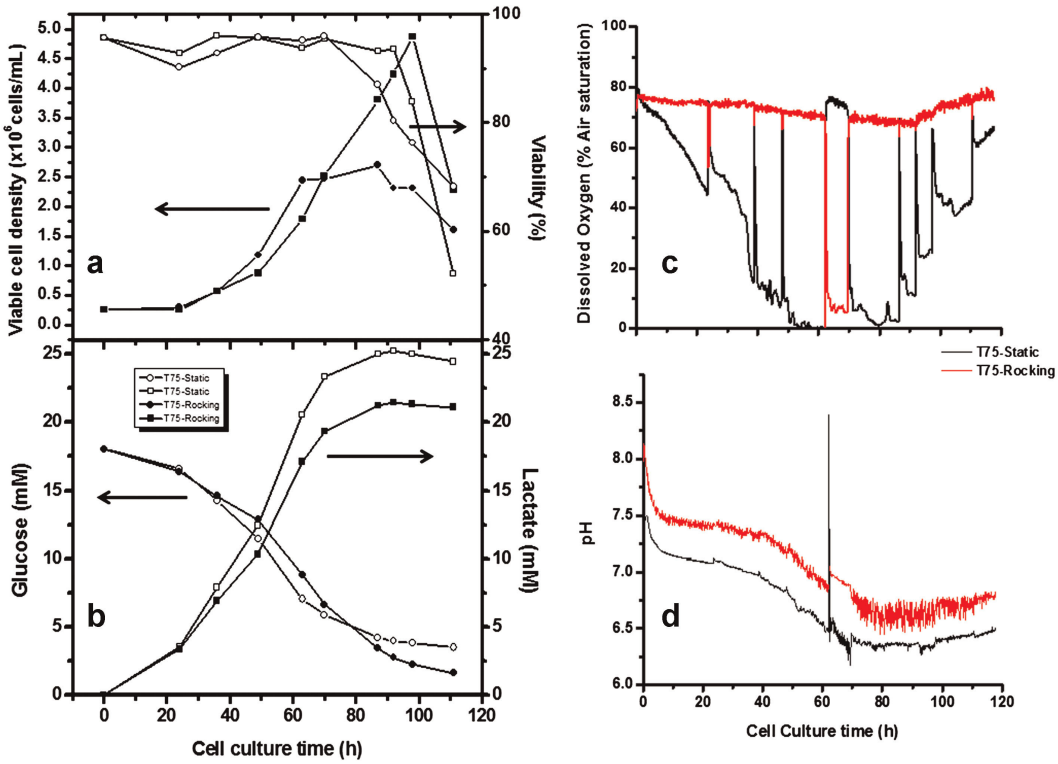

Figure 6. Cell culture comparability study between static and rocking T75-flasks after cell vial thaw. Maximum cell density and viability (**a**), glucose and lactate concentration (**b**), DO profile (**c**), and pH profile (**d**). Rocking T-flask at a k_La of 13.5 h^{-1} (20 mL and 10 rpm) show superior cell culture performance showing higher VCD, less lactate production, more optimal pH and DO profile as well. In the 60–70 h interval DO and pH coasters were swamped to verify if the readings were similar. We observed no significant difference between both sensors. [Color figure can be seen in the online version of this article, available at http://wileyonlinelibrary.com/bit]

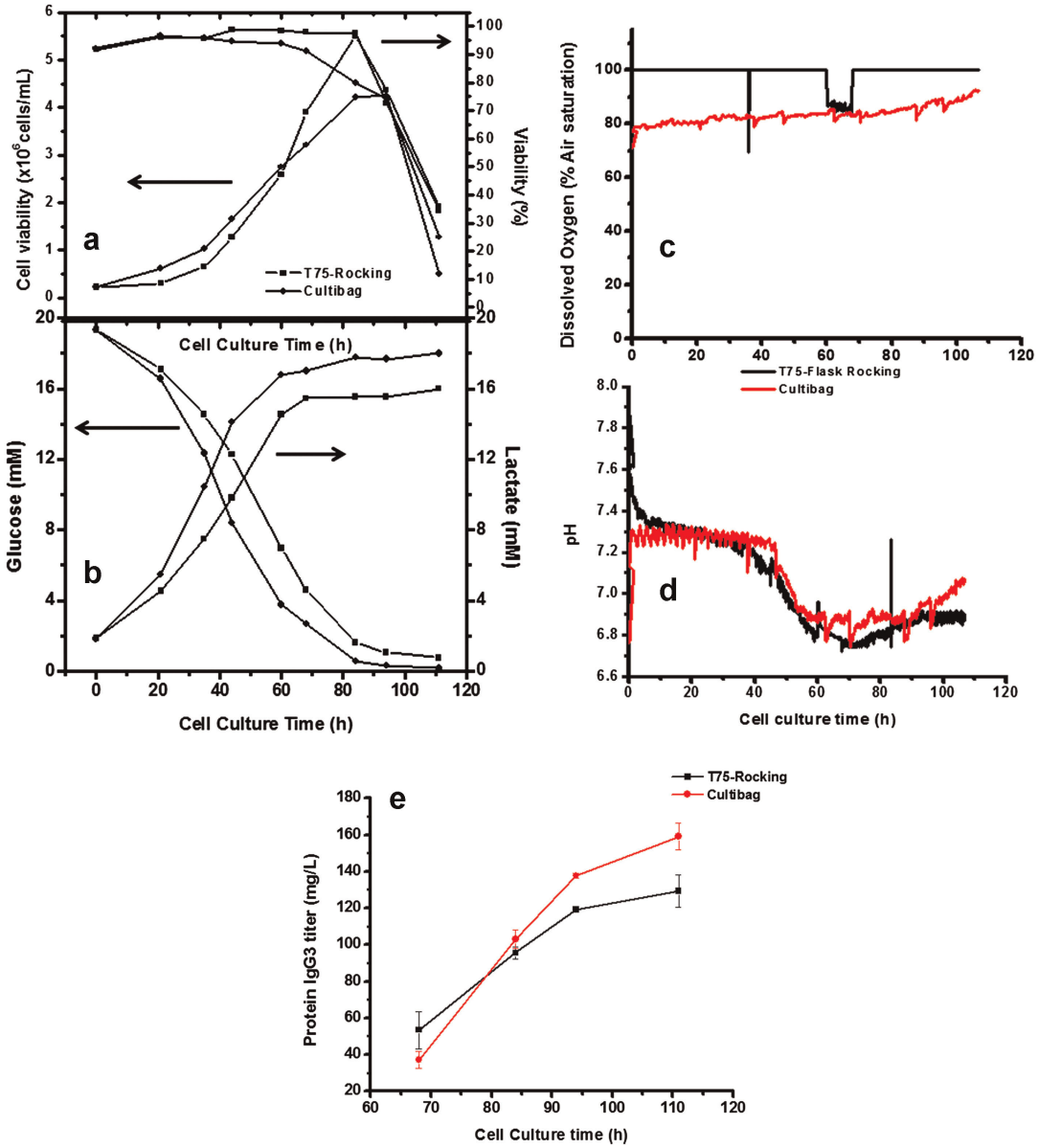

Figure 7. Scale-down comparability study between rocking T75-flask and a 10 L wave bioreactor at a matched k_La of 13.5 h^{-1}. Maximum cell density and viability (**a**), glucose and lactate concentration (**b**), DO profile (**c**), pH profile (**d**), and antibody production (**e**). Rocking T-flask show similar DO levels and maximum cell density to the wave bioreactor. In the 60–70 h interval, other DO and pH coasters were used temporarily to verify if the readings were similar. They were 17% DO and 0.1 pH units different, respectively. At the end of the culture the absolute titer difference was maximal of 19% between both systems, within the error of ELISA assay. [Color figure can be seen in the online version of this article, available at http://wileyonlinelibrary.com/bit]

Table I. Cell culture comparability study between sensor enabled rocking T75-flask and a 10 L Cultibag® at a matched k_La of 13.5 h^{-1}.

	Rocking T75-flasks filling volume = 20 mL	Cultibag filling volume = 2 L	Percentage difference
Maximum VCD ($\times 10^6$ cells/mL)	5.19 ± 0.45	4.27 ± 0.02	+22%
Maximum q_{Glc} (mmol/cell h)	$3.91 \times 10^{-10} \pm 2.24 \times 10^{-11}$	$4.88 \times 10^{-10} \pm 1.62 \times 10^{-10}$	−20%
Growth rate (day^{-1})	0.82 ± 0.16	0.97 ± 0.05	−15%
Maximum q_{Lac} (mmol/cell h)	$4.25 \times 10^{-10} \pm 6.72 \times 10^{-11}$	$5.74 \times 10^{-10} \pm 1.91 \times 10^{-10}$	−26%
Maximum protein titer (mg/L)	127.53 ± 2.49	167.25 ± 11.51	−24%
Maximum protein productivity (μg/$\times 10^6$ cell/day)[a]	9.0 ± 2.55	16.20 ± 7.64	−44%

[a]Estimated by (1) plotting the cumulative production of MAb against the integrated viable cell density (iVCD) and (2) estimating the slope of a linear regressive fit of the data.

the Cultibag (Table I) but with no apparent statistical significance difference.

Discussion

Bioprocess Implications

Major applications of wave bioreactors include clone screening, seed inoculum production, and small and medium scale manufacture (Eibl et al., 2010). However such applications have been prototyped at the mL-scale only in shaken (Chen et al., 2009) and stirred minibioreactors (Kondragunta et al., 2010). In this work a novel rocking disposable cell culture device at the mL-scale (<100 mL) with disposable DO and pH monitoring capabilities is presented. The device is small, inexpensive and can be integrated in a highly parallel fashion within a rocking train platform before larger disposable-wave bioreactors stage. In particular, our study suggests that sensor enabled rocking T25-flasks are relatively small in size and can potentially be used as high-throughput cell culture devices. As an example, rocking T-flasks could be used in clone stability studies performed under different DO levels conditions, obtained by manipulating k_La, to further investigate the impact of oxygen on protein titer and product quality attributes. Such cell culture platform technology can significantly contribute to reduce costs and speed up timescales of bioprocess development.

Scale Down

When operating at matched k_La operating conditions, our study shows that sensor enabled rocking T-flasks can mimic important cell performance parameters (i.e., VCD and protein titer) as well as environmental conditions (i.e., DO and pH profiles) of wave-type bioreactors but with the benefit of a smaller scale. However, as shown in Table I, the maximum protein productivity still differs by 44% between the two systems. Table I also shows that the cell line used in this work exhibits a negative correlation between cell growth and protein productivity. It can be hypothesized that this result can be due to hydrodynamic stress difference present in the rocking T-flask and the Cultibag, respectively. Al-Rubeai and Emery (1990) observed that high hydrodynamic stress conditions can result in high protein productivity presumably because of a much extended stationary growth phase (Persson and Emborg, 1992). Data obtained in this work suggests that the hydrodynamic stress in the wave bioreactor model (operated at 25 rpm and 4.5°) can be higher than in the rocking T75-Flask (at 10 rpm and 7.5°) and this may have caused the higher productivities observed. The length scales difference of both systems may also contribute to some extent to the shear stress difference. The liquid inside the wave bioreactor travels a longer distance and has higher mass (approximately 100-fold difference) than the liquid inside the T-Flask. As a result, in the wave bag, the energy released after the collision between the liquid in downward movement and the bag wall at the end-side of the length scale is larger than the energy released in the T-flask. This hypothesis is being further investigated in our laboratory using PIV (Particle-Image Velocimetry) coupled with analysis of protein glycosylation profile. Another possibility is that the T-flasks are rigid and a small scale bag made of the same flexible material as the larger scale system may be a better scale down choice. Finally, we have not considered the CO_2 removal efficiency in both systems and variations therein may also be a factor in final product titer.

Cell Passaging and Inoculum Expansion

Our study shows that sensor enabled PSDs can help optimize the inoculum expansion during routine manufacturing stages. For example, in the case of the hybridoma cell line cultured in static T-flasks, cells can be passaged into fresh media before a critical DO (0%) level is reached if real-time DO profile data is monitored instead of off-line parameters such as VCD. As suggested by Bristow and Hill (2008), hypoxia (0% DO levels) has a negative effect on genetic stability and overall culture health, thus we hypothesize that passaging cells during inoculum expansion based on DO profile data can increase the cell line genetic stability. Our data suggest that, in order to avoid hypoxic conditions, cells in static T-flasks should be passaged by day 2 (see Fig. 6). In contrast, rocking T-flasks never reached 0% DO levels and they can easily be passaged by 3½ days with cell viability profile remaining above 90% (Fig. 7a).

Mass Transfer

For the first time, our optical DO sensor technology has allowed a quantitative determination of the mass transfer capabilities of rocking T-flasks. Additionally, it allowed comparison of oxygen transfer capabilities of rocking T-flasks with shaken T-flasks and other PSDs (CultiFlask 50®, Spinner Flasks and SuperSpinner D 1000®). Our study shows that at the mL-scale (<100 mL), optical DO sensors can aid elucidating the oxygen transfer capabilities of other more complicated PSDs such as CultiFlask50 to further support (or reject) vendor claims of superior oxygen transfer rates. In the particular case of rocking T-flasks, our mass transfer study allowed to determine k_La correlations that would help process engineers to determine the design space conditions for an entire upstream process platform at constant k_La (Flores et al., 1997). The empirical correlation (Equation 2) developed in this study can also be applied to investigate the relative contribution of the convection term in bioreactor systems using alternative mixing methods.

Conclusions

This work shows that disposable cell culture devices such as T-flasks can be readily equipped with patch-based optical sensors, giving these devices important monitoring capabilities usually found in fully instrumented bench-scale bioreactors. A detailed mass transfer characterization of rocking T-flasks demonstrated that they have superior

oxygen transfer capabilities and at very low *Re* numbers than any other PSDs investigated in this study. Furthermore, a mass transfer correlation that accounts for convection and diffusion contributions to the gas liquid mass transfer coefficient k_La has also been proposed. This empirical correlation is based on easily measured parameters such as flask diameter, initial surface area to volume ratio and rocking speed. We propose a potential application of rocking T-flasks as scale-down model of bench-scale wave bioreactors providing similar DO profiles, maximum cell density and protein titers despite the very different scales. Our study suggests that sensor enabled rocking T-flasks are a promising upstream bioprocess tool for clone screening studies, clone stability studies, inoculum expansion, and scale-down model studies.

Nomenclature

A/V	initial surface area to volume ratio (cm^{-1})
D	rocking T-flask length scale (m)
D_f	flask diameter (m)
D_i	impeller diameter (m)
dCO_2	dissolved carbon dioxide
DO	dissolved oxygen
ELISA	enzyme-linked immunosorbent assay
iVCD	integral viable cell density
k_La	overall volumetric mass transfer coefficient (h^{-1})
N	rocking speed (s^{-1} or h^{-1})
PSDs	Process Scouting Devices
Re_f	flask Reynolds number ($Re_f = D^2\rho N/\mu$)
Re_i	impeller Reynolds number ($Re_i = D_i^2\rho N/\mu$)
V	filling volume (m^3)
VCD	maximum cell density ($\times 10^6$/mL)

Greek Symbols

ρ	liquid density (kg/m^3)
μ	dynamic viscosity ($N\,s/m^2$)

Funding from Sartorius-Stedim Biotech is gratefully acknowledged. G. Rao has an equity position in Flurometrix. Views expressed in this article are those of the authors and not necessarily of the US FDA or the US government. Discussion of the individual cell culture devices does not constitute endorsement by the US FDA or the US government. Authors thank Bhargavi Kondragunta and Shaunak Uplekar for their assistance with wave bioreactor cell culture experiments as well as insightful discussions with Erik Read. Authors also thank Priyanka Gupta for her assistance in preparing this manuscript.

References

Al-Rubeai M, Emery AN. 1990. Mechanisms and kinetics of monoclonal antibody synthesis and secretion in synchronous and asynchronous hybridoma cell cultures. J Biotechnol 16(1–2):67–85.

Anderlei T, Zhang W, Papaspyrou M, Büchs J. 2004. Online respiration activity measurement (OTR, CTR, RQ) in shake flasks. Biochem Eng J 17(3):187–194.

Bambot SB, Holavanahali R, Lackowicz JR, Carter JM, Rao G. 1993. Phase fluorometric sterilizable optical sensor. Biotechnol Bioeng 43:1139–1145.

Bristow RG, Hill RP. 2008. Hypoxia, DNA repair and genetic stability Nat Rev 8(3):180–192.

Brown AM. 2001. A step-by-step guide to non-linear regression analysis of experimental data using a Microsoft Excel spreadsheet. Comp Prog Meth Biomed 65:191–200.

Chen A, Chitta R, Chang D, Amanullah A. 2009. Twenty-four well plate miniature bioreactor system as a scale-down model for cell culture process development. Biotechnol Bioeng 102(1):148–160.

Dutton RL, Scharer JM, Moo-Young M. 1998. Descriptive parameter evaluation in mammalian cell culture. Cytotechnology 26:139–152.

Eibl R, Kaiser S, Lombriser R, Eibl D. 2010. Disposable bioreactors: The current state-of-the art and recommended applications in biotechnology. Appl Microbiol Biotechnol 86:41–49.

Flores ER, Perez F, de la Torre M. 1997. Scale-up of *Bacillus thuringiensis* fermentation based on oxygen transfer. J Ferment Bioeng 83:561–564.

Funke M, Buchenauer A, Schnakenberg U, Mokwa W, Diederichs S, Mertens A, Müller C, Kensy F, Büchs J. 2010. Microfluidic biolector—Microfluidic bioprocess control in microtiter plates. Biotechnol Bioeng 107(3):497–505.

Ge X, Hanson M, Shen H, Kostov Y, Brorson KA, Frey DD, Moreira AR, Rao G. 2006. Validation of an optical sensor-based high-throughput bioreactor system for mammalian cell culture. J Biotechnol 122:293–306.

Glicklis R, Merchuk JC, Cohen S. 2004. Modeling mass transfer in hepatocyte spheroids via cell viability, spheroid size, and hepatocellular functions. Biotechnol Bioeng 86:672–680.

Gramer M, Poeschl DM. 2000. Comparison of cell growth in T-flasks, in micro hollow fiber bioreactors, and in an industrial scale hollow fiber bioreactor system. Cytotechnology 34:111–119.

Gupta A, Rao G. 2003. A study of oxygen transfer in shake flasks using a non-invasive oxygen sensor. Biotechnol Bioeng 84(3):351–358.

Harms P, Kostov Y, French JA, Soliman M, Anjanappa M, Ram A, Rao G. 2006. Design and performance of a 24-station high throughput microbioreactor. Biotechnol Bioeng 93(1):6–13.

Heath C, Kiss R. 2007. Cell culture process development: Advances in process engineering. Biotechnol Prog 23:46–51.

Hermann R, Lehmann M, Büchs J. 2003. Characterization of gas-liquid mass transfer phenomena in microtiter plates. Biotechnol Bioeng 81(2):178–186.

Kensy F, Zimmermann HF, Knabben I, Anderlei T, Trauthwein H, Dingerdissen U, Büchs J. 2005a. Oxygen transfer phenomena in 48-well microtiter plates: Determination by optical monitoring of sulfite oxidation and verification by real-time measurement during microbial growth. Biotechnol Bioeng 89(6):698–708.

Kensy F, John GT, Hofmann B, Büchs J. 2005b. Characterisation of operation conditions and online monitoring of physiological culture parameters in shaken 24-well microtiter plates. Bioprocess Biosyst Eng 75:75–81.

Kondragunta B, Drew JL, Brorson KA, Moreira AR, Rao G. 2010. Advances in clone selection using high-throughput bioreactors. Biotechnol Prog 26(4):1095–1103.

Kostov Y, Harms P, Randers-Eichhorn L, Rao G. 2001. Low-cost microbioreactor for high-throughput bioprocessing. Biotechnol Bioeng 72(3):346–352.

Linek V, Kordac M, Moucha T. 2006. Evaluation of the optical sulfite oxidation method for the determination of the interfacial mass transfer area in small-scale bioreactors. Biochem Eng J 27:264–268.

Lu C, Gonzalez C, Gleason J, Gangi J, Yang JD. 2007. A T-flask based screening platform for evaluating and identifying plant hydrolysates for a fed-batch cell culture process. Cytotechnology 55:15–29.

Mikola M, Seto J, Amanullah A. 2007. Evaluation of a novel wave bioreactor® cellbag for aerobic yeast cultivation. Bioprocess Biosyst Eng 30:231–241.

Persson B, Emborg C. 1992. A comparison of simple growth vessels and a specially designed bioreactor for the cultivation of hybridoma cells. Cytotechnology 8:179–187.

Randers-Eichhorn L, Bartlett RA, Frey DD, Rao G. 1996. Noninvasive oxygen measurements and mass transfer considerations in tissue culture flasks. Biotechnol Bioeng 51:466–478.

Shuler ML, Kargi F. 2001. Selection, scale-up, operation, and control of bioreactors. In: Amundson NR, editor. Bioprocess engineering. Basic concepts, 2nd edn. New Jersey: Prentice-Hall Publishing. 294 p.

Singh V. 1999. Disposable bioreactor for cell culture using wave-induced agitation. Cytotechnology 30:149–158.

Vallejos JR, Brorson KA, Moreira AR, Rao G. 2010. Dissolved oxygen and pH profile evolution after cryovial thaw and repeated cell passaging in a T-75 flask. Biotechnol Bioeng 105(6):1040–1047.

Vallejos JR, Brorson KA, Moreira AR, Rao G. 2011. Integrating a 250 mL-spinner flask with other stirred bench-scale cell culture devices. A mass transfer perspective. Biotechnol Prog 27(3):803–810.

Van't Riet K. 1979. Review of measuring methods and results in nonviscous gas-liquid mass transfer stirred vessels. Ind Eng Chem Process Des Dev 18(3):357–364.

Finally, the sensor technology allowed us to quickly characterize the engineering performance of a new spinner flask called the SuperSpinner that had been introduced to the market by Sartorius. This device was equipped with a novel membrane oxygenator that was attached to the impeller. The studies that were done were similar to the previous two papers and demonstrated that the non-invasive sensor technology provided a robust and easy to implement tool to provide new insights into process development at the laboratory scale. Shaunak Uplekar, a graduate student and João, an exchange student from Portugal contributed to this work along with the other authors.

ARTICLE

BIOTECHNOLOGY and BIOENGINEERING

A Case Study in Converting Disposable Process Scouting Devices Into Disposable Bioreactors as a Future Bioprocessing Tool

José R. Vallejos,[1] Shaunak Uplekar,[1] João F. da Silva,[1] Kurt A. Brorson,[2] Antonio R. Moreira,[1] Govind Rao[1†]

[1]Center for Advanced Sensor Technology, Department of Chemical, Biochemical and Environmental Engineering, University of Maryland, Baltimore County, 1000 Hilltop Circle, Baltimore, Maryland 21250; telephone: 410-455-3415; fax: 410-455-1049; e-mail: grao@umbc.edu

[2]Office of Biotechnology Products, Center for Drug Evaluation and Research, Food and Drug Administration, 10903 New Hampshire Ave, Silver Spring, Maryland, 20993

ABSTRACT: In this study, we perform mass transfer characterization (k_La) on a novel mechanically driven/stirred Process Scouting Device, PSD, (SuperSpinner D 1000®, SSD) and demonstrate that this novel device can be viewed as disposable bioreactor. Using patch-based optical sensors, we were able to monitor critical cell culture environmental conditions such as dissolved oxygen (DO) and pH in SSD for comparison to a 1 L standard spinner (SS) flask. We also coupled these mass transfer studies with mixing time studies where we observed relative high mixing times (5.2 min) that are typically observed in production scale bioreactors. Decreasing the mixing time 3.5-fold resulted in 30% increase in k_La (from 2.3 to 3.0 h^{-1}) and minimum DO level increased from 0% to 20% for our model hybridoma cell line. Finally, maximum viable cell density and protein titer stayed within ±20% of historical data, from our standard 5 L stirred bioreactor (Biostat®) operated under active DO control.

Biotechnol. Bioeng. 2012;109: 2790–2797.

KEYWORDS: disposable bioreactors; optical sensors; spinner flasks; mass transfer; mixing; seed train

Introduction

Disposable cell culture Process Scouting Devices (PSDs) are widely used in laboratory scale studies and seed culture generation. Driven by the need to reduce validation costs, novel disposable PSDs have been recently designed, but they typically lack engineering characterization and online monitoring, thereby limiting their utility in bioprocessing. Disposable cell culture technology (devices and sensors) can fairly be considered to represent the next generation of upstream bioprocessing technology (Rao et al., 2009). Static and shaken non-instrumented disposable cell culture devices (also known as Process Scouting Devices, PSDs) have been available for many years. However, the development of low cost disposable dissolved oxygen (DO) and pH patch-based sensors (Kostov et al., 2001) has made it possible to convert disposable PSDs into disposable bioreactors. However, the lack of engineering characterization and online monitoring of these devices is limiting their further application for bioprocessing. In this study, we have enabled a non-instrumented novel PSD (SuperSpinner D 1000®) with low cost disposable DO and pH sensors matching k_La with a culture in a standard 1-L spinner flask and compared cell performance with historical data from a fully instrumented laboratory-scale bioreactor under active DO control.

Recently, a wide variety of novel mechanically driven disposable bioreactors have been created that are (i) wave-mixed, (ii) stirred, (iii) orbitally shaken, (iv) vertically oscillating, (v) pneumatically driven, and (vi) hybrid systems (Eibl et al., 2010). Large scale, stirred disposable bioreactors of up to 2,000 L have been developed (Xcellerex, Marlborough, MA). At the other end, the SuperSpinner D 1000® [mechanically driven/stirred PSD (Schmale, 2008)] is the smallest (i.e., 1 L maximum) non-instrumented disposable stirred bioreactor available (Sartorius AG, Goettingen, Germany). Despite its increasing use in seed expansion applications, the SuperSpinner D 1000® lacks engineering characterization to evaluate oxygen transfer capabilities (i.e.,

[†]Director of Center for Advanced Sensor Technology (CAST).
José R. Vallejos's present address is Martek Biosciences Corporation (a DSM Nutritional Lipids Division) in Kingstree, South Carolina, USA.
Correspondence to: G. Rao
Contract grant sponsor: Sartorius-Stedim Biotech
Received 17 November 2011; Revision received 12 April 2012; Accepted 16 April 2012
Accepted manuscript online 30 April 2012;
Article first published online 17 May 2012 in Wiley Online Library (http://onlinelibrary.wiley.com/doi/10.1002/bit.24541/abstract)
DOI 10.1002/bit.24541

mass transfer), mixing efficiency, power per volume unit requirements, shear stress and hydrodynamic characterization, and other engineering parameters that would help to integrate it (i.e., via a scale-up strategy) with a train of large-scale disposable bioreactors. As a background, a few engineering characterization studies (Aunins et al., 1989; Sucosky et al., 2004; Vallejos et al., 2011) have been carried out on SS flasks, but none for SuperSpinner D 1000®. This information gap makes it harder to evaluate the full potential of disposable PSDs in several bioprocessing applications. As a result, disposable spinner flasks (SuperSpinner D 1000®) have primarily been proposed for cell culture seed development bioprocessing applications.

In a SuperSpinner D 1000® device, a hollow-fiber membrane is wound around a stir bar with iron core at the tip. This creates a tumbling type of agitation when the stir bar is rotated by a magnetic driven unit. These spinner flasks are disposable and use bubble-free aeration. The basic design was first proposed by Lehmann et al. (1988) and Heidemann et al. (1994) and later adapted by Sartorius. The early publications, Heidemann et al. (1994) proposed a direct relationship between volumetric mass transfer coefficient (k_La), membrane length (i.e., polypropylene membrane) and gas flow at constant temperature (20°C) and constant agitation speed (35 rpm). The prototyping work of Heidemann et al. (1994) used a Duran® flask with an electrode probe inserted in the SuperSpinner device. Our goal is to allow integration of SuperSpinner D 1000® (and other non-instrumented PSDs) device with larger stirred bioreactors typically equipped with active process control (i.e., DO and pH) for such applications as pre-clinical studies, seed train development, and production of glycoproteins (Eibl et al., 2010).

In this study, we investigated mass transfer, mixing, and cell performance of a SuperSpinner D 1000® equipped with patch-based optical sensors and bench marked against a standard 1 L spinner flask and historical data obtained in our laboratory in a 5 L bench-scale stirred bioreactor (Biostat®).

Materials and Methods

Experimental Set-Up

Spinner flasks with inside affixed DO and pH patches were placed on top of a magnetic stirrer (Bellco Glass, Inc, Vineland, NJ). The DO and pH patches were obtained from Fluorometrix (Stow, MA) and used as previously described in other PSDs mass transfer studies (Gupta and Rao, 2003; Randers-Eichhorn et al., 1996; Vallejos et al., 2011). Figure 1 depicts the LEDs for excitation and photo detector for light detection positions. All cell culture studies were carried out inside a CO_2 incubator.

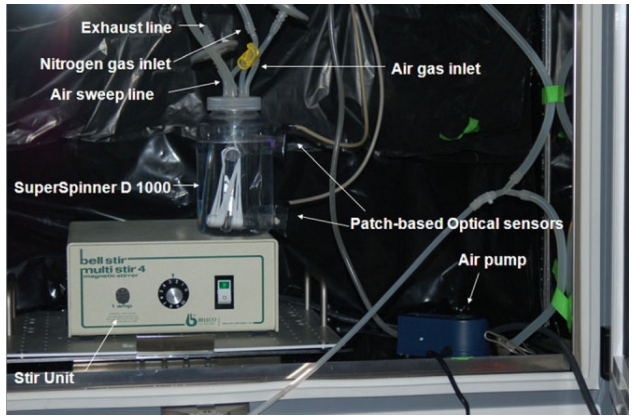

Figure 1. Mass transfer experimental set-up. SuperSpinner D 1000 mounted on the top of a stir unit, air pump (Elite 801®), optical sensors, and gas tubing connections.

Volumetric Mass Transfer Coefficient Measurements and Correlations

For a standard 1 L Spinner flask, a gas tubing line was connected to an inlet in one of the arms of the flask using a 2-port sampler assembly (Bellco Glass, Inc) and for SuperSpinner D 1000® the gas tubing line was connected to the gas inlet port. In some cases where a spinner flask was filled to the maximum working volume, a second patch was placed close to the liquid surface (i.e., top). The reader should read Vallejos et al. (2011) for details on the techniques of volumetric mass transfer coefficient measurements and correlation in small scale devices. Briefly, deionized water at 37°C was gassed out with nitrogen and when DO reached 0% agitation was stopped and the headspace was flushed with air. After 45 s of flushing with air, the DO reading in the headspace reached saturation levels and agitation was set at the desired rate. This method is mostly known as the "gassing out" method and more details can be found in textbooks (Shuler and Kargi, 2001). The response time of the optical sensor was disregarded due to the low k_La observed in this study and it was considered negligible (Van't Riet, 1979).

The volumetric mass transfer coefficient (k_La) model equation used to correlate our experimental data is as follow:

$$k_La = mV^aN^b \quad (1)$$

Nonlinear regression analysis was used to fit the k_La experimental data from this study to Equation (1), allowing us to estimate the empirical constants (m, a, b). Where "m" is an empirical constant that allows unit equivalency between both sides of Equation (1). Additionally, "a" and "b" are empirical constants that correlate k_La to volume and agitation speed, respectively. We used equations based

on the method proposed by Brown (2001) and a macro embedded in Excel (Microsoft®) spreadsheet.

Mixing Time Experiments

We used a high definition video recorder camera model HDR-CX 110 (Sony Corporation, Tokyo, Japan) to visually monitor mixing. By observing the mixing of a fluorescein-based dye (fluorescein disodium salt, Sigma–Aldrich, St. Louis, MO) in DI (deionized) water in both SuperSpinner D 1000® and 1 L SS flask we were able to estimate the mixing time (estimated by visual observation as the time to reach homogeneity).

Cell Culture Experiments

A non-adherent SP2/0-based mouse/hybridoma (2055.5) secreting an IgG3 antibody was used in this study with culture parameters identical to those reported in Vallejos et al. (2010). A single CD Hybridoma AGT™ (Invitrogen, Carlsbad, CA) lot was employed for all studies. The inoculum seed was prepared in a 5 L glass vessel inside a Class II Type A/B3 sterile hood (The Baker Company, Inc., Sanford, ME) and then split into the two spinners to ensure that the same starting culture was used for both devices. Prior to sterilization, patches were attached to the SS flask wall and autoclaved at 121°C for 22 min. In the case of SuperSpinner D 1000®, sterile forceps were used to attached pre-autoclaved patches to this pre-sterilized PSD inside a laminar flow hood. Protein titer was measured following a standard ELISA protocol on the frozen supernatant as previously described by Kondragunta et al. (2010).

Results

Mass Transfer

Our patch-based DO sensor enabled us to estimate the volumetric mass transfer coefficient k_La in SuperSpinner D1000® and a SS flask. In this study, we observed that the 1 L SS flask and the SuperSpinner D 1000® (SSD) flask show many k_La matching points (Fig. 2). These data points, aside for the 300-mL filling volume case, may be considered the design space where cell culture performance comparability studies (i.e., at matched k_La) between both systems can be investigated. At 300 mL, only about 42% (i.e., length ratio) of the aeration membrane in SuperSpinner D 1000® is submerged in the liquid. This reduces the mass transfer area, thus providing a lower k_La than SS at the same volume (Fig. 2). As more liquid is added to SSD more mass transfer area is available thus enhancing k_La.

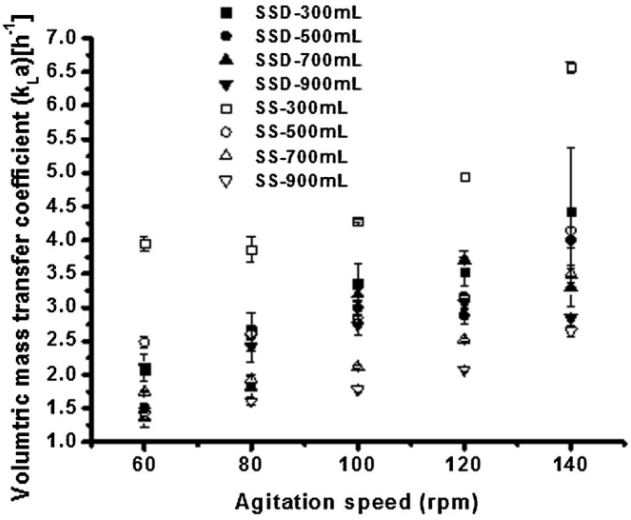

Figure 2. Experimental volumetric mass transfer coefficient in SuperSpinner D 1000 (SSD) and a 1 L standard spinner flask (SS). At the same filling volume of 300 mL (open square symbol) SS provides a significantly higher k_La than SSD (closed square symbol). It also shows some k_La matching points in the range of 500–700 mL between SSD and SS. These can be used as design space for comparability study between both systems. These experimental data are expanded upon in Figure 3 using empirical Equation (1).

We also estimated the coefficients for Equation (1) and obtained the following values

$$k_La = 0.047 \cdot V^{-0.19} N^{0.87} \quad \text{(SuperSpinner D 1000 flask, [SSD])} \tag{2}$$

$$k_La = 0.028 \cdot V^{-0.68} N^{0.94} \quad \text{(1 L-standard spinner flask, [SS])} \tag{3}$$

and its shows that mass transfer in the 1 L SS flask is more sensitive to volume change than SuperSpinner D 100® as given by the absolute values of coefficients 0.68 and 0.19, respectively. This could be due to the different type of aeration, surface aeration in SS versus free bubbling (i.e., submerged aeration) in SSD with the former being less efficient supplying oxygen as the volume increases.

We plotted our model Equations (2) and (3) in a 3D plot (Fig. 3), and observed that at lower filling volumes (i.e., 300 mL), the SS flask has significantly higher (up to 96%) k_La than SuperSpinner D 1000®. This observation is in agreement with our experimental data shown in Figure 2 and furthermore our model equations also predict that above 600 mL the SSD flask has higher k_La than the SS flask. As the liquid filling volume in SuperSpinner D 1000® is increased, more sections of the aeration membrane are submerged in the liquid thus increasing the mass transfer area. At 300 mL, the surface area to volume ratio is 42.87 and

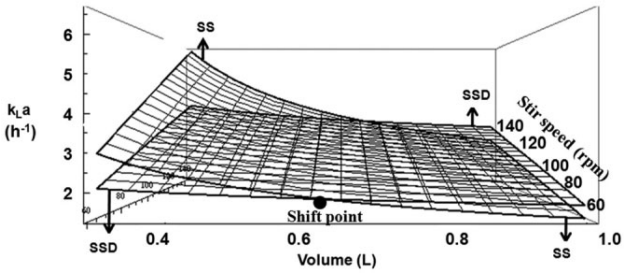

Figure 3. k_La comparability between Superspinner D 1000 (SSD) and 1 L standard spinner (SS) in the range of 300 mL to 1 L and 60–140 rpm. Data generated from model Equation (1). A shift point around 630 mL can be observed. Before this shift point (lower filling volumes), SS is more efficient, providing higher k_La. Above 630 mL a shift takes place, and SSD starts to become more efficient at mass transfer.

$36.7\ m^{-1}$ for SS and SuperSpinner D 1000®, respectively. However, at 900 mL this ratio is 14.3 and 12.2 for SS (surface aeration) and SSD (submerged aeration), respectively. This is in agreement with the well known fact that at similar surface area to volume ratio, submerged aeration is more efficient than surface aeration enhancing k_La (Chisti and Jauregui-Haza, 2002).

The convenient application nature of our DO patch-based optical sensor allowed us to place two patches inside SuperSpinner D 1000® and SS flasks operated at their maximum recommended working volumes. Figure 4b shows that at 60 rpm and 800 mL working volume the difference between k_La at the bottom and top sections reaches about 25%. We observed this to happen only to SSD but not to SS thus we hypothesized that mixing in the axial flow can be inefficient under these conditions in the SuperSpinner D 1000®. As a result we proceeded to investigate mixing in both spinner flasks using a tracer-based method as described in the Materials and Methods section.

Mixing Time

Figure 5a shows that mixing in the axial direction is inefficient at 60 rpm for SuperSpinner D 1000® and it takes about 311 s (5.2 min) to reach homogeneity (as evidenced by uniformity in dye concentration in the entire liquid volume). In fact, during the first 15 s we observed two un-mixed regions (dye concentration in the bottom section) showing that the gravitational force is higher than the impeller pumping capacity in the axial direction at 60 rpm. These segregated poorly mixed regions also have been observed in other systems (Vallejos et al., 2005; Zalc et al., 2002) and they are known as Poincaré sections where mixing is limited to diffusion. These segregated regions were absent in the SS flask where the rotating paddle impeller can distribute the dye in the entire vessel more efficiently than the oscillating impeller in the SuperSpinner D 1000®. The inefficient mixing time observed in our very small SSD is similar to those found in the much larger 5,000 L bioreactors (Xing et al., 2009) suggesting that the SuperSpinner D 1000® under these conditions (800 mL and 60 rpm) could be used as a scale-down model of manufacturing-scale vessels where mixing times can be very long.

Dissolved Oxygen and pH Monitoring in SuperSpinner D 1000® and a 1 L-Standard Spinner Flask at Matched k_La

Using our optical sensor enabled k_La data, we set a k_La of $2.3\ h^{-1}$ for our culture comparison. This allowed us to operate the SS flask (i) between the maximum agitation speed (140 rpm) feasible for the SS flask, avoiding stronger vortexes and (ii) the minimum stir speed for SuperSpinner

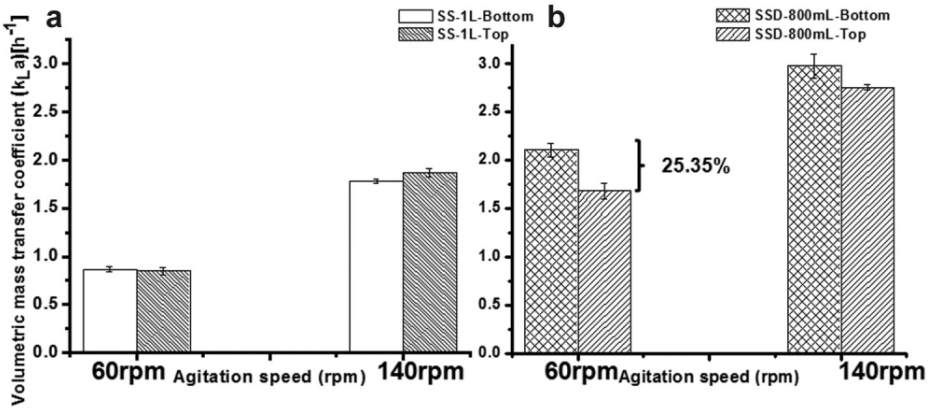

Figure 4. Local k_La in the top and bottom sections of SuperSpinner D 1000 (SSD) and 1 L standard spinner flask (SS). At low agitation speed of 60 rpm a k_La difference of up to 25% between top and bottom sections is observed (**b**).

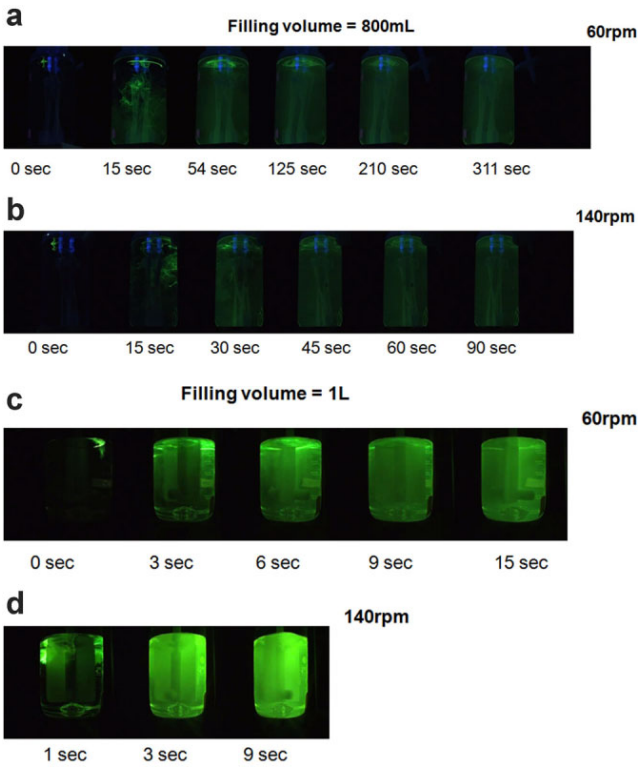

Figure 5. Mixing time in SuperSpinner D 1000 (SSD, **a**,**b**) and standard spinner flasks (SS, **c**,**d**) at a filling volume of 800 mL and 1 L at 60 rpm (a,c) and 140 rpm (b,d), respectively. Inefficient mixing as evidenced by poorly mixed segregated regions in the SSD axial axis is observed. Large mixing time (311 s, 5.2 min) at 60 rpm is also observed for SSD. Increasing agitation speed up to 140 rpm in SSD decreased mixing time down to 90 s (1.5 min). SS shows lowest mixing time of 9 and 3 s at 60 and 140 rpm, respectively.

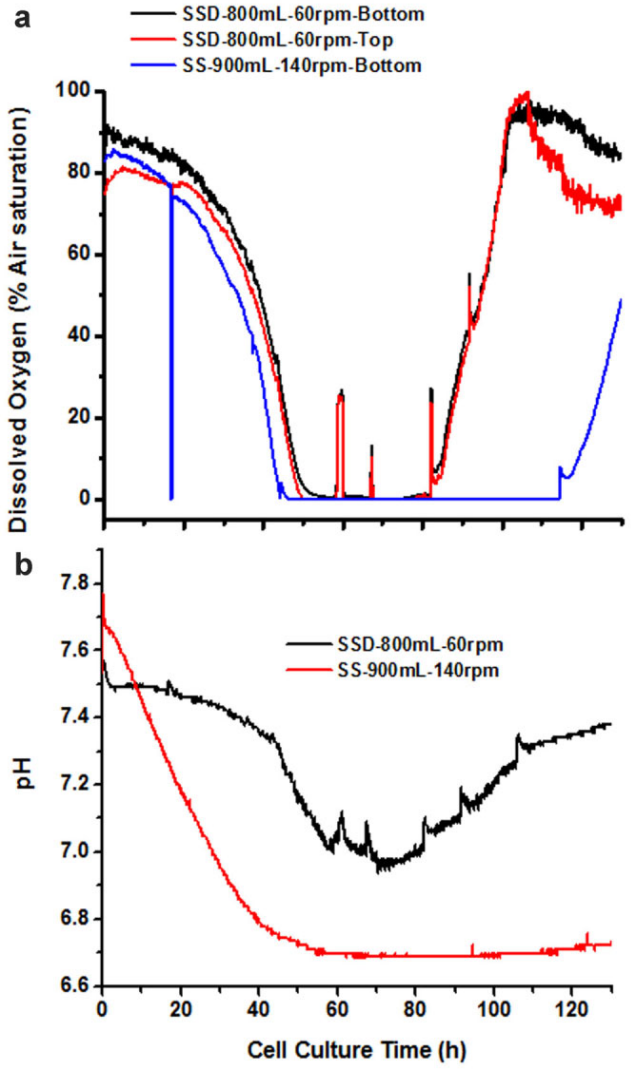

Figure 6. Dissolved oxygen and pH profiles for SuperSpinner D 1000 and 1 L standard spinner flask. Critical DO (**a**) levels (**b**) of 0% are reached in both systems at a matched k_La of 2.3 h^{-1}.

D 1000® (60 rpm), avoiding over mixing. Figure 6a shows that SuperSpinner D 1000® and SS flask reached sub-optimal DO levels (i.e., 0%) about the same time when run at matched k_La. In addition, cells in SuperSpinner D 1000® entered the death phase faster than cells in SS flasks (as evidenced by an earlier drop in cell viability for SSD, see Fig. 7) which could be caused by the type of aeration in the SSD (submerged). The same phenomenon has been observed in previous studies in our laboratory (unpublished data). We have observed that under sparged air conditions in spinner flasks; our cells exhibit a faster death rate than under headspace aeration in the same flasks. The pH profiles (i.e., minimum pH reached) for SuperSpinner D 1000® and standards spinner flask are similar to other systems previously cultured and monitored inside CO_2-incubator conditions (Vallejos et al., 2010). According to Table I, the maximum cell density reached in SuperSpinner D 1000® showed an 18.9% difference with respect to 1 L SS flasks which is within the ±20% commonly accepted industry variation criterion (Chen et al., 2009). For maximum protein titer analysis, we terminated the culture when viable cell percentage reached 80% (Harding et al., 2000) and we observed (Table I) that both spinners have similar maximum protein titer (136.4 vs. 127.6 mg/L).

We also tested the SuperSpinner D 1000® at a higher k_La (3.0 h^{-1}, $\sigma \pm 0.13$; 140 rpm) and observed a change in DO profile. Figure 8 shows that the minimum DO reached under this new k_La was about 20% (verified in a repeated run, data not shown) thus avoiding the sub-optimal DO levels observed in Figure 6 and these data are summarized in Table I. We compared our SuperSpinner D 1000® (at 20% DO levels) maximum viable cell density and protein titer data with historical data generated in our laboratory using Biostat® under active DO control (i.e., 30%) and observed that both end points are within the ±20% criterion (Table I). Based only on traditional endpoints such as maximum viable cell density and protein titer (Table I),

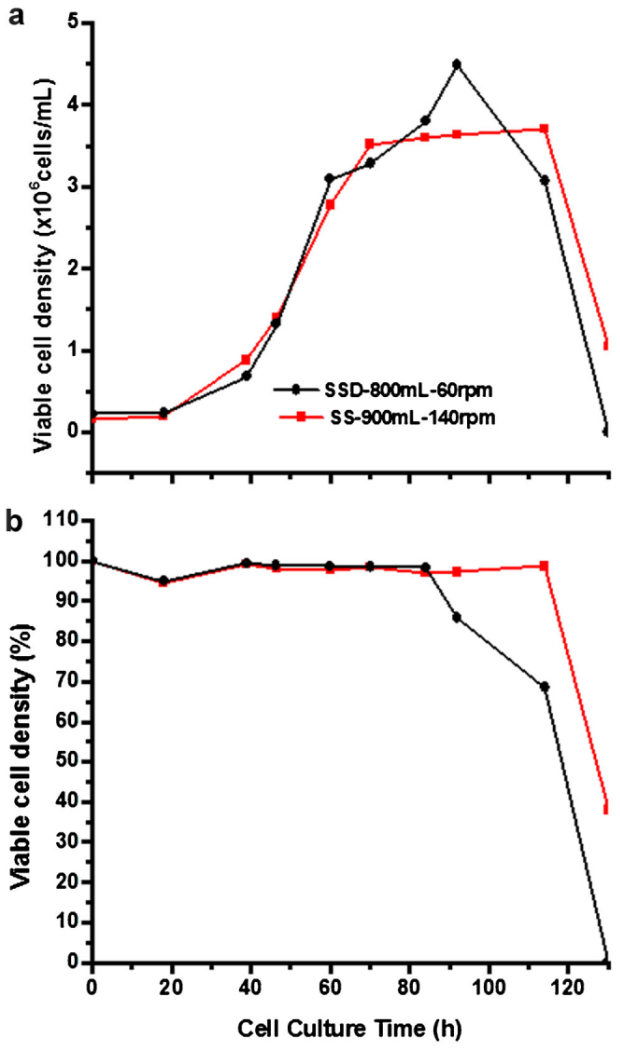

Figure 7. **a**: Viable cell density (VCD) and (**b**) viable cells (%) for SuperSpinner D 1000 (SSD) and 1 L standard spinner flask (SS) at matched k_La. Similar VCD profiles are observed in both systems. Viability drops faster in SSD and it could be the result of the "free bubble" oxygen supply method as compare to headspace in SS. We have also observed that this viability dropping rate worsen when continuous sparging (air or oxygen) is supplied.

SuperSpinner D 1000® (at 0% and 20% DO levels) and SS flasks can be considered potential scale down models of Biostat®. Based on these promising data, we are currently evaluating scale-down equivalency (i.e., growth rate, protein titer and glycosylation) between SSD and our Biostat® using DoEs and relevant statistical tools (e.g., two-one-side test; TOST).

Discussion

Bioprocess Implications

Our study has at least three important bioprocess implications. First, it illustrates the importance of monitoring critical process conditions such as DO during early R&D studies that are often carried out in non-instrumented PSDs. Our data support our hypothesis that less time and resources could be used when for example, selecting the right clone if DO profile at the clone selection stage is known. Serrato et al. (2004) observed that heterogeneous conditions in DO affect *N*-glycosylation but not protein titer suggesting that the current approach of using only off-line end points in non-instrumented PSDs is suboptimal as it may hide relevant environmental conditions (i.e., DO) that would surface at subsequent early process optimization stages. We propose that SSD can be used, for example, to realistically investigate CO_2 removal efficiency, for example, by strains selected in Microbioreactors. Second, our study shows the importance of a data-driven process (i.e., engineering characterization and on-line monitoring of environmental conditions) during the selection of cell culture devices. Until now, little published engineering characterization is available for disposable PSDs such as SuperSpinner D 1000®. Our study reveals (Table I) that after defining the design space (i.e., k_La), the SuperSpinner D 1000® (at 20% DO levels) can potentially function as a scale-down model for bench-scale bioreactors (at 30% DO levels) mimicking DO levels, maximum cell density and protein titer. Our study increases the number of potential candidates of disposable stirred-based scale-down tools for early optimization studies. This implies that a seamless, data-driven,

Table I. Comparability study between SuperSpinner D 1000, a 1 L standard spinner flask and historical data of a 5L bench scale bioreactor (Biostat®).

	N, rpm (filling volume)	Mixing time	k_La (h^{-1})	Minimum DO levels (%)	Maximum VCD ($\times 10^6$ cells/mL)	Protein IgG3 titer (mg/L)
SuperSpinner D 1000	60 (800 mL)	3.5 min	2.3	0	4.49	136.4 (+4.9%)[a]
1 L-standard spinner	140 (900 mL)	3 s	2.3	0	3.71	127.6 (−1.9%)[a]
SuperSpinner D 1000	140 (800 mL)	60 s	3.0	20	3.9	105.6 (−18.8%)[a]
Biostat®[b] (Active DO control)	220 (4.5 L)	4 s	2.5[c]	30	4.5	130

[a]Percentage difference with respect to Biostat®.
[b]Laboratory historical data.
[c]Estimated from the oxygen mass balance of $dC/dt = OUR - OTR$ and using a $C^* = 1.42 \times 10^{-3}$ mmol O_2/mL (oxygen was used to control DO at 30%), $q_{O_2} = 5.6 \times 10^{-10}$ mmol/cell h (Vallejos et al., 2010), $X_v = 4.5 \times 10^6$ cells/mL.

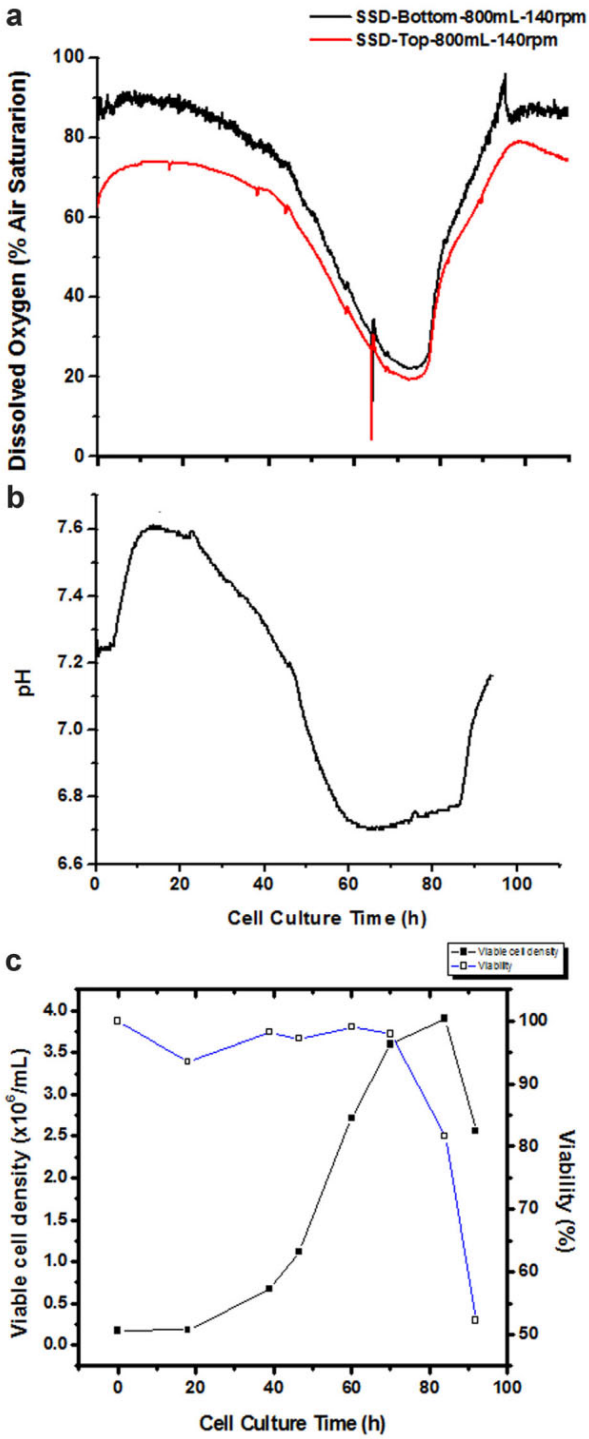

Figure 8. **a**: Dissolved oxygen, (**b**) pH profile, and (**c**) Viable cell density (VCD) and viable cells (%) for SuperSpinner D 1000 (SSD) at a k_La of 3 h^{-1} (800 mL, 140 rpm). DO is kept above 20%.

process transfer can be devised to link currently non-instrumented PSDs (such as SuperSpinner D 1000®) with bench scale-bioreactors. Finally, our study suggests that SuperSpinner D 1000® can be integrated with other fully instrumented bioreactors in a seed development train under "active" DO control. By choosing the correct operational conditions (i.e., k_La), the SuperSpinner D 1000® can mimic the DO profile levels of fully instrumented bioreactors avoiding reaching sub-optimal DO levels (i.e., 0%) for our cell line model.

Mixing Time

Mixing time studies in SuperSpinner D 1000® helped us with understanding the local k_La difference between the top and bottom sections of the vessel at a relative low agitation speed (i.e., 60 rpm) and maximum recommended working volume (i.e., 800 mL). We observed that under these conditions industrial relevant mixing time (5.2 min) is likely to be found in SuperSpinner D 1000® and it had significant effect on the DO and pH profiles but not on the maximum VCD and protein titer. A 3.5-fold reduction in mixing time resulted in a 30% increase in k_La (from 2.3 to 3.0 h^{-1}) and the pH decreased from 7.0 to 6.7 (verified in a repeated run which was within a 0.1 pH unit difference, data not shown). Since lactate concentrations at 2.3 and 3.0 h^{-1} were very similar (data not shown), we hypothesized that CO_2 removal at shorter mixing time (90 s and 140 rpm) is less efficient in SuperSpinner D 1000® under these conditions resulting in the pH decrease. This can be due to the increase in liquid turbulence and oxygen flow (from the gas membrane to the liquid) that reduces the CO_2 flow into the gas membrane keeping more CO_2 in the liquid. We are currently investigating these observations further using our optical-based CO_2 sensors.

Mass Transfer

Our optical-based DO sensor technology allowed determining quantitatively for the first time the mass transfer capabilities of this novel mechanically driven/stirred PSD. Our study shows that optical-based DO sensors can aid elucidating the oxygen transfer capabilities of novel PSDs and further support (or reject) the claim that these PSDs are significantly superior to re-usable cell culture flasks or other disposable PSDs. In the particular case of the SuperSpinner D 1000®, our mass transfer study allowed to determine k_La correlations that would help cell culture scientists to define the design space conditions where matching k_La points can be selected in order to develop, for example, an entire upstream process platform at constant k_La (Flores et al., 1997).

Conclusions

Our study shows that novel disposable cell culture devices such as SuperSpinner D 1000® can be readily equipped with patch-based optical sensors, giving these devices similar monitoring capabilities as fully instrumented bench-scale

bioreactors. We established a mass transfer correlation based on easily measured parameters (liquid volume and impeller agitation speed), showing that a design space can be selected for SuperSpinner D 1000® where it can operate in a cell culture train with matched k_La to subsequent upstream manufacturing stages. Based on our promising, but preliminary data, we proposed a potential application of SuperSpinner D 1000® as a scale-down model of bench-scale stirred bioreactors providing similar DO profiles at both scales. We hypothesized that even at this small scale (SuperSpinner D 1000®, 800 mL), mixing times similar to those at large scale can also be modeled.

G. Rao has an equity position in Flurometrix. Views expressed in this article are those of the authors and not necessarily of the US FDA or the US government. Discussion of the individual cell culture devices does not constitute endorsement by the US FDA or the US government. We thank Bhargavi Kondragunta for providing historical laboratory data from Biostat® cell cultures.

Nomenclature

DO	dissolved oxygen
DoE	design of experiment
k_La	overall volumetric mass transfer coefficient (h^{-1})
N	stir speed (s^{-1} or min^{-1})
PSDs	process scouting devices
SS	standard spinner flask
SSD	superspinner D 1000 flask
V	filling volume (m^3)
VCD	maximum cell density ($\times 10^6$/mL)

Greek Symbols

σ	standard deviation

References

Aunins JG, Woodson BA, Jr., Hale TK, Wang DIC. 1989. Effect of paddle impeller geometry on power input and mass transfer in small-scale animal cell culture vessels. Biotechnol Bioeng 34:1127–1132.

Brown AM. 2001. A step-by-step guide to non-linear regression analysis of experimental data using a Microsoft Excel spreadsheet. Comp Prog Meth Biomed 65:191–200.

Chen A, Chitta R, Chang D, Amanullah A. 2009. Twenty-four well plate miniature bioreactor system as a scale-down model for cell culture process development. Biotechnol Bioeng 102(1):148–160.

Chisti Y, Jauregui-Haza UJ. 2002. Oxygen transfer and mixing in mechanically agitated airlift bioreactors. Biochem Eng J 10:143–153.

Eibl R, Kaiser S, Lombriser R, Eibl D. 2010. Disposable bioreactors: The current state-of-the art and recommended applications in biotechnology. Appl Microbiol Biotechnol 86:41–49.

Flores ER, Perez F, de la Torre M. 1997. Scale-up of *Bacillus thuringiensis* fermentation based on oxygen transfer. J Ferment Bioeng 83:561–564.

Gupta A, Rao G. 2003. A study of oxygen transfer in shake flasks using a non-invasive oxygen sensor. Biotechnol Bioeng 84(3):351–358.

Harding CL, Lloyd DR, McFarlane CM, Al-Rubeai M. 2000. Using the mycrocyte flow cytometer to monitor cell number, viability, and apoptosis in mammalian cell culture. Biotechnol Prog 16(5):800–802.

Heidemann R, Riese U, Lütkemeyer D, Büntemeyer H, Lehmann J. 1994. The Super-Spinner: A low cost animal cell cultura bioreactor for the CO_2 incubator. Cytotechnol 14:1–9.

Kondragunta B, Drew JL, Brorson KA, Moreira AR, Rao G. 2010. Advances in clone selection using High-throughput bioreactors. Biotechnol Prog 26(4):1095–1103.

Kostov Y, Harms P, Randers-Eichhorn L, Rao G. 2001. Low-cost microbioreactor for high-throughput bioprocessing. Biotechnol Bioeng 72(3):346–352.

Lehmann J, Vorlop J, Büntemeyer H. 1988. Bubble-free reactors and their development of continuous culture with cell recycle. Anim Cell Technol 3:221–237.

Randers-Eichhorn L, Bartlett RA, Frey DD, Rao G. 1996. Noninvasive oxygen measurements and mass transfer considerations in tissue culture flasks. Bioetchnol Bioeng 51:466–478.

Rao G, Moreira A, Brorson K. 2009. Disposable bioprocessing: The future has arrived. Biotechnol Bioeng 102(2):348–356.

Schmale K. 2008. SuperSpinner D1000: Efficient cell cultivation for the Lab-scale production of biomass and recombinant proteins. Nat Methods (5: Application Notes).

Serrato JA, Palomares LA, Meneses-Acosta A, Ramirez OT. 2004. Heterogeneous conditions in disolved oxygen affect *N*-glycosylation but not productivity of a monoclonal antibody in hybridoma cultures. Biotechnol Bioeng 88(2):176–188.

Shuler ML, Kargi F. 2001. Selection, scale-up, operation, and control of bioreactors. In: Amundson NR, editor. Bioprocess engineering. Basic concepts, 2nd edition. New Jersey: Prentice-Hall Publishing. p 294.

Sucosky P, Osorio DF, Brown JB, Neitzel GP. 2004. Fluid mechanics of a spinner-flask bioreactor. Biotechnol Bioeng 85(1):34–346.

Vallejos JR, Kostov Y, Ram A, French JA, Marten MR, Rao G. 2005. Optical analysis of liquid mixing in a minibioreactor. Biotechnol Bioeng 93(5):906–911.

Vallejos JR, Brorson KA, Moreira AR, Rao G. 2010. Dissolved oxygen and pH profile evolution after cryovial thaw and repeated cell passaging in a T-75 flask. Biotechnol Bioeng 105(6):1040–1047.

Vallejos JR, Brorson KA, Moreira AR, Rao G. 2011. Integrating a 250 mL-spinner flask with other stirred bench-scale cell culture devices. A mass transfer perspective. Biotechnol Prog 27(3):803–810.

Van't Riet K. 1979. Review of measuring methods and results in nonviscous gas-liquid mass transfer stirred vessels. Ind Eng Chem Process Des Dev 18(3):357–364.

Xing Z, Kenty BM, Li ZJ, Lee SS. 2009. Scale-up analysis for CHO cell culture process in large-scale bioreactors. Biotechnol Bioeng 103(4): 733–746.

Zalc JM, Szalai ES, Alvarez MM, Muzzio FJ. 2002. Using CFD to understand chaotic mixing in laminar stirred tanks. AIChE J 48(10):2124–2134.

The 2-liter shake flask turns out to be a process development tool widely used in fermentation and seed train development. We wanted to better understand some of the limitations in the system, as it is clearly one of these designs that was scaled-up empirically. I imagine that after the Erlenmeyer flask (which was an ideal chemist's tool to allow addition of different chemicals and mixing by swirling the flask) was deployed for fermentations, somebody thought that building larger ones would be a simple way to scale up and so today, you have shake flasks ranging from 100 mL to 2 Liter volumes. However, unlike sparged bioreactors, the shake flask suffers from severe mass transfer limitations due to the exchange surface being limited to the liquid surface and the film that forms during swirling agitation. Furthermore, as we had seen earlier, the type of closure exerts an enormous influence on headspace oxygen transfer.

We wanted to get a better understanding of the physiological environment and set about an ambitious study that would quantify both the liquid phase and the headspace process parameters. The next paper describes these results for a multitude of measurements, as were able to use oxygen, pH, CO_2 sensors for both liquid and headspace monitoring. Another interesting experiment was to see if sweeping the headspace would provide for more oxygen transfer and allow for greater working volumes to be used.

The results show that metabolism can be greatly affected by the culture conditions. In particular, we were able to observe extended oscillatory metabolism under certain conditions. Importantly, none of this behavior is obvious to just casual observation, which is the current state-of-the-art.

Real-Time Monitoring of Shake Flask Fermentation and Off Gas Using Triple Disposable Noninvasive Optical Sensors

Xudong Ge
Center for Advanced Sensor Technology, Dept. of Chemical, Biochemical and Environmental Engineering, University of Maryland Baltimore County, Baltimore, MD 21250

Govind Rao
Center for Advanced Sensor Technology, Dept. of Chemical, Biochemical and Environmental Engineering, University of Maryland Baltimore County, Baltimore, MD 21250

DOI 10.1002/btpr.1528
Published online February 28, 2012 in Wiley Online Library (wileyonlinelibrary.com).

Bioprocess development is a data-driven process requiring a large number of experiments to be conducted under varying conditions. Small-scale upstream bioprocess development is often performed in shake flasks because they are inexpensive and can be operated in parallel. However, shake flasks are often not equipped to accurately monitor critical process parameters such as pH, dissolved oxygen, and CO_2 concentrations. Therefore, there is no definitive information on oxygen supply of growing cells, CO_2 formation, and pH changes. Here we describe several shake flask fermentations where all three parameters are monitored by disposable noninvasive optical sensors. The sensitive element of these sensors is a thin, luminescent patch affixed inside the flask. Small electronic devices for excitation and fluorescence detection are positioned outside the shake flask for noninvasive monitoring. By measuring the process parameters throughout the course of the E. coli *fermentations, we obtain information that is not routinely available in shake flask fermentations. For example, for cultures with only a few millimeters liquid depth, oxygen limitation can occur at relatively low agitation speeds. Under certain conditions oscillations in dissolved oxygen can occur. An increase in shaker speed and a decrease in culture volume can increase the oxygen availability and reduce the duration of oxygen limitation.* © 2012 American Institute of Chemical Engineers *Biotechnol. Prog.*, 28: 872–877, 2012
Keywords: real-time monitoring, shake flask fermentation, disposable, noninvasive, optical sensor

Introduction

Shake flasks are widely used in upstream bioprocess development because they are inexpensive and can be operated in parallel. However, although several studies have dealt with the oxygen availability in shake flasks and its effects on cell growth and product formation during the past decades,[1–7] shake flasks are still usually not equipped to accurately monitor critical process parameters such as pH, dissolved oxygen and CO_2 concentrations because of the lack of suitable and convenient means to measure these process parameters in situ. Conventional probes have been used to monitor these critical process parameters in shake flask fermentations since 1970s.[8,9] However, it is often difficult to insert these cumbersome probes into shake flasks while trying to maintain aseptic conditions. As these probes are expensive and nondisposable, their cleaning, sterilization, and calibration between experiments are still relatively time-consuming. Because the above parameters are usually not monitored in routine shake flask fermentations, there is no definitive information on the oxygen supply of growing cells, the CO_2 evolution, and pH changes. With the invention of disposable noninvasive sensors, this situation might be changed quickly in the future. The disposable noninvasive sensors for pH, DO, and CO_2 used in this study were developed by the authors' laboratory.[10–20] All patches share a similar multilayer structure with a sensitive dye immobilized in the responsive layer of the sensing patch. The disposable sensing patches can be attached to the bottom or inside wall of any transparent bioreactors. A small device for illuminating the patch and detecting the fluorescence can then be positioned outside to measure the analyte concentration in the shake flask noninvasively. This provides a lot more information about the bioprocess than routine shake flask fermentations while greatly reducing the chance of contamination. As different sensing patches with the same composition responded consistently, only a few patches randomly selected from a whole batch are used for calibration. After that, a calibration code is generated and the users can use the other sensing patches from the same batch directly with no need for calibration. Additionally, as the cost for each patch is almost negligible compared to other costs, the patches are disposable. There is no need for cleaning, sterilization or recalibration. Weigl et al.[21] have previously described a triple sensor in a flow-cell format, which is not convenient for in situ

Correspondence concerning this article should be addressed to G. Rao at grao@umbc.edu.

bioprocess monitoring. Our approach makes the measurements directly in the bioreactor. This can save a lot of time for process setup and significantly speed up the development process.[22] In this article, we describe several shake flask *E. coli* fermentations monitored by the disposable sensors. By using three different sensors together, more information about the process such as cell oxygen uptake rate and CO_2 evolution rate, etc. can be revealed that cannot be obtained in routine shake flask fermentations. The novelty is the simultaneous monitoring of O_2, pH, and CO_2 which we have not described before. In addition, the article describes simultaneously measuring oxygen and CO_2 in the headspace or the off gas, and this is again novel, as it allows for off-gas measurements using inexpensive sensors.

Materials and Methods

Disposable noninvasive optical sensors

The DO, CO_2, and pH disposable sensors used in this study were developed by the authors' laboratory.[10–20] All sensors share a similar multilayer structure: a responsive layer, an optical isolation layer, a support layer, and an adhesive layer. The responsive layer in the DO sensor is a layer of silicone rubber with an oxygen-responsive fluorophore (tris-(bathophenanthroline) ruthenium(II) chloride) immobilized in it. The adhesive layer is a layer of silicone adhesive used for attaching the patches to the inside wall or bottom of the shake flask. The optical isolation layer is a hydrophobic membrane that has dual functions to prevent background fluorescence from affecting the fluorescence measurements and to prevent a stagnant water film from forming in the isolation layer. The formation of a stagnant water film can greatly prolong the response of the sensor. The support layer is a layer of polyester to enhance the mechanical strength of the patches. When the fluorophore is excited by an intensity-modulated light source, the intensity of the resulting emission appears at the same frequency but with lower modulation and a phase shift. Because the fluorescence of the fluorophore is quenched in the presence of oxygen, the phase shift will change in response to a change in DO concentration. The phase shift of the resulting emission is related to the oxygen concentration by:

$$\frac{\tan(\phi_0)}{\tan(\phi)} = 1 + Ksv[O_2] \tag{1}$$

where ϕ and ϕ_0 are the phase shift in the presence and absence of oxygen, respectively, Ksv is the Stern-Volmer constant and $[O_2]$ is the oxygen concentration.[23]

The responsive layer in the CO_2 sensing patches is a layer of silicone rubber with a pH-responsive fluorophore (HPTS) and an organic base (cetyl trimethyl ammonium hydroxide) immobilized in it.[19,20] All other layers in the CO_2 sensing patches are the same as in the DO sensing patches. The responsive layer in the pH sensing patches is a hydrogel-white backing composite layer with 6,8-dihydroxypyrene-1,3-disulfonic acid disodium salt (DHDS) covalently immobilized in it. The white backing serves as both a support for the hydrogel and an optical isolator from the background fluorescence. Unlike the DO and CO_2 sensing patches, the white backing in the pH sensing patches is highly hydrophilic so that hydrogen ions can enter the patches to induce a signal change. The support and adhesive layers in the pH sensing patches are also the same as in the DO patches.

Although DHDS has two hydroxyl groups while HPTS has only one, the immobilized DHDS is an analog to HPTS because one of the two hydroxyl groups in DHDS has been used during covalent immobilization. Both possess two excitation maxima at wavelength of 405 nm and 460 nm, corresponding to the protonated form and deprotonated form of the fluorophores. When a change in pH or CO_2 concentration breaks the dissociation equilibrium, the amount of the fluorophore in one of the two forms will increase while the other will decrease until a new equilibrium is reached. Correspondingly, the ratio of the two excitation maxima will change. For the pH disposable sensing patches, the ratio of the two excitation maxima (R) is related to the pH value by:

$$R = \frac{R_{acid}10^{-pH} + R_{basic}K^I_{app}}{10^{-pH} + K^I_{app}} \tag{2}$$

where R_{acid} and R_{basic} are the ratio of the two excitation maxima for the protonated form and deprotonated form of the fluorophore, respectively, K^I_{app} is the apparent dissociation constant of the fluorophore at ionic strength I. For the CO_2 disposable sensing patches, the ratio of the two excitation maxima (R) is related to the CO_2 concentration ($[CO_2]$) by:

$$[CO_2] = A + BR + CR^2 \tag{3}$$

where A, B, and C are constants.

The validation of these optical sensors was performed previously by comparing with standard industrial electrochemical probes,[22] and excellent consistency was confirmed. When pH and DO measurements obtained with the optical sensors were compared to measurements from the standard probes, the accuracy was sufficient to prohibit any significant impact on growth, production kinetics, and protein product quality.

Calibration of the disposable sensors

As different sensing patches with the same composition responded consistently, for each batch of newly prepared sensing patches, only a few randomly selected patches are used for calibration. After that, a calibration code is generated and all other patches of the same batch can be used directly by entering the calibration code into the software and no actual calibrations are required. To calibrate the patches, the patches have to be first autoclaved at 121°C for 25 minutes. The DO sensing patches have a responsive range from 0 to 21% (Figure 1). They were calibrated in PBS by sequentially measuring the phase shift at 0, 4.2, 8.4, 12.6, 16.8, and 21% O_2 concentrations. The gas mixtures with desired O_2 concentrations were obtained by mixing pure N_2 and air through two flowmeters (FM4332 and FM4333, Advanced Specialty Gas Equipment Corp., South Plainfield, NJ). The gas mixture was bubbled through the PBS buffer until the desired concentration was achieved. The temperature during calibration was 37°C. The CO_2 sensing patches have a responsive range from 0.0 to 20.0% CO_2 (Figure 1). They were also calibrated in PBS buffer. The gas mixtures containing 0.0–20.0% CO_2 were sparged into the calibration vessel sequentially, and the ratio of the fluorescence intensities at each CO_2 concentration was measured. The pH sensors have a responsive range from pH 6.0 to 8.5 (Figure 1). They were calibrated using six PBS buffers of known pH and a constant ionic strength of 0.15M with phosphate buffering species at 73 mM and sodium chloride added to

achieve the desired ionic strength. The pH of the buffers was verified with an AR25 Dual Channel pH/Ion Meter (Fisher Scientific, Pittsburgh, PA) before calibration. The temperature was also maintained at 37°C all the time.

Instrumentation

The instrumentation to measure the phase shift of the DO sensing patches uses a blue LED (Sharp Electronics Corp.) with a shortpass filter (Schott, Germany), and a PIN photodiode (BPW32, Vishay, France) with a longpass filter (Andover Corporation, NH). The LED is driven with a simple transistor driver that is controlled by the reference of an in-house built lock-in amplifier and modulated at 10 kHz. The photodetector output is connected to the signal input of the lock-in, and phase is measured.[24]

The pH and CO_2 coasters are miniature dual wavelength fluorometers specifically designed to measure the excitation ratio of the patch in small form factor. It consists of two commercially available LEDs with emissions at 400 (Bivar, Irvine, CA) and 450 nm (Nichia, Japan), respectively. The "red tail" in the LED emission is filtered using a common short pass filter BG-12 (Schott, Germany). The emission detection is performed by a photodiode, filtered with a band pass filter (center wavelength 550 nm, 40 nm FWHM). The LED light is modulated at ~10 kHz, which helps to suppress the influence of the ambient light. The light intensity is converted into a voltage by a transimpedance amplifier, and the fluorescence amplitude is quantified using an on-board synchronous detector. The LEDs are fired sequentially, and the fluorescence intensity is measured. The digital control and the analog-to-digital conversion are performed by a U12 LabJack digital acquisition (DAQ) card (LabJack Corporation, Lakewood, CO). The digital signals are recorded by a computer, which also calculates the emission ratio.

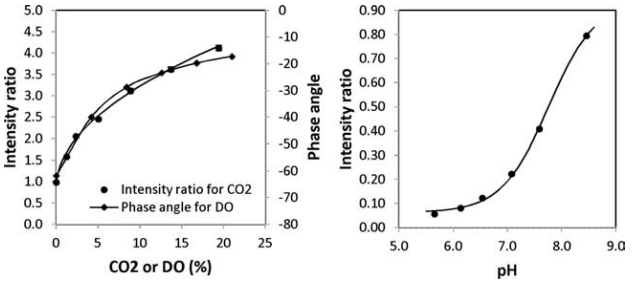

Figure 1. Calibration curves of the DO, pH, and CO_2 sensors.

Shake flask fermentations

The fermentation experiments were carried out at 37°C in 2-L shake flasks shown in Figure 2. The seed NM303 *E. coli* culture was prepared by inoculating 50 mL of LB medium with a single colony and incubated at 37°C in a 250-mL shake flask with shaking at 260 rpm (Orbit Environ Shaker, Lab-line Instruments; Melrose Park, IL) for 8–10 h. In the first experiment (Figure 2, left), three disposable sensing patches, which were used to measure the pH, dissolved O_2 and CO_2 concentrations in the culture, were attached to the bottom of the flask. Two disposable sensing patches, which were used to measure the O_2 and CO_2 concentrations in the off gas, were attached to the bottom of a glass vessel. The shake flask and the glass vessel were then filled with DI water and autoclaved at 121°C for 25 min. About 500 mL of LB medium was added and inoculated with 25 mL of the seed inoculums prepared above. The shake-flask was then placed on a bench-top shaker (CERTOMAT®BS-1, Sartorius, Germany) with three coasters positioned under the flask with adhesive tape for online measurement of pH, dissolved O_2 and CO_2 concentrations in the culture, and two coasters under the glass vessel for online measurement of O_2 and CO_2 concentrations in the off gas. The shake flask was briefly agitated at 260 rpm, and then maintained at 150 rpm for the rest of the time. Because the coasters were attached to the flask, the shaking of the flask did not affect the fluorescence measurements. LB medium did not interfere with the fluorescence measurements due to the optical isolation layer of the sensors. During the fermentation, the culture was aerated through the headspace at 26.6 mL min^{-1} from a lab air supply. Nearly 1.0 mL of broth sample was taken from the flask every 30–66 min for biomass analysis. The cellular optical density (OD) was measured with a Hewlett Packard 8452A Diode Array Spectrophotometer at 600 nm.

In the second experiment (Figure 2, right), the shake flask was covered with milk filters. Three disposable sensing patches were attached to the bottom of the flask for online measurement of pH, dissolved O_2 and CO_2 concentrations in the culture. Two disposable sensing patches for O_2 and CO_2 were attached to the wall of the flask for measuring O_2 and CO_2 concentrations in the headspace. The shake flask was then filled with DI water and autoclaved. 50 mL of LB medium was added and inoculated with 1 mL of the seed inoculums. The shake-flask was then placed on the benchtop shaker with three coasters positioned under the flask for online measurement of the pH, dissolved O_2 and CO_2 concentrations in the culture, and two coasters fixed on the wall

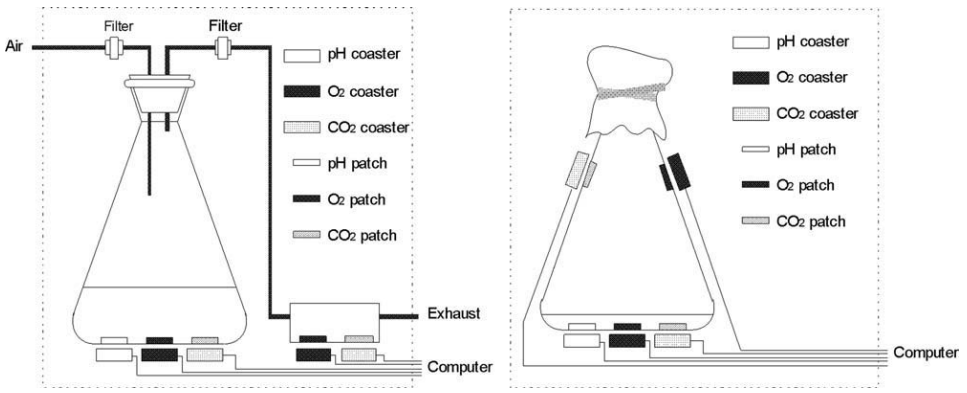

Figure 2. Setup for *E. coli* fermentation with continuous air supply (left) or milk-filter as closure (right).

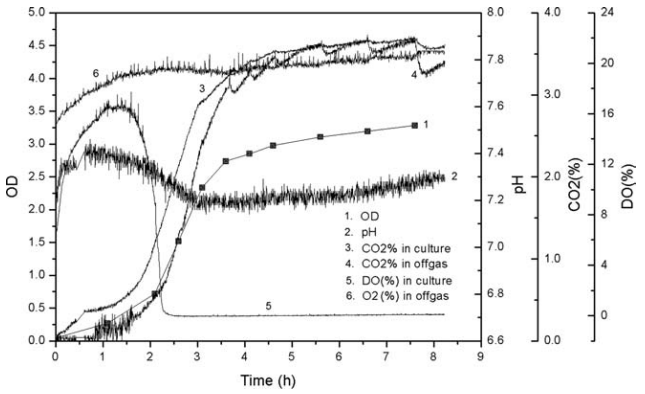

Figure 3. *E. coli* fermentation with continuous air supply at 26.6 mL min^{-1} in a 2-L shake flask (Figure 2, left) at 37°C and 150 rpm. About 500 mL of LB medium was inoculated with 25 mL of seed inoculums.

The stationary height of the culture is ~30 mm.

outside the flask for online measurement of O_2 and CO_2 concentrations in the headspace.

Results and Discussion

Shake flasks are widely used in small-scale upstream bioprocess development but no process parameters except temperature and agitation are monitored because of the lack of convenient means to measure these parameters in situ. In the first experiment, we studied the use of disposable sensing patches in NM303 *E. coli* fermentation with continuous air supply. Figure 3 shows the profiles of the process parameters during the fermentation conducted in a 2-L shake flask at 37°C and 150 rpm with continuous air supply at 26.6 mL min^{-1} as shown in Figure 2 (left). It can be seen that the pH value of the culture remains relatively constant and the pH change during the whole process is <0.3 pH units. The DO concentration at the beginning of the fermentation is low because much of the oxygen dissolved in the media is removed during autoclaving. In the lag phase of the fermentation, the bacteria cells consume less oxygen than the diffusion rate from the gas phase to the media. So the DO concentration increases gradually and reaches its maximum at about 1.5 h. After the cell growth enters the exponential phase, the cells consume more and more oxygen, and the DO concentration drops abruptly. At about 2.5 h, the fermentation becomes oxygen diffusion-limited and this oxygen-limiting condition persists until the end of the fermentation, which lasts about 8 h. The CO_2 concentration profiles follow the OD profile and reach steady state when the cell growth reaches the stationary phase. The zigzag shape of the CO_2 concentration profile in the off gas is caused by sampling. From the steady-state CO_2 concentration in the off gas (3.68%), the respiration rate of the cells can be calculated to be 4.4 mmol/(h−L).

Figure 4 shows the profiles of the process parameters during the *E. coli* fermentation conducted in a 2-L shake flask at 37°C and 150 rpm with no continuous air supply as shown in Figure 2 (right). In shake flask fermentations, oxygen availability is greatly dependent on the surface area to liquid volume ratio. As the surface area to liquid volume ratio is small in the fermentation shown in Figure 3, oxygen-limiting conditions persist since the early stage of the exponential phase till the end of the process. To increase the oxygen availability,

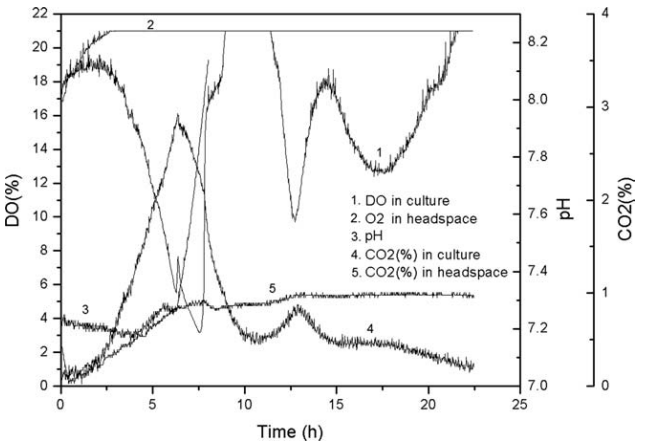

Figure 4. *E. coli* fermentation in a 2-L shake flask with milk filter as closure (Figure 2, right) at 37°C and 150 rpm.

About 50 mL of LB medium was inoculated with 1 mL of seed inoculums. The stationary height of the culture is <3 mm.

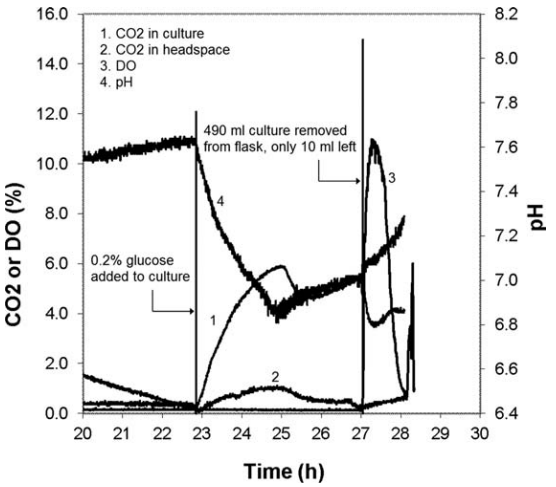

Figure 5. Effect of glucose addition and culture removal on pH, dissolved CO_2 concentration in culture, and CO_2 concentration in headspace at late stage of an *E. coli* fermentation carried out in a 2-L shake flask (Figure 2, right) at 37°C and 150 rpm.

About 500 mL of LB medium was inoculated with 25 mL of seed inoculums. The initial stationary height of the culture is ~30 mm. After removal of most of the culture, the new stationary height of the culture is only 1 mm.

we used only 50 mL of LB medium in this experiment and inoculated it with only 1 mL of seed inoculums. The stationary height of the culture is only 3 mm. As expected, the DO concentration in the culture is never depleted. Instead, it oscillates down and up three times. This phenomenon was also observed by other researchers in yeast fermentations[25–28] and bacterium fermentations.[29-33] In the fermentation shown in Figure 4, the oxygen availability is much higher than that in the fermentation shown in Figure 3 because of the much higher surface area to liquid volume ratio. As a result, the cells grow much faster and deplete the energy source in 7.5 h. Just before the depletion of the energy source, the pH of the culture shoots up above the upper limit of pH sensor. The increasingly more basic media neutralize the dissolved CO_2 and its concentration declines abruptly. After that, the cells

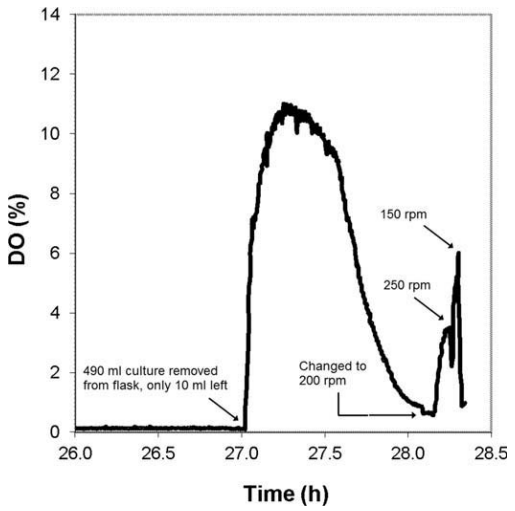

Figure 6. Effect of culture removal and change in agitation speed on the DO concentration in the culture at late stage of an *E. coli* fermentation carried out in a 2-L shake flask (Figure 2, right) at 37°C.

Other conditions are the same as in Figure 5.

begin to die until some of the cells find a new metabolic pathway and begin to multiply quickly.

In the fermentation shown in Figures 5 and 6, we measured the effect of glucose addition, culture removal, and change in agitation speed on the process parameters. The fermentation was carried out in a 2-L shake flask with no air supply at 37°C and 150 rpm. About 500 mL of LB medium was inoculated with 25 mL of seed inoculums. Twenty two hours after the beginning of the fermentation, 0.2% glucose was added to the culture. It can be seen that it immediately induces a rebound of CO_2 concentration both in the culture and headspace. The rebound of CO_2 concentration in the culture, in turn, induces a decline in pH. Twenty seven hours after the beginning of the fermentation, most of the culture is removed from the shake flask. The initial stationary height of the culture is ~30 mm. After the removal of most of the culture, the new stationary height of the culture in the shake flask is estimated to be only 1 mm (the estimation is based on the 10-mL culture volume measured after the fermentation). As expected, the DO concentration begins to increase after the removal of most of the culture. However, as the cells grow much rapidly because of higher oxygen availability, the DO concentration begins to drop again. Two hours later, it unexpectedly drops to almost zero. This result tells us that fermentations with a stationary height as low as 1 mm can become oxygen limited at low agitation speed because of the low solubility of oxygen in water. At 28.2 h, the speed of the shaker is increased incrementally from 150 to 200 rpm, and then to 250 rpm. It can be seen that the DO concentration increases accordingly. When the agitation speed is changed back to 150 rpm, the DO concentration also returns to its original value.

In all the fermentations, fouling was not observed most likely due to the Teflon-like backing on the patch. Although the patches can be reused for several times with little change in sensitivity, the patches are designed for only one use. This can save a lot of time used for cleaning and sterilization, and increase the development efficiency. As shown above, the monitoring of shake flask fermentation using triple noninvasive optical sensors provides a lot of information about the bioprocess which can not be obtained in routine shake flask fermentations. To the best of our knowledge, this is the first successful attempt to monitoring all three important process parameters in situ noninvasively with disposable noninvasive sensing patches in shake flasks.

Conclusions

Monitoring of shake flask fermentations using triple disposable noninvasive optical sensors was studied. The sensors are thin luminescent patches that can be affixed inside the flask. Small electronic devices for excitation and detection of the fluorescence are positioned outside the shake flask to noninvasively monitor the pH, dissolved oxygen, and CO_2 concentrations in situ. By measuring the process parameters throughout the course of the *E. coli* fermentations, we obtained information about the bioprocess that may not be obtained in routine shake flask fermentations. For instance, the pH of the culture can either remain relatively stable or change greatly depending on the fermentation conditions. For cultures with only a few millimeters liquid depth an oxygen limitation can occur at relatively low agitation speed. Under certain conditions oscillation can occur. An increase in shaker speed and a decrease in culture volume increase the oxygen availability and reduce the duration of oxygen limitation.

Acknowledgments

Unrestricted funding from Sartorius-Stedim Biotech is gratefully acknowledged. The authors dedicate this article to Professor Antonio Moreira for introducing them to the world of regulatory science.

Literature Cited

1. Dahlgren ME, Powell AL, Greasham RL, George HA. Development of scale-down techniques for investigation of recombinant *Escherichia coli* fermentations: acid metabolites in shake flasks and stirred bioreactors. *Biotechnol Prog*. 1993;9:580–586.
2. Visser W, Scheffers WA, Batenburg-van der Begte WH, van Dijken JP. Oxygen requirements of yeasts. *Appl Environ Microbiol*. 1990;56:3785–3792.
3. Tunac JB. High-aeration capacity shake-flask system. *J Ferment Eng*. 1989;68:157–159.
4. McDaniel LE, Bailey EG. Effect of shaking speed and type of closure on shake flask cultures. *Appl Microbiol*. 1969;17:286–290.
5. Schultz JS. Cotton closure as an aeration barrier in shaken flask fermentations. *Appl Microbiol*. 1964;12:305–310.
6. Gaden EL. Improved shaken flask performance. *Biotechnol Bioeng*. 1962;4:99–103.
7. Smith CG, Johnson MJ. Aeration requirements for the growth of aerobic microorganismms. *J Bacteriol*. 1954;68:346–350.
8. Vasala A, Panula J, Bollók M, Illmann L, Hälsig C, Neubauer P. A new wireless system for decentralized measurement of physiological parameters from shake flasks. *Microb Cell Fact.* 2006;5:8.
9. Phillip HH. Continuous monitoring of oxygen concentrations in air-purged shake-flask fermentations. *Appl Microbiol*. 1970;19:551–554.
10. Bambot SB, Holavanahali R, Lakowicz JR, Carter GM, Rao G. Phase fluorometric sterilizable optical oxygen sensor. *Biotechnol Bioeng*. 1994;43:1139–1145.
11. Sipior J, Bambot S, Romauld M, Carter GM, Lakowicz JR, Rao G. A lifetime-based optical CO_2 gas sensor with blue or red excitation and stokes or anti-stokes detection. *Anal Biochem*. 1995;227:309–318.
12. Bambot S, Holavanahali R, Lakowicz JR, Carter GM, Rao G. Optical oxygen sensor using fluorescence lifetime measurement. *Adv Exp Med Biol*. 1994;361:197–205.

13. Kermis HR, Kostov Y, Harms P, Rao G. Dual excitation ratiometric fluorescent pH sensor for noninvasive bioprocess monitoring: development and application. *Biotechnol Prog*. 2002;18: 1047–1053.
14. Kermis HR, Kostov Y, Rao G. Rapid method for the preparation of a robust optical pH sensor. *Analyst*. 2003;128:1181–1186.
15. Sipior J, Randers-Eichhorn L, Lakowicz JR, Carter GM, Rao G. Phase fluorometric optical carbon dioxide gas sensor for fermentation off-gas monitoring. *Biotechnol Prog*. 1996;12:266–271.
16. Chang Q, Randers-Eichhorn L, Lakowicz JR, Rao G. Steam-sterilizable, fluorescence lifetime-based sensing film for dissolved carbon dioxide. *Biotechnol Prog*. 1998;14:326–331.
17. Kostov Y, Harms P, Pilato RS, Rao G. Ratiometric oxygen sensing: detection of dual-emission ratio through a single emission filter. *Analyst*. 2000;125:1175–1178.
18. Kostov Y, Van Houten KA, Harms P, Pilato RS, Rao G. Unique oxygen analyzer combining a dual emission probe and a low-cost solid-state ratiometric fluorometer. *Appl Spectrosc*. 2000; 54:864–868.
19. Ge X, Kostov Y, Rao G. High-stability noninvasive autoclavable naked optical CO_2 sensor. *Biosens Bioelectron*. 2003;18:857–865.
20. Ge X, Kostov Y, Rao G. Low-cost noninvasive optical CO_2 sensing system for fermentation and cell culture. *Biotechnol Bioeng*. 2005;89:329–334.
21. Weigl BH, Holobar A, Trettnak W, Klimant I, Kraus H, O'Leary P, Wolfbeis OS. Optical triple sensor for measuring pH, oxygen and carbon dioxide. *J Biotechnol*. 1994;32:127–138.
22. Hanson MA, Ge X, Kostov Y, Brorson KA, Moreira AR, Rao G. Comparisons of optical pH and dissolved oxygen sensors with traditional electrochemical probes during mammalian cell culture. *Biotechnol Bioeng*. 2007;97:833–841.
23. Lakowicz JR. *Principles of Fluorescence Spectroscopy*, 2nd ed. New York: Kluwer Academic; 1999.
24. Harms P, Kostov Y, French JA, Soliman M, Anjanappa M, Ram A, Rao G. Design and performance of a 24-station high throughput microbioreactor. *Biotechnol Bioeng*. 2006;93:6–13.
25. Beuse M, Kopmann A, Diekmann H, Thoma M. Oxygen, pH value, and carbon source induced changes of the mode of oscillation in synchronous continuous culture of *Saccharomyces cerevisiae*. *Biotechnol Bioeng*. 1999;63:410–417.
26. Hjortso MA, Nielsen J. Population balance models of autonomous microbial oscillations. *J Biotechnol*. 1995;42:255–269.
27. Satroutdinov AD, Kuriyama H, Kobayashi H. Oscillatory metabolism of *Saccharomyces cerevisiae* in continuous culture. *FEMS Microbiol Lett*. 1992;77:261–267.
28. Xu Z, Tsurugi K. A potential mechanism of energy-metabolism oscillation in an aerobic chemostat culture of the yeast *Saccharomyces cerevisiae*. *FEBS J*. 2006;273:1696–1709.
29. Ahrens K, Menzel K, Zeng A, Deckwer W. Kinetic, dynamic, and pathway studies of glycerol metabolism by *Klebsiella pneumoniae* in anaerobic continuous culture: III. Enzymes and fluxes of glycerol dissimilation and 1,3-propanediol formation. *Biotechnol Bioeng*. 1998;59:544–552.
30. Anderson DC, Swartz J, Ryll T, Lin N, Snedecor B. Metabolic oscillations in an *Escherichia coli* fermentation. *Biotechnol Bioeng*. 2001;72:212–218.
31. Daugulis AJ, McLellan PJ, Li J. Experimental investigation and modeling of oscillatory behavior in the continuous culture of *Zymomonas mobilis*. *Biotechnol Bioeng*. 1997;56:99–105.
32. Menzel K, Zeng AP, Biebl H, Deckwer WD. Kinetic, dynamic, and pathway studies of glycerol metabolism by *Klebsiella pneumoniae* in anaerobic continuous culture: I. The phenomena and characterization of oscillation and hysteresis. *Biotechnol Bioeng*. 1996;52:549–560.
33. Zeng AP, Menzel K, Deckwer WD. Kinetic, dynamic, and pathway studies of glycerol metabolism by *Klebsiella pneumoniae* in anaerobic continuous culture: II. Analysis of metabolic rates and pathways under oscillation and steady-state conditions. *Biotechnol Bioeng*. 1996;52:561–571.

Manuscript received Oct. 29, 2011, and revision received Jan. 31, 2012.

Chapter Four: Minibioreactors

Instrumenting process scouting devices can clearly help understand the cellular environment while they are growing. But would it not be much better to replicate the actual environment present in the industry standard workhorse, the stirred tank bioreactor? It was this question that started the journey to figure out how to design a system that not only could be used to match, for example, the oxygen transfer characteristics of the bioreactor, but could also behave like one in miniature in terms of other parameters such as mixing time, shear stress experienced by cells etc.

The first paper describes how we converted a standard optical cuvette into a milliliter-scale bioreactor. This paper received the Gaden Award from Wiley in 2002 as the most influential paper published in Biotechnology & Bioengineering in 2001. The title perhaps should have used the word "minibioreactor" instead of "microbioreactor."

This technology also spurred the widespread use of miniature bioreactors. The current market leader is the AMBR system and uses single use minibioreactors that look similar to our very first system described in the paper that follows. Indeed, it appears that these words stated in the abstract written 20 years ago "*The low cost of the microbioreactor, detection system, and the small volume of the fermentation broth provide a basis for development of a multiple-bioreactor system for high-throughput bioprocess optimization*" proved to be prophetic!

Low-Cost Microbioreactor for High-Throughput Bioprocessing

Yordan Kostov, Peter Harms, Lisa Randers-Eichhorn, Govind Rao

Department of Chemical and Biochemical Engineering, University of Maryland Baltimore County, Baltimore, Maryland 21250; telephone: (410) 455-3415; fax: (410) 455-1049; E-mail: grao@umbc.edu and Medical Biotechnology Center, University of Maryland Biotechnology Institute, Baltimore, Maryland 21201-1503

Received 1 July 2000; accepted 17 October 2000

Abstract: The design of a microbioreactor is described. An optical sensing system was used for continuous measurements of pH, dissolved oxygen, and optical density in a 2 mL working volume. The K_La of the microbioreactor was evaluated under different conditions. An *Escherichia coli* fermentation in both the microbioreactor and a standard 1 L bioreactor showed similar pH, dissolved oxygen, and optical density profiles.

The low cost of the microbioreactor, detection system, and the small volume of the fermentation broth provide a basis for development of a multiple-bioreactor system for high-throughput bioprocess optimization. © 2001 John Wiley & Sons, Inc. *Biotechnol Bioeng* **72**: 346–352, 2001.
Keywords: microbioreactor; optical sensing; fermentation

INTRODUCTION

The human genome sequence is complete. While the sequencing of the human genome has been a mammoth task, many have pointed out that this effort pales in comparison to what lies ahead. The next step is to identify what turns these genes on and what proteins they express. Fermentation and cell culture will play a critical role in elucidating these factors. The method of choice to produce proteins is by cloning and expression in a suitable host and optimizing its production in a bioreactor. Assuming there are 50–100,000 human genes, these will first have to be cloned into various hosts (*E. coli*, yeast, CHO, BHK, and other workhorses). Then an enormous permutation of culture conditions will have to be evaluated to identify critical factors that turn these genes on. Following this, the identity of the proteins produced will have to be determined. Clearly, the ability to culture cells in controlled environments is crucial to this venture. The heart of any fermentation/cell culture (bioprocess) operation is an instrumented bioreactor capable of pH, temperature, and dissolved oxygen measurement and control. Bioprocess development is currently hampered by a paucity of high-throughput techniques to evaluate the effect of operational/nutritional parameters on cell growth and product formation in a systematic and statistically significant manner. Currently available instrumented bioreactors are expensive and bulky, thus making bioprocess development inefficient as large numbers of simultaneous experiments simply cannot be conducted. Recent advances in optical sensor technology provide a possible solution.

Traditionally, bioprocess technology has been critical to the development and availability of new drugs and vaccines. Additionally, bioprocesses are important in a wide variety of industries besides pharmaceuticals—food industry, ecology, water treatment, etc. (Arroyo et al., 2000; Bakoyianis and Koutinas, 1996; Bylund et al., 2000; Handa-Corrigan et al., 2000; López-López et al., 1999; McIntyre et al., 1999; Pressman et al., 1999; Yang et al., 2000). For bioprocess optimization in the pharmaceutical industry, significant numbers of fermentations are needed under varying environmental and nutritional conditions. This is expensive and time-consuming in practice, as this type of research is typically performed in shake flasks (with practically no control of the bioprocess parameters) or in small (1–3 L) bioreactors (Tholudur et al., 1999). In order to decrease the number of experiments required for optimization, mathematical modeling of the bioprocess is used (Alvarez-Ramirez et al., 1999; Boon et al., 1999; Cooney et al., 1999; Tholudur et al., 1999). However, this approach also requires a significant number of fermentations for establishing process parameters. It is sobering to contemplate the fact that bioreactor technology has changed little since the first successful bioproduct—penicillin. All the cell culture drugs approved to date (e.g., insulin, tPA, erythropoeitin, monoclonals, interferon, etc.) are based on bioreactor production. These were based on, at most, a few known genes. The task of going after several thousand target genes based on the human genome is truly staggering.

Thus a technology for fast, reliable, and inexpensive parallel bioprocessing is strongly desirable. One possible solution is to try to scaledown the volume of the bioreactor while preserving its control capabilities. Plate readers offer the opportunity for studies of parallel bioprocesses (Li et al., 2000), but they can read one or two parameters (absorbance

Correspondence to: Dr. Govind Rao
Contract grant sponsors: Genentech, Merck, and Pfizer.

and/or fluorescence) and are not equipped with chemical sensors or actuators for bioprocess control.

A key requirement for any bioprocess is the ability to measure process parameters, as well as to supply nutrients, oxygen, and pH correctors. Typically, pH, dissolved oxygen (DO), and optical density (OD) are monitored continuously. In small volumes (1–2 mL or less) it is difficult (or impossible) to use standard industrial probes because of their dimensions. There are miniaturized versions of these sensors (Liu and Neuman, 1982; Suzuki et al., 1991; Zhong et al., 1992) but their fabrication is rather sophisticated and they are expensive. Another problem is the fact that standard Clark-type oxygen probes consume oxygen (Lee and Tsao, 1979). In small volumes they will compete with respiring cells and distort the measurements.

One option for overcoming these problems is to use the emerging technology of optical chemical sensing (Bambot et al., 1994; Randers-Eichhorn et al., 1997; Xu et al., 1998). As these sensors are typically based on equilibrium principles, they do not interfere with the measured process. Their physical dimensions could be very small. Last, but not least, the cost of the measuring equipment (readout devices) is very low (Kostov et al., 1998, 2000) and the sensors themselves are sufficiently inexpensive to be disposable.

In this work, we describe an approach for scaling *down* the working volume of the bioreactor to 2 mL. The design and evaluation of the performance of the microbioreactor are presented. Three parameters—pH, DO, and OD—were continuously measured by means of optical sensors. A test fermentation was performed in the microbioreactor and the results were compared with those from a fermentation in a standard 1-L bioreactor. The results provide a basis for the development of highly parallel bioprocessing that can be successfully performed and monitored in small volumes.

MATERIALS AND METHODS

pH Measuring Channel

The excitation of the dye was performed consecutively by two light-emitting diodes (LEDs): blue LNG992CFBW (Panasonic, Secaucus, NJ), and UV NSHU590E (Nichia America, Mountville, PA). The emission of the blue LED was filtered with a 460 ± 15 nm bandpass filter (12.5 mm diameter); the UV LED was used without filtering. The fluorescence emission was observed by a large active area PIN photodiode S1223-01 (Hamamatsu, Bridgewater, NJ) through a 520 ± 5 nm interference filter. The filters used in all channels were from Intor (Sorocco, NM). The photodiode current was converted to voltage and amplified by transimpedance and lock-in amplifiers made in-house. The design of the amplifiers is described elsewhere (Kostov et al., 2000). The LEDs were switched on and off by transistor switches. LED control and the measurement of the output signal from the lock-in amplifier were done by the ADC/DAC board (described below). Calibration of the channel was performed using media with the dissolved indicator. The pH of the solution for the calibration was adjusted by titration with 1 M HCl or NaOH.

DO Measuring Channel

For excitation of the O_2 patch, a second blue LED was used. Its emission was also filtered with a 460 ± 15 nm filter. The detection of the emission from the sensor was performed by an avalanche photodiode module C5460 (Hamamatsu, Bridgewater, NJ) with a mounted 590 ± 20 nm bandpass interference filter. Additionally, the channel uses the red LED from the optical density channel as a reference for determination of the phase delays associated with the electronics. The phase measurements were made using an SR844 RF lock-in amplifier (Stanford Research Systems, Sunnyvale, CA). The output of the SR844 was measured by the ADC board. The LEDs were controlled by a special transistor driver.

The calibration curve was obtained by blending a controlled flow of air (supplied by an aquarium air pump) and pressurized nitrogen (Airgas Mid-Atlantic, Baltimore, MD). The percentage of oxygen was calculated as a function of the gas flow.

OD Measuring Channel

The optical density channel consisted of a red ultrabright LED LTL 4268 UR (Lite-on, Milpitas, CA) and photodiode detector (PIN photodiode coupled to transimpedance amplifier). An interference filter 600 ± 5 nm was positioned in front of the photodiode. The LED and the detector were placed on opposite sides of the cuvette, as shown in Figure 1. The output signal was measured directly from the ADC board. Calibration of the channel was performed using the seed culture. Out-of-calibration data were calculated using linear extrapolation.

Data Collection System

The data collection system recorded four parameters: intensities of HPTS fluorescence under UV and blue excitation, phase shift of the O_2 sensor fluorescence, and the intensity of the light transmitted through the media at 600 nm. The sensors are controlled and monitored by a 166 MHz Pentium computer equipped with a National Instruments PCI-6111E multiple input/output card. A program was written in Labview that sequentially enables each channel and measures the output of the sensor. The 370 nm LED is turned on and after a few seconds 500 intensity measurements are acquired in 5 sec and averaged. The 370 nm LED is turned off and the process is repeated for the 460 nm measurement of pH. For optical density, the ambient light is measured 1,000 times in 10 ms. The red LED is turned on and another 1,000 points are taken almost immediately. The red LED is then turned off and another 1,000 ambient light readings are

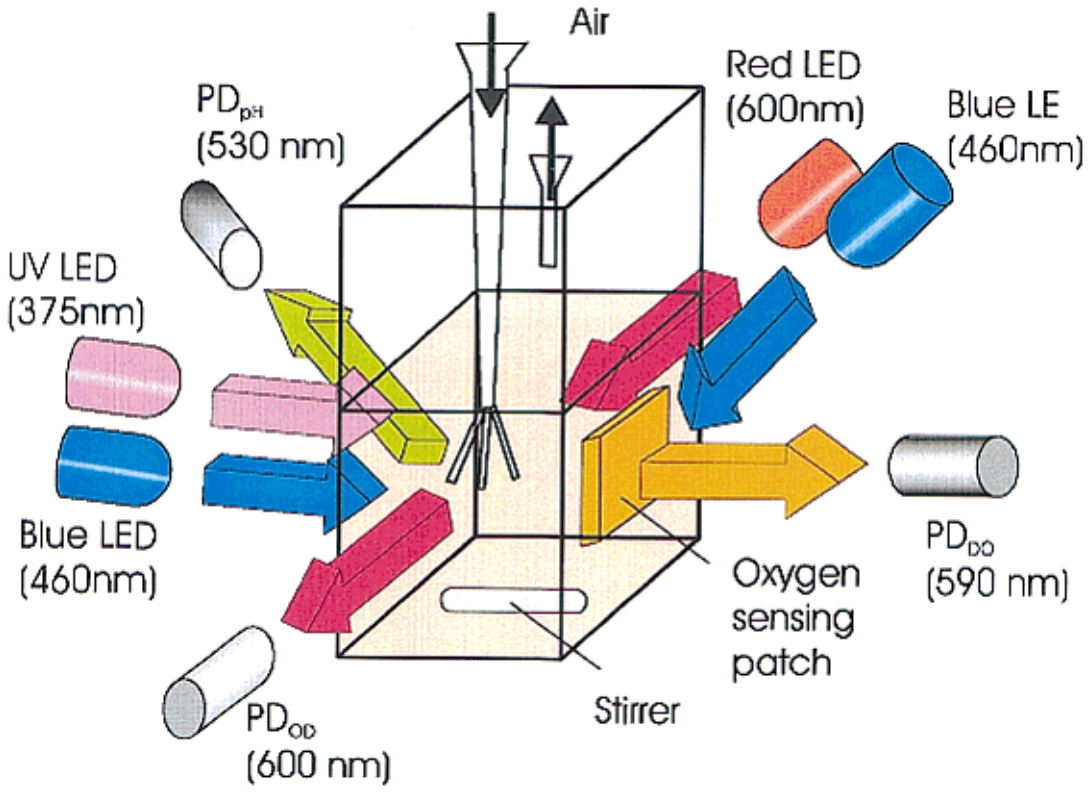

Figure 1. Cuvette-based microbioreactor. At the left cuvette wall, blue and UV LED together with 530 nm photodetector are used to measure pH; at the right cuvette wall, blue LED, oxygen sensing patch, and 590 nm photodetector are used to measure dissolved oxygen; red LED and 600 nm photodetector are used to measure optical density through the front and back wall. The air supply inlet and outlet are positioned at the corners of the cuvette. LEDs are fired in succession to prevent crosstalk (for clarity, figure not to scale).

taken. The process is repeated if the standard error is too high or if the ambient light measurements are substantially different. Dissolved oxygen is measured by turning on the blue LED, waiting 5 sec, and acquiring 100 phase measurements over 2 sec. Each measurement cycle takes just under 45 sec.

Fermentation in a 1-L Fermentor

The overnight seed culture consisted of a 0.5% inoculum of *Escherichia coli* strain JM105 frozen stock in LB media (10 g/L NaCl, 10 g/L tryptone, 5 g/L yeast extract, pH 7.2) incubated at 30°C with shaking at 260 rpm (model G24, New Brunswick Scientific, Edison, NJ). Fermentations were carried out in a New Brunswick BioFlo III fermentor containing 1 L buffered LB (10 g/L NaCl, 10 g/L tryptone, 5 g/L yeast extract, 4 g/L K_2HPO_4, 0.5 g/L KH_2PO_4, pH 7.2) and 15 mL of 0.15 g/L sterilized solution of HPTS in deionized water. The fermentor was inoculated with 10% seed culture. Aeration, agitation, and temperature were controlled at 1 vvm, 300 rpm, and 25°C, respectively. Dissolved oxygen and pH were not controlled. Data of continuous readings were logged every 20 sec on a Mac II computer using a Strawberry Tree data acquisition system and Workbench software (Strawberry Tree, Sunnyvale, CA).

Optical density values representative of the bacterial growth were measured offline with a Hewlett-Packard 8452A Diode Array spectrophotometer at 600 nm.

Fermentation in the Cuvette

The cuvette and the oxygen sensing film were sterilized with 70% ethanol for 5 min. The cap with mounted inlet, outlet, and tubing was heat-sterilized. The sensing film was attached to the wall with sterilized grease to fit in the window in the black tape and the cuvette was sterilized again with ethanol. 2.25 mL of the same buffered LB media, 0.25 ml of the same seed culture, and 37.7 μL of 0.15 g/L sterilized solution of HPTS in deionized water were added and the cap was attached. The assembly was performed in a laminar flow hood. The assembled microbioreactor was transferred into the holder with the sensing system. Aeration and agitation were controlled at 2 vvm and 300 rpm, respectively. The fermentation was performed at room temperature of 25°C.

RESULTS AND DISCUSSION

Microbioreactor Design

The working vessel was a disposable polystyrene cuvette, 1 × 1 cm, with a total volume of 4 mL. To avoid contamina-

tion during the process, it was equipped with a silicone rubber cap. The cap had an inlet for air delivery and outlet for the exhaust air. They were positioned at the corners of the cuvette to avoid overlapping with the optical path for optical density measurements. The inlet was connected to an air sparger (Fig. 1). It was fabricated from a 100 mL plastic pipette tip. Three tubes with inner diameters of 0.25 mm were positioned at the end of the tip. The tubes were glued using epoxy resin. The outlet consisted of a short piece of a 16-gauge syringe needle. The air was supplied by an aquarium pump, passed through a regulator for low gas flow rates and filtered using a syringe filter (Millex-GV, 0.22 μm; Millipore, Bedford, MA). Stirring was executed by a small magnetic stir bar and magnetic stirrer. The K_La of the cuvette was adjusted to be approximately equal to the K_La of the 1-L fermentor operated at 300 rpm agitation and 1 vvm aeration (21 h^{-1}).

Positioning of the Measuring System

The cuvette was large enough to accommodate the required optics and electronics and no optical fibers were needed. The use of conventional optics allowed for increased signal levels, as practically all the excitation light is coupled to the sensors. All solid-state light sources and detectors, low-cost optical filters. and electronics were used. As some of the components (especially the filters) were bigger than the cuvette wall, more attention was paid to the proper spatial placement of the optical modules around the cuvette in order to avoid crosstalk between the channels. The positioning of the basic components for each channel is also shown in Figure 1.

pH Measurements

The pH measurements were performed using a ratiometric pH-sensitive dye: 1-hydroxypyrene-3,5,7-sulfonic acid, (HPTS; Sigma, St. Louis, MO), pKa = 7.2. A sterilized solution of HPTS was directly introduced into the culture media. Front-face geometry was used for fluorescence detection (Fig. 2A). The dye has two excitation peaks, 400 and 450 nm. When excited at these wavelengths, the ratio of the fluorescence emissions at 520 nm of the dye depends on pH. The ratiometric approach avoids interference from turbidity changes during the process and provides accurate measurements of pH. The longer wavelength is easily excitable using a blue LED; however, until recently there were no UV LEDs, which precluded the use of this indicator in low-cost systems. The pKa of HPTS (7.2) makes it appropriate for use with neutral-range bioprocesses. HPTS is a nontoxic indicator, used for blood gas measurements in vivo (Zhang et al., 1995). Its addition to the media did not influence cell growth. The calibration curve of the pH channel is shown in Figure 3A. The pH was calibrated by measuring the intensity ratio of the solution as the pH was changed and verified on a benchtop pH meter. The use of semiconductor light sources and detectors allowed us to design a very compact and low-cost detection system. To our knowledge, this is the first all-solid-state ratiometric instrument that operates in the UV/blue range.

One possible problem for future applications could be the range of the emission spectrum of HPTS—its emission maximum is positioned at 520 nm. With increased use of GFP (which possesses a very similar emission spectrum) for product quantification, it could be desirable to use pH sen-

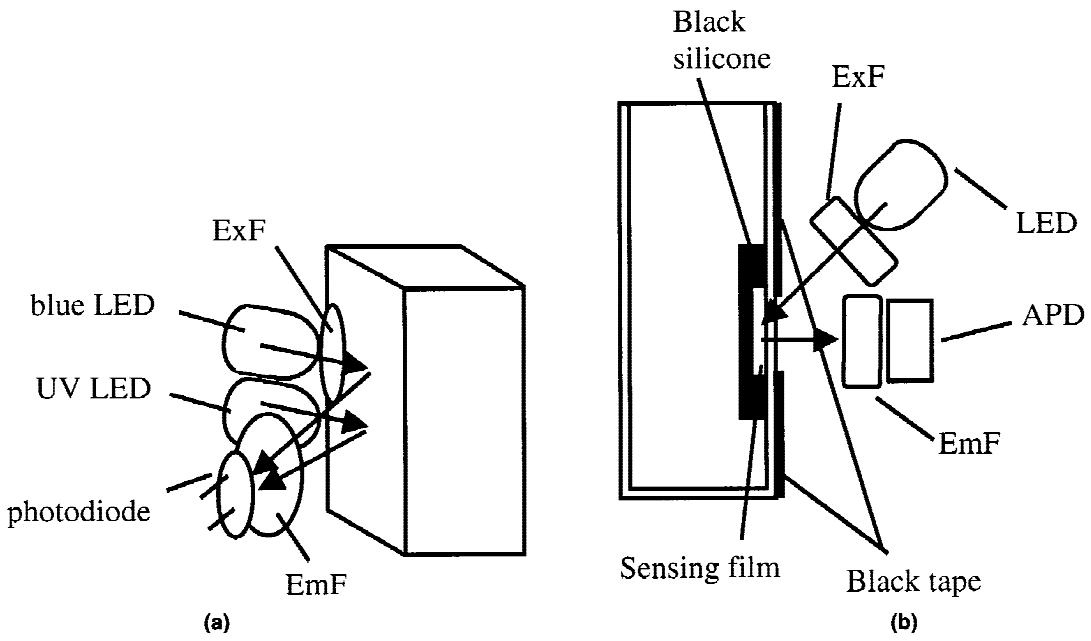

Figure 2. **a**: Optical configuration of the pH channel. **b**: Optical configuration of the oxygen sensing channel. LED — light emitting diode; APD — avalanche photodiode module; ExF — excitation filter; EmF — emission filter (for clarity, figure not to scale).

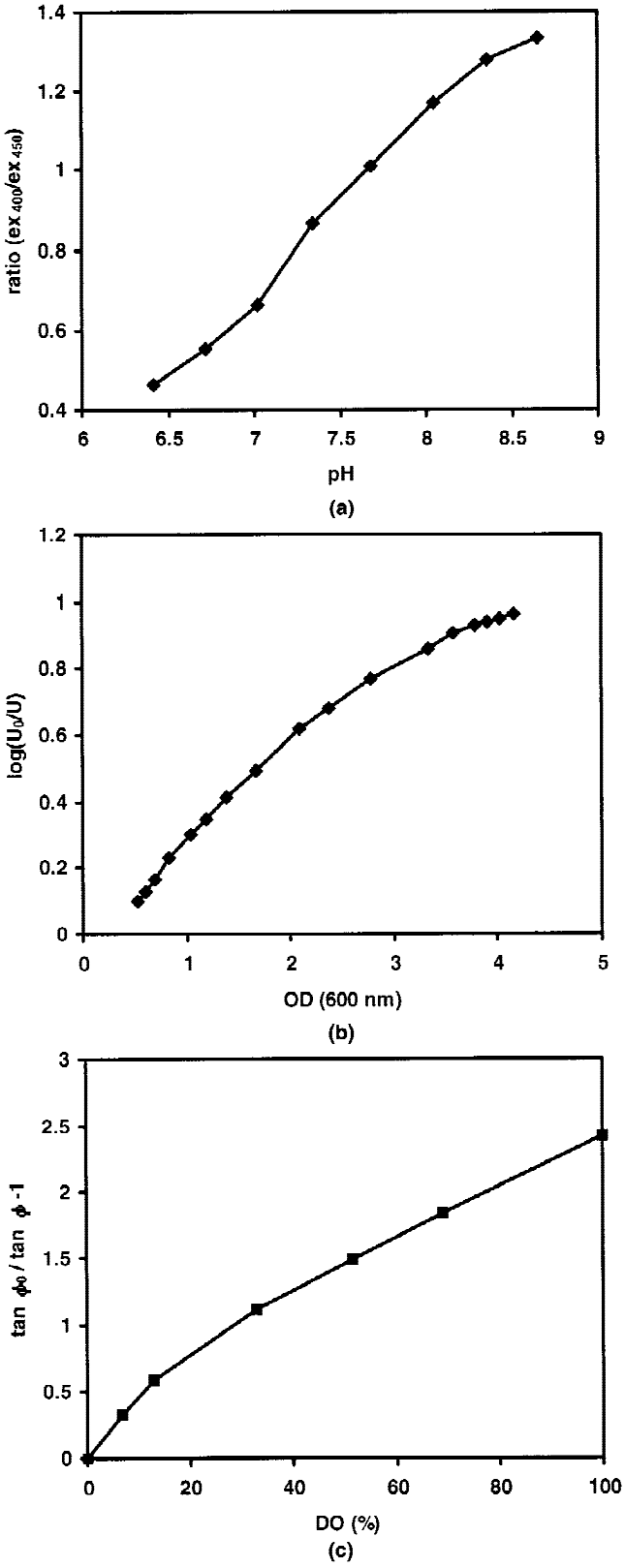

Figure 3. Calibration curves of the channels. **A**: pH channel. **B**: OD channel. **C**: DO channel.

sitive dyes that emit at longer wavelengths. While the approach of adding indicator directly to the culture medium worked for our proof-of-principle purposes, it is undesirable for long-term use. An immobilized indicator would be preferable for reasons of improved optical isolation, as well as eliminating undesirable interactions with growth medium components and/or cells.

OD Measurements

The OD channel was realized using the simplest possible means. The absorbance of the cell suspension was directly measured using a 600-nm LED. Its calibration curve is shown in Figure 3B. As expected, it does not follow Beer's law, and the sensitivity rapidly decreases with the increase in OD. The highest measurable optical density is limited by the noise of the photodetector. For this particular setup the maximum OD detected was approximately 9 (results not shown).

To ensure that pH and OD did not affect each other, their values were verified by offline measurements in the beginning and at the end of the process. The results are shown on the respective figures (Fig. 4A,C) with pH and OD profiles. Offline pH and OD values agreed very well with their online ones and demonstrate stable operation (no drift) over the period of operation.

DO Measurements

The DO channel was positioned on the opposite wall of the cuvette to the pH channel. It uses a ruthenium-based oxygen sensor, Ru(diphenylphenanthroline)$_3^{2+}$ immobilized in silicone rubber (Bambot et al., 1994). The optical configuration of the components is shown in Figure 2B. This silicone film was attached to the cuvette wall using silicone grease (high-vacuum grease; Dow Corning, Midland, MI). This successfully prevents the sensor patch from peeling off the wall and penetration of media between the film and the photodetector. The patch was covered by a layer of black silicone (GE 312A; General Electric, Waterford, NY) for optical isolation from the fermentation media. The wall of the cuvette was covered with black tape (with a window for the sensor) to prevent excitation of the media.

Oxygen detection was performed using frequency domain detection of ruthenium fluorophore lifetime. In this technique, the excitation light is modulated and the lifetime is measured by determination of the phase shift between excitation light and fluorescence emission. This is a well-established method for oxygen detection (Bambot et al., 1994) and relies on the reversible quenching of fluorescence emission due to oxygen binding. Its greatest advantage is the fact that the measurements are equilibrium based and do not consume oxygen. Calibration was achieved by using an air-nitrogen blending setup and recording the phase shift going from nitrogen to air. The calibration curve of the device is presented in Figure 3C.

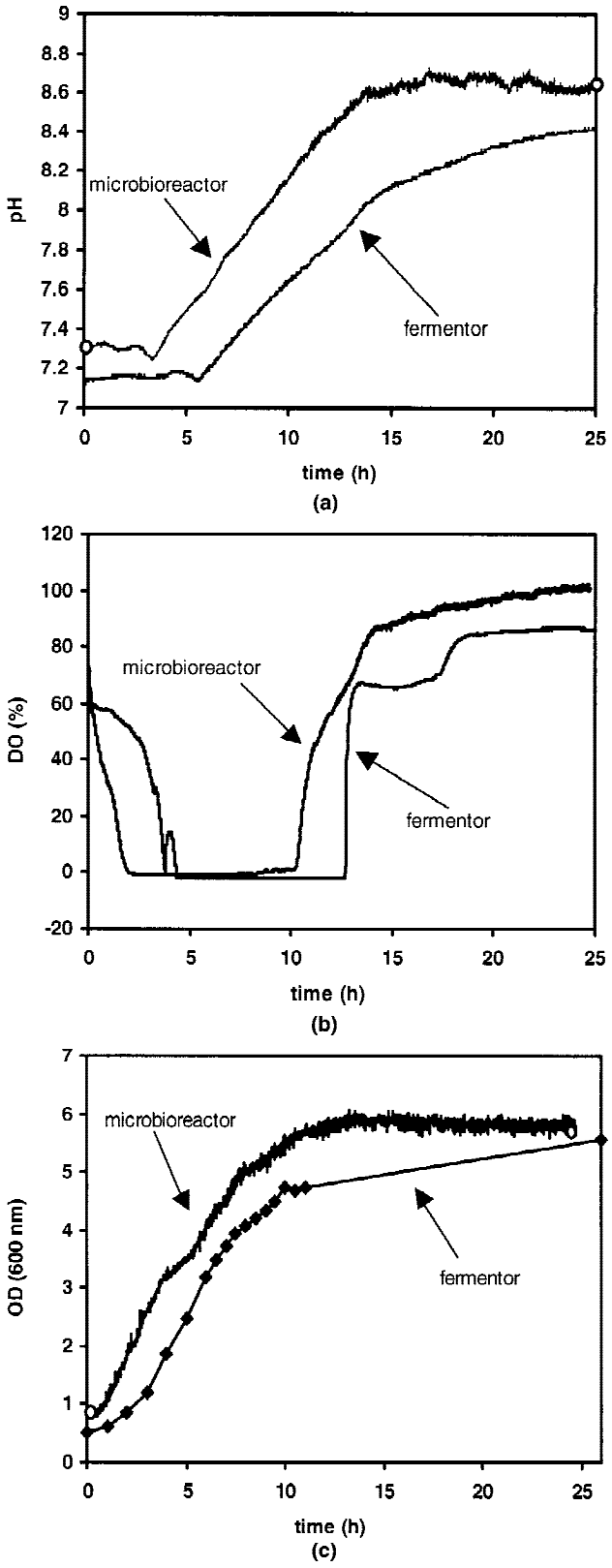

Figure 4. Time profiles of microbioreactor variables and comparison with a standard 1-L bioreactor. **A**: pH profiles. The circles in the beginning and at the end represent the pH values measured with a standard pH meter. **B**: DO profiles. **C**: OD profiles. The circles in the beginning and at the end of the process represent the values measured by spectrophotometer after dilution.

The increased thickness of the sensor resulted in an increased response time of the sensor—up to 2 min. While this is not a problem for bioprocess measurements, it created problems in measurements of the K_La. For this reason, K_La was determined using a sensor without the protective layer with a much shorter response time of 20 sec.

Preserving the value of K_La is a particular problem when scaling a bioprocess (up or down). In our case, it was determined that matching the air flow and the stirring rate resulted in K_La values that were substantially lower than the values obtained in the 1-L bioreactor ($K_La = 9.8\ h^{-1}$ in the microbioreactor; $21\ h^{-1}$ in the 1-L bioreactor). Furthermore, variation of the stirring rate had very little effect on K_La. One possible explanation of this finding is the difference in the positioning of the sparger and the stirrer. In a normal bioreactor, the stirrer is positioned in the escape path of the air bubbles. Stirring adds a significant horizontal component to their trajectory, increasing the total time of their presence in the solution. This effect is much less pronounced when the stirrer is below the sparger.

Another option for K_La variation is changing the air flow rate. The transfer coefficient of the microbioreactor was determined at 1, 2, and 3 vvm. K_La was $9.8\ h^{-1}$, $27.5\ h^{-1}$, and $44.4\ h^{-1}$, respectively. Transfer coefficients of the microbioreactor and the bioreactor were very close at an air flow rate of 2 vvm in the microbioreactor.

An additional advantage of the ruthenium complex is its long lifetime (microseconds)—this permits low frequency modulation (76 kHz in this case) which reduces the circuit cost to $100 or so. In contrast, short lifetime (tens of nanoseconds) fluorophores demand high-frequency modulation (tens to hundreds of MHz), where costs and complexity rise by an order of magnitude or more.

Microbioreactor Performance

The performance of the microbioreactor was finally tested by parallel fermentations of *E. coli* in the microbioreactor and a 1-L Bioflo III (New Brunswick Scientific) fermentor. Both were inoculated at the same time from the same seed culture after setting them to run under identical K_La—the fermentor was run at 300 rpm and 1 vvm aeration ($21\ h^{-1}$). This K_La was arbitrarily chosen as agitation/aeration above this level led to foaming in the microbioreactor. Clearly, this was more due to the ad hoc fabrication of the aeration system and an inefficient magnetic stir-bar served as the agitator. As mentioned above, oxygen delivery to a growing culture is the most critical parameter in bioreactor operation—this is largely due to the extremely poor solubility of oxygen in an aqueous phase (8 mg/L at 35°C in distilled water). Comparing the performance of two bioreactors (say, during scale-up) requires that all parameters be identical, especially the K_La, since a process with a higher K_La will invariably result in higher cell density due to greater oxygen availability. Comparison of the resulting profiles is shown in Figure 4. As can be seen, the profiles of pH, dissolved oxygen, and optical density are very similar in both pro-

cesses. The patterns of oxygen depletion during the exponential growth, as well as the recovery of the dissolved oxygen to 100% at the end of the process, are similar and reproducible in both cases. The correlation coefficient between the OD of the two fermentations was 0.984, indicating very similar growth profiles in the two cultures. However, all the specific points of the microbioreactor process occurred approximately 2 h earlier. Additional investigation showed that after 1 h of operation the microbioreactor heated up by approximately 3°C above the ambient temperature due to Joule heating (the cuvette was not equipped for temperature control). Thus, while the cells in the 1-L bioreactor were cultivated at 25°C, the microbioreactor process was at 28°C. Since the optimal growth temperature for *E. coli* is 37°C, the temperature elevation may explain the slightly increased cell growth rate and decreased lag time in the microbioreactor. One solution to the problem would be the use of a small thermoelectric device for temperature control.

This work has shown that a bioprocess could be successfully performed and followed in small volumes. The use of semiconductor light sources and detectors allowed us to design a very compact and low-cost detection system. All the parts used and the circuit components necessary to obtain a signal were obtained for a cost of less than $400. In the near future, we intend to develop feedback loops for temperature and air-flow control, use an immobilized pH indicator, and select an appropriate indicator with wavelengths that are different from GFP, so that it will be possible to simultaneously measure the cell mass and the product.

The sensors and actuators used allow for an even further decrease of the reactor volume.

Given the low cost of the detection system used (<$400), as well as the small volumes of the bioprocess, it seems possible to develop a system where many bioprocesses (96 or more) could be run in parallel for lower cost than one bench-scale bioreactor. This will greatly reduce both the cost and the development time for optimizing new or established bioprocesses and lead to high-throughput bioprocessing. In addition, it could dramatically improve microbial isolation and cultivation of new species, as enormous numbers of experimental conditions could be attempted on a massively parallel scale.

This work was supported by unrestricted gifts from Genentech, Merck, and Pfizer to Dr. Rao. Peter Harms was supported by an NSF graduate fellowship.

References

Alvarez-Ramirez J, Meraz M, Monroy O. 1999. Mathematical analysis of proportional-integral control for fixed bed bioreactors. J Chem Technol Biotechnol 74:78–84.

Arroyo M, Torres-Guzmán R, de la Mata I, Castillón MP, Acebal C. 2000. Activation and stabilization of penicillin V acylase from Streptomyces lavendulae in the presence of glycerol and glycols. Biotechnol Prog 16:368–371.

Bakoyianis V, Koutinas AA. 1996. A catalytic multistage fixed-bed tower bioreactor in an industrial-scale pilot plant for alcohol production. Biotechnol Bioeng 49:197–203.

Bambot SB, Holavanhali R, Lakowicz JR, Carter GM, Rao G. 1994. Phase fluorimetric sterilizable optical oxygen sensor. Biotechnol Bioeng 43: 1139–1145.

Boon MA, Janssen AEM, van der Padt A. 1999. Modelling and parameter estimation of the enzymatic synthesis of oligosaccharides by β-galactosidase from Bacillus circulans. Biotechnol Bioeng 64:558–567.

Bylund F, Castan A, Mikkola R, Veide A, Larsson G. 2000. Influence of scale-up on the quality of recombinant human growth hormone. Biotechnol Bioeng 69:119–128.

Cooney MJ, Goh LT, Lee PL, Johns MR. 1999. Structured model-based analysis and control of the hyaluronic acid fermentation by Streptococcus zooepidemicus: physiological implications of glucose and complex-nitrogen-limited growth. Biotechnol Prog 15:898–910.

Handa-Corrigan A, Hayavi S, Ghebeh H, Mussa NA, Chadd M. 1998. Novel porous matrix and bioreactors for high density cultures of insulinoma cell lines: insulin secretion and response to glucose. J Chem Technol Biotechnol 71:51–56.

Kostov Y, Comte A, Scheper T. 1998. Solid state luminescence phase-shift oxygen sensor for biotechnology. Chem Biochem Eng Q 12:201–205.

Kostov Y, Albano CR, Rao G. 2000. All solid state GFP sensor. Biotechnol Bioeng 70:473–477.

Lee YH, Tsao GT. 1979. Dissolved oxygen electrodes. In: Ghose TK, Fiechter A, Blackebrough N, editors. Advances in biochemical engineering. Berlin: Springer-Verlag. p 35.

Li J, Wang S, VanDusen WJ, Schultz HA, Herber WK, Chae HJ, Bentley WE, Rao G. 2000. Green fluorescent protein in *Saccharomyces cerevisiae*: real time studies of the *GAL1* promotor. Biotechnol Bioeng 70:187–196.

Liu CC, Neuman MR. 1982. Fabrication of miniature pO_2 and pH sensors using microelectronic techniques. Diabetes Care 5:275–277.

López-López A, Expósito E, Antón J, Rodríguez-Valera F, Aldaz A. 1999. Use of Thiobacillus ferrooxidans in a coupled microbiological-electrochemical system for wastewater detoxification. Biotechnol Bioeng 63:79–86.

McIntyre JJ, Bunch AW, Bull AT. 1999. Vancomycin production is enhanced in chemostat culture with biomass-recycle. Biotechnol Bioeng 62:576–582.

Pressman JG, Georgiou G, Speitel GE Jr. 1999. Demonstration of efficient trichloroethylene biodegradation in a hollow-fiber membrane bioreactor. Biotechnol Bioeng 62:681–692.

Randers-Eichhorn L, Albano CR, Sipior J, Bentley WE, Rao G. 1997. On-line green fluorescent protein sensor with LED excitation. Biotechnol Bioeng 55:921–926.

Suzuki H, Sugama A, Kojima N, Takei F, Ikegami K. 1991. A miniature Clark-type oxygen electrode using a polyelectrolyte and its application as a glucose sensor. Biosens Bioelectron 6:395–400.

Tholudur A, Ramirez WF, McMillan JD. 1999. Mathematical modeling and optimization of cellulase protein production using Trichoderma reesei RL-P37. Biotechnol Bioeng 66:1–16.

Xu Z, Rollins A, Alcala R, Marchant RE. 1998. A novel fiber optic pH sensor incorporating carboxy SNAFL-2 and fluorescent wavelength-ratiometric detection. J Biomed Mater Res 39:9–15.

Yang J-D, Angelillo Y, Chaudhry M, Goldenberg C, Goldenberg DM. 2000. Achievement of high cell density and high antibody productivity by a controlled-fed perfusion bioreactor process. Biotechnol Bioeng 69:74–82.

Zhang S, Tanaka S, Wickramasinghe TABD, Rolfe P. 1995. Fiber-optical sensor based on fluorescent indicator for monitoring of physiological pH values. Med Biol Eng Comput 33:152–156.

Zhong L, Han J, Li G, Cui D, Fan J, Yang X. 1992. Miniature urea sensor based on H(+)-ion sensitive field effect transistor and its application in clinical analysis. Chin J Biotechnol 8:57–65.

I was not happy with the fact that although a successful demonstration in terms of the identical fermentation behavior at the liter and milliliter scale, the microbioreactor looked like a cuvette. Surely we could do better? And could we have some more working volume so that the system could be sampled? The next few papers show how we achieved these goals and importantly, also show that from the cells' point of view, their productivities change if they are selected from a well-plate versus a stirred tank design. And if their ultimate use in production is in a stirred tank, we felt that the minibioreactor should in fact be engineered to perform exactly like a lab- and large scale one. This is pretty much the standard around which process development labs in industry use, where a laboratory scale 1-10 liter bioreactor used to replicate the environment and operating conditions at the pilot and manufacturing scale (100-1000s of liter volumes).

However, in order to achieve this, the hydrodynamics of larger scale bioreactors needed to be replicated at the small scale. We had available a novel confocal sensor that could accurately make non-invasive measurements of fluorescent tracers at a single point in space (https://doi.org/10.1021/bp050117x). Using this tool, and with my colleague Mark Marten's help along with two enterprising undergraduates Joey French and Arun Ram, we were able to show that a 12.5 mL bioreactor could in fact replicate mixing seen in large scale bioreactors.

Optical Analysis of Liquid Mixing in a Minibioreactor

Jose R. Vallejos,[1] Yordan Kostov,[1] Arun Ram,[2] Joseph A. French,[3] Mark R. Marten,[1] Govind Rao[1]

[1]Center for Advanced Sensor Technology, Department of Chemical and Biochemical Engineering. University of Maryland at Baltimore County, Baltimore, Maryland 21250; telephone: (410)-455-3400; fax: (410) 455-1049; e-mail: grao@umbc.edu
[2]Department of Computer Science and Electrical Engineering, University of Maryland at Baltimore County, Baltimore, Maryland
[3]Department of Physics, University of Maryland at Baltimore County, Baltimore, Maryland

Received 27 June 2005; accepted 24 October 2005

Published online 29 November 2005 in Wiley InterScience (www.interscience.wiley.com). DOI: 10.1002/bit.20785

Abstract: A novel optical sensor was used to study mixing and mean circulation time in a model minibioreactor (12.5 mL stirred vessel, equipped with a paddle impeller). Rotational rates in the range of 10–1,000 rpm corresponding to Reynolds number between 14 and 1,350 were studied. Results suggest that depending on the impeller rotational speed, mixing times up to 214 ± 87 s can be reproducibly achieved. The minibioreactor was operated in the transitional regime, and it was determined that the non-dimensional form for mixing time, $N\Theta_M$ was linearly dependent on Reynolds number. A linear correlation between mean circulation time and the inverse of rotational speed was also determined. The mean circulation time dependence on rotational speed in the 12.5 mL stirred vessel is similar to those found in large-scale stirred vessels. These results suggest that mixing and circulation times found in large-scale reactors can be replicated in minibioreactors. © 2005 Wiley Periodicals, Inc.

Keywords: mixing; minibioreactor; high throughput; bioprocessing; scale up

INTRODUCTION

Minibioreactors designed for use in the pharmaceutical industry have the potential to both increase process development rates and to reduce costs (Lye et al., 2003). If these benefits are achieved in the early stages of drug discovery (i.e., during screening and development phases), they have the potential to significantly reduce overall product development cost. To date, a number of mini- and microbioreactors have been described in the literature. For example, Kostov et al. (2001) described a 2 mL working volume cuvette-based microbioreactor equipped with pH, dissolved oxygen, optical density sensors for continuous measurement of process variables. Maharbiz et al. (2004) described an array of eight 250 μL reactors capable of temperature and pH control and as well as optical density measurement. Zanzotto et al. (2004) used a microbioreactor with volumes in the range of 5–50 μL with integrated sensors for online measurement of optical density, dissolved oxygen, and pH during growth of *Escherichia coli*. Elmahdi et al. (2003) measured pH during microscale fermentation by inserting a micro-pH probe into a 7 mL well in a microtiter plate. Finally, Doig et al. (2005) used three different microplates (24, 96, and 384 wells) with working volumes between 65 and 1,182 μL to measure $k_L a$ during growth of *Bacillus subtilis.*

With the development of these miniaturized bioreactors, numerous questions regarding mixing at small scales emerge. For example, is mixing behavior in small-scale stirred vessels similar to that in large-scale stirred vessels? What roles do convection, diffusion, and eddy scales play during mixing processes in microbioreactors? Is it reasonable to expect large circulation times in small-scale stirred vessels? To date, the study of mixing and flow in minibioreactors has primarily been conducted using computational fluid dynamic (CFD) simulations (Lamping et al., 2003), and relatively few experimental studies have been carried out.

In contrast, mixing and hydrodynamics have been studied extensively at lab and large scale (Barneveld et al., 1987; Bittorf and Kresta, 2000; Hall et al., 2004; Nere et al., 2003). As a measure of overall degree of bioreactor agitation, a number of authors have used mixing time (Marten et al., 1997; Papagianni et al., 2003; Vasconcelos et al., 1995) or the time required to reach homogeneity after addition of a soluble tracer. Most of the current mixing operations in bioreactor applications are turbulent but laminar and transitional scenarios are becoming industrially more relevant (Alvarez et al., 2005).

The aim in this study was to begin to characterize agitation in a minibioreactor, operated in the transitional regime, by studying both mixing time (Θ_M) and mean circulation time

Correspondence to: Govind Rao or Mark Marten
Contract grant sponsors: Fulbright; NIH; Merck & Co.
Contract grant numbers: U104336; RR018608

($\bar{\Theta}_C$). To accomplish this, a 12.5 mL stirred vessel for high throughput cell culture fermentation was used as a model system. Mixing time is defined as the time required for the system to reach 95% of its final value after addition of a miscible tracer. Circulation time is defined as the time interval between successive passes of a fluid element through a fixed point in the vessel. A novel optical sensor is used to assess both mixing and circulation times. Then, correlations between mixing time and Reynolds number and between mean circulation time and impeller rotational are compared with correlations determined in large-scale stirred vessels.

MATERIALS AND METHODS

The vessel used was a glass vial with a footprint identical to that of a single well in a 24-well plate. In addition, it consists of a stainless steel cap, shaft with impeller, coupling and driving motor (See Fig. 1). In all our experiments, florescein disodium salt was used as a tracer. The vessel geometry and impeller position for the bioreactor are presented in Table I. Since standard dimensions do not exist for bioreactors, our studies were done in normalized conditions of H to D ratios. The Reynolds number defined as $\mathrm{Re} = ND^2\rho/\mu$ was varied ranging from 14 to 1,350, where N is the rotational speed (s^{-}), D is the impeller diameter (m), ρ is liquid density (kg/m^3) and μ is the viscosity (Pa.s).

A drop of dye (i.e., 10 μL) was injected in the vessel without disturbing the system. The drop of tracer was gently placed on the surface of the liquid (i.e., water) at approximately 3 mm near the impeller shaft. The time at which the tracer is added to the vessel is considered as the initial time ($t = 0$). A confocal optical sensor that was previously validated (Vallejos et al., 2005) was used during the experiments. The optical sensor transmits a signal to an Analog-to-Digital Converter (LabJack, www.labjack.com),

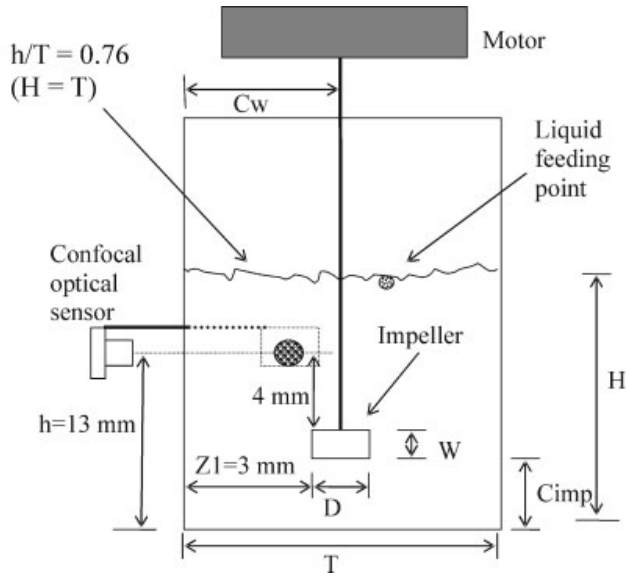

Figure 1. Vessel geometrical parameters. The most important geometrical parameters of the 12.5 mL stirred vessel are indicated.

Table I. Vessel geometrical parameters.

Reactor size	T(mm)	D(mm)	D/T	W/D	C_{imp}(mm)	C_w/T
12.5mL	17	9	0.53	0.44	8.8	0.5

Table I presents the most important geometry parameters of the 12.5 mL stirred vessel.

which finally transmits the digital signal to a PC equipped with LabView software. On the PC, the signal is displayed in millivolts versus time.

The signal (X_t) was normalized by dividing it by its final value (X_f) using the following equation (Khang and Levenspiel, 1976):

$$E = \frac{X_t}{X_f} \tag{1}$$

where X_t is the actual signal transmitted by the confocal sensor (mV) and X_f is the final value of the signal transmitted by the confocal sensor (mV).

A total of 20 runs for each rotational speed were performed. For each run, mixing time was determined as the time needed for the amplitude of the oscillations to become less than 5% of steady state value. Following this, the mean value was computed. Mean circulation time was calculated using the following equation (Roberts et al., 1995):

$$\bar{\Theta}_C = \frac{\sum_{i=1}^{n} t_i}{n} \tag{2}$$

where t_i is the time between two consecutive circulations peaks (sec) and n is the number of circulation peaks (t_i) detected.

The stirred vessel was equipped with a single paddle impeller. A 31.5 mm model 2111-13-02 motor (Lin Engineering) drove the impeller.

Mixing Time Studies

A ratio of $H/T = 1$ was used and the working volume was 3.9 mL, this geometrical ratio (i.e., $H/T = 1$) is commonly used in industrial fermentors or stirred tanks. In order to achieve the ratio, the vessel was filled up with liquid to 1/3 of the total height. Mixing time was studied at a fixed location with coordinates (h, $Z1$, $R1$) (13, 3, 9) in mm. See Figure 1 for more details.

Circulation Time Studies

Circulation time studies were performed at a fixed location and only the liquid height (H) was changed. Circulation time at two different H/T ratios (i.e., $H/T = 1$ and $H/T = 2$) was studied. In the case where $H = T$, the conditions employed are as described above. In the second hydrodynamic case $H = 2T$

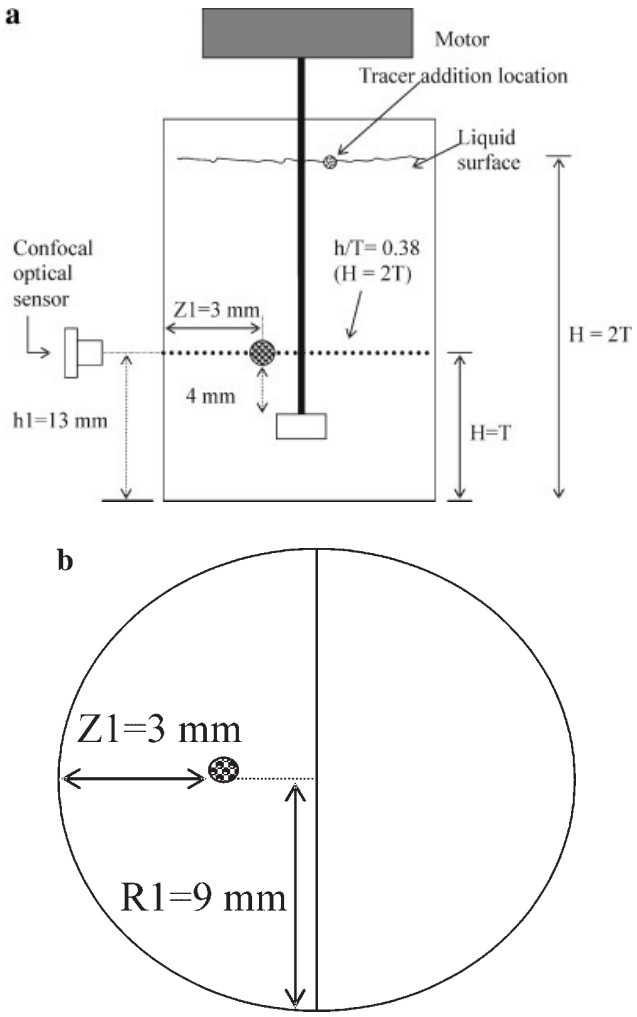

Figure 2. Circulation time measurement location. Figure shows the locations in the stirred vessel where circulation time was measured. (a) Cross-sectional view; (b) top view.

(i.e., 7.8 mL working volume), the sensor was kept at the same position as in $H = T$ (Fig. 2).

RESULTS AND DISCUSSION

Mixing Time

The 12.5 mL stirred vessel was primarily operated in the transitional regime (i.e., $10 < \mathrm{Re} < 10^4$). It was observed that the vessel was perfectly mixed (i.e., after mixing time was reached, no stagnant zones were seen in the minibioreactor) over the range of $14 < \mathrm{Re} < 1{,}350$. However, in the range $14 < \mathrm{Re} < 41$ the presence of doughnut-like segregated regions (i.e., Poincaré sections or isolated mixing regions (IMR)) were visually observed in the 12.5 mL stirred vessel. These segregated regions eventually disappeared as mixing progressed. It is well known that Poincaré sections can create barriers to efficient mixing. Zalc et al. (2002) reported the presence of Poincaré sections for a 0.24 m diameter stirred tank for $20 < \mathrm{Re} < 40$. Poincaré sections may also negatively

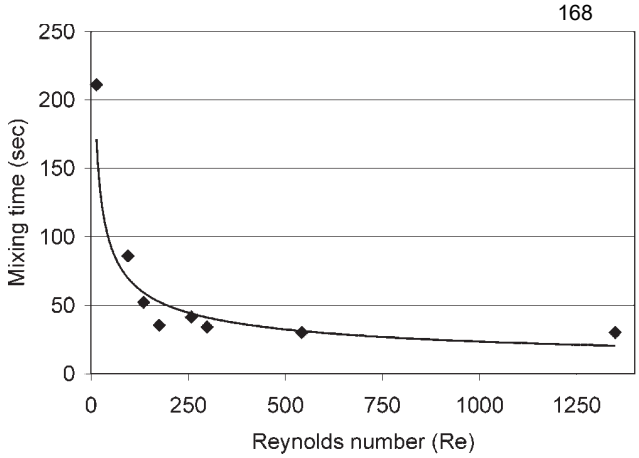

Figure 3. Mixing in the 12.5 mL stirred vessel as a function of Re. (◆) Experimental data. (—) Power correlation from experimental data. Figure shows how mixing in the stirred vessel is dependent on Reynolds number vessel. The experimental data fits a power curve of the form $Y = aX^b$. For the 12.5 mL model bioreactor $a = 568$, $b = -0.46$ with an $r^2 = 0.86$.

affect the mixing efficiency in the 12.5 mL stirred vessel. As these isolated mixing regions are known not to exchange significant fluid with the outside active mixing region (Ohmura et al., 2003), this may be responsible for the relative large mixing time of 214 ± 87 s determined in the minibioreactor at $\mathrm{Re} = 13.5$. For $\mathrm{Re} > 41$, no Poincaré sections were observed.

Figures 3 and 4 show experimentally measured mixing time values and non-dimensional mixing time as a function of Reynolds numbers, respectively. After $\mathrm{Re} = 176$ (i.e., 130 rpm), mixing time in the 12.5 mL vial seems to reach a constant value of approximately 34 s. It appears that at $\mathrm{Re} = 176$, the maximum pumping capacity of the impeller has been achieved such that additional increases in rotational speed have little effect on mixing time. Figure 4 shows a linear (i.e., $r^2 = 0.99$) dependency of the non-dimensional ($\mathrm{N}\Theta_\mathrm{M}$) form of mixing time on Reynolds number. This implies that the product, $\mathrm{N}\Theta_\mathrm{M}$, in the small-scale 12.5 mL stirred vessel is not constant in the transition regime. Nienow

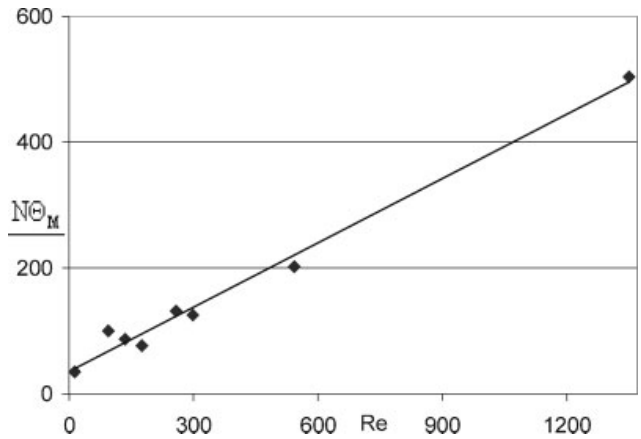

Figure 4. Non-dimensional form of mixing as a function of Re. Figure shows the dependence of the non-dimensional mixing form on Reynolds number.

DOI 10.1002/bit

(1997) has observed that when convection is controlling, the product $N\Theta_M$ is constant under turbulent regime. Sano and Usui (1985) experimentally found that $N\Theta_M$ is independent of Re in the turbulent regime (i.e., $Re > 5 \times 10^3$), and only depends on the geometrical shape of the impeller. Since a linear dependency of the non-dimensional form of mixing ($N\Theta_M$) on Re was determined in the 12.5 mL stirred vessel, it may suggest convection is not always controlling the mixing process. In the transition regime, both laminar and turbulent flow elements exist. In the laminar regime, turbulence is not relevant but chaos is the only mechanism for mixing (Alvarez et al., 2005). The presence of chaotic mixing may also be responsible not only for the relative large mixing time values but also for the segregated regions observed in the minibioreactor for $Re < 41$. Since chaotic mixing is very sensitive to initial conditions, the tracer injection point may have a significant effect on the mixing time when laminar flow is predominant. Studies of mixing with different tracer injection location are under way to study its influence.

Mean Circulation Time

Case 1. $H = T$

Circulation peaks at two agitation speeds are shown in Figure 5. It was determined that as rotational speed is increased, mean circulation time is decreased. For example, at lower rotational speed (i.e., 10 rpm), the circulation peaks are more separated between each other than at 30 rpm. This leads to larger mixing time values and circulation time (i.e., 41 s).

Interestingly, the number of peaks before homogenization in the vessel is reached at 10 rpm, is similar to the number reported in the literature for large-scale stirred vessels. For example, Nienow (1997) when describing the bulk flow model reported that the system was homogenized after about five circulation peaks. Similarly, at 10 rpm in a 12.5-mL-stirred vessel five circulation peaks are required before homogenization is achieved. At 30 rpm, 24 circulation peaks were seen in the region near the impeller. As the rotational speed is increased, the number of circulation peaks is increased and the mean circulation time decreases. Above 130 rpm (data not shown), no more circulation peaks were observed.

Case 2. $H = 2T$

As it was for the first case (i.e., $H = T$), the results for $H = 2T$ show that mean circulation time is inversely proportional to increasing rotational speed. The results for the case when $H = 2T$ also show that for a given rotational speed mean circulation time increases by increasing the liquid height. Results are shown in Figure 6.

It has been previously demonstrated in moderately large stirred tanks that $\bar{\Theta}_C$ is inversely proportional to the impeller speed (Holmes et al., 1964; Middleton, 1979; Roberts et al., 1995). Figure 6 shows the same type of dependence of mean circulation time on rotational speed for the 12.5 mL vessel as it was for the 8–785 L vessels used by Holmes et al. (1964). Our results show that as the rotational speed is increased, the circulation time decreases in the 12.5 mL stirred vessel.

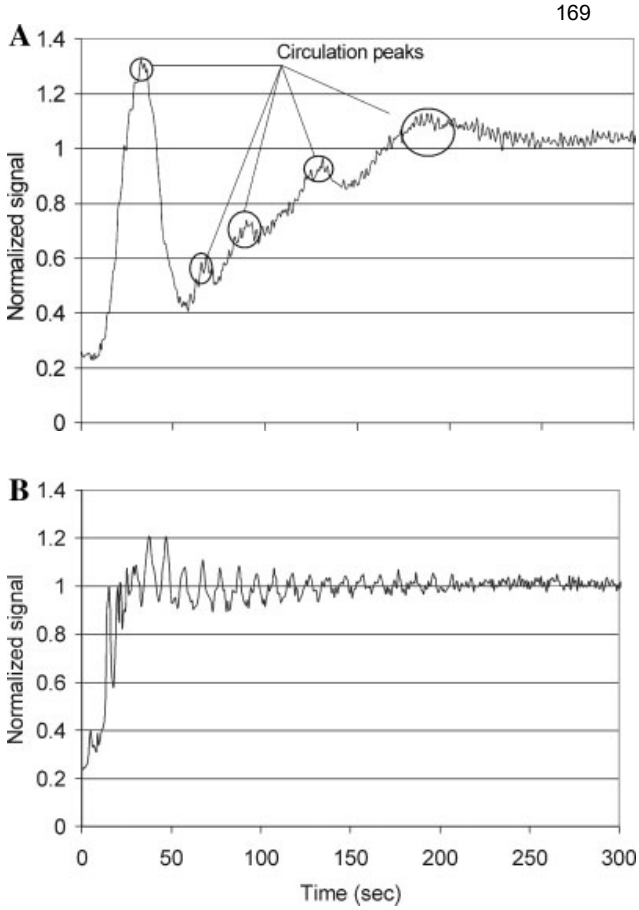

Figure 5. Mixing and circulation at 10 and 30 rpm. Figure shows how mixing and circulation time is achieved in the stirred vessel at a rotational speed of (**A**) 10 and (**B**) 30 RPM.

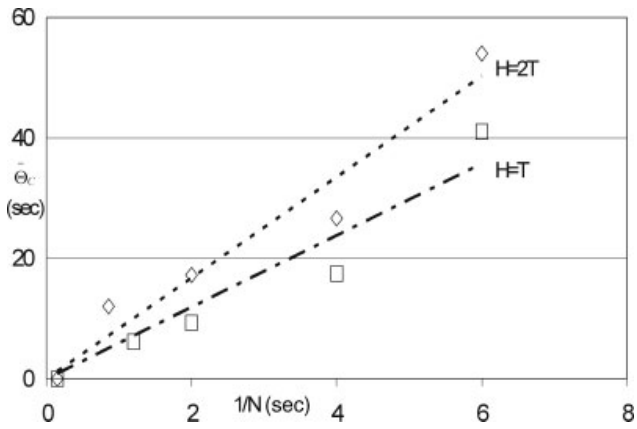

Figure 6. Influence of impeller speed and liquid height on circulation time. Figure shows the influence of impeller speed and liquid height on circulation time. (- - -◇) $H = 2T$. (_._.□) $H = T$.

For the case where $H = T$, Holmes et al. (1964) suggested that:

$$\bar{\Theta}_C \sim N^{-1}(T/D)^2 \quad (3)$$

or

$$\bar{\Theta}_C = k(T/D)^2(1/N) \quad (4)$$

In the particular case of the 12.5 mL vessel equipped with a single paddle impeller, for $H = T$, k was found to be 1.67 with a correlation coefficient (r^2) of 0.9244. For the case $H = 2T$, k was found to be 2.35 with a correlation coefficient (r^2) of 0.9476. Roberts et al. (1995) present values of k for Rushton and pitched blade turbines of 0.64 and 0.88, respectively. These results are in some extent unexpected as the flow regimes in our small scale minibioreactor differ considerably from the large scale bioreactor (Roberts et al., 1995). In our case, the flow varies from predominantly laminar to predominately turbulent, while in the big reactors the flow is fully turbulent. Still, results at small scale are comparable with those at large scales where the same pattern for circulation time as a function of rotational speed has been observed.

CONCLUSIONS

In summary, the 12.5 mL stirred vessel was operated in the Re range of $14 < \mathrm{Re} < 1{,}350$. The stirred vessel is completely mixed for the entire range of Re. Isolated mixing regions were seen in the minibioreactor for $\mathrm{Re} < 41$ but disappeared before mixing time were reached. The non-dimensional form of mixing time, $N\Theta_M$, for the 12.5 mL stirred vessel operated in the transition regime is linearly dependent on the Reynolds number. Mean circulation time in the stirred vessel is inversely proportional to the impeller rotational speed. This dependency of mean circulation time on impeller rotational speed is similar to those previously reported (Holmes et al., 1964; Middleton, 1979; Roberts et al., 1995). Depending on the rotational speed and the liquid height chosen, mean circulation times of 54 and less than 1 s were found in the stirred vessel. Finally, it was verified experimentally that mean circulation time is proportional to the liquid height.

The results suggest that the mixing behavior of large tanks can be replicated at the small-scale bioreactors although the hydrodynamic conditions at both scales are different. The implications are that non-ideal cultivation conditions existing in large-scale bioreactors may be conveniently studied in minibioreactors and large numbers of experiments may be readily conducted.

NOMENCLATURE

C_{imp}	Clearance (mm)
C_w	Impeller clearance from vessel sidewall (mm)
D	Diameter of the agitator (mm)
E	Normalized signal dimensionless
Fl	Impeller flow number dimensionless
H	Liquid height (mm)
n	Number of t_i detected
N	Impeller speed (rpm)
Re	Reynolds Number dimensionless
T	Internal diameter of the vessel (mm)
t_i	Time between two consecutive circulations peaks (sec)
X_t	Actual signal transmitted by the confocal sensor (mV)
X_f	Final value of the signal transmitted by the confocal sensor (mV)
W	Width of the impeller (mm)

Greek Letters

barΘ_C	Mean circulation time (sec)
Θ_M	Mixing time (sec)

References

Alvarez MM, Guzmán A, Elías M. 2005. Experimental visualization of Mixing pathologies in laminar stirred tank bioreactors. Chem Eng Sci 60:2449–2457.

Barneveld JV, Smit W, Oosterhuis NMG, Pragt HJ. 1987. Measuring the liquid circulation time in a large gas-liquid contactor by means of a radio pill. 2. Circulation time distribution. Ind Eng Chem Res 26:2192–2195.

Bittorf KJ, Kresta SM. 2000. Active volume of mean circulation for stirred tanks agitated with axial impellers. Chem Eng Sci 55:1325–1335.

Doig S, Pickering SCR, Lye GJ, Baganz F. 2005. Modelling surface aeration rates in shaken microtrite plates using dimensionless groups. Chem Eng Sci 60:2741–2750.

Elmahdi I, Baganz F, Dixon K, Harrop T, Sugden D, Lye GJ. 2003. pH control in microwell fermentations of *S. erythrae* CA340: Influence on biomass growth kinetics and erythromycin biosynthesis. Biochem Eng J 16:299–310.

Hall JF, Barigou M, Simmons MJH, Stitt EH. 2004. Mixing in unbaffled high-throughput experimentation reactors. Ind Eng Res 43:4149–4158.

Holmes DB, Voncken RM, Dekker JA. 1964. Fluid flow in turbine-stirred, baffled tanks-I. Circulation time. Chem Eng Sci 19:201–208.

Khang SJ, Levenspiel O. 1976. New scale-up and design method for stirrer agitated batch mixing vessels. Chem Eng Sci 31:569–577.

Kostov Y, Harms P, Randers-Eichhorn L, Rao G. 2001. Low-cost microbioreactor for high-throughput bioprocessing. Biotechnol Bioeng 72(3):346–352.

Lamping SR, Zhang W, Allen B, Shamlou PA. 2003. Design of a prototype miniature bioreactor for high throughput automated bioprocessing. Chem Eng Sci 58:747–758.

Lye GJ, Ayazi-Shamlou P, Baganz F, Dalby PA, Woodley JM. 2003. Accelerated Design of Bioconversion Process Using Automated Microscale Processing Technique. Trends Biotechnol 21(1):29–37.

Maharbiz MM, Holtz WJ, Howe RT, Keasling JD. 2004. Microbioreactor Arrays with Parametric Control for High-Throughput Experimentation. Biotechnol Bioeng 85(4):376–381.

Marten MR, Wenger KS, Khan SA. 1997. In: Nienow AW, editor. 4th International Conference on Bioreactor & Bioprocess Fluid Dynamics. Bury St Edmonds, UK: Mechanical Engineering Publications.

Middleton JC. 1979. Measurement of Circulation within Large Mixing Vessels. Third European Conference on Mixing. April 4th–6th.

Nere NK, Patwardhan AW, Joshi JB. 2003. Liquid-phase mixing in stirred vessels. Turbulent flow regime. Ind Eng Chem Res 42:2661–2698.

Nienow AW. 1997. On impeller circulation and mixing effectiveness in the turbulent flow regime. Chem Eng Sci 52:2557–2565.

Ohmura N, Makino T, Kaise T, Kataoka K. 2003. Transition of organized flow structure in a stirred vessel at low Reynolds Numbers. J Chem Eng J 36(12):1458–1463.

DOI 10.1002/bit

Papagianni M, Mattey M, Kristiansen B. 2003. Design of a tubular loop bioreactor for scale-up and scale-down of fermentation processes. Biotechnol Prog 19:1498–1504.

Roberts RM, Gray MR, Thompson B, Kresta SM. 1995. The effect of impeller and tank geometry on circulation time distribution in stirred tanks. Tans IChem 73 Part A:78–86.

Sano Y, Usui H. 1985. Interrelations among mixing time, power number and discharge flow rate number in baffled mixing vessles. J Chem Eng J 18:47–52.

Vallejos JR, Kostov Y, Marten MR, Rao G. 2005. A novel noninvasive confocal optical sensor to study mixing. Biotechnol Prog 21:1531–1536.

Vasconcelos JMT, Alves SS, Barata JM. 1995. Mixing in Gas-Liquid Contactors agitated by multiple turbines. Chem Eng Sci 50(14):2343–2354.

Zalc JM, Szalai ES, Alvarez MM, Muzzio FJ. 2002. Using CFD to understand chaotic mixing in laminar stirred tanks. AIChE J 48(10): 2124–2134.

Zanzotto A, Szita N, Boccazzi P, Lessard P, Sinskey AJ, Jensen KF. 2004. Membrane-aerated microbioreactor for high-throughput bioprocessing. Biotechnol Bioeng 87(2):243–254.

The logical evolution of the previous two papers was to construct a high throughput system with miniature stirred tanks and the following paper describes this melding of optics, electronics and mechanical systems. We enlisted a mechanical engineering colleague, Anjanappa and his student Mohammed Soliman. This resulted in what I believe to have been the first ever demonstration of a 24 mini stirred tank system where pH, oxygen and optical density were simultaneously monitored in an *E. coli* fermentation. It also showed that this sort of high-density system would have never been possible without optical sensor technology enabling it.

Design and Performance of a 24-Station High Throughput Microbioreactor

Peter Harms,[1] Yordan Kostov,[1] Joseph A. French,[2] Mohammed Soliman,[3] M. Anjanappa,[3] Arun Ram,[4] Govind Rao[1]

[1]Department of Chemical and Biochemical Engineering, Center for Advanced Sensor Technology, University of Maryland at Baltimore County, Baltimore, Maryland 21250; telephone: (410)-455-3400; fax: (410)-455-1049; e-mail: grao@umbc.edu
[2]Department of Physics, University of Maryland at Baltimore County, Baltimore, Maryland; e-mail: grao@umbc.edu
[3]Department of Mechanical Engineering, University of Maryland at Baltimore County, Baltimore, Maryland
[4]Department of Computer Science and Electrical Engineering, University of Maryland at Baltimore County, Baltimore, Maryland

Received 5 July 2005; accepted 6 September 2005

Published online 22 November 2005 in Wiley InterScience (www.interscience.wiley.com). DOI: 10.1002/bit.20742

Abstract: Two prototype 24-unit microbioreactors are presented and reviewed for their relative merits. The first used a standard 24-well plate as the template, while the second consisted of 24-discrete units. Both systems used non-invasive optical sensors to monitor pH and dissolved oxygen. The systems were used to cultivate *Escherichia coli*. Both designs had their merits and the results obtained are presented. In addition, dissolved oxygen control was demonstrated at the milliliter scale and 24 simultaneously monitored fermentations were successfully carried out. These results demonstrated high quality high throughput bioprocessing and provide important insights into operational parameters at small scale. © 2005 Wiley Periodicals, Inc.

Keywords: high throughput; non-invasive; fluorescence; fermentation; cell culture; bioreactor

INTRODUCTION

Microscale culture technology has evidenced a great deal of recent interest. The advantages of being able to replicate laboratory-scale stirred tank bioreactors at small scale are rather obvious, as one can economically conduct large numbers of cultivation experiments under controlled conditions. As a first step, we previously demonstrated the comparability of data from a liter and milliliter-scale *Escherichia coli* fermentation (Kostov et al., 2001).

Subsequently, several studies examining various designs and other aspects of microscale culture have been carried out. A number of research groups have used standardized well plates as reactors, and have added some type of sensing. The simplest used a standard plate reader to measure a pH sensitive dye in the growth medium (Girard et al., 2001). A more advanced system coated the well bottoms of 96-well plates with fluorescent oxygen sensors, again performing measurements with a commercial plate reader (John et al., 2003). The plate reader has a built-in shaker, but still can only provide k_La values up to 40/h. With an improved shaker, the k_La could easily exceed 200/h (Hermann et al., 2002). Another promising study used optical measurements of dissolved oxygen and cell mass, and achieved k_La's of 100–400/h (Lamping et al., 2003).

In other studies, Maharbiz et al. (2004) demonstrated an array of eight 250 μL reactors based on printed circuit board technology that controlled temperature, pH, and measured optical density. Zanzotto et al. (2004) utilized a microbioreactor with volumes in the range of 5–50 μL with integrated optical sensors for on-line measurement of optical density, dissolved oxygen, and pH during growth of *E. coli*. Elmahdi et al. (2003) measured pH during microscale fermentation by inserting a micro-pH probe into a 7 mL well in a microtrite plate. As mentioned earlier, Hermann et al. (2002) have characterized the mass transfer characteristics of well plates. Puskeiler et al. describe a 48-well milliliter scale bioreactor array. Finally, Doig et al. (2005) used three different microplates (24-, 96-, and 384-wells) with working volumes between 65 and 1,182 μL to measure k_La during growth of *Bacillus subtilis.*

In this paper, we present the results from two prototype high throughput milliliter scale bioreactors. Both designs utilize individually driven impeller agitated units, and appear like miniature stirred tanks. One was based using a standard 24-well plate as the footprint, while the other employs a discrete miniature stirred tank design. In both cases, each unit had its independent agitator in the form of a DC or a stepper motor. A major reason for us to utilize the stirred tank approach is the large body of previous experience in design and use of such systems for cell and microbial culture and for the achievability of convective mixing. While agitated well plates do offer convective mixing, each well cannot be individually addressed. In terms of the footprint, the motivation was to utilize a 24-well plate architecture given its widespread commercial deployment. During the course of this design's testing and validation, it became apparent that

Correspondence to: Govind Rao
Contract grant sponsors: NIH; Merck Research Laboratories
Contract grant number: RR018608

a discrete miniature bioreactor design would also offer advantages and so both types were fabricated and tested as described next.

MATERIALS AND METHODS

Sensors and Instrumentation

In all cases, optical sensors were used to measure pH and DO as previously described (Kermis et al., 2002; Kostov et al., 2001). Cell mass was monitored by turbidity, and provision was also included to allow fluorescence intensity measurements of green fluorescent protein (GFP), which can be used to monitor protein expression and organism stress (Lu et al., 2003). The GFP sensor was not used in the studies reported in this paper and is mentioned for completeness. Figure 1 shows the generic scheme for the sensors and instrumentation. For the 24-well plate system, Figure 2a and b show the entire board assembly and how the sensor patches were placed in each well. Further details are in Harms [2004].

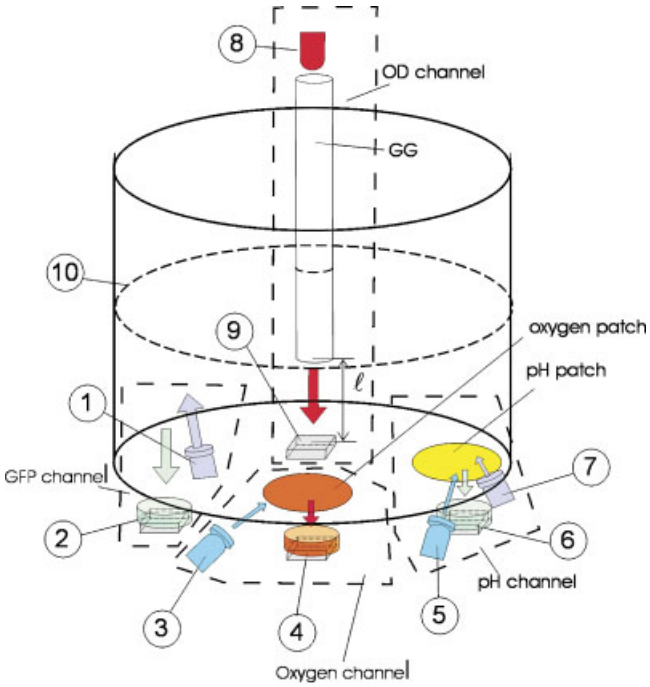

Figure 1. Schematic of the positioning of the optical sensors around a single well in a 24-well microplate. The light source and the detectors are not drawn to scale. Interference filters are positioned in front of the LEDs and photodiodes (represented here by small disks). A pinhole is installed in front of every detector for better collection of the light (not shown). The spatial positioning is selected in such way that the excitation light from one channel creates minimum interference to the other channels. The glass optical guide GG extends below the liquid level to achieve constant light path length *l* for OD measurements. 1, excitation UV LED for the GFP channel; 2, detection photodiode for the GFP channel; 3, excitation blue LED for the oxygen channel. 4, detection photodiode for the oxygen channel; 5, 7, excitation blue and UV LEDs for the pH channel; 6, detection photodiode for the pH channel; 8, red LED for the OD channel; 9, detection photodiode for the OD channel; 10, the liquid level. For the discrete microbioreactor, the lightguide was discarded and OD was measured across the diameter of the vial (not shown). [Color figure can be seen in the online version of this article, available at www.interscience.wiley.com.]

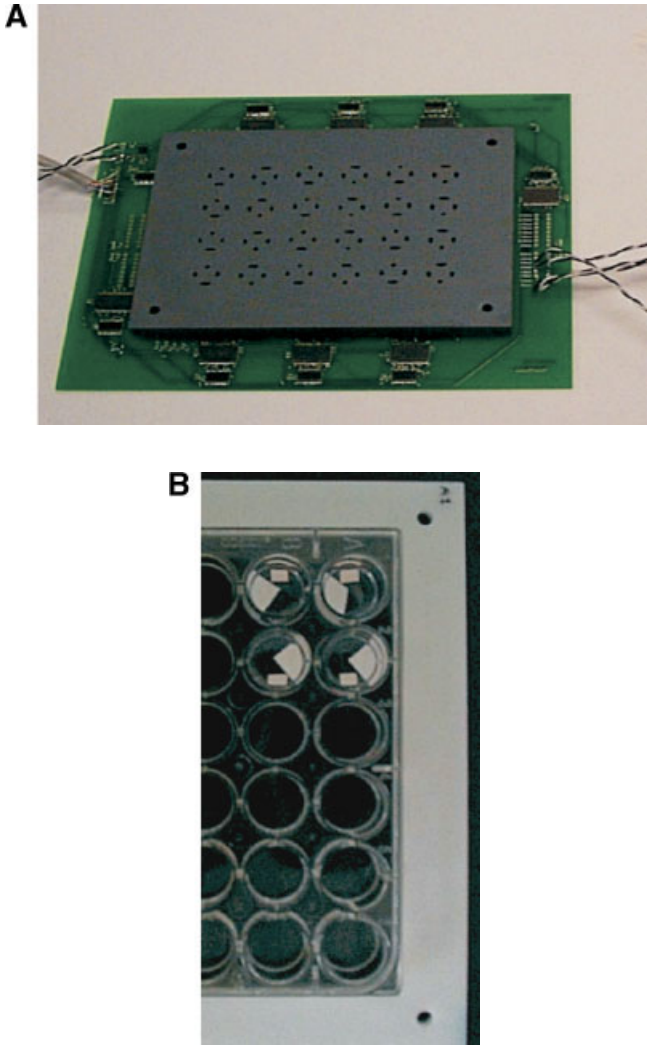

Figure 2. **A**: Measurement board and (**B**) patch placement in a microwell plate. [Color figure can be seen in the online version of this article, available at www.interscience.wiley.com.]

24-Well Plate System

For the 24-well plate system, k_La's were determined by the sulfite oxidation method as adapted for microtiter plates by Hermann et al. (2001, 2002). The reactors were filled with 1 mL of a solution of 0.5 M sodium sulfite, 0.012 M sodium phosphate, <1 μM cobalt sulfate, and the pH indicator dye HPTS, adjusted to pH 8. Once all of the reactors were filled, agitation and aeration were started and held constant. As the sulfite is oxidized, the solution pH drops, causing an optical change of the HPTS. The k_La is inversely proportional to the time taken for this change, which ranged from 2 to 26/h.

Also for the 24-well plate system, *E coli* JM105 was grown on LB media in the reactor system. Cells were taken from an overnight shake flask culture. The overnight culture (0.5 mL) was added to 12 mL of fresh media to provide

a starting OD of about 0.2. One milliliter of this culture was aliquoted into each reactor, after which the reactors were assembled and monitoring and controls were started. Six reactors were run simultaneously using wells B1 through B6. pH control was not used in this experiment. Since the well plate was not sealed, ethanol sterilization was used and the fermentations were run in a laminar flow hood.

Discrete Microbioreactor System

For the individual microbioreactor design, Figure 3a–c show the details of each microbioreactor, its instrumentation, and the entire assembly with 24-independent stirred vessels. The vessel used was a flat-bottomed transparent vial. The bottom of the vial has a footprint identical to that of a single well in a standard 24-well plate.

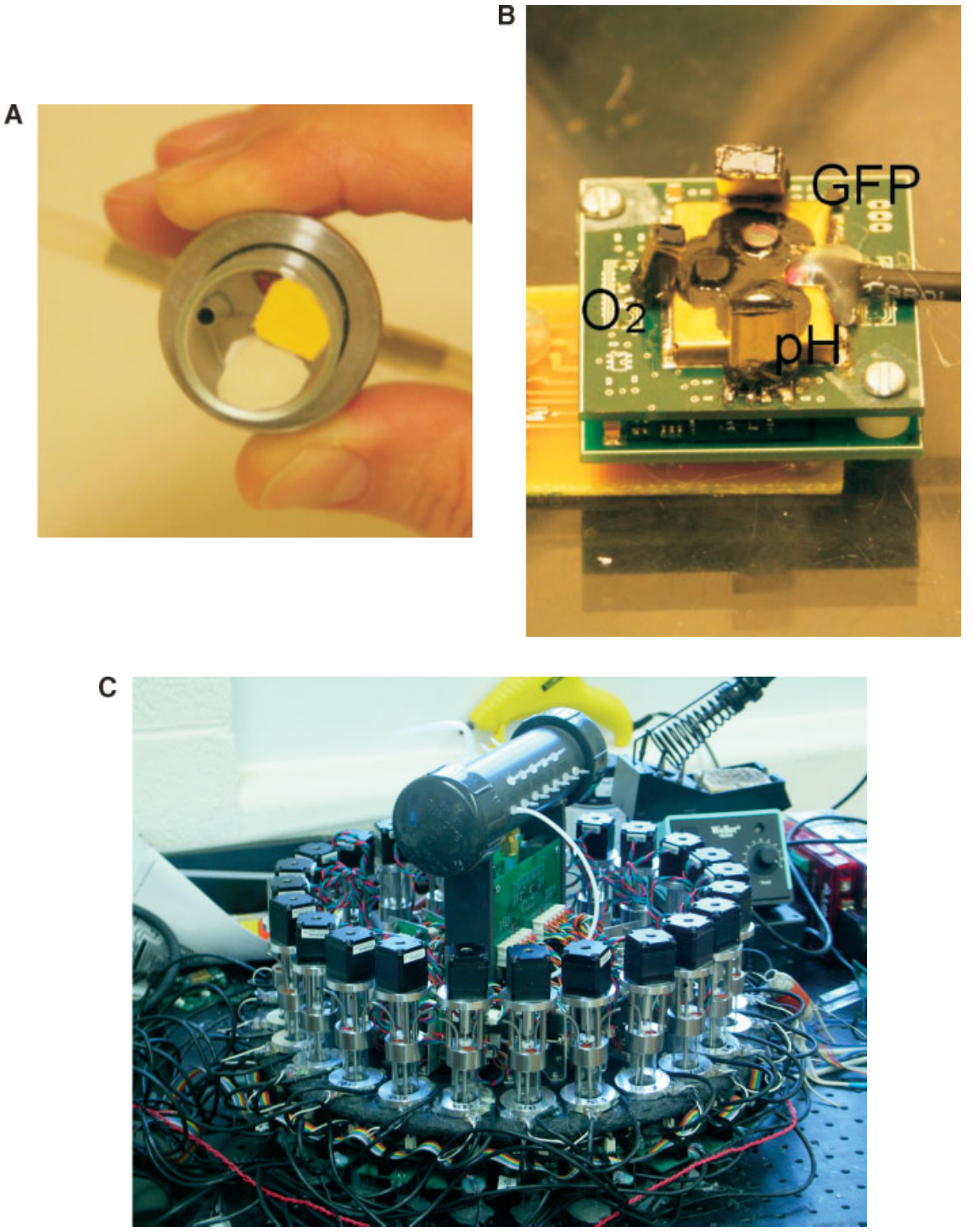

Figure 3. **A**: Sensor board, (**B**) patch placement, and (**C**) 24-discrete unit high throughput bioreactor.

In the discrete system, every bioreactor was equipped with an individual sterilizable cap. This allowed the individual units to be autoclaved and also permitted operation outside a laminar flow hood. Another significant difference from the plate design was the use of stepper motors for agitation control. At low speeds (10 rpm) the stepper motors offer greatest accuracy, while still offering maximum agitation speed of 1,000 rpm. A dedicated microcontroller for each motor allowed for individual rpm control of every bioreactor both through hardware and software. A third difference was that every bioreactor used a dedicated sensor board. All sensor boards (i.e., bioreactors) were sampled simultaneously. The total readout time of the sensors for all bioreactors was approximately 25 s. In contrast, the 24-well plate sensor board had a latency of several minutes between samples when all 24 stations are sampled, as the data were serially processed through a single bus.

Other than a strain variation (in this experiment, a GFP harboring *E. coli*), other culture conditions were the same as for the well plate experiment.

For data acquisition and control, LABView (National Instruments, Austin, TX) was used to write the routines in both systems.

RESULTS AND DISCUSSION

24-Well Plate Format

Oxygen Transfer

The results of k_La measurements in the 24-well plate system are shown in Figure 4. There is a wide scatter in observed k_La values, particularly above 1,000 rpm. Some scatter is certainly expected due to noise in the sensor, but most of the variation could be caused by differences between the reactors (due to difficulties in consistently making identical hand made units) and inequality of the sparge gas flow rates. The sparge gas distribution is governed primarily by the pressure drop through the sterile filters, which shows some variation, even from the same manufacturing lot.

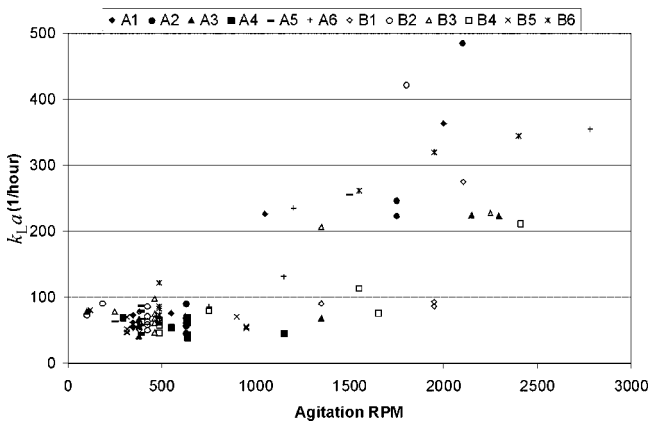

Figure 4. k_La measurements in a 24-well plate microbioreactor.

The k_La curve appears to be flat until some critical agitation, above which k_La increases rapidly. If surface aeration is dominant (Humphrey, 1998), then increasing agitation would have a minimal effect until a vortex is formed. This vortex would increase the surface area, which would increase the k_La. The change in surface area has been measured photographically in shaken 96-well plates and similar k_La curves were generated (Hermann et al., 2002). Because the agitation speeds can be very high, up to 2,800 rpm, the baffling effect of the heater and needles for sparging, temperature monitoring, and cell mass measurement is not sufficient to prevent vortex generation.

The wide range of achievable k_La's indicates that dissolved oxygen control is possible. However, the odd non-linear shape of the k_La curve and, more importantly, the high degree of scatter in the data, makes it difficult to find and tune a good oxygen control algorithm. Rather than performing the iterative testing of controller algorithms and settings, for later experiments, the control was set to the simplest method, namely on–off control, which provides proof of controllability but not accurate control.

In this implementation of on–off control, the agitation was switched between either a low speed (500 rpm) or a high speed (2,000 rpm). A traditional on–off controller would use zero as one of the agitation values, but that would prevent the reactor from being well-mixed, which would affect the readings from the oxygen sensor. As the oxygen sensor provides the input to the controller, this must be avoided. Bacterial cultures using this on–off control are discussed next.

Oxygen Control Versus Uncontrolled Cultures

Two sets of triplicate cultures were conducted to demonstrate oxygen control. Wells B1, B2, and B3 were run with on–off DO control and a setpoint of 20% as described earlier. Wells B4 and B6 were run without control. Well B5 experienced a temperature control malfunction and is not shown. Figure 5 shows DO and pH profiles from the 2-wells.

Reactors B4 and B6 were run without oxygen control at a constant agitation of 500 RPM. The dissolved oxygen profile shown in Figure 5a starts around 100% and approaches zero when the oxygen demand exceeds the oxygen supply, and then returns to 100% as the cells approach stationary growth phase. The curves are very similar between the two reactors, but B4 is oxygen limited for 10.2 h, while B6 is only limited for 8.6 h. This is a clear indication of a difference in k_La, even though the reactors were operated at identical agitation rates. Their pH profiles, shown in Figure 5b, show a slight drop and then rise.

Reactors B1, B2, and B3 were run with on–off oxygen control, with a setpoint of 20%.

Figure 6a shows a detailed view of the dissolved oxygen profile with oxygen control enabled. With the on–off control used here, the obvious oscillations are exactly as expected. These oscillations are caused entirely by the controller, and do not represent the behavior of the organism (Andersen

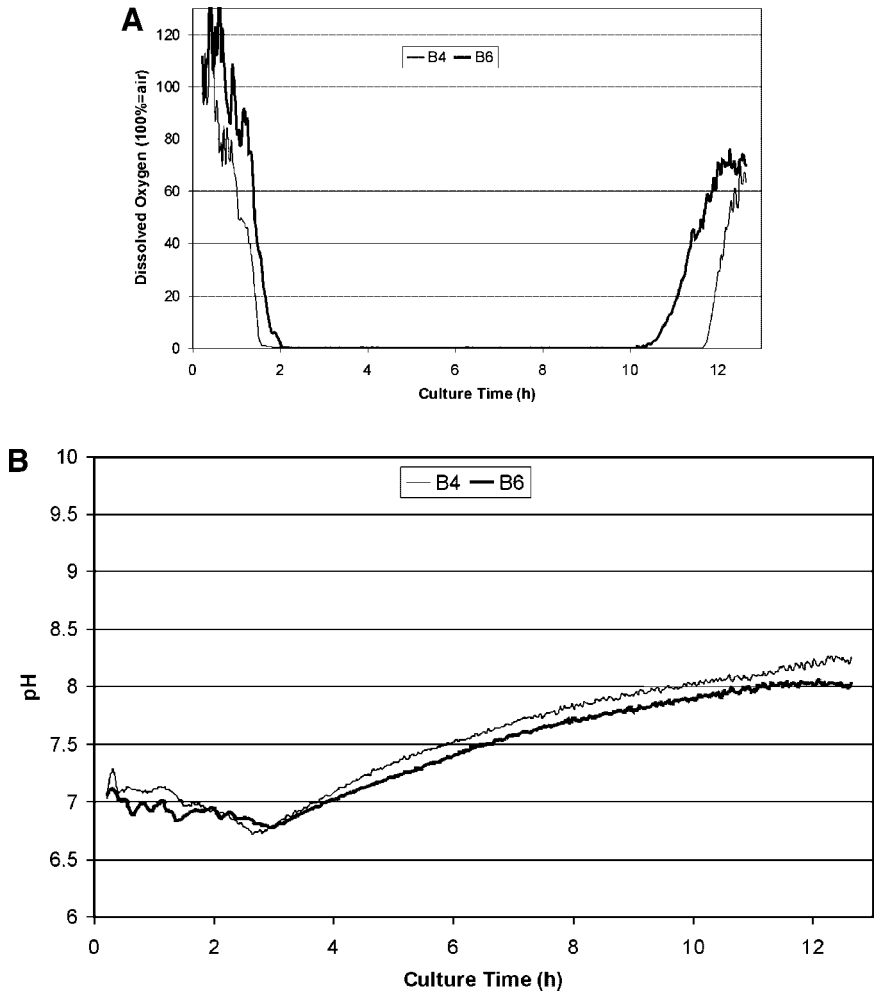

Figure 5. **A**: Dissolved oxygen profile from reactors B4 and B6. Both reactors were operated at a constant 500 rpm. **B**: pH profile of reactors B4 and B6. Both reactors were operated at a constant 500 rpm.

et al., 2001). The oxygen controller oscillates when the oxygen demand is greater than the oxygen supply at the low agitation but less than the supply at the high agitation, which also indicates rapid growth. An average oxygen concentration may help visualization of the data. As the period is about 10 min, a reasonable window for averaging is about 30 min. Because the magnitude of oscillation is very high, simple averaging is not a good choice. Instead, the data was passed through a 4th order Butterworth low-pass filter with a time constant of 30 min (15 samples). This has the advantage of smoothing the oscillations without needing to average an even multiple of the oscillatory period. The smoothed dissolved oxygen data are shown in Figure 6b and show that the control was successful in maintaining average DO close to the setpoint in all three microbioreactors.

While the smoothing makes it is easier to identify the major growth phases, it does not accurately represent the cells' true environment. Figure 6c shows a single cycle along with calculated values for the bulk oxygen concentration. The calculations assume a constant OUR and use previously calculated values of $k_L a$ (68 and 300/h) and patch response time (100 s). They also include a 120 s dead time introduced by the software between measuring the phase of the oxygen patch and outputting the new agitation speed. The expected deadtime for the software is only about 60 s, but it should vary from well to well depending on the order of taking measurements. The model fits the data remarkably well. If this model is correct, it indicates that the patch response time and sampling interval are much too long for proper use of this control algorithm. The bulk oxygen concentration does not stay at an average level, but oscillates between an excess of oxygen and complete oxygen starvation.

A major issue with bioreactor scale-up is that as volumes increase, mixing becomes worse, and cells are subjected to transients in oxygen concentration and chemical composition, with frequent oscillations in substrate, product, and waste. While studies have attempted to reproduce this effect using multiple linked bioreactors (Sandoval-Basurto et al., 2005), the parallel miniature bioreactor system could be used to control the cells' microenvironment directly and rapidly. A change in mixing at a large scale could be simulated by a

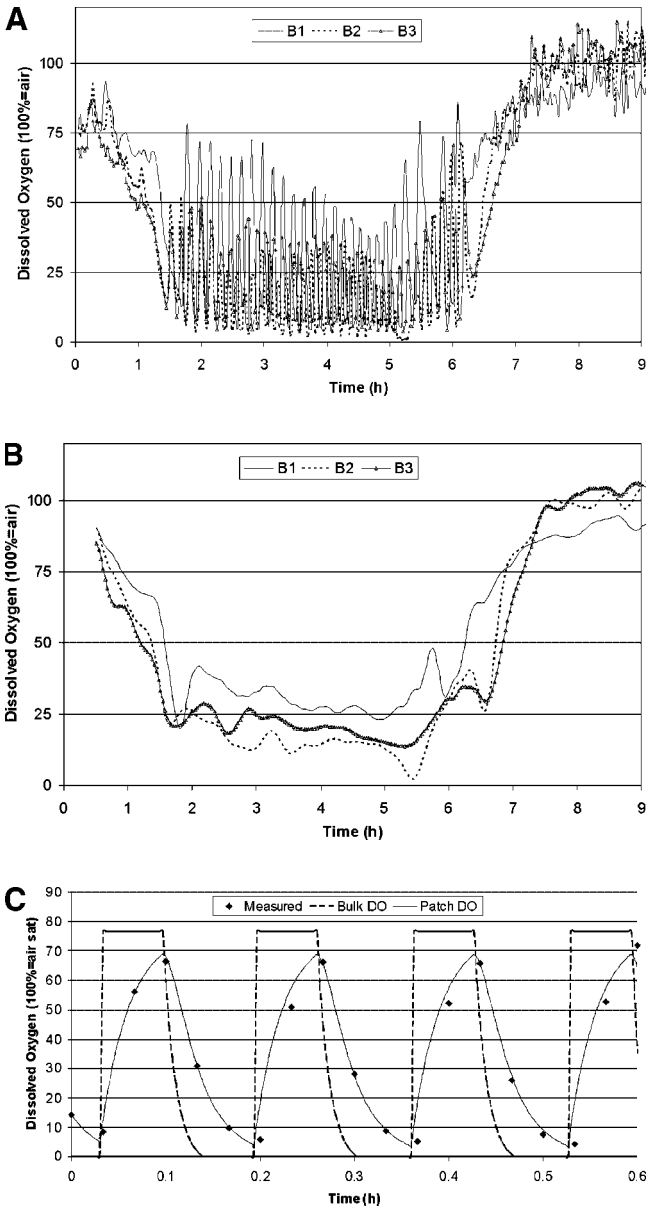

Figure 6. **A**: Original and (**B**) filtered views of dissolved oxygen under on–off control. The filtering removes most of the oscillations, showing a slight downward trend between 2 and 6 h for all three reactors. **C**: Modeled behavior of a reactor with on–off control of dissolved oxygen. The oxygen levels in the patch closely resemble the measured data, but do not accurately represent the bulk dissolved oxygen due to the slow patch response. The cells may be oxygen limited for a significant fraction of the time, but it is not apparent from the measured data.

change in the control cycle time and sampling rate in the miniature system. With a proper setup, the system could resemble either a bench-scale fermenter or a production-scale fermenter, which could be greatly beneficial to bioprocess characterization and operational qualification from a regulatory standpoint.

The DO controlled cultures had similar pH curves as shown in Figure 7. After 6.5 h, the consistently high dissolved oxygen concentration indicates that the cells stopped rapid growth. This observation is confirmed by the leveling off seen in the pH data. Compared to the uncontrolled cultures, the

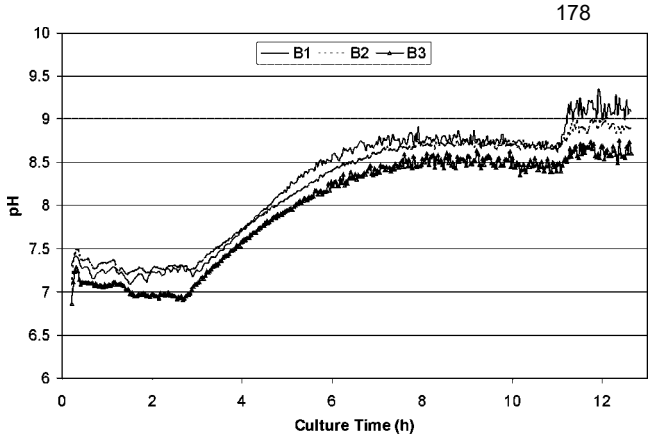

Figure 7. pH profile of reactors B1, B2, and B3. The reactors used on–off control of oxygen, providing higher growth rates than reactors B4 and B6. Growth was completed at about 7 h.

experiments with DO control show greater consistency and repeatability in the fermentation. Clearly, improved control at the microscale is a necessary feature in order to replicate the utility of laboratory scale bioreactors.

24-Discrete Microbioreactors

The parallel plate architecture did present some drawbacks. A robotic sampler (available for both pH control and nutrient addition) was ineffective due to the large numbers of tubes and wiring harnesses that clogged the available space above the microwell plate. Furthermore, having all the sensors on a single board proved to be a major problem when a short circuit on one part of the board resulted in the entire board becoming non-functional. It was experiences such as this that led to the single microbioreactor and modular sensor board design shown in Figure 2.

Given the variations in sparged aeration that were observed, we decided to test operational consistency and sensor performance by operating the 24-discrete units also under surface aeration. As can be clearly seen in Figure 8a, the fermentations showed virtually identical oxygen profiles, other than minor variations. In each case, cell growth results in oxygen consumption that results in the oxygen sensor reading zero oxygen as the cells continue to grow microaerobically. Upon substrate exhaustion, respiration ceases and oxygen values revert to the equilibrium value seen prior to the fermentation.

The pH data corroborated the oxygen profiles. Deprived of oxygen, the cells grew microaerobically. Under such conditions, they produce acetate, which results in sharp pH drops and this is exactly what was observed. Later, the cells utilize the acetate as a carbon source, which results in a gradual pH rise until the end of the fermentation. One microbioreactor's pH channel (number 3) was noticeably noisier than the rest, but nevertheless showed a trend similar to the others. Microbioreactor 20 also did not perform like the rest and we believe that one of the LED's (pH is a ratiometric measurement using two LEDs) was not aligned correctly.

Another important observation needs to be noted here. In contrast to the microwell plate, the pH data are significantly more inconsistent in the discrete microbioreactors. We attribute this to the surface characteristics of the vessel. The bottom of a microwell plate was nearly perfectly flat. In contrast, the bottoms of the glass vials employed in the discrete design have a slight curvature and manifest irregularities that vary from vial to vial. Consequently, the light path of the excitation LEDs is variant, leading to inconsistent readings between the vials. These observations are being quantitatively documented and will be reported separately.

Finally, Figure 8c shows optical density data from the discrete microbioreactors. As can be seen, the data are highly scattered, so meaningful comparisons between microbioreactors are not possible. The trend for each individual trace shows the expected increase in optical density exhibited by a growing culture. Optical density did not work consistently—at this point in time, we believe that these measurements are too susceptible to minor changes in alignment and bubble interferences to be anything more useful than a relative measure of growth. In the case of GFP, the initial experiments used cells with very low expression levels and consequently

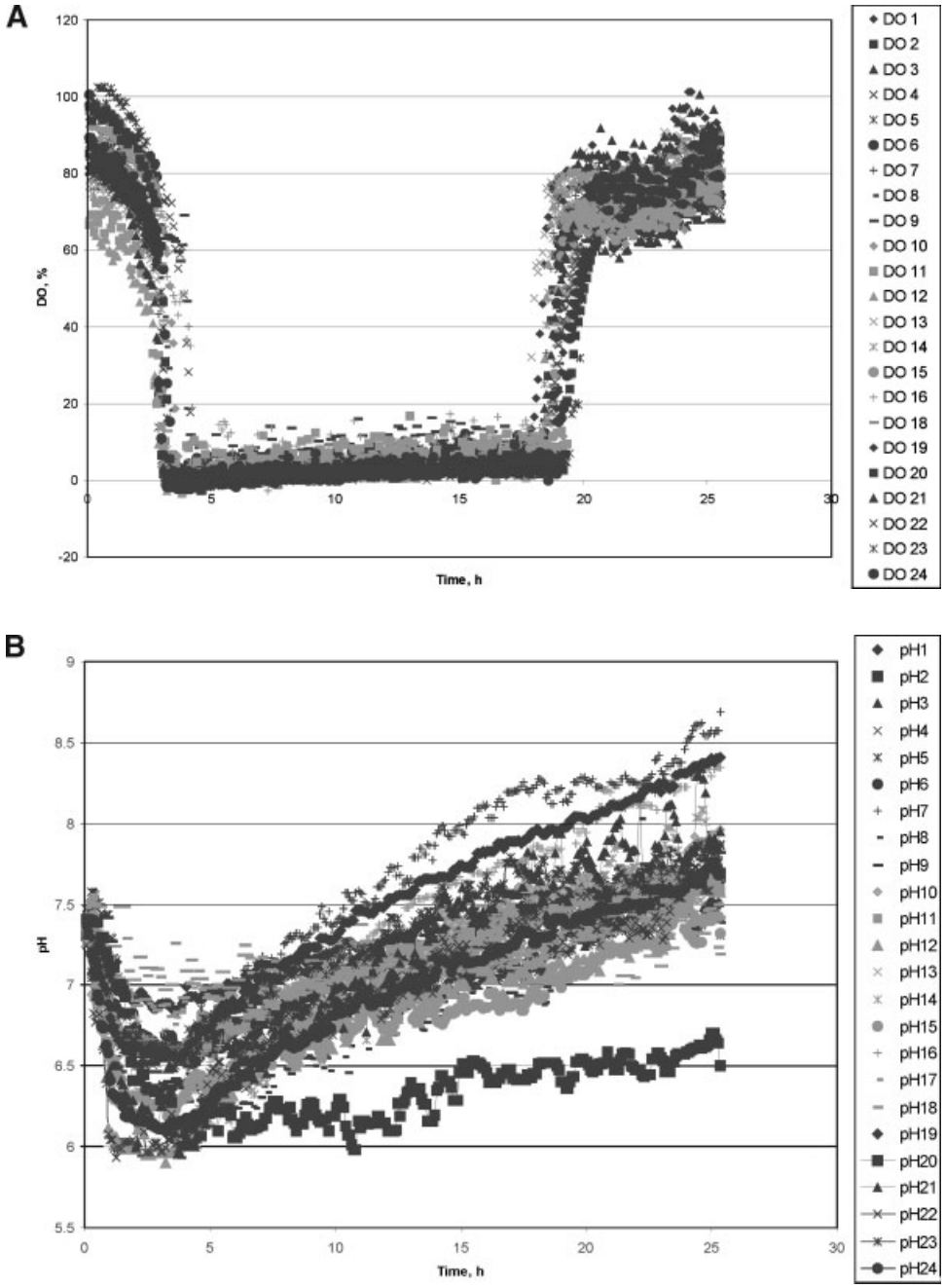

Figure 8. **A**: Dissolved oxygen profiles from 24 simultaneous fermentations conducted in individual microbioreactors. **B**: pH profiles from corresponding microbioreactors. **C**: Optical density profiles from 16 microbioreactors.

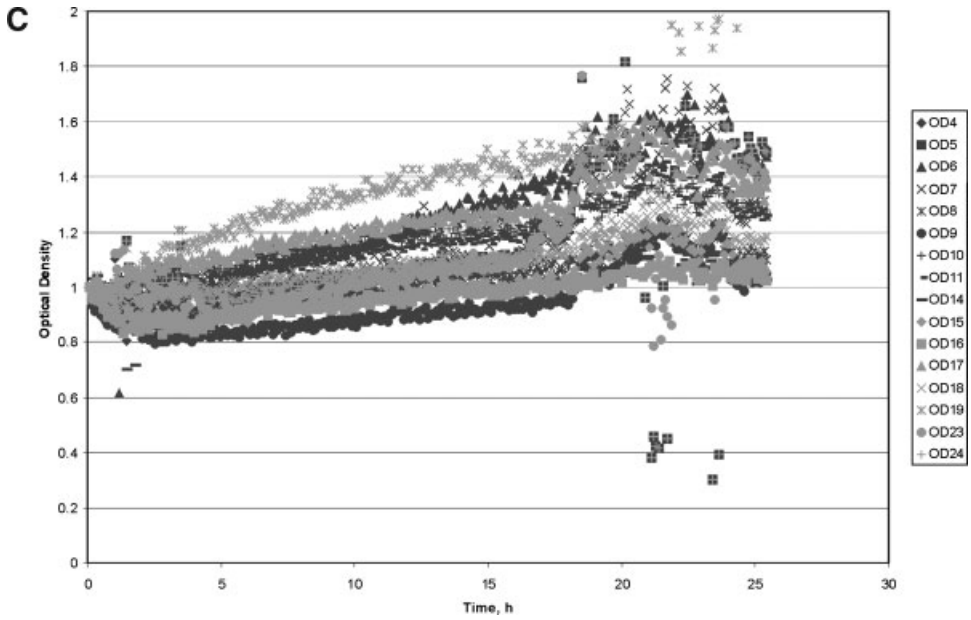

Figure 8. (*Continued*)

the signals were not much greater than the noise. Future experiments will address GFP measurements.

CONCLUSIONS

We have demonstrated an important advance in the further development of high throughput bioprocessing. The feasibility of controlled microbioreactor operation as well as the consistency of multiple experiments at the small scale has been demonstrated. It is hoped that these advances will lead to high throughput bioreactor systems that will be indistinguishable operationally from traditional larger scale bioreactors.

Peter Harms was supported by an NSF Graduate Fellowship.

References

Andersen DC, Swartz J, Ryll T, Lin N, Snedecor B. 2001. Metabolic oscillations in an *E. coli* fermentation. Biotechnol Bioeng 75:212–218.

Doig S, Pickering SCR, Lye GJ, Baganz F. 2005. Modelling surface aeration rates in shaken microtrite plates using dimensionless groups. Chem Eng Sci 60:2741–2750.

Elmahdi I, Baganz F, Dixon K, Harrop T, Sugden D, Lye GJ. 2003. pH control in microwell fermentations of *S. erythrae* CA340: Influence on biomass growth kinetics and erythromycin biosynthesis. Biochem Eng J 16:299–310.

Girard P, Jordan M, Tsao M, Wurm FM. 2001. Small-scale bioreactor system for process development and optimization. Biochem Eng J 7:117–119.

Harms P. 2004. Parallel miniature bioreactors in a twenty-four well plate. Ph.D. Thesis, UMBC.

Hermann R, Lehmann M, Büchs J. 2002. Characterization of gas–liquid mass transfer phenomena in microtiter plates. Biotechnol Bioeng 81: 178–186.

Hermann R, Walther N, Maier U, Büchs J. 2001. Optical method for the determination of the oxygen-transfer capacity of small bioreactors based on sulfite oxidation. Biotechnol Bioeng 74:355–363.

Humphrey A. 1998. Shake flask to fermentor: What have we learned? Biotechnol Prog 14:3–7.

John GT, Klimant I, Wittman C, Heinzle E. 2003. Integrated optical sensing of dissolved oxygen in microtiter plates: A novel tool for microbial cultivation. Biotechnol Bioeng 81:829–836.

Kermis HR, Kostov Y, Harms P, Rao G. 2002. Dual excitation ratiometric fluorescent pH sensor for noninvasive bioprocess monitoring: Development and application. Biotechnol Prog 18:1047–1053.

Kostov Y, Harms P, Randers-Eichhorn L, Rao G. 2001. Low-cost microbioreactor for high-throughput bioprocessing. Biotechnol Bioeng 72:346–352.

Lamping SR, Zhang H, Allen B, Shamlou PA. 2003. Design of a prototype miniature bioreactor for high throughput automated bioprocessing. Chem Eng Sci 58:747–758.

Lu C, Bentley WE, Rao G. 2003. Observations of oxidative stress in aerobic *Escherichia coli* fermentations. Biotechnol Bioeng 83:864–870.

Maharbiz MM, Holtz WJ, Howe RT, Keasling JD. 2004 . Microbioreactor arrays with parametric control for high-throughput experimentation. Biotechnol Bioeng 85:376–381.

Sandoval-Basurto EA. Guillermo Gosset, Francisco Bolivar, Octavio T Ramirez. 2005. Culture of *Escherichia coli* under dissolvedoxygen gradients simulated in a two-compartment scale-down system: Metabolic response and production of recombinant protein. Biotechnol Bioeng 89:453–463.

Zanzotto A, Szita N, Boccazzi P, Lessard P, Sinskey AJ, Jensen KF. 2004. Membrane-aerated microbioreactor for high-throughput bioprocessing. Biotechnol Bioeng 87:243–254.

Now that miniature bioreactor use with optical sensors is widespread, it seems hard to believe that there was so much resistance to their use initially. One of the frequent questions that we got was “how do you know if the optical sensors are not affecting cellular metabolism?” To answer this, we embarked on the following study in collaboration with FDA. Doug Frey and his student Hong Shen also joined the effort. We were able to extensively validate the sensor performance in a multiple bioreactor format. More importantly, we were able to do a genomic study and show that transcription was similar in bioreactors that were optically monitored versus control.

Available online at www.sciencedirect.com
SCIENCE DIRECT®
Journal of Biotechnology 122 (2006) 293–306
Journal of BIOTECHNOLOGY
www.elsevier.com/locate/jbiotec

Validation of an optical sensor-based high-throughput bioreactor system for mammalian cell culture

Xudong Ge [a], Michael Hanson [a,b], Hong Shen [a], Yordan Kostov [a], Kurt A. Brorson [b], Douglas D. Frey [a], Antonio R. Moreira [a], Govind Rao [a,*]

[a] *Center for Advanced Sensor Technology, Department of Chemical and Biochemical Engineering, University of Maryland, Baltimore County, 1000 Hilltop Circle, Baltimore, MD 21250, United States*
[b] *Office of Biotechnology Products, Center for Drug Evaluation and Research, Food and Drug Administration, 8800 Rockville Pike, Bethesda, MD 20892, United States*

Received 17 August 2005; received in revised form 27 October 2005; accepted 7 December 2005

Abstract

Cell culture optimization is a labor-intensive process requiring a large number of experiments to be conducted under varying conditions. Here we describe a high-throughput bioreactor system that allows 12 mini stirred-tank bioreactors to be operated simultaneously. All bioreactors are monitored by low-cost minimally invasive optical sensors for pH and dissolved oxygen. The sensors consist of single-use patches affixed inside the bioreactors and monitored optically from the outside. Experimental results show that different sensing patches with the same composition respond consistently. The discrepancy between different pH sensors is less than 0.1 pH units over most of their responsive range. The discrepancy between different dissolved oxygen sensors is less than 10% over the whole range from 0% to 100% dissolved oxygen. The consistency of the sensing system ensures that only an initial one-time calibration is required for the sensing patches. After that, a calibration code is generated and sensing patches of the same composition can be used directly. This greatly reduces the time and cost required for monitored multi-bioreactor operations. We used SP2/0 myeloma/mouse hybridoma cell cultures to demonstrate reactor performance consistency. Transcriptional profiling, HPLC analysis, viable cell count, and viability inspection show that the presence of sensing patches and the use of optical monitoring have no apparent effect on the metabolism of the cells.

Keywords: Optical sensor; Non-invasive; High-throughput bioreactor; Mammalian cell culture; Transcriptional profiling

1. Introduction

Although much progress has been made in the biotechnology industry, the development of bioprocesses is still rather labor-intensive and inefficient. In

* Corresponding author. Tel.: +1 410 455 3432; fax: +1 410 455 6500.
E-mail address: grao@umbc.edu (G. Rao).

0168-1656/$ – see front matter © 2006 Elsevier B.V. All rights reserved.
doi:10.1016/j.jbiotec.2005.12.009

order to bring a high quality product to the market as soon as possible, it is highly desirable to optimize the bioprocess expeditiously. Bioprocess optimization typically involves three major tasks: strain selection, media formulation, and selection of critical process parameters. Strain selection is to select the best producing colony from an early stage culture. Media formulation is developed to find the best combination of different nutrients such as sugars, amino acids, vitamins, minerals, and hormones. Because there are so many different nutrients, the combinational possibilities are enormous. Selection of critical process parameters is done to identify the ideal conditions and the allowable range for each variable. Some of the parameters are pH, dissolved oxygen (DO), feeding strategy, culture temperature, seeding cell density, induction time, and harvest time. In each of the above three tasks, a large number of experiments under varying conditions have to be conducted in order to determine the best colony or the optimal environmental and nutritional conditions.

The most commonly used devices for bioprocess optimization are laboratory-scale bioreactors and shake flasks. Laboratory-scale bioreactors equipped with various types of probes can provide more information about the bioprocesses than shake flasks. However, because experiments performed with laboratory-scale bioreactors are more labor-intensive and time-consuming, many compromises are often made during process optimization in order to keep the number of experiments down. Thus, there is a good chance that the optimal conditions may be missed. Even with compromises, process optimization could take more than a hundred runs, and often could last a year or more. Although process optimization performed in shake flasks is less labor-intensive and expensive, the conditions are generally not monitored, and only agitation and temperature are controlled. Thus, such studies can only provide limited information about the bioprocess.

To speed the process of new products going to the market, the development of fully instrumented high-throughput bioreactors that enable a large number of experiments in a short period of time is of great significance. Several companies and research groups are developing high-throughput bioprocessing devices for process optimization, and some are commercially available. Infors AG (Bottmingen/Basel, Switzerland) developed a Sixfors system, which is basically six laboratory-scale fermenters set side-by-side on a large platform. The advantages of this system over six individual fermenters are in reactor uniformity and a unified control. DASGIP (Jülich, Germany) developed a parallel shake flask system modified to accept DO and pH electrodes for process control. These systems use industry standard sensors for process monitoring or control. As these probes are expensive and non-disposable, their cleaning, sterilization, and calibration between experiments are still relatively time-consuming. Weuster-Botz et al. developed a gas-inducing milliliter-scale bioreactor system with a maximum of 48 stirred-tank reactors arranged in a bioreaction block (Puskeiler et al., 2005; Weuster-Botz et al., 2005). DO concentration was monitored online with fluorometric sensor spots immobilized onto the reactor bottom. OD and pH were monitored by automatically taking samples into commercially available microtiter plates, which were then transported to a plate reader. Maharbiz et al. (2004) presented an array of eight 250 μl microbioreactors each with closed-loop temperature control, adjustable oxygen supply generated electrochemically, and continuous pH and OD monitoring. Another approach to the development of high-throughput bioprocessing devices is the use of standard well plates supplemented with some type of sensing as microbioreactors (Girard et al., 2001; John et al., 2003; Lye et al., 2003). Measurements of process parameters were performed with commercial plate readers. Zanzotto et al. (2004, 2005) developed a membrane-aerated microbioreactor with only 5–50 μl working volume using commercially available sensor foils for pH and DO monitoring. The microbioreactor was successfully used in gene expression analysis. Since mass transport at this scale is diffusive rather than convective as in larger-scale fermentors, it is unclear whether this will be a scalable approach. Mass transfer into microtiter places with a view to high-throughput bioprocessing applications has been characterized (Hermann et al., 2002). Bioprocessors (Woburn, MA) have recently introduced a system capable of several hundred simultaneous cultivations at the hundred microliter scale. Both these systems by virtue of a high surface to volume ratio are capable of high volumetric mass transfer coefficients.

In this paper, we report the validation of an optical sensor-based stirred-tank high-throughput bioreactor system. This system can hold twelve 30-ml bioreactors with the two most important parameters (pH and

DO) being monitored by disposable optical sensors. The advantages of stirred-tank bioreactors include their wide applications in bioprocessing and the existence of a vast body of previous experience in design and scale-up. Miniature stirred tanks using optical sensors have been analyzed for their suitability in high-throughput bioprocessing (Lamping et al., 2003; Harms et al., 2006). Optical sensors have the advantages of being non-invasive, easily miniaturized, and low cost (Ge et al., 2003, 2004; Harms et al., 2002; Kostov et al., 2001). As sensing patches with the sample composition have the same analyte response, only a one-time calibration of the entire sensor lot is necessary. This allows for far simpler operation in practice, as sensors need not be calibrated individually. In this paper, the reliability and consistency of the sensing system, which is the basis of so-called calibration-free sensing, were evaluated. The performance of the bioreactors was evaluated with SP2/0 myeloma/mouse hybridoma cell cultures, and the possible effect of the sensor patches and excitation light on the metabolism of cells was examined. Although this system was not equipped with control capabilities, it provides an important first validation of the effect of optical monitoring on cell growth and product formation.

2. Materials and methods

2.1. The high-throughput bioreactor (HTBR) system

The HTBR system is shown in Fig. 1. The system consists of 12 mini stirred-tank bioreactors equipped with disposable DO and pH optical sensing patches (only 1 bioreactor and its agitation motor are shown), a detector board, a gas distributor, a turntable and is a commercial product made by Fluorometrix (Stow, MA). The turntable is hollow and also serves as a water bath. The bioreactors are 30 mm in diameter and 78 mm in height with a working volume of approximately 30 ml (Fig. 2). All the bioreactors were positioned on a turntable, which was driven by a stepper motor underneath it. Agitation was provided by two 6 mm × 18 mm paddles powered by the agitation motors. Each bioreactor has a fluorescence-based pH patch and a DO patch on the bottom, allowing on-line measurement of the two most important process parameters (Kermis et al.,

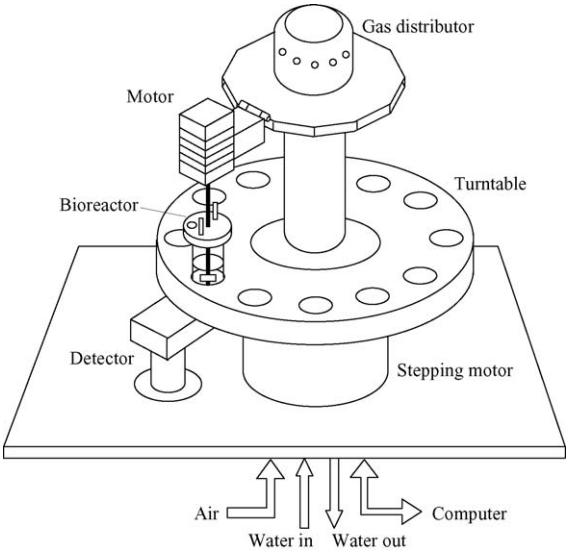

Fig. 1. High-throughput bioreactor (HTBR) system. The system can hold 12 stirred-tank bioreactors, but only one is shown here.

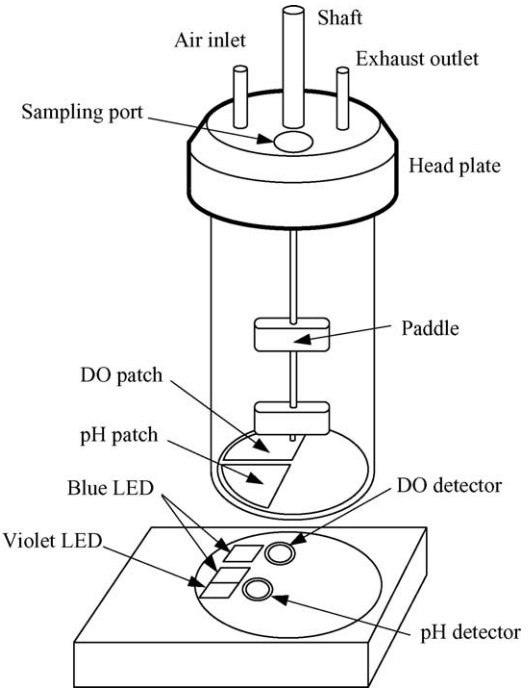

Fig. 2. The bioreactor and the monitoring system. Interference filters are positioned in front of the LEDs and photodiodes (not shown). Note that the sensing patches were affixed on the bottom while the LEDs and detectors were positioned outside. The advantage of this strategy is that the measurement is only partially invasive, but appropriate alignment of each patch to its corresponding optics is required.

2002, 2003; Tolosa et al., 2002). There are currently no closed-loop controls for pH and DO. This feature will be added to the next generation of the HBTR system. Temperature was controlled at 37 °C by circulating water between a refrigerated constant temperature circulator (Polyscience, Niles, IL) and the turntable. The inlet air, nitrogen and carbon dioxide were supplied from laboratory air supply, N_2 and CO_2 cylinders, respectively. Gas mixtures were obtained by blending different gases through two flowmeters (FM4332 and FM4333, Advanced Specialty Gas Equipment Corp., South Plainfield, NJ). The gas mixture thus obtained was sent to the gas distributor, which consists of a single inlet chamber with 12 outlets. Individual bioreactors connect to each outlet through plastic or rubber tubing followed by a 0.2-μm filter, and then to a sparger that delivers air into the media. There is currently no ability to individually meter air flow into each reactor.

The system was controlled by a computer equipped with a LabJack U12 card (LabJack Co., Lakewood, CO) using a custom LabVIEW program. Agitation speed could be adjusted continuously from 10 rpm to 1000 rpm in each bioreactor. Process parameters in one bioreactor were measured one at a time. After all the process parameters for one bioreactor were measured, the turntable rotated the next bioreactor above the detector. One measurement cycle takes from approximately 20 s to 4 min, depending on how many bioreactors are monitored.

For the present, only the optical sensing patches were made of disposable materials. The vessels were made of glass and the headplates were made of stainless steel. The current reactor is designed such that the glass vial with patches can be discarded after a single use. In the future, the reaction vessels and the accessories will be molded from biologically compatible disposable materials. Thus, the entire bioreactor including the optical sensing patches will be completely disposable. This development will significantly decrease the time and labor involved in performing experiments.

2.2. DO and pH monitoring

The oxygen sensor patches used in this study were provided by Lumet LLC (Bethesda, MD). The Lumet patches have three different layers: a responsive layer, an adhesive layer, and a white backing layer. The responsive layer is a layer of silicone rubber with an oxygen-responsive fluorophore immobilized in it (Tolosa et al., 2002). The adhesive layer is used for attaching to the bottom of the bioreactor. The white backing layer is designed to prevent autofluorescence from the growth media from affecting the fluorescence measurements.

The fluorophore immobilized in the DO patches is a long-lifetime fluorophore (Kostov et al., 2000b,c; Tolosa et al., 2002; Van Houten et al., 1998). When the fluorophore is excited by an intensity-modulated light source, the intensity of the resulting emission appears at the same frequency but with lower modulation and a phase shift. Because the fluorescence of the fluorophore is quenched in the presence of oxygen, the phase shift will change in response to a change in DO concentration.

The instrumentation to measure the phase shift uses a blue LED (Sharp Electronics Corp.) with a shortpass filter (Schott, Germany), and a PIN photodiode (BPW32, Vishay, France) with a longpass filter (Andover Corporation, NH). The LED was driven with a simple transistor driver that was controlled by the reference of an in-house built lock-in amplifier and modulated at 10 kHz. The photodetector output was connected to the signal input of the lock-in, and phase was measured (Harms et al., 1999).

The calibration of the DO patches was done in PBS buffers (pH 7.2). Six bioreactors with DO sensing patches were used for the calibration. The bioreactors were each added 20 ml of PBS buffer, and then placed on the turntable at positions 1, 3, 5, 7, 9, and 11, respectively. The gas mixture with desired O_2 content was obtained by mixing air and nitrogen whose flow rates were adjusted by flowmeters. The gas mixture bubbled through the PBS buffer. The temperature was maintained at 37 °C all the time.

The pH sensor patches used in this study were developed by the authors' laboratory (Kermis et al., 2002, 2003). They also have three different layers: an adhesive layer, a responsive layer, and a support layer. The adhesive layer has the same functions as the DO patches. The responsive layer is a hydrogel-white backing composite layer with the sensing fluorophore 6,8-dihydroxypyrene-1,3-disulfonic acid disodium salt (DHPDS) covalently immobilized in it. The white backing serves as both a support for the hydrogel and an optical isolator from the autofluorescence from the

media. Because the mechanical strength of the hydrogel is weak, an additional support layer (polyester film) was added between the adhesive layer and the responsive layer to enhance the patch's mechanical strength. Because of the high stability of the dye, the pH sensing patches can last 2 months with little drift.

The responsive fluorophore (DHPDS) immobilized in the pH patches possesses two excitation maxima at wavelength of 405 nm and 465 nm, corresponding to the protonated and deprotonated forms of the fluorophore. As a change in pH breaks the dissociation equilibrium of the fluorophore, the amount of the fluorophore in one of the two forms will increase while the other will decrease until a new equilibrium is reached. Correspondingly, the ratio of the two excitation maxima (R) will change.

The two excitation sources for the pH patches were a blue LED and a violet LED with a shortpass filter. The emission was filtered by a bandpass filter (Intor Inc., Socorro, NM) before reaching a PIN photodiode. The photocurrent was amplified by a transimpedance stage and a simple lock-in amplifier, both of which were developed in-house (Kostov et al., 2000a).

The pH sensors were calibrated using PBS or bicarbonate buffers of known pH and a constant ionic strength of 0.15 M with phosphate or carbonate buffering species at 73 mM and sodium chloride added to achieve the desired ionic strength. The pH of the buffers was verified with an AR25 Dual Channel pH/Ion Meter (Fisher Scientific, Pittsburgh, PA) before calibration. The temperature was also maintained at 37 °C all the time.

2.3. Cell culture

A SP2/0 based myeloma/mouse hybridoma cell line (2055.5) secreting an IgG3 antibody specific for the *Neisseria meningitides* capsular-polysaccharide (MCPS) (Rubinstein and Stein, 1988) was maintained in a 250-ml spinner flask (Kontes, Vineland, NJ) in CD Hybridoma protein-free media (Gibco Brand, Carlsbad, CA) supplemented with 2 mM glutamine (HyClone, Laboratories Inc., Logan, UT), 100 U/ml penicillin (HyClone), 100 μg/ml streptomycin (HyClone), 1 g/l PF-68 (MP Biomedicals, LLC, Aurora, OH), and 3.5×10^{-4}% β-mercaptoethanol (v/v) (Sigma, St. Louis, MO, USA). The flask was kept in a water-jacketed incubator (Napco, Winchester, VA) at 37 °C and 50% relative humidity with a headspace CO_2 composition of 5% in air.

Before performing the cell cultures on the HTBR, the air inlets and outlets of all vessels were covered with 0.22 μm syringe filters (Millex-GV, Millipore, Bedford, MA, USA). All vessels were then steam sterilized at 121 °C for 25 min. Upon cooling, each vessel was first rinsed with media and then filled with 35 ml of cell culture media inoculated with 0.1×10^6 cells/ml of media in a laminar flow hood. To explore the effect of patches and excitation lights (460 nm and 405 nm) on cell growth and culture environment, the experiment was carried out with cells being grown in three different situations. Among the 11 vessels used, vessels 1–5 had sensing patches and were monitored [patch(+)/light(+)], vessels 7–9 had no patches and were not monitored [patch(−)/light(−)], vessels 10–12 had no patches but were illuminated with excitation light like the monitored vessels [patch(−)/light(+)]. Vessel 6 was not used. The temperature and agitation speed was controlled at 37 °C and 300 rpm in all vessels. The vessel headspace was open to the atmosphere via 0.22 μm syringe filters. All light(+) vessels were illuminated every 30 min for monitoring or comparison. Samples were taken once a day with syringes through the sampling port on the vessels. Cells in the samples were counted using a hemocytometer, and viability was determined using the trypan blue exclusion method. At 45 h, 5 ml of culture were withdrawn from each of the bioreactors for transcriptional profiling. Final culture supernatants from the 11 reactors were analyzed using a high-throughput size-exclusion chromatography system.

Although the bioreactors were equipped with air spargers for culture aeration, it was found to be difficult to realize uniform air distribution among the bioreactors since individual needle valves were not employed for each reactor. This has also been previously observed in our prior work (Harms et al., 2006). As the main goal of the present study was to check the consistency and repeatability of the sensing system, and its effects on the cells, other factors affecting the growth of the cells such as non-uniform air distribution were deliberately avoided. Thus, no aeration other than by diffusion through the inlet and outlet filters was provided in the cell culture. Further studies using homogeneous air distribution among bioreactors are being conducted.

2.4. Transcriptional profiling

2.4.1. RNA extraction, reverse transcription, and DNA microarray hybridization

Total RNA from monitored [patches(+)/lights(+)] and control [patches(−)/lights(−)] cultures was extracted with Trizol (Gibco Brand) and chloroform (Mallinckrodt, Phillipsburg, NJ) and purified using the RNeasy Mini-Prep kit (Qiagen Inc., Valencia, CA). An indirect experimental design utilizing common reference RNA was used in the microarray study. For each DNA microarray, the following procedure was carried out. mRNA in 20 μg of total RNA [from cultured cells or a murine reference pool (Becton, Dickinson, and Co., Franklin Lakes, NJ)] was primed with 0.05 μg/μl oligo-dT^{20} (FDA/CBER Core Facility, Bethesda, MD) on ice for 10 min following a 10 min incubation at 70 °C. Primed mRNA was reverse transcribed to cDNA with 0.02–0.05 mM dNTPs (Invitrogen, Carlsbad, CA) and 3.33 U/μl reverse transcriptase (Stratagene, La Jolla, CA) in 1× first strand buffer (Stratagene) with 0.01 M DTT (Sigma) in a reaction at 42 °C lasting for 90 min. Non-reverse transcribed RNA and excess reaction reagents were removed using a MinElute PCR Purification Kit (Qiagen). The purified cDNA was fluorescently labeled with either Cy3 (reference cDNA) or Cy5 (culture cDNA) dyes (Amersham, Piscataway, NJ) for 90 min in 0.1 M $NaHCO_3$ (pH 9) coupling buffer (Sigma). Residual dye was removed afterwards with the same PCR Purification Kit.

Microarrays (16,896 spots, including positive/negative controls, and genes, some multi-spotted) obtained from the NCI/CBER microarray facility were pre-hybridized with 5× SSC buffer (American Bioanalytical, Natick, MA), 1% BSA (w/v) (Sigma), and 0.1% SDS (w/v) (Sigma) for 1 h, washed in DEPC-treated H_2O (MP Biomedicals, Irvine, CA) and isopropanol (American Bioanalytical) and spin-dried at 100 × *g* for 5 min in a table top centrifuge (Beckman, Fullerton, CA). Purified labeled cDNA from a single reactor was mixed with purified labeled cDNA from the reference pool and 32 μl of hybridization buffer (Ambion, Austin, TX), forming the hybridization solution, which was stored in the dark at 42 °C until usage. Immediately prior to hybridization, MAUI hybridization mixers (Biomicro, Salt Lake City, UT) were affixed to the microarray slide surfaces. Hybridization solution was injected into the mixers and the microarrays were placed into the MAUI hybridization chamber (Biomicro) for hybridization overnight at 42 °C.

2.4.2. Scanning, image processing, and data analysis

The microarrays were washed with 1× SSC (0.05% SDS) and 0.1× SSC, each for 4 min, and scanned for Cy3 and Cy5 signal intensities using a GenePix 400B microarray scanner (Axon, Union City, CA). Image processing (automatic and manual spot selection/rejection) was carried out using GenePix Pro 6.0 (Axon).

Using BRB ArrayTools software (http://linus.nci.nih.gov/BRB-ArrayTools.html, National Cancer Institute, Bethesda, MD), genes on individual arrays were filtered out according to their background subtracted fluorescence intensities. Ratios of the Cy5 and Cy3 signals were log-transformed and then normalized with a Lowess smoother, which takes into consideration dye intensity biases (Yang et al., 2002). Microarrays were carried out for four monitored and three control reactors. ArrayTools was then used to compare gene expression in the two groups of arrays by carrying out a Class Comparison analysis. The analysis utilizes a random-variance *t*-test (Wright and Simon, 2003) to identify genes that are differentially expressed (p-value <0.001) as a result of a change in culture conditions which, in this case, is the presence of the HTBR sensing system (DO and pH patches and excitation lights of varying wavelengths).

2.5. Size-exclusion chromatography

The size-exclusion chromatographic experiments were performed on an Ultimate HPLC instrument coupled to a FAMOS autosampler (LC Packings—Dionex, Sunnyvale, CA, USA) and controlled by Chromeleon software Version 6.6 (Dionex). The columns used were a 3.5 cm × 0.46 cm (i.d.) Super SW guard column and a 30 cm × 0.46 cm (i.d.) TSK-GEL Super SW3000 separation column placed in series (TosohBioscience, Montgomeryville, PA, USA). The samples from the micro-bioreactors were filtered through 0.2 μm polysulfone filters (Millipore) and stored in a 96 deep well plate in the FAMOS with the cooling system adjusted to 8 °C. A 100-μl sample loop was used for sample injection, and a conventional UZ-view flow cell with a 10 μl volume was used for UV detection.

The flow rate in the experiments was controlled at 0.1 ml/min, and the column effluent was monitored at both 260 nm and 280 nm. The eluent buffer was composed of 100 mM sodium phosphate and 300 mM sodium chloride (Sigma) at pH 7, and was degassed by vacuum filtering using a 47 mm diameter nylon membrane filter with 0.2 μm pores (Whatman, Clifton, NJ, USA).

3. Results and discussion

3.1. Mechanical stability

For a high-throughput bioreactor system, the most important feature is the parallel operation of process monitored bioreactors. To produce meaningful results, the sensing system of the parallel bioreactors must behave consistently, and all bioreactors must have comparable performance under the same conditions. This is especially important for the high-throughput bioreactor system described here, as the ultimate goal of our present study is a completely disposable system with calibration-free sensing capability. As long as the sensing system and the performance of the bioreactors are reliable and repeatable, other actions like closed-loop control, nutrient feeding, etc. can be performed with little difficulty. While the above comments apply to any bioreactor equipped with conventional DO and pH sensors, another very important question must be answered for optically monitored bioreactors. It is important to demonstrate that the blue and violet light used for sensor excitation has no measurable effect on the growth of the cells, their gene expression and the product quality. Because the success of the HTBR system and of optical monitoring in general is greatly dependent on these features, a major part of this work was devoted to the clarification and validation of these two aspects (i.e. consistency of operation and non-interference of the optical sensors).

The mechanical performance of the system was first evaluated by running the system continuously for several days. The temperatures inside different bioreactors were identical and no appreciable fluctuations were observed. The shafts of the agitators wobbled a little but their speeds were even, and the transition was smooth when the speed was adjusted from 10 rpm to 1000 rpm. The slight wobble of the shafts could be overcome by improving the bearing structure and the manufacturing precision.

3.2. Reliability and repeatability of the sensing system

To check the reliability and repeatability of the sensing system, six vessels with DO and pH sensing patches were used. The responsive layer of the DO sensing patches is a layer of silicone rubber with an oxygen-responsive fluorophore immobilized in it. For a single-emitting fluorophore, the phase shift (N) of the resulting emission when excited by an intensity-modulated light source applies (Lakowicz, 1999; Tolosa et al., 2002),

$$\frac{\tan(N_0)}{\tan(N)} - 1 = K_{SV}[Q] \quad (1)$$

where N_0 is phase shift of the fluorophore in the absence of the quencher, K_{SV} is the Stern Volmer constant, and [Q] is the concentration of the quencher. However, because there are dual-emitting species (Kostov et al., 2000b,c), the fluorophore in the DO patches does not completely follow the above linear equation. Here we used a non-linear equation to fit the DO calibration data,

$$P = \frac{\tan(N_0)}{\tan(N)} - 1 \quad (2)$$

$$[O_2]\,(\%) = AP^2 + BP \quad (3)$$

where $[O_2]$ is the DO concentration, A and B are constants shown in Fig. 3.

The calibration data and the fitted curve are shown in Fig. 3. It can be seen that a second-order polynomial fits the calibration data very well. The accuracy and consistency of the sensors is shown in Fig. 4. It can be seen that the six different DO patches gave consistent results with an average relative error of 9.0% from the real values. The fluctuation of the DO readings at 48.5% and 100.0% was caused by the instability of the flowmeters. To check if the cell culture media affect the calibration, the DO readings in PBS buffer and in cell culture media were compared at several different DO concentrations. The DO readings in PBS buffer were $0.1 \pm 0.1\%$, $9.8 \pm 0.3\%$, $25.0 \pm 0.6\%$, $27.8 \pm 0.4\%$, and $100.1 \pm 3.4\%$ while in cell culture media they were $0.0 \pm 0.0\%$, $9.4 \pm 0.1\%$, $24.6 \pm 0.4\%$, $27.7 \pm 0.5\%$, and $99.8 \pm 10.2\%$. Statistical analysis

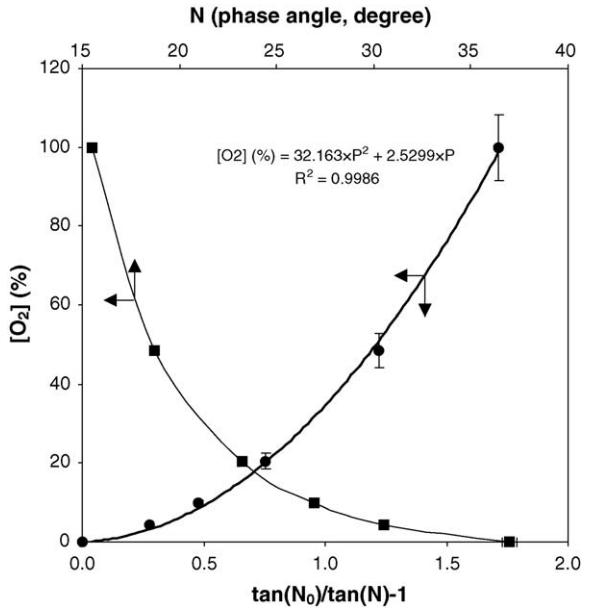

Fig. 3. Calibration of the dissolved oxygen patches. Calibration was done in PBS at 37 °C using six vessels each with a DO sensing patch. Gas mixtures of known composition were passed through each vessel. The error bars shown in the figure stand for the standard deviation of the six different readings, which are 0.4%, 0.8%, 2.0%, 4.4%, and 8.3% at DO concentrations from 4.3% to 100.0%. Divided by the corresponding DO concentrations, these deviations gave an average relative error of 9.0% from the real values.

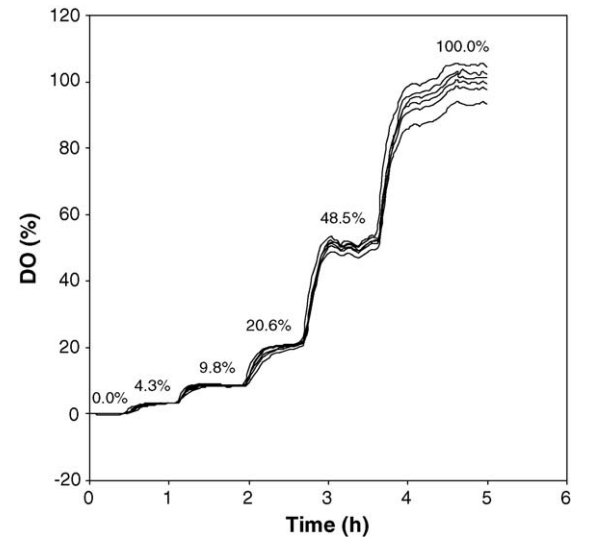

Fig. 4. Consistency of DO measurements in six different vessels.

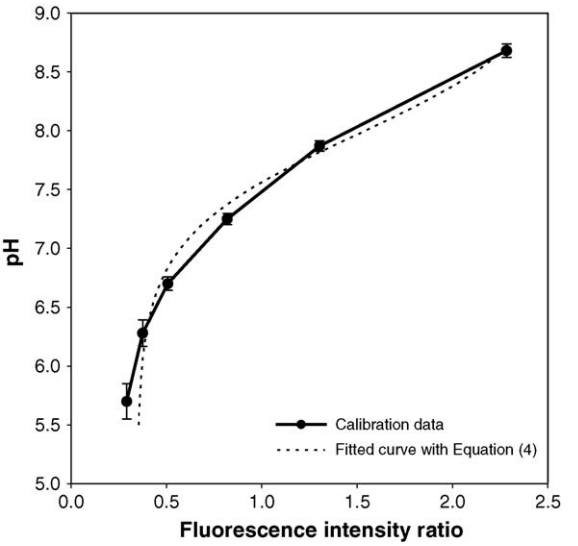

Fig. 5. Calibration of the pH patches. Calibration was done in PBS or bicarbonate buffers of known pH at a constant ionic strength of 0.15 M at 37 °C using six vessels each with a pH sensing patch. The error bars stand for the standard deviation of the six different readings, which are 0.15, 0.11, 0.06, 0.05, 0.05, and 0.06 pH units, respectively, from pH 5.70 to 8.68.

showed that there was no significant difference between the two sets of readings. The average 90% response time of the DO sensors is 12.6 min from air to nitrogen, and 10.8 min from nitrogen to air. Although not very rapid, these response times are more than sufficient for monitoring the slow DO changes typical of cell cultures.

The calibration data of the pH patches is shown in Fig. 5. The error bars represent the average deviations of the readings of the six sensors. For this kind of pH sensor, the following equation is often used to fit the calibration data (Kermis et al., 2003):

$$R = \frac{[H^+]R_{min} + K_{app}R_{max}}{[H^+] + K_{app}} \quad (4)$$

where R_{max} and R_{min} are the ratios of the two excitation maxima (460 nm/405 nm) for the deprotonated and protonated forms of the fluorophore, respectively, $[H^+]$ is the molar concentration of the hydrogen ions, and K_{app} is the apparent association constant of the fluorophore. The fitted line for Eq. (4) is shown in Fig. 5 (the dotted line). It can be seen that although it is more convenient to use, this equation can introduce big errors

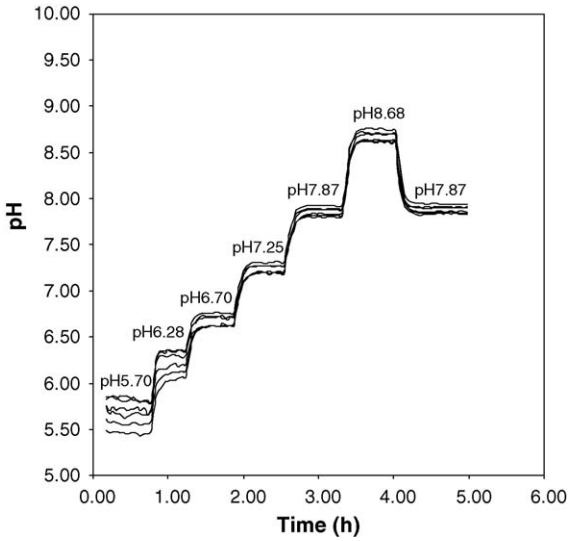

Fig. 6. Consistency of pH measurements in different vessels.

under pH 6.0. To avoid this problem, the pH values were calculated by linear interpolation.

The consistency of the sensors is shown in Fig. 6. It can be seen that all six sensors gave very similar results at pH above 6.5. At pH below 6.0, the sensitivity of the sensors is lower, and the consistency of the sensors decreases because a small error in intensity measurement can cause a relatively large error in pH. The average deviation of the sensors is 0.15, 0.11, 0.06, 0.05, 0.05, and 0.06 pH units, respectively, from pH 5.70 to 8.68. The maximum deviation is 0.23, 0.16, 0.07, 0.06, 0.06, and 0.07 pH units, respectively. Variance analysis showed that no significant difference existed between the 12 different positions on the turntable at 95% confidence level. Thus, the reasons for this discrepancy are limited to the patches and the bioreactors. Factors that may affect the consistency of the readings of different sensors include the uniformity of the patches, the size and alignment of the patches, the shape of the bioreactor bottoms, etc. Although the consistency of the readings is already quite good especially at pH above 6.5, it can be further improved by optimizing these factors. The average 90% response time is 5.4 min from pH 6.28 to 7.87, and 2.4 min from pH 7.87 to 6.28, which is rapid enough for cell culture monitoring. To confirm that the calibration done in PBS is applicable to cell culture, the pH of the fresh media was measured with the HTBR and the AR25 Dual Channel pH/Ion Meter. The two devices showed similar results, which were 8.8 ± 0.1 for the HTBR and 8.90 for the pH meter.

From the results shown above, it can be seen that different sensing patches with the same composition responded consistently. This is of great significance because it implies that the sensing patches need to be calibrated only once. After that, a calibration code is generated and the sensing patches with the same composition can be used directly for the next culture with no need for recalibration. Unlike optical probes in which the relative positions of the components are fixed, the detectors and the sensing patches used in this study were separate (Fig. 2). The advantage of this strategy is that the measurement is only partially invasive. Because the patches are autoclavable, they can be steam sterilized with the bioreactors. There is no direct contact between the external instrumentation and the culture during the process. This greatly reduces the chance of contamination. However, as the two components are separate, the alignment of the two is important. To obtain repeatable results, the sensing patches need to be positioned at the same positions right above the detector board (Fig. 2).

3.3. Performance consistency of bioreactors

To check the consistency of bioreactor's performance and the effect of the excitation light on the cell growth, cell cultures experiments were conducted in the system. The batch cell cultures lasted approximately 70 h. Samples were taken once a day for cell count and viability inspection. During the microscopic (400×) inspection of the samples, no visually detectable contamination was found in any of the 11 vessels during the cell culture.

Fig. 7 shows the DO and pH profiles in the five monitored vessels during the cell cultures. It can be seen that the cultures in all five bioreactors behaved almost identically. All DO and pH profiles followed the same trend, with only a 2.7% average difference in DO concentration, and a 0.09 unit average difference in pH. The oxygen levels were all continuously decreasing with time until totally depleted at approximately 40 h. The oxygen-limiting conditions persisted for 5 h. At 45 h, 5 ml of culture was withdrawn from each of the five bioreactors for transcriptional profiling. The withdrawal of 5 ml of culture sucked the same volume of

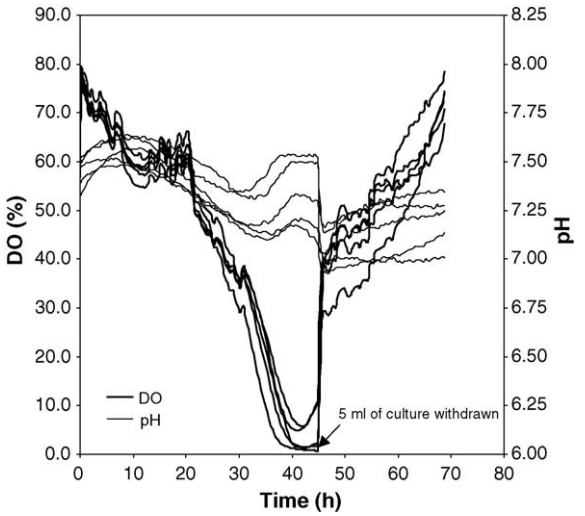

Fig. 7. DO and pH profiles in myeloma/mouse hybridoma cell cultures.

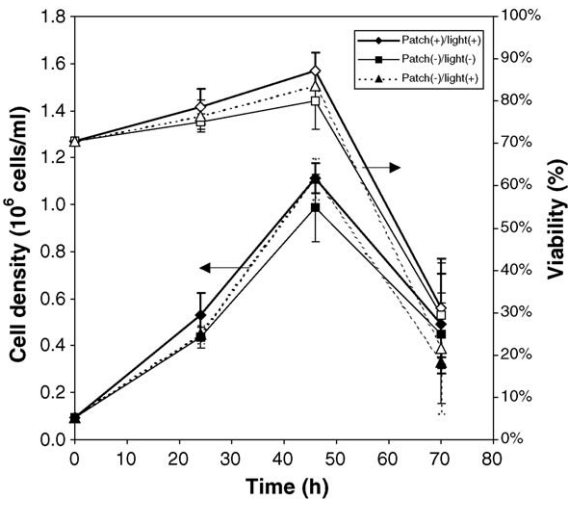

Fig. 8. Cell density profiles and viability profile in monitored and control myeloma/mouse hybridoma cell cultures.

air into the bioreactor, increasing the oxygen concentration in the headspace abruptly. This abrupt increase again induced an abrupt increase in DO concentration in the media. The subsequent gradual increase in DO concentration was caused by the lowered oxygen consumption as more and more cells began to die in the decline phase due to the depletion of energy or nutrient source. The pH increase during the first 10 h was likely caused by the gradual release of the CO_2 from the media, which was previously in equilibrium with 5% CO_2 when kept in the incubator. The culture became increasingly more acidic in the subsequent 20 h because the cells produced increasing amount of CO_2 as they grew. At the last stage of the exponential growth phase, the production of CO_2 by the cells slowed down, and pH began to increase again. The abrupt decrease in pH after the 5 ml of culture was withdrawn was probably caused by the escape of ammonia from the media. As the major nutrient and energy source for mammalian cell culture, glutamine could be metabolized through several different pathways, resulting in different energy output and ammonia release (Genzel et al., 2005). The ammonia thus formed likely accumulated in the medium and in the headspace above the media. The introduction of fresh air due to the sample withdrawal diluted the ammonia concentration in the headspace, causing the release of ammonia from the media. We are designing experiments to verify this observation definitively.

As the sensing patches were in contact with the cultures, and the patches were illuminated with excitation light once every 30 min, it was important to check if they have an effect on the cell growth. Fig. 8 shows the viable cell densities in cultures growing under three different conditions ([patch(+)/light(+)], [patch(−)/light(−)], and [patch(−)/light(+)]) and the viabilities of the cells. It can be seen that the viable cell densities and the viabilities of the cells in the three different situations are quite similar. *F*-test and Student's *t*-test showed that there was no significant difference between the three groups of data. The viable cell densities and the viabilities of the cells in three different situations all reached maximum at 46 h, consistent with the DO profiles. After that, cell lysis dominated in the process, the viable cell densities and the viabilities of the cells both began to decrease.

3.4. DNA microarray analysis

DNA microarrays are a powerful technique to simultaneously monitor the activity of a large percentage of the cell transcriptome. Thus, it is exquisitely sensitive to changes in the cell culture state and can be sued to definitively demonstrate culture consistency. DNA microarray analysis showed nearly identical gene expression profiles between cultures with and without monitoring. For example, in Fig. 9, the same portion of two different arrays is shown. One array

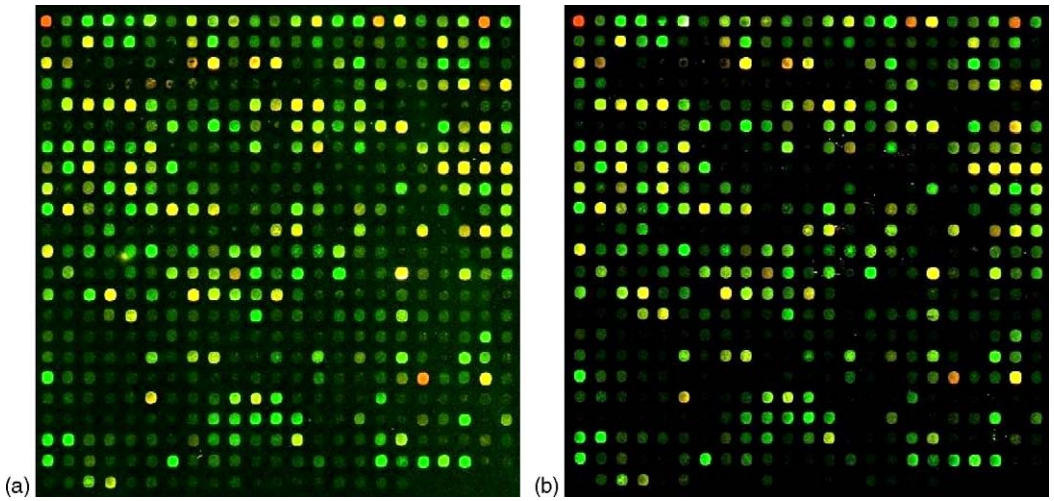

Fig. 9. The same portion from two different arrays, one from a control culture (a) and the other from a monitored culture (b). Red spots are indicative that the reactor cDNA present there is more abundant than the reference cDNA. Green spots designate the opposite. Yellow spots mean that the cDNA levels between the reactor and the reference pool are about equal. (For interpretation of the references to color in this figure legend, the reader is referred to the web version of the article.)

is from a monitored culture and the other is from a control. As can be seen, in that portion of the arrays the two samples show great similarity.

The similarity in the two expression profiles can also be seen by plotting the average logarithmic ratio of fluorescent signals $[\overline{\log_i}(\text{Cy5}/\text{Cy3})]$ for each gene in the monitored cultures versus the average ratio in the control cultures, as in Fig. 10. In this plot, if the expression of a gene is the same in both situations, the data point should fall along the middle diagonal line, also known as the identity line, or $y = x$. The two lines in the plot above and below the identity line represent thresholds for two-fold differential expression. For this experiment less than 1% of the genes in the analysis (14,005 genes passed the signal intensity filter) exhibited an average differential expression of two-fold or greater. However, using the average expression value across a series of experimental replicates does not take into consideration important statistical aspects, such as the number of samples and the variability within the groups.

Conversely, the Class Comparison analysis in ArrayTools does take these and other statistically relevant pieces of information into consideration when determining if genes are differentially expressed. To do so, it uses a random-variance *t*-test, which is an improvement over the standard separate *t*-test as it permits sharing information among genes about within-class variation without assuming that all genes have the same variance (Wright and Simon, 2003). Genes were considered statistically significant if their *p*-value

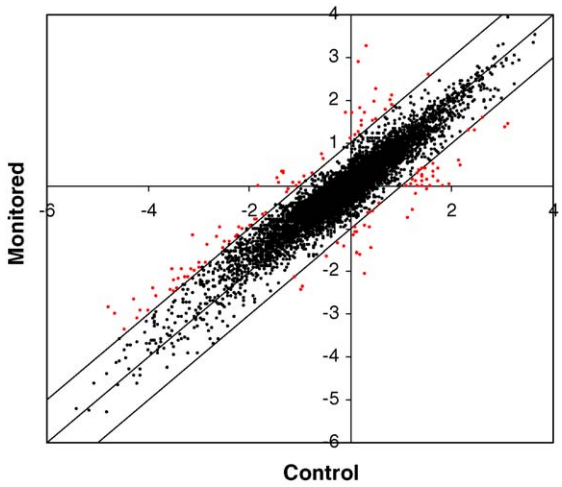

Fig. 10. A scatterplot of the average logarithmic ratio of fluorescent signals $[\overline{\log_i}(\text{Cy5}/\text{Cy3})]$ of each gene in the monitored reactors vs. the average in the control reactors. Red spots are genes whose average expression is two-fold up or down. Total of 14,005 genes in the analysis, 128 of which are red. (For interpretation of the references to color in this figure legend, the reader is referred to the web version of the article.)

was less than 0.001. A stringent significance threshold was used to limit the number of false positive findings. This is necessary in the situation present here where with the number of genes, one would expect as many as 14 false positives. Here the Class Comparison analysis returned no statistically significant differentially expressed genes, further supporting the conclusion that the sensing instrumentation does not impact the cellular physiology of the cultures.

3.5. Size-exclusion chromatography

Final culture supernatants from the 11 reactors were analyzed using a high-throughput size-exclusion chromatography system. The chromatograms of the 11 reactors were compared to the chromatogram (data not shown) of the sterile media itself. Shown in Fig. 11 is the portion of the reactor chromatograms that is unique to the cell culture, i.e. none of peaks shown were present in the media chromatogram. Fig. 11 shows a variety of peaks spanning a retention time from 20 min to 45 min. As the detector is measuring the absorbance at 280 nm, the identities of the different peaks could be a wide variety of proteins, such as cellular products and metabolites, or nucleic acid. Regardless of the peak identities, it is obvious from the similarity in trends that the cell culture environment was nearly identical in all 11 reactors.

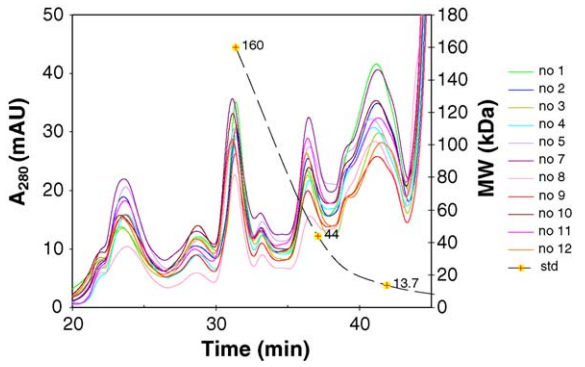

Fig. 11. A plot of a portion (retention time = 20–45 min) of the 11 reactor final supernatant size-exclusion chromatograms (reactor #6 not used) showing the absorbance at 280 nm (left axis). Three standard proteins: mouse IgG, ovalbumin, and RNase with molecular weights (right axis) of 160 kDa, 44 kDa, and 13.7 kDa, respectively, are plotted at their respective retention times. Reactors 1–5 [patches(+)/lights(+)], 7–9 [patches(−)/lights(−)], and 10–12 [patches(−)/lights(+)].

Table 1
The size-exclusion chromatographic retention times and final antibody titers of the 11 reactors

Configuration	Reactor no.	Retention time (min)	Antibody titer (mg/l)
Patch(+)/light(+)	1	31.38	94
	2	31.39	84
	3	31.43	80
	4	31.39	84
	5	31.26	92
		31.37 ± 0.06[a]	87 ± 6[a]
Patch(−)/light(−)	7	31.14	109
	8	31.29	75
	9	31.33	77
		31.25 ± 0.10[a]	87 ± 19[a]
Patch(−)/light(+)	10	31.18	109
	11	31.09	90
	12	31.14	86
		31.14 ± 0.04[a]	95 ± 12[a]
		31.27 ± 0.12[b]	89 ± 11[b]

Average = mean ± standard deviation.
[a] Average.
[b] Total average.

By using a mouse IgG standard (Southern Biotech, Birmingham, AL), the peak at the retention time of ∼31 min was identified as our anti-MCPS IgG_3 product peak. The product peaks for each reactor were integrated and the areas were compared to the standard area to determine the final antibody titer in each reactor. The retention time for each product peak was measured as well. The results are summarized in Table 1. Statistical analysis shows that the retention time has no significant difference between the monitored [patches(+)/lights(+)] and the control [patches(−)/lights(−)], and there is also no significant difference between the light only group [patches(−)/lights(+)] and the control [patches(−)/lights(−)]. Based on the limited variation in retention time, no observable aggregation or fragmentation of the product is suspected. Also it appears that the sensing system has no inhibitory effect on the organism's total IgG_3 production capability.

4. Conclusion

This paper described a disposable optical sensor-based high-throughput bioreactor system for bioprocess development and optimization. All bioreactors

were monitored by low-cost disposable optical sensors for pH and dissolved oxygen. Results showed that all sensors in different bioreactors behaved consistently, and all bioreactors had similar performance under the same conditions. The discrepancy between different pH sensors was less than 0.1 pH units in most of their responsive range. The discrepancy between different dissolved oxygen sensors was less than 10% in the whole range from 0% dissolved oxygen to 100%. Because the sensors behave consistently, only a one-time initial calibration was required. After that, the sensing patches with the same composition could be used directly without need for further calibration. SP2/0 myeloma/mouse hybridoma cell cultures grown in the bioreactors exhibited consistent reactor performance. Transcriptional profiling and HPLC analysis showed that the sensing patches and the optical sensing system had no apparent deleterious effects on cellular physiology at the transcript level and on product quality.

Acknowledgements

This work was sponsored by NSF Grant BES0091705 and unrestricted funding from Merck & Co. The technology described in this paper has been licensed to Fluorometrix, in which some of the authors (X.G., Y.K., and G.R.) have an equity position. We thank Ruth Cordoba-Rodriguez for a careful review of this manuscript. Microarray analyses were performed using BRB ArrayTools developed by Dr. Richard Simon and Amy Peng. Views expressed in this article are those of the authors and not necessarily those of the US FDA or the US Government. Discussion of individual cell culture devices does not constitute an endorsement by the US FDA or US Government. Michael Hanson is partially funded by a PDA Pre-Doctoral Fellowship.

References

Ge, X., Kostov, Y., Rao, G., 2003. High-stability non-invasive autoclavable naked optical CO_2 sensor. Biosens. Bioelectron. 18, 857–865.

Ge, X., Kostov, Y., Rao, G., 2004. Low-cost noninvasive optical CO_2 sensing system for fermentation and cell culture. Biotechnol. Bioeng. 89 (3), 329–334.

Genzel, Y., Ritter, J.B., Konig, S., Alt, R., Reichl, U., 2005. Substitution of glutamine by pyruvate to reduce ammonia formation and growth inhibition of mammalian cells. Biotechnol. Prog. 21 (1), 58–69.

Girard, P., Jordan, M., Tsao, M., Wurm, F.M., 2001. Small-scale bioreactor system for process development and optimisation. Biochem. Eng. J. 7, 117–119.

Harms, P., Kostov, Y., Rao, G., 2002. Bioprocess monitoring. Curr. Opin. Biotechnol. 3, 124–127.

Harms, P., Sipior, J., Ram, N., Carter, G.M., Rao, G., 1999. Low-cost phase-modulation measurements of nanosecond fluorescence lifetimes using a lock-in amplifier. Rev. Sci. Instrum. 70, 1535–1539.

Harms, P., Kostov, Y., French, J.A., Soliman, M., Anjanappa, M., Ram, A., Rao, G., 2006. Design and performance of a 24 station high throughput microbioreactor. Biotechnol. Bioeng. 93 (1), 6–13.

Hermann, R., Lehmann, M., Büchs, J., 2002. Characterization of gas-liquid mass transfer phenomena in microtiter plates. Biotechnol. Bioeng. 81, 178–186.

John, G.T., Klimant, I., Wittman, C., Heinzle, E., 2003. Integrated optical sensing of dissolved oxygen in microtiter plates: a novel tool for microbial cultivation. Biotechnol. Bioeng. 81, 829–836.

Kermis, H.R., Kostov, Y., Harms, P., Rao, G., 2002. Dual excitation ratiometric fluorescent pH sensor for noninvasive bioprocess monitoring: development and application. Biotechnol. Prog. 18, 1047–1053.

Kermis, H.R., Kostov, Y., Rao, G., 2003. Rapid method for the preparation of a robust optical pH sensor. Analyst 128, 1181–1186.

Kostov, Y., Albano, C.R., Rao, G., 2000a. All solid-state GFP sensor. Biotechnol. Bioeng. 70, 473–477.

Kostov, Y., Harms, P., Pilato, R.S., Rao, G., 2000b. Ratiometric oxygen sensing: detection of dual-emission ratio through a single emission filter. Analyst 125, 1175–1178.

Kostov, Y., Van Houten, K.A., Harms, P., Pilato, R.S., Rao, G., 2000c. Unique oxygen analyzer combining a dual emission probe and a low-cost solid-state ratiometric fluorometer. Appl. Spectrosc. 54, 864–868.

Kostov, Y., Harms, P., Randers-Eichhorn, L., Rao, G., 2001. Low-cost microbioreactor for high-throughput bioprocessing. Biotechnol. Bioeng. 72, 346–352.

Lakowicz, J.R., 1999. Principles of Fluorescence Spectroscopy, second ed. Kluwer Academic/Plenum Publishers, New York.

Lamping, S.R., Zhang, H., Allen, B., Shamlou, P.A., 2003. Design of a prototype miniature bioreactor for high throughput automated bioprocessing. Chem. Eng. Sci. 58, 747–758.

Lye, G.J., Ayazi-Shamlou, P., Baganz, F., Dalby, P.A., Woodley, J.M., 2003. Accelerated design of bioconversion process using automated microscale processing technique. Trends Biotechnol. 21 (1), 29–37.

Maharbiz, M.M., Holtz, W.J., Howe, R.T., Keasling, J.D., 2004. Microbioreactor array with parametric control for high-throughput experimentation. Biotechnol. Bioeng. 85 (4), 376–381.

Puskeiler, R., Kaufmann, K., Weuster-Botz, D., 2005. Development, parallelization, and automation of a gas-inducing milliliter-

scale bioreactor for high-throughput bioprocess design (HTBD). Biotechnol. Bioeng. 89, 512–523.

Rubinstein, L.J., Stein, K.E., 1988. Murine immune response to the *Neisseria meningitidis* group C capsular polysaccharide. II. Specificity. J. Immunol. 141 (12), 4357–4362.

Tolosa, L., Kostov, Y., Harms, P., Rao, G., 2002. Noninvasive measurement of dissolved oxygen in shake flasks. Biotechnol. Bioeng. 80 (5), 594–597.

Van Houten, K.A., Heath, D.C., Barringer, C.A., Rheingold, A.L., Pilato, R.S., 1998. Functionalized 2-pyridyl-substituted metallo-1,2-enedithiolates. Synthesis, characterization, and photophysical properties of (dppe)M{S_2C_2(2-pyridine(ium)) (CH_2CH_2OR'')} and (dppe)M[{S_2C_2(CH_2CH_2-N-2-pyridinium)}]$^+$ (R'' = H, acetyl, lauroyl; M = Pd, Pt; dppe = 1,2-bis(diphenylphosphino)ethane). Inorg. Chem. 37, 4647.

Weuster-Botz, D., Puskeiler, R., Kusterer, A., Kaufmann, K., John, G.T., Arnold, M., 2005. Methods and milliliter-scale device for high-throughput bioprocess design. Bioprocess. Biosyst. Eng. 28 (2), 109–119.

Wright, G.W., Simon, R.M., 2003. A random variance model for detection of differential gene expression in small microarray experiments. Bioinformatics 19 (18), 2448–2455.

Yang, Y.H., Dudoit, S., et al., 2002. Normalization for cDNA microarray data: a robust composite method addressing single and multiple slide systematic variation. Nucleic Acids Res. 30 (4), e15.

Zanzotto, A., Boccazzi, P., Gorret, N., Van Dyk, T.K., Sinskey, A.J., Jensen, K.F., 2005. In situ measurement of bioluminescence and fluorescence in an integrated microbioreactor. Biotechnol. Bioeng. 93 (1), 40–47.

Zanzotto, A., Szita, N., Boccazzi, P., Lessard, P., Sinskey, A.J., Jensen, K.F., 2004. Membrane-aerated microbioreactor for high-throughput bioprocessing. Biotechnol. Bioeng. 87 (2), 243–254.

Bhargavi Kondragunta joined the lab and we pursued the further development of the minibioreactor system. Jessica Drew was an undergrad who also got her Master's degree and worked on the project. We sought to see if there was value to using the minibioreactors for clone selection, which is traditionally done in well plates. Our hypothesis was that if you picked a high yielding clone from a well plate for further use in bioreactors, you may not get the best clonse simply because the well plate environment is quite different from a stirred tank.

It turns out that this was indeed the case as the following paper demonstrated.

Advances in Clone Selection Using High-Throughput Bioreactors

Bhargavi Kondragunta
Center for Advanced Sensor Technology, University of Maryland, Baltimore County, Baltimore, MD 21250
Dept. of Chemical and Biochemical Engineering, University of Maryland, Baltimore County, Baltimore, MD 21250
Div. of Monoclonal Antibodies, Center for Drug Evaluation and Research, Food and Drug Administration, Silver Spring, MD 20903

Jessica L. Drew
Center for Advanced Sensor Technology, University of Maryland, Baltimore County, Baltimore, MD 21250
Dept. of Chemical and Biochemical Engineering, University of Maryland, Baltimore County, Baltimore, MD 21250

Kurt A. Brorson
Div. of Monoclonal Antibodies, Center for Drug Evaluation and Research, Food and Drug Administration, Silver Spring, MD 20903

Antonio R. Moreira and Govind Rao
Center for Advanced Sensor Technology, University of Maryland, Baltimore County, Baltimore, MD 21250
Dept. of Chemical and Biochemical Engineering, University of Maryland, Baltimore County, Baltimore, MD 21250

DOI 10.1002/btpr.392
Published online January 29, 2010 in Wiley Online Library (wileyonlinelibrary.com).

Effective clone selection is a crucial step toward developing a robust mammalian cell culture production platform. Currently, clone selection is done by culturing cells in well plates and picking the highest producers. Ideally, clone selection should be done in a stirred tank bioreactor as this would best replicate the eventual production environment. The actual number of clones selected for future evaluation in bioreactors at bench-scale is limited by the scale-up and operational costs involved. This study describes the application of miniaturized stirred high-throughput bioreactors (35 mL working volume; HTBRs) with noninvasive optical sensors for clone screening and selection. We investigated a method for testing several subclones simultaneously in a stirred environment using our high throughput bioreactors (up to 12 clones per HTBR run) and compared it with a traditional well plate selection approach. Importantly, it was found that selecting clones solely based on results from stationary well plate cultures could result in the chance of missing higher producing clones. Our approach suggests that choosing a clone after analyzing its performance in a stirred bioreactor environment is an improved method for clone selection. © 2010 American Institute of Chemical Engineers *Biotechnol. Prog.*, 26: 1095–1103, 2010
Keywords: high-throughput, mini-bioreactors, subcloning, noninvasive, optical, sensors

Introduction

Therapeutic proteins have an annual global market of ~US $33 billion, and it is expected to increase to US $70 billion by 2010.[1] The success of engineered therapeutic monoclonal antibodies in particular has spurred considerable interest in developing improved manufacturing strategies, including initial selection of high-producing stable antibody expressing clones in a cost-effective and high-throughput manner. Effective subclone selection, typically done after transfection, is central to obtaining stable cell lines for manufacturing. In addition, subcloning of hybridomas must also be done periodically to remove low and nonproducing cells that arise as a result of chromosome loss and mutation in the heavy chain of the antibody.[2] In many cases, nonproducers have been found to proliferate faster than those cells that are producing higher antibody titers[3] and overtake the culture.

The traditional method of subclone selection is by limiting dilution (LD) cloning in 96-well plates, generally the most economical and simplest method.[4] The highest producing clone is chosen based on ELISA results from the stationary well plates. In some cases, cells are selected based on specific productivity of membrane IgG expression of individual cells by cell sorting.[5] Data from other groups has indicated that the selection methods based on productivity from a single point resulted in a high chance of selecting an unstable cell line.[6] Clone selection should be based not only on higher titers in 96-well cultures, but also on compatibility with the actual production culture such as batch or fed-batch processes. A major drawback with the 96-well plate approach is time and expense; developing and qualifying such stable cell lines with proven higher antibody productivity is a major undertaking in a commercial environment that

Statements in this article represent the views of the authors and do not constitute official positions or policies of the Food and Drug Administration or the U.S. Government.

Correspondence concerning this article should be addressed to Govind Rao at grao@umbc.edu

takes about 6–12 months. Also 96-well plates and subsequent T-flasks are generally not instrumented, and can not be monitored for critical parameters like percent DO (percent dissolved oxygen in liquid media) and pH.

Typically the number of clones selected in 96-well culture that are transitioned to bioreactors are few (typically < 4), since it is inefficient and expensive to scale up a large number of clones to bench-scale. Thus, a large number of clones are left out before knowing how well they would perform in a stirred environment. Although small scale devices such as shake flasks and spinners have been used to screen clones and thus increase this number, the inability to monitor and possibly control DO and pH are strong drawbacks. For example, DO variations can greatly affect glycosylation profiles.[7]

Miniaturization and parallelization of monitored cell culture is a key goal for bioprocess research. Examples of miniaturized devices include microfabricated fiber optic sensors for DO, pH, and cell density[8] used in a 6-mL miniaturized bioreactor[9] and a 50-μL bioreactor.[10] Another is a 250-μL bioreactor with commercial ion-selective field effect transistor (ISFET) pH sensor chip.[11] Third is a reaction block for 48 magnetically mixed miniaturized 5–10-mL scale bioreactors with control for pH and substrate addition.[12] Additional advances in high-throughput technology have included a 24-well plate mini-bioreactor system,[13] a 150-μL membrane aerated microbioreactor,[14] and chambers with gas diffusion through polymethylpentene membranes for cell culture.[15] Efforts were made for developing instrumented shake flasks which can monitor real-time DO and pH.[16-19] The shake-flasks from DASGIP (Julich, Germany) and TAP (UK) have the ability to control pH. Pioneering work was done using disposable, noninvasive optical sensors[20] which were integrated and validated for high-throughput applications.[21-23] Finally, glucose sensors have been developed that can give on-line measurements in the micro molar range[24] and can be used in miniaturized bioreactors.

The high-throughput bioreactors (HTBR) technology is different from similar high-throughput technologies; it not only has the critical functional aspect of mixing comparable to bench-scale bioreactors,[25] but also includes the disposable optical sensors. These functionalities make it an ideal system for bridging the gap between early stages of clone selection in well plates, and its future use in bioreactors. With the use of disposable optical sensors in a stirred environment, the performance of individual clones can be more thoroughly understood by monitoring real-time DO and pH profiles. In this study we demonstrated that this is possible by selecting subclones based on their performance in the high-throughput bioreactors, not just from 96-well plates alone. These results were compared to those from stationary well plate cultures alone.

Materials and Methods

Cell culture

An Sp2/0 myeloma based mouse hybridoma cell line (2055.5) secreting an anti-meningitidis-capsular–polysaccharide (anti-MCPS) IgG3[26] was used as the experimental cell line. The parental hybridoma clone was obtained from Dr. K. Stein (CBER/FDA) in 2002 for subsequent subcloning experiments. The cells were maintained in T-Flasks (Corning, Lowell, MA) and 250-mL spinner flasks (Kontes, Vineland, NJ) in a 5% CO_2 incubator (Napco, Winchester, VA) at 37°C, in chemically defined (CD) hybridoma media (Invitrogen, Carlsbad, CA) and passaged every 3–4 days. Each 1 L of CD media was additionally supplemented with 8 mM of L-Glutamine (Invitrogen, Carlsbad, CA) and 3.5×10^{-4} % β-mercaptoethanol (v/v; Sigma, St. Louis, MO) as described in Table 1. 10% of fetal calf serum (FCS; HyClone, Laboratories, Logan, UT) was added to the media during subcloning and passaging of selected clones. Cell density and viability were determined using a hemocytometer with trypan blue dilution, and Volupac (Sartorius AG, Germany) was used to measure the packed cell volume (PCV) after spinning the cell sample at 2,500 rpm for 1 min. The glucose and lactate were measured with the YSI 2700 SELECT Biochemistry Analyzer (YSI, Yellow Springs, OH).

Table 1. 12-Unit HTBR Station Cell Culture Operational Parameters

Cell Culture Operational Parameter	Values
Working volume (mL)	35
Seeding density (cells/mL)	2.5×10^5
Starting pH	7.2 ± 0.2
Impeller speed (rpm)	150
Sample volume (mL)	0.5
DO	Allowed to follow natural trend due to cell growth
Temperature (°C)	37
Cell culture medium	CD Hybridoma with 10% Fetal calf serum, 8 mM L-glutamine and 3.5×10^{-4} % β-mercaptoethanol (v/v)

The batch run of 6 days was used a standard procedure. pH was manually controlled on Day 0 to bring it within 7.2–7.4. For the impeller speed and air flow-rate used, the $k_L a$ by gassing out method was 0.9 h^{-1}.

High-throughput bioreactor system

HTBR System Description. The HTBR system (Fluorometrix, MA) was designed and manufactured in-house[23]; it consists of a rotating platform that can hold up to 12 miniature bioreactors on its outer edge. The turntable is hollow, and when connected to an external water bath, provides temperature control for the mini-bioreactors. Each of the mini-bioreactors (Figure 1) is composed of a stainless steel headplate and a glass vial with a 35 mL working volume, and has been previously illustrated in a schematic.[23] The headplates have an inlet and an outlet for gas exchange, a rubber septum for sampling, and a shaft with two impellers. Each shaft can be connected with an overhead motor which is capable of stirring up to 1,000 rpm; in these studies it was operated at 150 rpm. Twelve individual rotameters can be manually set up to deliver air and carbon dioxide gas mixtures up to 40 mL/min. The system shines a light emitting diode (LED) up through the bottom of the glass vessel of the mini-bioreactor. Two optical sensor patches are positioned in the reactor, which emit fluorescence based on analyte levels. The fluorescence is quantified by detectors on the other side of the glass which interfaces with the Labview software (Fluorometrix).

Two optical sensors, one for DO and one for pH[20] were used. Each sensor is a patch with 3 layers; a responsive layer, a backing layer which helps reduce interference from the media in the fluorescence reading and an adhesive layer. The calibration of the DO and pH patches has been described previously.[21]

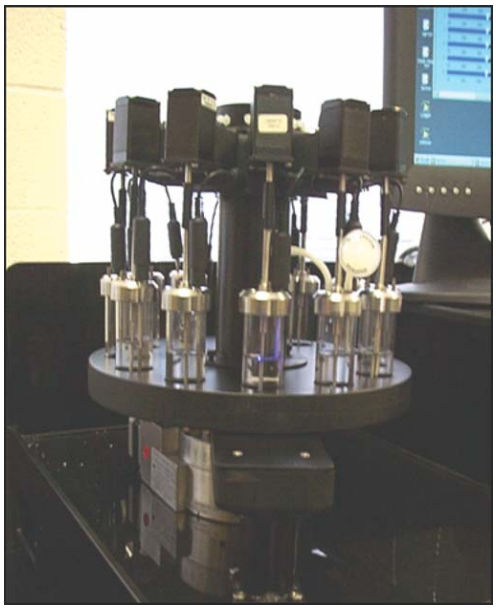

Figure 1. Twelve-unit HTBR station with 35 mL working volume glass vessels.

HTBR Cell Culture. For the experiments reported here 12 mini-bioreactor vessels with 35 mL working volume each were used. Vacuum grease was added around the impeller shaft and opening in the head plate to help seal the connection. The assembly of the reactor began with affixing of the patches at the bottom of the glass vessel, followed by attaching 0.22-μm venting filters (Sartorius) to the gas in- and outlet ports. After assembly, water was added to each vessel, and they were steam sterilized at 121°C for 25 min. After the mini-bioreactors had cooled to room temperature they were inoculated in a laminar airflow hood with $\sim 2.5 \times 10^5$ cells per ml in 35 mL total volume, using the seed from stationary T-flasks. During the first 4 h after inoculation, pH was monitored and CO_2 was added via head-space at 3.7 mL/min to all the vessels to bring the pH down to a range of 7.2–7.4 (Table 1). At the beginning of the culture the pH control range was 7.2 ± 0.2. However, by following the natural trend without control, just as they would in a shake-flask, they remained within physiological conditions (i.e., >6.60, even during the peak growth phase of the culture).

A continuous air-overlay at 5 mL/min to the head-space was maintained starting from Day 2 to the end of the run to allow culture oxygenation. Before Day 2, diffusion of air through the bioreactor vent filters was the source of oxygen supply to the cells. Samples were taken daily for 6 days (0.5 mL per day) with a 19 gauge 1½″ sterile needle. The rubber septum was sterilized with 70% ethanol before the sample was withdrawn. The sample was used for measuring (1) cell count and viability, (2) ELISA (Enzyme-Linked ImmunoSorbent Assay), (3) glucose and lactate concentration, and (4) packed cell volume and percent biomass using Volupac (Sartorius AG, Germany).

Limited dilution cloning

For this work, we chose a SP2/0-based mouse hybridoma cell line, 2055. We had previously observed that this 15-year old clone was somewhat unstable in CD media. For example, right after thaw it produced around 60 mg/L of IgG3 protein in batch culture, but productivity declined over a 1 month culture period to about 30 mg/L, thus it was an ideal model for our experiment. Parental 2055 hybridoma cells were plated at 1 cell/well (as assessed by trypan staining) using standard limited dilution methods. Because of inefficient survival of isolated cells, this level of seeding results in a net seeding level of <0.3–0.5 cells/well, ensuring clonality of the majority of the wells.

Briefly, hybridoma cells were allowed to grow for 72 h after which the cell suspension was diluted to a final cell density of 1×10^3 cells per mL in CD medium (Invitrogen, CA) supplemented with 10% Fetal Calf Serum (HyClone, Laboratories, Logan, UT) and 8 mM L-Glutamine (Invitrogen, CA). From this, serial dilutions were made until a final cell density of 5 cells/mL was achieved. The final diluted cell suspension was dispensed using an eight-channel pipette in 200 μL aliquots into five 96-well tissue culture treated U-bottomed microplates (Corning, Lowell, MA) at a final concentration of 1 cell/well in CD medium with 10% FCS and allowed to incubate at 37°C in a 5% carbon dioxide incubator for 12 days. Supernatant samples were removed for recombinant antibody quantification using ELISA. Surviving clones (12 in total) were transferred into T-25 tissue culture flasks (Corning) and allowed to grow in fresh media. Cells were monitored periodically until there was enough culture to inoculate the high-throughput mini-bioreactors (<5 mL inoculum per reactor).

ELISA

An ELISA was used to quantitate supernatant IgG3 titer levels[27] in 96-well plates (Labcor, Anjou, QC, Canada). The plates were coated with 2 μg/mL goat anti-mouse-κ affinity purified antibody (Southern Biotech, Birmingham, Alabama) in 0.015 M bicarbonate buffer, pH9.0 and incubated for 1 h. The plates were washed and then blocked with PBS/1% Fish gelatin (Fisher, Pittsburgh, PA) for 1 h, followed by washing. An initial 200-fold dilution was performed for each of the samples prior to loading. The reference standard used was mouse IgG3 (Pharmingen, CA) at concentrations of 2,500 ng/mL and 50 ng/mL. A 3-fold dilution series of test samples and purified mouse IgG3 standards was performed directly in the wells. The plates were incubated for at least one hour and then washed. Five milliliters of developing reagent, goat anti-mouse antibody alkaline phosphatase (Southern Biotech, Birmingham, Alabama) was added per plate after 1:2,000 dilution. The plates were incubated for 1 h and then washed. Finally, the 4-methylumbelliferyl phosphate substrate buffer (Sigma, St. Louis, MO) was added and plates were scanned using a Spectramax M5 (Molecular Devices, Sunnyvale, CA) plate reader. Plate readings were taken after 20 and 30 min post substrate addition in a top-down fashion at an excitation of 360-nm and emission of 450-nm. SoftMax 5.0 software was used to analyze the data.

Experiments in high-throughput bioreactors

Control HTBR Run. To verify individual reactors were uniform in functionality, control cultures were run in each of the 12 vessels. This was to rule out contribution from vessel-by-vessel variation, if the subclones themselves were observed to be growing differently. For this experiment, a vial of a subclone termed "C14," described later, was thawed and passaged in CD media with 10% FCS for 2 weeks,

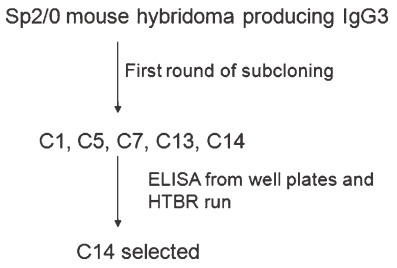

Figure 2. Schematic of Experiment I.

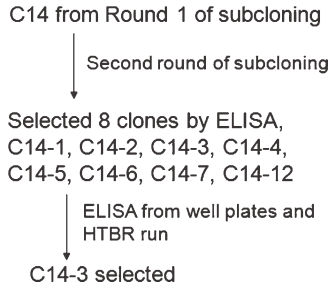

Figure 3. Schematic of Experiment II.

to obtain enough inoculum for 12 mini-bioreactors. Each of the twelve mini-bioreactors was inoculated using the operating parameters described in Table 1. The bioreactors environmental and operational parameters are as previously described in "HTBR Cell Culture" section. Standard deviation was computed at each time-point across all 12 reactors. Coefficient of variation (%CV) was computed as the ratio of the standard deviation to the mean. An average standard deviation and %CV was then computed across all time points.

Experiment I. To demonstrate the utility of the HTBR for selection of stable clones with high productivity, the SP2/0 cells were subcloned using LD cloning and then grown in the HTBR. Five clones were selected from 96-well plates based on their ELISA results, and frozen until further testing. These were denoted as C1, C5, C7, C13, and C14 (Figure 2).

To determine if these 5-well plate selected clones performed differently in a stirred bioreactor environment (i.e., did they secrete higher/lower titers of antibody), they were thawed and seeded into the HTBR in triplicate using the operational parameters described in Table 1. Clone C1, which was a nonproducer, was also included as a negative control. To scale up the cell density to an acceptable level to seed the HTBR, the subclones were briefly cultured in T-flasks (<2 weeks) as described previously.

Experiment II. This experiment was done to further confirm the hypothesis tested in Experiment I, with minor modifications. The HTBR system was employed for initial screening of up to 12 clones in one run, using the same LD protocol as the first round of subcloning. C14 cells were subcloned with one cell per well in three 96-well plates (Figure 3) and protein titers were measured by ELISA. The main difference from Experiment 1 was that the scale-up time from well plates to mini-bioreactors was minimized (scaled-up directly from 96-well plates. The seed was scaled-up in 10 days to inoculate the HTBRs using operational parameters described in Table 1.

Results

To test the HTBR as a system for clone selection, we set up two rounds of subcloning to evaluate differences in productivities and growth of subclones in 96-well plates and the HTBRs. We also ran a control experiment to validate that the HTBR vessels themselves are uniform in their ability to support hybridoma cultures.

Table 2. Average %CV for Growth and Environmental Parameters for the Control Batch Run Using Clone C14 in All 12 HTBRs

Growth and Environmental Parameters from Control Run	%CV from Control Run with 1.2-HTBRs with Clone C14
Viable cell density	9.0
%DO	5.5
pH	1.1
ELISA	11.1

In all cultures, we supplemented the media in the HTBR with 10% fetal calf serum. Cloning in 96-well plates is often very difficult in the absence of serum. Single, isolated cells in culture may need unknown factors present in serum that are not needed when in dense contact cultures, like an established production culture. Since the early/mid-1990s, the standard for biotech production cultures is to use serum-free or protein-free media. However, our system is designed to mimic a very early phase of product development, cell line screening. ICH Q7 (2000) essentially defines biotech GMPs (Good Manufacturing Practices) as starting at the working cell-bank stage, long after cell line screening. Thus, GMP approaches applicable for production cultures do not necessarily apply to cell line screening.

Experiment I

This first HTBR clone selection experiment was conducted with the five clones from 96-well plates, C1, C5, C7, C13, and C14 (Figure 4). The cultures were healthy and viable for 6 days in the batch mode. The critical parameters pH, DO, and glucose remained within a range consistent with culture survival, although some fluctuations were seen in DO and pH as the cultures are uncontrolled.

The HTBR allowed detection of differences between clones mainly using on-line DO profiles. Although some variability in DO profiles was observed during exponential phase, most variability was observed during the stationary phase of the culture on Days 4 and 5. In this phase of culture, DO profiles of all the clones started to trend upwards, mirroring the slow-down in cell growth and drop in viability. The differences in DO profiles clearly showed the clones that survived longer in culture vs. the clones that lost viability earlier. For example, the DO profile of clone C5 came up much earlier than that of the other clones which correlated with the drop in its viability profile by Day 4. Whereas the DO profiles of clones C13 and C14 came up the last, which is in agreement with the higher cell densities and higher viabilities towards the end of the batch culture. Although the DO was recorded to be close to 0% during exponential growth, there was sufficient oxygen to keep the culture viable, mainly due to continuous headspace aeration. Overall, the HTBR allowed monitoring of this key cell culture parameter at a cell-line selection stage where it is typically not performed (i.e., during early clone selection). By monitoring DO consumption at this early stage, more informed decisions can be made concerning which clone to ultimately choose.

The pH trends were monitored to ensure that they stayed within physiological limits for the entire length of the run. A response was observed in culture pH when there was CO_2

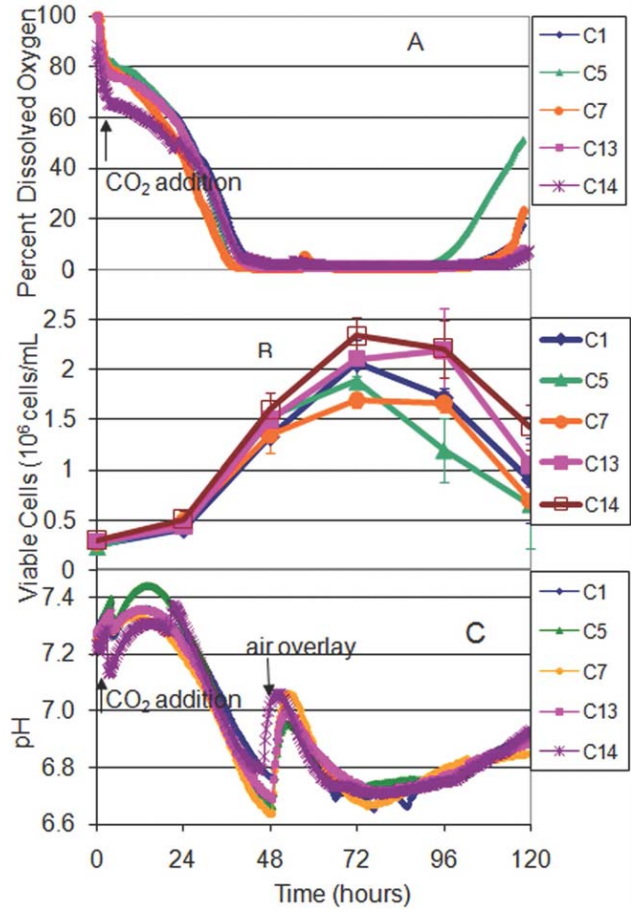

Figure 4. DO, cell growth, and pH profiles from Experiment I for the first set of subclones C1, C5, C7, 13, and C14.

A: Average Percent dissolved oxygen profiles of subclones. The error bars were not included for better picture clarity. The majority of the data (>70%) was within one standard deviation. B: Average viable cell density by cell counting with a hemocytometer and trypan blue for the subclones. The error bars reflect one standard deviation. C: Average pH profiles of subclones. Error bars were not included to allow meaningful data interpretation.

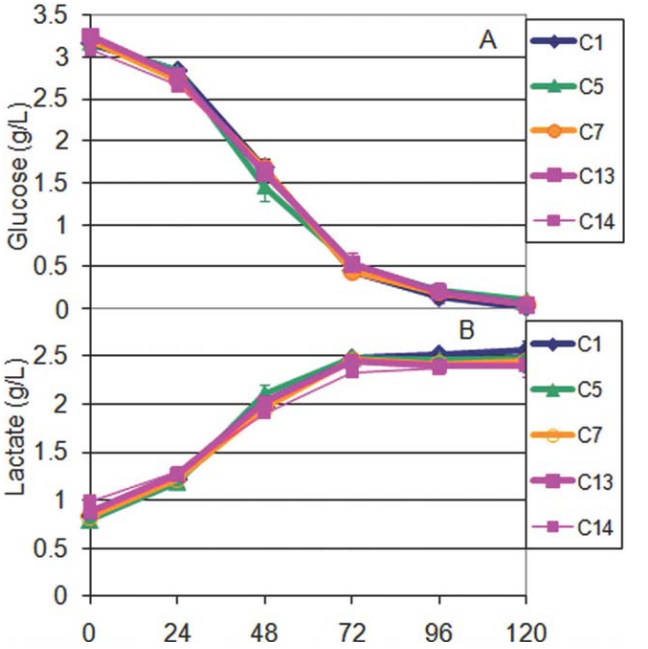

Figure 5. A: Average Glucose concentration measurements from Experiment I using YSI 2700 glucose analyzer. Error bars are one standard deviation, for the batch run for 120 h. B: Average lactate concentration measurements, with error bars reflecting one standard deviation.

Table 3. Average IgG3 Concentration Produced by Clones from Well Plates and Day 5 of the Batch Culture (Peak Titer) in Experiment I

Subclone ID	IgG3 Concentration from 96-Well Plates (mg/L)	AverageIgG3 Concentration from Triplicate HTBR Runs for Subclones (mg/L)
C1	0	0
C5	10.1	126.6
C7	19.8	150.8
C13	55.4	157.5
C14	60.8	167.3

addition to the head-space, as well as when air overlay was started to the HTBR culture. The glucose and lactate concentration profiles (Figure 5) for all of the clones were found to be very similar. This information is also useful for early clone selection in that it indicates that other parameters, like DO should be focused instead on during the decision making process.

The average antibody titers of the subclones from the initial stationary well plates were compared with the average Day 5 titers of the clone from HTBR runs (Table 3). From the well plate ELISA, clone C14 was determined to be the highest producer, with C13 close behind. It is known that the cell densities are variable in well plates, but still clones are selected based on higher ELISA values from the supernatant. All titer levels in HTBRs were much higher than in well plates as the peak cell density reached is much higher in the HTBRs. The ELISA results from Day 5 of the HTBR run shows that although C14 is still a high producer, C7 and C13 also have very similar productivities with less than 13% difference between the clones. Clone C1, a nonproducer from well plates worked as negative control in the HTBRs. For each subclone run in triplicate in the HTBRs, the standard deviation was computed for all the cell culture parameters on each day, following which an average standard deviation and %CV was obtained for all the days in culture. The average %CV measurements for cell culture growth parameters of the subclones is shown in Table 4, with majority of the data (>67%) within one standard deviation.

This information can be key for the decision making process during clone selection. By verifying that cell density and key cell culture parameters remain in an acceptable range and culturing the clones in stirred environment, more uniform levels of IgG expression was observed between clones. All of the clones reached similar peak cell densities in the HTBRs, thus removing cell density as a variable as in 96-well plates. Thus, use of the HTBR prevented an overemphasis on high expression by one particular clone that may have resulted from a 96-well plate artifact, rather than actual higher specific productivity.

Experiment II

In this experiment, there was extreme heterogeneity in the growth and DO profiles of the subclones (Figures 6 and 7A),

Table 4. Summary of Average %CV of Cell Culture Environmental and Growth Parameters of Triplicate HTBR Runs from Experiment I

	Coefficient of Variation (%CV) for Cell Culture Growth Parameters of Each Clone from Experiment I					
Subclone ID	Viable Cell Density	Percnet DO	pH	Titer	Glucose	Lactate
C1	5.26	4.51	0.954	N.A.	4.15	1.15
C5	2.93	0.994	1.41	15.36	5.57	2.75
C7	7.80	3.06	0.840	5.81	6.92	2.64
C13	3.46	3.39	0.55	1.55	8.14	1.66
C14	12.71	2.61	1.39	7.87	6.68	2.98

The average standard deviation is for the entire length of the batch run, from Day 0 to Day 5, with sampling at 20-min interval in HTBRs.

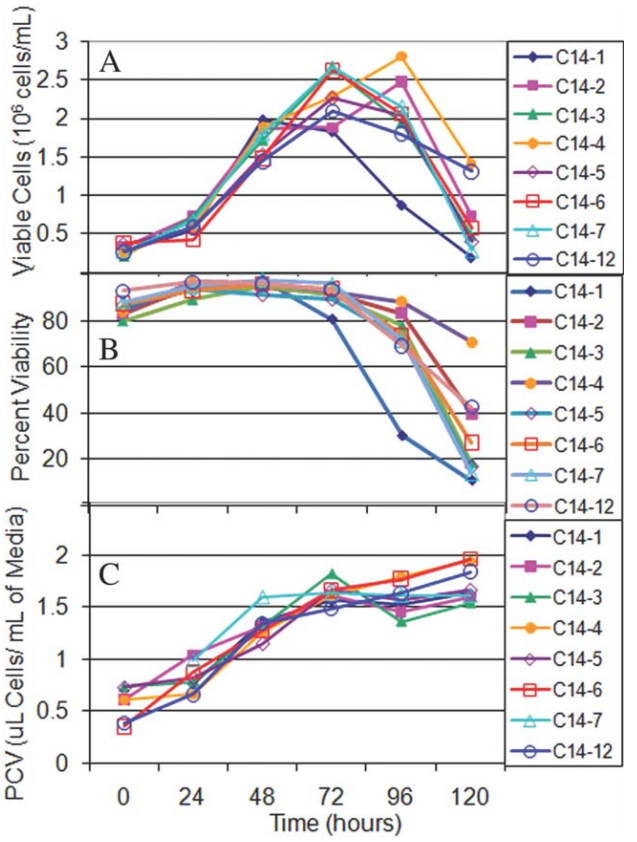

Figure 6. A: Viable cell density by cell counting with a hemocytometer and trypan blue for the eight surviving clones from Experiment II. Each of the subclones was in singlicate in the HTBRs for 6 days in batch mode. B: Percent viability of the subclones. C: PCV determined by Sartorius Volupac measurement of volume cells/mL of media.

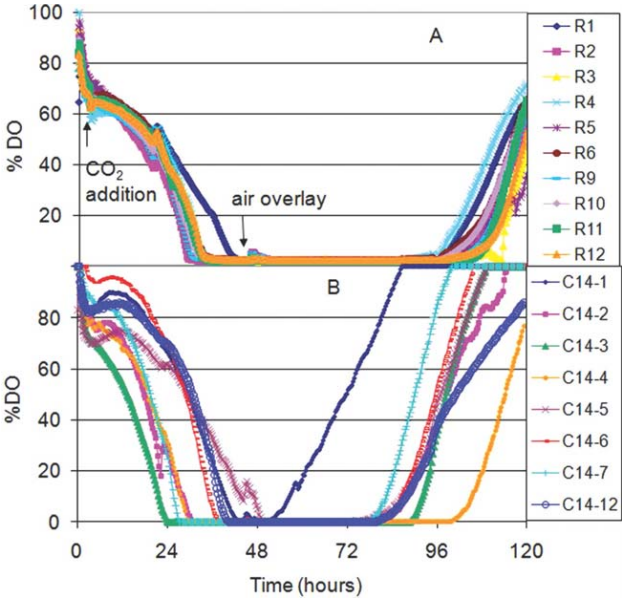

Figure 7. A: DO profiles measured by optical sensor patches for the Experiment II subclones. The individual HTBRs are labeled from R1 to R12. (B) DO profiles from the control experiment using the C14 clone in all 12 HTBRs in a batch culture for 120 h.

compared to those from the control experiment (Figure 7B). C14-8 and C14-9 did not grow in stirred HTBRs, and two others, C14-10 and C14-11 were discarded due to poor growth in T-flasks scale-up stage itself. In general, the differences in growth and viability could be fairly well predicted by the differences in DO profiles. For example, the DO profile of C14-1 came up the fastest which coincided with the quick and sharp drop in the culture viability during the later part of the batch run. In contrast, the DO profile for C14-12 started decreasing much later compared to the other clones, which corresponded with the slower growth initially. The glucose and lactate concentration profiles themselves (Figure 8) were not very good indicators of the differences in growth of the subclones, as there were no noticeable differences between the profiles for various clones. The fact that the HTBR allowed detection of variability in growth and DO profile allowed (1) early elimination of clones not amenable to a stir tank environment and (2) early identification of key parameters for focus during clone selection (i.e., growth and DO, not glucose).

The most important result from this experiment is the comparison of peak IgG3 concentrations from the HTBR runs vs. the well plate results (Figure 9). The highest producers from the stirred HTBR culture were not the same as those from well plates. The second round of subcloning helped pick a slightly higher producer, although certainly not as dramatic of an increase as the first round of subcloning provided. The results from the HTBR run showed that C14-3 is the highest producer, with C14-12 following closely behind. Clone C14-4 was a very fast grower, but had one of the lowest productivities. Thus, the HTBR allowed identification of the most promising clone C14-3.

Control run

Using the same batch of seed culture of C14 clone in 12 different HTBRs resulted in very similar profiles for cell growth (Figure 10). The peak productivity in the batch culture on Day 5 was used for comparison. For the control run in 12 HTBRs, the standard deviation was computed for all the cell culture growth and environmental parameters on each day, following which the %CV was obtained.

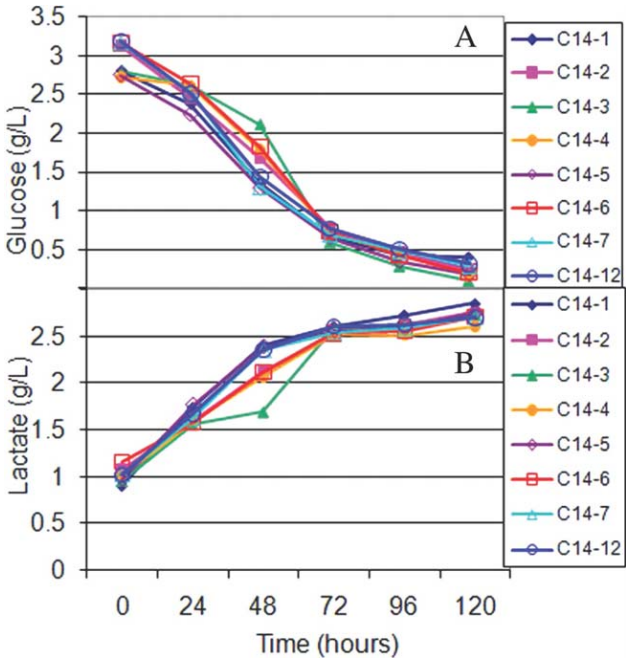

Figure 8. A: HTBR glucose concentrations from YSI 2700 measurements for the subclones from Experiment II. B: Lactate concentrations.

The %CV for growth parameters in Table 2 show that using the same seed in all the HTBRs resulted in very similar growth and productivities. To calculate average %CV for DO data, the data under 5%DO was not used, as the measurement accuracy was low at the very low DO levels. The minimum variability seen here was also observed in earlier studies validating the HTBR (Ge et al., 2006). For example, %DO profiles for C14 cell growth in all 12 HTBRS were very tight together (Figure 7A), and >70% of the data was within one standard deviation.

The minimal vessel-to-vessel variability in the HTBR supports the hypothesis that differences seen in Experiments I and II are due to clonal differences, not instrument artifacts.

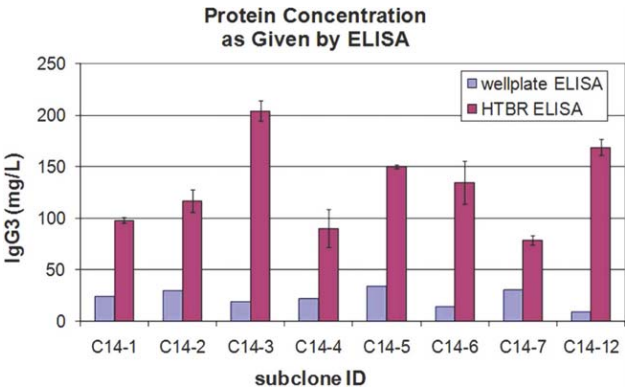

Figure 9. Comparison of protein concentrations between 96-well plates cultures and HTBR cultures from Experiment II. Peak titers from Day 5 of the batch culture are presented for the HTBR run, and 2-week titer from wells are presented for 96-well plates. C14-3 and C14-12 were found to be higher producers from HTBR runs, whereas C14-5 and C14-7 were the highest producers from the 96-well plates.

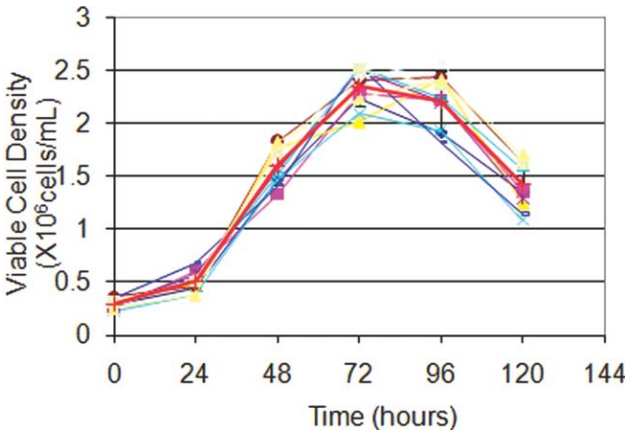

Figure 10. Viable cell densities of C14 clone in the control HTBR run with 12 reactors. The average profile is highlighted.

Discussion

In this study, we found that while selecting clones from the well plate alone can identify a good producer, clone selection in stirred environment is a better approach. For example, in Experiment I, there were substantial differences in the initial well plate ELISA results, but the differences between productivities of subclones greatly diminished in the more controlled environment of the HTBRs. In Experiment II, the very lowest producer and the third lowest producer from well plates turned out to be the highest two antibody producers in the stirred mini-bioreactors. In this case, the order of productivities was completely different in the HTBRs vs. the stationary well plate cultures. If we had used the traditional well plate method alone, we would have not picked the highest producers.

The advantage of on-line monitoring for percent DO and pH by the HTBRs is that these key parameters are very sensitive to environmental changes and cell growth. The most important difference between routine cell counts and DO monitoring is that the DO is monitored continuously and real-time. Having the DO information along with cell count helps the experimenter understand if the "slow" or "fast" growth is inherent to the cell-line or for example, if there was a problem with the air/oxygen supply for part of the run. Our suggestion is that the DO profile along with cell counts and productivity give an overall idea about the growth characteristics of the subclone. Thus, differences between clones or process conditions are readily apparent in a way not feasible in 96-well plates or conventional T-flasks. The DO profile differences from Experiments I and II provided clear insights on cell growth unobtainable in traditional systems: the faster the cell grows initially, the quicker their DO profile decreases; the longer they survive towards the end of the culture, the slower or later their DO profile starts to increase again. The profiles from the control run using C14 in 12 different HTBRs had tight DO trends (Figure 7B). Although glucose and lactate were measured, their trends could not be as clearly correlated to growth differences observed between the subclones, as clearly as the DO profiles did. For example, C14-1 in Experiment II which had a drop in viability by Day 2 showed no difference in glucose profile compared to other subclones, although this was clearly observed from the DO profile. Only by culturing and selecting clones in the HTBR were these key differences apparent.

While performing these experiments under controlled DO and pH would be ideal, the main purpose of our experiments was to compare the subclones performance in monitored stirred environments, as early as possible in the selection process. All of the subclones were compared under the same set of operating conditions, and the best performers under a common set of conditions were selected. The idea is the test the clones coming out of 96-well plates as soon as possible in the stirred HTBRs. Although the HTBR is currently not controlled, our monitoring results indicate that the two most important parameters, DO and pH, remained within levels consistent with cell survival. The next logical step for final selection of the highest producing clone from the screening study would be to use the HTBR with control capability which is currently under development.

The HTBRs are definitely an improvement over shake flasks, which are currently being used to test subclones obtained from 96-well plates. The HRBRs are more comparable to bench-scale bioreactors with their precise monitoring capability and micro-environment, but currently without the control aspect. Shake flasks are typically not monitored, and in addition, the HTBRs allow some amount of manual control. For example, we had CO_2 introduced in our HTBRs at the beginning of the run, and monitored to get the pH within our starting range 7.2 ± 0.2. This kind of precise control is more difficult with unmonitored shake flasks. Another advantage of the HTBR over traditional shake flasks is that all of the sampling was done without stopping the impeller or the overlay gassing.

The set-up time for HTBRs is fairly short with the disposable nature of the probes, making it a viable alternative to shake-flasks and even bench-scale bioreactors. Also, the patches are calibrated as a whole manufactured lot, and do not need calibration prior to every run.

Overall, our experiments lead us to conclude that the current 96-well plate based method of subclone selection is lacking an important step (i.e., highly parallel selection in a monitored, stirred environment). Stirred environment is completely different compared to stationary systems, for cell growth and productivity. The higher mass transfer of oxygen as well as other key nutrients in stirred systems plays a vital role in changing the metabolism of the cell. The physical (well mixed with higher mass transfer) as well as biochemical environment of the cells (availability of nutrients) in stirred systems make them a better choice for clone selection. Hence, it is imperative to select the final clone in a stirred system. Ideally, clones should be tested in a bioreactor-like environment, with as much monitoring as possible. By monitoring growth and production of clones in mini-bioreactors the selection of the best clone can be made based on how the clones perform in an environment similar to the production methods. HTBRs can be used as an initial winnowing down tool for selection from a few dozen clones before final clone selection under controlled serum-free conditions.

Conclusions

This study showed the power of the HTBR for clone selection. In particular, high IgG3 producing hybridoma clones identified after a 6 day run in high-throughput bioreactors differed from those identified in an initial 96-well plate. Hence, it can be concluded that a stirred bioreactor environment affects antibody production by hybridoma clones in a manner different than a stationary one, making clone selection in a stirred environment the superior choice. Although selection in stirred tanks was previously limited by the costs involved in scale-up and testing in earlier versions of lab scale bioreactors, use of the smaller scale HTBR makes this easier, cheaper, and quicker vs. moving through the traditional route of scaling up subclones to stationary T-flasks and spinners, and eventually to lab-scale bioreactors.

Acknowledgment

The authors acknowledge the support from Sartorius-Stedim Biotechnology and Fluorometrix. GR has an equity position in Fluorometrix.

Literature Cited

1. Browne S, Al-Rubeai M. Selection methods for high-producing mammalian cell lines. *Trends Biotechnol*. 2007;25:425–432.
2. Frame K, Hu W. The loss of antibody productivity in continuous culture of hybridoma cells. *Biotechnol Bioeng*. 1990;35: 469–476.
3. Ritter Mal H. *Monoclonal Antibodies: Production, Engineering, and Clinical Application*. *Postgraduate Medical Science Series*, Vol. 3. New York, NY: Cambridge University Press; 1995:500.
4. Barnes L, Moy N, Dickson A. Phenotypic variation during cloning procedures: Analysis of the growth behavior of clonal cell lines. *Biotechnol Bioeng*. 2005;94:530–537.
5. Böhm E, Voglauer R, Steinfellner W, Kunert R, Borth N, Katinger H. Screening for improved cell performance: selection of subclones with altered production kinetics or improved stability by cell sorting. *Biotechnol Bioeng*. 2004;88:699–706.
6. Barnes L, Bentley C, Dickson A. Characterization of the stability of the recombinant protein production in the GS-NS0 expression system. *Biotechnol Bioeng*. 2001;73:261–270.
7. Serrato J. A. PLA, Meneses-Acosta A, Ramirez OT. Heterogenous conditions in dissolved oxygen affect N-glucosylation but not productivity of a monoclonal antibody in hybridoma cultures. *Biotechnol Bioeng*. 2004;88:176–188.
8. Junker BH, Wang DIC, Hatton TA. Fluorescence sensing of fermentation parameters using fiber optics. *Biotechnol Bioeng*. 1988;32:55–63.
9. Lamping SR, Zhang H, Allen B, Shamlou PA. Design of a prototype miniature bioreactor for high throughput automated bioprocessing. *Chem Eng Sci*. 2003;58:747–758.
10. Zanzotto A, Szita N, Boccazzi P, Lessard P, Sinskey AJ, Jensen KF. Membrane-aerated microbioreactor for high-throughput bioprocessing. *Biotechnol Bioeng*. 2004;87:243–254.
11. Maharbiz M, Holtz WJ, Howe RT, Keasling JD. Microbioreactor arrays with parametric control for high-throughput experimentation. *Biotechnol Bioeng*. 2004;85:376–381.
12. Puskeiler R, Kaufmann K, Weuster-Botz D. Development, parallelization and automation of a gas-inducing milliliter-scale bioreactor for high-throughput bioprocess design (HTBD). *Biotechnol Bioeng*. 2005;89:512–523.
13. Isett K, George H, Herber W, Amanullah A. Twenty-four-well plate miniature bioreactor high-throughput system: assessment for microbial cultivations. *Biotechnol Bioeng*. 2007;98:1017–1028.
14. Zhang Z, Szita N, Boccazzi A, Sinskey AJ, Jensen KF. A well-mixed, polymer-based microbioreactor with integrated optical measurements. *Biotechnol Bioeng*. 2005;93:286–296.
15. Diao J, Young L, Zhou P, Shuler M. An actively mixed minibioreactor for protein production from suspended animal cells. *Biotechnol Bioeng*. 2008;100:72–81.
16. Chen A, Chitta R, Chang D, Amanullah A. Twenty-four well plate miniature bioreactor system as a scale-down model for cell culture process development. *Biotechnol Bioeng*. 2009;102: 148–160.
17. Gupta A, Rao G. A study of oxygen transfer in shake flasks using a non-invasive oxygen sensor. *Biotechnol Bioeng*. 2003;84:351–358.

18. Weuster-Bolz D, Altenbach-Rehem J, Arnold M. Parallel substrate feeding and pH-control in shaking-flasks. *Biochem Eng J*. 2001;7:163–170.
19. Wittmann C, Kim HM, Heinzle E. Characterization and application of an optical sensor for quantification of dissolved oxygen in shake-flasks. *Biotechnol Lett*. 2003;25:377–380.
20. Kermis Hr. KY, Harms P, Rao G. Dual excitation ratiometric fluorescent pH sensor for noninvasive bioprocess monitoring: development and application. *Biotechnol Prog*. 2002;18:1047–1053.
21. Hanson M, Ge X, Kostov Y, Brorson K, Moreira M, Rao G. Comparisons of optical pH and dissolved oxygen sensors with traditional electrochemical probes during mammalian cell culture. *Biotechnol Bioeng*. 2007;97:833–841.
22. Harms P, Kostov Y, French J, Rao G. Design and performance of a 24-station high throughput microbioreactor. *Biotechnol Bioeng*. 2005;93:6–13.
23. Ge X, Hanson M, Shen H, Kostov Y, Brorson K, Frey D, Moreira M, Rao G. Validation of an optical sensor-based high throughput bioreactor system for mammalian cell culture. *Biotechnol Prog*. 2006;122:293–306.
24. Ge X, Rao G, Tolosa L. On the possibility of real-time monitoring of glucose in cell culture by microdialysis using a fluorescent glucose binding protein sensor. *Biotechnol Prog*. 2008;24:691–697.
25. Vallejos J, Kostov Y, Ram A, French J, Marten M, Rao G. Optical analysis of liquid mixing in a minibioreactor. *Biotechnol Bioeng*. 2006;93:906–911.
26. Rubinstein LJ, Stein KE. Murine immune response to the *Neisseria meningitidis* group C capsular polysaccharide. II. Specificity. *J Immunol*. 1988;141:4357–4362.
27. Brorson KA, Krasnokutsky MV, Stein KE. Immunoglobulin isotype switching in xid mice. *Mol Immunol*. 1995;32:487–494.

Manuscript received July 9, 2009, and revision received Oct. 14, 2009.

Chapter Five: Scale-up-down Using Sentinel Genes

So clearly, one can make a minibioreactor behave like a larger scale bioreactor. But exactly how do the cells behave? Afterall, the ultimate goal of a scale-up/down studies is to ensure that no matter what the scale, the cells behave in the same manner in terms of their metabolism. So it came down to measuring the cellular response at the genetic level. We set out to ask if one could create a scale-less operating paradigm, where the gene expression profiles would match over a typical multiday batch culture. We were fortunate to have access to the entire mouse genome chip at FDA and in a collaboration, were able to identify a few key genes that we dubbed “sentinel” genes that could be used to fingerprint a successful scale up/down operation. The next two papers detail these efforts.

The first paper was a foundational discovery study. Bhargavi was joined by Shaunak Uplekar, another Ph.D student. Together with Han, Joshi and Puri from FDA, we were able to pick a handful of genes that showed potential to be used as markers of cell status.

Genomic Analysis of a Hybridoma Batch Cell Culture Metabolic Status in a Standard Laboratory 5 L Bioreactor

Bhargavi Kondragunta
Center for Advanced Sensor Technology and Dept. of Chemical and Biochemical Engineering, University of Maryland, Baltimore County, 1000 Hilltop Circle, Baltimore, MD 21250

Div. of Cellular and Gene Therapy, Center for Biologics Evaluation and Research, Food and Drug Administration, 29 Lincoln Dr, Bethesda, MD 20892

Jing Han, and Bharat H Joshi
Div. of Cellular and Gene Therapy, Center for Biologics Evaluation and Research, Food and Drug Administration, 29 Lincoln Dr, Bethesda, MD 20892

Kurt A. Brorson
Div. of Monoclonal Antibodies, Center for Drug Evaluation and Research, Food and Drug Administration, 10903 New Hampshire, Silver Spring, MD 20903

Raj K. Puri
Div. of Cellular and Gene Therapy, Center for Biologics Evaluation and Research, Food and Drug Administration, 29 Lincoln Dr, Bethesda, MD 20892

Shaunak Uplekar, Antonio R. Moreira, and Govind Rao
Center for Advanced Sensor Technology and Dept. of Chemical and Biochemical Engineering, University of Maryland, Baltimore County, 1000 Hilltop Circle, Baltimore, MD 21250

DOI 10.1002/btpr.1605
Published online September 18, 2012 in Wiley Online Library (wileyonlinelibrary.com).

Currently, there is a gap in the knowledge of the culture responses to controlled bioreactor environment during the course of batch cell culture from early exponential phase to stationary-phase. If available, such information could be used to designate gene transcripts for predicting cell status and as a quality predictor for a controlled bioreactor. In this study, we used oligonucleotide microarrays to obtain baseline gene expression profiles during the time-course of a hybridoma batch cell culture in a 5 L bench-scale bioreactor. Gene expression changes that were up or down modulated from early-to-late in batch culture, as well as invariant gene profiles with significant expression were identified using microarray. Typical cellular functions that seemed to be correlated with transcriptomics were oxidative stress response, DNA damage response, apoptosis, and cellular metabolism. As confirmatory evidence, microarray findings were verified with a more rigorous semiquantitative gene-specific Reverse transcriptase-polymerase chain reaction (RT-PCR). The results of this study suggest that under predefined bioreactor culture conditions, significant gene changes from lag to log to stationary phase could be identified, which could then be used to track the culture state.
 Biotechnol. Prog., 28: 1126–1137, 2012
Keywords: cell culture, genomic, time-course, sparged bioreactor, microarrays

Introduction

It is well recognized that in order to ensure consistent product quality (e.g. glycosylation[1,2]), critical cell culture environmental parameters such as dissolved oxygen (DO), pH, CO_2 levels are controlled using set-points during a bioreactor process. Several changes in the culture environment can occur owing to varying requirement for aeration, and possibly agitation in cultures, in order to maintain set-point control for temperature, %DO and pH (CO_2 gas for acid control) in a bioreactor. For example, as cultures grow and become more dense, the culture's aeration and agitation requirements increase, and remain high until death phase. In addition, there could be other bioreactor environmental stress factors[3–8] that could result in apoptosis.[9,10] These include gas sparging in culture media, high gas entrance velocity at the sparger site, increased hydrodynamic forces by air bubble bursting at the liquid surface or foaming, insufficient mixing at high cell densities, energy dissipation of impeller stream and possible reactive oxygen species formation, during the course of bioreactor culture. Increasing levels of apoptosis in cell culture has been associated with lower productivity, product quality, and cell

Additional Supporting Information may be found in the online version of this article.

Correspondence concerning this article should be addressed to G. Rao at grao@umbc.edu or R.K. Puri at Raj.Puri@fda.hhs.gov.

growth. Although bubble-free membrane aerated reactors have been developed[11] to overcome bubbling-related problems, sparging with oxygen, air, CO_2, and/or nitrogen is the preferred method for %DO and pH control in bioreactor cultures,[12] to allow for a faster gas exchange into the culture medium. This is also an important distinction between the bioreactor environment and incubator cultures where mostly surface aeration is used for oxygenation.

With the recent upsurge of genomics and proteomics, several studies showing transcriptional changes as a result of cell culture medium and/or process improvements have been reported using mouse, Chinese hamster ovary (CHO), and human cell lines. However, the focus of these studies has been mainly for improving cell productivity by either medium and/or process improvements, but not for measuring cell physiological changes in a controlled bioreactor, as inputs to obtain genomic profiles as standards to predict culture reproducibility, and act as additional inputs to product quality. As shown below, the majority of the transcriptomic studies have been conducted in an incubator culture environment, with focus on improving productivity under various scenarios. For example, addition of sodium butyrate to increase specific productivity of recombinant proteins in CHO, and hybridoma cells grown in T-flasks, showed gene expression changes in protein processing machinery in both cell types.[13] While others correlated transcriptomics to histone modifications and lipid metabolism changes induced by sodium butyrate, in mouse hybridoma and CHO cells grown in T-flasks.[14] Recent studies also include the effect of lower culture temperature (33°C) to improve productivity in CHO[15,16] and Monocyte activated killer (MAK) hybridoma cells in spinner-flasks showing changes in the transport and signaling pathways,[17–19] and genomic profiling for CHO and NS0 in 500 mL shake-flasks[20] to identify pathways associated with high producers,[21] and effect of ammonium on glycosylation gene expression in 1 L spinners.[22] A study profiling cellular metabolism genes was also reported in 293-HEK cells using membrane-aerated bioreactors.[23]

The goal of microarray analysis is to identify differentially expressed genes (DEGs), i.e., a list of genes with expression levels statistically, and more importantly, biologically different between two or more sets of the representative transcriptomes. The plethora of available methods[24] for obtaining DEGs increases confusion and continuing debate on the appropriate choice of methods for identifying reliable DEG lists. Although with the numerous statistical methods available, there might be no single best way. Several recent studies focused on obtaining a consistent set of DEGs using various microarray data analysis techniques and measurement platforms, particularly on the need for calibrated reference RNA samples[25,26] and "gold standard" datasets (e.g., by quantitative real-time polymerase chain reaction (qRT-PCR)) as part of the effort for quality control of microarray data.[27,28]

Some researchers have recommended the use of a fold-change-ranking, in addition to a nonstringent *P*-cutoff as a baseline practice to generate more reproducible DEG lists, where the *P* criterion balances sensitivity (probability of successfully identifying a real effect) and specificity (probability of successfully rejecting a nonexistent effect). Other statistically based methods such as maximum likelihood estimation methods for 2-color arrays have been described in literature.[29] As microarrays measure a large number of genes simultaneously, a necessity for multiple correction method arises,[30] including Bonferroni correction of *P*-value, and false discovery rate. Although for analysis of variance (ANOVA) and *t*-test methods used here, multiple correction methods were not included, stringent *P*-values were used to capture most of the significant changes.

In this study, we measured the time-course transcriptomic profiles of cells due to changes in bioreactor environment with culture progression. To achieve this we have used oligonucleotide microarrays to identify gene expression changes from early exponential to stationary phases of growth, in a controlled cell culture bioreactor. We have then verified a subset of modulated genes using RT-PCR.

Materials an Methods

Cell culture

A Sp2/0 myeloma based mouse hybridoma cell line (2055.5) secreting an anti-*meningitidis*-capsular–polysaccharide IgG3[31] was used as the experimental cell line. The parental hybridoma clone was a kind gift from Dr. K. Stein (CBER/FDA). The original line was subsequently subcloned, with 17 subclones evaluated for higher titers and stable production.[32] During studies cells were maintained in T-flasks (Corning, Lowell, MA) and 250 mL spinner flasks (Kontes, Vineland, NJ) in a 5% CO_2 incubator (Napco, Winchester, VA) at 37°C, in chemically defined (CD) hybridoma media (Invitrogen, Carlsbad, CA) being split every 3 to 4 days. Each 1 L of CD media was additionally supplemented with 8 mM of L-Glutamine (Invitrogen, Carlsbad, CA) and 3.5×10^{-4}% β-mercaptoethanol (v/v) (Sigma, St. Louis, MO). Cell density and viability were determined using a hemocytometer with trypan blue exclusion. Culture glucose and lactate were measured with the YSI 2700 SELECT Biochemistry Analyzer (YSI, Yellow Springs, OH). Enzyme linked immunosorbent assay (ELISA) was used for product titer, previously described in our earlier studies.[33]

5 L bioreactor set-up and experimental protocol

The batch culture was conducted in a 5 L water-jacketed, round-bottomed glass vessel (Braun B, Melsungen, Germany). Temperature was controlled at 37°C set-point. A continuous air-overlay at 0.03 VVM (volume gas/reactor volume/minute) to the head-space was used to maintain positive pressure in the vessel and to drive out any accumulated gases such as Ammonia and CO_2. Vessel aeration was through a ring sparger to bubble gas through the culture broth from below the impellers. Gas sparge rate was set to be 0.022 VVM through a ring sparger at the bottom of the vessel. The agitation rate was set at 220 RPM with two of the 2-blade 45° pitched impellers, spaced at 0.91 D_i (impeller diameter) apart and 0.25 D_i from the bottom of the agitator shaft. The ratio of liquid height to diameter (H/T ratio) of the vessel was 1.5.

Consecutive bioreactor runs were conducted for three biological replicates, each starting from a vial thaw, followed by seed scale-up for 6–8 passages prior to 5 L experimentation. Each of these bioreactor runs were separated by several weeks' time to allow for randomness in the experimental conditions. The 5 L bioreactor with 4.5 L working volume was inoculated at $2.0 \pm 0.5 \times 10^5$ cells/mL. Samples were taken twice daily for 5 days. The bioreactors were sampled approximately every 12 h, both for RNA extraction and cell growth measurements. The RNA extraction was performed immediately, and stored at −80°C. Microarrays were run specifically

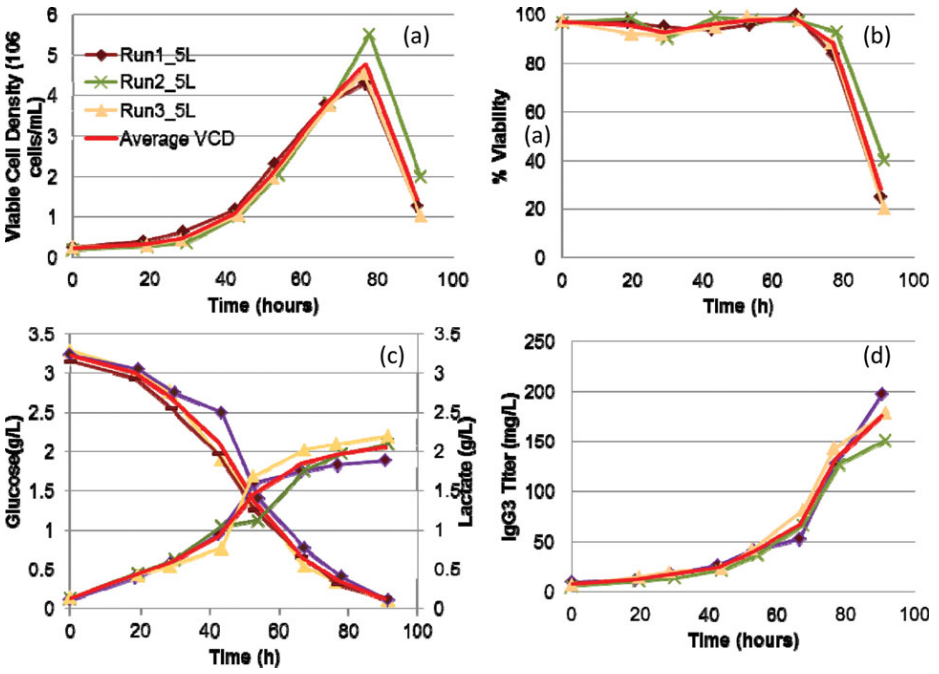

Figure 1. Cell growth and productivity profiles of SP2/0 cell line in 5 L oxygen sparged batch culture.

(a) Viable cell density profiles of three biological replicates along with the average cell density profile. (b) % viability profiles of the three biological replicates. (c) Glucose and lactate concentration measurement profiles in the batch culture. (d) Sp2/0 cell-line produced IgG3 expression profiles in batch culture.

for four groups of RNA samples, from day 1 (18–19 h), day 2 (42–44 h), day 3 (66–68 h), and day 3.5 (90–92 h) time-points of culture, for the three sets of biological replicates. These samples ranged from early exponential, to late stationary/early death phase. In this case, we define early-exponential and part-lag phase as day 1, peak exponential as day 2, late exponential as day 3 and stationary/early death phase as day 3.5. The day 0 samples at inoculation were not included in the microarray analysis, which would cover the early lag phase.

%DO and pH control for 5 L bioreactor systems

The set-point for %DO was set at 30% air saturation, and that for pH was set at 7.2. Culture DO control was achieved by bubbling or sparging pure oxygen through the culture fluid, using a ring sparger, along with maintaining a set impeller speed at 220 RPM. At the beginning of the culture, %DO was allowed to decrease naturally with cell growth until it reached 30%, at which point the control action was automatically initiated. Intermittent oxygen sparging at 0.022 VVM into the culture fluid controlled by the Braun PID controller, was used to maintain a 30% DO set-point for the remainder of the run (profiles can be found in the Figure 1, Supporting Information). There was no base control used during the run, the pH was allowed to decrease within physiological levels during the batch run. Culture pH was controlled at a set-point of 7.2 using CO_2 overlay at 0.007 VVM for acid control. No base control was used as the cultures remained within physiological range, which was above 6.8 pH units during the batch culture.

Microarray hybridization procedure

The steps involved in running microarrays and analyzing data using biostatistics packages from NCI are described in the sections below. Epoxy coated microarray slides (Operon Biotechnologies, Huntsville, AL, now MWG Biotech AG) printed at CBER/FDA on Gene Machines Omnigrid Arrayer (San Carlos, CA) and labeled as Mm-35K-V4.0p5 were used for the studies presented here. These chips used Strategene's replicated alien controls. The procedure used for microarrays is briefly described below.

Probe Preparation. Total RNA from the cells was extracted with Trizol (Gibco Brand, Carlsbad, CA) and chloroform (Mallinckrodt, Phillipsburg, NJ), and purified using the RNeasy Mini-Prep Kit (Qiagen Inc., Valencia, CA). A 2-color method or indirect experiment method was used where cDNA from the bioreactor time-point and from an all-inclusive universal mouse reference RNA pool (Becton, Dickinson, and Co., Franklin Lakes, NJ) was cohybridized on the microarray slide. The RNA concentration was adjusted to 10 μg in 12 μL using RNAse free water, and was denatured by incubation at 70°C for 10 min along with 2 μL oligo dT primer (0.05 μg/μL oligo-dT), following which it was quickly chilled on ice for 10 min. Then a total of 22 μL of the reverse transcriptase reagents, with 3.33 U/μL of reverse transcriptase (Stratagene, La Jolla, CA) in a first strand buffer (Stratagene) supplemented with 0.01 M DTT (Sigma) and 0.02–0.05 mM dNTPs (Invitrogen, Carlsbad, CA) were added and incubated at 42°C for 90 min for reverse transcription of the primed mRNA. At the end of the 90 min, the final volume was adjusted to 60 μL with RNAase free water.

RNA Quality Assessment on Agilent Bioanalyzer. Prior to processing RNA samples on microarrays, the samples were run on a RNA nanogel, as well as quantified using a Nanodrop ND-1000. The ratios A260/280, and A230/280 were measured and those with ratio of 1.7–2.1 were acceptable. The RNA integration number (RIN) was used to assess the integrity of RNA from the electrophoretic trace, and includes

effect of degradation products. The factor was 8.0 – 10 for all the samples, the ideal RIN being 10.

Dye Coupling and probe Clean-up. After reverse transcription of mRNA to cDNA, the cDNA was purified by removing the remaining t-RNA and r-RNA using the MinElute (Qiagen) kit. The probe was eluted using 12 μL of elution buffer. Prior to fluorescence labeling with spectrally similar dyes, Cy3 and Hyper 5, 5 μL of coupling buffer (0.2 M $NaHCO_3$, pH 9) was added to each sample. Here 15 μL each of Cy3 dye for the reference, and Hyper5 dye (Amersham, Piscataway, NJ) for the test samples, were added and incubated in the dark for 90 min. Residual dye was removed afterward using the same MinElute PCR Purification Kit. Following incubation, the probe was cleaned up to remove residual dye using the Qiagen MinElute kit.

Hybridization. Epoxy coated glass slides with 36,055 oligonucleotide mouse genome chip purchased from Operon were used. The Maui mixing chamber (Biomicro, Salt Lake City, UT) was used for hybridization, with flow-volume of 42 μL. Ambion hybridization buffer was preheated to 42°C and 24 μL of the buffer was added to 24 μL of the clean coupled probe, and injected into the Maui hybridization chamber (Biomicro). The slide was incubated overnight at 42°C.

Microarray Slide Washing, Scanning and Image Processing. After the overnight hybridization period, the MAUI mixers were disassembled and the arrays were washed in series with 1× (Saline sodium citrate) SSC (0.05% (Sodium dodecyl sulfate) SDS) and 0.1× SSC, each for 4 min. The arrays were then scanned for Cy3 and Hyper5 fluorescent emission intensities using a GenePix 4000B microarray scanner (Axon, Union City, CA) with 5 μm resolution. Laser power was set at 100% and photomultiplier tube (PMT) gain was set between 610 and 700, to view the spots clearly. Also, signal intensities observed from the intensity histograms from either Hyper5 or Cy3 were used to adjust the PMT gain for each of the signals, such that the signal bias was minimized. The fluorescence histograms were used to observe the quality of data obtained from each channel, and determine if the array could be included in the analysis. Image processing, consisting of automatic and manual spot selection/rejection, and spot identification (gridding) was carried out using GenePix Pro 6.0 software (Axon).

Intensity Based Spot Filtering for Background Correction. Filters were used to reduce the noise level, such as mean signal intensity > 100, signal to background ratio > 1 standard deviation, and fold-change > 1.5. Spot diameter was chosen between 25 μm to 100 μm. Datasets with $> 70\%$ genes found were used for the analysis. Another filter used was the method of setting the signal above background threshold of ± 1 standard deviation from the mean signal, where the signal was calculated as the mean intensity minus the median background. Spot mapping was done to NCI Production Gene Array List (GAL) files. In addition, 25 genes that were not found by mapping to the GAL file were omitted from the gene analysis to avoid false positives.

Statistical analysis

Microarray Data Normalization and Array Selection. Normalization removes systematic variability of the dataset. As two dyes, Hyper5 and Cy3 are used to obtain the signal of the sample and reference; there is a possibility of dye induced intensity bias. Lowess normalization[34] was used on the raw data to correct for intensity based bias in 2-color data. Lowess smoothing was applied using Madb (microarray database from Advanced Technology Center at NCI/CCR, the Bioinformatics and Molecular Analysis Section, NIH) software, which adjusts the ratio of Hyper5 (red)/Cy3 (green) by applying the lowess correction.

1-way ANOVA and Paired Unequal Variance t-tests for Differentially Expressed Genes. Our method for detecting differential gene expression was by using statistical hypothesis testing methods such as 1-way ANOVA followed by *post hoc* paired unequal variance *t*-tests between groups. In addition, unequal variance *t*-tests were also run on the initial normalized data as well to capture changes that could have been missed out by the parametric F-statistic based 1-way ANOVA. To discuss which genes exhibited significant expression changes from beginning to end of batch culture, we performed 1-way ANOVA analysis comparing the mean values of log gene expression ratios at each timepoint using Madb software (Microarray Database, madb.nci.nih.gov). To obtain a subset of significant gene expression changes between any two time-points in culture, we used unequal variance *t*-test method from Madb software (Gene list and pathways can be found in Table 1, Supporting Information). Our strategy using the *t*-test comparing two time-points clearly shows the nature of the change, i.e., up or downregulation of the gene, and helps obtain subsets of genes that varied between specific group pairs. This method also eliminates the necessity for the gene to be significantly expressed (based on data filters) at all four time-points, as required for the 1-way ANOVA analysis. From all the possible combinations of paired *t*-tests, in this case we chose to present the transcriptomic changes at peak exponential (day 2), late exponential (day 3), and late stationary/early death (day 3.5) relative to the early exponential (day 1) sample set. By both of these methods most of the significant gene expression changes could be captured. In addition to these methods, significance analysis of microarrays time-course analysis and K-means clustering approaches from Madb software were also used to obtain subgroups of significantly expressed genes (data not shown).

RT-PCR protocol

cDNA Preparation. RNA from a −80°C freezer was reconstituted on ice and a final dilution of 2 μg in 10 μL of RNAse free water was made. A master mix of 4 μL of 10× PCR gold buffer, 8 μL of 25 mM $MgCl_2$, 12 μL of 10 mM dNTPs (made by adding equal amounts of dGTP, dATP, dCTP, dTTp) and 2 μL of oligo dT (all reagents from Applied Biosystems, CA) were made. As a next step, 2 μL of RNAse inhibitor and 2 μL of Reverse transcriptase (RT) enzyme and water were added to the master mix, and mixed by pipetting for 4–5 s. Immediately the diluted RNA was added and vortexed gently for 2–3 s and spun down. The 40 μL reaction mixture was held for 10 min at room temperature, following which it was set on a reaction block at 42°C for 60 min. When the reaction was complete, the cDNA was spun down and stored at −20°C, as it is relatively stable compared to the RNA that has to be stored at −80°C at all times.

RT-PCR Reaction. A master mix of 5 μL of a 10× PCR gold buffer (Applied Biosystems, Foster City, CA), 2 μL of 25 mM $MgCl_2$ solution along with 0.5 μL each of forward and reverse primers, and 0.5 μL of Amplitaq gold polymerase were

Table 1. Genes Classified by Gene Ontology (GO) Subgroup using GOFFA Functionality from ArrayTrack™ Software

1-way ANOVA, Intensity>200, P<0.01 (111 genes)		
Gene Ontology Functional Class (number of genes)	Gene Function/Activity	Gene Transcripts
Catalytic activity (32) (GO:0003824)	Oxidoreductase activity (9) (GO:0016491)	Txnrdl, Aldh2, Cox6al, Idhl, Prdx5, Cox7a21, Ndufs8
	Hydralase activity (13)(GO:0016740)	Apexl, Ssu72, Dynll1, Eef2, Pgam1, Pmpcb, Ddxl
	Lyase activity (3) (carbon-oxygen and carbon-carbon) (GO:0016829)	Apex1, Odc1, Umps
	Transferase activity (6) (GO:0016740)	Ext2, Git2, Umps, Nck2, Hadhb, Gstm5
Binding (52) (GO:0005488)	Cofactor binding (GO:0048037) (3)	Ero1lb, Idh1 (NAD or NADH binding), Txnrd1(NADP or NADPH binding)
	Ion binding (GO:0043167) (19)	Magnesium ion binding-Apex1, Idh1, Nuclt9, Calcium ion binding - Anxa6,Transition metal ion binding - Birc2, Cycs, Dnaja1, Git2, Man2b, Mt1, Mt2, Ndufs8, Pmpcb
	Metal cluster binding (GO:0051540)(1)	Ndufs8
	Nucleic acid binding (GO:0003676) (15)	Apex1, Ddx1, Eef2, Elk3, Pa2g4, Qars, Rps20, Sfrs2, Ssrp1, Tufm
	Protein binding (GO:0005515) (23)	Arpc3, Birc2, CD74, CD99, Cite, Cstb, Dnaja1, Dynll1, Erol1b, Fas, Hspa9, Pa2g4, Qars, Sfrs2
Antioxidant activity (2) (GO:0016209)	Peroxidase activity (GO:0004601)(1)	Prdx5
	Thioredoxin-disulfide reductase activity (GO:0004791)(1)	Txnrd1
Transcription regulator activity (9)	Transcription factor activity(GO:0030528, 0006355, 0045449)	Elk3, Pa2g4, Morf4l2, Mbtd1, Rblcc1, 5srpl, Ybx1
Cellular processes (GO:00099 87) (62)	Cell cycle (GO:0007049)(3)	Ccpg1, Rb1cc1, Vps4b
	Cell communication (GO:0007154)(11)	Dnaja1, Fas, Git2, Mras, MT1, MT2, Olfr5, Rab2a, Ptplad1, Tom1l1
	Cell death (GO:0008219) (8)	Bok, Cycs, Fas, Itm2b, Qars, Rb1cc1
Cellular metabolism (GO:0044237)(41)	Aminoacid metabolism (GO:0006519)	Idh1, Odc1
	Macromolecule metabolic process (GO:0044260)(30) DNA repair, replication (GO:0006259) mRNA processing (GO:0006397) Protein metabolic process (GO:0044267)(16)	Apex1, Morf4l2, Smc6, Ssrp1 Sfrs2, Sfrs3, Ssu72, Ssrp1, Ybx1 CD74,Cuedc2, Dnaja1, Eef2, Rpll9, Rpl22l1, Rpl39, Rps20, Sumo2, Uspl1, Tufm
	Carbohydrate metabolism (GO:0044262)	Idh1, Pgam1
	Cellular catabolic process (GO: 0044248)	Cuedc2, Hadhb, Idh1, Nudt9, Pgam1, Rb1cc1, Sumo2, Uspl1
	Nitrogen compound metabolism and regulation(20)(GO: 0034641,0051171) Nucleotide, nucleic acid metabolism (GO:0006139), 18	Dynll, Odc1, Umps, Atpif, Pa2g4 Aim, Apex1, Atpif1, Elk3, Mbtd1, Morf4l2, Nudt9
	Oxygen and ROS metabolism (G0:0006800)	Cycs
Regulation of cellular processes (GO:0050794)(31)	Signal transduction (GO:0007165)(11)	Dnaja1, Fas, Git2, Mras, Mt1, Rab2a
	Regulation of cellular metabolism (GO:0031323)(10)	Atplf1, Dynll1, Elk3, Mbtd1, Morf4l2, Pa2g4
Cellular response to stimulus (GO:0051716)(6)	Response to DNA damage (GO:0034984)(4)	Apex1, Ssrp1, Morf4L2, Smc6
	Response to starvation (GO:0009267)(1)	Rb1cc1

The list of genes were obtained by 1-way ANOVA analysis of microarray gene findings from four groups of biological replicates. Genes were found to be significantly expressed at all time-points from beginning to end of batch culture with *P*-value cut off of 0.01.

prepared for the RT-PCR reaction. After adding the enzyme the contents were mixed without vortexing, by pipetting. 10 μL of prepared cDNA was added to the mixture along with RNAse free water to make a 50 μL reaction mixture. This reaction mixture was combined by 2–3 s of gentle vortexing and quick spin, prior to loading on the PCR machine. All reagents were maintained on ice prior to the reaction. The PCR cycle had a denaturation step at 94°C for 45 s, annealing step at 56°C for 30 s and extension at 72°C, for 55 seconds.

Gel Staining and Semiquantitation. PCR product was run on a 2% Agarose gel in a 1× (Tris-base, acetic acid, Ethylenediamine tetra acetic acid) TAE buffer (100V for 45 min) with ethidium bromide. Quantity One 4.6.6 Chemdoc XRS from Biorad Instruments was used to capture the live image using Trans UV light exposure. Image focus and exposure time was adjusted to capture image for semiquantitation. The Quantity One software was used to obtain band area and back-ground subtracted intensity for the test genes, which were divided by the back-ground subtracted intensity of the β-actin control.

Results

Cell growth and environmental parameters in 5 L model bench-scale system

The model system used in this study was a 5 L batch bioreactor culture, which transitioned between early log, exponential and stationary phase of growth over a course of 3.5 days (viability > 85%), while cultures were terminated after 4 days. As can be seen in Figure 1, the 5 L profiles for cell growth, %viability and metabolites consumption were typical for a hybridoma batch culture. The cell viability dropped rapidly at the tail end of the culture. Glucose was mostly consumed over time, with lactate was slightly over 2 g/L by the end of batch culture. The

Table 2. Primer Sequences, Entrez gene IDs and a Brief Description of the Gene Functions for the List of Genes Chosen for RT-PCR Verification

Gene Name	Entrez Gene ID	Description	Primer Sequence
Hspa9	Heat shock 70kDa protein 9 (15526)	Role in cell proliferation, stress response, protein folding, protein export from nucleus	FW: TGTCAAGGAGTTCAAGAGA BW:ATGGTAAGGTATGGCAAGT
ACTB	Actin, beta (11461)	Highly conserved proteins that are involved in cell motility, structure, and integrity	FW: CACCTTCTACAATGAGCTGCG BW: TGCTTGCTGATCCACATCTGC
Sod1	Superoxide dismutase 1(20655)	Response to superoxide, free radical induced apoptosis pathway (BioCarta);	FW: GAACCAGTTGTGTTGTCA BW: CAGCCTTGTGTATTGTCC
Arpc3	Actin related protein complex,3	Control of actin polymerization in cells; protein binding	FW: GGCATACCACTCTTCTCT BW: CTGTCCGCTTCATTCTTAA
Atpif1	ATPase inhibitory factor 1(11983)	ATPase inhibitor activity	FW: TCGGATAGCATGGATACG BW: TGGTGGTCAATCTCATCTT
CD74	Major histocompatibility complex,(16149)	MHC class II protein binding, protein complex assembly, intracellular protein transport	FW: CGACCTCATCTCTAACCAT BW:TACAGGAAGTAAGCAGTGG
Cycs	Cytochrome c, somatic (13063)	Apoptosis, activation of caspase activity	FW: GGAGGCAAGCATAAGACT BW: TTGTTGGCATCTGTGTAAG
Txnrd1	Thioredoxin reductase 1(50493)	Reduces thioredoxins, plays a role in selenium metabolism and protection against oxidative stress	FW:GATGAAGAGCAGACCAATG BW: CACAACAGCCATATTCCAA
Rpl19	Ribosomal protein L19 (19921)	Translation; translational elongation	FW: CCTGTGACTGTCCATTCC BW: TCCTCATCCTTCTCATCCA
Odc1	Ornithine decarboxylase 1 (18263)	Argininеand Proline Metabolism (IPA); positive regulation of cell proliferation;	FW: ATAAGGATGCGTTCTATGTTG BW: CTCACTATGGCTCTGCTAT
Ssrp1	Structure specific recognition protein 1(20833)	DNA replication; DNA repair; regulation of transcription	FW:TATGACGATTATGCTGACTCT BW: TCTGCCACATCTTCTTCTT
Sumo2	(170930)	Small ubiquitin-related protein 1 conjugation, SUMO ligase activity	FW: AGAGGCATACACCACTTAG BW: TGTCTGTTTCGTTGATTGG

Most of the selected genes belong to oxidative stress response, apoptosis, cellular metabolism and protein binding functional categories.

product titer seems to be highest at the day 3 time-point. The mean specific productivity and standard deviation for this cell-line that could be supported by the animal-free CD-medium was 24.7 $\pm$ 0.64 pg/cell/day, and the mean integral viable cell density at peak culture of 5.2 $\times$ 10^6 $\pm$ 0.246 cells/mL/h.

Microarray exploration for significantly expressed gene transcript profiles during culture

Our strategy was to use microarrays to identify specific genes, both which varied, and also which had invariant expression levels as the culture transitioned from lag to log to stationary phases. Based on statistical background and spot filtering total of 14,589 genes were found to be expressed at some level in the samples tested. The filters were set to low limits to capture most of the gene expression changes during the time-course, especially since some of the statistical analysis used required the gene to be expressed at all time-points to be included in the analysis.

To restrict our analysis to genes where expression changes clearly and reproducibly occurred, a *P*-value cutoff of 0.01 was chosen for the ANOVA analysis. Using this cutoff for the 6634 initial set of genes resulting from ANOVA analysis, the significant gene expression changes across the four groups yielded 111 genes. Out of the 111 significant genes, 44 genes were up-regulated, while 48 genes were down-regulated, and 19 genes went up and down during the course of batch culture (Gene identity and expression ratios shown in Tables 2 and 3, Supporting Information). As a broad screen the fold-change filter was not set to obtain the significant genes, as even a modest fold-change, but highly reproducible, could be biologically relevant. Although the microarray analysis results in an approximation of gene expression variations, choosing a very stringent *P*-value for microarray data might lose some of the significant genomic changes, while choosing a low significance *P*-value may result in an overabundance of genomic

Table 3. Gene Regulation and Fold Changes During Culture Progression by Microarrays (MA) and RT-PCR

Gene ID	Change During Batch Culture	Fold-Change by MA	Fold-Change by RT-PCR
Sod1	Upregulated	2.32	1.65
Cycs	Upregulated	2.78	2.42
CD74	Downregulated	5.32	1.52
Atpif1	Downregulated	2.27	1.76
Txnrd1	Downregulated	3.13	1.58
Odc1	Downregulated	7.42	1.43

variations which could include some noise. For example, further ANOVA analysis with a less stringent *P*-value cutoff of 0.05, along with a fold-change filter set at 1.5, and signal intensity >200, yielded more genes, 365 using ArrayTrack™ (National Center for Toxicological Research, FDA) software. This less stringent *P*-value might be especially necessary to obtain a larger gene set to study in a functional category of interest. A volcano plot of this data showing the significant gene number, using a combination of specific fold-change and *P*-value cut off can be found in Figure 2. The volcano plot gives the option of viewing the gene scatter plot using two filters simultaneously, such as fold-change and *P*-value that was used in this case. The set of DEGs obtained depend on the filter cutoff values selected. The number of genes with significant variation determined by unequal variance *t*-tests using a *P*-value < 0.05 was found to be 50 genes for the pair day 2 to day 1 (early culture), 123 genes for day 3 to day 1 (mid culture), and 212 genes for day 3.5 to day 1 (late culture).

As a next step, functional pathway analysis of the DEGs over the course of the culture were categorized using gene ontology for functional analysis (GOFFA) and Kyoto Encyclopedia of Genes and Genomes databases accessed using ArrayTrack™ software. Table 1 shows the gene ontology functional groups obtained using the GOFFA functionality from ArrayTrack™ and the relevant genes that were significantly expressed from ANOVA analysis, along with the number of genes in each category. The significant genes seem to

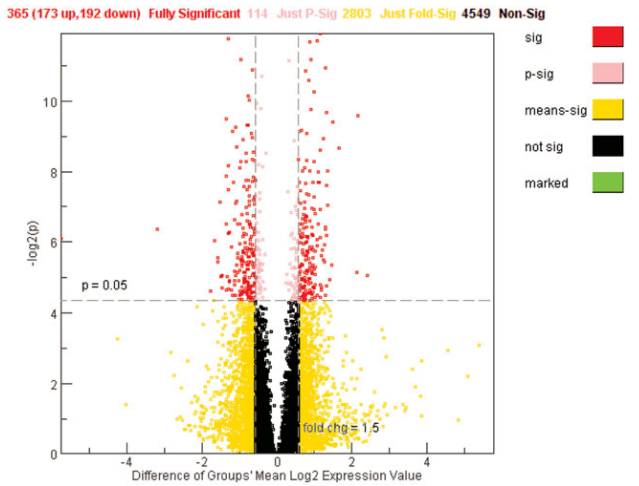

Figure 2. Volcano plot of 1-way ANOVA results showing the number of significant genes with *P*-value cutoff at 0.05 and a fold-change filter at 1.5 to capture most changes. The reference used was the universal mouse standard in the two-color assay.

Out of the 365 significant genes, 173 were up-regulated and 192 were down-regulated.

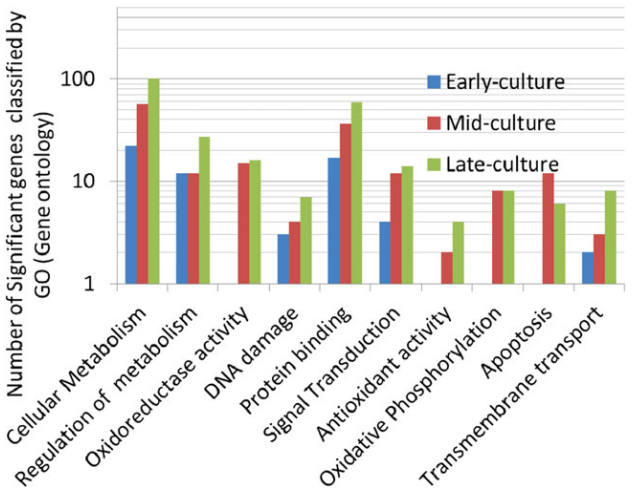

Figure 3. Number of genes obtained from microarrays by unequal variance *t*-tests at each of the early (day 2), mid (day 3) and late culture (day 3.5) time-points in comparison to the day 1 as reference.

These findings are shown above as number of genes in each functional category from early to late in culture. The number of genes obtained by GOFFA analysis and plotted on a semilog plot.

fall mainly in categories "cellular metabolism," "protein binding," and "regulation of cellular processes."

Many of these genes fall into categories consistent with culture evolution over time. For example, the number of genes (Figure 3) related to cellular metabolism, regulation of metabolism, signal transduction (Mt1, Eif6,) protein binding, DNA damage repair (Apex1, Sod1, Morf4l2), and transmembrane transport showed an increase in number from early to late culture *t*-test subgroups. It was observed that the gene transcripts involved in cellular functions predicted to change their expression levels as culture ages, such as oxido-reductase activity related genes Aldh3a, Fth1, Fth2, Ppx3, Prdx5, Sod1, Txnrd1, antioxidant activity related genes Prdx5, Sod1, Gpx3, apoptosis related genes Cycs, Fas, Sod1 and oxidative phosphorylation related genes Atp5h, Cox8a, Ndufa7, seem to be elevated at the later time-points in culture. The percentage of genes involved in various cellular functions, from early to late in culture is shown in the pie-chart in Figure 4. The percentage of gene transcripts in each of the functional categories such as cellular metabolism, protein binding and signal transduction were relatively unchanged when comparing early to late in batch culture, although the actual number of significantly expressed genes by the unequal variance *t*-tests increased with culture progression. Also, the percent metabolism regulation genes were found to drop, from beginning to end of culture. Some of the genes related to cellular functions such as apoptosis did not show up in early exponential, but were significantly expressed at later time-points, as would be expected.

RT-PCR verification of microarray findings

To validate our microarray results and identify genes that can be precisely tracked as markers for culture state, we developed PCR primers for Sod1, Cycs, Hspa9, CD74, Atpif1, Arpc1b, Odc1, Rpl19, Txnrd1, Sumo2, Ssrp1 gene transcripts. Table 2 shows the primer sequences for the 11 genes chosen for RT-PCR verification and semiquantitation, resulting in PCR products of <150 bp. These genes were selected based on their relevant biological function described above along with their level of expression from microarray analysis. We chose to focus on the apoptosis,[9] damage protection, protein folding,[35] amino acid metabolism, and cellular metabolism[36–38] pathways because from a functional stand-point, it is easy to surmise that they may be involved in cellular transitions as cell adapts not only to the stresses of the changing bioreactor environment, but also to slower growth and nutrient depletion with culture progression.

Genes with variable and invariant expression over time-course of culture verified by RT-PCR

In general, we found reasonable agreement between profiles resulting from microarrays and RT-PCR techniques, as seen in Table 3 where the direction of changes could be matched between the RT-PCR and microarray findings. This can be also evidenced by visual inspection (see Figures 5 and 6). The fold-changes during the course of culture in the PCR assay were measured using β-actin as a housekeeping reference. Although absolute number of fold-changes from early to late in culture obtained from microarray results could not be compared using the semiquantitation technique by PCR, there was good agreement with the trends such as up or downregulation of the gene expression from both methods. For RT-PCR data, the significance of fold-change during culture progression was predicted using *P*-value statistical analysis across the four time-points. Table 4 shows the *P*-value statistics generated by 1-way ANOVA analysis for the four groups of time-points, as well as the Kristal-Wallis analysis that does not assume Gaussian distribution of the RT-PCR semiquantitation data. It should be noted that only those fold-changes which showed significance by both analyses were concluded as being definitely up or down-regulated, while the remaining were categorized as invariant profiles. Also, the microarray results represented in log ratios tend to compress the fold-changes.

Some of the gene expression results verified included the following observations which made intuitive sense from a biological standpoint. The expression for Sod1 and Cycs genes

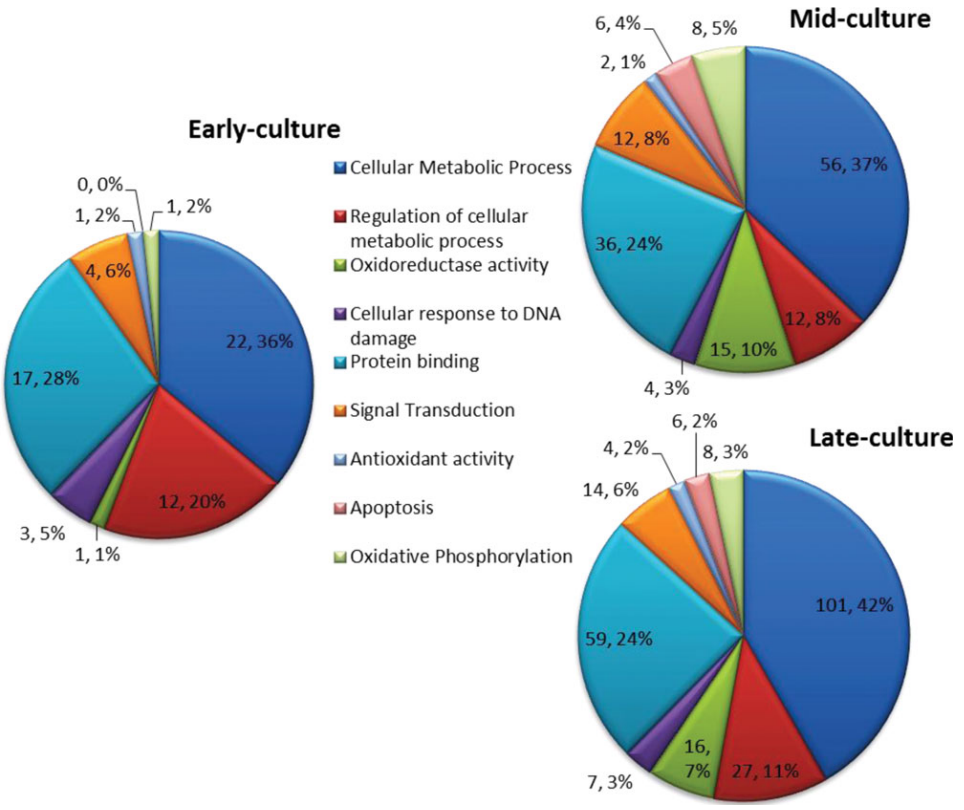

Figure 4. Pie-charts showing the percentage of genes that were found in each gene ontology category.

In this plot the X-axis is the functional category and the Y-axes are the percentage of total gene transcripts in each category, and the number of significant genes. The percent changes during early culture at peak exponential (day 2), midculture during late exponential/early stationary (day 3), and late culture, stationary/early death (day 3.5) are presented, with respect to the early exponential (day 1) sample. The genes related to several cellular functions were summarized using ArrayTrack™ software.

(Figure 5) was found to be up-regulated from beginning to end of culture, as measured by both microarrays and RT-PCR. Thus, apoptosis genes appear to be good candidates to track culture state as cells transition during batch culture in a controlled bioreactor. Also, the gene Txnrd1 that reduces thioredoxins[39] and plays a protective role against oxidative stress had a fairly constant expression during majority of the culture period from day 1 to 3, but down-regulated when viability started to drop toward the end of culture. Other transcripts, CD74 involved in protein complex assembly and protein binding, Odc1 involved in arginine and proline metabolism and regulation of cell proliferation, were initially downregulated, but upregulated towards later part of culture. Atpif1 gene was constant until late exponential, but upregulated during stationary phase of culture.

In contrast to the above genes, some of the gene expression profiles were mostly constant as determined by statistical analysis (Table 4) during the entire course of the batch culture (Figure 6). It is to be noted that these genes were identified from microarray ANOVA analysis with stringent *P*-value, however fold-change criteria was not set to be able to capture small enough, but reproducible, and hence biologically relevant transcripts. By RT-PCR, the expression of these genes was virtually constant during the course of culture, and were assigned as invariant, but significantly expressed at each time-point. Genes such as Hspa, Arpc3, Sumo 2, Ssrp1, and RPl19, had relatively constant expression during the culture duration, compared to the genes classified as variable during the course of cell culture.

Discussion

There could be several advantages to having the ability to track and predict the culture status in a bioreactor by analyzing a subset of marker genes. If this were the case, the impact of changes on cell growth and product in bioreactor culture environment could be discerned by the up or down-regulation of these genes. The impact of changes due to relevant bioreactor environment issues including mixing, mode of aeration, and changes due to bioreactor scale-up, can be predicted. In addition, such gene data could be extended to cell line engineering to overcome negative environmental effects. Our model 5 L system coupled with the microarray analysis was run to attain this goal.

Strategies for obtaining differential gene expression

A widely used approach for obtaining differential expression is to simply compare fold-change between the test sample and the control. In general, the sensitivity and reliability of the fold-change filter might be applicable mostly to the larger and the most robust changes in gene expression, but might be questionable for smaller changes. A smaller fold-change that is reproducible, and not influenced by noise and other such factors, might be biologically important. For instance, with at least two-fold change criteria, if the conditions in the study do not affect enough genes to induce this change, very few genes might be selected, resulting in low sensitivity, and causing the loss of valuable gene

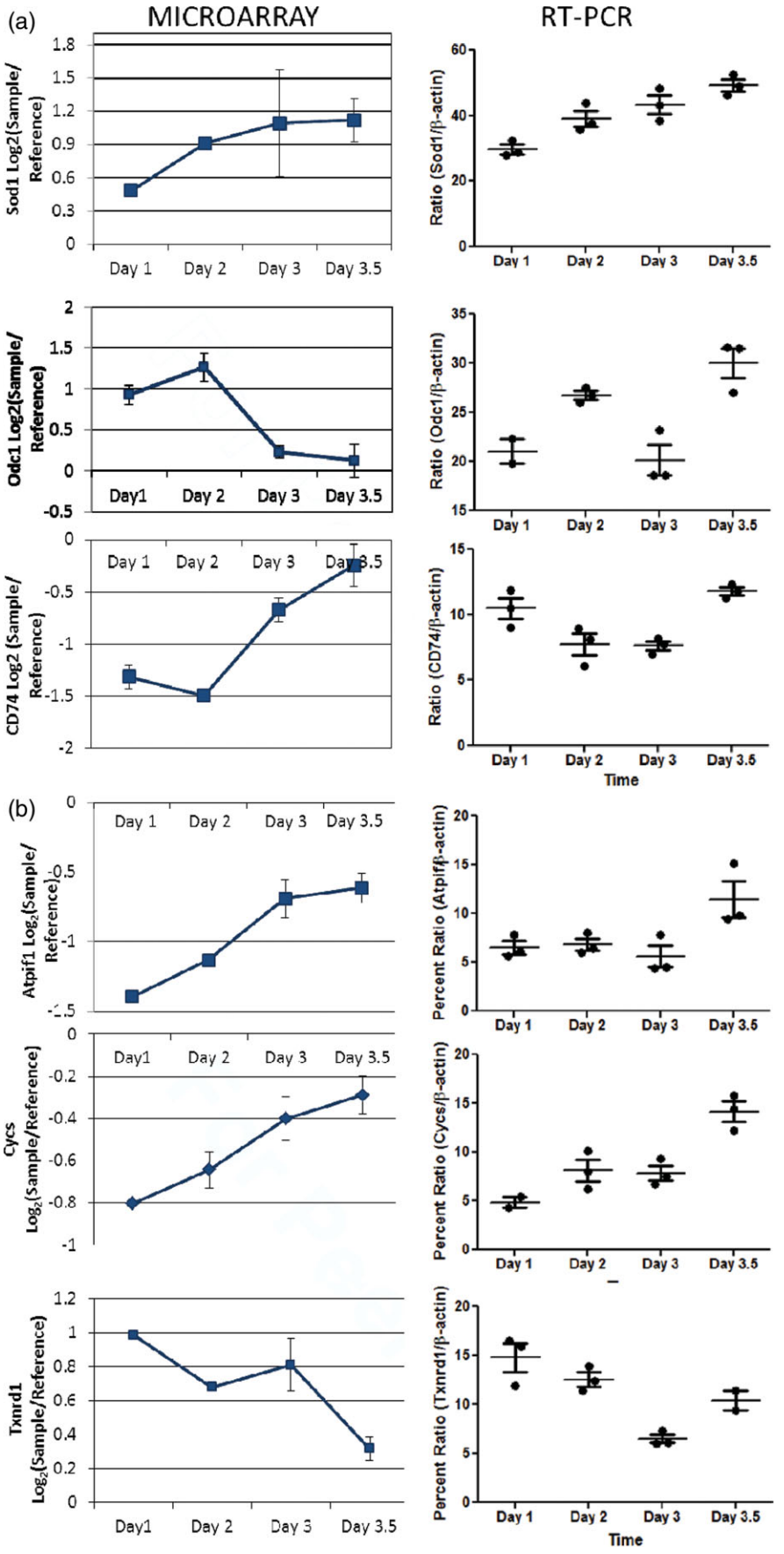

Figure 5. Profiles of genes with variable expression both from microarray analysis (left) and RT-PCR semiquantitation(right) from early to late in 5 L batch cell culture are shown for (a) Sod1, Odc1 and CD74 genes and (b) Atpif1, Cycs and Txnrd1.

Variable genes confirmed by semiquantitative PCR analysis, using the ratio of expression with a house-keeping gene β-actin as a reference for comparison and microarray data were expressed as log ratios of gene expression with universal mouse reference are shown here. Note the general concurrence in expression trends between microarrays and PCR.

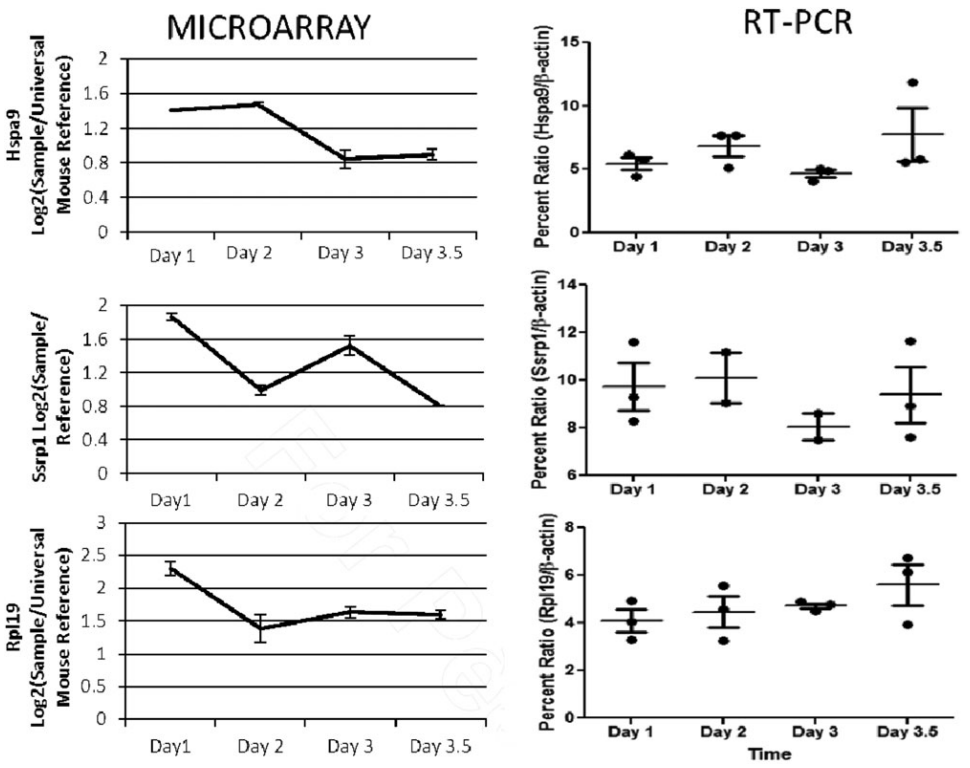

Figure 6. Examples of invariant gene profiles without statistically significant variation during culture such as Hspa9, Ssrp1, Rpl19, by microarrays, by microarrays (left), confirmed by semiquantitative RT-PCR analysis (right).

PCR semiquantitation shown using the ratio of expression with a house-keeping gene β-actin as a reference for comparison, and microarray data expressed as log ratios of gene expression with universal mouse reference. Profiles of gene expression by both methods, from early to late in batch culture are shown.

Table 4. RT-PCR Semi-Quantitation Statistics such as the *P*-values from 1-way ANOVA, as well as the Kruskal-Wallis Analysis that does not Assume Gaussian Distribution of Data, are Shown Here

Gene ID	1-way ANOVA *P*-Value	F Value	R^2	ΔGroup Means Significance by ANOVA	Kruskal-Wallis (KW test) *P*-Value	KW Test ΔGroup Medians Significance
Sod1	0.0015	14.14	0.84	Yes	0.027	Yes
CD74	0.0036	10.69	0.80	Yes	0.034	Yes
Atpif	0.0284	5.15	0.66	Yes	0.063	No
Cycs	0.0018	15.59	0.87	Yes	0.042	Yes
Txnrd1	0.0026	13.72	0.85	Yes	0.045	Yes
Odc1	0.0027	13.44	0.85	Yes	0.039	Yes
Hspa9	0.3147	1.39	0.34	No	0.132	No
Rpl19	0.3861	1.15	0.30	No	0.622	No
Arpc1b	0.0228	5.61	0.67	Yes	0.070	No
Sumo2	0.0641	3.86	0.62	No	0.093	No
Ssrp1	0.6556	0.57	0.22	No	0.442	No

Significance of fold-change predicted by both kinds of statistical analysis for the PCR data is shown here.

information. In our case with the log transformed data, the fold-change filter for *t*-tests set was 1.5 with log base 2 as a method of capturing strongly expressed genes. Fold-changes measured were generally lower in the typical batch cell culture, especially without any intervened changes such as media, osmolality, or temperature etc. Also, in our case with the two color-array, the reference used for all the samples was a universal mouse reference. Hence, setting a stringent fold-change filter was not particularly useful in our case, as we were looking for changes across the time-course samples.

In contrast to the fold-change approach, statistical hypothesis-testing based approaches such as ANOVA or *t*-tests can reveal genes that show highly significant changes across the time-course. Using 1-way ANOVA analysis, we examined whether the gene variability between the various time-points in the culture was higher than the variability within the biological replicates themselves, at each time-point. Several assumptions such as uniformity of variance of errors and normality of data were made prior to ANOVA analysis,[40] which although might be valid for some genes, others might deviate. Log transformation of the data was done to stabilize the variance and make the data more amenable to such parametric testing by 1-way ANOVA. Hence, the log ratios presented here show reduced fold-difference between the time-points, unless transformed back to ratios. Also, a common universal mouse reference was used for this multiple groups test in the timecourse.

At low expression, microarrays tend to have a lower signal to noise ratio, resulting in high variance. When there is low expression/high variance for a gene at one or more time-points in the ANOVA analysis, it causes the gene to be

not included, with the chosen P-value of <0.01. However, using an unequal variance t-test between any two groups of samples only, such changes could be captured. Hence, this method of unequal variance paired t-tests along with 1-way ANOVA allows for identification of a larger subset of genes[41] that could be biologically relevant.

Gene profiles for culture state analysis

Profiles of some genes were determined to vary from beginning to end of culture (Figure 5), while others were invariant in culture (Figure 6) based on the results of 1-way ANOVA, as well as the Kruskal-Wallis statistical analysis of the RT-PCR results (shown in Table 4). Their status could shed light on the physiological state of the cells in a sparged bioreactor environment. In addition, such gene profiles would be valuable for comparing a process change. An example of variable gene expression profiles was the increase in Sod1 gene expression from day 1 to day 3.5 in culture. One could conjecture that this could result from an increase in free-radical stress on cells due to sparging pure oxygen into the culture fluid for %DO control, especially with increased demand for bubbling as culture grows. Sod1 gene is involved in converting superoxide radicals to molecular oxygen and hydrogen peroxide (Free-radical induced apoptosis pathway, BioCarta.com), and is also involved in Nrf2-mediated oxidative stress pathway (Ingenuity Pathway Analysis, www.ingenuity.com). This makes Sod1 a particularly useful candidate for surrogate tracking of culture state in a controlled bioreactor, where oxidative stresses are expected. As the cultures were not fed, it is expected that cells undergo apoptosis as a result of nutrient starvation,[42] which was confirmed by our observed upregulation of apoptosis related gene Cycs.

Expression of several metabolic genes changed over time as expected to occur with nutrient depletion over the duration of batch culture. Upregulation of Atpif1 gene at the end of the culture is consistent with a reduction in nucleotide metabolism. As protein expression was highest during the stationary/late-stationary part of the culture (Figure 5), an increase in CD74, a protein complex assembly related gene could be expected in the later part of culture. This argues that this gene is useful for culture analysis. The upregulation of the Odc1 metabolism gene toward the end of the culture is consistent with the cell metabolic machinery being still intact, and could prolong if the culture was fed with nutrient supplemented media. Oxidative phosphorylation pathway related genes Cox8a, Ndufa7, Ndufs8 were all upregulated toward the end of culture. As these genes are involved in energy generation process, their upregulation correlates with increasing energy generation with culture progression. Such correlations of metabolic changes under different culture conditions with gene expression changes have also been shown in a recent study using embryonic stem cells.[43] RT-PCR findings suggest that the profiles of protein binding genes such as Arpc3, and protein folding gene Hspa9 (Figure 6) were mostly unchanged during the culture period, suggesting despite apoptosis and nutrient starvation, there was no negative impact on the batch culture. Comparing to other published DEG lists for other cell lines such as hybridoma and CHO[16,44,45] some overlapping genes were found. Examples include ribosomal proteins (Rpl family), protein folding chaperone (Hspa), cytoskeleton elements (Arpc), translation regulation genes (Eifs), Cytochrome c oxidase (Cox), Cytochrome c somatic (Cycs), growth arrest and DNA-damage -inducible alpha (GADD45), Heme oxygenase (Hmox), and metabolism gene Isocitrate dehydrogenase (Idh). As both the microarrays, and RT-PCR results are only good approximations of gene findings, the transcriptomic profiles from this study need to be further confirmed by a more rigorous qRT-PCR (quantitative) approach. Also, varying bioreactor conditions that could change the expression of these genes selectively to confirm their functionality in culture is part of a future study from our laboratory.

Conclusions

Our studies indicate that a subset of significantly expressed genes related to several important cellular functions in a bioreactor can be identified and genomic profiles can be obtained. The genes that were found to be up or downregulated in a bioreactor could depict the cell status as the culture transitions from early exponential to late stationary phases of growth. These gene profiles could be used to track the culture state, for process reproducibility and inputs to product quality in a changing bioreactor environment with set-point control. Any relationship to product quality needs to be specifically studied to fully understand the effect of variations in gene profiles. This study serves as a starting point for delineating relevant transcriptomic profiles that could be used to track cell status in a bioreactor environment.

GEO accession

GSE33062-Genomic analysis for predicting cell culture status in a sparged bench-scale 5 L bioreactor.

Acknowledgments

This work would not have been achieved without scientific support from Amy X Yang and Toshio Fujisawa (CBER, FDA), and Mike Hanson (UMBC). The UMBC authors gratefully acknowledge funding from Sartorius-Stedim Biotechnology. Support from CDER/FDA Critical Path Project #1500 contributed to the completion of this study. They dedicate this article to Prof. Raj Mutharsan, for his pioneering work on intracellular analytes measurement to assess cell physiological state.

FDA Disclaimer: Views expressed in this article are not endorsed by the FDA, and are of the authors only.

Literature Cited

1. Nam JH, Zhang F, Ermonval M, Linhardt RJ, Sharfstein ST. The effects of culture conditions on the glycosylation of secreted human placental alkaline phosphatase produced in Chinese hamster ovary cells. *Biotechnol Bioeng*. 2008;100:1178–1192.
2. Restelli V, Wang MD, Huzel N, Ethier M, Perreault H, Butler M. The effect of dissolved oxygen on the production and the glycosylation profile of recombinant human erythropoietin produced from CHO cells. *Biotechnol Bioeng*. 2006;94:481–494.
3. Meier SJ, Hatton TA, Wang DI. Cell death from bursting bubbles: role of cell attachment to rising bubbles in sparged reactors. *Biotechnol Bioeng*. 1999;62:468–478.
4. Michaels JD, Mallik AK, Papoutsakis ET. Sparging and agitation-induced injury of cultured animals cells: do cell-to-bubble interactions in the bulk liquid injure cells?*Biotechnol Bioeng*. 1996;51:399–409.
5. Kioukia N, Nienow AW, AlRubeai M, Emery AN. Influence of agitation and sparging on the growth rate and infection of insect cells in bioreactors and a comparison with hybridoma culture. *Biotechnol Prog*. 1996;12:779–785.
6. Zhu Y, Cuenca JV, Zhou W, Varma A. NS0 cell damage by high gas velocity sparging in protein-free and cholesterol-free cultures. *Biotechnol Bioeng*. 2008;101:751–760.

7. Alrubeai M, Singh RP, Goldman MH, Emery AN. Death mechanisms of animal-cells in conditions of intensive agitation. *Biotechnol Bioeng*. 1995;45:463–472.
8. Ryu JS, Lee GM. Application of hypoosmolar medium to fed-batch culture of hybridoma cells for improvement of culture longevity. *Biotechnol Bioeng*. 1999;62:120–123.
9. Krampe B, Al-Rubeai M. Cell death in mammalian cell culture: molecular mechanisms and cell line engineering strategies. *Cytotechnology*. 2010;62:175–188.
10. Majid FAA, Butler M, Al-Rubeai M. Glycosylation of an immunoglobulin produced from a murine hybridoma cell line: the effect of culture mode and the anti-apoptotic gene, bcl-2. *Biotechnol Bioeng*. 2007;97:156–169.
11. Lehmann J, Vorlop J, Büntemeyer H. Bubble-free reactors and their development of continuous culture with cell recycle. In: Spier RE, editor. *Animal Cell Biotechnology*. London: Academic Press Limited; 1988;221–238.
12. Chisti Y. Animal-cell damage in sparged bioreactors. *Trends Biotechnol*. 2000;18:420–432.
13. Yee JC, de Leon Gatti M, Philp RJ, Yap M, Hu WS. Genomic and proteomic exploration of CHO and hybridoma cells under sodium butyrate treatment. *Biotechnol Bioeng*. 2008;99:1186–1204.
14. De Leon Gatti M, Wlaschin KF, Nissom PM, Yap M, Hu WS. Comparative transcriptional analysis of mouse hybridoma and recombinant Chinese hamster ovary cells undergoing butyrate treatment. *J Biosci Bioeng*. 2007;103:82–91.
15. Thaisuchat H, Baumann M, Pontiller J, Hesse F, Ernst W. Identification of a novel temperature sensitive promoter in CHO cells. *BMC biotechnol*. 2011;11:51.
16. Doolan P, Meleady P, Barron N, Henry M, Gallagher R, Gammell P, Melville MW, Sinacore M, McCarthy K, Leonard M, Charlebois T, Clynes M. Microarray and proteomics expression profiling identifies several candidates, including the valosin-containing protein (VCP), involved in regulating high cellular growth rate in production CHO cell lines. *Biotechnol Bioeng*. 2010;106:42–56.
17. Baik J, Lee M, An S, Yoon S, Joo E, Kim Y.Park H, Lee G. Initial transcriptome and proteome analyses of low culture temperature-induced expression in CHO cells producing erythropoietin. *Biotechnol Bioeng*. 2006;93:361–371.
18. Kantardjieff A, Jacob NM, Yee JC, Epstein E, Kok YJ, Philp R, Betenbaugh M, Hu WS. Transcriptome and proteome analysis of Chinese hamster ovary cells under low temperature and butyrate treatment. *J Biotechnol*. 2010;145:143–159.
19. Yee JC, Gerdtzen ZP, Hu WS. Comparative transcriptome analysis to unveil genes affecting recombinant protein productivity in mammalian cells. *Biotechnol Bioeng*. 2009;102:246–263.
20. Nissom PM, Sanny A., Kok YJ, Hiang YT, Chuah SH, Shing TK, Lee YY, Wong KT, Hu WS, Sim MY, Philp R., Transcriptome and proteome profiling to understanding the biology of high productivity CHO cells. *Mol Biotechnol*. 2006;34:125–140.
21. Charaniya S, Karypis G, Hu WS. Mining transcriptome data for function-trait relationship of hyper productivity of recombinant antibody. *Biotechnol Bioeng*. 2009;102:1654–1669.
22. Chen P, Harcum S. Effects of elevated ammonium on glycosylation gene expression in CHO cells. *Metab Eng*. 2006;8:123–132.
23. Lee YY, Wong K, Nissom PM, Wong DC, Yap MG. Transcriptional profiling of batch and fed-batch protein-free 293-HEK cultures. *Metab Eng*. 2007;9:52–67.
24. Shi L, Jones WD, Jensen RV, Harris SC, Perkins RG, Goodsaid FM, Guo L, Croner LJ, Boysen C, Fang H, Qian F, Amur S, Bao W, Barbacioru CC, Bertholet V, Cao XM, Chu TM, Collins PJ, Fan XH, Frueh FW, Fuscoe JC, Guo X, Han J, Herman D, Hong H, Kawasaki ES, Li QZ, Luo Y, Ma Y, Mei N, Peterson RL, Puri RK, Shippy R, Su Z, Sun YA, Sun H, Thorn B, Turpaz Y, Wang C, Wang SJ, Warrington JA, Willey JC, Wu Jie, Q, Zhang L, Zhong S, Wolfinger RD, Tong W. The balance of reproducibility, sensitivity, and specificity of lists of differentially expressed genes in microarray studies. *BMC Bioinformatics*. 2008;9:S10.
25. Pine PS, Rosenzweig BA, Thompson KL. An adaptable method using human mixed tissue ratiometric controls for benchmarking performance on gene expression microarrays in clinical laboratories. *BMC Biotechnol*. 2011;11:38.
26. Shi L, Tong W, Fang H, Scherf U, Han J, Puri RK, Frueh FW, Goodsaid FM, Guo L, Su Z, Han T, Fuscoe JC, Xu ZA, Patterson TA, Hong H, Xie Q, Perkins RG, Chen JJ, Casciano DA. Cross-platform comparability of microarray technology: intra-platform consistency and appropriate data analysis procedures are essential. *BMC Bioinformatics*. 2005;6:S12.
27. Yang AX, Mejido J, Bhattacharya B, Petersen D, Han J, Kawasaki ES, Puri RK. Analysis of the quality of contact-pin fabricated oligonucleotide microarrays. *Mol biotechnol*. 2006; 34:303–315.
28. Petersen D, Chandramouli GVR, Geoghegan J, Hilburn J, Paarlberg J, Kim CH, Munroe D, Gangi L, Han J, Puri R, Staudt L, Weinstein J, Barrett JC, Green J, Kawasaki ES. Three microarray platforms: an analysis of their concordance in profiling gene expression. *BMC Genomics*. 2005;6:63–77.
29. Chen Y, Bittner M. Ratio-based decisions and the quantitative analysis of cDNA microarray images. *J Biomed Optics*. 1997;2:364–374.
30. Osier M, Zhao H, Cheung K. Handling multiple testing while interpreting microarrays with the Gene Ontology Database. *BMC Bioinformatics*. 2004;6:124.
31. Rubinstein LJ, Stein KE. Murine immune response to the Neisseria meningitidis group C capsular polysaccharide. *I. Ontogeny. J Immunol*. 1988;141:4352–4356.
32. Kondragunta B, Drew JL, Brorson KA, Moreira AR, Rao G. Advances in clone selection using high-throughput bioreactors. *Biotechnol Prog*. 2010;26:1095–1103.
33. Yang YH, Dudoit S, Luu P, Lin DM, Peng V, Ngai J, Speed TP. Normalization for cDNA microarray data: a robust composite method addressing single and multiple slide systematic variation. *Nucleic Acids Res*. 2002;30:e15.
34. Speed TP. *Statistical analysis of gene expression microarray data*. Boca Raton. Chapman & Hall/CRC; 2003.
35. Lee DH, Kim SG, Kweon DH, Seo JH. Folding machineries displayed on a cation-exchanger for the concerted refolding of cysteine- or proline-rich proteins. *BMC Biotechnol*. 2009;9:27.
36. Burleigh SC, van de Laar T, Stroop CJ, van Grunsven WM, O'Donoghue N, Rudd PM, Davey GP. Synergizing metabolic flux analysis and nucleotide sugar metabolism to understand the control of glycosylation of recombinant protein in CHO cells. *BMC Biotechnol*. 2011;11:95.
37. James DC, Freedman RB, Hoare M, Ogonah OW, Rooney BC, Larionov OA, Dobrovolsky VN, Lagutin OV, Jenkins N. N-glycosylation of recombinant human interferon-gamma produced in different animal expression systems. *Biotechnology*. 1995;13: 592–596.
38. Meleady P, Doolan P, Henry M, Barron N, Keenan J, O'Sullivan F, Clarke C, Gammell P, Melville MW, Leonard M, Clynes M. Sustained productivity in recombinant Chinese hamster ovary (CHO) cell lines: proteome analysis of the molecular basis for a process-related phenotype. *BMC Biotechnol.* 2011; 11:78.
39. Arner ES, Holmgren A. Physiological functions of thioredoxin and thioredoxin reductase. *Eur J Biochem.* 2000;267:6102–6109.
40. Draghici S. Statistical intelligence: effective analysis of high-density microarray data. *Drug Discov Today*. 2002;7:S55–S63.
41. Pavlidis P. Using ANOVA for gene selection from microarray studies of the nervous system. *Methods*. 2003;31:282–289.
42. Hwang SO, Lee GM. Nutrient deprivation induces autophagy as well as apoptosis in Chinese hamster ovary cell culture. *Biotechnol Bioeng*. 2008;99:678–685.
43. Sepulveda DE, Andrews BA, Papoutsakis ET, Asenjo JA. Metabolic flux analysis of embryonic stem cells using three distinct differentiation protocols and comparison to gene expression patterns. *Biotechnol Prog*. 2010;26:1222–1229.
44. Yoon SK, Song JY, Lee GM. Effect of low culture temperature on specific productivity, transcription level, and heterogeneity of erythropoietin in Chinese hamster ovary cells. *Biotechnol Bioeng*. 2003;82:289–298.
45. Bhattacharya B, Miura T, Brandenberger R, Mejido J, Luo Y, Yang AX, Joshi BH, Ginis I, Thies RS, Amit M, Lyons I, Condie BG, Itskovitz-Eldor J, Rao MS, Puri RK. Gene expression in human embryonic stem cell lines: unique molecular signature. *Blood*. 2004;103:2956–2964.

Manuscript received Mar. 20, 2012, and revision received Jul. 11, 2012.

Once the more sensitive genes (and as might be expected, most of them are related to cellular stress response) were identified, we were able to use this powerful tool to design a minibioreactor that would operate in a manner similar to a laboratory scale system right down to the genomic level. With new technologies that are now available for real-time transcript monitoring, I expect that a gene-chip sensor will guide next generation scaling efforts.

Bioreactor Environment-Sensitive Sentinel Genes as Novel Metrics for Cell Culture Scale-Down Comparability

Bhargavi Kondragunta
Center for Advanced Sensor Technology and Dept. of Chemical, Biochemical and Environmental Engineering, University of Maryland, Baltimore, MD 21250

Div. of Cellular and Gene Therapy, Center for Biologics Evaluation and Research, Food and Drug Administration, 29 Lincoln Drive, Bethesda, MD 20892

Div. of Monoclonal Antibodies, Center for Drug Evaluation and Research, Food and Drug Administration, Silver Spring, MD 20903

Bharat H. Joshi and Jing Han
Div. of Cellular and Gene Therapy, Center for Biologics Evaluation and Research, Food and Drug Administration, 29 Lincoln Drive, Bethesda, MD 20892

Kurt A. Brorson
Div. of Monoclonal Antibodies, Center for Drug Evaluation and Research, Food and Drug Administration, Silver Spring, MD 20903

Raj K. Puri
Div. of Cellular and Gene Therapy, Center for Biologics Evaluation and Research, Food and Drug Administration, 29 Lincoln Drive, Bethesda, MD 20892

Antonio R. Moreira and Govind Rao
Center for Advanced Sensor Technology and Dept. of Chemical, Biochemical and Environmental Engineering, University of Maryland, Baltimore, MD 21250

DOI 10.1002/btpr.1606
Published online September 18, 2012 in Wiley Online Library (wileyonlinelibrary.com).

Scale-down of bioreactors is currently done based on matching one or more measurable parameters such as k_La *and* P/V*, which could result in insufficient process comparability. Currently, there is a lack of genomic translational studies in cell culture scale-down, which could help delineate measurable cellular attributes for improved scale-down. In this study, we scaled-down from a typical bench-scale 5-L bioreactor to a novel high-throughput 35-mL minibioreactor based on matching oxygen transfer rate, which resulted in cell growth and product-related discrepancies using Sp2/0 cells. Performing DNA microarrays on time-course samples from both systems, we identified ~200 differentially expressed transcripts, presumably because of bioreactor aeration and mixing differences with scale-down. Evaluating these transcripts for bioreactor-relevant cellular functions such as oxidative stress response and DNA damage response, we chose 18 sentinel genes based on their degree of difference and functionality, which we further verified by quantitative real-time polymerase chain reaction (*qRT-PCR*). Tracking the differential expression of Sod1, Apex1, and Odc1 genes, we were able to correlate sparging-related damage and poor mixing, as possible causes for physiological changes such as prolonged culture in minibioreactors. Additionally, to verify our sentinel gene findings, we performed follow-up improved scale-down studies based on gene analysis and measured transcriptomic changes. As a result, qRT-PCR-based genomic profiles and cell growth profiles showed better convergence between the improved minibioreactor conditions and the model 5-L bioreactor. Our results broadly show that based on the knowledge from transcriptomic changes of sentinel gene profiles, it is possible to improve bioreactor scale-down for more comparable processes.* © 2012 American Institute of Chemical Engineers *Biotechnol. Prog.,* 28: 1138–1151, 2012
Keywords: sentinel genes, scale-down, minibioreactors, time-course

Introduction

Cell culture processes in bioreactors use rigorous environmental controls such as maintaining fixed set points for dissolved oxygen (DO), culture pH, aeration, and impeller agitation rates. Especially during the scale-down or vice versa, this is done to avoid undesirable changes in culture

This article is dedicated to the memory of Professor James E. Bailey.The findings and conclusions in this report are those of the author(s) and do not necessarily represent the views of the FDA. No endorsement of any vendor or technique is implied. G. Rao has an equity position in Fluorometrix.

Additional Supporting Information may be found in the online version of this article.

Correspondence concerning this article should be addressed to G. Rao at grao@umbc.edu or to Raj K. Puri at Raj.Puri@fda.hhs.gov.

environment. However, as a result of scale change, negative effects such as shear- and bubble-induced damage from gas sparging and agitation are known to occur that lead to process differences and could impact product quality. Changes in culture conditions can lead to, for example, altered glycosylation profiles, which can then drastically change the drug's pharmacokinetics.[1,2] Typical bioprocess scale-down is done by matching physical parameters between bioreactor systems, such as power per volume (P/V), oxygen mass-transfer coefficient ($k_L a$), mixing time, impeller tip speed, CO_2 removal, and impeller shear rate.[3–5] The first description of a scale-down to minibioreactors using constant $k_L a$ was reported a decade ago.[6] Although bioreactor scale change has been thoroughly studied using the above mentioned methods, it is still subjective,[7] mainly because of a gap in knowledge at the cellular level.

Currently, there are limited measurement strategies at the cellular level that could be used to adequately describe a process, such as cell growth and viability measurements. Bioreactor environmental parameters such as DO, culture pH, dissolved carbon dioxide, and oxygen uptake rate as well as metabolite measurements still fall short of explaining culture phenomena at the physiological level because of complexity of the cellular system. Using such measurements alone, one might be unable to accurately predict a pathway response or, for example, the relationship to other biochemical responses within the cell. Further, without sufficient knowledge at the cellular level, one could end up changing or optimizing several parameters, resulting in an iterative process before reaching the right parameter to adjust. In this study, we go beyond routine measurements such as cell growth, bioreactor engineering parameters, environmental parameters, and product titer as scale-down process comparisons, and present a time-course transcriptomic comparison between the two scales throughout the course of cell culture as a method for improving process matching upon scale change.

With the increasing affordability of microarrays as tools for measuring cell physiological changes, identifying cell-type-specific sentinel genes for culture scale-down optimization has become a possibility. The availability of complete genome sequences for mouse, human, and now hamster cell lines makes cell lines derived from these species excellent models for studying the underlying biochemical responses of cells to environmental perturbations. Currently, in mouse cell lines, an estimated 37,000 different transcripts can be tested by using microarrays. Microarrays have been used, for example, to identify cell confluence biomarker genes for human embryonic kidney-293 (HEK-293) cells maintained in CO_2 incubators,[8] thus identifying signal changes in adenoviral vector production due to phenotypic changes in cells. Gene sequencing for chinese hamster ovary (CHO), the most prevalent host cell-line for producing biological drugs, was undertaken by CHO genomics consortium,[9,10] and now the draft genomic sequence for CHO-K1's estimated 24,383 predicted genes is available.[11]

In this study, culture in a novel 35-mL high-throughput minibioreactor was compared to a typical 5-L bench-scale bioreactor after scale-down based on constant oxygen transfer rate (OTR) (Figure 1). The minibioreactor system used in this study had overhead mixing capability, along with ability to sparge gases into the culture medium. In the recent years, several high-throughput systems[12–16] have been reported as viable scale-down models for microbial and mammalian cell

Figure 1. 5-L bench-top bioreactor and the novel 35-mL minibioreactor tristation.

cultures. As a novel approach to explain scale differences, genomic microarrays were performed for both bioreactor systems to identify via an algorithm we present here a set of differentially expressed sentinel gene markers. Using process knowledge provided by the time-course transcriptomic changes, we applied improvements to the minibioreactors to reduce discrepancies.

Materials and Methods

Cell culture

A subclone of the Sp2/0 myeloma-based mouse hybridoma cell line (2055.5) secreting an anti-meningitidis-capsular–polysaccharide IgG3[17] was used for these studies. The original line was subsequently subcloned to obtain higher titers and a stable production cell line.[18] During studies, cells were maintained in T-Flasks (Corning, Lowell, MA) and 250-mL Spinner flasks (Kontes, Vineland, NJ) in a 5% CO_2 incubator (Napco, Winchester, VA) at 37°C, in chemically defined CD hybridoma media (Invitrogen, Carlsbad, CA) being split every 3–4 days. Each 1 L of CD media was additionally supplemented with 8 mM of L-glutamine (Invitrogen, Carlsbad, CA) and 3.5×10^{-4}% β-mercaptoethanol (v/v) (Sigma, St. Louis, MO).

Microarray gene expression analysis

Detailed microarray procedures and statistical analysis are described in our companion paper.[19] Epoxy-coated microarray slides (Operon Biotechnologies, Huntsville, AL, now MWG Biotech AG) printed at CBER, FDA on Gene Machines Omnigrid Arrayer (San Carlos, CA) at the NCI gene core array laboratory and labeled as Mm-35K-V4.0p5 were used for the studies presented here. These chips used Strategene's replicated alien controls. Madb (microarray database from Advanced Technology Center at NCI/CCR, the Bioinformatics and Molecular Analysis Section (BIMAS), NIH) software was primarily used for analysis. In addition, ArrayTrack™ (National Center for Toxicological Research, FDA) software was also used for microarray statistical analysis and to access gene pathways and functionality databases. Pathway analysis was done using GOFFA (gene ontology for functional analysis), KEGG (Kyoto Encyclopedia of Genes and Genomes), and Biocarta (Biocarta.com). Our method for detecting differential gene expression using statistical hypothesis testing methods such as analysis of variance (ANOVA) and t-tests is presented here. The experimental method was set up such that microarrays were run at four or more time points during the course of culture for each reactor type. It would be insufficient to analyze the physiological differences between the cultures of two

bioreactor systems using gene expression at a single time point. The mRNA levels could be upregulated or downregulated during different phases of the culture, namely the early exponential, late exponential, stationary, and late stages of cell culture. Hence, it would be important to study the genomic profiles, rather than expression at a single point.

Gene expression profiles were obtained by plotting log ratios of the test bioreactor sample to the universal mouse reference at several time points over the course of culture. The set of gene transcripts that showed differences between the two bioreactor systems was obtained by statistical analysis, where five groups of samples were analyzed for minibioreactors and four groups of samples were analyzed for 5-L bioreactors, with at least one sample point on each day of batch culture. The final sample collected was with viability $\geq$80% to ensure RNA quality for microarray processing. Significant gene expression profiles were identified using two analysis methods. The first method was by one-way ANOVA analysis to obtain significant changes over the culture period using several groups of samples during the time course. The second method was comparing gene expression differences at each time point between two groups of data, namely the 5-L bioreactor and minibioreactor culture samples, by unequal variance *t*-tests. In addition, other statistical methods such as hierarchical clustering and SAM time-course analysis (data not shown) methods were also looked into to obtain differential gene expression.

Quantitative RT-PCR methodology

The protocol used for the quantitative polymerase chain reaction (qPCR) reaction is as follows. For a 20 μL reaction, 10 μL of SYBR PCR Master Mix (Qiagen, MD), 0.5 μL each of forward and reverse primers, and 8 μL of water along with 1 μL of target gene cDNA were loaded per well. cDNA preparation procedure can be found in an earlier publication.[19] Wells were sealed and spun down, and stored on ice for up to 30 min before loading on the Biorad ICycler IQ5. The qRT-PCR cycle parameters had a denaturation step at 94°C for 45 sec, annealing step at 56°C for 30 sec, and extension at 72°C for 20 sec, for 40 cycles. The final PCR product was ~100–150 bp, and 50 ng of cDNA was loaded for the β-actin control for the PCR analysis.

The specificity of the primers was tested on agarose gels to observe single bands of the PCR product. Also, the annealing temperature used was tested in the range of 56–58°C before obtaining an optimum for the assay.

The threshold cycle, C_t was measured for a fixed amount (2 μL) of cDNA for all sentinel gene transcripts and compared to the C_t value of the cDNA for the endogenous reference, β-actin. To ensure that the concentration of cDNA would fall in the linear range and also to reduce the C_t difference between the test gene and β-actin, the endogenous control, the amount of cDNA of the bioreactor test samples used was adjusted such that the threshold cycle number difference did not exceed $\pm$2 cycles. Compared with β-actin housekeeping gene, Sod1 and Txnrd1 genes were highly expressed, as measured from initial qRT-PCR assays. Hence, in the qPCR reaction, a five-fold diluted amount of cDNA was used for these two gene transcripts to bring down the threshold cycle difference between the endogenous control and test gene to $\pm$1. Apex1 gene was also highly expressed, and 2.5-fold diluted amount of cDNA was used. Cycs gene had a lower expression compared with β-actin, and twice the amount of cDNA as the endogenous control was used for the PCR reaction. This method helped with minimizing the threshold cycle difference between the test gene and endogenous control, thus subtle changes in gene expression between the minibioreactor and bench-scale time-course gene expression could be accurately obtained. Based on our C_t measurements for the expression of the reference gene (β-actin), the mRNA was found to be stably and strongly expressed. This reference gene expression was measured across each of the culture samples for both the 5-L and the minibioreactor samples (data not shown).

In addition to the steps above, the following precautions were taken to ensure high-quality qRT-PCR data. As RNA integrity is a major factor in the qPCR analysis, its degradation was minimized by storage in -80°C freezer and paying attention to handling and storage in small aliquots. High degree of pipetting accuracy was realized as absolutely essential for high-quality qPCR data. Also, utmost care was taken to avoid dust during qPCR experimentation.

Both Nanodrop 1000 and Bioanalyzer nanogels were used to confirm RNA quality as previously described.[19] In addition, RNA samples were adequately diluted before quantitation for samples at higher concentrations (>2000 ng/μL). For very low concentrations of RNA, an alternate fluorescence-based detection method such as Qubit Fluorometer from Invitrogen would be a better choice than Nanodrop, although in our case the very low concentration samples were omitted from further processing.

PCR data analysis

For data normalization, β-actin,[20] GAPDH,[21,22] or other housekeeping genes (HKG) are routinely used. An endogenous control is a transcript that is present at a constant amount in total RNA, whose levels are a means of normalizing differences in the amount of total RNA loaded in each reaction. In this case, we have used mouse β-actin that is inherent to cell cytoskeleton as the housekeeping gene. Culture samples with viability of >80% were used with this endogenous control. The constant expression of this gene was verified by measuring its threshold cycle time, C_t, using the three biological replicate samples, along with three technical replicates at each biological replicate, at all time points in culture. An average of the technical replicates at each of the biological replicate point was taken, followed by group statistics using the three biological replicates data, and finally taking an average at each time point. For the three test systems under consideration, namely the 5-L control, the initial minibioreactor, and the improved minibioreactor, the average C_t values at each time point were obtained using the same method as described above for β-actin. As a next step, the ΔC_t is calculated for each C_t value by using the following equations.

$$\Delta C_t = C_t(\text{Test Gene}) - C_t(\beta - \text{actin})$$

$$\text{Expression Ratio of the gene of interest to the endogenos control}, \beta - \text{actin} = 2^{-\Delta C_t}$$

An average of three biological replicates data along with standard deviation as the *Y* error bars was plotted for test systems. Statistical significance of the differential gene expression results was inferred using *p*-values for transcriptomic expression data obtained in culture. In this case, *p*-values were obtained for the one-way ANOVA and *t*-test analysis of the replicates data at each time point.

Table 1. Calculated Scale-Down Parameters, Height to Diameter Ratio, Impeller to Vessel Diameter Ratio, Tip Speed, Reynolds Number, Mass-Transfer Coefficient, and Mixing Time for 5-L Bioreactor and Minibioreactor

Reactor Type	Impeller Type	$D_{impeller}/D_{vessel}$	H/T (Liquid Height/ Vessel Diameter	Reynolds Number	Impeller Tip Speed (m/s)	k_L a (h^{-1})	OTR mmol $O_2 mL^{-1}h^{-1}$	t_{mixing} (s)
5L	45° pitched blade −2	0.45	1.4	1.89E+04	2.64E-01	2	4.28×10^{-4}	4
Initial MBR	Flat paddles −2	0.67	2.2	8.08E+02	4.50E-02	9.8	4.4×10^{-4}	10
Improved MBR	45° pitched blade −3	0.5	2.2	6.18E+02	4.76E-02	2	4.28×10^{-4}	4

High-throughput minibioreactors

Minibioreactor Vessel Setup. The minibioreactors closely resemble a typical bench-top bioreactor with overhead motor-driven impellers. The minibioreactor tristation module consists of a stainless steel head plate assembly and a glass reactor vessel, to the bottom of which the DO and pH sensing patches are affixed.[23] Each sensor is a patch with three layers: a responsive layer, a backing layer that helps reduce interference from the media in the fluorescence reading, and an adhesive layer.

The calibration of the DO and pH patches has been described previously.[24] Although the DO and pH sensor patches need not be calibrated each time before use, a simple 30-sec measurement of the electronic offsets used for calculating calibration constants was recommended approximately once a month. It also has the capability for CO_2 sensing using optical sensors. Each tristation module is $\sim 6.5'' W \times 9.5'' H \times 9.5'' D$. Head plate assembly sealing is ensured by the use of an O-ring and spring seals separated by a close-tolerance Teflon spacer. Vacuum grease was added around the impeller shaft and opening in the head plate to further help seal the connection. Each reactor has a total volume of about 40 mL, with a working volume of 10–30 mL. Four 0.22-μm vent filters (Sartorius, Germany) are attached to the gas in and outlet ports. Post-assembly, water was added to each vessel, and they were steam sterilized at 121°C for 30 min. As a method to avoid filter wetting, an external 30-mL outgas vessel with water at room temperature equipped with an overhead filter served as a condenser. This method not only ensured sterility but also served as a visual indicator of gas flows, where the entry of gases into the minibioreactor could also be verified by the bubbling taking place in the external vessel. Evaporation at this scale was minimal, and no compensation was made.

Impeller and sparger setup in minibioreactors

Initial Setup. The initial minibioreactors using Teflon paddle impellers resulted in radial mixing. The Teflon paddles had a $D_{impeller}/D_{vessel}$ ratio of 0.67 and were placed at 0.25 $D_{impeller}$ from the bottom of the shaft, and the distance between the two impellers was 0.9 $D_{impeller}$. The reactors also had the ability for gas sparging directly into the culture media through a 316 stainless tube sparger 1/16″ diameter placed closer to the vessel wall.

Improved Setup. The improved minibioreactors used three 316 stainless, 45° pitched-blade, upward pumping impellers (Mound Manufacturing, Dayton, OH), and distance between the impellers was 0.9 $D_{impeller}$. The impellers and spargers were custom manufactured by laser welding for precision and finish. The $D_{impeller}/D_{vessel}$ ratio was 0.45, similar to the 5-L bioreactor (Table 1). A 316 stainless L-sparger with the outside diameter of 0.095″ was used. Three 100–200 μm holes, 3 mm apart were drilled on a flattened horizontal section (thickness was reduced to 0.005″) of the cylindrical wall of the L-sparger, facing the impeller. The sparger had a removable threaded plug at the end submerged in liquid for cleanability of the sparger element. The sparger holes were positioned directly under the impeller in the improved minibioreactor design.

Initial minibioreactor aeration

A major challenge in the minibioreactor operation was to obtain a stable % DO and pH control in the 35 mL working volume. As three gases, air, CO_2, and nitrogen, were used for controlling both the DO (% DO) and pH in the initial setup, the gas distribution (sparge or overlay) along with proportional-intergral-derivative control (PID) loop tuning was crucial for the success of the feedback control. Choice of sparged gases into the liquid media, versus overlay gases, for example, CO_2 and nitrogen, in the vessel head space and air in sparge generally improved the stability of pH and % DO set points within ±5% variation. For example, % DO overshoot during the early lag and late-stationary phase with lower oxygen demand was observed when nitrogen was used in sparge and an oscillatory % DO response was observed. To overcome these problems, aeration in the minibioreactors consisted of sparging air alone, while having CO_2 and N_2 gases in the head-space overlay. Needle valves were metered using a single low-flow rotameter operating in the range of 0.1–30 mL/min to set gas flow rates to both the sparger and head space. Maximum allowable sparge rate into the minibioreactor vessel without flooding is 30 mL/min. Sparge rate for air was 10–15 mL/min and an overlay at 6 mL/min for CO_2 and 15 mL/min for N_2 gas. A summary of the vessel geometry and physical parameters is included in the Supporting Information.

Improved minibioreactor aeration

A similar aeration strategy as the initial setup was used, except that pure oxygen was used in a cascade mode, along with air and nitrogen, for % DO control. The improved minibioreactor mostly eliminated the need for nitrogen using precise loop tuning, where nitrogen was used only at the tail end of culture to overcome DO overshoot. A future design with mass-flow meters would lead to a more precise gas metering and control. An L-shaped pipe sparger with 100–150 μm holes was placed with flow under the impeller. PID loop tuning was done for sparging pure oxygen at 5 mL/min, along with adjusting the sampling interval between 15 and 60 sec, to allow for sufficient controller response time.

Minibioreactor control

In comparison to its predecessor, the HTBR system,[24,25] this minibioreactor system had the advantage of PID feedback control. Independent control for temperature, pH, % DO, agitation, and nutrient addition could be achieved in each of the minibioreactors within the tristation unit. The minibioreactor control system consisted of proprietary software and a USB interface module with DAQ and digital IO

cards. Peltier devices were used for temperature control, with heating range up to 40°C. The pH control was could be achieved either by CO_2 addition (used for this study) or by acid/base (by precision miniature peristaltic pumps mounted on the tristation) control, and the patch responsive range is 5.5–8.5 pH units. Agitation control was achieved by a DC stepping motor, which drives the reactor shaft with a range of 10–1000 rpm.

Scale-down to minibioreactors

Initial Scale-Down. The initial scale-down was based on similar OTR[26–28] to ensure that both the 5 L (Braun B, Melsungen, Germany) and minibioreactor would have similar rate of change of % DO concentration to reach the set point. Two different gases, air in the minibioreactor cultures and pure oxygen in the 5-L cultures, were used for % DO control. The reason for using different gases was that air sparge with paddle mixing was sufficient to maintain 30% DO set point in the minibioreactors. However, pure oxygen sparge was necessary in the 5 L to maintain the DO set point. In general, this need for using pure oxygen for DO control would be especially true as the scale increases from milliliter to liter scale. Hence, k_La could not be matched as air was used for k_La measurements in both the 5 L and minibioreactor. The OTR, which is a product of the DO concentration gradient in the liquid phase and the mass-transfer coefficient, was matched instead. The OTR was obtained by

$$\frac{dC_L}{dt} = k_La\left(C_L^* - C_L\right).$$

For initial scale-down, the 5-L operating conditions were preset at 220 rpm, 50 mL/min sparge, 150 mL/min overlay, and k_La was measured to be 2 h^{-1} and OTR was 4.28×10^{-4} mmol O_2/mL/h. The dynamic gassing out method[29] was used with nitrogen/air to measure k_La and obtained as the slope of $\ln(1 - C/C^*)$ versus time, with 30% DO as a cutoff for slope determination to ensure linear range of probe response. In case of head-space aeration, the response was delayed by time taken to replace nitrogen in the gas lines. The OTR was calculated using the maximum solubility of oxygen in liquid phase C_L^* of 2.14×10^{-4} mmol O_2/mL at 37°C temperature and atmospheric pressure, and percent saturation value being 100% for air and 476% when using pure oxygen.

The minibioreactor operating conditions for rpm and air flow rate were determined by matching OTR in the two systems.

$$\mathrm{OTR} = k_La_{5L}(C^*_{\mathrm{oxygen}} - C_L) = k_La_{(\mathrm{MBR})}(C^*_{\mathrm{air}} - C_L).$$

By matching OTR and using known $k_La_{(5\ L)}$, theoretical C^* for oxygen and air, the unknown $k_La_{(\mathrm{MBR})}$ was obtained. Using this value, the unknown rpm and air-sparge rate in the minibioreactor were set for scale-down runs.

Scale-Down After Improvements to Minibioreactor Mixing and Aeration. In the improved minibioreactor, oxygen was used for % DO control as in the 5 L, giving the same C^*; hence, k_La was matched as the scale-down parameter (Table 1) in this case. This k_La in the minibioreactor was used to obtain the operating conditions rpm and air-sparge rates. In addition, mixing characteristics were also compared before and after improvements to the minibioreactor. Contrary to the supposition that the paddle impellers (in the initial minibioreactor design) were adequate at the 35-mL scale for uniform mixing, fluorescein dye mixing studies[30] found stratification in tracer distribution at the minibioreactor operating speed of 150 rpm (based on matching OTR) before achieving complete mixing. Using the mixing model obtained from tracer studies, mixing time was compared between the minibioreactor and the 5 L (Supporting Information). Although rpm could be increased to overcome stratification paddle, it was found to be detrimental to cell growth (data not shown) and hence was not adopted. Thus, even at this 35-mL miniature scale radial mixing by paddles was clearly insufficient, and the need was seen for axial mixing. Following the design change to the axial impellers in the minibioreactor, mixing characteristics could be better matched with the 5-L bioreactor.

Scale-down comparability study protocol

The bioreactor systems chosen for this scale-down comparison study were the (1) novel minibioreactor tristation equipped with noninvasive optical sensors along with ability to control % DO, pH, and temperature and (2) model 5-L bench-top stirred-tank bioreactor with similar control capability. For identifying sentinel gene markers using microarray comparison of the initial scale-down, we performed stringent biological replicates. To achieve this, three independent vial thaws, followed by seed-scale-up and bioreactor runs that were separated by a few weeks at a time, were carried out to increase the randomness of the replicate samples. In the experiments reported here, to reduce discrepancy in the inoculation density as well as the inoculum culture between the 5-L model bioreactor and minibioreactor test system, the 5 L was first inoculated at $2.0 \pm 0.5 \times 10^5$ cells per milliliter. The culture was allowed to mix well for up to 30 min in the 5-L bioreactor, following which culture was transferred in a sterile manner to minibioreactors. A continuous air overlay at 0.03 VVM to the head space was maintained for positive pressure and to drive out any accumulated gases such as CO_2 and nitrogen. For sterile sampling of the minibioreactors, the rubber septum was sterilized with 70% ethanol before the sample was withdrawn. Samples were taken twice daily (0.5 mL/day) with a 19-gauge $1\frac{1}{2}''$ sterile needle. The sample was used for measuring cell count and viability using a hemocytometer with trypan blue dye, ELISA for IgG3 titer, glucose and lactate concentration by YSI 2700, and cell pellet for RNA extraction. In addition, for analysis by microarrays and quantitative RT-PCR, five groups of samples were taken from the initial minibioreactor (initial MBR) along with four groups of samples from the 5-L control bioreactor, with a final viability cutoff of $\geq$80% to ensure RNA quality. Additional sampling was required for the minibioreactor, which stayed viable for a longer period. Samples were taken at the same time points, except at the end of culture, where the final sample collected for the 5 L had to end at day 3 pm as the viability dropped rapidly toward the end of run. Although for time-based transcriptomic data, processing more samples would be desirable, the higher cost of the assays led to minimizing the number of samples taken. For RNA extraction, cell pellets of a minimum of 3×10^6 total cells were collected.

Tracer mixing study in minibioreactors and 5 L

Mixing characteristics such as uniform mixing versus stratification were measured for both the initial paddle impellers and the improved pitched-blade impellers using a dye-

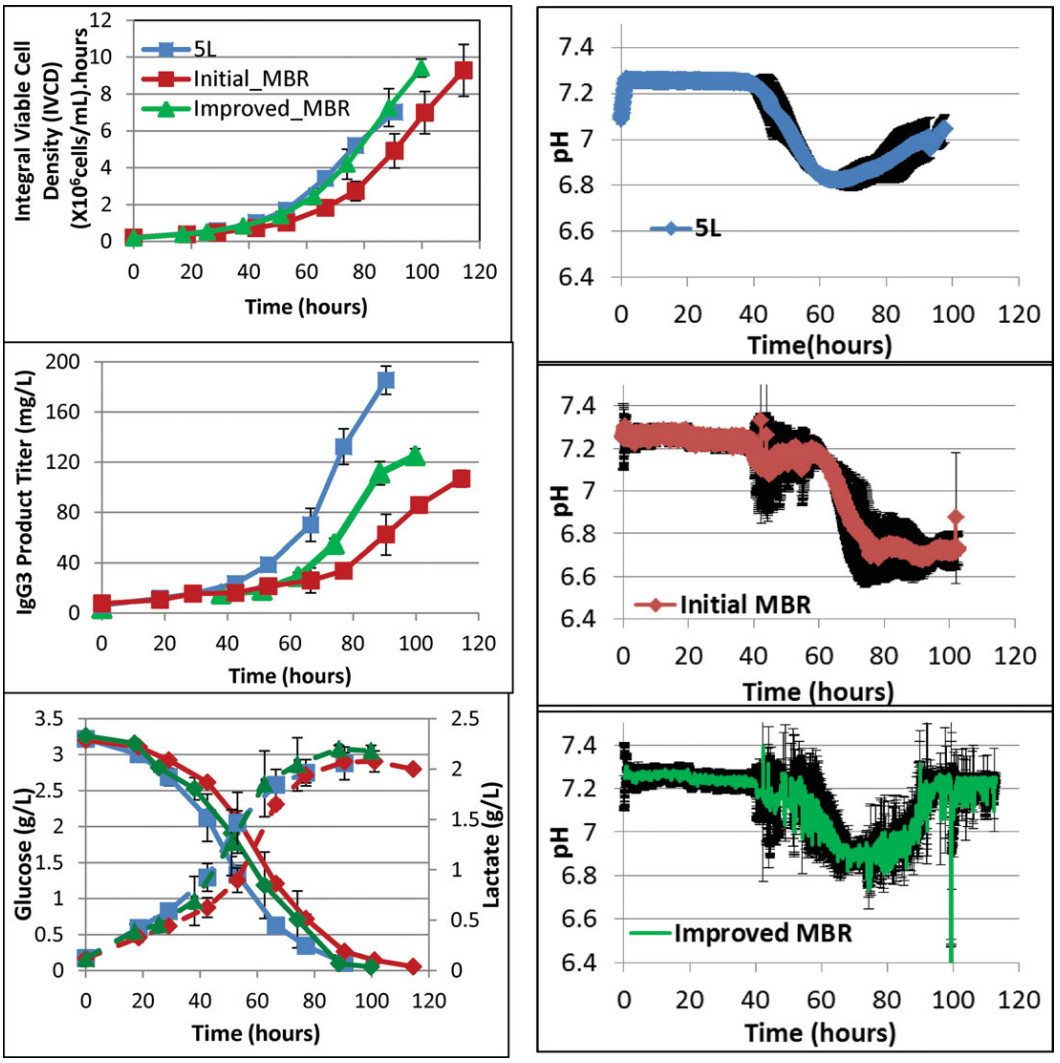

Figure 2. Comparison of cell culture growth and product parameters such as IVCD, IgG3 product titer, and culture pH of the 5-L bioreactor (blue) and scale-down to initial minibioreactor (red) and improved minibioreactor (green).

Average of three biological replicate scale-down studies is plotted here along with their standard deviation for the *Y* error bars.

based method (data in Supporting Information). A tracer-mixing study was conducted using a visual method (Sony Handycam HDR-CX130) with fluorescein sodium salt. Uniformity of mixing was determined by comparing four 50 × 50 pixel squares in regions above and below the impellers using RGB saturation uniformity in Image J software. Mixing models that correlated mixing time (θ_M) to the various *H*/*T* ratios and impeller Reynolds number[30] (*Re*) in the minibioreactors and the 5-L bioreactor were used to obtain θ_M at the operating *Re*, and hence the rpm in each case. This was done for both the initial minibioreactors with paddle impellers and the improved minibioreactors with pitched impellers.

Results

Initial scale-down from 5-L bioreactor to 35-mL minibioreactor

Our efforts to develop a better scale-down strategy were spurred by a difficult scale-down from a bench-scale bioreactor to the very small volume prototype device at the milliliter scale developed in our laboratory (Figure 1). In spite of the inherent differences in the vessel geometrical ratios (Table 1) between the 5-L bioreactor and the novel minibioreactor, our initial hypothesis as that scale-down based on matching a physical parameter such as the OTR could ensure comparable growth.

In this case, our initial scale-down based on similar OTR resulted in differences in both cell growth and product profiles between the two systems (Figure 2). This was mainly evidenced by a ~24 h initial growth lag, along with a more subtle, but subsequent slower growth in the exponential phase (day 3) in the initial minibioreactors compared with 5 L. In addition, there was increased longevity of 30 h in the minibioreactor cultures compared with the 5-L control bioreactors.

These growth differences were reflected in product accumulation, where the maximum IgG3 expression was in the later part or stationary phase of batch culture for the 5-L system, in contrast to the initial minibioreactors where the product accumulation tapered off at 50% lower value. Other commonly measured parameters did not explain the differences. The % DO profiles (data in Supporting Information) reflected the cell growth during the early log phase until the 30% DO set point was reached, followed by control at the

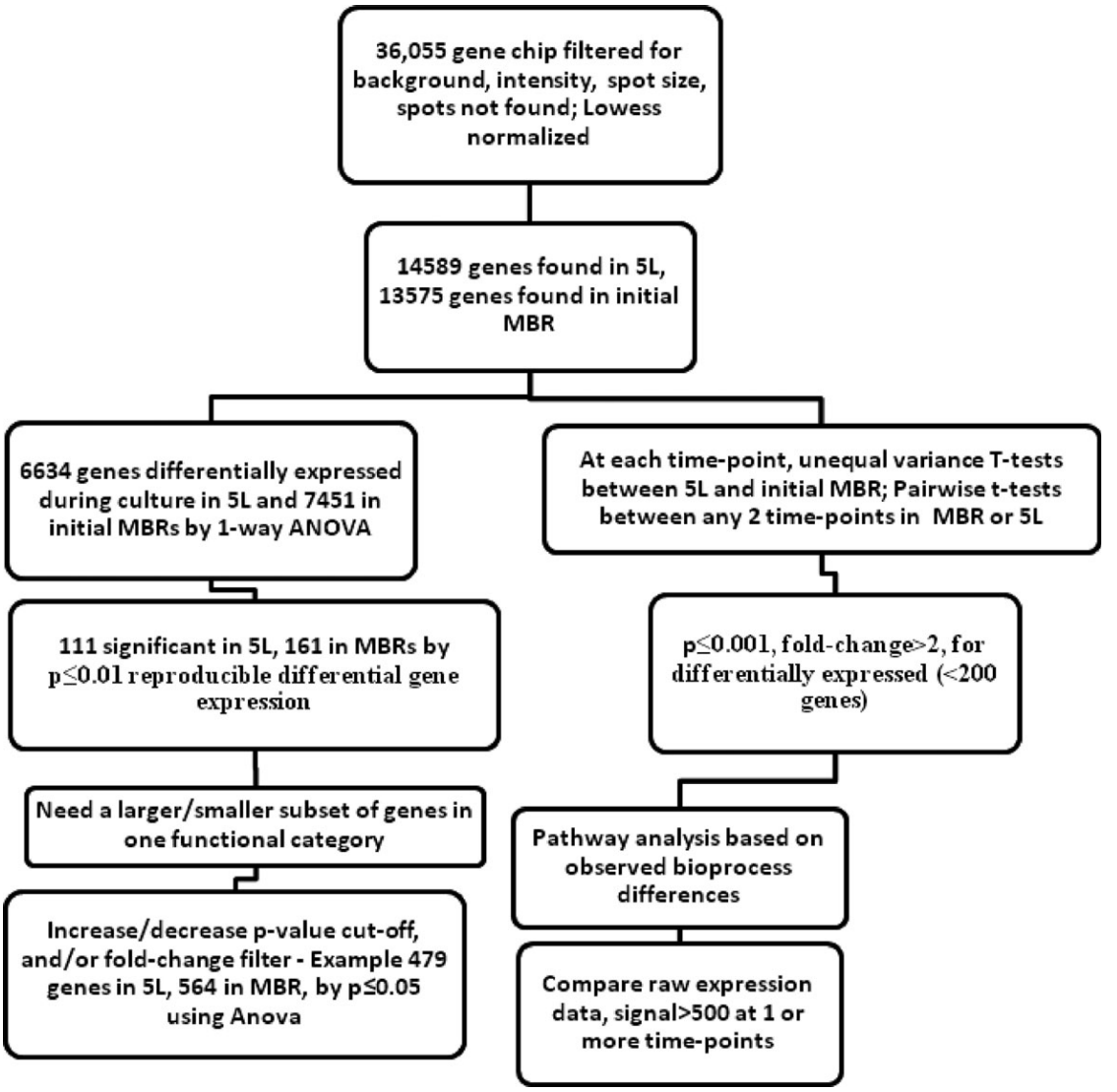

Figure 3. Genomic approach of identifying sentinel genes combining microarray statistical analysis in conjunction with pathway analysis.

set point until termination of culture. There were no noticeable significant differences in glucose and lactate concentration profiles between the two bioreactor systems, aside from possible lactate consumption in the minibioreactors as evidenced by a slight decrease in lactate concentration toward the end of culture. Although the terminal pH of the initial minibioreactor cultures was lower compared with that in 5 L, it could be explained by CO_2 compensation. The strategy of intermittent nitrogen overlay used to overcome an undesirable % DO overshoot, especially in the later part of the culture to maintain a fixed % DO set point in the 35-mL minibioreactor, seemed to have resulted in CO_2 stripping and subsequent CO_2 compensation to maintain the pH set point.

Identifying sentinel genes depicting cellular response to initial scale-down

To analyze this insufficient scale-down using a more cell physiology-driven approach, we set out to identify sentinel genes following the strategy shown in Figure 3. The hypothesis was that knowledge of differential gene expression patterns would enhance the understanding of the effect of bioreactor environment on cell cultures. Post the initial scale-down described above, microarray gene expression analysis was done as depicted by the flow sheet. Applying background filters and Lowess normalization to the 36,055 gene chip results, 14,589 genes were found to be expressed in the 5 L and 13,575 genes in the minibioreactor. Applying one-way ANOVA, 6634 genes were found to be differentially expressed across the culture time points in the 5 L and 7451 in the minibioreactor. The idea then was to use *p*-value statistics to obtain a smaller manageable subset (<200) of differentially expressed gene transcripts. To obtain a suitable number of gene transcripts, we typically set the stringency of the *p*-value filter to 0.01 or lower and fold-change filters to 2 or higher to obtain 111 differentially expressed genes in the 5 L and 161 genes in the minibioreactor. In addition, the two bioreactor systems were compared using unequal variance *t*-tests at each culture phase, with a *p*-value cutoff of $\leq$0.001 to obtain <50 genes at each time point. These gene sets from both 1-way ANOVA and t-tests were then winnowed to <20 genes as markers or "sentinel genes" based on their functional

Table 2. Biochemical Functional Pathways Relevant to Process-Related Differences Observed for Initial Scale-Down from the 5-L Bioreactor to the Minibioreactors

Gene Ontology and Functional Pathway Categories used for Sentinel Gene Identification	
Steeper viability drop in 5L system versus initial minibioreactor	Apoptosis positive regulation Apoptosis protection/prevention DNA damage/response, DNA binding Oxidative stress
Growth lag in initial MBRs-differences in cell metabolism, insufficient mixing, possible CO_2 differences	Cellular metabolism regulation Negative regulation of metabolic process TCA cycle Amino acid metabolism Transcription regulation
Larger bubbles, lesser bubble-residence time, resulting in almost continuous sparging during peak exponential growth in initial MBRs	Free-radical damage, Response to stimulus, stress Cellular cytoskeleton organization, actin polymerization Membrane part, integral to membrane Structural constituent of ribosome
Lower product titer in initial MBRs	Intracellular protein transport Protein folding, binding, glycosylation
Pathways not included for this scale-down comparison	Signal transduction, receptor signaling Cell activation Enzyme regulator activity

Table 3. List of 18 Sentinel Genes Using Microarray Statistical Analysis from 5-L Bioreactor and Minibioreactor

Gene Name (Entrez ID)	Gene Description	Gene Ontology	Primer Sequence
Hspa9 (15526)	Heat shock 70 kDa protein 9	Stress response, protein folding, protein export from nucleus	FW: TGTCAAGGAGTTCAAGAGA BW: ATGGTAAGGTATGGCAAGT
Sod1 (20655)	Superoxide dismutase 1	Response to superoxide, free-radical-induced apoptosis pathway (BioCarta)	FW: GAACCAGTTGTGTTGTCA BW: CAGCCTTGTGTATTGTCC
Arpc3 (56378)	Actin-related protein complex 3	Control of actin polymerization in cells, protein binding	FW: GGCATACCACTCTTCTCT BW: CTGTCCGCTTCATTCTTAA
Atpif1 (11983)	ATPase inhibitory factor 1	ATPase inhibitor activity	FW: TCGGATAGCATGGATACG BW: TGGTGGTCAATCTCATCTT
CD74 (16149)	Major histocompatibility complex	MHC class II protein binding, protein assembly, intracellular protein transport	FW: CGACCTCATCTCTAACCAT BW: TACAGGAAGTAAGCAGTGG
Cycs (13063)	Cytochrome c, somatic	Apoptosis, activation of caspase activity	FW: GGAGGCAAGCATAAGACT BW: TTGTTGGCATCTGTGTAAG
Txnrd1 (50493)	Thioredoxin reductase 1	Reduces thioredoxins, protection against oxidative stress	FW: GATGAAGAGCAGACCAATG BW: CACAACAGCCATATTCCAA
B4Galnt4 (330671)	Beta-1,4-*N*-acetyl-galactosaminyl transferase 4	GalNAc transferase activity	FW: TTGAGCCTGGAGAATGTT BW: GGTAGAAGCACTTGTTGTC
Apex1 (11792)	Apurinic/apyrimidinic endonuclease 1	Damaged DNA binding, positive regulation of DNA repair, cellular response to hydrogen peroxide, oxidoreductase activity	FW: CCAGAGACCAAGAAGAGTAA BW: CCACATTCCAGGAGCATA
PigP (56176)	Phosphatidylinositol glycan anchor biosynthesis, class P (Pigp)	Glycosylphosphatidylinositol (GPI)-anchor biosynthesis	FW: TCCTTATCACAGTTGTAATTGG BW: GGCATCCTCTTGGTAGTT
Ddost (13200)	Dolichyl-di-phosphooligosaccharide-protein glycotransferase	Protein amino acid N-linked glycosylation via asparagine	FW: GACCACCACAACTATGATG BW: CTTCAGCAGGTTCTCAGT
Galnt14 (71685)	UDP-*N*-acetyl-alpha-D-Galactosamine: polypeptide *N*-acetylgalactosaminyltransferase 14	Catalysis of the reaction: UDP-*N*-acetyl-D-galactosamine + polypeptide = UDP + *N*-acetyl-D-galactosaminyl-polypeptide	FW: GTGGTTCTTGCTCTATGC BW: CGCAATCCATATCCTGAAC
Pdhb (68263)	Pyruvate dehydrogenase (lipoamide) beta (Pdhb)	Pyruvate metabolism, acetyl CoA biosynthesis from pyruvate, TCA cycle, glycolysis/gluconeogenesis	FW: AATACGGTGACAAGAGGAT BW: TAGGTGAGATGATTATACA
Cs (12974)	Citrate synthase	Shuttle for transfer of acetyl groups from mitochondria to the cytosol (Biocarta), TCA cycle, glyoxylate and dicarboxylate metabolism (KEGG)	FW: AATCAGGAGGTGCTTGTC BW: GGTAGAAGCACTTGTTGTC
Rpl19 (19921)	Ribosomal protein L19	Translation, translational elongation	FW: CCTGTGACTGTCCATTCC BW: TCCTCATCCTTCTCATCCA
Odc1 (18263)	Ornithine decarboxylase 1	Arginine and proline metabolism (IPA), positive regulation of cell proliferation	FW: ATAAGGATGCGTTCTATGTTG BW: CTCACTATGGCTCTGCTAT
Ssrp1 (20833)	Structure-specific recognition protein 1	DNA replication, DNA repair, regulation of transcription	FW: TATGACGATTATGCTGACTCT BW: TCTGCCACATCTTCTTCTT
Sumo2 (170930)	SMT3 suppressor of mif	Small ubiquitin-related protein 1 conjugation, SUMO ligase activity	FW: AGAGGCATACACCACTTAG BW: TGTCTGTTTCGTTGATTGG
ACTB (11461)	Actin, beta	Highly conserved proteins that are involved in cell motility, structure, and integrity	Qiagen

(a)

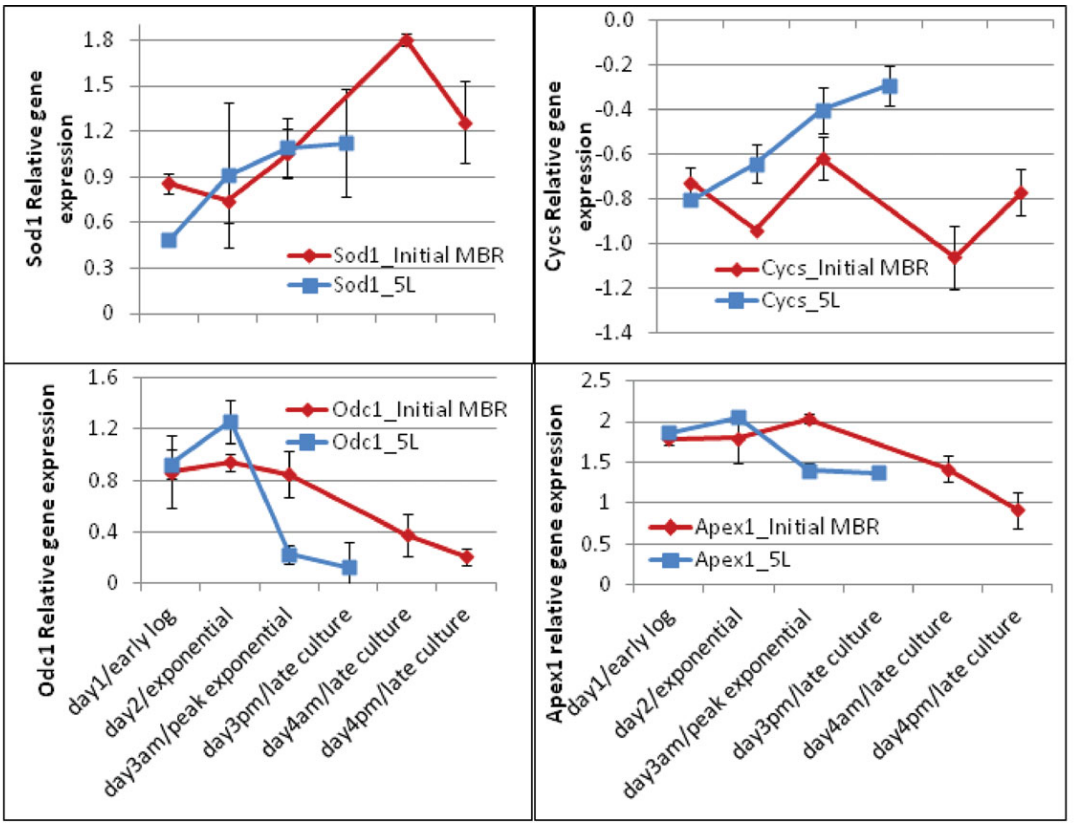

(b)

Culture Time-point	Day 1/early exponential	Day 2 / exponential	Day 3am/ peak exponential	Day 3pm /late exponential	Day 4pm /late culture
Time (h)	18-20	42-44	66-68	90-92	101-103

Figure 4. Microarray results for the gene expression profile comparison of the 5-L bioreactor (blue) with the initial minibioreactor (red) postinitial scale-down.

The relative gene expression is the log ratio of the sample to the universal mouse reference at each time point. Here, each point represents the mean of three biological replicates and error bars are 1 standard deviation from the mean. Log expression ratios of gene transcripts from the time-course culture samples were labeled using Hyper5 dye for the samples and Cy3 dye for the mouse reference. Profiles of free-radical damage repair gene Sod1, DNA damage repair gene Apex1, apoptosis-related gene Cycs, as well as arginine and proline metabolism gene Odc1 are shown. (b) The culture time points at which genomic data were collected are shown in hours.

relevance to cell culture and their fold change from expression patterns.

Additionally, the gene expression of these chosen genes was verified from raw data to ensure a strong signal for at least one or more time points in culture to increase their chance of being detected by a more specific PCR assay, compared with a broad screen microarray analysis. Importantly, the bioreactor observations were correlated to likely cellular functions[31–34] (Table 2), which is a key to choosing relevant process-specific sentinel genes (Table 3). Specifically, transcriptional changes belonging to relevant cellular functions such as apoptosis, oxidative stress, free-radical damage, glycosylation, aerobic respiration, and metabolism in a bioreactor environment were identified by gene ontology and pathway analysis of the significant genes.

It should be noted that while using microarrays for measuring transcriptomic changes between the 5-L and initial scale-down MBR batches, it is not unusual to have lower fold changes for differential gene expression during culture time course,[35] because the system was not stressed particularly by a specific additive or a notable process change.

Examples of microarray time-course profiles comparing the 5-L bioreactor with the minibioreactor after initial scale-down are shown in Figure 4. The microarray profiles of the other sentinel genes have also been plotted for comparison.[36] Close attention was paid to either upregulation or downregulation of gene transcripts at one or more time points during culture and further confirmed by qRT-PCR analysis. These changes were then compared to the discrepancies found in culture growth and product titer between the two systems. This exercise identified genes such as Sod1, Apex1, and Cycs as sentinel genes. From qRT-PCR results (Figure 5), upregulation of damage protection genes, such as Sod1, free-radical protection in later part of culture, and Apex1, apoptosis protection gene during late exponential phase, was found in the initial minibioreactors, but not in the 5-L culture. Also, apoptosis gene, Cycs gene, was upregulated in the 5-L bioreactor (Figure 6) toward the later part of the culture, but was mostly invariant in the minibioreactor. Fold-changes of gene expression from qRT-PCR analysis between the minibioreactor and 5 L were obtained during the time-course (Table 4).

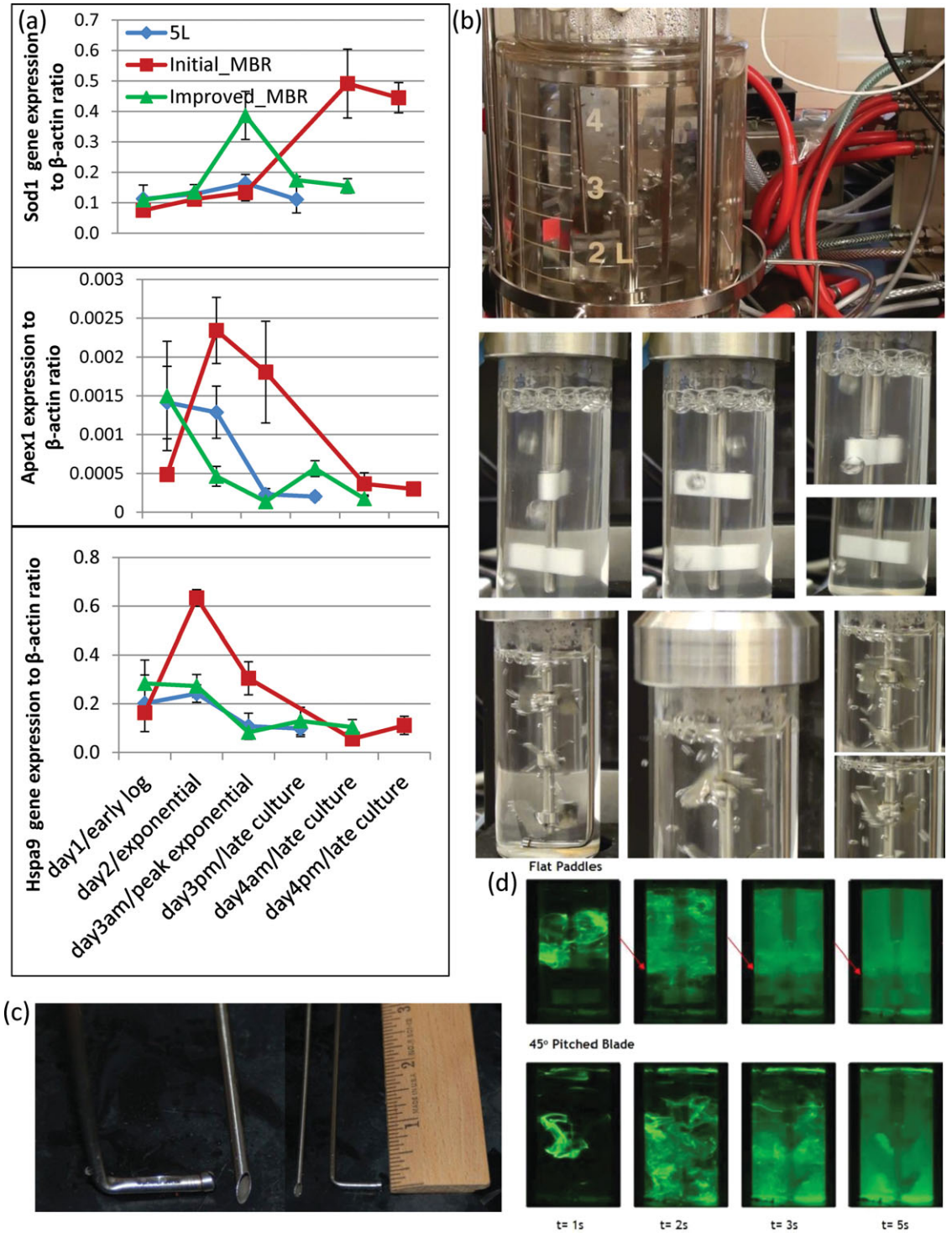

Figure 5. **(a) Cell culture process implications of Sod1, Apex1, and Hspa9 relative gene expression profiles with respect to *β*-actin endogenous gene expression by qRT-PCR are shown for the 5-L, initial minibioreactor, and improved minibioreactor cultures.The points on the qRT-PCR profiles are an average of three biological replicates, each with three technical replicates, and the *Y* error bars are 1 standard deviation from mean. Note better agreement (convergence) between blue and green lines versus red. (b) Gas-dispersion images on the right (top to bottom) show the three systems under consideration, at their respective operating conditions for impeller speed and sparge rate—(i) 5-L control system with pitched impellers and a ring sparger, (ii) initial minibioreactor with paddle impeller and open-tube sparger, and (iii) improved minibioreactor with pitched impellers and L-shaped, drilled-pipe sparger. (c) Images of the 316 stainless sparge pipes used in the minibioreactors. (d) The images of tracer mixing study in the minibioreactors using the 45° pitched impellers clearly show better mixing and elimination of segregation or poorly mixed areas as observed from using paddle impellers.**

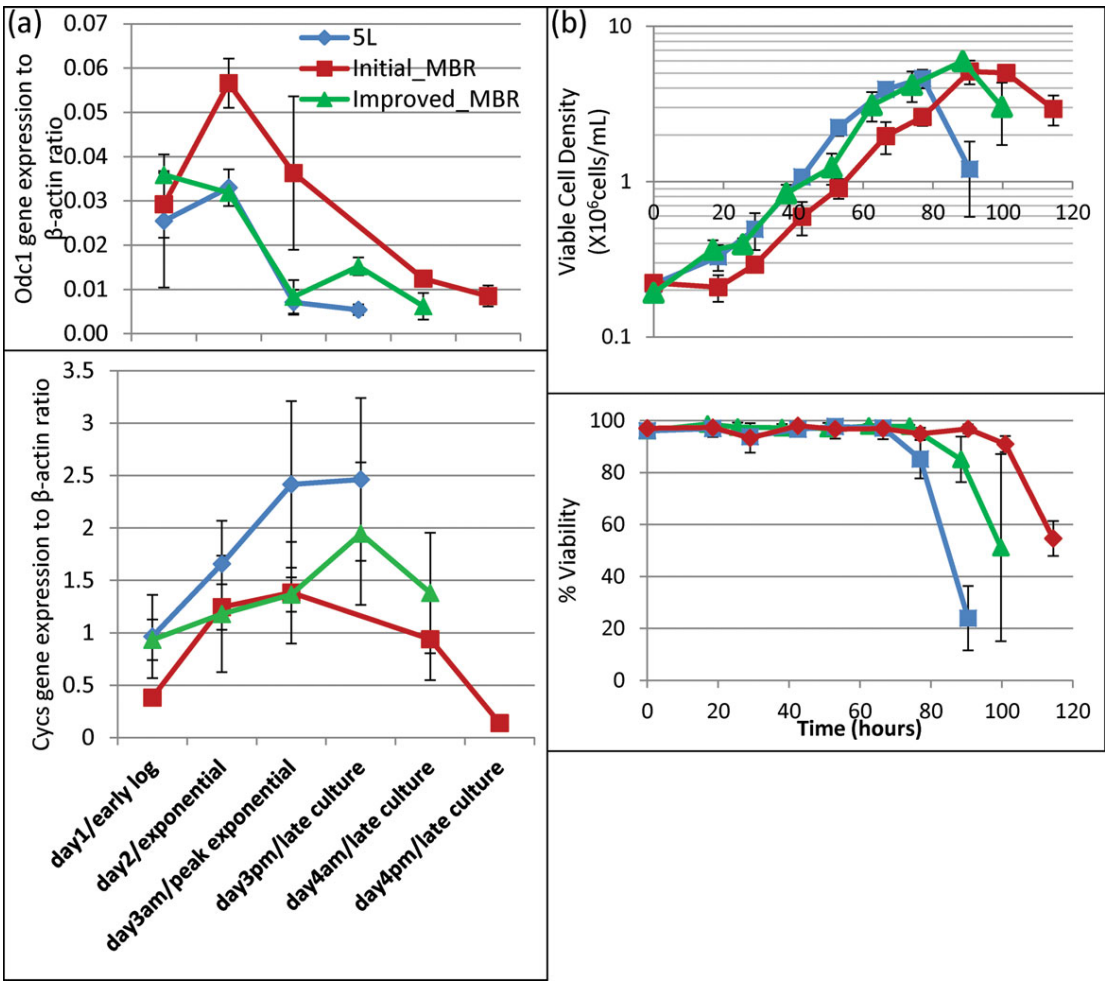

Figure 6. **(a) qRT-PCR results of Cycs and Odc1 relative gene expression profiles with respect to *β*-actin are shown for the 5-L (blue), initial minibioreactor (red), and improved minibioreactor (green). The points are an average of three biological replicates, each with three technical replicates, and the *Y* error bars are 1 standard deviation from mean. (b) Comparison plots of viable cell density and % viability to describe process implications of these gene findings.**

Table 4. Fold Changes and *p*-Values from qRT-PCR, comparing the 5-L Bioreactor and Minibioreactor Cultures

Gene Name	Fold-Change of Initial MBR with Respect to 5L Control	Gene Regulation	Culture Time-Point	*p*-Value
Sod1	3.0	Upregulated	Late culture/day 4am	0.018
Apex1	8.2	Upregulated	Peak exponential/day 3am	0.003
Hspa9	2.3	Upregulated	Exponential/day 2am	0.0000217
Cycs	1.8	Down-regulated	Peak exponential/day 3am	0.1
Odc1	4.8	Upregulated	Peak exponential/day 3am	0.02
Pdhb	3.3	Down-regulated	Late culture/day 3pm	0.1

Although some of the *p*-values for the comparison were above 0.05, they were still included as significant differences as they could be biologically relevant. In general, genes with lower expression intensity had higher variability in fold change.

Improved minibioreactor scale-down for driving toward culture comparability with the control 5-L system

For improved understanding at the cellular level, expression differences of the identified sentinel genes were correlated to specific bioreactor process differences. Based on such correlations, corresponding process differences were addressed by modifications made to the minibioreactor for improving scale-down. For example, at the transcriptomic level, upregulation of DNA damage protection gene Sod1 in the later culture stage occurred in the initial minibioreactors (Figure 5). We hypothesized that these could be attributed to higher bubble-induced damage using the existing tube sparger and insufficient mixing. The growth lag could also be attributed to insufficient mixing. To address these issues, minibioreactor impeller and sparger design as well as DO control modifications were made to obtain an "improved' minibioreactor (improved MBR). Upon comparing cell growth profiles of improved minibioreactor with 5-L bioreactor, the growth lag that was previously observed in the initial minibioreactor scale-down was eliminated (viable cell semi-log plot in Figure 6). The improved minibioreactor culture profiles were closer to those of the 5-L bioreactor culture, compared with initial minibioreactor scale-down, with a variation of ±25% for peak cell density and integral viable cell

density (IVCD) and within ±30% for IgG3 titer. Variation of ±20% has been reported by other researchers[37,38] while comparing 24-well high-throughput shaken reactors to bench scale using a CHO cell line. Closer alignment was seen in the pH profiles of the improved scale-down minibioreactors displaying a similar profile as that of the 5-L bioreactor, with the pH increasing toward the end of culture, and remained in range compatible with cell growth and survival due to pH control.

Sentinel gene expression profiles comparison between the 5-L control bioreactor, the initial minibioreactor, and improved minibioreactor cultures

As a next step, we set out to verify if the sentinel genes identified would also be predictive of the improved scale-down using the modified minibioreactor. Mainly, if there would be similar improvement in the transcriptomic profiles such that they would be convergent with those of the 5 L when compared with the initial scale-down. Figure 5 captures the likely cell culture effects we propose for the upregulation of Sod1, Apex1, and Hspa9 genes in our initial minibioreactor system compared with those in the 5-L bioreactor. The qRT-PCR results of Sod1, Apex1, and Hspa9 indicate that the initial minibioreactor profiles clearly deviated from the 5-L control, thus supporting the observation of insufficient scale-down and their roles as sentinel genes to predict this. Especially, the free-radical damage protection gene Sod1 was upregulated from day 3 pm to day 4 am, concomitant with increased aeration requirements for DO control at peak exponential cell growth in the initial minibioreactors. Importantly, we observed that in the initial minibioreactor, which used air sparging for % DO control, there was an almost-continuous sparging at peak cell growth.

Another factor in the initial minibioreactor runs that could have resulted in higher free-radical damage was the higher bubble surface-area per unit culture volume due to larger bubbles and lower bubble residence time from the open tube sparger (by visual images; Figure 5b). This effect was further intensified with increased bubbling during exponential phase. We attribute these phenomena to have possibly contributed to the upregulation of damage response genes such as Sod1 and upregulation of DNA damage protection gene Apex1 during the exponential growth phase in the initial minibioreactors. Also, higher heat-shock protein Hspa9 gene expression observed in the exponential phase of the initial minibioreactors that argues for a stress response of hybridoma cells to the nonconducive environment. Importantly, the improved scale-down upon optimizing the minibioreactor mixing and aeration parameters resulted in profiles of all these sentinel genes that were closer to those of the 5-L control compared with the initial scale-down profiles.

Figure 6 shows our proposed cell culture process inferences of Cycs, Odc1, and Pdhb gene expression changes between the two bioreactor systems. The upregulation of the apoptosis-related gene Cycs in 5-L bioreactor seems to correlate with the sharp decline in viability starting by day 3 pm/late-culture sample at ~80 h, along with decreased cell growth profiles, and observed higher cell debris at the end of 5-L culture. This is expected late in batch culture because of byproduct accumulation such as lactate, CO_2, and/or nutrient starvation. However, in the initial minibioreactor scale-down culture, this apoptosis gene had a lower expression ratio and was fairly unchanged during the course of culture, which also correlated with higher culture viability over the duration of the run, along with a more gradual drop in viability.

The higher Odc1, amino acid metabolism gene expression in initial MBR runs, argues for a higher usage of alternate source(s) of energy such as amino acids or lactate anaerobically, rather than glucose alone. Interestingly, this presumed higher arginine, proline, and glutathione metabolism gene expression in initial minibioreactors was concomitant with increased longevity (culture stayed viable 24–30 h longer than in the 5-L bioreactor) and higher IVCD in the initial MBR, when compared with the 5-L control, using the same growth media. In comparison, the IVCDs of the improved scale-down minibioreactor were convergent with those from 5 L, while the culture stayed viable for ~10 h longer, which was more in line with the 5-L bioreactor compared with the 24–30 h longer, as in the initial scale-down. Also, higher Pdhb gene expression in the 5 L involved in converting glucose to pyruvate aerobically rather than to lactate anaerobically, pointed at higher aerobic metabolism in 5 L (data not shown). Upon shifting to the improved minibioreactor for scale-down, these discrepancies were reduced resulting in better convergence overall, also seen in the qRT-PCR profiles with 5-L control. In addition to the above observations, profiles of sentinel genes related to other functional categories such as protein transport and glycosylation were also measured (data not shown) for the model bioreactor systems.[36]

Discussion

Here, we propose that a set of "sentinel genes" can be identified using transcriptomics with a goal of better scaling down (or up) of cell culture. The validity of our sentinel gene findings was verified by qRT-PCR, and gene expression profiles that were predictive of improved minibioreactor scale-down were compared with earlier minibioreactor scale-down experiments. As an example, based on their functions, we surmise that Sod1 and Apex1 gene upregulation to prevent higher superoxide free-radical and DNA damage resulted in an antiapoptotic protective effect in the initial minibioreactor scale-down culture and was supported by a concomitant lower apoptosis gene Cycs expression. These genes were more convergent in the better scaled experiments.

The putative altered expression of anti-apoptotic genes in the initial scale-down minibioreactor cultures over the time course as well as versus the 5-L bench-scale system could play a crucial role in altering cell physiology in the minibioreactors, as our results broadly suggest (Figure 7). Antiapoptotic gene expression seemed to help increase culture longevity and IVCD in minibioreactor cultures, more for initial scale-down than for improved case. It is to be noted that even when glucose measured close to 0–0.2 g/L (was near the limit of detection of our YSI system), cell density was sustained at its peak for over 12 h at $\geq 5.5 \times 10^6$ cells per milliliter. Following this, cell viability did not dramatically change because of the lack of carbon source in the minibioreactors. Rather, the cell viability came down gradually suggesting that an alternate carbon source was used. This is consistent with our observed upregulation of Odc1 expression, a gene involved with metabolism. Similar amino acid and lactate consumption profiles were observed in other systems by researchers using antiapoptotic cell strains.[39] Apoptotic proteins have been found to control cellular metabolism and energy homeostasis.[40] It is possible that the energetics of the cells in the initial minibioreactors were

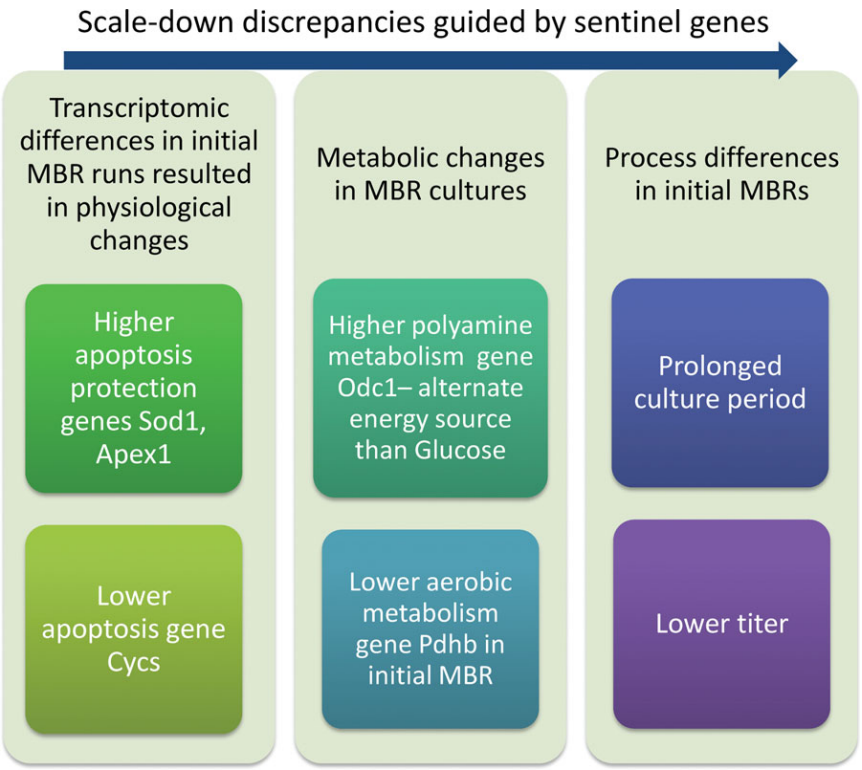

Figure 7. Scale-down discrepancies analyzed at the cellular level in the initial minibioreactors using sentinel genes profiles.

concentrated on apoptosis protection and increased metabolism, rather than on protein production.

A second case of a sentinel gene where the expression pattern was consistent with observations in our culture involved the TCA cycle gene Pdhb (data not shown). The average expression was higher in the 5-L bioreactor by four-fold compared with initial MBR, although with a lower *p*-value.[36] The lower expression of this gene in the initial minibioreactor scale-down suggests that there may have been lower aerobic metabolism in the initial MBRs compared to the 5-L bioreactor. It is possible that measuring this gene expression could serve as an indication of aerobic metabolism, in addition to pCO_2 measurements. This approach of measuring a gene expression during aerobic metabolism might be more accurate in the case of minibioreactors, as CO_2 could be easily affected by sparging in the 35 mL culture volume. Thus, such case studies using sentinel genes provided a deeper process understanding of the minibioreactor scale-down (Figure 7).

Conclusions

We have used a novel approach of identifying transcriptomic changes between the high-throughput minibioreactors and the model 5-L bioreactor for guiding scale-down comparability by providing better understanding at the cellular level. These changes could be particularly correlated to mixing, gas dispersion, and oxygen transfer differences between the bioreactor systems. Upon optimizing these parameters, we found evidence of the minibioreactor sentinel gene profile convergence with the model 5-L system, supported by improved growth parameters comparability between the 5-L bench-top and minibioreactor system, thus strengthening the functionality of gene findings and demonstrating that a rational function-based sentinel gene approach can be applied to improve bioreactor scale change.

GEO Accession

GSE33063—Process-sensitive sentinel genes as novel cell culture comparability metrics

Acknowledgments

UMBC authors acknowledge funding in part from the PDA Fellowship and Sartorius Stedim Biotech. Special thanks to Amy Yang and Toshio Fujisawa, CBER, Shaunak Uplekar and Joao Da Silva, graduate students from the Department of Chemical and Biochemical Engineering, UMBC, for their scientific support. Support from CDER/FDA Critical Path Project # 1500 contributed to the completion of this study.

Literature Cited

1. Chirino A, Mire-Sluis A. Characterizing biological products and assessing comparability following manufacturing changes. *Nat Biotechnol*. 2004;22:1383–1391.
2. Kunkel JP, Jan DCH, Jamieson JC, Butler M. Dissolved oxygen concentration in serum-free continuous culture affects N-linked glycosylation of a monoclonal antibody. *J Biotechnol*. 1998;62:55–71.
3. Xing Z, Kenty BM, Li ZJ, Lee SS. Scale-up analysis for a CHO cell culture process in large-scale bioreactors. *Biotechnol Bioeng*. 2009;103:733–746.
4. Varley J, Birch J. Reactor design for large scale suspension animal cell culture. *Cytotechnology*. 1999;29:177–205.
5. Yang JD, Lu C, Stasny B, Henley J, Guinto W, Gonzalez C, Gleason J, Fung M, Collopy B, Benjamino M, Gangi J, Hanson M, Ille E. Fed-batch bioreactor process scale-up from 3-L to 2500-L scale for monoclonal antibody production from cell culture. *Biotechnol Bioeng*. 2007;98:141–154.

6. Kostov Y, Harms P, Randers-Eichhorn L, Rao G. Low-cost microbioreactor for high-throughput bioprocessing. *Biotechnol Bioeng*. 2001;72:346–352.
7. Humphrey A. Shake flask to fermentor: what have we learned? *Biotechnol Prog*. 1998;14:3–7.
8. Han J, Farnsworth RL, Tiwari JL, Tian J, Lee H, Ikonomi P, Byrnes AP, Goodman JL, Puri RK. Quality prediction of cell substrate using gene expression profiling. *Genomics*. 2006;87: 552–559.
9. Jayapal KP, Wlaschin K, Hu WS, Yap MG. Recombinant protein therapeutics from CHO cells—20 years and counting. CHO Consortium: SBE Special Edition. 2007:40–47.
10. Kantardjieff A, Nissom PM, Chuah SH, Yusufi F, Jacob NM, Mulukutla BC. Developing genomic platforms for Chinese hamster ovary cells. *Biotechnol Adv*. 2009;27:1028–1035.
11. Xun X, Nagarajan H, Lewis NE, Pan S, Cai Z, Liu X. The genomic sequence of the Chinese hamster ovary (CHO)-K1 cell line. *Nat Biotechnol*. 2011;29:735–741.
12. Isett K, George H, Herber W, Amanullah A. Twenty-four-well plate miniature bioreactor high-throughput system: assessment for microbial cultivations. *Biotechnol Bioeng*. 2007;98: 1017–1028.
13. Maharbiz MM, Holtz WJ, Howe RT, Keasling JD. Microbioreactor arrays with parametric control for high-throughput experimentation. *Biotechnol Bioeng*. 2004;86:485–490.
14. Puskeiler R, Kaufmann K, Weuster-Botz D. Development, parallelization, and automation of a gas-inducing milliliter-scale bioreactor for high-throughput bioprocess design (HTBD). *Biotechnol Bioeng*. 2005;89:512–523.
15. Siurkus J, Panula-Perala J, Horn U, Kraft M, Rimseliene R, Neubauer P. Novel approach of high cell density recombinant bioprocess development: optimisation and scale-up from microliter to pilot scales while maintaining the fed-batch cultivation mode of *E. coli* cultures. *Microbial Cell Factories*. 2010;9:35.
16. Wen Y, Zang R, Zhang XD, Yang ST. A 24-microwell plate with improved mixing and scalable performance for high throughput cell cultures. *Process Biochem*. 2012;47:612–618.
17. Rubinstein LJ, Stein KE. Murine immune response to the Neisseria meningitidis group C capsular polysaccharide I. Ontogeny. *J Immunol*. 1988;141:4357–4362.
18. Kondragunta B, Drew JL, Brorson KA, Moreira AR, Rao G. Advances in clone selection using high-throughput bioreactors. *Biotechnol Prog*. 2010;26:1095–1103.
19. Kondragunta B, Han J, Joshi BH, Brorson KA, Puri RK, Uplekar S, Moreira AR, Rao G. Genomic analysis of a hybridoma batch cell culture metabolic status in a standard laboratory 5 L bioreactor. *Biotechnol Prog*. 2012;9:110–130.
20. Bas A, Forsberg G, Hammarstrom S, Hammarstrom ML. Utility of the housekeeping genes 18S rRNA, beta-actin and glyceraldehyde-3-phosphate-dehydrogenase for normalization in real-time quantitative reverse transcriptase-polymerase chain reaction analysis of gene expression in human T lymphocytes. *Scand J Immunol*. 2004;59:566–573.
21. Abu J, Batuwangala M, Symonds P. Expression of RAR beta2 gene by real-time RT-PCR: differential expression in normal subjects compared to cervical cancer patients normalised against GAPDH as a housekeeping gene. *Eur J Obstet Gynecol Reprod Biol*. 2008;140:295–296.
22. Barber RD, Harmer DW, Coleman RA, Clark BJ. GAPDH as a housekeeping gene: analysis of GAPDH mRNA expression in a panel of 72 human tissues. *Physiol Genomics*. 2005;21:389–395.
23. Kermis HR, Kostov Y, Harms P, Rao G. Dual excitation ratiometric fluorescent pH sensor for noninvasive bioprocess monitoring: development and application. *Biotechnol Prog*. 2002;18: 1047–1053.
24. Ge X, Hanson M, Shen H, Kostov Y, Brorson KA, Frey D, Moreira AR, Rao G. Validation of an optical sensor-based high throughput bioreactor system for mammalian cell culture. *J Biotechnol*. 2006;122:293–306.
25. Hanson M, Ge X, Kostov Y, Brorson KA, Moreira AR, Rao G. Comparisons of optical pH and dissolved oxygen sensors with traditional electrochemical probes during mammalian cell culture. *Biotechnol Bioeng*. 2007;97:833–841.
26. Hanson MA, Brorson KA, Moreira AR, Rao G. Comparisons of optically monitored small-scale stirred tank vessels to optically controlled disposable bag bioreactors. *Microbial Cell Factories*. 2009;8:44.
27. Bellucci JJ, Hamaker KH. Evaluation of oxygen transfer rates in stirred-tank bioreactors for clinical manufacturing. *Biotechnol Prog*. 2011;27:368–376.
28. Hortsch R, Stratmann A, Weuster-Botz D. New milliliter-scale stirred tank bioreactors for the cultivation of mycelium forming microorganisms. *Biotechnol Bioeng*. 2010;106:443–451.
29. Tribe LA, Briens CL, Margaritis A. Determination of the volumetric mass transfer coefficient (kLa) using the dynamic 'gas out-gas in' method: analysis of errors caused by dissolved oxygen probes. *Biotechnol Bioeng*. 1995;46:388–392.
30. Silva JD. Mixing characterization in novel high throughput minibioreactors: scale-down modeling from bench-scale. Masters Thesis, University of Maryland, Baltimore County, 2010.
31. Burleigh SC, van de Laar T, Stroop CJ, Grunsven W, O'Donoghue N, Rudd PM, Davey GP. Synergizing metabolic flux analysis and nucleotide sugar metabolism to understand the control of glycosylation of recombinant protein in CHO cells. *BMC Biotechnol*. 2011;11:95.
32. Meleady P, Doolan P, Henry M, Barron N, Keenan J, O'Sullivan F, Gammell P, Melville MW, Leonard M, Clynes, M. Sustained productivity in recombinant Chinese hamster ovary (CHO) cell lines: proteome analysis of the molecular basis for a process-related phenotype. *BMC Biotechnol*. 2011;11:78.
33. Krampe B, Al-Rubeai M. Cell death in mammalian cell culture: molecular mechanisms and cell line engineering strategies. *Cytotechnology*. 2010;62:175–188.
34. Hwang SO, Lee GM. Nutrient deprivation induces autophagy as well as apoptosis in Chinese hamster ovary cell culture. *Biotechnol Bioeng*. 2008;99:678–685.
35. Thomas R, Paredes CJ, Mehrotra S, Hatzimanikatis V, Papoutsakis ET. A model-based optimization framework for the inference of regulatory interactions using time-course DNA microarray expression data. *BMC Bioinformatics*. 2007;8:228.
36. Kondragunta B. Bioprocess convergence using sentinel genes for process parameter tuning. PhD Dissertation, University of Maryland, Baltimore County, 2011.
37. Chen A, Chitta R, Chang D, Amanullah A. Twenty-four well plate miniature bioreactor system as a scale-down model for cell culture process development. *Biotechnol Bioeng*. 2009;102:148–160.
38. Amanullah A, Otero JM, Mikola M, Hsu A, Zhang J, Aunins J, Schreyer HB, Hope JA, Russo AP. Novel micro-bioreactor high throughput technology for cell culture process development: reproducibility and scalability assessment of fed-batch CHO cultures. *Biotechnol Bioeng*. 2010;106:57–67.
39. Dorai H, Kyung YS, Ellis D, Kinney C, Lin C, Jan D, Moore G, Betenbaugh MJ. Expression of anti-apoptosis genes alters lactatemetabolism of chinese hamster ovary cells in culture. *Biotechnol Bioeng*. 2009;103:592–608.
40. Majors BS, Betenbaugh MJ, Chiang GG. Links between metabolism and apoptosis in mammalian cells: applications for anti-apoptosis engineering. *Metab Eng*. 2007;9:317–326.

Manuscript received Mar 20, 2012, and revision received July 11, 2012.

Epilogue/Conclusion: Out of the Box!

We are now entering the brave new world of personalized cell therapy. New technologies for process monitoring will be required. In particular, since the entire bioreactor contents will go back into the patient, the bar for sensor technologies will get higher. The conventional patch-based sensors may not be suitable, as the potential for unknown leachable/extractables and the optical energy interference with the cells/media are additional risk factors.

So with this in mind, we created technology that permits completely non-invasive monitoring. In one instance, the patches go outside a diffusible surface and in the other, a silicone tubing loop serves to transport the analyte outside the bioreactor for analysis. I believe that this approach has the potential to create all kinds of novel sensing opportunities.

The first study was born out of our work to develop sensors for neonatal monitoring. The idea was to measure various analytes diffusing across the skin. Because it is hard to conduct experiments on fragile babies, we thought that using a bioreactor as a surrogate system would be ideal. So Priyanka Gupta, a Master's student used a Teflon bag bioreactor where oxygen sensor patches were mounted both inside (as in all our previous studies) and outside the diffusible bag. The outside patch was then sealed with a piece of plastic to effectively allow diffusion only from inside the bag to the patch. Much to our astonishment, the system worked quite well and the sensors outside the bag tracked the oxygen levels in the bag during cell culture, albeit with longer response times.

This paves the way for truly non-invasive measurements in systems like cell therapy culture bags, where one would not want sensor patches with potential leachables/extractables in contact with the cells intended for delivery to a patient.

A Completely Noninvasive Method of Dissolved Oxygen Monitoring in Disposable Small-Scale Cell Culture Vessels Based on Diffusion Through Permeable Vessel Walls

Priyanka A. Gupta, Xudong Ge, Yordan Kostov, and Govind Rao
Center for Advanced Sensor Technology, Dept. of Chemical, Biochemical and Environmental Engineering, University of Maryland, Baltimore County, Baltimore, MD 21250

DOI 10.1002/btpr.1838
Published online November 22, 2013 in Wiley Online Library (wileyonlinelibrary.com)

Disposable cell culture vessels are extensively used at small scales for process optimization and validation, but they lack monitoring capabilities. Optical sensors that can be easily adapted for use in small-scale vessels are commercially available for pH, dissolved oxygen (DO), and dissolved carbon dioxide (DCO_2). However, their use has been limited due to the contamination and compatibility issues. We have developed a novel solution to these problems for DO monitoring. Oxygen diffusion through permeable vessel wall can be exploited for noninvasive monitoring. An optical oxygen sensor can be placed outside the oxygen permeable vessel wall thereby allowing oxygen diffusing through the vessel wall to be detected by the sensor. This way the sensor stays separate from the cell culture and there are no concerns about contaminants or leachants. Here we implement this method for two cell culture devices: polystyrene-made T-75 tissue culture flask and fluorinated ethylene propylene (FEP)-made Vuelife® cell culture bag. Additionally, mammalian and microbial cell cultures were performed in Vuelife® cell culture bags, proving that a sensor placed outside can be used to track changes in cell cultures. This approach toward noninvasive monitoring will help in integrating cell culture vessels with sensors in a seamless manner. *Biotechnol. Prog.*, 30:172–177, 2014
Keywords: optical sensors, noninvasive monitoring, mammalian cell culture, dissolved oxygen, disposable cell culture vessels

Introduction

At small scales (0.1–100 mL), the majority of cell culture vessels lack even the most basic online monitoring techniques that are being used at the bench and industrial scales. In recent years, fluorescence-based patch sensors for pH, pO_2, and pCO_2 have become commercially available. These patches essentially have a fluorescent dye immobilized in a polymer matrix. They are affixed inside the vessel with the electronics required for measurement placed outside. This is minimally invasive as except for the patch, which is very thin, the rest of the system is located outside and the measurement is made noninvasively through the transparent vessel wall. These sensors can be useful in scaling up from lab to bench scale and beyond,[1,2] and in developing small-scale platforms for process optimization.[3–7] However, despite the potential advantages of implementing this technology, they have not been widely adopted for use in industry and academia. There are two main reasons for this. First, there are concerns regarding the effects of the patch on cell cultures. Even though the sensing dye is immobilized in polymer matrix, there are chances that the dye might leach and cause toxicity. Studies conducted in our lab show that the pH and DO patches have no apparent negative effects on the cellular physiology at the transcript level and on the product quality of Hybridoma cell culture.[8] But the same cannot be predicted for other more sensitive cell lines. Other than the dye, polymer matrix and the optical isolator layer contacting the cell culture need to be biocompatible as well. Certain cell lines may be too sensitive for use of patch sensors. The second reason is the limited variety of devices which come equipped with these sensors. Manufacturers consider the process of integrating vessels with sensors disruptive to their manufacturing process. Commercially available systems come only for micro titer plates (SensorDish Reader® by Applikon Biotechnology) and shake flasks (Shake Flask Reader by PreSens, SENSOLUX® by Sartorius Stedim Biotech). Other vessels like T-flasks, spinner bottles, and spin-tubes have to be equipped with sensors in the lab. Some cell lines may require special treatment, like for adherent cell lines, the patch needs to be treated with protein to make cells adhere to it.[9] This is often a very tedious task, requiring many steps that need to be implemented carefully. Other than that, patch introduction can also be a source of contamination.

We have conceived a potential solution to these problems for DO monitoring. Our novel approach avoids the placement of any sensing material altogether inside the vessel, making monitoring truly noninvasive. As most of small-scale cell culture vessels are made of disposable polymers, a sensor patch can be placed outside the vessel wall and sealed completely. Dissolved oxygen (DO) in the cell culture will

Correspondence concerning this article should be addressed to G. Rao at grao@umbc.edu.

diffuse through the wall and be detected by the sensor patch. This way the patch remains separate from the cell culture, so there is no possibility of contamination or leaching of dye into the cell culture. For those cell culture vessels that have thick polymer walls, mounting the patch directly outside the vessel wall would be impractical due to the much prolonged response time. In this case, the wall thickness could be reduced by creating a cubical cavity in the wall. The patch can then be placed inside this cavity and sealed with a sealing material.

To test the feasibility of this idea, we implemented it for two types of cell culture vessels: tissue culture flask and Vuelife® cell culture bag. The former had to be modified for its wall thickness; the latter had thin enough walls to allow for reasonable response times. Further, mammalian and microbial cell cultures were performed in Vuelife® cell culture bags.

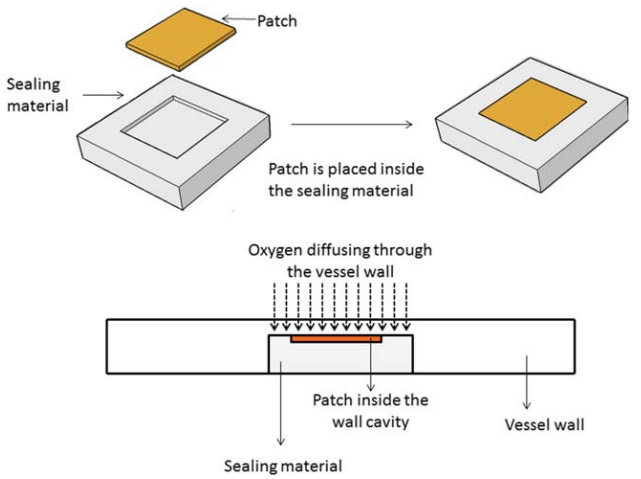

Figure 1. Schematic showing placement of the sensor patch.

The sensor patch is placed inside a transparent sealing material and placed outside the vessel. Oxygen diffusing through the vessel wall is then detected by the sensor patch.

Materials and Methods

Optical system

Our sensor system is composed of three different components: the sensing patch, the electronics, and the National Instruments' LabVIEW program. The patch consists of four layers. The topmost layer is an acrylic copolymer and acts as an optical isolator. The sensing layer is located below it, which has the fluorescent dye Tris(4,7-diphenyl-1,10 phenanthroline) ruthenium(II) dichloride immobilized in a silicone matrix. This layer is supported by a third polyester layer below it. The patch is attached to the vessel by a fourth adhesive layer. These patches were prepared in our lab. A large sheet of sensing material was prepared initially, which was then cut into smaller patches. The electronics were housed in a coaster which contained light emitting diodes (LEDs) for photoexcitation and photodiode for light detection. The coaster system was manufactured by Fluorometrix Corporation (currently marketed by Scientific Industries, Inc.). The LabVIEW program was used to log in the data online.

The sensor is based on the fluorescence quenching of the dye molecule. The emission intensity and lifetime of the molecule is inversely proportional to oxygen concentration. DO was measured using phase fluorometry. In this, a sinusoidally modulated light was used for exciting the fluorophore. The signal, thus, emitted was phase shifted with respect to the original excitation. Phase shift (Φ) is related to the lifetime by the following equation:

$$\tan\Phi = \omega\tau \quad (1)$$

where, ω is the angular frequency related to frequency (f) by: $\omega = 2\pi f$. Hence, phase shift decreases with increasing oxygen concentration. For our patches, phase shift varied approximately between $-18°$ and $-62°$.

In this article, the response time (T_{90}) is defined as the time taken by the sensor to reach 90% of its final phase shift value when the oxygen concentration changes from 0% air saturation to 100% air saturation. The response time of our sensor patch was approximately 60 s.

Cell culture vessels

T-75 tissue culture flasks were purchased from Corning Life Sciences. Fluorinated ethylene propylene (FEP) autoclavable cell culture bags of ABCS series were provided by American Fluoroseal Corporation. One side of these bags was 76.2 μm thick and the other side was 127 μm thick. Two different sizes of FEP cell culture bags were used: ABCS-32 and ABCS-72. ABCS-72 had a volume capacity of 72 mL and ABCS-32 had a volume capacity of 32 mL, when liquid filled in the bags was 1 cm thick in the middle.

Installing and sealing the patch outside the cell culture vessel

T-flask. CNC milling machine model 3501 from Little-MachineShop.com was used to create the cavity in the T-flask wall. A 50% ethanol–water mixture was used as a coolant to avoid polystyrene from melting during milling. It was not possible to measure the cavity wall thickness during milling. Hence, after the experiments were over, the cavity wall was broken from the flask and its thickness was measured. The time required to mill a cavity depended on the number of passes and feed rate used, but in general the time varied between 2 and 4 h. After the cavity was made, a patch was inserted and sealed inside it. Sealing material should be relatively impermeable to oxygen so that the sensor is quenched only by the oxygen diffusing from inside the vessel. To seal the patch, a 1.5 mm thick poly(methyl methacrylate) (PMMA) cap was used. PMMA was used for the ease of machining and its low oxygen permeability $\left(0.07\times10^{-13}\,\frac{\text{cm}^3}{\text{cm}^2}\frac{\text{cm}}{\text{sPa}}\right)$.[10] A PMMA cap to fit the cavity was modeled using laser cutting. Patch was placed inside the well in the cap. This cap was then inserted in the cavity and secured there with an adhesive (Figure 1).

Vuelife® Cell Culture Bags. FEP bags were not modified for their thicknesses. Patches were placed in 3 mm thick PMMA caps and attached directly outside the bags (Figure 1). Silicone adhesive tape (manufactured by Adhesive Research) was used for patch attachment. FEP has nonstick properties, so to improve its bondability, the bag was corona treated in a Harrick PDC-32G Plasma Cleaner. An exposure time of 5 min was found optimal. The silicone adhesive tape came in three layers, with the silicone adhesive layer sandwiched between two polyester nonadhesive layers. This adhesive layer is applied to the PMMA cap and the cap is

then firmly pressed against the surface of the bag. To remove any air bubbles present the setup was pressurized in a vice for 12 h.

Response time experiments

The cell culture vessel with the sensor patch installed was mounted on top of an oxygen coaster. First, nitrogen was passed through the cell culture vessel until the phase shift values leveled off, and nitrogen was then switched to air. The phase shift at the patch was recorded every 15 s. For the T-flask, after the experiment was over, the cavity wall was broken and its thickness was measured. For Vuelife® bags, this experiment was done for both thicknesses, and their response times were compared.

Gas flow rate was maintained at 313 mL/min. For a vessel volume of 75 mL, time required to fill the vessel would be approximately 14 s. Thus, the time required to fill the vessel was assumed negligible in comparison to the expected response times.

Cell culture experiments

Cell culture experiments will give insight into patch behavior in dynamic culture environments. DO profiles obtained from the patches placed outside and inside were compared for mammalian and microbial cell cultures.

Bag Preparation. Bags were equipped with sensors both inside and outside. Outside patches were attached with the help of silicone adhesive tapes. After the bag was corona treated and the outside patch attached to the bag, a small slit was made in the bag to insert a patch inside. After the patch was affixed at its place, the cut was closed with an autoclavable adhesive tape. Both patches were from the same batch and were assumed to have the same properties. A quarter of the bag was then filled with de-ionized (DI) water and autoclaved at 121°C for 22 min at 14 psi.

Mammalian Cell Culture. Mammalian cell culture was carried out in ABCS-32 bags. Two bags were used for the experiment. One bag had a patch inside it and another bag had a patch attached outside it. Both patches were monitored at the same location. The PMMA cap held the outside patch in its place. A PMMA plate with same dimensions as the PMMA cap was attached to the bag with the inside patch (Figure 2). This was done to ensure that the two patches were photobleached at the same rate. The cell line used was a nonadherent SP2/0-based myeloma/mouse (2055.5) secreting IgG3 antibody specific for the *Nisseria meningitides* capsular-polysaccharide (MCPS). About 1 L CD Hybridoma GT™ (Invitrogen, Carlsbad, CA) stock media solution supplemented with 8 mM L-glutamine (GIBCO) and 2×10^{-4}% β-mercaptoethanol (v/v) (Sigma, St. Louis, MO) was prepared and stored at 4°C. The cell culture was carried out in a CO_2 incubator at 37°C, 5% CO_2 in air. Cells were taken from a static T-flask and cultured in FEP bags at an initial cell concentration of 0.2×10^6 cells/mL. Each bag was inoculated with 30 mL of cell culture from the same inoculum to make sure that the initial conditions were approximately the same in the two bags. Data logging rate was 5 min.

Once the culture was started, it was left undisturbed and apart from DO measurements no other sampling was done. Cell counting, for inoculating cells, was done using a hemocytometer and viability was determined using trypan blue exclusion method. Glucose and lactate were measured at the end of cell culture using the YSI 2700 Chemistry Analyzer.

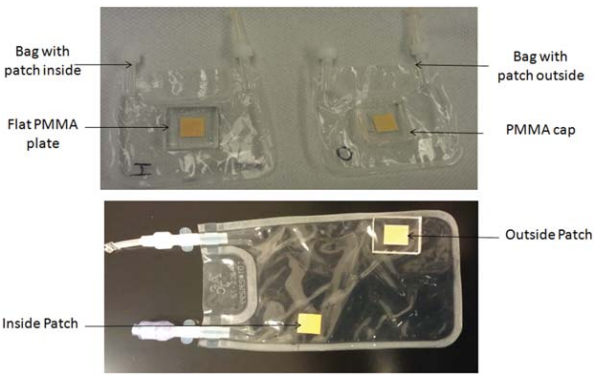

Figure 2. Pictures showing the configuration of the inside and outside patches for cell culture experiments.

Picture on the top shows two similar ABCS-32 bags used for the mammalian cell culture experiment, one has a patch outside and the other has a patch inside the bag. Below is a picture of an ABCS-72 bag used for microbial cell culture experiment. Inside and outside patches were monitored in the same bag and were placed on diagonally opposite ends of the bag.

Microbial Cell Culture. Experiments were carried out in ABCS-72 bags. Two coasters could be accommodated under an ABCS-72 bag, so both patches were monitored simultaneously in the same bag. Inside and outside patches were placed on the opposite ends of the bag (Figure 2). Glutamine binding protein (QBP) producing strain of *Escherichia coli* (NMJ30) was used for microbial cell culture. One liter of Luria-Bertani media was prepared for use in cell culture (5 g yeast extract, 10 g tryptone, and 10 g NaCl). About 40 mL of media was inoculated with one single *E. coli* colony from an agar plate. The culture was incubated at 37°C with orbital shaking at 120 rpm.

Results

Response time experiments

A tissue culture flask and an FEP cell culture bag were equipped with sensors outside for noninvasive DO monitoring. Initial experiments were conducted to estimate response times for the sensor integrated vessels.

The T_{90} for the flask-sensor system was approximately 2.51 h. The overall sensitivity was also reduced as the system stabilizes at a phase shift of around $-30°$ when air is being passed through the flask, compared with $-18°$ for just the patch. This is because the overall oxygen permeability of the new flask-patch system is lower than the oxygen permeability of the patch and the sensitivity of a sensor increases with an increase in permeability values.[11] Hence, for a sensor outside the T-flask, the phase shift will change from $-60°$ to $-30°$ for a change in DO percentage from 0% to 100%.

The thickness of the cavity wall, after breaking it from the flask, was found out to be 75 μm. The diffusion coefficient of oxygen in polystyrene varies from 2×10^{-7} to 4.3×10^{-7} cm^2/s.[12–14] The time required by oxygen to diffuse through the T-flask wall can be roughly estimated by using the following equation:[15]

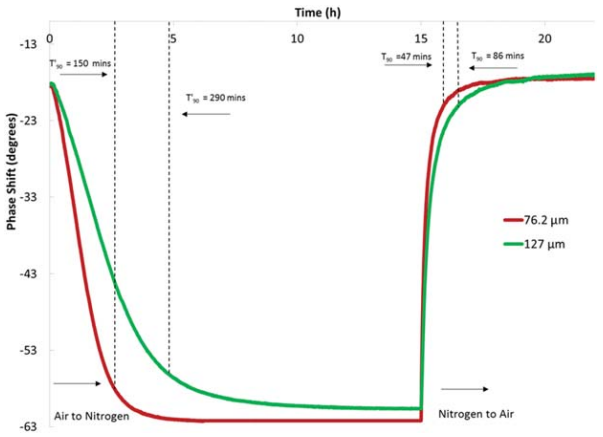

Figure 3. Results of the response time experiments for patches attached outside the 127- and 76.2-μm thick sides of the FEP bag.

Nitrogen and air were alternately passed through the FEP bag. Time required for air to nitrogen transition was longer than that required for nitrogen to air transition. Response time of 76.2 μm thick layer (47 min) was much smaller than that of 127 μm thick layer (86 min).

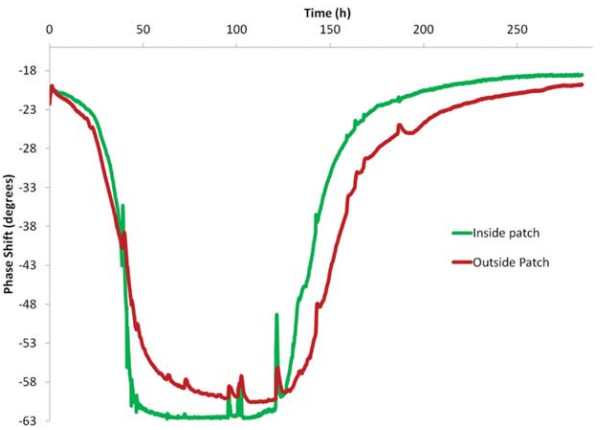

Figure 4. Phase shift profiles obtained for inside and outside patches during the mammalian cell culture.

A mammalian cell culture experiment was carried out in two separate ABCS-32 bags under similar conditions. One bag had a patch attached on the outside and another had a patch inside. Phase shifts were monitored at both patches and compared. In general, the outside patch was able to track the changes happening in the cell culture.

$$\frac{(\Delta x)^2}{D} = \Delta t \tag{2}$$

where, Δx is the wall thickness, Δt is the time taken for diffusion, and D the diffusion coefficient. This equation is used for estimating the time taken by a gas to diffuse through a very thin polymer film. The response time obtained through experiments is more than what is estimated from Eq. 2 (around 5 min). This could be either because the sealing was imperfect, leading to air pocket formation, or because the actual diffusion coefficient was lower than the values reported in literature.[12–14]

Milling cavities into T-flask was found to be impractical for further experiments. It was not possible to know the thickness of the cavity wall until after the experiment was over, after which the wall had to be broken from the flask and measured. Moreover, the wall was prone to cracking, sometimes requiring several attempts to obtain an intact cavity wall. Hence, for providing proof of concept, T-flask was replaced with a Vuelife® cell culture bag. An experiment was conducted to compare the behavior of outside sensors for two different bag thicknesses, 76.2 and 127 μm. Two separate bags were prepared, one with a patch attached outside the 76.2 μm layer and another with a patch outside the 127 μm layer. Response times were calculated for both air to nitrogen (T'_{90}) and nitrogen to air transitions (T_{90}). For air to nitrogen transition, the response times (T'_{90}) for the 127 and 76.2 μm thick layers were 290 and 150 min, respectively. For nitrogen to air transition (T_{90}, response time used to characterize the sensor system here), the values were 86 and 47 min for the 127 and 76.2 μm layers, respectively. Diffusion of air out of the patch took much longer than diffusion of air into the patch as evident from the response time graph (Figure 3). The difference between the two response times is 204 min for the 127 μm thick layer and 103 min for the 76.2 μm thick layer. Thus, the thicker the bag layer the greater the difference. When the difference is small (the inside sensor), the reading of the sensor is irrelevant to the trend of the concentration changes. However, when the difference is large (the outside sensor), the same readings may not necessarily mean the same concentrations, depending on whether the concentration is increasing or decreasing. As the difference is large for the outside sensor, it should be considered when interpreting the results. Since thinner bag walls resulted in shorter response times, the rest of the experiments were carried out with the patch attached outside the 76.2 μm thick side of the bag. Two more response time studies for the thinner layer yield a mean response time of 55 min with a standard deviation of 7.5 min.

Mammalian cell culture experiment

Even though the response time was relatively long, compared with only 1–2 min for only the patch, cell culture experiments were conducted to see if the patch outside could track the changes happening inside the cell culture. Since mammalian cells have long doubling times between 12 and 24 h, the outside patch sensor was tested in a mammalian cell culture first. Mammalian cell culture was performed in two separate bags with one having a patch inside and another outside under similar conditions. For comparison, the phase shifts at the patches during the cell culture were plotted against time (Figure 4). DO percentages were not compared since patch calibration did not take the resistance due to an additional FEP layer into account. The phase shift shown by the outside patch will depend on the rate at which oxygen concentration changes inside the cell culture. For slow changes, the values shown by the outside patch will be closer to those shown by the inside patch, but for fast changes they will be farther away. Since the experiment was carried out in different bags, glucose and lactate concentrations were measured at the end of cell culture to ensure that the cells experienced similar conditions in the two bags. Results for this are shown in Table 1. Lactate and glucose concentrations in the two bags were close to each other, and thus, conditions in the bags can be considered to be similar.

The outside patch followed the inside patch quite well. When the oxygen decreased, the phase shift at both patches also decreased, and when the oxygen concentration increased, the phase shifts also increased. Between 0 and 38 h, the phase shift at the outside patch is always lower than that at the inside patch. From 38 to 95 h the values at the outside patch are greater than those at the inside patch. This

is because the outside patch is not fast enough to respond to the sudden decline in oxygen concentrations. The difference in the phase shifts at the patches may not be translated into a big difference in DO percentage, since the patches are more sensitive at low oxygen concentration. Hence at low concentrations, small changes in concentration results in bigger phase shift changes. From 111 h onward, when the oxygen concentration is increasing in the culture, phase shift is always lower at the outside patch. This is because the slower outside patch cannot catch up with the phase shift at the inside patch. The Pearson correlation between the outside and the inside patch phase shifts is 96.95%. If the Pearson correlation is calculated for only times between 0 and 95 h, when oxygen concentration is declining, and it is calculated to be 98.81%. This experiment shows that the outside patch can be used to show all the phases of a DO profile.

Microbial cell culture experiment

Microbial cells, whose doubling times can be as low at 20 min, grow faster than mammalian cells, and thus also consume oxygen faster. Experiments were conducted to see how well the outside patch can track the changes in microbial cell cultures. The results are presented in Figure 5. After 2.5 h, when oxygen starts decreasing rapidly, the outside patch starts lagging with phase shift values higher than those at the inside patch. When the inside patch phase shift has already dropped to $-62°$ at 3 h, the phase shift at the outside patch is still $-36°$, reaching the same phase shift at about 5.5 h. The Pearson correlation between the inside and outside patches during 2.5–5.5 h is 86.53%. This is very low when compared with 98.81% for the mammalian cell culture.

Discussion

The bioprocess implications of monitoring DO have already been discussed by us before.[16–18] Here, we demonstrated a novel approach to monitor DO, which simplifies the use of optical sensors for disposable cell culture vessels. This method has several advantages over the previous method of inserting the sensor patch inside the vessel. A culture can be monitored for DO irrespective of cell line sensitivity or dye toxicity. Vessels integrated with sensors in this fashion would also provide full containment for pathogenic cell culture studies. This method can also be used to remedy calibration drifts due to photobleaching. Since the sensor is located outside, there is a possibility that it can be replaced during the cell culture without causing any contamination. In addition, no special care need be taken to validate leachables/extractables from the patches, as they are mounted outside the reactor. This is becoming an important consideration in the use of polymeric materials used in disposable bioreactor fabrication.[19–21] Moreover, this format is more convenient and easier to used by the end user since it does not require any changes in the current cell culture practices. Since the total cost of the patch and the additional sealing material is no more than 20 cents, the addition of this monitoring capability will not significantly increase the cost of the cell culture experiments. Apart from T-flasks and FEP bags, other disposable vessels can also be equipped with DO monitoring capabilities in a similar way. The diffusion coefficient of the vessel material will determine the extent of modification needed to obtain a particular response time. The various polymers used in disposable vessels and the thickness required to reach a 10 min response time are given in Table 2. Disposable bag reactors (Cellbag bioreactor by General Electric and Biostat® Cultibag RM by Sartorius), which use polymers with high gas barrier properties,[22] cannot be used as is, but can be adapted for monitoring with some modifications. For example, short response times can be obtained if the sensor can be sandwiched between the more permeable fluid contacting layer and the gas barrier layer. Another solution to overcome the limitations of vessel material could be to graft a more permeable polymer on the vessel where the sensor is installed.

Even though the response times obtained here were long compared with conventional patch-based sensors with

Table 1. Lactate and Glucose Concentrations in the ABCS-32 Bags at the End of the Mammalian Cell Culture Experiment

	Bag with the Inside Patch	Bag with the Outside Patch
Lactate (g/L)	1.49 ± 0.02	1.50 ± 0.03
Glucose (g/L)	0.696 ± 0.003	0.633 ± 0.010

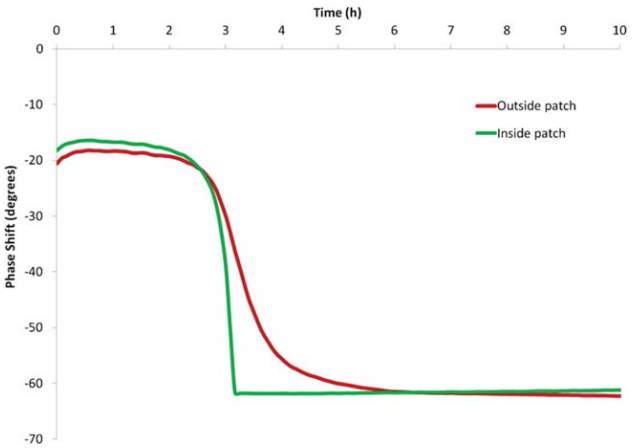

Figure 5. Phase shift vs. time plots obtained on monitoring inside and outside patches during a microbial cell culture experiment in an ABCS-72 bag.

Table 2. Different Polymers Used in Disposable Cell Culture Vessels and Their Relevant Properties

Polymer	Cell Culture Vessel	D^* (cm^2/s) × 10^7	$P^\dagger$ (mL cm/cm^2 s Pa) × 10^{13}	$d^\ddagger$ (μm)
Polystyrene	Petri dish, T-flask, Spinner flask	2–4.3[12–14]	1.8 at 25°C[14]	109–160
FEP	Vuelife cell culture bags	1.73[23]	3.2 at 25°C[24]	102
Polycarbonate	Shake flasks, SuperSpinner D 1000®	0.24–0.55[13]	0.8–1.2 at 23°C[25]	38–57
Low density polyethylene (LDPE)	Cellbag bioreactors, Cultibags (Fluid contact layer)	4.5 at 23°C[26]	1.5–1.6 at 25°C[14]	164
Ethylene vinyl alcohol (EVOH)	Cellbag bioreactors, cultibags (noncontact layer)	0.0072 at 23°C[26]	0.018–0.052 at 20°C[27]	6.6

*D is the diffusion coefficient of vessel material.
†P is the permeability of vessel material.
‡d is the vessel wall thickness through which oxygen diffuses in 10 min, as calculated from Eq. 2.

response times <60 s, the point here was not to obtain short response times, but to demonstrate that changes in a cell culture can be monitored by a patch outside. Our study was limited by the vessel wall thickness achievable in the lab. Response time can be decreased by reducing wall thickness. Reducing wall thickness by half should result in approximately four times shorter response times.

For a sensor integrated with a cell culture vessel in such a fashion, the overall response time will be longer and the sensitivity lower as compared with "only the sensor." However, the minimum necessary accuracy and precision required in dynamic environments will depend on monitoring goals. This approach can also be extended to carbon dioxide monitoring. Carbon dioxide patches, just like oxygen patches, can be placed outside for completely noninvasive monitoring. Implementation of this method to a wider range of vessels would require mechanical and polymer engineering to obtain thin cavity walls for fast analyte detection. Other analytes like protons, glucose, etc., can also be monitored noninvasively if the vessel wall is designed to include a small area permeable to these analytes.

Conclusions

Here a novel, completely noninvasive method of monitoring DO was implemented in T-flasks and FEP cell culture bags. Additionally, experiments were conducted with two different types of cell cultures: mammalian and microbial. It was found that the method would be more suited for slow growing but very sensitive cell cultures. This method of manufacturing sensors integrated with vessels will remove the barrier to immediate use of these sensors.

Acknowledgments

We dedicate this article to the memory of Dr. Joseph E. Qualitz, co-founder of Fluorometrix. His vision helped to create affordable noninvasive sensor technology for bioprocess monitoring. Funding from Sartorius-Stedim Biotech is gratefully acknowledged. Authors would also like to thank *American Fluoroseal* Corporation, for generously supplying ABCS series Vuelife® bags for this study. G.R., Y.K., and X.G. declare a conflict of interest as consultants to Fluorometrix.

Literature cited

1. Hanson MA, Ge X, Kostov Y, Brorson KA, Moreira AR, Rao G. Comparisons of optical pH and dissolved oxygen sensors with traditional electrochemical probes during mammalian cell culture. *Biotechnol Bioeng*. 2007;97:833–841.
2. Vallejos JR, Brorson KA, Moreira AR, Rao G. Integrating a 250 ml-spinner flask with other stirred bench-scale cell culture devices: a mass transfer perspective. *Biotechnol Prog*. 2011;27: 803–810.
3. Kostov Y, Harms P, Randers-Eichhorn L, Rao G. Low-cost microbioreactor for high-throughput bioprocessing. *Biotechnol Bioeng*. 2001;72:346–352.
4. Zanzotto A, Szita N, Boccazzi P, Lessard P, Sinskey AJ, Jensen KF. Membrane-aerated microbioreactor for high-throughput bioprocessing. *Biotechnol Bioeng*. 2004;87:243–254.
5. Kensy F, John GT, Hofmann B, Buechs J. Characterisation of operation conditions and online monitoring of physiological culture parameters in shaken 24-well microtiter plates. *Bioprocess Biosyst Eng*. 2005;28:75–81.
6. Zhang Z, Szita N, Boccazzi P, Sinskey AJ, Jensen KF. A well-mixed, polymer-based microbioreactor with integrated optical measurements. *Biotechnol Bioeng*. 2006;93:286–296.
7. Kirk TV, Szita N. Oxygen transfer characteristics of miniaturized bioreactor systems. *Biotechnol Bioeng*. 2013;110:1005–1019.
8. Ge X, Hanson M, Shen H, Kostov Y, Brorson KA, Frey DD, Moreira AR, Rao G. Validation of an optical sensor-based high-throughput bioreactor system for mammalian cell culture. *J Biotechnol*. 2006;122:293–306.
9. Bambrick LL, Kostov Y, Rao G. In vitro cell culture pO2 is significantly different from incubator pO2. *Biotechnol Prog*. 2011; 27:1185–1189.
10. McKeen LW. Permeability properties of plastics and elastomers. In: Polyolefins, Polyvinyls and Acrylics, Waltham, Massachusetts: William Andrew; 2012:186–187.
11. Badocco D, Mondin A, Pastore P, Voltolina S, Gross S. Dependence of calibration sensitivity of a polysulfone/Ru(II)-tris(4,7-diphenyl-1,10-phenanthroline)-based oxygen optical sensor on its structural parameters. *Anal Chim Acta*. 2008;627:239–246.
12. Gao Y, Ogilby PR. A new technique to quantify oxygen diffusion in polymer films. *Macromolecules*. 1992;25:4962–4966.
13. Gao Y, Baca AM, Wang B, Ogilby PR. Activation barriers for oxygen diffusion in polystyrene and polycarbonate glasses: effects of low molecular weight additives. *Macromolecules*. 1994;27:7041–7048.
14. Rharbi Y, Yekta A, Winnik MA. A method for measuring oxygen diffusion and oxygen permeation in polymer films based on fluorescence quenching. *Anal Chem*. 1999;71:5045–5053.
15. Liu T, Teduka N, Kameda M, Asai K. Diffusion timescale of porous pressure-sensitive paint. *AIAA J*. 2001;39:2400–2402.
16. Gupta A, Rao G. A study of oxygen transfer in shake flasks using a non-invasive oxygen sensor. *Biotechnol Bioeng*. 2003;84:351–358.
17. Vallejos JR, Brorson KA, Moreira AR, Rao G. Dissolved oxygen and pH profile evolution after cryovial thaw and repeated cell passaging in a T-75 flask. *Biotechnol Bioeng*. 2010;105:1040–1047.
18. Vallejos JR, Uplekar S, Silva JF, Brorson KA, Moreira AR, Rao G. A case study in converting disposable process scouting devices into disposable bioreactors as a future bioprocessing tool. *Biotechnol Bioeng*. 2012;109:2790–2797.
19. Wood J, Mahajan E, Shiratori M. Strategy for selecting disposable bags for cell culture media applications based on a root-cause investigation. *Biotechnol Prog*. 2013. doi: 10.1002/btpr.1802.
20. Skidmore K, Hewitt D, Kao, Y-H. Quantitation and characterization of process impurities and extractables in protein containing solutions using proton NMR as a general tool. *Biotechnol Prog*. 2012;28:1526–1533.
21. Hammond M, Nunn H, Rogers G, Lee H, Marghitoiu AL, Perez L, Nashed-Samuel Y, Anderson C, Vandiver M, Kline S. Identification of a leachable compound detrimental to cell growth in single-use bioprocess containers. PDA J Pharm Sci Technol 2013;67:123–134.
22. Barbaroux M, Sette A. Properties of materials used in single-use flexible containers: requirements and analysis. BioPharm International. November, 2006. Available at: http://www.biopharminternational.com/biopharm/article/articleDetail.jsp?id=423541. Accessed on June 3, 2013.
23. Lighton JRB. Measuring metabolic rates: a manual for scientists. In: Aquatic Oxygen Analysis. New York, New York: Oxford University Press; 2008:47–61.
24. American Fluoroseal Corporation. Permeability of AFC standard bags to N_2, O_2, CO_2, H_2O. Available at: http://www.toafc.com/document-library/technical-information/about-permeability/. Accessed March 30, 2013.
25. Massey LK. Permeability properties of plastics and elastomers. In: Polycarbonate. Norwich, New York: Plastics Design Library; 2003:177–179.
26. Yam KL. The Wiley encyclopedia of packaging technology. In: Barrier Polymers. USA: Wiley; 2010:105.
27. Mokwena KK, Tang J. Ethylene vinyl alcohol: a review of barrier properties for packaging shelf stable foods. *Crit Rev Food Sci Nutr*. 2012;52:640–650.

Manuscript received Jun. 5, 2013, and revision received Oct. 25, 2013.

Extending the non-invasive monitoring concept further, we show how a simple silicone loop in the bioreactor can pick-up oxygen and CO_2 and that coupled with a rate-based monitoring algorithm, provides very accurate measurements of these two critical process parameters linked to respiration. Madhubanti Chatterjee was the Ph.D. student whose primary project was to develop non-invasive neonatal sensors and we used her apparatus to achieve the same capability with cell culture and she was assisted by Shaunak Uplekar and Manohar Pilli.

ARTICLE

BIOTECHNOLOGY and BIOENGINEERING

A Unique Noninvasive Approach to Monitoring Dissolved O_2 and CO_2 in Cell Culture

Madhubanti Chatterjee, Xudong Ge, Shaunak Uplekar, Yordan Kostov, Leah Croucher, Manohar Pilli, Govind Rao

Center for Advanced Sensor Technology, Department of Chemical, Biochemical and Environmental Engineering, University of Maryland, Baltimore County, 1000 Hilltop Circle, Baltimore, Maryland 21250; telephone: 410 455 3415; fax: 410 455 6500; e-mail: grao@umbc.edu or xge1@umbc.edu

ABSTRACT: Although online monitoring of dissolved oxygen (DO) and carbon dioxide (DCO_2) is highly desirable in bioprocesses, small-scale bioreactors are usually not monitored due to the lack of suitable sensors. Traditional electrochemical sensors are usually not used because they are bulky and invasive. Disposable optical sensors are small and only partially invasive, but there are concerns regarding the toxicity of the patch and the phototoxicity of the illuminating light. Here we present a novel, noninvasive, rate-based technique for monitoring DO and DCO_2 in cell cultures. A silicone sampling loop which allowed the diffusion of O_2 and CO_2 through its wall was inserted inside a bioreactor, and then flushed with N_2 until the CO_2 and O_2 inside the loop were completely removed. The gas inside the loop was then allowed to recirculate through gas impermeable tubing to the O_2 and CO_2 sensors. We have shown that by measuring the initial diffusion rate we were able to determine the partial pressures of the two gases in the culture. The technique could be readily automated and measurements could be made in minutes. It was tested in demonstration experiments by growing murine hybridoma cells in a T-flask and a spinner-flask at 37°C. The results were comparable to those measured with commercially available fluorescence-based patch sensors. These results show that the rate-based method is an effective way to monitor small-scale cell cultures. This measurement mechanism can be easily built into disposable cell culture vessels for facile use.

Biotechnol. Bioeng. 2015;112: 104–110.

KEYWORDS: noninvasive; rate-based; sensor; dissolved oxygen; CO_2; cell culture

Introduction

Cell culture refers to the process by which prokaryotic or eukaryotic cells are grown in vitro, ideally under controlled environmental conditions. Cell culture technology finds applications in various areas including investigation of cell biology, relationships between disease causing agents and cells, effects of drugs on cells, genetic engineering and gene therapy. Perturbations in oxygen and CO_2 levels in the culture medium can cause unexpected changes in cell metabolism. It can affect the quality of the product (Pizarro et al., 2009) and be used as a quality indicator. CO_2, a product of cell respiration, influences the metabolic activity of cells. An excess of CO_2 can act as a toxin to the culture and needs to be constantly controlled and observed (Shang et al., 2003). Due to the low solubility of oxygen in water, dissolved oxygen (DO) concentration can become a limiting substrate for cell growth. On the other hand, a dissolved CO_2 (DCO_2) level above 20% is considered to be growth inhibitory for mammalian cells which necessitates an effective aeration strategy during scale-up of bioprocesses. Hence, the careful monitoring of DO and DCO_2 allows assessing the culture conditions (Bambot et al., 1993; Ge et al., 2004; Gupta and Rao, 2003; Harms et al., 2002; Kostov et al., 2001).

Recent developments show the effectiveness of commercial small-scale shaken systems with instrumented controllable micro- and mini-bioreactors where each reactor is designed as a single-use bioreactor (Barrett et al., 2010; Betts and Baganz, 2006; Chen et al., 2009). These systems are often equipped with disposable optical sensors for continuous monitoring or controlling of pH and DO. Optical sensors have a lot of advantages over traditional electrochemical sensors like high sensitivity, easy miniaturization, and free of electromagnetic interference, etc. In addition, the measurement made with patch sensors is only minimally invasive as except for the patch, which is affixed inside the bioreactor, the measurement is made noninvasively through the transparent vessel wall. These characteristics make them an ideal choice as sensors in these small-scale platforms for process optimization (Kensy et al., 2005; Kirk and Szita, 2013; Kostov

G. Rao, Y. Kostov, and X. Ge declare a conflict of interest. The non-invasive sensors used were developed in CAST and commercialized by Fluorometrix.

Correspondence to: Govind Rao or X. Ge

Contract grant sponsor: National Institutes of Health and General Electric
Contract grant number: 1R41HD072901-01
Received 14 May 2014; Revision received 7 July 2014; Accepted 18 July 2014
Accepted manuscript online 31 July 2014;
Article first published online 12 September 2014 in Wiley Online Library (http://onlinelibrary.wiley.com/doi/10.1002/bit.25348/abstract).
DOI 10.1002/bit.25348

et al., 2001; Zanzotto et al., 2004; Zhang et al., 2006). However, despite these advantages, there are concerns regarding the effects of the patch on cells. Even though the sensing dye is immobilized in polymer matrix, there are chances that the dye might leach and cause toxicity. Studies conducted in our lab show that the pH and DO patches have no apparent negative effects on the cellular physiology at the transcript level and on the product quality of hybridoma cell culture (Ge et al., 2006). But the same cannot be predicted for other more sensitive cell lines. Certain cell lines may be too sensitive for use of patch sensors (Ceroni et al., 2011; Quaranta et al., 2012; Yashchuk et al., 2007). Some cell lines may require special treatment, like for adherent cell lines, the patch needs to be treated with protein to make cells adhere to it (Bambrick et al., 2011). This is often a very tedious task, requiring many steps that need to be implemented carefully. In addition, it is not clear if repeated application of radiant energy affects cell or medium conditions, especially in small volumes. Finally, the vast majority of cell culture experiments are performed in simple, disposable vessels such as petri dishes, T-flasks and spinner flasks, which do not lend themselves to being easily monitored.

Here we report an alternative method to monitor DO and DCO_2 in cell cultures. A silicone sampling loop which allowed diffusion of oxygen and CO_2 through its wall was inserted inside the cell culture flask, and then flushed with nitrogen until the CO_2 and O_2 inside the loop were completely removed. The gas inside the loop was then allowed to recirculate through gas impermeable tubing to the DO and DCO_2 sensors. By measuring the initial diffusion rates of these two gases, we were able to determine their partial pressures in the culture. This technique was tested in mammalian cell cultures in a T-flask and a spinner-flask at 37°C. Results demonstrate that the sampling loop did not show any toxicity to the cells, and the measurement results were comparable to those of the aforesaid DO and DCO_2 optical patch sensors.

Materials and Methods

Experimental Setups and Measurement Procedures

The experimental setup is shown in Figure 1. The T-flask contained a silicone rubber sampling loop (Bellco Biotechnology, Vineland, NJ), which was immersed in the culture and used to collect the diffusing gases (CO_2 and O_2) from the cell cultures. The sampling loop is 250 mm long with an inner diameter of 0.32 mm. The diffusing gases from the cultures were transported to the sensors by gas impermeable tubing. The inlet of the sampling loop was connected to either a N_2 supply (N_2 flush stage) or the outlet of the O_2 sensor (recirculation stage) through a 4-way valve. The outlet of the sampling loop was connected to the inlet of the CO_2 sensor through a pump. For making a measurement, the system was first purged with N_2 to drive away any trace of CO_2/O_2 present in the loop. The valve was then switched to recirculation. The CO_2 concentration in the loop was monitored by LI-820 CO_2Analyzer (LI-COR, Lincoln, NE).

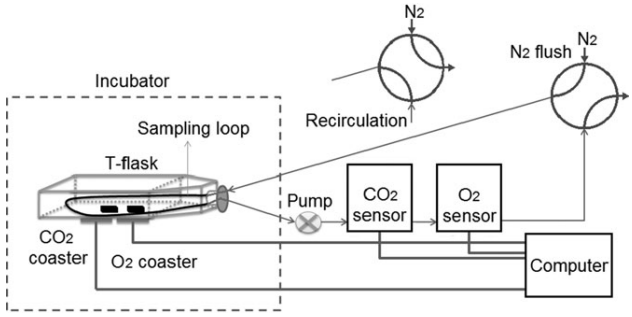

Figure 1. The experimental setup for measuring dissolved oxygen and carbon dioxide in a mammalian cell culture conducted in a T-flask.

The O_2 concentration was monitored by oxy. IQ Panametrics Oxygen Transmitter (GE, St. Marys, PA). The results were recorded on a laptop computer, and the initial diffusion rates were calculated by fitting the concentration profile in the first 2 min to a linear equation.

Calculation of the Initial Diffusion Rate

The mass balance equation for the whole recirculation system including the sampling loop, the inside volumes of the pump and the sensors, and the tubing can be written as follows

$$V\frac{dC}{dt} = kA(C_g - C) \tag{1}$$

where V is the total volume of the system, C is the O_2/CO_2 concentration in the sampling loop, t is time, k is the mass transfer coefficient, A is the total mass transfer area, and C_g is the O_2/CO_2 concentration in the culture. At the beginning of the recirculation ($t=0$), the O_2/CO_2 concentration in the sampling loop is zero. Thus,

$$C_g = \frac{V}{kA}\frac{dC}{dt}\bigg|_{t=0} = a\frac{dC}{dt}\bigg|_{t=0} \tag{2}$$

where $a = V/kA$. From the above equation, it can be seen that the O_2/CO_2 concentration in the culture is linearly proportional to their initial diffusion rate through the silicone sampling loop. By monitoring the O_2/CO_2 concentration in the sampling loop and calculating the initial diffusion rate, their concentration in the culture can be determined. The initial diffusion rate can be calculated by fitting the gas concentration trend line in the first 2 min to a linear equation.

Mammalian Cell Culture

The cell line used in this experiment was non-adherent SP2/0-based myeloma/mouse (2055.5) secreting IgG3 antibody

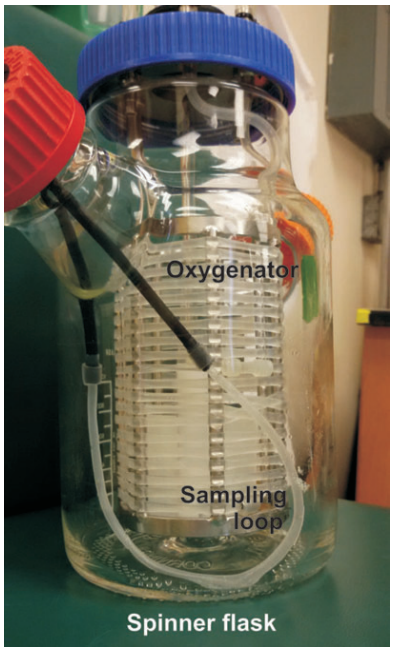

Figure 2. The spinner flask with a coil oxygenator and a silicone sampling loop.

specific for the Neisseria meningitides capsular-polysaccharide (MCPS). One liter of CD Hybridoma GTTM (Invitrogen, Carlsbad, CA) stock media solution supplemented with 8 mM L-glutamine(GIBCO) and 2×10^{-4} % β-mercaptoethanol (v/v) (Sigma, St. Louis, MO) was prepared and stored at 4°C. Fifty milliliters of this media was added into a re-closable T-flask (polystyrene, growth area 115 cm^2, max volume 100 mL, TPP, St. Louis, MO 63088) (Fig. 1). Cells were thawed from liquid nitrogen and introduced into the T-flask to inoculate the culture media at an initial cell concentration of 0.2×10^6 cells/ml. Figure 2 shows the spinner flask with a coil oxygenator and a silicone sampling loop. The sampling loop is the same size as that used in the T-flask. For the culture conducted in the spinner-flask, 825 mL of media was added and inoculated at an initial cell concentration of 0.25×10^6 cells/mL. The cell cultures were monitored in an incubator at 37°C and 5% CO_2 for one week. DO and DCO_2 were measured by the patch sensors every 5 min and the data were stored on a laptop computer. The rate-based measurement was made every 2–3 h by purging N_2 and switching the 4-way valve to the recirculation mode.

Optical Measurement System

The optical patch sensor system is comprised of a sensing patch and electronics used to illuminate the patch and detect the fluorescence. The measurement procedures were programmed using Lab VIEW (National Instruments). The DO patch consists of four layers (Bambrick et al., 2011; Ge et al., 2006; Tolosa et al., 2002). The upper layer is an optical isolator made up of acrylic copolymer. The immediate lower sensing layer is made up of the fluorescent dye tris(4,7-diphenyl-1,10phenanthroline) ruthenium(II) dichloride immobilized in a silicone matrix. This layer is held by an underlying third polyester layer, which is attached to the T-flask by a fourth adhesive layer. The CO_2 patch also has four layers (Ge et al., 2003; Ge et al., 2004). The second sensing layer contains a pH sensitive dye immobilized in a silicone rubber together with an organic base for CO_2 sensing. The top optical isolator, the polyester support layer, and the adhesive layer are all the same as the DO patch. These patches were prepared in our lab. Both DO and DCO_2 patches were autoclaved at 120°C for 25 min and then placed on the inside of the T-flask or the spinner-flask with sterile forceps by removing the adhesive liner that protects the adhesive layer from the patches. The electronics built in the DO coaster contains a blue light emitting diode for photo-excitation. The CO_2 coaster has a blue light emitting diode and a violet light emitting diode. Both coasters have a photodiode for light detection. The coaster systems were manufactured by Fluorometrix Corporation(currently marketed by Scientific Industries, Inc.). The LabVIEW program was used for continuous data monitoring online.

Sensor Calibration

The rate-based method was calibrated at 37°C by bubbling the gas mixture through the cell culture media. The gas mixtures with desired O_2/CO_2 concentrations were obtained by mixing pure N_2 and air/CO_2 through two flowmeters (FM4332 and FM4333, Advanced Specialty Gas Equipment Corp., South Plainfield, NJ). After the gas mixture reached equilibrium with the media, the O_2/CO_2 diffusion rate across the sampling loop was measured following the procedure described in the Experimental setups and measurement procedures. The diffusion rate was measured at 0.0%, 25.0%, 50.0%, 75.0%, and 100.0% (air saturation) in the bubbling gas stream for O_2, and 0.0%, 3.0%, 5.0%, 10.0%, and 20.0% for CO_2.

Results and Discussions

The rate-based method described in this paper measures the concentrations of DO and DCO_2 in cell cultures by measuring their initial diffusion rates across a silicone sampling loop immersed in the cell culture media. Since each measurement starts with purging the sampling loop with N_2 to remove the O_2/CO_2 originally present in the system, the O_2/CO_2 concentration in the sampling loop is zero before the recirculation begins. During the recirculation, O_2/CO_2 diffuses across the sampling loop and its concentrations in the system increase with time. After sufficient time, the O_2/CO_2 concentrations in the sampling loop will reach equilibrium with the DO/DCO_2 in the media. Figure 3 shows the typical O_2/CO_2 concentration profiles in the sampling loop during the measurement. It can be seen that

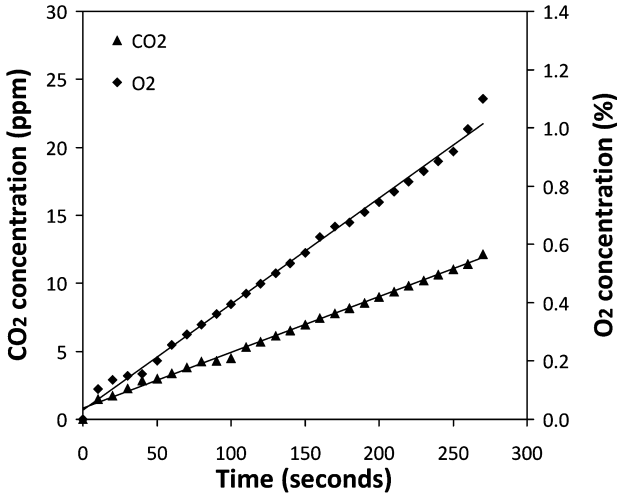

Figure 3. Typical O_2/CO_2 concentration profiles during a single measurement.

the O_2/CO_2 concentrations in the sampling loop increase linearly with time in the first few minutes after recirculation commences. By fitting the concentration profile in the first 2 min to a linear equation, the initial diffusion rate can be obtained.

Figures 4 and 5 show the correlation of the initial diffusion rates across the sampling loop vs. the concentrations in the bubbling gas stream. It can be seen that the O_2/CO_2 concentration in the bubbling gas stream is linearly proportional to the initial diffusion rate. The slope of the line is determined by the volume of the system, the surface area of the sampling loop and the mass transfer resistance of the sampling loop to the O_2/CO_2. Figures 4 and 5 show that the slope of the line is a constant at a constant temperature for a given system. Thus, by measuring the initial O_2/CO_2 diffusion rate across the sampling loop, the O_2/CO_2 level in the media can be obtained.

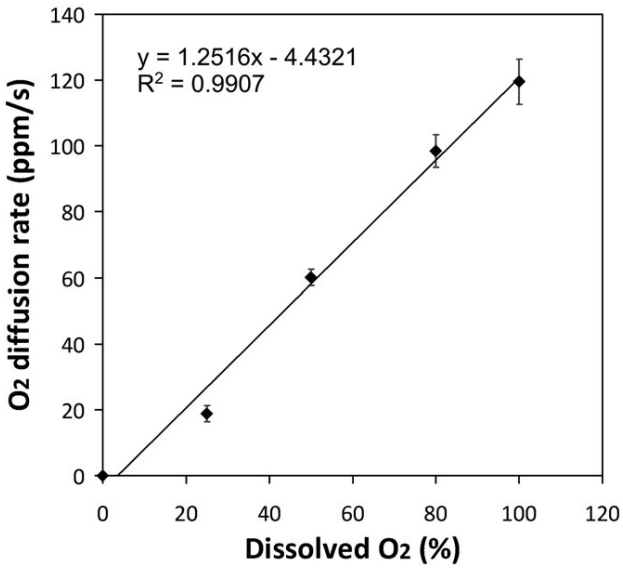

Figure 4. The initial diffusion rate of O_2 across the sampling loop vs. the readings of the DO patch. The error bars are the standard deviations of three repeated measurements.

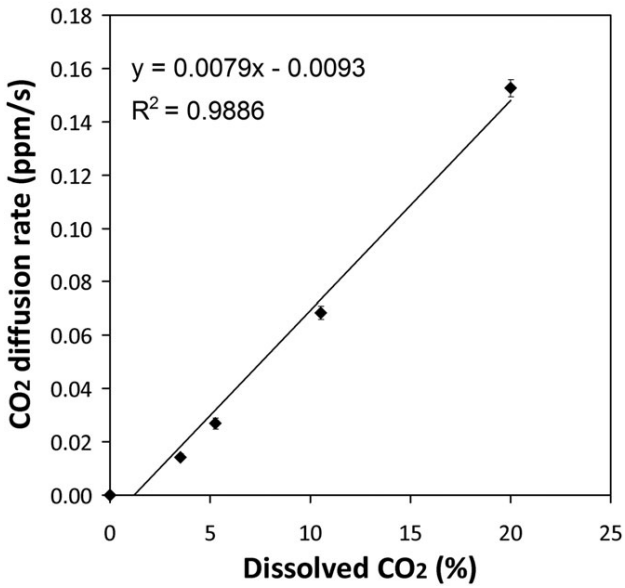

Figure 5. The initial diffusion rate of CO_2 across the sampling loop vs. the readings of the DCO_2 patch. The error bars are the standard deviations of three repeated measurements.

After calibration, the system was tested in mammalian cell cultures under static and agitated conditions. For this purpose, a T-flask and a spinner-flask were respectively used in an incubator maintained at 37°C. The culture was monitored for seven days. Figure 6 shows the DO and DCO_2 profiles in the T-flask measured by the rate-based method as well as by the DO and DCO_2 patch sensors. Figure 7 shows the DO and DCO_2 profiles in the spinner-flask measured by the rate-based method as well as by the DO and DCO_2 patch sensors. The cell density and viability profiles in the spinner-flask cell culture is shown in Figure 8. It can be seen that from the beginning of the cultures until 70 h, the cultures were growing and consumed increasingly more O_2. Both DO sensors showed the gradual decrease in DO concentration in the cultures. As expected, both DCO_2 sensors showed a gradual increase in DCO_2 concentration during this stage. At late stage of the cultures, the cells began to die and consumed proportionately less O_2. In both cases, the DO concentration in the cultures gradually increased while the DCO_2 concentration in the culture began to gradually decrease. O_2 limitation is a common phenomenon in microbial cell

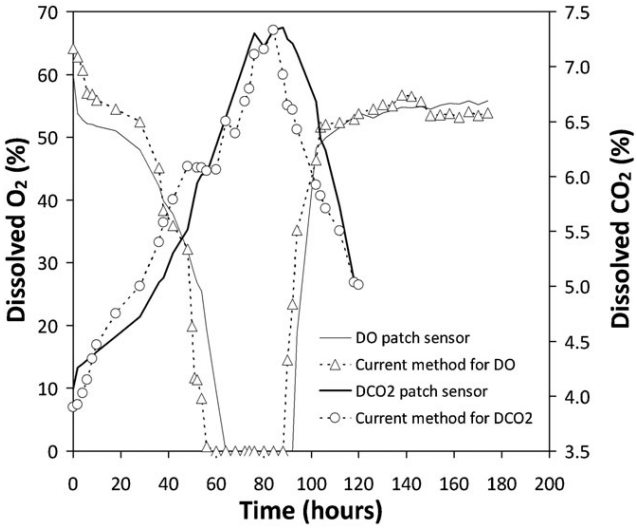

Figure 6. The DO and DCO_2profiles measured by the rate-based method during the mammalian cell culture in a T-flask as compared to the readings of DO and DCO_2 patch sensors.

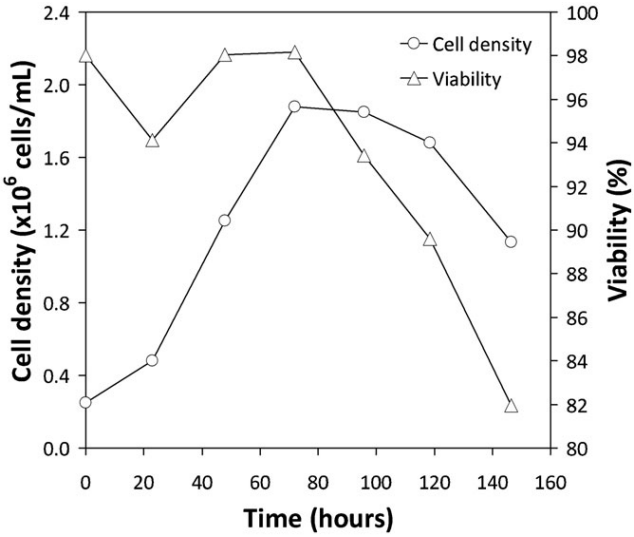

Figure 8. The density and viability of the cells in the spinner-flask cell culture.

culture even with vigorous shaking. Although mammalian cells do not divide as fast as microbial cells and consume less O_2, the process still became O_2-limited between 60–90 h for the T-flask culture and between 58–102 h for the spinner-flask culture due to the low solubility of O_2. Despite slow stirring, the O_2-limiting condition lasted longer in the spinner-flask due to the smaller specific mass transfer area for oxygen. Throughout the process, the rate-based approach followed the patch sensor quite well. The correlation coefficients between the rate-based results and the patch sensor results for the T-flask culture are 0.947 and 0.953 for DO and DCO_2, respectively. The correlation coefficients between the rate-based results and the patch sensor results for the spinner-flask culture are both 0.999 for DO and DCO_2. The readings of the two different methods were more consistent for the spinner-flask as the media was better mixed due to slow stirring. These results demonstrate that the noninvasive rate-based method is an effective way to monitor small-scale bioreactors.

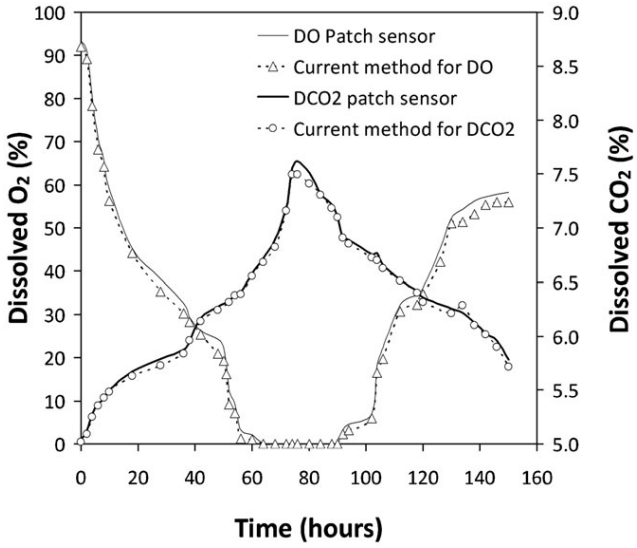

Figure 7. The DO and DCO_2 profiles measured by the rate-based method during the mammalian cell culture in a spinner-flask as compared to the readings of a DO and DCO_2 patch sensors.

The major advantage of the rate-based method described here is that it is completely noninvasive. There is no direct sensor-media contact except the biocompatible silicone sampling loop. At the early stage of the culture, the cell viability was as high as 98% (Fig. 8), showing that the silicone sampling loop did not affect the cells. Electrochemical probes are not commonly used in small-scale bioreactors mainly due to their invasive nature. Patch sensors have some advantages over traditional electrochemical probes in that they are usually disposable and only partially invasive. However, there are concerns regarding the effect of the patches on the cells, especially extremely sensitive cells. Media components such as vitamins may also be deteriorated if exposed to the illuminating light for a long time. We have reported a completely noninvasive approach to monitoring the DO and DCO_2 in disposable small-scale cell culture vessels based on the diffusion through the permeable vessel walls (Gupta et al., 2014). This approach is noninvasive and applicable to monitoring culture processes of extremely sensitive cells. However, this method depends on the mass transfer equilibrium across the vessel wall. The response time is relative long (>30 min) due to the additional mass transfer

resistance of the wall. Thus, this method can only be used in slowly growing cell cultures. Comparatively, the rate-based method described here does not require attainment of mass transfer equilibrium. On the contrary, only the initial diffusion rate in the first few minutes is measured. Thus, the measurements can be made much faster. Although all the measurements made in this work were done manually by switching a 4-way valve, the measurement procedure can be easily automated and each measurement can be made in 2 min. Additionally, the silicone (or other suitable permeable biocompatible material such as Teflon) can be easily built into disposable small-scale bioreactors like T-flasks, cell culture bags, etc. A single instrument could easily be multiplexed and built into the incubator. These disposable small-scale cell culture platforms can be put to immediate use for noninvasive monitoring of DO and DCO_2 in the culture and allow for greater precision in experimental design. For instance, one would no longer have to sample a cell population for deciding when to split cells or feed media- it could be done by simply observing the respiratory profile. In other cases, data on cellular respiration can be continuously obtained- for example, one may see patterns shift during stem cell differentiation (Cechin et al., 2014). As the sampling loop was designed only for single use and the culture lasted less than a few days, sensor drift caused by biofouling was not found. We will investigate if the sensor is affected by biofouling in long-term cell culture processes.

One of the limitations for the described approach is that it cannot measure the process continuously. Because the sensor measures the process parameters periodically, the response time of the sensor equals to the time needed for each measurement, which is 2 min in this case. For cell cultures with high oxygen uptake rates, the DO concentration may decrease rapidly while being measured. In this case, the measured initial diffusion rate may be overestimated or delayed. Thus, for fast-changing processes, this approach may not be fast enough, especially for control purposes. Additionally, as a sampling loop has to be inserted into the culture, this technique may not be applicable to microbio reactors like multi-well plates. Another limitation for the described approach is that each measurement can deplete a small amount of O_2 from the culture by diffusion through the silicone sampling loop. This is undesirable because it can lower the DO in the culture and inhibit the growth of the cells. So, the sampling loop should be so designed that each measurement takes away only negligible amount of O_2. The sampling loop should be minimally permeable but permeable enough to catch the trend of diffusion.

Conclusion

We present a novel, rate-based technique for monitoring DO and DCO_2 in cell cultures. By measuring the initial diffusion rate across a silicone sampling loop immersed in the culture media, the partial pressures of these two gases in the culture can be determined. This technique can be readily automated and measurements can be made in minutes. Demonstration experiments conducted with murine hybridoma cells in a T-flask and a spinner-flask at 37°C show that it can provide comparable results with fluorescence-based patch sensors. It is noninvasive and especially useful for cultures of sensitive cells. The described measurement mechanism can be easily built in disposable cell culture vessels for immediate use of these sensors.

The authors acknowledge the support of National Institutes of Health through STTR Grant # 1R41HD072901-01 and General Electric.

References

Bambot SB, Holavanahali R, Lackowicz JR, Carter JM, Rao G. 1993. Phase fluorometric sterilizable optical sensor. Biotechnol Bioeng 43: 1139–1145.

Bambrick LL, Kostov Y, Rao G. 2011. In vitro cell culture pO2 is significantly different from incubator pO2. Biotechnol Prog 27:1185–1189.

Barrett TA, Wu A, Zhang H, Levy MS, Lye GJ. 2010. Microwell engineering characterization for mammalian cell culture process development. Biotechnol Bioeng 105(2):260–275.

Betts JI, Baganz F. 2006. Miniature bioreactors: Current practices and future opportunities. Microbial Cell Factories 5:21.

Cechin S, Alvarez-Cubela S, Giraldo JA, Molano RD, Villate S, Ricordi C, Pileggi A, Inverardi L, Fraker CA, Domínguez-Bendala J. 2014. Influence of in vitro and in vivo oxygen modulation on β cell differentiation from human embryonic stem cells. Stem Cells Transl Med 3(3):277–289.

Ceroni P, Leebdev AY, Marchi E, Yuan M, Esipova TV, Beigamini G, Wilson DF, Busch TM, Vinogradov SA. 2011. Evaluation of phototoxicity of dendritic porphyrin-based phosphorescent oxygen probes: An in vitro study. Photochem Photobiol Sci 10(6):1056–1065.

Chen A, Chitta R, Chang D, Anianullah A. 2009. Twenty-four well plate miniature bioreactor system as a scale-down model for cell culture process development. Biotechnol Bioeng 102(1):148–160.

Ge X, Hanson M, Shen H, Kostov Y, Brorson KA, Frey DD, Moreira AR, Rao G. 2006. Validation of an optical sensor-based high through put bioreactor system for mammalian cell culture. J Biotechnol 122: 293–306.

Ge X, Kostov Y, Rao G. 2003. High-stability non-invasive autoclavable naked optical CO2 sensor. Biosens Bioelectron 18(7):857–865.

Ge X, Kostov Y, Rao G. 2004. Low-cost noninvasive optical CO_2 sensing system for fermentation and cell culture. Biotechnol Bioeng 89(3): 329–334.

Gupta A, Rao G. 2003. A study of oxygen transfer in shake flasks using a non-invasive oxygen sensor. Biotechnol Bioeng 84(3):351–358.

Gupta PA, Ge X, Kostov Y, Rao G. 2014. A complete noninvasive method of dissolved oxygen monitoring in disposable small-scale cell culture vessels based on diffusion through permeable vessel walls. Biotechnology Progress 30(1):172–177.

Harms P, Kostov Y, Rao G. 2002. Bioprocess monitoring. Current Opinion in Biotechnology 13:124–127.

Kensy F, John GT, Hofmann B, Buechs J. 2005. Characterisation of operation conditions and online monitoring of physiological culture parameters in shaken 24-well microtiter plates. Bioprocess and Biosyst Eng 28: 75–81.

Kirk TV, Szita N. 2013. Oxygen transfer characteristics of miniaturized bioreactor systems. Biotechnol Bioeng 110:1005–1019.

Kostov Y, Harms P, Randers-Eichhorn L, Rao G. 2001. Low-cost microbioreactor for high-throughput bioprocessing. Biotechnol Bioeng 72(3):346–352.

Pizarro SA, Dinges R, Adams R, Sanchez A, Winter C. 2009. Bio manufacturing process analytical technology (PAT) application for downstream processing: Using dissolved oxygen as an indicator of product quality for a protein refolding reaction. Biotechnol Bioeng 104(2):340–351.

Quaranta M, Borisov SM, Klimant I. 2012. Indicators for optical oxygen sensors. Bioanal Rev 4(2–4):115–157.

Shang L, Jiang M, Ryu CH, Chang HN, Cho SH, Lee JW. 2003. Inhibitory effect of carbon dioxide on the fed-batch culture of ralstoniaeutropha: Evaluation by CO_2 pulse injection and autogenous CO_2 methods. Biotechnol Bioeng 83(3):312–320.

Tolosa L, Kostov Y, Harms P, Rao G. 2002. Noninvasive measurement of dissolved oxygen in shake flasks. Biotechnol Bioeng 80(5):594–597.

Yashchuk VM, Kudrya VY, Losytskyy MY, Tokar VP, Yarmoluk SM, Dmytruk IM, Prokopets VM, Kovalska VB, Balanda AO, Kryvorotenko DV, Ogul'chansky TY. 2007. The optical biomedical sensors for DNA detection and imaging based on two-photon excited luminescent styryl dyes: Phototoxic influence on the DNA. Proc SPIE 6796: doi: 10.1117/12.778096.

Zanzotto A, Szita N, Boccazzi P, Lessard P, Sinskey AJ, Jensen KF. 2004. Membrane-aerated microbioreactor for high-throughput bioprocessing. Biotechnol Bioeng 87:243–254.

Zhang Z, Szita N, Boccazzi P, Sinskey AJ, Jensen KF. 2006. A well-mixed, polymer-based microbioreactor with integrated optical measurements. Biotechnol Bioeng 93:286–296.

Finally, Viki Chopda joined the lab as a postdoc. Working with Tim Holzberg, a Master's student and Brandon Folio, an undergraduate, we were able to push the CO_2 sensor application and demonstrate that the non-invasive sensor could be used to automatically measure the CO_2 with simple components and also realize CO_2 control in a minibioreactor. Michael Tolosa helped setup all the hardware that was critical to make the measurements.

Received: 18 July 2019 | Revised: 10 December 2019 | Accepted: 13 December 2019

DOI: 10.1002/bit.27253

ARTICLE

BIOTECHNOLOGY BIOENGINEERING WILEY

Real-time dissolved carbon dioxide monitoring I: Application of a novel in situ sensor for CO_2 monitoring and control

Viki R. Chopda | Timothy Holzberg | Xudong Ge | Brandon Folio | Michael Tolosa | Yordan Kostov | Leah Tolosa | Govind Rao

Department of Chemical, Biochemical and Environmental Engineering, Center for Advanced Sensor Technology, University of Maryland, Baltimore, Maryland

Correspondence
Govind Rao, Department of Chemical, Biochemical and Environmental Engineering, Center for Advanced Sensor Technology (CAST), University of Maryland, Baltimore, MD 21250.
Email: grao@umbc.edu

Funding information
Bill and Melinda Gates Foundation

Abstract

Dissolved carbon dioxide (dCO_2) is a well-known critical parameter in bioprocesses due to its significant impact on cell metabolism and on product quality attributes. Processes run at small-scale faces many challenges due to limited options for modular sensors for online monitoring and control. Traditional sensors are bulky, costly, and invasive in nature and do not fit in small-scale systems. In this study, we present the implementation of a novel, rate-based technique for real-time monitoring of dCO_2 in bioprocesses. A silicone sampling probe that allows the diffusion of CO_2 through its wall was inserted inside a shake flask/bioreactor and then flushed with air to remove the CO_2 that had diffused into the probe from the culture broth (sensor was calibrated using air as zero-point calibration). The gas inside the probe was then allowed to recirculate through gas-impermeable tubing to a CO_2 monitor. We have shown that by measuring the initial diffusion rate of CO_2 into the sampling probe we were able to determine the partial pressure of the dCO_2 in the culture. This technique can be readily automated, and measurements can be made in minutes. Demonstration experiments conducted with baker's yeast and *Yarrowia lipolytica* yeast cells in both shake flasks and mini bioreactors showed that it can monitor dCO_2 in real-time. Using the proposed sensor, we successfully implemented a dCO_2-based control scheme, which resulted in significant improvement in process performance.

KEYWORDS

bioprocess monitoring and control, dissolved carbon dioxide, mini bioreactor, process analytical technology, shake flask, surface aeration intensification

1 | INTRODUCTION

Carbon dioxide (CO_2) is an inevitable by-product of respiration processes and as such always present in aerobic and anaerobic bioprocesses. This holds true for the fermentative production of various range of products using microbes or mammalian cells. CO_2 and its hydrated counterpart HCO_3^- are well known to interact with cellular metabolism via several ways such as (a) acidifying internal pH, (b) their role as substrate or product in various chemical reactions, (c) altering physiological properties of proteins (Blombach & Takors, 2015). In fact, it is reported that an excess of CO_2 can act as a toxin to the culture and needs to be constantly controlled and observed (Shang et al., 2003). High dissolved carbon dioxide (dCO_2) also leads to decreased glucose, lactate, and glutamine specific metabolite rates. Increased dCO_2 causes perturbation in intracellular pH, thereby affecting pH-dependent enzymatic

reactions. For example, phosphofructokinase, which is a rate-limiting enzyme in the glycolytic pathway, is inhibited by low intracellular pH. Thus, dCO_2 has a direct impact on metabolic pathways (McIntyre & McNeil, 1997).

A dCO_2 level above 20% is reported to be a growth inhibitory factor for certain microbial as well as mammalian cells which necessitates an effective aeration strategy during scale-up of bioprocesses (Blombach & Takors, 2015). However, excessive stripping of dCO_2 is also detrimental to cell growth, which suggests that there is likely an optimal level of dCO_2 for cell culture (Mostafa & Gu, 2003). The organism used for production, the product of interest and the required quality of the product will certainly determine this optimal dCO_2 value. The concentration of dissolved oxygen (DO) and carbon dioxide vary over time due to respiration of the cells and hence these parameters can give the true metabolic signature of the culture broth if monitored in real-time. In addition, as an intrinsic property, partial CO_2 pressure of shake flask, benchtop lab-scale bioreactor, and the production bioreactor will differ significantly as it is an inherent consequence of high absolute pressure and mixing conditions. Hence, dCO_2 concentrations must be analyzed carefully and thoroughly during scale-up and technology transfer activities (Matsunaga, Kano, Maki, & Dobashi, 2009; Mitchell-Logean & Murhammer, 1997; Mostafa & Gu, 2003). The real-time dCO_2 values will be useful not only for optimizing but also for reproducing culture conditions independent of scale (Ahuja, Shilpa Jain, & Ram, 2015). Thus, the careful monitoring and control of DO and dCO_2 are needed in assessing the culture conditions (Ge, Kostov, & Rao, 2003; Gupta & Rao, 2003).

With Food and Drug Administration's process analytical technology (PAT) drive and rigorous quality requirements especially in biologics manufacturing (Food and Drug Administration, 2004), the attention towards continuous process supervision and real-time control is greater than ever (Chopda, Gomes, & Rathore, 2016; Gomes, Chopda, & Rathore, 2015; Gomes, Chopda, & Rathore, 2018). Despite this fact, small-scale processes are still lagging in terms of generating real-time data due to a lack of suitable online sensors. Traditional electrochemical sensors are usually not used because they are bulky and invasive. Disposable optical sensors are small and only partially invasive, but there are concerns regarding the toxicity of the patch and the phototoxicity of the illuminating light (Ge & Rao, 2012; Ge, Kostov, & Rao, 2005; Gupta & Rao, 2003). Over the past decade, new sensor technologies have become available to monitor the performances of shake flasks and small-scale fermentation systems (Table 1). Among these, the oxygen transfer rate (OTR) device and respiration activity monitoring system (RAMOS) measure OTR and respiration activities (not direct O_2 and CO_2 concentration) in the headspace of a shake flask and not the dissolved CO_2. Furthermore, these systems use two pipes inserted instead of culture plug with ports for inlet and outlet for aeration and exhaust, respectively (Anderlei & Büchs, 2001; Anderlei, Zang, Papaspyrou, & Büchs, 2004; Scheidle, Klinger, & Büchs, 2007; Seletzky et al., 2007). Another system, BCpreFerm can measure O_2 and CO_2 concentration

TABLE 1 Monitoring devices for shake flask cultures

Phase	Sensor name/description	References
Liquid (culture broth)	SENBIT system—uses Clarke type electrode to measure O_2 and pH	Vasala et al. (2006)
	Fluorescent illuminator & detector—immobilized optical sensor used to monitor O_2 and pH	Flitsch, Ladner, Lukacs, and Büchs (2016) Gupta and Rao (2003) Schneider, Schütz, John, and Heinzle (2010) Tolosa et al. (2002) Wittmann, Kim, John, and Heinzle (2003)
	Bioprocess monitoring 60—measures O_2 and pH	Kuhner: BPM-60
	InPro®5000, Mettler-Toledo	Chen et al. (2008) Srinivasan, Feng, and Lin (2012)
	Fiber optic dCO_2 sensor-YSI 8500	Lander and Kruglyak (1995)
	Kurt-Schwabe-Institut Meinsberg electrochemical CO_2 probe	Frahm et al. (2002)
	In situ sensor—diffusion rate-based measurement	Chatterjee et al. (2015)
Gas (headspace)	OTR device—measures OTR in the headspace	Anderlei and Büchs (2001)
	RAMOS—measures OTR in the headspace with penetrating the optical sensor	Anderlei et al. (2004)
	BCpreFerm system for shake flasks—dual CO_2 and O_2 sensors that attach to two outlets on a tri-outlet shake flask. Infrared-based measurements	BlueSens gas sensor GmbH
Liquid and gas	Used RAMOS to measure in the headspace and rotating flexi-tube optical sensor to monitor dissolved O_2, CO_2, and culture pH	Hansen, Jacob, Luchterhand, and Büchs (2012)
	Fluorescence-based method for monitoring CO_2 and O_2 in the culture broth and in the headspace of an Erlenmeyer flask and broth pH as well	Ge and Rao (2012)
	Circulation direct monitoring and sampling system—a system that continuously extracts and measures liquid (by electrode) and gas-phase samples	Takahashi et al. (2017) Takahashi and Aoyagi (2018a, 2018b, and 2018c)

Abbreviations: dCO_2, dissolved carbon dioxide; OTR, oxygen transfer rate; RAMOS, respiration activity monitoring system.

in the headspace of shake flask with a culture plug but not the dissolved CO_2 (BlueSens gas sensor GmbH). In all these three systems sensors or a measuring device rotates with the shake flask which may sometime cause drifts in the signal. The fluorescence-based method has been reported to measure O_2 and CO_2 in the headspace as well as in culture broth. The effect of fluorescent pigment has always been debated (Ge et al., 2005; Gupta & Rao, 2003). Takahashi et al. developed a circulation-based direct monitoring and sampling system with a circulation bypass component in the measuring site tilted in such a way that cells do not accumulate and the air bubbles are well dispersed (Takahashi & Aoyagi, 2018a, 2018b; Takahashi, Sawada, & Aoyagi, 2017). However, it is critical to prevent cells from clumping to avoid the clogging of the liquid circulation part.

In this article, we describe a novel method that correlates the concentration of dissolved CO_2 in culture broth with the initial diffusion rate of the CO_2 across a gas-permeable tubing. Silicone tubing was fully immersed in the culture medium through which CO_2 gas diffuses which was then circulated to a CO_2 sensor equipped with a custom-designed microcontroller pump and valves, located outside of the cell culture vessel. We have decided to select two model organisms for this study having distinct respiration activities. Baker's yeast was selected because it is well-known for its Crabtree effect. Through its Crabtree or overflow metabolism, yeast cells can switch from purely oxidative metabolism to a respiro-fermentative metabolism even under fully aerobic conditions as soon as glucose exceeds the critical concentration of about 0.1 g/L (Kasperski & Mis kiewicz, 2008). On the other hand, we have also selected a recombinant yeast *Yarrowia lipolytica P01g-Leu*, which is Crabtree-negative organism. The details of strain and culture conditions are given in the respective section.

The implementation of our novel sensor in monitoring dCO_2 in shake flask and in mini bioreactors was demonstrated using yeast fermentation as a case study. We were able to demonstrate the distinct dissolved CO_2 profile for these selected two organisms and further demonstrated a control strategy to control the metabolism. We believe that the enabling PAT at such small scale of operation will allow users to develop a scaled-down model of pilot-scale bioreactor operations. This will not only make the process development cost-effective and faster but also expected to follow a smoother transition of scale-up and technology transfer activities.

2 | MATERIALS AND METHODS

2.1 | Dissolved CO_2 sensor

This novel method correlates dCO_2 concentration in cell culture with the initial diffusion rate of the CO_2 across gas-permeable silicone tubing, which was provided by Sartorius (Goettingen, Germany) and originally used for aeration in bioreactors (BB-8848017). Silicone tubing (ranging from 4 to 6 cm in length) allows for the diffusion of CO_2 across its wall when fully immersed in the culture medium and connected to a CO_2 sensor (K30 CO_2 sensor from CO2Meter.com). The sensor is a fast-response infrared CO_2 sensor, which has a measurement range of 0–10,000 ppm with a precision of 20 ppm. The sensor is designed to output digitized values in serial format (RS 232). It is connected to a computer via serial-to-USB converter (i.e., FT232 from Future technology). The system is equipped with two 3-way valves and a pump, which are located outside of the cell culture vessel. The gas pump is a microdiaphragm pump produced by Parker (Hollis, NH), which provides a flow rate of up to 800 ml/min. The 3-way valves are solenoid valves produced by the Lee Company (Westbrook, CT). They require only a very small power to operate (~3 mWh/actuation), have small dimensions (<2″ in any direction). Versilon F-5500-A tubing, which is reported to have significantly low CO_2 diffusivity, was used to connect the system components together (shown as black lines in Figures 1–3). The electronics for activating the valves and digitizing the readings of the sensors are controlled by a dedicated microcontroller, which is also responsible for communicating the data to the computer (Ge et al., 2018). The program is written in LabVIEW, which controls the valves, reads the sensors, logs the data, and calculates the slopes in real-time. All the time intervals are user adjustable so as to allow flexibility of the software.

Before a measurement cycle, ambient air outside the culture vessel was pumped into the system (Air IN) and allowed to flow out through a separate outlet (Air OUT). This process purges any CO_2 in the tubing system and returns it to normal atmospheric levels (~400 ppm). After the purging process is complete, the valves close, allowing CO_2 from the culture to diffuse across the gas-permeable

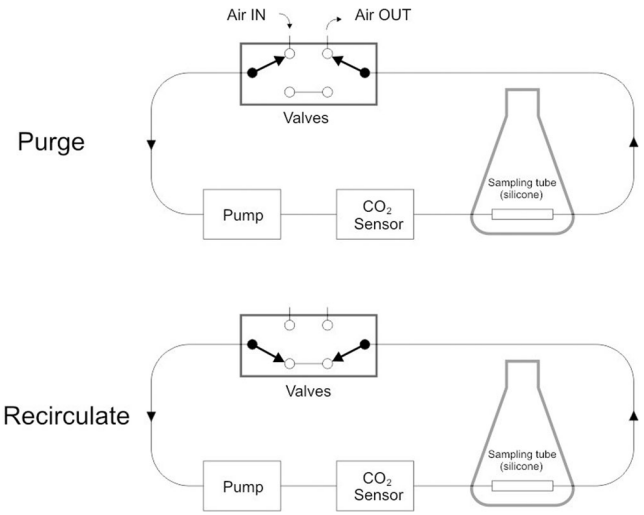

FIGURE 1 Illustration of the operational working of the dissolved carbon dioxide sensor. In the purge mode, the ambient air outside the culture vessel was pumped into the system (Air IN) and allowed to flow out through a separate outlet (Air OUT). This process purges any CO_2 in the tubing system and returns it to normal atmospheric levels (~400 ppm). On the other hand, in recirculation mode, the Air IN valve closes, allowing CO_2 from the culture to diffuse across the gas-permeable tubing into the system. The pump recirculates the diffused gas through the CO_2 sensor

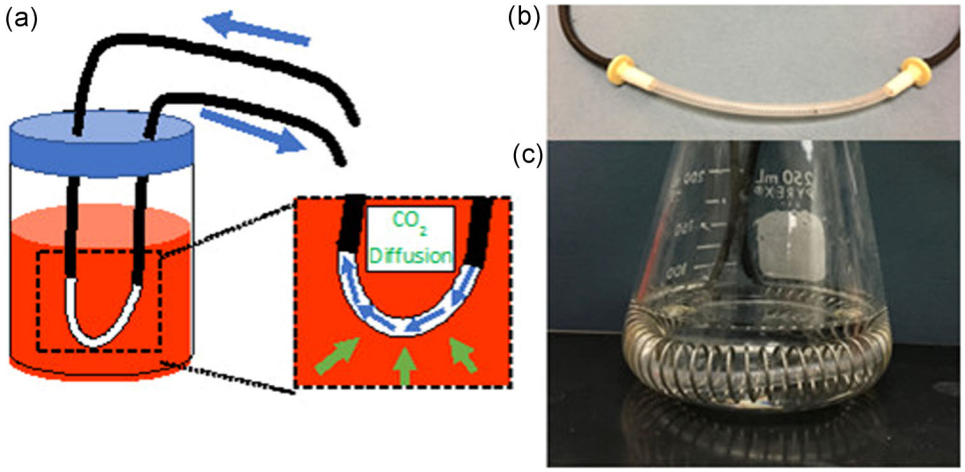

FIGURE 2 (a) Close-up view of airflow within the silicone sampling tube for dissolved carbon dioxide measurements inside a flask. CO_2 in the culture diffuses across the silicone sampling tube (green arrows) and enters the flow of air (blue arrows), which comes out of the sampling tube and returns back to the sensor. (b) Close-up view of assembled silicone sampling tube with spring inside to prevent kinking. (c) Assembled silicone sampling tube ready for measurement inside a shaker flask. The coil surrounding it prevents the tube from shifting while the flask is being shaken [Color figure can be viewed at wileyonlinelibrary.com]

tubing into the system. The pump recirculates the diffused gas through the CO_2 sensor. The purge and recirculate modes of operation and sensor setup are illustrated in Figure 1. The measurement principle and the operation procedure have been described in detail previously (Chatterjee et al., 2015).

Figure 2 shows the sensor design for use in a simple cell culture vessel (such as a shake flask), while Figure 3 shows the design for use in a mini bioreactor. The major difference between the two setups is in the direction of airflow through the silicone tubing. We have used a standard Erlenmeyer shake flask of 250 ml capacity with a sponge cap and 25 mm shaking diameter. For a shake flask, the silicone tubing was connected to the gas-impermeable Versilon tubing with simple luer fittings. A spring was inserted through the tube to avoid blockages, bents or kinks.

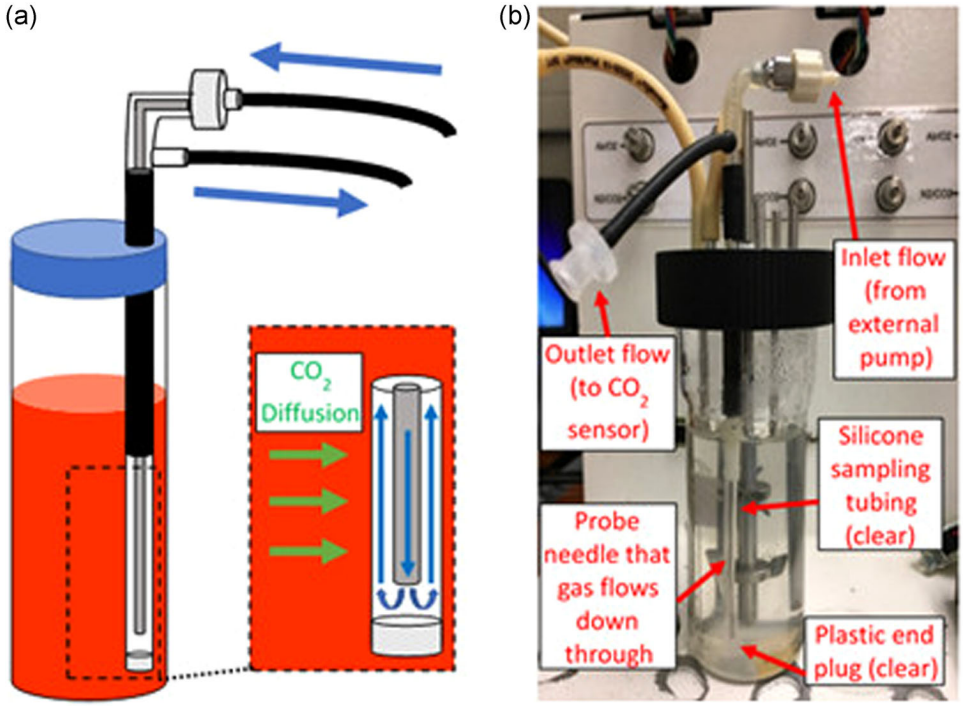

FIGURE 3 (a) Close-up view of airflow within the probe for dissolved carbon dioxide measurements inside a mini bioreactor. CO_2 in the culture diffuses across the silicone sampling tube (green arrows) and enters the flow of air (blue arrows), which comes out of the needle and back up into the probe housing before exiting out of the side outlet. (b) Measurement probe inside an assembled mini bioreactor vessel [Color figure can be viewed at wileyonlinelibrary.com]

For shake flask, aseptic sampling was carried out through a Versilon tube inserted in it so as to have minimal disturbance in O_2 and dCO_2 balance, which might change significantly if sampling carried out by conventional way of opening the culture plug (Takahashi and Aoyagi, 2018c). A cylindrical mini bioreactor (2.5 cm inner diameter) of 100 ml capacity was used for controlled feeding experiments. For the mini bioreactor, a probe construct was used that is similar in design to typical PAT probes used in larger bioreactors. Figure 3 outlines the direction of airflow through the top of the probe, down through a needle that is surrounded by silicone tubing, back up through the needle housing, and out the side of the probe. This allows for diffusion rate measurements to be collected in a narrow culture vessel with a low volume.

2.2 | Sensor characterization

After the prototype was built, the characteristics of the sensor such as sensitivity, the limit of detection (LOD), and so forth were studied. To avoid the accumulation of CO_2 in the system, the purge stage should last long enough. After some initial experiments, the following durations were determined to be the most appropriate: 30 s for the purge stage and 60 s for the recirculation stage. During the recirculation stage, the sensors were read every 2 s and the readings were recorded in the computer. The initial diffusion rate (the slope of the rising CO_2 concentration) was calculated by fitting the readings to a linear equation 15 s after the beginning of the recirculation and when there was a streak of five consecutive rising readings. After that, the slope was updated for every new sensor read until the end of the recirculation stage. The measurement cycle would repeat until it was stopped by pressing the stop button.

The calibration of the sensor was done by pumping in a known concentration of CO_2 into a flask filled with cell culture media at the same temperature and agitation speed as what will be used for cell growth. The sensor was calibrated up to 20% dCO_2 because most bioprocesses generally have dCO_2 levels lower than that. The sensing range of the sensor can be extended to 100% dCO_2 if a smaller size or less permeable sampling tube is used. For zero calibration point, the sensor was flushed with air and the reading of the sensor was considered as the baseline of the signal. The gas mixtures with desired CO_2 concentrations were obtained by mixing pure CO_2 and air through two mass flow controllers (Model #: 32907-63; Cole-Parmer Instrument Company, Vernon Hills, IL). After the gas mixture reached equilibrium with the media, the CO_2 diffusion rate across the sampling tube was measured following the procedure described above. By repeating this process for several concentrations of CO_2, a calibration curve could be constructed that is used to determine the dCO_2 concentration in cell culture based on the measured diffusion rate. The presence of moisture can affect the sensitivity of the sensor and hence it is recommended that after autoclaving, keep the sensor in purge mode for 2–3 hr.

2.3 | Strains and culture conditions

The developed sensor was used to monitor dCO_2 in both baker's yeast and *Y. lipolytica P01g-Leu* fermentations. DO was monitored by an optical sensor that is provided by Scientific Industries, Inc. The detailed description of the DO optical sensor can be found in the literature (Tolosa, Kostov, Harms, & Rao, 2002). The cultures were sampled once a day for optical density measurement.

2.3.1 | Baker's yeast fermentation

Fleischmann's Active Dry Yeast (*Saccharomyces cerevisiae* yeast, also known as baker's yeast) was used in these experiments and was directly added to yeast extract–peptone–dextrose (YPD) media incubated in shaker flasks and mini bioreactors. The media was prepared using individual components obtained from Sigma-Aldrich. For sensor characterization (proof-of-concept) run, the concentrations were as: 10 g/L of yeast extract, 20 g/L of each peptone and dextrose. For the control experiments, the dextrose concentration was reduced to 3 g/L deliberately while other components were at the same concentrations. The lower initial dextrose concentration gave us the flexibility to test the CO_2 control strategy by adding additional glucose. The initial yeast dry mass and the YPD media concentration were noted for each experiment involving this strain. Dry yeast (0.2 g) was added to 50 ml of YPD media in a shake flask and allowed to grow at 30°C at 250 rpm for 4 hr. This grown inoculum was further used to start the experiments with the desired initial inoculum density.

2.3.2 | *Y. lipolytica P01g-Leu* fermentation

Y. lipolytica is classified as an oleaginous yeast species because of its ability to accumulate lipids in large quantities (Xu, Qiao, & Stephanopoulos, 2017). We used a genetically modified version of a leucine auxotroph strain (*P01g-Leu*) that requires a leucine complementation pathway to grow (Xu, Qiao, Ahn, & Stephanopoulos, 2016). This strain was engineered for flavonoid biosynthesis (*P01g* with flavonoid pathway). The *P01g-Leu* strain was cultured in the YPD media because of its inability to synthesize leucine (leucine is needed in the culture media to grow). Three hundred microliters of glycerol stock were added to 5 ml of YPD media in 50 ml Falcon tube and allowed to grow at 30°C at 250 rpm for 20–24 hr. This preculture was further used to inoculate the shake flask culture with the desired starting optical density.

3 | RESULTS

3.1 | Sensor characterization

Figure 4 shows the calibration curve for the K30-based dCO_2 sensor, which was used in the later fermentation experiments. For comparison, the calibration curves for two different dCO_2 sensor systems built with LI-820 CO_2 gas analyzers (Bravo-01 and Bravo-04) were also provided. It can be seen that all three calibration

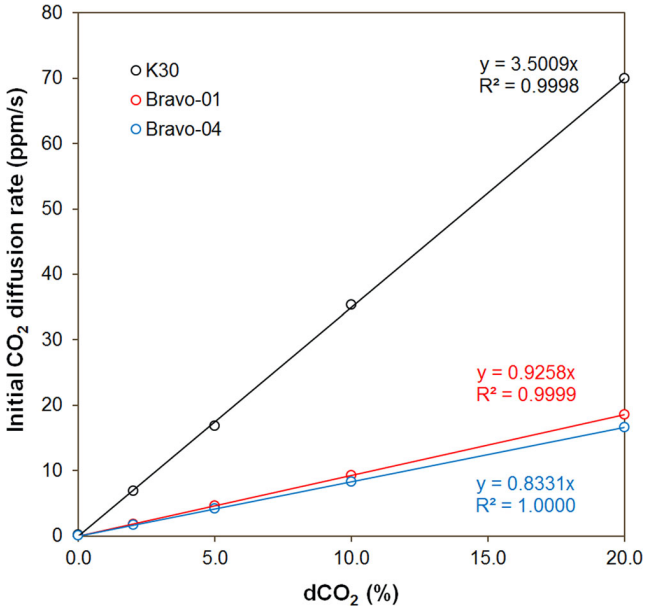

FIGURE 4 Calibration curves for three different prototypes showing the initial diffusion rate of CO_2 through the sampling tube versus dissolved carbon dioxide concentration. K30 was built with a K30 CO_2 sensor. Bravo-01 and Bravo-04 were built with a LI-820 CO_2 gas analyzer. The calibrations were performed in triplicate. The standard deviations are given as error bars, which are invisible because they are smaller than the symbols [Color figure can be viewed at wileyonlinelibrary.com]

curves fit very well to a linear equation with a negligible *y*-intercept (correlation coefficient $R^2 \approx 1.0$).

The slope of the lines represents the sensitivity of the sensor. According to our previous studies (Chatterjee et al., 2015), the sensitivity of the rate-based sensor is affected by the mass transfer coefficient of CO_2 in the sampling tube material (k), the total mass transfer area of the sampling tube (A), and the internal volume of the sensor system (V):

$$\left.\frac{dC}{dt}\right|_{t=0} = \frac{kA}{V} d\mathrm{CO_2} \quad (1)$$

Although the K30 CO_2 sensor has much lower precision than the LI-820 CO_2 gas analyzer (20 vs. 1 ppm), the K30-based dCO_2 sensor has a much higher sensitivity than the LI-820-based dCO_2 sensor (~3.5 vs. ~0.9 ppm/%) due to its much lower volume. Increasing the mass transfer area (the size) of the sampling tube can increase the amount of CO_2 diffusing into the system. As a result, a higher signal will be detected at the same dCO_2 level. Thus, the sensitivity of the system will be increased. Using a more permeable material for the sampling tube, the sensitivity of the system can be increased. However, using a too permeable material could saturate the CO_2 sensor, resulting in erroneous readings.

The LOD of the sensor, which is the lowest dCO_2 that the sensor can reliably measure is defined as three times of baseline signal noise divided by the sensitivity. This value was determined by conducting multiple baseline diffusion rate measurements and calculating the standard deviation for the dataset. Because LOD is inversely proportional to the sensitivity, any measures discussed above that can increase the sensitivity of the sensor can improve its LOD. In addition to modifying the parameters shown in Equation (1), the lengths of time for each stage of the measurement cycle could also affect the LOD. The length of the purge stage is important because it needs to be long enough to fully remove the CO_2 buildup from the system before the measurement stage begins. Increasing the duration of the recirculation stage can increase the repeatability (decrease the noise) of the measurement, so it can improve the LOD. However, increasing the recirculation duration will make the measurement cycles longer. In the tests described in this paper, the flush stage lasted 30 s and the recirculation stage lasted 60 s. So each measurement cycle lasted 1.5 min. For most applications, 1.5-min measurement intervals are fast enough, but for applications where accuracy is the highest priority, the duration of the recirculation can be increased for better accuracy. At the above conditions, the LOD was calculated to be 0.04% for Bravo-01, 0.13% for Bravo-04%, and 0.05% for K30. As mammalian cell cultures are usually maintained at 5% CO_2, the dCO_2 in bacteria and yeast fermentations can be higher due to faster growth rate, the described dCO_2 sensor is sensitive enough for monitoring dCO_2 concentration in fermentations.

3.2 | Shake flask monitoring

Experiments were performed using baker's yeast and *Y. lipolytica P01g-Leu* strain at shake flask scale in batch mode using YPD media. Process data for these preliminary experiments were successfully collected for multiple parameters, including DO, dCO_2, and optical density (OD). The experiments were started with ~0.2 and 0.5 initial optical density for baker's yeast and yeast *Y. lipolytica P01g-Leu*, respectively. Both cultures were grown at 30°C at 250 rpm. The profiles are depicted in Figure 5. It was observed that there was a sharp rise in dCO_2 concentration in the baker's yeast culture without a concomitant drop in O_2 consumption. In contrast, the *Y. lipolytica P01g-Leu* strain showed a steady increase in dCO_2 concentration with a decline in DO concentration (Figure 5a–c). Figure 5c shows the overlap of the dCO_2 trend for both yeasts where the significant distinction in their metabolic pattern can be seen. The initial sharp rise in dCO_2 concentration (first 7 hr) in the case of baker's yeast was probably due to the Crabtree effect where respire-fermentative glucose metabolism led to the production of CO_2 and ethanol (Chopda, Rathore, & Gomes, 2013; Chopda, Rathore, & Gomes, 2015; Persad, Chopda, Rathore, & Gomes, 2013). Thereafter, dCO_2 concentration decreased indicating exhaustion of glucose. From 9 to 20 hr, there was around 2% increase in dCO_2 concentration which indicates that the produced ethanol was being consumed (Figure 5a). In contrast, the yeast *Y. lipolytica P01g-Leu* followed a respiratory metabolism and therefore, dCO_2 rose steadily with a concomitant drop in DO concentration. The overall dCO_2 concentration was higher in yeast *Y. lipolytica P01g-Leu* compared with baker's yeast. As shown in Figure 5c, the fermentation period after 48 hr showed a higher OD in baker's yeast, which was around 3.5 even after starting with a lesser initial OD (the first data point was somewhat fluctuating

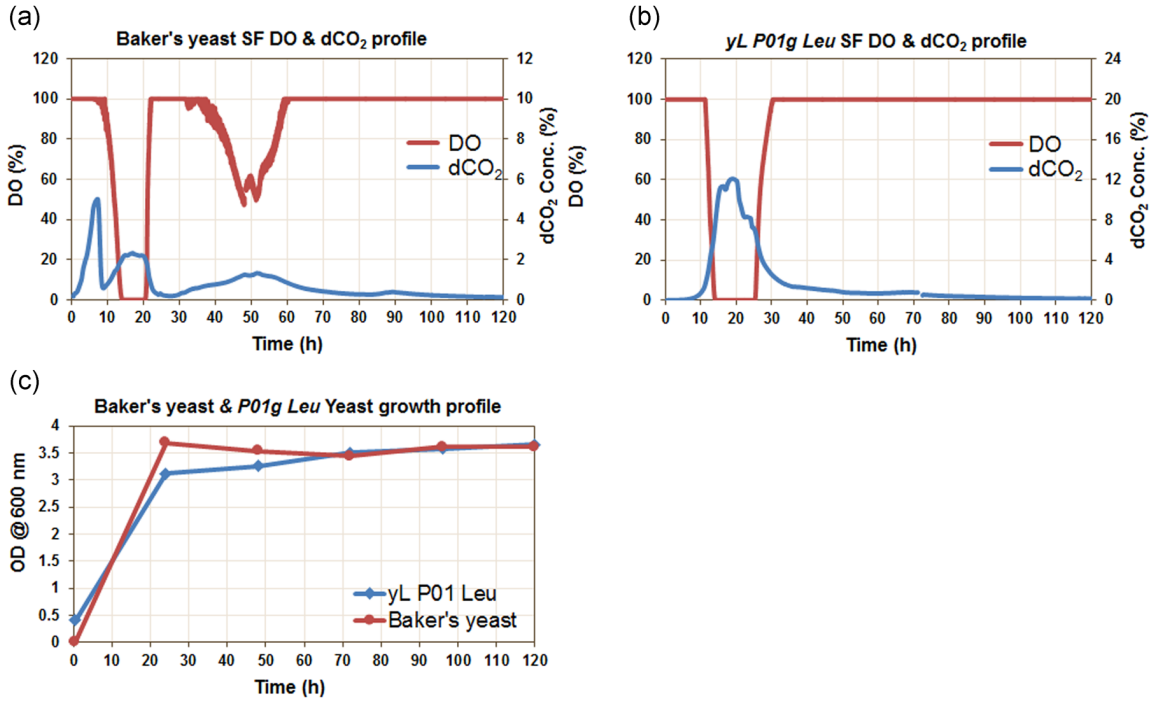

FIGURE 5 Fermentation profiles monitored in shake flask cultivation. (a) Dissolved oxygen (DO) and dissolved carbon dioxide (dCO_2) profile for batch baker's yeast culture; (b) DO and dCO_2 profile for batch *Yarrowia lipolytica P01g-Leu* yeast culture; (c) optical density (OD) profile for both yeast strains [Color figure can be viewed at wileyonlinelibrary.com]

due to the small number and probably sampling error), compared with the OD in *Y. lipolytica P01g-Leu* yeast, which was around 3.3 even after starting with a higher initial OD of 0.5. This may suggest a higher CO_2 concentration (~12%) in the case of *Y. lipolytica P01 Leu* yeast might have inhibited cell growth compared with the baker's yeast fermentation where dCO_2 concentration reached only 5%. This is in accordance with various literature data that have shown a similar inhibitory impact of higher CO_2 levels (Blombach & Takors, 2015). In addition, a similar distinct dCO_2 pattern in the Crabtree positive and negative strains was observed when measured in headspace by the RAMOS system (Anderlei et al., 2004).

3.3 | dCO_2 control by controlled glucose feeding

The concentration of glucose is critical in the baker's yeast culture as excessive glucose may turn on the Crabtree effect even in oxidative conditions. As glucose metabolism yields to biomass, CO_2 and water, we gave the target setpoint for the dCO_2 by keeping glucose in feedback control (on–off control). In the first condition, we controlled the dCO_2 levels at 10% for 4–8 hr using 400 g/L glucose and then turned off the controller for the remaining process duration. In other conditions, we controlled the dCO_2 levels at 10% and 6% for 4–24 hr using 400 and 200 g/L glucose feed concentration, respectively. The choice of maintaining a set of dCO_2 values using a certain concentration of glucose solution has been taken from our preliminary experimentation (data not included) while testing the sensor.

From Figure 6a–c we can see that the feedback control was able to maintain the dCO_2 levels around the set target. The experiment in which feeding was performed for only 4–8 hr showed that dCO_2 levels oscillated at around 10% and thereafter declined as the feeding was stopped (Figure 6a). This condition resulted in lower biomass concentration and reached only OD around 8 (Figure 6a). The experiment in which dCO_2 maintained at around 10% (4–24 hr), DO remain relatively at lower levels (5–10%) as shown in Figure 6b and OD reached to 14.5. In the third case, we reduced the concentration of the feed solution and set the dCO_2 levels to around 6%. With controlled glucose addition, dCO_2 remained well controlled at the desired set point of 6%, which led to significantly higher biomass (OD reached 25.2) as shown in Figure 6c). The biomass yield over glucose in the case of 400 g/L glucose fed (for 4–24 hr) experiments was estimated to be 0.47 OD/g-glucose while in the case of 200 g/L glucose fed (for 4–24 hr), it was estimated to be 1.0 OD/g-glucose. With a 4% lower target dCO_2 concentration, the biomass yield was increased by 114% (Figure 6a–c). This can be explained by the fact that with the condition in which 10% dCO_2 was maintained, the more glucose pumped into the bioreactor in an oxidative condition might have led to more ethanol formation (Crabtree effect) as a byproduct, which resulted in low biomass concentration (OD = 14.5). In contrast, the other condition in which dCO_2 was maintained to only 6% was able to maintain the culture in the respiratory regime and resulted in more biomass. Thus, a dCO_2-based feeding strategy can allow us to drive the bioprocess in a certain metabolic path. It is very important to track dCO_2 concentration through various stages of biomanufacturing from

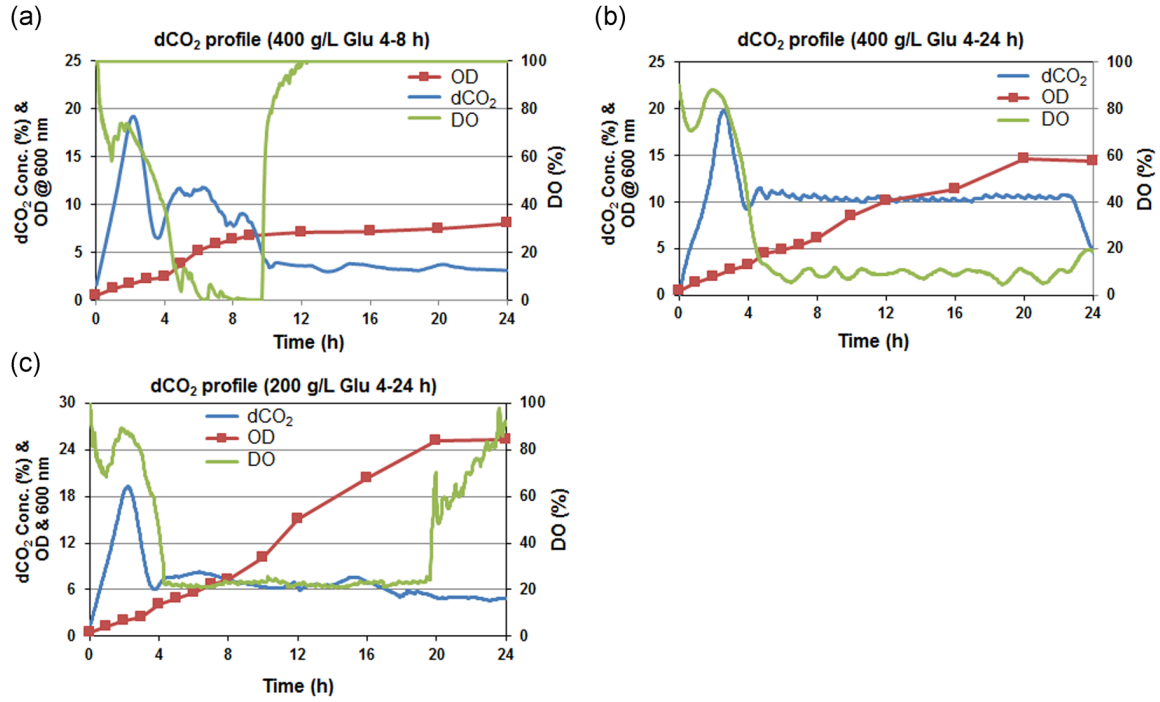

FIGURE 6 Fermentation process profiles monitored in recombinant baker's yeast culture in a mini bioreactor. (a) Dissolved oxygen (DO), optical density (OD), and dissolved carbon dioxide (dCO_2) profile for dCO_2 at 10% 4–8 hr with 400 g/L glucose feed; (b) DO, OD, and dCO_2 profile for dCO_2 at 10% 4–24 hr with 400 g/L glucose feed; (c) DO, OD, and dCO_2 profile for dCO_2 at 6% 4–24 hr with 200 g/L glucose feed [Color figure can be viewed at wileyonlinelibrary.com]

inoculum development in shake flask to seed generation at the benchtop bioreactor scale to industrial production scale to monitor culture conditions.

4 | DISCUSSION

DO-based control strategies are more popular in bioprocessing because oxygen is considered as an important substrate in metabolism. In addition, robust sensors to monitor DO in real-time are available at various scales of operation (Chopda, Pathak, Batra, Gomes, & Rathore, 2016; Chopda et al., 2013; Priyanka, Roy, Chopda, Gomes, & Rathore, 2019). However, due to the mass transfer limitation in bioprocesses, pure oxygen must be supplied to fulfill the requirement of DO (Carloni et al., 2009; Priyanka et al., 2019). This often leads to sensor responses at the extreme of their detection limits (either 0 or 100) resulting in oscillation or drift in the signal. For example, in Figure 5, it is hard to predict the existence of the Crabtree metabolism of the organism solely from DO response. In the growth phase, the DO signal went to 0 value and when the cells entered the stationary phase, the DO signal rose to 100% (Figure 5). On the other hand, dCO_2 provides a more nuanced response that can be correlated to biomass production. This is due to CO_2 being the final product of respiration both in microbial as well as in mammalian processes. It has a strong impact on cell metabolism in multiple ways as discussed in Section 1 of this paper. Thus, the real-time dCO_2 profile can give the true metabolic signature of a process. However, until now, CO_2 is mostly monitored in the exhaust gas, which itself cannot give real-time culture broth conditions as the information captured is filtered through the headspace. This means there exists an inherent lag in relaying the dCO_2 concentrations to the gaseous phase CO_2 (Chopda et al., 2015). Very few sensors are available in the market which can measure dCO_2 concentration, and most will not fit in small-scale systems such as shake flasks or mini bioreactors.

Here we have presented the application of a novel, noninvasive, rate-based technique for monitoring dCO_2 in bioprocess. By Fick's law of diffusion, the diffusion rate should be proportional to the concentration of dCO_2 in the broth. We have shown that by measuring the initial diffusion rate we were able to determine the partial pressure of dCO_2 in the culture. The technique could be readily automated, and measurements could be made in minutes. It needs to be mentioned that CO_2 exists in several different forms when it is dissolved in water (CO_2 [aq], H_2CO_3, HCO_3^-, CO_3^{2-}), dependent on the pH. The developed method measures only CO_2 (aq), the unreacted form of dissolved CO_2. When pH changes significantly, the changes in pH should be taken into consideration to accurately determine the CO_2 evolution rate.

The dCO_2 sensor was tested in demonstration experiments by growing baker's yeast and *Y. lipolytica* cultures. These results show that distinct changes in the metabolism of an organism can be captured using dCO_2 signatures, suggesting that the rate-based method is an effective way to monitor dCO_2 levels in small-scale systems. Furthermore, we have tested a control strategy based on dCO_2 concentration by controlled glucose feeding in the feedback

loop. Different dCO_2 profiles gave very distinct results in terms of biomass formation in baker's yeast mini bioreactor culture. The lowered concentration of dCO_2 resulted in a significant increase in biomass productivity (Figure 6). The experiment performed for sensor characterization (Figure 5) is the run in which no dCO_2 control was implemented that resulted in a maximum OD of around 3.5 at around 24 hr. On the other hand, all the dCO_2 controlled experiments (Figure 6) yielded a higher OD. The highest OD of 25.2 was achieved when dCO_2 was controlled at 6%, which is almost a seven-time increase in OD compared with uncontrolled conditions. Many researchers have used off-gas measurements to estimate the biomass in the reactor. The substrate demand is then determined according to the amount of biomass. However, this method is still an "open loop" control strategy and may lead to a lag in control action (Muthuswamy & Srinivasan, 2003; Valentinotti et al., 2003). Other case studies in the benchtop, as well as large scale bioreactors, emphasize the important role of dCO_2 monitoring and its significant impact on cell growth and protein production (Mitchell-Logean & Murhammer, 1997; Mostafa & Gu, 2003).

A similar phenomenon occurring in shake flask culture, where the performance of the shake flask in terms of biomass growth and product concentration was significantly affected by dCO_2 concentrations, was reported (Takahashi & Aoyagi, 2018a, 2018b). In one of the more interesting findings, researchers have shown that opening the shake flask closure for sampling allows diffusion of gases into the atmosphere, such that CO_2 concentrations decrease temporarily in the broth as well as in the headspace, thereby significantly impacting the community structure of soil microbes (Takahashi & Aoyagi, 2018b). A study conducted by McIntyre and McNeil (1997) concluded that culture is more vulnerable to CO_2 inhibition in the lag phase. In addition, during the inoculation step, the culture can experience many pressures due to the significant differences in the environment of a shake flask and in the bioreactor conditions. Monitoring dCO_2 levels across all scales of biomanufacturing will enable control of the culture environment to prevent any severe shock to the growing cells.

We believe that the studies presented in this paper using our in situ dCO_2 sensor proves the criticality and importance of monitoring and control of dCO_2. Monitoring dCO_2 will not only indicate real-time culture conditions but also give the critical process information for taking effective control decisions should deviations occur. We also showed that the proposed sensor is flexible in configuration and can be easily fit in shake flasks and other small-scale mini bioreactors. This will enable us to extract more process information even from small-scale systems thereby accelerating process development many folds.

5 | CONCLUSION

Shake flask and the small-scale fermentation processes are generally hindered by the scarcity of in-line sensors. We have identified that there is a need to develop a portable dCO_2 sensor for such small-scale fermentation due to the significant effect of dCO_2 on the overall metabolism and the subsequent scale-up activities. In this manuscript, we present a novel, rate-based technique for monitoring dCO_2 in cell cultures by measuring the initial diffusion rate across a silicone sampling tube immersed in the culture media. Demonstration experiments conducted with baker's yeast and *Y. lipolytica* yeast cells in both shake flasks and mini bioreactors show that it can monitor dCO_2 in real-time. Using the proposed sensor, we successfully implemented a dCO_2-based control scheme, which resulted in significant improvement in process performance. Through the implementation of dCO_2 based control strategy, we have shown that by controlling dCO_2 at various levels we can direct the metabolic fate of the process in real-time. In the future, our efforts will be directed towards using the developed dCO_2 based control scheme to reduce the disparity that exits across the different scales of operation.

ACKNOWLEDGMENT

The present work was conducted under the sponsorship and generous support of the Bill and Melinda Gates Foundation.

ORCID

Xudong Ge http://orcid.org/0000-0003-1733-398X
Govind Rao http://orcid.org/0000-0001-6140-7582

REFERENCES

BlueSens gas sensor GmbH. BCpreFerm—Whole Gas Analysis System. Retrieved from https://www.bluesens.com/products/analysis-systems/bcpreferm

Kuhner BPM-60. Retrieved from https://www.kuhner.com/en/product/add-ons/online-measurement/bpm-60.html

Ahuja, S., Jain, S., & Ram, K. (2015). Application of multivariate analysis and mass transfer principles for refinement of a 3-L bioreactor scale-down model—when shake flasks mimic 15,000-L bioreactors better. *Biotechnology Progress*, *31*(5), 1370–1380.

Anderlei, T., & Büchs, J. (2001). Device for sterile online measurement of the oxygen transfer rate in shaking flasks. *Biochemical Engineering Journal*, *7*, 157–162.

Anderlei, T., Zang, W., Papaspyrou, M., & Büchs, J. (2004). Online respiration activity measurement (OTR, CTR, RQ) in shake flasks. *Biochemical Engineering Journal*, *17*, 187–194.

Blombach, B., & Takors, R. (2015). CO_2—intrinsic product, essential substrate, and regulatory trigger of microbial and mammalian production processes. *Frontiers in Bioengineering and Biotechnology*, *3*, 1–11.

Chatterjee, M., Ge, X., Uplekar, S., Kostov, Y., Croucher, L., Pilli, M., & Rao, G. (2015). A unique noninvasive approach to monitoring dissolved O_2 and CO_2 in cell culture. *Biotechnology and Bioengineering*, *112*, 104–110.

Chen, Y., Krol, J., Huang, W., Cino, J. P., Vyas, R., Mirro, R., & Vaillancourt, B. (2008). dCO_2 on-line measurement used in rapamycin fed-batch fermentation process. *Process Biochemistry*, *43*, 351–355.

Chopda, V. R., Gomes, J., & Rathore, A. S. (2016). Bridging the gap between PAT concepts and implementation: An integrated software platform for fermentation. *Biotechnology Journal*, *11*, 164–171.

Chopda, V. R., Pathak, M., Batra, J., Gomes, J., & Rathore, A. S. (2016). Enabler for process analytical technology implementation in *Pichia pastoris*

fermentation: Fluorescence based soft sensors for rapid quantitation of product titer. *Engineering in Life Sciences*, *17*(4), 448–457.

Chopda, VR, Rathore, AS, & Gomes, J. (2013). On-line implementation of decoupled input-output linearizing controller in baker's yeast fermentation. *IFAC Proceedings Volumes*, *46*(32), 259–264.

Chopda, V. R., Rathore, A. S., & Gomes, J. (2015). Maximizing biomass concentration in baker's yeast process by using a decoupled geometric controller for substrate and dissolved oxygen. *Bioresource Technology*, *196*, 160–168.

Food and Drug Administration (2004). Guidance for industry: PAT—A framework for innovative pharmaceutical development, manufacturing and quality assurance. Retrieved from http://www.gmp-compliance.org/guidemgr/files/PAT-FDA-6419FNL.PDF

Flitsch, D., Ladner, T., Lukacs, M., & Büchs, J. (2016). Easy to use and reliable technique for online dissolved oxygen tension measurement in shake flasks using infrared fluorescent oxygen-sensitive nanoparticles. *Microbial Cell Factories*, *15*, 1–11.

Frahm, B., Blank, H., Cornand, P., Oelssner, W., Guth, U., Lane, P., … Pörtner, R. (2002). Determination of dissolved CO_2 concentration and CO_2 production rate of mammalian cell suspension culture based on off-gas measurement. *Journal of Biotechnology*, *99*, 133–148.

Ge, X., Adangwa, P., Lim, J. Y., Kostov, Y., Tolosa, L., Pierson, R., … Rao, G. (2018). Development and characterization of a point-of care rate-based transcutaneous respiratory status monitor. *Medical Engineering & Physics*, *56*, 36–41.

Ge, X., Kostov, Y., & Rao, G. (2003). High-stability non-invasive autoclavable naked optical CO_2 sensor. *Biosensors and Bioelectronics*, *18*, 857–865.

Ge, X., Kostov, Y., & Rao, G. (2005). Low-cost noninvasive optical CO_2 sensing system for fermentation and cell culture. *Biotechnology and Bioengineering*, *89*, 329–334.

Ge, X., & Rao, G. (2012). Real-time monitoring of shake flask fermentation and off gas using triple disposable noninvasive optical sensors. *Biotechnology Progress*, *28*, 872–877.

Gomes, J., Chopda, V. R., & Rathore, A. S. (2015). Integrating systems analysis and control for implementing process analytical technology in bioprocess development. *Journal of Chemical Technology and Biotechnology*, *90*, 583–589.

Gomes, J., Chopda, V. R., & Rathore, A. S. (2018). Monitoring and control of bioreactor: Basic concepts and recent advances. *Bioprocess Technol Prod Biopharm Bioprod*, 201–237.

Gupta, A., & Rao, G. (2003). A study of oxygen transfer in shake flasks using a non-invasive oxygen sensor. *Biotechnology and Bioengineering*, *84*, 351–358.

Hansen, S., Jacob, I., Luchterhand, B., & Büchs, J. (2012). Development of a modified Respiration Activity Monitoring System for accurate and highly resolved measurement of respiration activity in shake flask fermentations. *Journal of Biological Engineering*, *6*(1), 11.

Kasperski, A., & Mis ´kiewicz, T. (2008). Optimization of pulsed feeding in a baker's yeast process with dissolved oxygen concentration as a control parameter. *Biochemical Engineering Journal*, *40*, 321–327.

Lander, E., & Kruglyak, L. (1995). Genetic dissection of complex traits: Guidelines for interpreting and reporting linkage results. *Nature Genetics*, *11*, 241–247.

Matsunaga, N., Kano, K., Maki, Y., & Dobashi, T. (2009). Culture scale-up studies as seen from the viewpoint of oxygen supply and dissolved carbon dioxide stripping. *Journal of Bioscience and Bioengineering*, *107*, 412–418.

McIntyre, M., & McNeil, B. (1997). Effects of elevated dissolved CO_2 levels on batch and continuous cultures of *Aspergillus niger A60*: An evaluation of experimental methods. *Applied and Environmental Microbiology*, *63*, 4171–4177.

Mitchell-Logean, C., & Murhammer, D. W. (1997). Bioreactor headspace purging reduces dissolved carbon dioxide accumulation in insect cell cultures and enhances cell growth. *Biotechnology Progress*, *13*, 875–877.

Mostafa, S. S., & Gu, X. (2003). Strategies for improved dCO_2 removal in large-scale fed-batch cultures. *Biotechnology Progress*, *19*, 45–51.

Muthuswamy, K., & Srinivasan, R. (2003). Phase-based supervisory control for fermentation process development. *Journal of Process Control*, *13*, 367–382.

Persad, A., Chopda, V. R., Rathore, A. S., & Gomes, J. (2013). Comparative performance of decoupled input-output linearizing controller and linear interpolation PID controller: Enhancing biomass and ethanol production in *Saccharomyces cerevisiae*. *Applied Biochemistry and Biotechnology*, *169*, 1219–1240.

Priyanka, Roy, S., Chopda, V., Gomes, J., & Rathore, A. S. (2019). Comparison and implementation of different control strategies for improving production of rHSA using *Pichia pastoris*. *Journal of Biotechnology*, *290*, 33–43.

Scheidle, M., Klinger, J., & Büchs, J. (2007). Combination of on-line pH and oxygen transfer rate measurement in shake flasks by fiber optical technique and Respiration Activity MOnitoring System (RAMOS). *Sensors*, *7*, 3472–3480.

Schneider, K., Schütz, V., John, G. T., & Heinzle, E. (2010). Optical device for parallel online measurement of dissolved oxygen and pH in shake flask cultures. *Bioprocess and Biosystems Engineering*, *33*, 541–547.

Seletzky, J. M., Noack, U., Hahn, S., Knoll, A., Amoabediny, G., & Büchs, J. (2007). An experimental comparison of respiration measuring techniques in fermenters and shake flasks: Exhaust gas analyzer vs. RAMOS device vs. respirometer. *Journal of Industrial Microbiology and Biotechnology*, *34*, 123–130.

Shang, L., Jiang, M., Ryu, C. H., Chang, H. N., Cho, S. H., & Lee, J. W. (2003). Inhibitory effect of carbon dioxide on the fed-batch culture of *Ralstonia eutropha*: Evaluation by CO_2 pulse injection and autogenous CO_2 methods. *Biotechnology and Bioengineering*, *83*, 312–320.

Srinivasan, S., Feng, S., & Lin, Y. H. (2012). Dissolved carbon dioxide concentration profiles during very-high-gravity ethanol fermentation. *Biochemical Engineering Journal*, *69*, 41–47.

Takahashi, M., & Aoyagi, H. (2018a). Practices of shake-flask culture and advances in monitoring CO_2 and O_2. *Applied Microbiology and Biotechnology*, *102*, 4279–4289.

Takahashi, M., & Aoyagi, H. (2018b). Monitoring of CO_2 and O_2 concentrations in the headspace of Sakaguchi flasks during liquid culture of microorganism. *Applied Microbiology and Biotechnology*, *102*, 6637–6645.

Takahashi, M., & Aoyagi, H. (2018c). Effect of intermittent opening of breathable culture plugs and aeration of headspace on the structure of microbial communities in shake-flask culture. *Journal of Bioscience and Bioengineering*, *126*, 96–101.

Takahashi, M., Sawada, Y., & Aoyagi, H. (2017). Development of a circulation direct sampling and monitoring system for O_2 and CO_2 concentrations in the gas–liquid phases of shake-flask systems during microbial cell culture. *AMB Express*, *7*, 163.

Tolosa, L., Kostov, Y., Harms, P., & Rao, G. (2002). Noninvasive measurement of dissolved oxygen in shake flasks. *Biotechnology and Bioengineering*, *80*, 594–597.

Valentinotti, S., Srinivasan, B., Holmberg, U., Bonvin, D., Cannizzaro, C., Rhiel, M., & von Stockarb, U. (2003). Optimal operation of fed-batch fermentations via adaptive control of overflow metabolite. *Control Engineering Practice*, *11*(6), 665–674.

Vasala, A., Panula, J., Bollók, M., Illmann, L., Hälsig, C., & Neubauer, P. (2006). A new wireless system for decentralised measurement of physiological parameters from shake flasks. *Microbial Cell Factories*, *5*, 8.

Wittmann, C., Kim, H. M., John, G., & Heinzle, E. (2003). Characterization and application of an optical sensor for quantification of dissolved O_2 in shake-flasks. *Biotechnology Letters*, *25*, 377–380.

Xu, P., Qiao, K., Ahn, W. S., & Stephanopoulos, G. (2016). Engineering *Yarrowia lipolytica* as a platform for synthesis of drop-in transportation fuels and oleochemicals. *Proceedings of the National Academy of Sciences of the United States of America*, *113*(39), 10848–10853.

Xu, P., Qiao, K., & Stephanopoulos, G. (2017). Engineering oxidative stress defense pathways to build a robust lipid production platform in *Yarrowia lipolytica*. *Biotechnology and Bioengineering*, *114*(7), 1521–1530.

How to cite this article: Chopda VR, Holzberg T, Ge X, et al. Real-time dissolved carbon dioxide monitoring I: Application of a novel in situ sensor for CO_2 monitoring and control. *Biotechnology and Bioengineering*. 2019;1–11. https://doi.org/10.1002/bit.27253

With the new multiplexed CO_2 sensor, we were able to revisit the early shake flask work and demonstrate that surface aeration intensification not only improves oxygen transfer to shake flasks, but also helps remove denser-than-air CO_2 efficiently, leading to improved growth and recombinant protein production. Lynn Wong joined this effort.

Received: 19 July 2019 | Revised: 10 December 2019 | Accepted: 13 December 2019

DOI: 10.1002/bit.27252

BIOTECHNOLOGY BIOENGINEERING WILEY

ARTICLE

Real-time dissolved carbon dioxide monitoring II: Surface aeration intensification for efficient CO_2 removal in shake flasks and mini-bioreactors leads to superior growth and recombinant protein yields

Viki R. Chopda | Timothy Holzberg | Xudong Ge | Brandon Folio | Lynn Wong | Michael Tolosa | Yordan Kostov | Leah Tolosa | Govind Rao

Department of Chemical, Biochemical and Environmental Engineering, Center for Advanced Sensor Technology, University of Maryland, Baltimore, Maryland

Correspondence
Govind Rao, Chemical, Biochemical & Environmental Engineering Director, Center for Advanced Sensor Technology (CAST), University of Maryland Baltimore County (UMBC), Baltimore, MD 21250.
Email: grao@umbc.edu

Funding information
Bill and Melinda Gates Foundation

Abstract

Mass transfer is known to play a critical role in bioprocess performance and henceforth monitoring dissolved O_2 (DO) and dissolved CO_2 (dCO_2) is of paramount importance. At bioreactor level these parameters can be monitored online and can be controlled by sparging air/oxygen or stirrer speed. However, traditional small-scale systems such as shake flasks lack real time monitoring and also employ only surface aeration with additional diffusion limitations imposed by the culture plug. Here we present implementation of intensifying surface aeration by sparging air in the headspace of the reaction vessel and real-time monitoring of DO and dCO_2 in the bioprocesses to evaluate the impact of intensified surface aeration. We observed that sparging air in the headspace allowed us to keep dCO_2 at low level, which significantly improved not only biomass growth but also protein yield. We expect that implementing such controlled smart shake flasks can minimize the process development gap which currently exists in shake flask level and bioreactor level results.

KEYWORDS

dissolved carbon dioxide, mini-bioreactor, shake flasks, surface aeration intensification

1 | INTRODUCTION

The mass transfer including oxygen supply and dissolved CO_2 (dCO_2) stripping is one of the critical factors which affect the performance of aerobic bioprocesses across the scale from shake flask to manufacturing level (Matsunaga, Kano, Maki, & Dobashi, 2009). Although shake flask cultures are aerobic, O_2 dissolved in the culture broth is generally insufficient for maximal cell growth. Similarly, high-density cultures in the bioreactor suffer from poor dissolved oxygen (DO) concentration. To counter these issues, variations have been evaluated such as having inner concavities or convexities in the flask (baffled flask) to increase the oxygen diffusion (Büchs, 2001) and by supplying pure oxygen or increasing back pressure in the bioreactor (Priyanka, Roy, Chopda, Gomes, & Rathore, 2019). However, these variations have their own limitations such as the former one creates a shear to the cells and the later one generates oxidative stress to the cells, both of which negatively affect the cell growth and the product produced. Accumulation of dCO_2 is another recurrent issue in large-scale production bioreactors and mostly ignored in shake flask cultivation (Jenzsch, Gnoth, Kleinschmidt, Simutis, & Lübbert, 2007; Mostafa & Gu, 2003). Although a significant portion of dCO_2 gets stripped through surface aeration in shake flasks, the rate of stripping is limited and largely determined by the closure material used and the liquid surface to volume ratio. Recently, a few case studies showed that dCO_2 has a significant impact on small-scale

production systems (Takahashi & Aoyagi, 2018a, 2018b). However, due to the lack of reliable portable sensors for shake flask and mini-bioreactor cultures, the parameters such as DO and dCO_2 are rarely measured and their impact at this small scale is not clearly understood (Chopda, Gomes, & Rathore, 2016; Chopda, Pathak, Batra, Gomes, & Rathore, 2017; Gomes, Chopda, & Rathore, 2015). Due to the process analytical technology drive, the last decade has witnessed advances in shake flask monitoring sensors which led to improved understanding of the effect of various parameters on the culture growth and overall metabolism (Ge, Kostov, & Rao, 2005 &, 2006; Hanson et al., 2007; Kermis, Kostov, Harms, & Rao, 2002; Tolosa, Kostov, Harms, & Rao, 2002; Vallejos, Brorson, Moreira, & Rao, 2010). Various researchers proved that as the success of large-scale operations is determined significantly by DO and dCO_2 concentrations, similarly, these parameters have a significant role at small scale bioprocessing system too (Blombach & Takors, 2015). Conventionally, oxygen supply and dCO_2 stripping are performed by gas sparging and agitation in large-scale cultures, because of their large mass transfer rate and operational simplicity (Mitchell-Logean & Murhammer, 1997). However, both gas sparging and agitation rates are restricted to low levels because of operational constraints (e.g., foaming, hydrodynamics) and biological limitations (e.g., shear sensitive cells). In case of shake flask, the culture is solely dependent on the orbital shaking and the limited surface aeration that occurs through the headspace for the DO supply and dCO_2 stripping. In fact, in one such case study, Takahashi and Aoyagi (2018b) showed that intermittent opening of culture plugs temporarily changes the CO_2 concentration in the headspace, which results in observable changes in microbial physiology. This indicates that in the culture vessel, the CO_2 gets accumulated without proper ventilation and further forms a blanket (CO_2 blanket theory), which hinders the effective gaseous mass transfer (Xing, Lewis, Borys, & Li, 2017). By intermittent opening, the culture plug may have allowed better gas transfer though temporarily, but it is significant enough to generate an observable impact on microbial physiology. This implicates that there is potential scope to optimize the shake flask and bioreactor cultures by regulating headspace gas distribution.

In this paper, we evaluated the impact of sparging air in the headspace of bio-reaction vessels such as shake flasks and mini-bioreactors using our novel rate-based sensor for in-situ dCO_2 monitoring. By introducing air in the headspace, the gaseous distribution in the headspace and the dissolved gas concentration in the liquid broth are expected to change. Our investigation proved that the surface aeration plays a critical role in shake flask process development. With controlled surface aeration in the shake flask and mini-bioreactor, we were able to improve not only the biomass growth but also the protein yield.

2 | MATERIALS AND METHODS

2.1 | *Yarrowia lipolytica* Po1g-Leu fermentation

Yarrowia lipolytica is classified as an oleaginous yeast species because of its ability to accumulate lipids in large quantities (Xu, Qiao, Ahn, & Stephanopoulos, 2016). We used genetically modified versions of the Po1g strain engineered for flavonoid biosynthesis (Po1g with flavonoid pathway). The Po1g-Leu strain was cultured in YPD broth. 300 µL of glycerol stock was added to 5 ml of YPD broth in 50 ml falcon tube and allowed to grow at 30°C and 250 rpm for 20-24 hr. This preculture was further used to inoculate the mini-bioreactor culture with the desired starting optical density. The volume of the mini-bioreactor is 100 ml with a working volume of 50 ml. The bioreaction was conducted in batch mode at 30°C and lasted for 48 hr. To avoid excessive foaming, the mini-bioreactor was bubble aerated at a flow rate of 20 cm^3/min.

2.2 | *Escherichia coli* fermentation

The gene *LivJ* from *E. coli* that codes for Leu/Ile/Val ABC transporter periplasmic binding protein was synthesized with a C-terminus 6xHis tag. The synthesized fragment was inserted into the MCS of the expression vector pET28a between *Nco*I and *Xho*I. The A177C mutant was generated via site-directed mutagenesis of the original construct. All plasmids were verified with sequencing. 300 µL of glycerol stock was added to 5 ml of Luria-Bertani (LB) media broth in 50 ml falcon tube and allowed to grow at 37°C and 250 rpm for 20-24 hr. This preculture was further used to inoculate the shake flask culture (50 ml culture in 250 ml flask) with the desired starting optical density at 200 rpm. At around 4 hr, 1 mM of IPTG was added as an inducer and at around 6 hr, a bolus of glucose feed (4 g/L culture) was added at once.

Cell pellets obtained from the fermentation process were thawed out on ice and resuspended with lysis buffer in the ratio 1 g of pellet to 10 ml of lysis buffer. The suspension was sonicated and then centrifuged at 10,000 rpm, 4°C to obtain the soluble fraction. Each sample of supernatant was added to a 10-ml bed of Ni-NTA resin that was pre-equilibrated. After binding, the resin bed was subjected to the following: five column volumes of binding buffer, and eight column volumes of wash buffer. The protein of interest was then eluted in three fractions. Finally, the protein concentration was quantified using a standard Bradford assay (Kruger, 2009).

All the yeast and bacteria fermentation processes were monitored for pH and DO using optical sensors developed by our group for shake flasks and mini-bioreactors (Scientific Industries Inc., Bohemia, NY). The details of the sensors can be found in the articles from our group (Hanson et al., 2007; Kermis et al., 2002; Kostov, Harms, Randers-Eichhorn, & Rao, 2001; Tolosa et al., 2002). The dCO_2 was monitored using the rate-based sensor also developed by our group (Chatterjee et al., 2015; Chopda et al., 2019).

2.3 | Surface aeration intensification

To intensify the surface aeration in the shake flask, standard-size holes (ϕ3.15 mm) were made in the culture plug for air in and out. Additional ports were made for CO_2 sensor in and out, and for sampling. The mini-bioreactor has the necessary ports for air in and out, and for installing the needle-shaped dCO_2 probe. The flow rate

of the air for overlay was set at 20 cm^3/min and the delivery pressure was set at 10 psig from the source. Air was supplied from the source to the culture vessel using proprietary fluoroelastomer Versilon™ F-5500-A tubing of internal diameter 1.57 mm.

3 | RESULTS

3.1 | Impact of culture plug and overlay on shake flask fermentation

The culture plug used in shake flask has a significant role in gaseous exchange in the headspace. Traditionally, cotton plugs and sponge caps are commonly used for shake flasks (Amoabediny & Buchs, 2010; Takahashi & Aoyagi, 2018a, 2018b, 2018c). The culture plug type and with or without surface air intensification conditions are expected to have significant effects on the gaseous mass transfer by altering the gaseous distribution in the vessel. Here we used dCO_2 as a monitoring parameter to evaluate the impact of culture plug and surface air intensification on the culture. Two different culture plugs, rubber septum cap and sponge cap, were evaluated using *E. coli* culture. The two experimental setups are demonstrated in Figure 1.

Figure 2 shows the dCO_2, DO, and optical density (OD) profiles for the 24-hr *E. coli* culture grown in shake flasks with rubber septum caps. The shake flasks have 0.2 μm sterile air filters acting as exhaust mimicking the standard bioreactor setup. It was observed that with and without intensified surface aeration, there was a significant difference in dCO_2 and DO concentration. The dCO_2 was found to be significantly less (>5 times lower) in the shake flasks with air overlay (dCO_2 < 20%) compared to the shake flask in which there was no overlay. The dCO_2 was so high in the no overlay condition that the sensor was got saturated and the concentration reached beyond the calibration range. The oxygen-limitation present in the shake flask with no overlay disappeared in the shake flask with air overlay due to the increased oxygen availability. The faster CO_2 removal and greater O_2 availability greatly improved the performance of the shake flask in terms of biomass growth and product concentration. The flask with intensified surface aeration was found to have 36% more biomass growth (8.3 OD) compared to the shake flask without intensified surface aeration, which reached only up to 6.1 OD. The wet cell weight (WCW) was increased by 43% with intensified surface aeration (Table 1). The recombinant protein production was analyzed and found that with air overlay the protein yield was increased by more than five times compared to the case in which there was no overlay kept (Table 1). These results show that surface aeration intensification plays a critical role in O_2 supply and CO_2 clearance in shake flasks with rubber septum caps, resulting in improved biomass growth and protein production.

We further tested the sponge caps as they are more commonly used. Figure 3 shows the dCO_2, DO and OD profiles for the 24-hr *E. coli* cultures grown in shake flasks with sponge caps. It was observed that with and without air overlay, there was also a big difference in dCO_2 concentrations as depicted in Figure 3c. The dCO_2 was found to be almost 50% less in the shake flasks in which overlay was kept with air compared to the shake flask in which there was no overlay. The sponge cap provided enough oxygen in both cases, evidenced by the absence of oxygen limitation. In contrast, when we used rubber septum with no overlay condition, the DO was reached to zero from 6 to 12 hr (Figure 2). With sponge caps, the flask with lower dCO_2 concentration found to have 33% more biomass growth (~12 OD) compared to the shake flask having a higher dCO_2 concentration (~9 OD). The WCW in both conditions with the sponge caps was found to be similar.

We further analyzed the recombinant protein production and found that with the air in overlay the protein yield was increased by 57% compared to the case in which there was no overlay kept (Table 2). This result shows the significance of the dCO_2 on the culture growth as well as on protein production despite the presence of sufficient oxygen. Surface aeration plays a critical role in CO_2 clearance from the headspace thereby enhancing the diffusion of CO_2 out of the broth. The resulting lower concentration of dCO_2 leads to improved biomass growth and protein production.

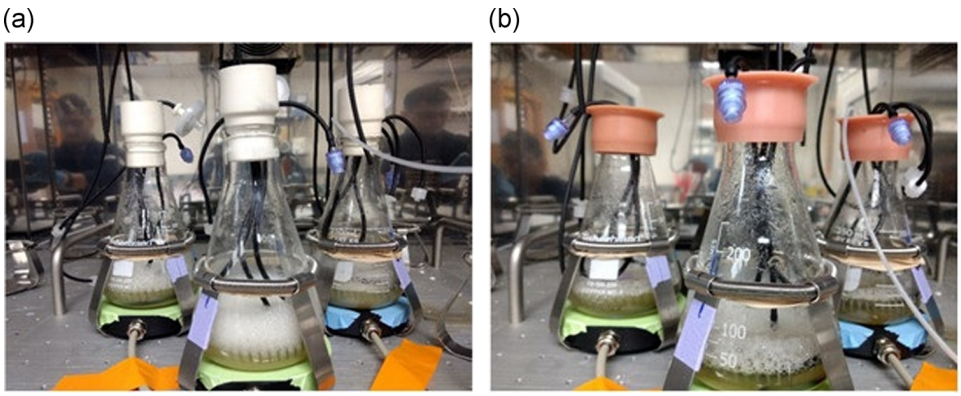

FIGURE 1 Demonstration of shake flask setup with coasters at the bottom for real-time pH and dissolved oxygen (DO) monitoring: (a) Shake flask with rubber septum cap and (b) shake flask with sponge cap. The dissolved CO_2 (dCO_2) measurement loop was housed in the spring coil on the bottom [Color figure can be viewed at wileyonlinelibrary.com]

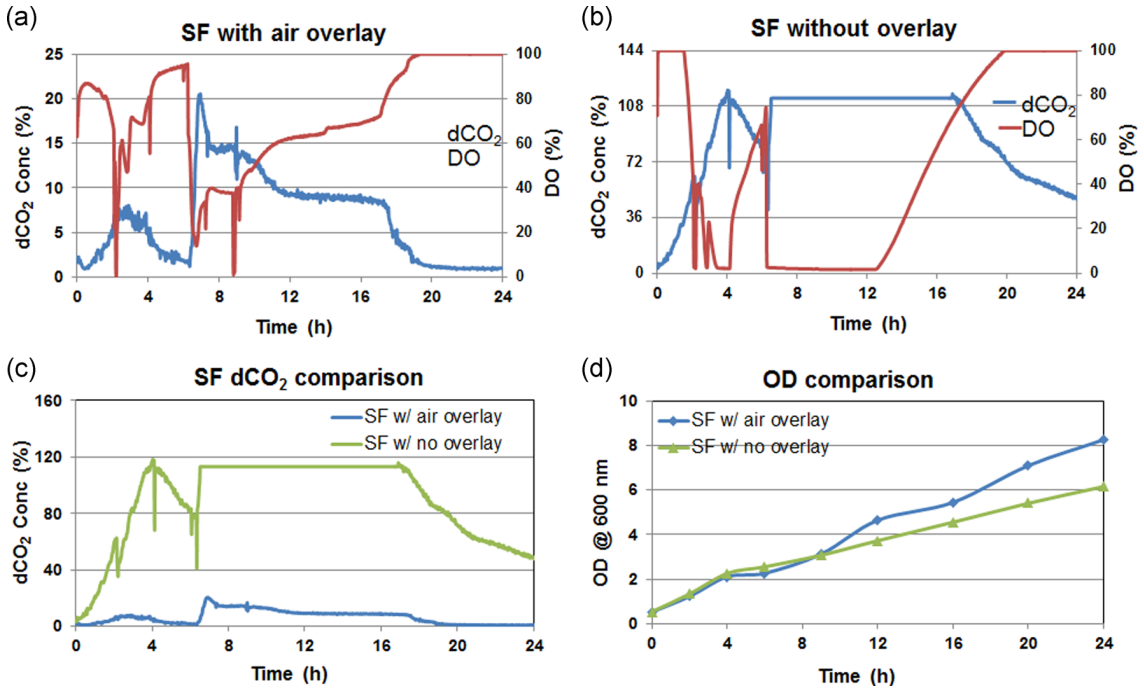

FIGURE 2 Process parameters monitored in *Escherichia coli* shake flask fermentation with rubber septum cap. (a) DO and dCO_2 profiles with air overlay. (b) DO and dCO_2 profiles with no overlay. (c) Comparison of dCO_2 profiles under different overlay conditions showing the significance of surface aeration. (d) Comparison of biomass growth showing the impact of surface aeration in the shake flask. dCO_2, dissolved CO_2; DO, dissolved oxygen; OD, optical density; SF, shake flask [Color figure can be viewed at wileyonlinelibrary.com]

3.2 | Impact of overlay on fermentations conducted in mini-bioreactors

One of the most important factors in bioreactor operations is mass transfer, which includes both oxygen supply and dCO_2 stripping. In the scale-up of industrial biomanufacturing, dCO_2 buildup is one of the most serious issues because of its significant impact on the culture condition as well as on the product production. However, excessive stripping of dCO_2 is also detrimental to cell growth, which suggests that there is likely an optimal level of dCO_2 for cell culture (Mostafa & Gu, 2003). The organism used for production and the product of interest will certainly determine this optimal dCO_2 value. Therefore, it is critical to monitor and control dCO_2 levels. We assessed the impact of keeping the air in the headspace (overlay) of the mini-bioreactor (50 ml working volume) for *Y. lipolytica* culture grown for 48 hr in batch mode at 30°C (Figure 4). It was observed that when air was sparged in the headspace of the mini-bioreactor, dCO_2 concentration was lowered in the culture broth indicating better stripping of dCO_2 from the vessel. The dCO_2 concentration with intensified surface aeration was almost reduced to half (2–3%) compared to the no overlay condition. The oxygen-limitation condition lasted about 6 hours shorter for the culture with air overlay. The lowering in the dCO_2 levels together with improved oxygen limitation resulted in higher growth and the OD reached above 10 compared to the only 8 OD in the case where no overlay. This indicates that the culture conditions are dependent on the interplay between DO and dCO_2, which is significantly affected by intensifying air in the overlay of a vessel.

TABLE 1 Recombinant protein production in the shake flask culture with rubber septum caps

Surface aeration	Protein yield (μg)	WCW (g)	Normalized protein yield (%)
No overlay	194.8	0.7	0.028
Air overlay	1587.6	1.0	0.159

Abbreviation: WCW, wet cell weight.

4 | DISCUSSION

O_2 supply and CO_2 stripping are two important factors in determining the success of biomanufacturing scale-up. They are two of the parameters that are challenging to replicate in the same way at different scales of manufacturing (Sieblist et al., 2011; Xing, Kenty, Li, & Lee, 2009). One can replicate constant glucose or any other metabolite concentration-based strategy or other scale-up strategies, but the concentration maintenance of dissolved gases across different scales is challenging due to the complexity of biological systems and the dynamic and hydrodynamic involved in the process (Chopda, Rathore, & Gomes, 2015; Gomes, Chopda, & Rathore, 2018; Persad, Chopda, Rathore, & Gomes, 2013). Researchers have evaluated different strategies to maintain DO supply and low dCO_2 level such as (1) sparge(a) rate, (2) agitator

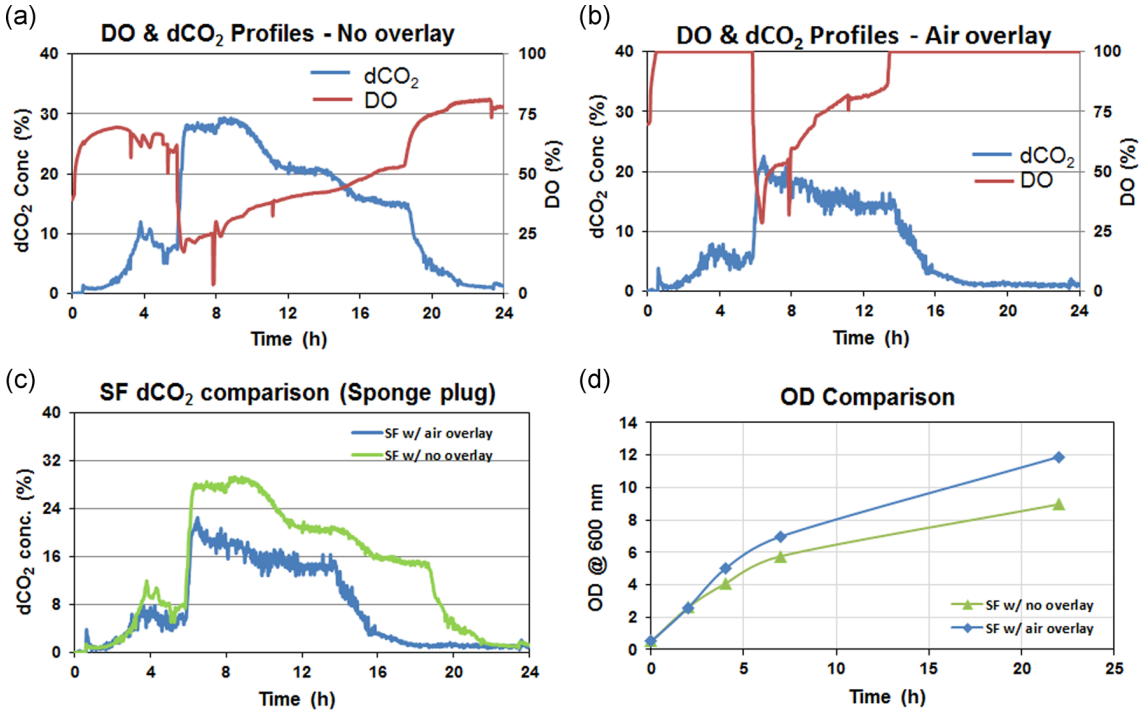

FIGURE 3 Process parameters monitored in *Escherichia coli* shake flask fermentation with sponge cap. (a) DO and dCO_2 profiles with no overlay. (b) DO and dCO_2 profiles with air overlay. (c) Comparison of dCO_2 profiles under different overlay conditions showing the significance of surface aeration. (d) Comparison of biomass growth showing the impact of surface aeration in the shake flask. dCO_2, dissolved CO_2; DO, dissolved oxygen; OD, optical density; SF, shake flask [Color figure can be viewed at wileyonlinelibrary.com]

speed, (3) impeller position, and (4) aeration rate at the headspace of bioreactor. All these methods are tested in standard bioreactor. Some of these like agitator speed and impeller position will not apply to the shake flask and may not be ideal choice to vary for shear sensitive cultures. However, we aim to have a general method which can be applied at all scales from shake flask to manufacturing bioreactor. We have tried sparging the culture in the shake flask, however, it foams out of the flask. Henceforth, we decided to evaluate the impact of sparging in headspace of shake flask, which to the best of our knowledge very few case studies are available on this concept (Takahashi & Aoyagi, 2018c). Further, we have monitored the impact of sparging in the headspace through our novel rate-based CO_2 sensor, which measures dCO_2 concentration in the culture broth.

Surface aeration through air overlay is common in cell culture at large scale to minimize the adverse effect of CO_2. However, in the small-scale systems, such as in shake flask and mini-bioreactor, it is generally assumed that surface aeration through headspace is sufficient for both oxygen supply and CO_2 stripping. But our results in this study showed that it is not true. Instead, sparging air in the headspace of shake flask and mini-bioreactor led to improved performance in terms of increased biomass growth and protein production. We also expect that this might be one of the reasons why most of the shake flask experiments are not reproducible at bioreactor level or why scale-up and technology transfer activity always has to consider a standard benchtop bioreactor. One interesting article (Matsunaga et al., 2009) suggests that it is not always valid to adjust the culture conditions based on only the constant k_{La}, which is the conventional approach. The evidence observed in CHO cultures shows that the dissolved gases concentration also holds the key to a successful scale-up (Matsunaga et al., 2009). As a result, it is important to consider surface aeration as a manipulative factor.

TABLE 2 Recombinant protein production in the shake flask culture with sponge caps

Surface aeration	Protein yield (μg)	WCW (g)	Normalized protein yield (%)
No overlay	1357	0.8	0.170
Air overlay	2137	0.8	0.267

Abbreviation: WCW, wet cell weight.

A similar impact of headspace aeration on dCO_2 concentration in the bioreactor has been reported (Mitchell-Logean & Murhammer, 1997; Mostafa & Gu, 2003). By sparging the air in the headspace, they were able to reduce dCO_2 concentration from 24 to 6 mM, which resulted in increased cell density for insect cell culture (Mitchell-Logean & Murhammer, 1997).

A study conducted by McIntyre and McNeil (1997) concluded that culture is more vulnerable to CO_2 inhibition in the lag phase. In addition, during the inoculation step, the culture can experience many stresses due to the significant differences in the environment of a shake flask and in the bioreactor conditions. Monitoring and regulating dCO_2 levels will allow us to control the culture

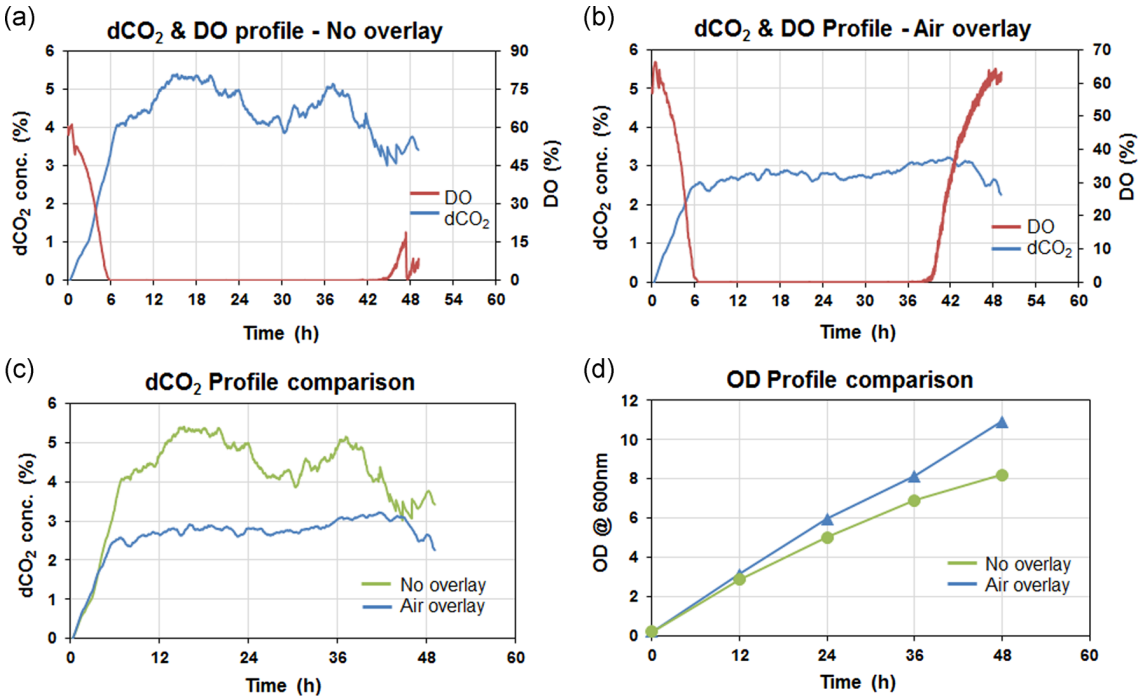

FIGURE 4 Process parameters monitored in recombinant *Yarrowia lipolytica Po1g Leu* yeast fermentation in mini-bioreactor (a) DO and dCO_2 profiles with no overlay (b) DO and dCO_2 profiles with air overlay. (c) Comparison of dCO_2 profiles under different overlay conditions showing the significance of surface aeration. (d) Comparison of biomass growth profiles showing the impact of surface aeration in the mini-bioreactor. dCO_2, dissolved CO_2; DO, dissolved oxygen; OD, optical density [Color figure can be viewed at wileyonlinelibrary.com]

environment to prevent any severe shock to the growing cells. Surface aeration intensification significantly enables us to manipulate this gas distribution. We believe that the shake flask and mini-bioreactor case studies presented in this paper using our proposed aeration modification will be an important factor to be considered in process development and scale-up activities.

5 | CONCLUSIONS

Our investigation proved that the surface aeration plays a critical role in shake flask process development. With controlled surface aeration in the shake flask, we were able to not only improve biomass growth but also reach higher protein yield. In addition, this study confirms and demonstrates the application of our novel noninvasive rate-based in-situ dCO_2 monitoring sensor in shake flask and in mini-bioreactor conditions.

ACKNOWLEDGMENTS

We would like to thank the Bill and Melinda Gates Foundation for generous support for this project.

ORCID

Xudong Ge http://orcid.org/0000-0003-1733-398X
Govind Rao http://orcid.org/0000-0001-6140-7582

REFERENCES

Amoabediny, G., & Büchs, J. (2010). Determination of CO_2 sensitivity of micro-organisms in shaken bioreactors. I. Novel method based on the resistance of sterile closure. *Biotechnology and Applied Biochemistry*, *57*(4), 157–166. https://doi.org/10.1042/ba20100211

Blombach, B., & Takors, R. (2015). CO_2–intrinsic product, essential substrate, and regulatory trigger of microbial and mammalian production processes. *Frontiers in Bioengineering and Biotechnology*, *3*, 108.

Büchs, J. (2001). Introduction to advantages and problems of shaken cultures. *Biochemical Engineering Journal*, *7*(2), 91–98.

Chatterjee, M., Ge, X., Uplekar, S., Kostov, Y., Croucher, L., Pilli, M., & Rao, G. (2015). A unique noninvasive approach to monitoring dissolved O_2 and CO_2 in cell culture. *Biotechnology and Bioengineering*, *112*(1), 104–110.

Chopda, V. R., Gomes, J., & Rathore, A. S. (2016). Bridging the gap between PAT concepts and implementation: An integrated software platform for fermentation. *Biotechnology Journal*, *11*(1), 164–171.

Chopda, V. R., Holzberg, T., Ge, X., Folio, B., Tolosa, M., Kostov, Y., … Rao, G. (2019). Real-time dissolved carbon dioxide monitoring I: Application of a novel in situ sensor for CO_2 monitoring and control. *Biotechnology and Bioengineering*, https://doi.org/10.1002/bit.27253

Chopda, V. R., Pathak, M., Batra, J., Gomes, J., & Rathore, A. S. (2017). Enabler for process analytical technology implementation in *Pichia pastoris* fermentation: Fluorescence-based soft sensors for rapid quantitation of product titer. *Engineering in Life Sciences*, *17*(4), 448–457.

Chopda, V. R., Rathore, A. S., & Gomes, J. (2015). Maximizing biomass concentration in baker's yeast process by using a decoupled geometric controller for substrate and dissolved oxygen. *Bioresource Technology*, *196*, 160–168.

Ge, X., Hanson, M., Shen, H., Kostov, Y., Brorson, K. A., Frey, D. D., … Rao, G. (2006). Validation of an optical sensor-based high-throughput bioreactor system for mammalian cell culture. *Journal of Biotechnology*, *122*(3), 293–306.

Ge, X., Kostov, Y., & Rao, G. (2005). Low-cost noninvasive optical CO_2 sensing system for fermentation and cell culture. *Biotechnology and Bioengineering*, *89*(3), 329–334.

Gomes, J., Chopda, V. R., & Rathore, A. S. (2015). Integrating systems analysis and control for implementing process analytical technology in bioprocess development. *Journal of Chemical Technology & Biotechnology*, *90*(4), 583–589.

Gomes, J., Chopda, V. R., & Rathore, A. S. (2018). Monitoring and control of bioreactor: Basic concepts and recent advances. *Bioprocessing Technology for Production of Biopharmaceuticals and Bioproducts*, 201–237.

Hanson, M. A., Ge, X., Kostov, Y., Brorson, K. A., Moreira, A. R., & Rao, G. (2007). Comparisons of optical pH and dissolved oxygen sensors with traditional electrochemical probes during mammalian cell culture. *Biotechnology and Bioengineering*, *97*(4), 833–841.

Jenzsch, M., Gnoth, S., Kleinschmidt, M., Simutis, R., & Lübbert, A. (2007). Improving the batch-to-batch reproducibility of microbial cultures during recombinant protein production by regulation of the total carbon dioxide production. *Journal of Biotechnology*, *128*(4), 858–867.

Kermis, H. R., Kostov, Y., Harms, P., & Rao, G. (2002). Dual excitation ratiometric fluorescent pH sensor for noninvasive bioprocess monitoring: Development and application. *Biotechnology Progress*, *18*(5), 1047–1053.

Kostov, Y., Harms, P., Randers-Eichhorn, L., & Rao, G. (2001). Low-cost microbioreactor for high-throughput bioprocessing. *Biotechnology and Bioengineering*, *72*(3), 346–352.

Kruger, N. J. (2009). The Bradford method for protein quantitation. In Walker J. M. (Ed.), *In The protein protocols handbook* (pp. 17–24). Totowa, NJ: Humana Press.

Matsunaga, N., Kano, K., Maki, Y., & Dobashi, T. (2009). Culture scale-up studies as seen from the viewpoint of oxygen supply and dissolved carbon dioxide stripping. *Journal of Bioscience and Bioengineering*, *107*(4), 412–418.

McIntyre, M., & McNeil, B. (1997). Dissolved carbon dioxide effects on morphology, growth, and citrate production in Aspergillus niger A60. *Enzyme and Microbial Technology*, *20*(2), 135–142.

Mitchell-Logean, C., & Murhammer, D. W. (1997). Bioreactor headspace purging reduces dissolved carbon dioxide accumulation in insect cell cultures and enhances cell growth. *Biotechnology Progress*, *13*(6), 875–877.

Mostafa, S. S., & Gu, X. S. (2003). Strategies for improved dCO_2 removal in large-scale fed-batch cultures. *Biotechnology Progress*, *19*(1), 45–51.

Persad, A., Chopda, V. R., Rathore, A. S., & Gomes, J. (2013). Comparative performance of decoupled input–output linearizing controller and linear interpolation PID controller: Enhancing biomass and ethanol production in *Saccharomyces cerevisiae*. *Applied Biochemistry and Biotechnology*, *169*(4), 1219–1240.

Priyanka, Roy, S., Chopda, V. R., Gomes, J., & Rathore, A. S. (2019). Comparison and implementation of different control strategies for improving production of rHSA using *Pichia pastoris*. *Journal of Biotechnology*, *290*, 33–43.

Sieblist, C., Hägeholz, O., Aehle, M., Jenzsch, M., Pohlscheidt, M., & Lübbert, A. (2011). Insights into large-scale cell-culture reactors: II. Gas-phase mixing and CO_2 stripping. *Biotechnology Journal*, *6*(12), 1547–1556.

Takahashi, M., & Aoyagi, H. (2018a). Monitoring of CO_2 and O_2 concentrations in the headspace of Sakaguchi flasks during liquid culture of microorganism. *Applied Microbiology and Biotechnology*, *102*(15), 6637–6645.

Takahashi, M., & Aoyagi, H. (2018b). Practices of shake-flask culture and advances in monitoring CO_2 and O_2. *Applied Microbiology and Biotechnology*, *102*(10), 4279–4289.

Takahashi, M., & Aoyagi, H. (2018c). Effect of intermittent opening of breathable culture plugs and aeration of headspace on the structure of microbial communities in shake-flask culture. *Journal of Bioscience and Bioengineering*, *126*, 96–101.

Tolosa, L., Kostov, Y., Harms, P., & Rao, G. (2002). Noninvasive measurement of dissolved oxygen in shake flasks. *Biotechnology and Bioengineering*, *80*(5), 594–597.

Vallejos, J. R., Brorson, K. A., Moreira, A. R., & Rao, G. (2010). Dissolved oxygen and pH profile evolution after cryovial thaw and repeated cell passaging in a T-75 flask. *Biotechnology and Bioengineering*, *105*(6), 1040–1047.

Xing, Z., Kenty, B. M., Li, Z. J., & Lee, S. S. (2009). Scale-up analysis for a CHO cell culture process in large-scale bioreactors. *Biotechnology and Bioengineering*, *103*(4), 733–746.

Xing, Z., Lewis, A. M., Borys, M. C., & Li, Z. J. (2017). A carbon dioxide stripping model for mammalian cell culture in manufacturing scale bioreactors. *Biotechnology and Bioengineering*, *114*(6), 1184–1194.

Xu, P., Qiao, K., Ahn, W. S., & Stephanopoulos, G. (2016). Engineering *Yarrowia lipolytica* as a platform for synthesis of drop-in transportation fuels and oleochemicals. *Proceedings of the National Academy of Sciences of the United States of America*, *113*(39), 10848–10853.

How to cite this article: Chopda VR, Holzberg T, Ge X, et al. Real-time dissolved carbon dioxide monitoring II: Surface aeration intensification for efficient CO_2 removal in shake flasks and mini-bioreactors leads to superior growth and recombinant protein yields. *Biotechnology and Bioengineering*. 2020;1–7. https://doi.org/10.1002/bit.27252

Bibliography

We have not added anything here, since the papers are the references and the bibliography cited in them acknowledge the efforts of many researchers whose work we have used to advance the field.

About the Author

Govind Rao is Professor of Chemical & Biochemical Engineering at the University of Maryland, Baltimore County. He obtained his Bachelor of Technology degree in Chemical Engineering from the Indian Institute of Technology, Madras in 1984. His Ph.D. degree was obtained from Drexel University in Chemical Engineering in 1987. He has been a faculty member at UMBC since 1987 and has served as Department Chair from 2000-2006. In 2006, he founded the Center for Advanced Sensor Technology (CAST) and has been serving as its Director since its inception.

CAST has pushed the envelope has focused on applications of fluorescence spectroscopy to create novel low-cost sensors for bioprocess, biomedical and environmental applications. CAST has developed patented next-generation sensors for low-cost non-invasive monitoring of oxygen, pH and pCO_2 in bioreactors. In addition, novel sensors for glucose and glutamine have been developed. The same non-invasive sensor technology developed for bioreactors is now being applied for neonatal monitoring where glucose and blood gases can be monitored at low cost. This technology is completely painless, as it relies on transdermal diffusion and so no blood draws are needed, thereby minimizing pain and infection risks to vulnerable infants. Another example of this is the development of a low-cost cardboard incubator that is currently in clinical trials in India. This single-use device costs <$5 and is coupled to a $200 servo-controller. The current focus in the CAST is a major effort to develop next generation bio-manufacturing technology and is aimed at producing protein-based therapeutics at the point-of-care. Cell-free systems are used to produce drugs in under 8 hours, compared to the several weeks that current processes enable. This technology was recently described in *Nature Biomedical Engineering* and demonstrates the potential to allow manufacturing of medicines anywhere in the world from a suitcase size device. It was recently featured on the cover of Chemical & Engineering News: https://cen.acs.org/magazine/96/09645.html and in Nature: https://www.nature.com/articles/d41586-019-03455-x.

Dr. Rao's research is targeted towards disruptive innovation, where the goal is to create paradigm shifts in the state-of-the-art. A major effort is the application of sensor technology to reduce healthcare costs and close disparity gaps by making innovative low-cost devices for use in low-resource settings. As part of this strategy, technology transfer and partnerships have been set up with entities in low-resource settings. Many industrial bioprocesses use patented sensor technologies developed by Dr. Rao. He has published over 180 papers in professional journals. His funding has come from several diverse sources including NSF, NIH, JDRF, DARPA, FDA, ONR, Bill and Melinda Gates Foundation and from several companies. Dr. Rao has given several invited Keynote and Plenary Lectures at various International Conferences and Corporations. He serves on various government and industry advisory panels.

He has received several awards. These include the Presidential Young Investigator Award from the National Science Foundation, Outstanding Teaching and Research Awards from UMBC, the Van Lanen Award from the American Chemical Society, the Gaden Award from Biotechnology & Bioengineering, the University System of Maryland Regents Award for Excellence in Research and he has been named a 2003 Innovator of the Year by the Maryland Daily Record. Dr. Rao has several patents, many of which have been licensed. Dr. Rao has served as the Chair of the Biotechnology Division of the American Chemical Society and on the Editorial Board of several prominent journals. In 2007, he was elected as a Fellow of the American Association for the Advancement of Science. In 2009, he was named as Editor of the PDA Journal of Pharmaceutical Science and Technology. In 2015 he received a "50 bright ideas" award from UMBC for the number of inventions filed and named an Eminent Engineer by Tau Beta Pi. He received the 2017 Pioneer Award from Connected World Magazine. The cardboard incubator won the 2019 Academic Pediatric Association Global Health Research Award. He has just been named 2019 Presidential Research Professor at UMBC.